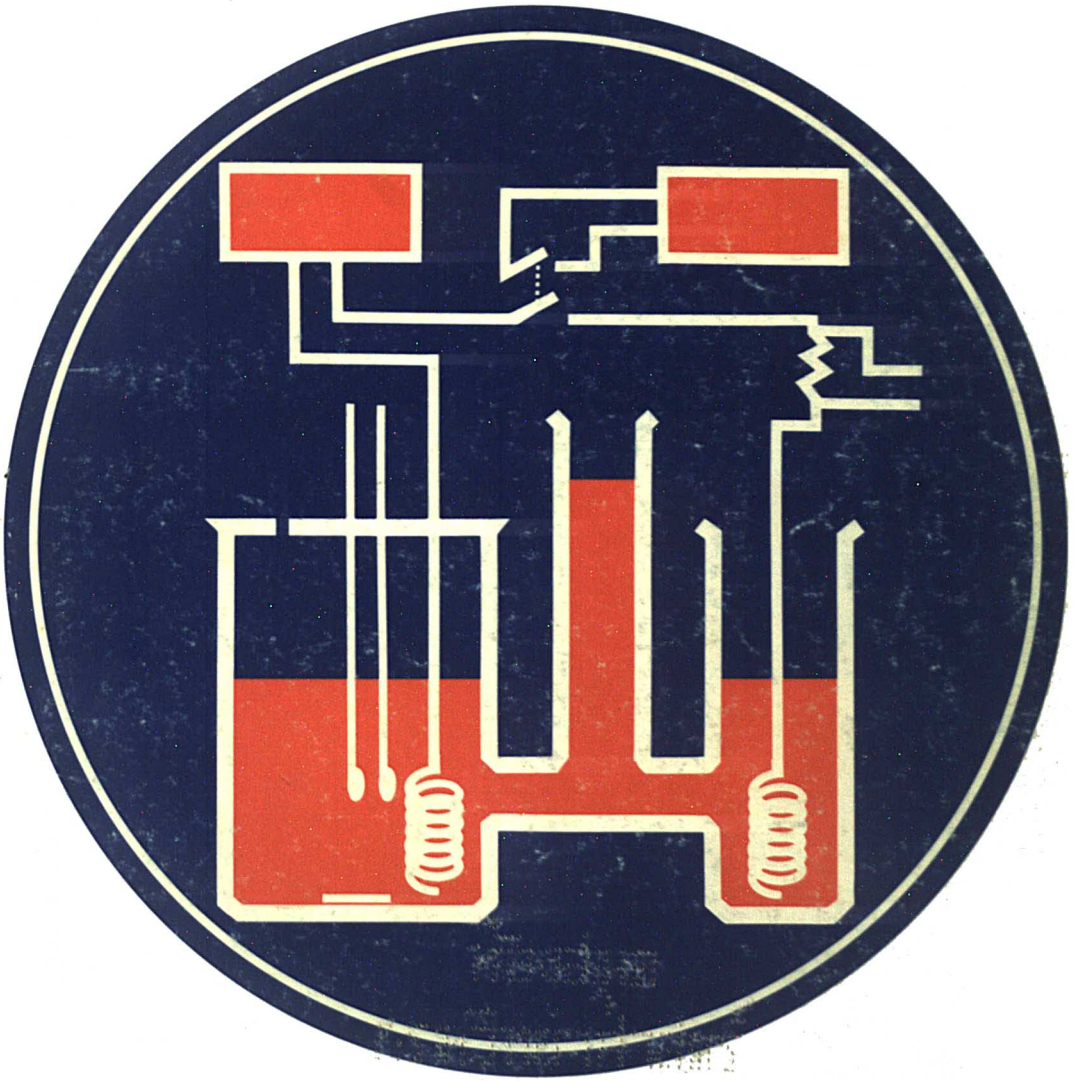
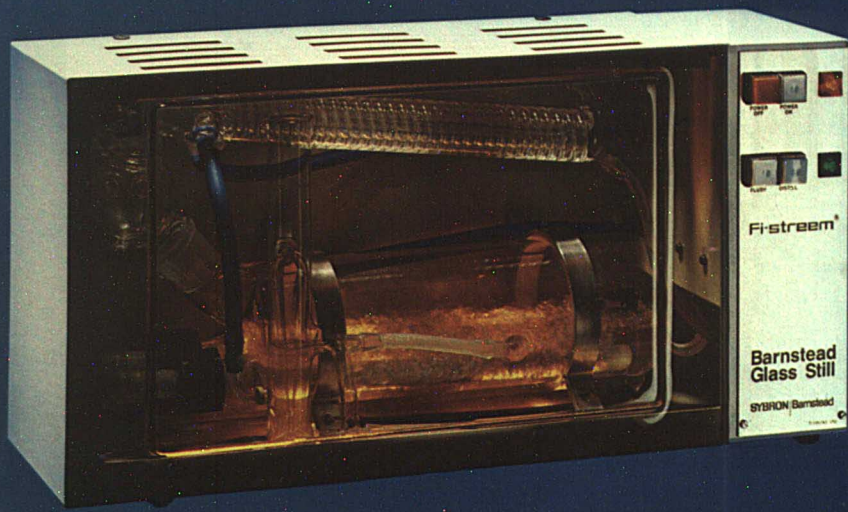
✓MARCH 1979

analytical chemistry



THE NEW BARNSTEAD GLASS STILL



IT'S WORTH LOOKING INTO

Here's a reliable, trouble-free source of high purity distilled water—in a compact fully automatic package that makes sense for the modern laboratory. Check this unbeatable combination of features:

High Purity.

Barnstead borosilicate glass stills produce sterile, pyrogen-free distillate with a specific resistance in excess of 2 megohms-cm (@ 25° C) depending upon feedwater quality. Total solids is typically as low as 0.1 mg/liter with SiO_2 content less than 5 ppb.

Fully Automatic.

A built-in distillate level monitor plus fail-safe low water protection enable continuous unattended operation with complete confidence. And since all controls are part of the still itself, you don't need a variety of expensive accessories for automatic operation.

Easy to Maintain.

These stills are designed so you know when to clean them . . . and they're built so you won't have to as often. The attractive acrylic safety cover lets you see the condition of the still at all times. A unique deconcentrator continuously removes scale-forming impurities to significantly reduce the need for cleaning. When periodic cleaning is required, you don't have to disassemble the still—a simple push button drain control makes the job quick and easy.

Exceptionally Compact.

Barnstead glass stills occupy only about 1/4th the space of other glass still systems. They blend nicely into the decor of any laboratory and can be conveniently bench or wall mounted.

Barnstead glass stills are available in single or double distilling modes; in output capacities of 4 or 8 liters per hour; and with a range of accessories including storage reservoirs, pretreatment kits and post-treatment polishing equipment. All models are CSA approved and are designed to meet OSHA requirements.

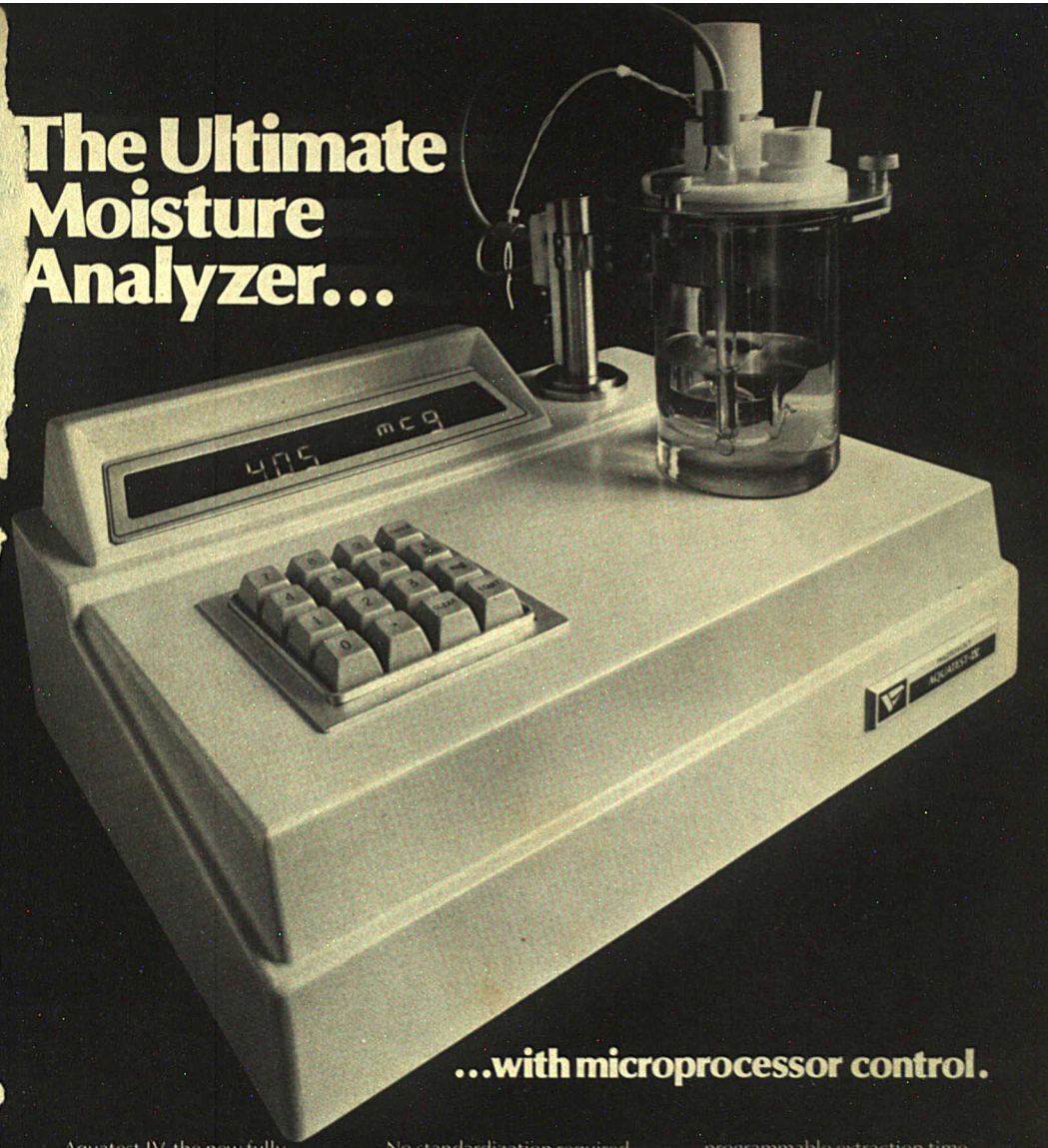
The glass still of the future is here today, available off-the-shelf from your laboratory supply distributor. For a closer look, contact Barnstead Company, Division of Sybron Corp., 225 Rivermoor St., Boston, MA 02132. (617) 327-1600.

4 liter/hr.— cat. no. A1040
8 liter/hr. — cat. no. A1042
4 liter/hr. double distiller — cat. no. A1056

SYBRON | Barnstead

CIRCLE 24 ON READER SERVICE CARD

The Ultimate Moisture Analyzer...



...with microprocessor control.

Aquatest IV, the new fully automated Karl Fischer titrator with digital readout, displays water content without calculations in ppm, percentages or micrograms.

No standardization required.

Aquatest IV automatically corrects for intertering reactions.

And has automatic blank correction when extracting, plus programmable extraction time.

For a free demonstration in your lab, call toll-free (800) 221-5182. In New York State, call collect (212) 989-0484.

After you lift a finger, you don't have to lift a finger.

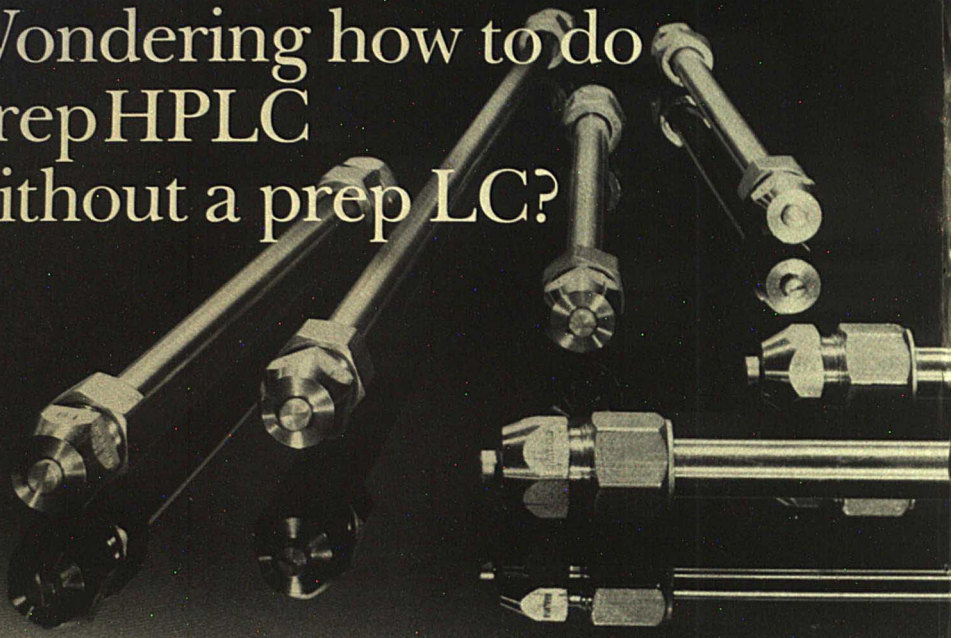
Photovolt Corporation

1115 BROADWAY, NEW YORK, N.Y. 10010

See us March 5-8 at the Pittsburgh Conference, Booths 712-714

CIRCLE 173 ON READER SERVICE CARD

Wondering how to do prep HPLC without a prep LC?



The new Partisil Magnum 9 prep columns — that's how.

Good news. You don't need thousands of dollars worth of dedicated prep LC system for preparative HPLC. Only your analytical LC and our new Partisil Magnum 9 prep columns. Excellent lab scale prep.

And you can have any, or all, Partisil phases (silica gel, amino-cyano, two reversed-phases, anion exchanger, cation exchanger) in the new Magnum 9 configuration; 50 cm or 25 cm long, 9.4 mm ID. You can load up to 2.5 grams of sample on a new Magnum 9 column.* Efficiencies of the best analytical columns: Magnum 9 packed with Partisil 10, N/M = 24,000 plates.

*Partisil Magnum 9 ODS-2; organics.

New Magnum 9 columns are fast, resolution is excellent. Simple scale-up from Partisil analytical columns — identical media. Final sample purity can be 99% or better. And Magnum 9 columns are **not** disposable types; you can regenerate them — an appreciable economic benefit, we think.

If you would like to know more, there's a new technical bulletin for the purpose. Write or call **Whatman Inc.**, 9 Bridewell Place, Clifton, New Jersey 07014. Tel: 201-777-4825.

Whatman

CIRCLE 239 ON READER SERVICE CARD

Volume 51, No. 3, March 1979
ANCHAM
51(3) 301A-426A/321-464 (1979)
ISSN 0003-2700

© Copyright 1979
by the American Chemical Society

Permission of the American Chemical Society is granted for libraries and other users to make reprographic copies for use beyond that permitted by Sections 107 or 108 of the U.S. Copyright Law, provided that the copying organization pay the appropriate per-copy fee through the Copyright Clearance Center, Inc. Educational institutions are generally granted permission to copy upon application to Office of the Director, Books and Journals Division, ACS, 1155 16th St., N.W., Washington, D.C. 20036.

Published monthly with review issue added in April and Laboratory Guide in August by the American Chemical Society, from 20th and Northampton Sts., Easton, Pa. 18042. Executive and Editorial headquarters, American Chemical Society, 1155 16th St., N.W., Washington, D.C. 20036 (202) 872-4600. Second class postage paid at Washington, D.C., and at additional mailing offices.

1979 Subscription prices—including surface postage

	1 yr	2 yr	3 yr
MEMBERS:			
Domestic	$12	$22	$30
Canada, Foreign	21	40	57
NONMEMBERS:			
Domestic	16	29	42
Canada	25	47	69
Other Foreign	33	61	89

Airmail and air freight rates are available from Membership & Subscription Services, ACS, P.O. Box 3337, Columbus, Ohio 43210 (614) 421-7230.

New and renewal subscriptions should be sent with payment to the Office of the Controller at the ACS Washington address.

Subscription service inquiries and changes of address (include both old and new addresses with ZIP code and *recent mailing label*) should be directed to the ACS Columbus address noted above. Please allow six weeks for change of address to become effective.

Claims for missing numbers will not be allowed if loss was due to failure of notice of change of address to be received in the time specified; if claim is dated (a) North America: more than 90 days beyond issue date, (b) all other foreign: more than one year beyond issue date; or if the reason given is "missing from files."

Microfilm and microfiche editions are available by single volume or back issue collection. Inquiries and payments to Microforms Program, ACS Washington address.

Single issues, current year, $3.00 except review issue and Labguide, $4.00; **back issues and volumes:** *write or call* Special Issues Sales, ACS Washington address (202) 872-4365.

Advertising Management: Centcom, Ltd., 25 Sylvan Road South, Westport, Conn. 06880 (203) 226-7131

analytical chemistry

CONTENTS

REPORT

Harvey Diehl of Iowa State University reviews the history and some recent high-precision electrochemical work on the evaluation of the faraday **318 A**

INSTRUMENTATION

Laser Raman molecular microprobe generates information about chemical bonds and molecular structure. Each component of a sample can be detected, identified, and located. Numerous applications are shown **414 A**

REGULATIONS

Licensing, registration, and certification programs attract widespread interest in today's regulatory atmosphere **333 A**

NEWS

Technical programs of interest to analytical chemists at the 177th ACS National Meeting in Honolulu, Hawaii, April 1-6, 1979, and at the 4th International Symposium on Column Liquid Chromatography in Boston, Mass., May 7-10, 1979, are given **337 A**

BOOKS

R. J. Highet and R. L. Clements review books on NMR spectrometry and paper and thin-layer chromatography **399 A**

EDITORS' COLUMN

The recent activities of the National Committee for Clinical Laboratory Standards illustrate concerted efforts toward regulation by voluntary consensus standards rather than by legislation **407 A**

EDITORIAL

Modifications of current PhD programs appear preferable to launching entirely new degree programs to meet the needs of industry **321**

Technical Contents/Briefs	**304 A**
Reader Survey	**314 A**
Call for Papers	**375 A**
Meetings	**376 A**
Short Courses	**376 A**
New Products	**388 A**
Chemicals	**392 A**
Manufacturers' Literature	**396 A**
Advertising Index	**424 A**
Author Index	**IBC**
Future Articles	**IBC**



Our cover depicts a coulometric titration cell, an apparatus used in this month's REPORT

ห้องสมุด กรมวิทยาศาสตร์บริการ
26 มี.ค. 2522

Briefs

Chronopotentiometry with Programmed Current 322

The electrolysis current is varied as the square-root of time resulting in additive transition times. The RSD is of the order of 1% at 5×10^{-4} M.

Li Hang Chow and Galen W. Ewing,* Department of Chemistry, Seton Hall University, South Orange, N.J. 07079

Anal. Chem., 51 (1979)

Experimental Evaluation of Recursive Estimation Applied to Linear Sweep Anodic Stripping Voltammetry for Real Time Analysis 327

The Kalman filter is experimentally evaluated and a critical comparison with other digital techniques indicates that it affords improved precision of analyte concentration estimates.

Paul F. Seelig and Henry N. Blount,* Brown Chemical Laboratory, The University of Delaware, Newark, Del. 19711

Anal. Chem., 51 (1979)

Correction for Background Current in Differential Pulse, Alternating Current, and Related Polarographic Techniques in the Determination of Low Concentrations with Computerized Instrumentation 337

Quadratic least squares fit of data at potentials removed from the wave of interest is used to predict the base line.

A. B. Bond* and B. S. Grabaric, Department of Inorganic Chemistry, University of Melbourne, Parkville, 3052, Victoria, Australia

Anal. Chem., 51 (1979)

Potentiometric Stripping Analysis in Non-Deaerated Samples 342

Potentiometric stripping analysis of Zn, Cd, Pb, Tl, Cu, and Bi can be performed in acidic non-deaerated samples using dissolved oxygen as oxidant. The optimum concentration range of analyte is 25–1000 μg/L.

Daniel Jagner, Department of Analytical Chemistry, University of Göteborg, Fack, S-402 20 Göteborg, Sweden

Anal. Chem., 51 (1979)

Optimization of the Analytical Oxidation of Dihydronicotinamide Adenine Dinucleotide at Carbon and Platinum Electrodes 346

Reproducible carbon electrode, prepared by covering the surface with electrochemically generated NAD^+, gives results at mM and μM levels by current measurement at a single potential.

Jacques Moiroux and Philip J. Elving,* Department of Chemistry, University of Michigan, Ann Arbor, Mich. 48109

Anal. Chem., 51 (1979)

*Corresponding author.

Neutral Carrier Sodium Ion-Selective Microelectrode for Intracellular Studies 351

The response to Na^+ activities is linear over the range 10^{-1}–10^{-3} M NaCl solutions, and the selectivities of H_3O^+, K^+, Mg^{2+}, and Ca^{2+} are adequate for reliable intercellular measurements.

R. A. Steiner, M. Oehme, D. Ammann, and W. Simon,* Department of Organic Chemistry, Swiss Federal Institute of Technology, Universitätstr. 16, CH-8092 Zurich, Switzerland

Anal. Chem., 51 (1979)

Reticulated Vitreous Carbon Flow-Through Electrodes 353

The material has low electrical resistance, large surface area, and a physically continuous structure. Solutions in the concentration range of 1–1000 μM produce currents from about 1–1000 μA, respectively, using flow rates from 0.5–25 mL/min.

A. N. Strohl and D. J. Curran,* Department of Chemistry, GRC Tower I, University of Massachusetts, Amherst, Mass. 01003

Anal. Chem., 51 (1979)

Introduction of Functiona Groups onto Carbon Electrodes via Treatment with Radiofrequency Plasmas 358

The functional groups provide sites for further attachment of molecules/ions using conventional chemical reactions. Results for the cases of oxygen and ammonia discharges are discussed in detail.

John F. Evans and Theodore Kuwana,* Department of Chemistry, The Ohio State University, 140 West 18th Avenue, Columbus, Ohio 43210

Anal. Chem., 51 (1979)

Metal-Ion Chelation Chromatography on Silica-Immobilized 8-Hydroxyquinoline 366

Selective separations of trace level concentrations of transition and lanthanide metal ions are achieved. The relation of chromatographic behavior to solution chelation equilibria is described.

John R. Jezorek and Henry Freiser,* Department of Chemistry, University of Arizona, Tucson, Ariz. 85721

Anal. Chem., 51 (1979)

4-(Pyridylazo)resorcinol-Based Continuous Detection System for Trace Levels of Metal Ions 373

As littel as 5 ng of metal ions can be spectrophotometrically determined in a flow system using PAR.

John R. Jezorek and Henry Freiser,* Department of Chemistry, University of Arizona, Tucson, Ariz. 85721

Anal. Chem., 51 (1979)

ORION's "no lemon" meters will suit you to a T-shirt.



Model 501: New, low-cost digital pH meter readable to 0.01 pH. Features ATC and digital reading of temperature.

Model 407A: Versatile, top-of-the-line analog meter for pH and specific ion work. Also available in battery-powered field version, with carrying case.

Model 201: A low-cost, hand-held digital that reads to 0.05 pH. Comes with carrying case and line adaptor to permit laboratory use.

Model 701A: Research-grade digital pH/mV meter with 0.001 pH resolution. Features ATC and digital output for interfacing to ORION printer. Comes with swing arm electrode holder.

901 Microprocessor Analyzer: Unique "thinking" meter offers unmatched simplicity of operation, makes electrode analysis faster, easier. Pushbutton standardization and blank correction. No calibration curves to draw.

The famous ORION "no lemon" T-shirt, yours with a demo of any ORION "no lemon" meter.

Ask for a demonstration of any ORION "no lemon" meter and receive a "no lemon" T-shirt, free!

Take your pick of the "no lemon" crop! These are just a few of ORION's pH and specific ion meters, priced from as little as $220. They're so reliable, each one comes with our famous "no lemon" guarantee: if your meter quits for any reason other than abuse within one year of purchase, we'll replace it with a brand new one. Immediately, and without charge. That's why we say, "ORION eats lemons!" Mail the coupon today for your demo and free T-shirt.



Please call me for a demo of (circle):
501 901 407A 201 701A

T-shirt size: ☐medium ☐large ☐extra-large

Name _____

Title _____ Phone ( ) _____

Organization _____

Street _____

City _____ State _____ Zip _____

ORION RESEARCH

380 Putnam Ave., Cambridge, MA 02139

Orion® "No lemon"®

CIRCLE 156 ON READER SERVICE CARD

Briefs

Lead, Cadmium, and Zinc Bis(diethyldithiocarbamate) and Diethyldithiocarbamic Acid as Reagents for Liquid–Liquid Extraction 376

The extraction constants (log K_{ex}) of $Pb(DDC)_2$, $Cd(DDC)_2$, and $Zn(DDC)_2$ for the system $H_2O/CHCl_3$ are found to be 7.94 ± 0.09, 5.77 ± 0.05, and 2.39 ± 0.02.

Sixto Bajo* and Armin Wyttenbach, Swiss Federal Institute for Reactor Research, 5303 Würenlingen, Switzerland *Anal. Chem., 51 (1979)*

Fluidic Logic Element Sample Switch for Correlation Chromatography 379

Sample injection system suitable for correlation chromatography is fabricated from two Coanda wall attachment fluidic bistable amplifiers to increase the S/N of a conventional FID.

Raymond Annino,* Department of Chemistry, Canisius College, Buffalo, N.Y. 14208, and **Marie-France Gonnord and Georges Guiochon,** Ecole Polytechnique, Laboratoire de Chimie Analytique Physique, Route de Saclay, 91128 Palaiseau Cedex, France *Anal. Chem., 51 (1979)*

Combination of Size Exclusion and Normal-Phase Partition Modes in High Performance Liquid Chromatography 382

The combined use of the two separation modes, illustrated with phthalate esters, alkylbenzenes, and ketones, may extend their advantages and compensate their disadvantages.

Sadao Mori* and Akira Yamakawa, Department of Industrial Chemistry, Faculty of Engineering, Mie University, Tsu, Mie 514, Japan *Anal. Chem., 51 (1979)*

Salting-Out Chromatography Applied to Separation and Analysis of Mixtures of Thioureas and Thioacetamide by High Performance Liquid Chromatography 385

A recovery of 99.3 ± 2.66% is obtained at the level of 160 ng/mL when the method is applied to field soil samples. Limits of detection are estimated to be 2.7 ng.

Akio Hashimoto, Water Quality Research Section, Kitakyushu Municipal Institute of Environmental Health Science, 1-2-1 Shinike, Tobataku, Kitakyushu City, 804, Japan *Anal. Chem., 51 (1979)*

High Gas Temperature Furnace for Species Determination of Organometallic Compounds with a High Pressure Liquid Chromatograph and a Zeeman Atomic Absorption Spectrometer 387

The furnace reduces chemical interference caused by $MgCl_2$, $CuCl_2$, and $CaCl_2$ such that two orders of magnitude more interferent can be tolerated.

Hideaki Koizumi,* Ralph D. McLaughlin, and Tetsuo Hadeishi, Lawrence Berkeley Laboratory, University of California, Berkeley, Calif. 94720 *Anal. Chem., 51 (1979)*

Gas–Liquid Chromatographic Study of the Thermodynamics of Solution in Dipropionitriles 392

GC equilibrium data on the three nitrile stationary phases over a limited temperature range (40–60 °C) for three solvents are determined.

R. K. Kuchhal and K. L. Mallik,* Indian Institute of Petroleum, Dehradun-248005, India *Anal. Chem., 51 (1979)*

Graphitized Carbon in Gas–Liquid–Solid Chromatography and Gas Chromatography/Mass Spectrometric Analysis of High Boiling Hydrocarbon Mixtures 400

C_4 to C_{40} hydrocarbons in natural samples can be resolved on columns packed with graphitized carbon black coated with poly(phenyl ether).

Paolo Ciccioli and John M. Hayes, Departments of Chemistry and Geology, Indian University, Bloomington, Ind., **Gianfranco Rinaldi and Kenneth B. Denson,** Department of Geology, Indiana University, Bloomington, Ind., and **Warren G. Meinschein,*** Department of Geology and School of Public and Environmental Affairs, Indiana University, Bloomington, Ind. *Anal. Chem., 51 (1979)*

Development and Characterization of a Miniature Inductively Coupled Plasma Source for Atomic Emission Spectrometry 408

The plasma source operates at low RF power levels and requires less argon support gas than conventional ICP sources.

R. N. Savage and G. M. Hieftje,* Department of Chemistry, Indiana University, Bloomington, Ind. 47401 *Anal. Chem., 51 (1979)*

Determination of Organic (Methyl) Mercury in Fish by Graphite Furnace Atomic Absorption Spectrophotometry 414

Addition of dithizone to toluene extract allows methyl mercury to be determined in the furnace with a detection limit of 0.08 μg Hg/g sample.

Gerald T. C. Shum,* Harry C. Freeman, and John F. Uthe, Department of Fisheries & the Environment, Fisheries and Marine Service, Technology Branch, 1707 Lower Water Street, P.O. Box 550, Halifax, Nova Scotia B3J 2S7 *Anal. Chem., 51 (1979)*

Fiber Optic Waveguides for Time-of-Flight Optical Spectrometry 417

A fiber optic waveguide can be used as the dispersing element in a time-of-flight optical spectrometer.

W. B. Whitten* and H. H. Ross, Analytical Chemistry Division, Oak Ridge National Laboratory, Oak Ridge, Tenn. 37830 *Anal. Chem., 51 (1979)*

A major breakthrough in HPLC sample injectors.

The unique 4-port design of this new HPLC sample injection valve offers you 7 significant advantages.



1. IMPROVED PRECISION AND REPRODUCIBILITY. Standard deviation of peak area in repetitive sampling <0.5%.

2. LONG VALVE LIFE. 30,000 operations at 6000 psi before any significant seal wear evidence.

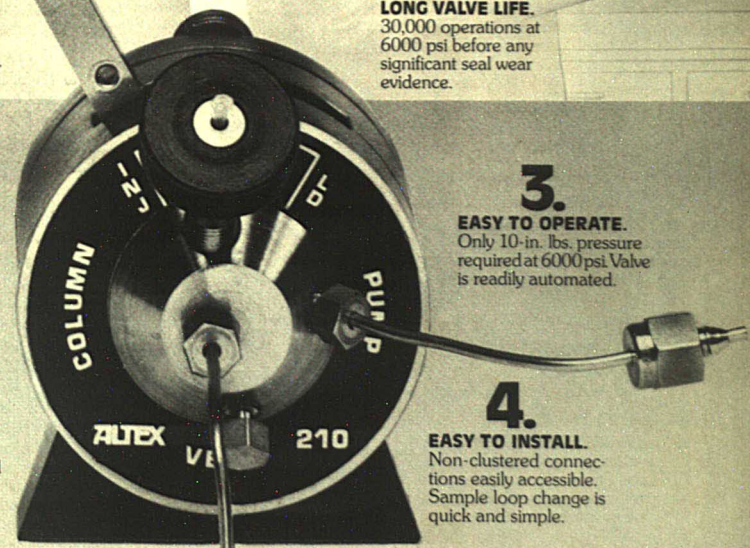
3. EASY TO OPERATE. Only 10-in. lbs. pressure required at 6000 psi. Valve is readily automated.

4. EASY TO INSTALL. Non-clustered connections easily accessible. Sample loop change is quick and simple.

5. CHOICE OF INLET PORTS. Inject with needle or luer-tipped syringe; or connect valve to any remote sampler system.

6. EVENT MARKER. This accessory will mark injection point on your chromatogram, start integrator or tell your Altex 420 Controller to start a program.

7. AUTOMATED OPERATION. Pneumatically-operated version is available for automated systems.



Let us send you a complete brochure documenting features and performance of this remarkable new injection valve.

ALTEX

ALTEX SCIENTIFIC INC.
A subsidiary of Beckman Instruments Inc.
1780 Fourth Street, Berkeley, California 94710, (415) 527-5900, Telex 33-5403

CIRCLE 1 ON READER SERVICE CARD

Briefs

Influence of Errors and Matching Criteria upon the Retrieval of Binary Coded Low Resolution Mass Spectra 420

Performance of the retrieval depends primarily on the extent of errors occurring in the coded spectra and is hardly affected by the matching criterion being used.

Geert van Marlen, Department of Analytical Chemistry, Delft University of Technology, Jaffalaan 9, Delft, The Netherlands, and **Auke Dijkstra* and Henk A. van't Klooster,** Department of Analytical Chemistry, State University of Utrecht, Croesestraat 77A, Utrecht, The Netherlands *Anal. Chem., 51 (1979)*

Application of Microporous Membranes to Chemiluminescence Analysis 424

Reagent addition rates of only μL/min into an analyte flow stream are obtained through microporous membranes. Co(II) determinations using luminol have a 10^{-10} M detection limit and ±3% RSD.

Vance Nau and Timothy A. Nieman,* School of Chemical Sciences, University of Illinois, Urbana, Ill. 61801 *Anal. Chem., 51 (1979)*

Trace Element Laser Microanalyzer with Freedom from Chemical Matrix Effect 428

In-situ sensitivity of about 1 ppm is achieved for chromium and the uncertainty in the measurement is 15–30%.

H. S. Kwong and R. M. Measures,* Institute for Aerospace Studies, University of Toronto, 4925 Dufferin Street, Downsview, Ontario M3H 5T6, Canada *Anal. Chem., 51 (1979)*

Resolution of the Optical Isomers of Dansyl Amino Acids by Reversed Phase Liquid Chromatography with Optically Active Metal Chelate Additives 433

Separation of D,L-dansyl amino acids with high efficiency and α values greater than 2.0 are achieved. Mechanistic details are described.

James N. LePage, Wolfgang Lindner, Geoffrey Davies, David E. Seitz, and Barry L. Karger,* Institute of Chemical Analysis and Department of Chemistry, Northeastern University, Boston, Mass. 02115 *Anal. Chem., 51 (1979)*

Effect of Oxygen on Composition of Light Hydrocarbons Evolved in Oil Shale Pyrolysis 435

Absolute and relative amounts of *n*-alkanes and 1-alkenes from C_1 to C_5 evolved during oil shale pyrolysis are measured by gas solid chromatography on Spherocarb.

Mark V. Robillard, Sidney Siggia, and Peter C. Uden,* Department of Chemistry, GRC Tower I, University of Massachusetts, Amherst, Mass. 01003 *Anal. Chem., 51 (1979)*

Membrane-Covered, Rotated Disc Electrode 439

The electrode evaluates mass transport in membranes.

David A. Gough* and John K. Leypoldt, Department of Applied Mechanics and Engineering Sciences, Bioengineering Group, University of California at San Diego, La Jolla, Calif. 92093 *Anal. Chem., 51 (1979)*

Amperometric Enzymatic Determination of Total Cholesterol in Human Serum with Tubular Carbon Electrodes 444

The method requires only 20 μL of sample, shows no interference from hemoglobin, bilirubin, or 4 mg/dL ascorbic acid, and gives a correlation coefficient of 0.995 with the Leffler method.

Younghee Hahn and Carter L. Olson,* College of Pharmacy, 500 West 12th Avenue, The Ohio State University, Columbus, Ohio 43210 *Anal. Chem., 51 (1979)*

Determination of Quinidine and Dihydroquinidine in Plasma by High Performance Liquid Chromatography 449

Plasma concentrations as low as 0.05 μg/mL can be measured with a RSD less than 10%. The minimum detectable quantity is 1 ng on column.

Berry J. Kline,* Vilma A. Turner, and William H. Barr, Department of Pharmacy and Pharmaceutics, Medical College of Virginia, Virginia Commonwealth University, Richmond, Va. 23298 *Anal. Chem., 51 (1979)*

Determination of Trace Silica in Industrial Process Waters by Flameless Atomic Absorption Spectrometry 452

The RSD of the test at the 25 μg/L SiO_2 level is 6.1%, and average recovery of silica added to various industrial waters is 102%.

Judith A. Rawa* and Earl L. Henn, Calgon Corporation, P.O. Box 1346, Pittsburgh, Pa. 15230 *Anal. Chem., 51 (1979)*

Fluorescence Photometric Determination of Disopyramide and Mono-*N*-dealkylated Disopyramide in Plasma after Separation by Thin-Layer Chromatography 455

The procedure is linear up to 10 mg/L and the calibration curve passes through the origin.

Ram N. Gupta,* Francis Eng, and Diane Lewis, Department of Laboratory Medicine, St. Joseph's Hospital, Hamilton, Ontario, Canada, and **Cyrus Kumana,** Department of Medicine, McMaster University, Hamilton, Ontario, Canada *Anal. Chem., 51 (1979)*

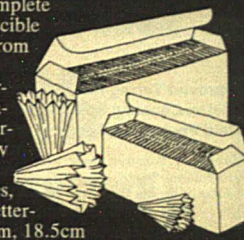
Put less time in to get more results out with S&S pre-pleated filter papers.

A pre-pleated S&S filter paper gives you twice the exposed surface area of an ordinary filter folded by hand into quadrants. You not only save time on folding, your solid–liquid separations move faster, and a series of filtrations can be set up and run in measurably shorter time. Solids are more dispersed over the surface of the paper, and clogging is reduced or eliminated. Because of this, these filters are widely used to recycle reagents in chemistry autoanalyzers.

Standard grades of S&S pre-pleated filters resist dilute acidic and alkaline solutions. Their wet-strength is high and their relatively high flash point permits filtration of hot gelatins, agar and other culture media without degeneration of the filter.

If you've been avoiding pre-pleated filters because they sometimes burst at the apex during critical filtrations, use S&S pre-pleated filters without fear. They're burst-proof under normal laboratory conditions.

S&S pre-pleated filters retain precipitates from coarse to fine in six standard grades and 10 standard diameters from 12.5 cm to 50.0 cm. Now, for phase separation requirements, they're also available in several sizes in 595hy ½ hydrophobic, silicone-impregnated for quick and complete separation of immiscible aqueous solutions from organic solvents.



For complete information and specifications, contact your nearby laboratory supply dealer. For a free sample pack of three grades, write to S&S on your letterhead, specifying 12.5cm, 18.5cm or 24.0cm diameter.

Schleicher & Schuell

Schleicher & Schuell, Inc.
Keene, New Hampshire 03431

Schleicher & Schüll GmbH, D-3354, Dassel, West Germany
Schleicher & Schüll AG, 8714, Feldbach ZH, Switzerland

CIRCLE 192 ON READER SERVICE CARD

FREE 3-PACK

75 pre-pleated filters — 25 each of three filtration speeds: Fast, Medium and Slow. Write to S&S on your letterhead. Be sure to specify 12.5cm, 18.5cm or 24.0cm diameter.

Briefs

Correspondence

Improved Timing Resolution in Time-Correlated Photon Counting Spectrometry with a Static Crossed-Field Photomultiplier 458

Vaughn J. Koester, Department of Physiology and Graduate Program in Physiology and Biophysics, University of Texas Health Center at Dallas, 5323 Harry Hines Boulevard, Dallas, Tex. 75235
Anal. Chem., 51 (1979)

Ligand Exchange Chromatography of Amino Acids on Copper(II) Modified Silica Gel with Ultraviolet Spectrophotometric Detection at 210 Nanometers 459

M. Caude and A. Foucault,* Laboratoire de Chimie Analytique de l'Ecole Superieure de Physique et de Chimie Industrielles de la ville de Paris, 10 rue Vauquelin, 75231 Paris, Cedex 05, France
Anal. Chem., 51 (1979)

Comments on Determination of Acetate in Biological Material by Vacuum Microdistillation and Gas Chromatography 461

Lawrence Sweetman, Department of Pediatrics M-009, University of California—San Diego, La Jolla, Calif. 92093
Anal. Chem., 51 (1979)

Aids for Analytical Chemists

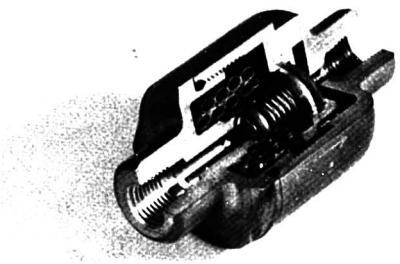
Simultaneous Determination of Trace Amounts of Hydrogen, Oxygen, Nitrogen, Carbon Monoxide, Carbon Dioxide, Methane, Ethane, Ethelene, and Acetelene by Two Gas Chromatographic Columns in Parallel and One Detector 462

Fikry F. Andrawes,* Lockheed Electronics Co., Inc., 1830 Nasa Road 1, Houston, Tex. 77058, and **Everett K. Gibson, Jr.,** SN7, Geochemistry Branch, NASA Johnson Space Center, Houston, Tex. 77058
Anal. Chem., 51 (1979)

Preparing Nitrogen Gas for Nitrogen-15 Analysis 463

Richard J. Volk* and William A. Jackson, Department of Soil Science, North Carolina State University, Raleigh, N.C. 27607
Anal. Chem., 51 (1979)

FLASH ARRESTOR PROTECTS ATOMIC ABSORPTION USERS



The 6103L flash arrestor minimizes the hazards of acetylene flashback that can occur with Atomic Absorption. Flashback in Atomic Absorption results when the flame at the instrument burner head reverses and travels back through the hose to the pressure regulator and/or cylinder.

Should a flashback occur, the shock wave preceding the flame automatically locks the Flash Arrestor valve shutting off the gas flow. The flame is then detoured through spiral tubing where it is extinguished .

The 6103 flash arrestor is reusable and can be employed on virtually every line through which a flammable gas flows. **Matheson, 1275 Valley Brook Avenue, P.O. Box E, Lyndhurst, NJ 07071.**

Circle 137 on Reader Service Card.

EXPANDED LINE OF CALIBRATION GAS MIXTURES

Matheson has expanded its broad line of gas mixtures in MATHESON PROCESSED ALUMINUM CYLINDERS to include a new cylinder size. The cylinder, designated as size 2R, contains approximately 80 cu.ft. of calibration gas standard and complements the 1R (150 cu.ft.) and 3R (30 cu.ft.) sizes, giving users a wider choice of cylinders for their calibration gas standards.

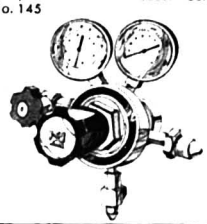
The new 2R cylinder is available to contain corrosive and toxic gas mixtures of hydrogen sulfide, benzene, carbonyl sulfide, oxides of nitrogen and certain mercaptans. These types of mixtures are routinely supplied by Matheson to calibrate analyzers used in monitoring industrial emission levels and ambient air pollution levels.

For a brochure that describes the calibration gas standards available in MATHESON PROCESSED ALUMINUM CYLINDERS, including concentration ranges and cylinder specifications, contact **Matheson, 1275 Valley Brook Avenue, P.O. Box E, Lyndhurst, NJ 07071.**

Circle 138 on Reader Service Card.

A Special Regulator For GC

The Matheson 3104 regulator is a high purity, two-stage regulator with a stainless steel diaphragm. Two-stage design provides even regulation regardless of cylinder pressure changes. Stainless steel diaphragm minimizes inboard leakage of air or water from the atmosphere, and does not outgas impurities into carrier or fuel gas systems. Five minute helium leak rate is $< 2 \times 10^{-9}$ ccs. Excellent for applications involving trace components. Circle Reader Service No. 145



Gas Miser

A device which allows one or more GCs to be set on standby during non-working hours. The flow of carrier gas is reduced with the flick of a switch without upsetting the equilibrium conditions of your instrument. Then normal operating conditions are resumed the same way.

Gas Miser, for the GC laboratory. Saves expensive time and carrier gas. Pays for itself in less than a year.
Circle Reader Service No. 146



High Purity Carrier Gases

Matheson makes carrier gases available in a variety of purity classifications – choose the specifications that most nearly meet your requirements. Routine analyses can be performed using Helium, High Purity, 99.995%. For more critical applications, you may choose Ultra High Purity 99.999% and Matheson Purity 99.9999%. For other applications, Argon, Hydrogen, and Nitrogen are all available in a variety of purities.
Circle Reader Service No. 147

Zero Gases

For the carrier gas, fuel gas, and oxidizer gas—all required for flame ionization and flame photometric gas chromatography-Matheson offers Ar, He, H_2, N_2, 40% H_2/60% N_2, and 40% H_2/60% He Zero Gases each having a total hydrocarbon content of less than 0.5 ppm (as CH_4). Air, Zero Gas is available with hydrocarbon content < 2.0 ppm. Circle Reader Service No. 148

Calibration Standards

When the level (TLV) of a toxic vapor is to be monitored the instrument must be accurate – for the physical well-being of those who may be exposed.

The only way to do this is to calibrate the instrument with an analyzed standard. Matheson pioneered such standards, accuracy traceable to NBS, if available, or to Matheson Primary standards. Calibration standards are readily available for: benzene, vinyl chloride, acrylonitrile, carbon monoxide. . . virtually any vapor forming material. Circle Reader Service No. 149



Gas Leak Detector

Simple to operate. Detects helium and other gases with great sensitivity. Enables you to check your entire GC system without the mess usually associated with leak detection solutions.

The smallest imaginable leak in your GC system can invalidate your results completely – especially if you're working with trace concentrations.

We recommend that one be handy in every instrument lab. Circle Reader Service No. 150



How to Succeed at Gas Chroma~tography

Gases – carrier gases, calibration gases, or fuel gases are key to good GC techniques. Matheson has equipment to help you improve this gas system and you should use it.

The wrong regulator or porous tubing can permit diffusion into the gas stream and influence results.

But some equipment will help in other ways like saving money or zeroing in on a defective connection.

Further, todays detectors are so sensitive that a welding grade of helium is counter productive.

To find out how you might improve the efficiency of your GC system, ask for our free wall chart describing methods that can be used with common and uncommon detectors in use today. Contact us for your copy.

Matheson®
Lyndhurst, NJ 07071

East Rutherford, NJ 07073
Morrow, Georgia 30260
Bridgeport, NJ 08014
Gloucester, Massachusetts 01930
Joliet, Illinois 60434
Dayton, Ohio 45424
La Porte, Texas 77571
Cucamonga, California 91730
Newark, California 94560
Dorsey, Maryland 21227
Gonzales, Louisianna 70737
Whitby, Ontario, Canada L1N 5R9
Edmonton, Alberta, Canada T5B 4K6
B 2431 Oevel, Belgium
6056 Heusenstamm, West Germany

Circle Reader Service No. 151

Here are 33 Johns-Manville chromatography products.

And a guide to help you use them.



J-M chromatography guide

The number of Johns-Manville chromatography supports, adsorbents and packings continues to grow.

With all these choices available, we'd like you to have this handy guide to help in selecting the right type and grade for your application.



Liquid Chromatography

There are 8 grades of Chromosorb® LC supports, adsorbents and packings to choose from.

LC-1 An inert diatomite-based support compatible with all liquid phases. Provides fast and efficient separation of a wide variety of polar compounds when used in a liquid-liquid chromatography mode.

LC-2 A pellicular packing having active porous silica layers permanently bonded to an inert spherical solid glass core. Versatile in separating various classes of compounds by selecting the right composition of the solvent system.

LC-3 A pellicular packing with alumina bonded to the surface of diatomite. Very efficient in the separation of polycyclic hydrocarbons, alkaloids, amines, aldehydes, ketones, surfactants and plasticizers.

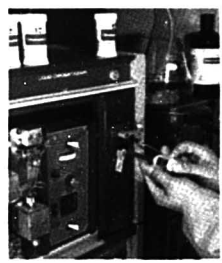
LC-4 Pellicular reverse phase packing with a monomolecular layer of octadecyltrichlorosilane chemically bonded to Chromosorb LC-2. Excellent separations of fused ring aromatic hydrocarbons, quinones, herbicides, barbiturates, steroids, food additives, etc.

LC-5 Pellicular reverse phase packing with a monomolecular layer of diphenyldichlorosilane chemically bonded to Chromosorb LC-2. Excellent separations for a wide variety of pharmaceutical and biomedical compounds.

NEW LC-6* A fully porous microparticulate silica offered in a 10 m particle size with a surface area of 300+ m^2/gm, and an average pore diameter of 130 angstroms. It offers exceptionally high efficiency, capacity, resolution and speed of analysis. Highly selective in separating close polarity compounds with an isocratic solvent system or in separating wider polarity range mixtures with gradient elution.

NEW LC-7* A reverse phase microparticulate HPLC column packing material prepared by chemically bonding an octadecyl group to Chromosorb LC-6 via Si-O-Si-C type bond. A closely controlled reaction provides a C_{18} nonpolar stationary phase of excellent performance in either partition or ion pair chromatography modes. Excellent in separating wide varieties of compounds used in pharmaceutical and food products.

NEW LC-8* A microparticulate polar-bonded phase HPLC column packing material prepared by chemically bonding a cyano-type group to a Chromosorb LC-6 silica surface. It complements Chromosorb LC-7 for reverse phase HPLC. Highly polar and very efficient in separating polar compounds.



Gas Chromatography

Century Series. This Chromosorb line is made up of 8 porous polymer supports in a broad range of mesh sizes. Each one is significantly different in function and retention characteristics.

101 Fast, efficient separation of free fatty acids, glycols, alkanols, alkanes, esters, ketones, aldehydes and ethers.

102 High surface area polymer causing no tailing of water, alcohols or most other oxygenated compounds. Useful for light and permanent gases and low molecular-weight compounds.

103 Fast, efficient separation of amines, alcohols, aldehydes, hydrazines and ketones.

104 For nitriles, nitro-paraffins, aqueous hydrogen sulphide, xylenols, oxides of nitrogen and ammonia.

105 Provides efficient separation of aqueous mixtures containing formaldehyde, acetylene from lower hydrocarbon and most gases and organic compounds in the boiling range up to 200° C.

106 Nonpolar surface retaining nonpolar organic compounds in a column for a longer time with respect to polar compounds. Highly efficient in resolving C_2-C_5 alcohols.

107 Intermediate polarity providing efficient separation of various classes of compounds in general and Formalin in particular.

108 Separation of gases and polar materials such as water, alcohols, aldehydes, ketones, glycols and others. Retention characteristics differ from other Century Series supports.

Diatomite Supports. Not only do we package diatomite supports in a wide variety of grades and treatments, but we quarry the raw material at the world's highest quality and most uniform deposit of diatomite at Lompoc, California. We're the only company that provides diatomite supports from the ground up.

Chromosorb A Developed specifically for use in preparative-scale gas chromatography. Good capacity to hold liquid phases (25% maximum), a structure that does not readily break down with handling and a surface that is not highly adsorptive.

Chromosorb G Developed for analysis of polar compounds, it has high column efficiency, good handling and non-friable characteristics. It is particularly useful when low loaded columns (max. 7%) are required in drug, steroid and pesticide analysis. Available with non-acid-washed (NAW), acid-washed (AW) and acid-washed dimethyldichlorosilane (AW-DMCS) treatments.

Chromosorb P Prepared from Johns-Manville firebrick, it can be used for both analytical and preparative-scale chromatography. High capacity to hold liquid phases (30% maximum). It has a hard surface that does not break down on handling. Primarily used for analysis of hydrocarbons and compounds of low polarity. NAW, AW, AW-DMCS and hexamethyldisilazane (HMDS) treatments available. AW-DMCS-treated Chromosorb P has sufficiently reduced surface activity for analysis of medium polar compounds.

Chromosorb W A flux-calcined support with a medium capacity to hold liquid phases (25% maximum) and a relatively non-adsorptive surface. This support is fragile and must be handled gently to prevent formation of fine particles which tend to lower column efficiency. Recommended for analysis of polar compounds. Available in NAW, AW, AW-DMCS and HMDS treatments.

Chromosorb G-HP and W-HP A special treatment after AW-DMCS treatment yields the most efficient and inert grades in the Chromosorb G and W series. For use in the analysis of steroids, bile acids, pharmaceutical and toxicological compounds, especially where trace analyses are required.

Chromosorb 750 The most inert and non-friable diatomite support in the line. It is both acid-washed and silanized. 750 is highly efficient and designed for analysis of biomedical compounds and pesticides. The hard surface generates a minimum amount of "fines" during coating and packing. The inert surface shows minimum adsorption and decomposition with polar compounds. Uniform distribution of the liquid phase film on the particle surface is easily achieved.

Chromosorb R-6470-1 A specially produced, fine particle support developed to coat the inner walls of capillary columns. It is produced from flux-calcined diatomaceous silica and has a surface area of 5-6m^2 per g. and a particle size range of 1-4 μ.

Chromosorb T Made from Teflon® 6 powder, it is used where a highly inert surface is needed to avoid tailing problems encountered with compounds such as water, hydrazine, sulfur dioxide, etc.

For technical information. For more specific information on performance and packing of Johns-Manville gas and liquid chromatography products, contact Jack Denboske, Filtration and Industrial Minerals Division, or Ed Hammel, International Division, Johns-Manville, Ken-Caryl Ranch, Denver, CO 80217, (303) 979-1000. Telex: Johnmanvil DVR 454404

* *To be released soon.*

Johns-Manville

CIRCLE 98 ON READER SERVICE CARD

free LC News

Foods & Beverages

Analyze & Purify Flavor Constituents



The flavor industry uses LC in research, product development, QC & blending, for non-destructive analysis and purification of flavor constituents.

CIRCLE 240 ON READER SERVICE CARD

Rapid Cleanup of Food Samples

A simple five-step procedure uses a SEP-PAK Cartridge to remove potential interferences from food samples to ensure precise quantitation and extend column life.



CIRCLE 241 ON READER SERVICE CARD

Chromatography Supplies Catalog



All new resource book includes comprehensive performance, price and ordering information for Waters' Chromatography Supplies product line.

CIRCLE 242 ON READER SERVICE CARD

Waters

The Liquid Chromatography People

Waters Associates, Inc.

Maple Street, Milford, MA 01757

(617) 478-2000

analytical chemistry

Reader Survey

Do you have trouble keeping up with developments in your field? How do you manage to keep on top of technical innovations? Is a formal certification program desirable to encourage professionals to improve their expertise? Please take a few minutes to give us your views by circling the appropriate numbers for your responses to the questions below on our Reader Service Card, page 385 A.

Results of this survey will appear in a future issue of the JOURNAL.

What is the main activity you undertake to keep up-to-date on technical developments in your field?

301 Reading journals and magazines
302 Attending conferences and meetings
303 Attending special seminars and short courses
304 Attending courses available locally in a college or university

To how many scientific journals (*not* free or controlled circulation) do you subscribe personally?

305 None
306 One
307 Two
308 Three
309 Four or more

How many controlled circulation (free) scientific publications do you receive in your own name?

310 None
311 One
312 Two
313 Three
314 Four or more

Have you been exposed to or had the opportunity to participate in any audio or visual/audio educational courses in your field?

315 Yes
316 No

Does your institution encourage continuing education?

317 Yes
318 No

Are you familiar with the certification program instigated by the American Institute of Chemists? See REGULATIONS, page 333 A, this issue.

319 Yes
320 No

Are you in favor of this sort of program for professionals?

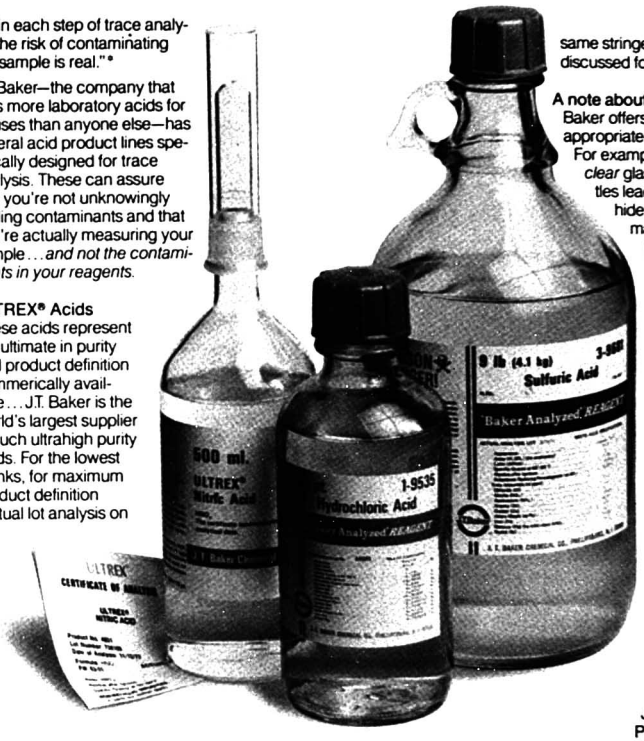
321 Yes
322 No

Trace Element Analysis: How to be sure that those traces are really in the sample... and not in the acid.

"...in each step of trace analysis the risk of contaminating the sample is real."*

J.T. Baker—the company that sells more laboratory acids for all uses than anyone else—has several acid product lines specifically designed for trace analysis. These can assure that you're not unknowingly adding contaminants and that you're actually measuring your sample...*and not the contaminants in your reagents.*

ULTREX® Acids
These acids represent the ultimate in purity and product definition commercially available...J.T. Baker is the world's largest supplier of such ultrahigh purity acids. For the lowest blanks, for maximum product definition (actual lot analysis on each certificate), for assurance that your work will not be compromised or jeopardized by impurities or uncertainties, no other acids can even begin to match ULTREX acids.



'Baker Analyzed'® Reagent Acids (BAR)
These acids—and all the other acids discussed here—are the only ones commercially available with the *actual lot analysis* on every container label. More than that: 'Baker Analyzed' Reagent acids are routinely subjected to more tests than required to meet ACS purity standards. BAR acids are ideal for demanding trace analysis and, as with all Baker acids intended for trace analysis, only your sample is an "unknown." *Currently available:* acetic, hydrochloric, hydrofluoric, nitric, perchloric, and sulfuric acids.

Baker Specialty Acids
- Sulfuric acid for the Babcock Milk Test (meets Food Chemical Codex specifications).
- Low-mercury acids: with mercury controlled to less than 5 ppb, they are especially suitable for mercury determinations. *Available:* sulfuric, perchloric, and nitric acids. Note that these specialty acids are also 'Baker Analyzed' Reagents and meet the same stringent specifications previously discussed for this grade.

A note about Baker acid containers
Baker offers a wide choice of safe and appropriate-to-the product containers. For example, our acids are always in *clear* glass, never brown. (Brown bottles leach impurities into the acid and hide discoloration and particulate matter.) Clear glass bottles with protective plastic coating are also available.

For more information
Check with your local Baker distributor (there are 120 stocking locations) or write or call J.T. Baker, Phillipsburg, New Jersey 08865, phone 201/859-2151 or use coupon below.

In the final analysis... the professional chooses J.T. Baker

J.T.Baker CHEMICALS

J.T. Baker Chemical Company
Phillipsburg, New Jersey 08865

* "Tracing the Elements," A.J. Barnard, Jr. and R.W. Dudley, *Industrial Research*, March 1973.

CIRCLE 18 ON READER SERVICE CARD

J.T. Baker Chemical Co.
Phillipsburg, N.J. 08865 · 201/859-2151

I'm interested in learning more about your acids for trace analysis:
- ☐ ULTREX® Ultrapure acids
- ☐ 'Baker Analyzed'® Reagent acids
- ☐ Sulfuric acid for the Babcock Milk Test
- ☐ Low-mercury acids.

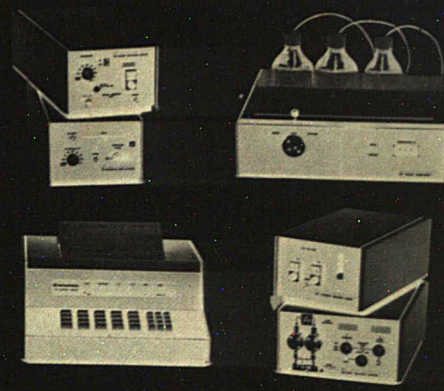
Name_____
Title_____
Department_____
Organization_____
Address_____
_____ Zip
Telephone_____ Ext.
Area Code

A new level in HPLC sophistication and simplicity.



Micromeritics proudly introduces its new 7500 microcomputer-based Liquid Chromatograph—a beautiful blend of engineering sophistication and operating simplicity.

We've taken the most advanced features available in HPLC today and packaged them so you can have the exact system to fit your specific application. Both gradient and isocratic integrated systems are available to accommodate rigorous quality control and methods development needs or the complex analysis functions of research and development laboratories.



Simple keyboard entry
All operating commands can be made from a single microcomputer-based control module. An alphanumeric display readout continually informs the operator of entry status for such parameters as flow rate, pressure limits, solvent concentration and column temperature.

Total analysis reporting
Comprehensive analysis reporting is achieved through a printer/plotter which not only gives you the chromatograms, but also a printout of gradient/solvent conditions, flow rate, pressure, temperature and operational status. Sample retention times, peak area and height, percent of concentration, sample and injection numbers can also be printed out.

Total automation
The 7500 system can be totally automated to give you unattended analysis around the clock. It can initiate 192 analyses of up to 64 samples . . . automatically.

Other advanced design features
The new 7500 also has an all new Ternary Solvent Mixer for more accurate and reliable low pressure solvent blending; a precision heated column compartment for faster more stable analysis; a new pulseless solvent delivery system; and a choice of three detectors—variable wavelength, fixed wavelength or refractive index.

Also available as components. Buy what you need now, and add more as you need it.

Available as components, too
And finally, you have the option of buying as much or as little of the system as you presently need. The 7500 system is also available as individual components. You can buy what you need now and add more later as you need it.

To learn more about the many features that separate the new 7500 from all the other HPLCs on the market, contact Micromeritics Instrument Corporation, 5680 Goshen Springs Road, Norcross, Georgia 30093 USA (404) 448-8282 TELEX: 70-7450.

micromeritics

EUROPEAN SALES OFFICE
2 Orchard Way
Eaton Bray
Bedfordshire
England
Telex 851-826249

AFRICA
North
Coultronics France S. A
Margency 95580 Andilly
France
Telephone 989-9030

South
Coulter Electronics PTY. Ltd
Transvaal
South Africa
Telephone 805-2046 55 56

ARGENTINA
Instrumentalia S R L
Buenos Aires
Telephone 85-3121 86-1436

AUSTRALIA
Townson & Mercer Ltd
Lane Cove N.S.W.
Telephone 428-1199

BELGIUM
Anais S. A
Namur
Belgium
Telephone 081-22 50 85

BRAZIL
Danon-Sociedade Importadora
Equipmentos Cientificos LTDA
Rio de Janeiro
Telephone 221-4480

DENMARK
Bie & Berntsen, Ltd
Roedovre
Telephone 45-294-8822

EASTERN EUROPE
Medata AB
Stockholm
Sweden
Telephone 08-303370

ENGLAND
Coulter Scientific Ltd
Hertsford
Telephone Harp 63151

FINLAND
OY Tamro AB
Helsinki
Telephone 90-544011

FRANCE
Coultronics France S.A.
Margency 95580 Andilly
Telephone 989-9030

GERMANY
Coulter Scientific GmbH
Gahlingsfad
West Germany
Telephone 02156-75501

GREECE
The GG Forum
Thessaloniki
Greece
Telephone 542-371

GUADELOUPE
Coultronics France S.A.
Margency 95580 Andilly
France
Telephone 989-9030

INDIA
Blue Star Limited
Bombay
Telephone 45-7887 or
45-6799

ITALY
Coulter Scientific S.p.A
Milano
Telephone 98-80-108

JAPAN
Shimadzu Seisakusho Ltd
Kyoto
Telephone (075)8111111

KUWAIT
Bader Sultan & Bros. Co
Kuwait
Telephone 421291 92 93

MALAYSIA
Delta Electronics SDN. BHD
Bangsar Baru
Kuala Lumpur
Telephone 943629

MARTINIQUE
Coultronics France S.A.
Margency 95580 Andilly
France
Telephone 989-9030

NETHERLANDS
Chemical Laboratory Instruments
Schindel
Netherlands
Telephone 04104-4035

NEW ZEALAND
Selby-Wilton Scientific, Ltd
Lower Hutt
Telephone 697-099

REUNION
Coultronics France S.A.
Margency 95580 Andilly
France
Telephone 989-9030

SPAIN
Izasa S.L
Barcelona 15
Telephone 2548100

SWITZERLAND
IG Instrumenten-Gesellschaft
Zurich
Telephone 0186331

TAIWAN
Vertex Corporation
Taipei, Taiwan
Telephone 752-645203

U.S.S.R.
Coultronics France S.A.
Margency 95580 Andilly
France
Telephone 989-9030

CIRCLE 143 ON READER SERVICE CARD

High-Precision Coulometry and the Value of the Faraday

Harvey Diehl
Department of Chemistry
Iowa State University
Ames, Iowa 50011

The high-precision chemical work in which I have been engaged has led to a new value for the faraday. The faraday is the fundamental constant interrelating chemistry and electricity. I will begin by discussing the particular characteristics of the electron which have led to our adoption of it as the fundamental primary standard in chemistry; I will review the recent history of work on the evaluation of the faraday, and then describe my own work on the coulometric titration of the highly purified organic base 4-aminopyridine which has led to a new value for the faraday. I will then pass to the curious events which followed the completion of this work and which led to the acceptance of the new value. Finally, I will discuss the various problems I am now tackling in an effort to reduce the uncertainty in the current value for the faraday from the estimated 4.9 parts per million (ppm) to less than 1 ppm. Throughout this discussion, the emphasis will be on the care taken to ensure the purity of the chemicals used and to guarantee the proper calibration of the various physical standards, although of necessity most of the detail must be omitted in a lecture and the interested listener referred to the published papers.

The electron is the only really pure chemical we have. There is presumably, and evidently, only one kind of electron and for the chemist the electron can be taken from a wire into a liquid, or the reverse, at any convenient and suitable potential over a range of some 5 V. This corresponds to a range of molar concentration of an electroactive species of some 80 orders of magnitude. The quantity of electrons delivered, that is, the product of current and time, can be measured relatively easily with great precision and accuracy, at the present time at the level of 0.1–0.2 ppm. And finally, the electron can be made to engage in a wide variety of electrode chemistry and this often at 100% current efficiency.

Quite clearly, then, our chemistry at the macro level should be based ultimately on the electron, just as the interpretation of much of our chemical and physical phenomena at the atomic and molecular level is based on the properties of the electron. At the macro level, at which we chemists work, then, one Avogadro's number of electrons, that is, one faraday of electricity, is one gram-equivalent-weight of electrons. In still other terms, one faraday of electricity is equivalent to 1 liter of a one normal solution of an oxidizing agent or a reducing agent, or by the right chemistry, to 1 liter of a one normal solution of an acid or of a base. The value of the faraday thus becomes of pivotal importance to the chemist, and the chemical methods for evaluating it provide the linkage between the faraday and our various primary standard chemicals.

For convenience, I have cast the three Faraday laws of electrolysis in mathematical form

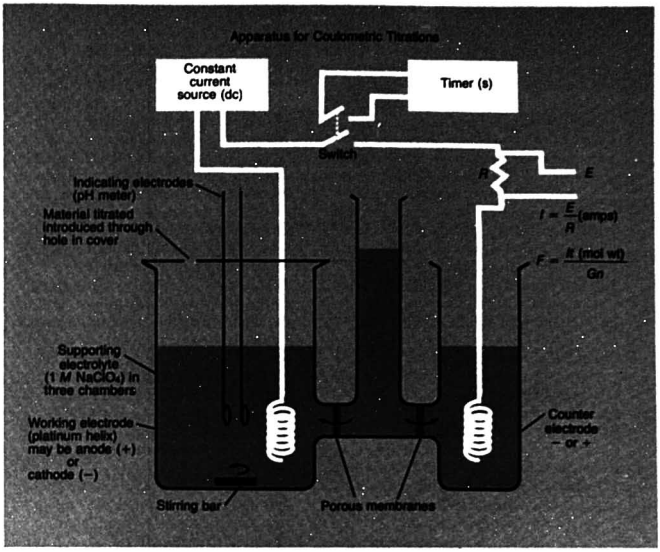
$$G = \frac{1}{F} It \frac{\text{mol wt}}{n} \qquad (1)$$

G is the mass of chemical changed at an electrode, in grams; I is the current, in amperes; t is the time, in seconds; n, the number of electrons involved in the change, is dimensionless. The proportionality factor, F, is designated as the *faraday* and is the quantity of electricity associated with one gram-equivalent-weight (Note 1), or one Avogadro's number of electrons, $F = N_A e^-$. The recent values for the faraday are given in Table I.

The Craig silver dissolution value (*1*) was the accepted value from 1960 on, as recalculated successively, for the shift of the atomic weight scale to carbon-12, for two changes in the definition of the ampere, for a determination of the isotope ratio in the silver used, for a change in the definition of the volt, and for a more generous statistical treatment than Craig gave his own data (Note 2). The physicists interested in the values of the various fundamental constants, given succes-

Presented at a symposium honoring Frank J. Welcher on the occasion of his retirement from Indiana University-Purdue University at Indianapolis, Ind., October 4, 1978.

0003-2700/79/0351-318A$01.00/0
© 1979 American Chemical Society



sively better values for various physical quantities, obtained the significantly lower value. This discrepancy, some 20 ppm, is some four times greater than the estimated uncertainty in the electrochemical value and ten times the estimated uncertainty in the calculated value. So confident had the physicists become by 1973 that they felt it necessary to reject (*4*) the Craig electrochemical value outright as "being subject to some serious error". It came, then, as a source of astonishment to them when the Iowa State University (ISU) value based on coulometric titrations of 4-aminopyridine was advanced in 1974, agreeing in most pleasant and surprising fashion with the Craig value. The 4-aminopyridine value is based on coulometric titrations at both the cathode and anode, and the electrode reactions involved are not only different in themselves but quite different in chemistry from the Craig anodic dissolution of silver. On completion of this work and during the editorial reviewing process, the ISU physical standards were subjected to meticulous recalibrations at the NBS and found to be correct. Suspicions of the physicists were further allayed by a repetition of the titrations themselves at NBS; the results were identical with the ISU results (*3, 5*). The physicists have now reinstated (*6*) the experimental, electrochemical value, largely, I suspect because of the remarkable agreement of the 4-aminopyridine value with the Craig value. We now have the curious state of affairs that the physicists believe the electrochemical value to be correct and have called for a re-examination of their own work, (*7*), and the chemists (that is, myself) believe there is an undisclosed error in the electrochemical work. An attack on the discrepancy is being mounted mutually and is bound to uncover new and unexpected phenomena. But at this level of accuracy, the going is not easy. Before describing this problem in more detail, I digress with a bit of history.

T. W. Richards, working at Harvard with G. P. Baxter and a line of brilliant students, was the one who carried the chemical determination of atomic weight to its greatest perfection. Such chemistry came to an abrupt halt when the mass spectrographers became able to measure atomic weights more easily and more accurately. The last chemical determinations of an atomic weight were reported in 1940.

About this same time, coulometric titrations (titrations affected by chemicals generated electrochemically) were introduced by Szebelledy and Smogyi. Such titrations underwent progressive extension and refinement during the following 30 years, principally by John Taylor and George Marinenko at NBS. My own entry into the field was brought on by a long fes-

Table I. Recent Values for the Faraday

F in 1972 NBS coulombs per g-equiv-wt (Uncertainty[a])	Worker, location, year, and method
96 486.72 (σ = 6.8 ppm)	Craig, Hoffman, Law, and Hamer (*1*). NBS. 1960. Anodic dissolution of silver, as recalculated (Note 2)
96 486.57	Diehl and coworkers (*2, 3*). Iowa State University. 1975, 1976. Titration of 4-aminopyridine
96 484.56 (σ = 2.8 ppm)	Cohen and Taylor (*4*). NBS. 1973. Calculation involving least-squares treatment of other physical data

[a] Combined random and systematic uncertainties expressed as the standard deviation of the mean, the systematic uncertainties being estimated at the 70% confidence level.

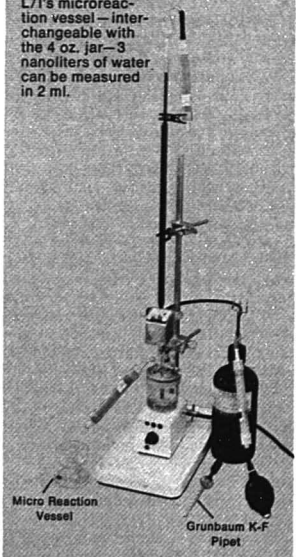
ห้องสมุด กรมวิทยาศาสตร์บริการ

Odorless water determinations

In the field and in the lab with one precision L/I aquametry apparatus.

L/I's instrument is so simple that untrained personnel can make a determination in 2 minutes with high precision. L/I guarantees 1% accuracy, 0.5% reproducibility over 90% of the range of the instrument (1 part/million to 100% water). **L/I's price is $505.00 complete** with one quart of K-F reagent, which is **$700 less** than comparable instruments.

L/I's 6" x 10" apparatus uses your Karl Fischer reagent bottle as a reservoir, eliminating the odors and hazards of transfer. The reaction vessel is an ordinary 4 oz. disposable "cream" jar. Using L/I's microreaction vessel—interchangeable with the 4 oz. jar—3 nanoliters of water can be measured in 2 ml.



LABINDUSTRIES
620 Hearst Ave.
Berkeley, CA 94710
Phone (415) 843-0220

CIRCLE 129 ON READER SERVICE CARD

tering argument about the merits of ammonium hexanitratocerate as a primary standard. Knoeck and I were able to settle that argument by a high-precision coulometric titration, taking advantage of an improved titration cell and electrical apparatus designed by E. L. Eckfeld and E. W. Shaffer, Jr. (*8*), of the Leeds and Northrup Co. Knoeck and I contributed (*9, 10*) to the field with a study of ammonium hexanitratocerate, potassium acid phthalate, and potassium dichromate (titrated both as an oxidizing agent and as an acid), and by the design of two new coulometric titration cells. The next step was a redetermination of the value of the faraday, work dictated not only by the logic of the chemical situation but by increasingly insistent intimations from the physicists that the existing value for the faraday might be wrong.

The faraday is what might be termed a *macro fundamental constant*. By its very nature, a direct, experimental evaluation of it must necessarily involve measurements on large quantities of materials, as opposed, say, to measurements at the atomic level such as mass spectrometry, radioactivity, the behavior of charged particles in high vacuum, and the diffraction of X-radiation from crystals. In this respect then, that is, in the highly precise manipulation of large amounts of chemicals and the precise measurement of physical quantities, evaluating the faraday is a modern-day throwback to the days of Richards and Baxter and their students. But with one further and very severe demand: mass must be measured in absolute terms. In the old atomic weight work, it was sufficient that a set of weights be calibrated so as to be internally consistent inasmuch as the work was all relative. In the faraday work, on the other hand, the weights used must be in terms of absolute mass and "traceable" to the International Kilogram so that the value obtained for the faraday will be on the same basis as other fundamental standards.

4-Aminopyridine was selected as our primary standard chemical from some several thousand compounds considered because it meets certain rigid requirements. In the final stage of purification it can be sublimed, thus ensuring the absence of solvent trapped within the crystal, a most insidious impurity and probably the greatest source of uncertainty in precision work (Note 3). The melting point is high so that the total impurity can be determined by the depression-of-the-freezing-point technique. It is sufficiently strong as a base to provide a satisfactory end-point. It is composed only of carbon, hydrogen, and nitrogen, elements for which the isotope ratios can be determined fairly readily so that the value for the faraday can rest directly on carbon-12.

The 4-aminopyridine was obtained in the final sublimation as long, needle-like crystals. The total impurity in this 4-aminopyridine was determined (*11*) by the depression-of-the-freezing-point method using a gold crucible, a platinum resistance thermometer, heat shields, highly sophisticated electronic temperature controls, precision electrical measuring devices, and a new method of handling the data. The basic equation for obtaining the mole fraction of impurity, $x = L_f(\Delta T)/RT_m^2$, requires a knowledge of the latent heat of fusion L_f, and the melting point, T_m; these properties and also the specific heats of the solid and liquid were measured. The conclusion drawn was that the total impurity in the 4-aminopyridine amounted to less than 10 ppm, a lower limit set by the thermodynamics involved and sensitivity, 0.001°, of the thermometer.

In the titration cell used, catholyte and anolyte are separated by two porous membranes (the details are shown in drawings in ref. *3*), and the electrolyte, 1 *M* sodium perchlorate, in the middle chamber is maintained at sufficient head to maintain flow into both the outer and inner chambers sufficient to counteract the normal migration of the electroactive species during electrolysis. The helix of platinum in the outer, working chamber could be made either positive or negative. In the titrations of 4-aminopyridine, it was used both ways.

The chemistries at the platinum working electrode are

As an anode:

$$2H_2O = 4H^+ + 4e^- + O_2$$

current efficiency: 102–104%

As a cathode:

$$H^+ + e^- = \tfrac{1}{2}H_2$$

or alternatively:

$$2H_2O + 2e^- = H_2 + 2OH^-$$

current efficiency: 100.0000%

The current efficiency at the anode in a sodium perchlorate electrolyte is not 100%, unfortunately. The reason, as we discovered, is a side reaction forming peroxyperchlorate, Cl_2O_8, a new species which deserves more attention than I have so far been able to give it. We were able to devise a working platinum anode which does have a current efficiency of 100.0000% in the generation of hydrogen ion. It is based on the oxidation of the hydrazinium ion:

$$N_2H_5^+ = N_2 + 5H^+ + 4e^-$$

We call it the *hydrazine-platinum anode* (*12*). Note the unusual integral

HPLC announcement:

A significant advance in solvent delivery...

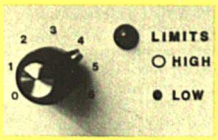
A great new pump from LDC

The new ConstaMetric III metering pump is a single modular unit designed specifically for HPLC use, not merely adapted from a general purpose pump. Naturally it's from LDC, with their preeminent Milton Roy pump engineering expertise.

Dual piston reciprocating pump

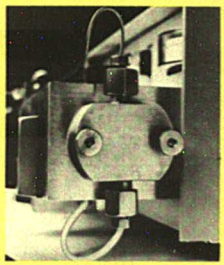


6,000 psi capability

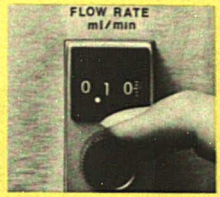


Hi-low limit shutdown

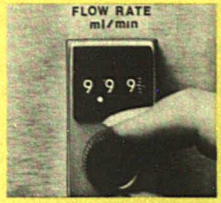
Gradient programmable

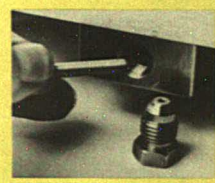


All solvent lines are external for quick servicing or leak detection



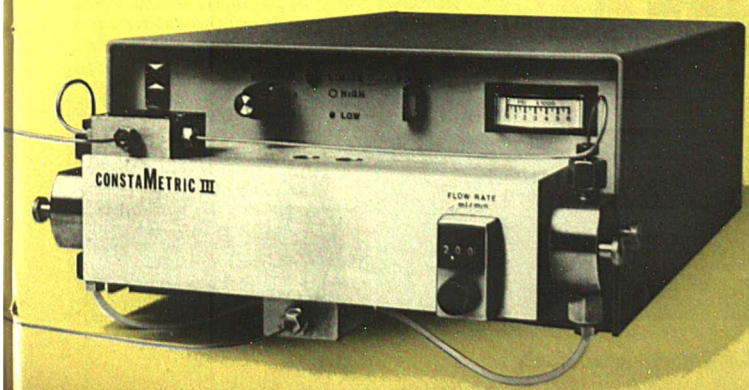
Adjustable flow rate 0.10 to 9.99 mL/min





Filter accessible for servicing

Send for the detailed ConstaMetric III brochure and complete LDC pump catalog.



LDC liquid chromatography

LABORATORY DATA CONTROL
Division of Milton Roy
P.O. Box 10235,
Riviera Beach, FL 33404
305/844-5241 telex 513479

European office:
LABORATORY DATA CONTROL
Milton Roy House, High Street
Stone, Staffs., ST15 8AR
England
Telephone
0785-83-3542
telex 36623

234

CIRCLE 126 ON READER SERVICE CARD

From Buchler... keeping pace with the age of discovery:

An ALL NEW digital power supply.

Buchler introduces the first laboratory power supply with large, bright L.E.D. digital readout and instant pushbutton selection of constant-*power*, constant-*voltage*, or constant-*current* modes.

The bright L.E.D. display means easy reading, even from across the room, without the distraction of dual or multifunction scales.

Overvoltage and overcurrent protection are built in; control circuits operate at low voltage for long life and reliability.

This is the only truly contemporary power supply. It's new from Buchler. Available through your leading laboratory supply house.

Buchler Instruments, Inc.

1327 16th Street, Fort Lee, N.J. 07024
(201) 224-3333 (212) 563-7844



Buchler Instruments: made in the United States, sales and service worldwide.

CIRCLE 21 ON READER SERVICE CARD

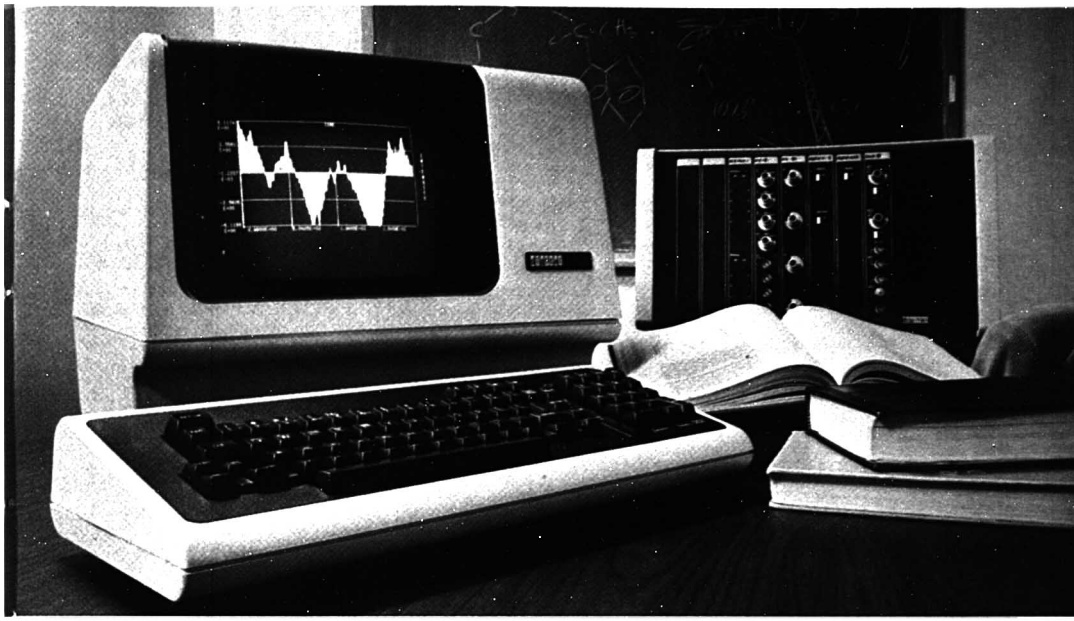
ratio of five hydrogen ions generated for each four electrons passed. We titrated the 4-aminopyridine with hydrogen ion generated at this anode. We also titrated the 4-aminopyridine by adding an excess of standard perchloric acid and back titrating the excess with hydroxide generated at the cathode. The perchloric acid was standardized coulometrically in the same way. Thus, the 4-aminopyridine was titrated coulometrically two ways, at the anode and at the cathode.

Masses of about 3 g of 4-aminopyridine were titrated. The main current, running for some 8 h, was in the neighborhood of 64 mA. The smaller current, used through the end-point regions at the beginning ("pretitration") and at the end of a titration, was approximately 6.4 mA. These currents were measured, of course, with high precision, actually by measuring the potential drop over a 20-ohm resistor with a Leeds and Northrup Type K5 potentiometer. The position of the end-point in the titration curves was determined by fitting a cubic equation to the data and setting the second derivative equal to zero (*13*).

To calculate a value for the faraday from our data, it is necessary to know the molecular weight of 4-aminopyridine, and of course, with the same accuracy as in the remainder of the work. For the atomic weights of carbon and hydrogen, we took the values, H = 1.00797 ± 0.00001 and C = 12.01115 ± 0.00005, from the "1961 Table of Atomic Weights" rather than from later tables in which the numbers have been rounded off for general use and the ± figure represents, not the uncertainty in the value, but the range which encompasses all values of the isotope mixture ever reported. For nitrogen, we calculated a value, N = 14.00672 ± 0.00001, from certain works of the 1960's on the isotope ratio of nitrogen and rejected other work not applicable to our 4-aminopyridine. The molecular weight of 4-aminopyridine used was 94.11702 with an uncertainty of 0.00003. When this work on the faraday was initiated, it was intended to determine the isotope ratio of the three elements in the specific 4-aminopyridine used; unfortunately this part of the program was never carried out.

It is barely possible, of course, for an analytical chemist of the Richards, Willard, Lundell, Wichers stripe to get through a lecture without presenting an extensive table of results. However, I will forego my contribution to deference to tradition. The published papers (*2, 3*) give the data in detail so that the interested reader, perhaps some future individual with a new theoretical approach which needs checking, can repeat the calculations. The bottom lines of the respective tables

THINK MINC.



Digital made the computer easy-to-use and easy-to-interface. And you can buy it on a desk-top calculator budget.

Plug MINC in, turn it on, and you can plot charts, solve complex engineering and statistical problems, control instruments and acquire data. You have complete, ready-to-run BASIC software—true computer functionality. It's as easy as that. MINC's built around Digital's proven PDP-11 microcomputer. MINC has its own graphics terminal, one million character dual floppies and three serial line interfaces.

And MINC makes interfacing easy. Hooking up a lab instrument is as simple as plugging in a single connector to the IEEE Bus interface or one of the seven optional input/output modules. When you finish your experiment, you unplug the connector and wheel the MINC cart to the next job.

And, if you need more on-line data storage, there's the new DECLAB-11/MNC that combines the functionality and ease-of-use of MINC with 10 million character, random access disk drives, powerful FORTRAN software and Digital's versatile RT-11 operating system.

If you'd like the whole story on these easy-to-use systems, write Laboratory Data Products Group, Digital Equipment Corporation, Marlborough, Massachusetts 01752. Telephone (617) 481-9511, Ext. 6969. European headquarters: 12, av. des Morgines, 1213 Petit-Lancy/Geneva. In Canada: Digital Equipment of Canada, Ltd.



DECLAB-11/MNC



MINC

digital

CIRCLE 46 ON READER SERVICE CARD

INNOVATIVE GAS CHROMATOGRAPHS FROM SHIMADZU

One of the world's oldest and largest manufacturers of gas chromatographs, Shimadzu, spent more than a quarter century developing and perfecting these instruments. The performance of Shimadzu's fine line of gas chromatographs and related equipment is outstanding. And the very latest electronics technology is used to ensure high reliability with easy maintenance.

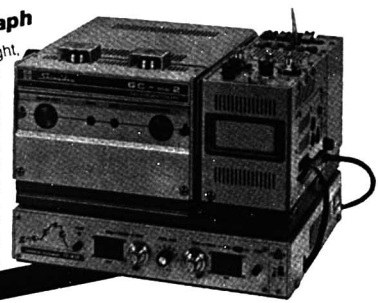


Chromatopac C-R1A Recording Data Processor

Only the C-R1A can calculate calories, vapour pressure, specific gravity of liquid, deviations from standard values, mole concentration (%) — weight concentration (%) and others in addition to the standard routines. A thermal plotter printer for chromatograms, recording of names of components is equipped. Up to 393 peak∫area∫as well as measurement of peak heights or∫average peak heights can be processed. There is also an all new grouping function and a self-diagnostic function.

GC-MINI 2 Gas Chromatograph

Although very compact and lightweight, this GC system has the performance of much larger and more expensive types. Outstanding stability, sensitivity and accuracy are ensured by dual column flow and on-column/on-detector system, two different kinds sensors system in column oven, and contamination free type detector. And a unique oven temperature control system can maintain the oven at room temperature, even when the injection port temperature is high. Maintenance is also easier because the four main modules can be disassembled and the electric control broken down to its five sub-units.



See SHIMADZU at the Pittsburgh Conference, Booths No.1409-1416

• ***Write today for more information on these and other Shimadzu labor and cost saving instruments.***

SHIMADZU SCIENTIFIC INSTRUMENTS, INC.

SHIMADZU SCIENTIFIC INSTRUMENTS, INC.
9147 Red Branch Road, Columbia, Md. 21045, U.S.A. Phone: (301)596-6078 Telex: 87459
SHIMADZU (EUROPA) GmbH
4000 Düsseldorf 1, Duisburger Weyer Str.1 F.R. Germany Phone: (0211)314061 Telex: 08586839
SHIMADZU SEISAKUSHO LTD.
1 Tokitsuyo Kuwabaracho, Nakagyo-ku, Kyoto 604 Japan Telex: 05422166

CIRCLE 189 ON READER SERVICE CARD

Table II. Results of Coulometric Titrations of 4-Aminopyridine Leading to a Value for the Faraday

Work done at Iowa State University (ISU) and repeated at the National Bureau of Standards (NBS)

	F in 1972 NBS coulombs per g-equiv-wt (Uncertainty[a] in ppm)	
	ISU	NBS
Anodic oxidation[b] at hydrazine-platinum anode	96 486.40 (6.2)	96 486.58 (2.3)
Cathodic reduction[c]	96 486.78 (2.3)	96 486.53 (2.7)

[a] Standard deviation of the mean combining the random errors with the systematic errors estimated at the 70% confidence level (one standard deviation). [b] Direct titration with hydrogen ion generated at the anode. [c] Back titration with hydroxy ion generated at the cathode after addition of excess perchloric acid.

are given here, in Table II, that is the values obtained for the faraday and an estimate of the combined random and systematic uncertainties. As you see, the results obtained at ISU and NBS were identical, the average being the value reported in Table I, 96 486.57 1972 NBS coulombs per gram-equivalent-weight. The agreement between the ISU-4-aminopyridine value and the earlier NBS-Craig-silver dissolution method is striking. The discrepancy, however, between the direct, experimental, electrochemical value and the calculated value now becomes a matter of real concern.

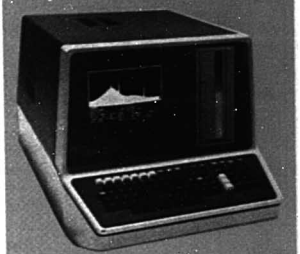
It would, perhaps, have been wise to have terminated this work at this stage. The new value is after all two orders of magnitude better than the accuracy and precision characteristic of essentially all chemical work, industrial, clinical, and academic. But while the policy of quitting while you are ahead is sound in playing a market, scientific research has not only many of the elements but much of the irresistible lure of gambling. The physicists report that a backlog of experimental and theoretical work has accumulated because a high-precision value for the faraday is lacking. Moreover, they are serious enough about the business to undertake an exhaustive re-examination of the various experimental measurements used in arriving at their value. The chemists can hardly do less. Then too, it may well be that the discrepancy does lie in the chemical work. If so, however, the fault is something common to the electrolysis of aqueous solutions involving such diverse reactions as the anodic dissolution of silver, the anodic generation of hydrogen ion, and the cathodic generation of hydroxyl ion. Because the calculated value is smaller than the direct, electrochemical value, it appears as if a very small portion of the electricity passing through the electrochemical cell does so without effecting a chemical change at the electrodes. Sufficient unexplained phenomena, having to do principally with the change in pH through the equivalence-point region, had been observed during our own work to keep us intrigued. And in addition, some astonishing and quite unorthodox results of simple electrolysis experiments have been reported during the immediate past few years by the Indian chemist Palit (*14*), work which has been unconscionably ignored by the electrochemists. The Palit observations may indeed strike directly at our assumption of 100.0000% current efficiency in our faraday experiments. The pressure, though, to do better comes from the physicists. Almost without making a deliberate decision, I slipped into an effort to reduce the uncertainty in the electrochemical value to less than 1 ppm.

A necessary prelude to such an effort is a re-examination of the uncertainties in the various measurements involved in the determination just completed (ref. 3, page 511) and steps to reduce the uncertainty in each to less than 1 ppm. The uncertainties in the standards of emf and resistance are estimated to be 0.2 ppm. By a modification of the electrical measuring circuit, it has been possible to eliminate the potentiometer and replace it with a simple null point detector good to 0.2 ppm. We have acquired a new constant current source, based on the Kroeger-Rhinehart circuit (*15*), stable to 0.5 ppm and have devoted considerable effort to eliminating from the circuits electrical pick-up noise, transients arising during switching, and grounding effects. As with the electrical measurements, the measurement of time, previous uncertainty 0.2 ppm, is above reproach, although we have acquired a new timing device and are arranging to key it to the color TV broadcast timing which is reported (*16*) to be good to a few parts per billion. With this apparatus we hope to confirm the 4-aminopyridine value by

EXAMINE...
Spectral Data



In addition to the most versatile and sensitive multichannel detectors the OMA 2 offers uniquely powerful examination and analysis.



OMA® 2...
The 1215 Console helps you examine your data by
1) Displaying data and reference information simultaneously
2) Storing numerous reference spectra in non-volatile diskette memory

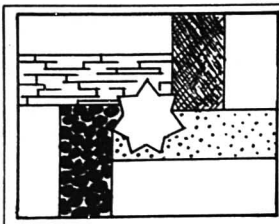
DATA MANIPULATION FEATURES INCLUDE:
1) Programmable Savitsky Golay smooth (3, 5, 7, 9, 11 pts)
2) Shift of data
3) Algebraic manipulation + − / * as well as log and exp functions
4) Keystroke entry of model functions
5) Interactive fitting by use of standard programming capability

For more information on the OMA 2 System, write or call today.

EG&G PARC

EG&G PRINCETON APPLIED RESEARCH, P. O Box 2565, Princeton, NJ 08540; Phone: 609/452-2111. 496

CIRCLE 172 FOR ADDITIONAL INFORMATION ONLY



Analytical Chemistry of Liquid Fuel Sources

Tar Sands, Oil Shale, Coal, and Petroleum

Advances in Chemistry Series No. 170

Peter C. Uden and Sidney Siggia, *Editors*
University of Massachusetts

Howard B. Jensen, *Editor*
Laramie Energy Research Center

Based on a symposium cosponsored by the Divisions of Petroleum Chemistry and Analytical Chemistry of the American Chemical Society

With today's critical need to utilize all available fossil energy sources, this timely research collection on various aspects of liquid fuel analysis and characterization takes on tremendous importance.

Twenty-one papers offer a clear and concise presentation of specific advances in analytical methodology and instrumentation ranging from high-resolution gas and liquid chromatography to electron microprobe, carbon-13 NMR, EPR, and computer modeling.

CONTENTS

Spontaneous Combustion Liability of Subbituminous Coals • Analysis of Five U.S. Coals • Organic Constituents in Solvent-Refined Coals • Analysis of SRC, Recycle Solvents, and Coal Liquefaction Products • Structural Characterization of Solvent Fractions • New Techniques for Measuring PNA • Characterization of Mixtures of Polycyclic Aromatic Hydrocarbons • Chromatographic Studies on Oil Sand Bitumens • Petroleum Asphaltenes, • Organometallic Complexes in Domestic Tar Sands • In Situ Reverse Combustion • Cretaceous Shales of Marine Origin • Green River and Devonian Oil Shales • Oil Shale Analysis for Element Balance Studies • Chromatographic Analysis of Oil Shale and Shale Oil • Olefin Analysis in Shale Oils • Hydro-Treating Response of Coal, Shale, and Petroleum Liquids • Oil Shale and Solvent-Refined Coal Materials Analysis • Chemical Class Fractionation of Fossil-Derived Materials • Residual Fractions Analysis • SRC Comparison with Petroleum Residua

342 pages (1978) $32.00 Clothbound
LC 78-10399 ISBN 0-8412-0395-4

SIS/American Chemical Society
1155 16th St., N.W./Wash., D.C. 20036

Please send _____ copies of *Advance 170 Analytical Chemistry of Liquid Fuel Sources* (ACH 0395-4) at $32.00 per copy.

☐ Check enclosed for $_____. ☐ Bill me.
Postpaid in U.S. and Canada plus 75¢ elsewhere. California residents please add 6% state use tax.

Name _____

Address _____

City _____ State _____ Zip _____

the titration of another pure chemical and to pass to titrations in nonaqueous solvents. These measurements have so far been delayed because of other formidable difficulties.

In principle, improving the uncertainty in the molecular weight, 3 ppm, really a matter of measuring isotope ratios, can be solved with existing technology. Establishing the purity of a chemical to one in 10^6, however, has not yet been solved. The limit on the depression-of-the-freezing-point method is about 10 ppm mol %. In the 4-aminopyridine work I placed the uncertainty in the purity at 3 ppm on the basis of a knowledge of the likely impurities and their effects (ref. 2, page 724). Our understanding of the phenomena at the region of the equivalence-point at this level is certainly faulty, and although we have so far managed by virtue of the cancellation of errors by making the conditions in the pre- and final titrations identical, this is not good science. The one aspect of this attack on the faraday at the 1 ppm level in which we have had some success is in the measurement of mass.

Although the uncertainty in the measurement of mass was estimated (3) at 1 ppm, I now believe this to be wrong and the measurement of mass to be the greatest source of uncertainty in the work. The problems arise both from the dissemination of mass from the platinum-iridium International Kilogram down to the stainless steel working weights and from the correction for the buoyancy of air on the chemicals and on the weights. I shall discuss the latter first.

The correction for the buoyancy of air is calculated by

$$M = W_o|[1 - (d_a/d_w)]/[1 - (d_a/d_o)]| \quad (2)$$

from a knowledge of the densities of the object (d_o), the weights (d_w), and the air (d_a), M being the mass of the object and W_o the sum of the weights when the object is weighed in air. The density of air is calculated from a knowledge of the prevailing temperature (t, in °C), barometric pressure (P_{bar}), and relative humidity (RH) by

$$d_a = \frac{0.001293[P_{bar} - 0.3780P_{H_2O}(RH/100)]}{(1 + 0.0036609t)(760.0)} \quad (3)$$

P_{H_2O} being the vapor pressure of water at the temperature t. This equation is derived from the ideal gas law and the law of additivity of partial pressures; the numbers given incorporate the latest values for the gas constant and the molecular weights of air and water. To obviate making the measurements and the calculation at each weighing, use is made in routine work of a sealed glass globe, the volume of which has been measured and the weight of which in air of known density has been measured. From any subsequent weighing the density of air at the time can be obtained by a bit of simple arithmetic. This "Baxter's globe," which has been around since the 1920's (*17*), gives a density of air good to one part per thousand (ppt) or so. When I attempted to push the accuracy by using a larger globe, electrostatic effects became so serious as to vitiate the results. Good results were obtained with a commercial, spherical "float" of stainless steel which was polished anodically and provided with

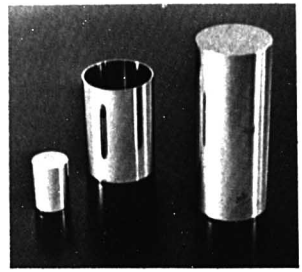


Figure 1. Hollow, evacuated cylinder of stainless steel and counterweights used to determine density of air by a simple weighing and to show that moist air conforms to gas laws



Figure 2. "Vacuum Weighing Bottle" used to determine in a vacuum the mass of the hollow cylinder, counterweight, and other weights

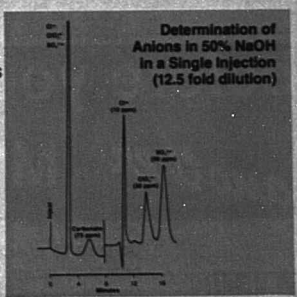
ION CHROMATOGRAPHY BREAKTHROUGH!

A simple and rapid means of analyzing complex mixtures containing both organic acids and inorganic ions at trace levels.



The dual system Ion Chromatograph 16 utilizes newly developed ion exchange columns which allow separation and detection of all ions in complex mixtures with pK_a less than (approximately) 7. This includes inorganic ions such as chloride, nitrate and sulfate as well as organic acids such as C_1-C_{10} carboxylic acids, organic phosphonic and sulfonic acids, and carbonic acid.

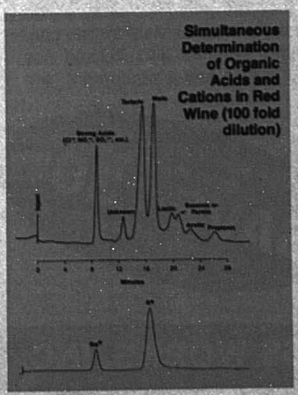
The Dionex IC 16 is extremely versatile. Just dilute the sample and in the most complex matrix you can determine • a host of strong acids or their salts such as inorganic ions • Weak acids or their salts such as organic carboxylic acids in a single sample analysis • anions and cations simultaneously with a single sample injection (because the ion Chromatograph 16 is actually *two* systems in one).



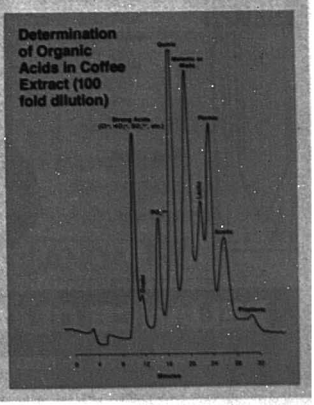
Determination of Anions in 50% NaOH in a Single Injection (12.5 fold dilution)

There's more. The IC 16 includes auxiliary valves which allow the use of additional chromatographic detectors such as UV. Pre- or post columns can be used individually or coupled with this dual system and you can even use column gradients. Let your imagination run wild!

For information on this Dionex innovation, call or circle the appropriate reader service number.



Simultaneous Determination of Organic Acids and Cations in Red Wine (100 fold dilution)



Determination of Organic Acids in Coffee Extract (100 fold dilution)

For information regarding applications of IC, circle the appropriate number:

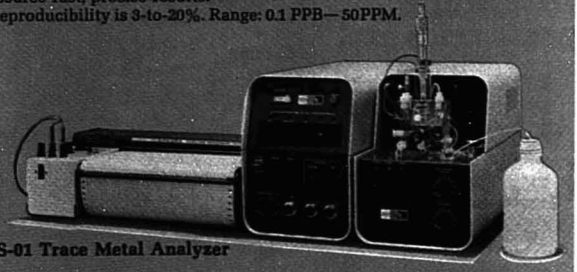
Air Pollution	50	Brine Analysis	54
Water Pollution	51	Power Production	55
Elemental Analysis	52	Quality Control	56
Soil Analysis	53	IC 16	57

DIONEX

Ion Chromatography Systems
In the U.S.: 1228 Titan Way
Sunnyvale, CA 94086
Phone (408) 737-0700
In Europe: c/o 4, The Buchan, Camberley, Surrey, GU15 3XB England.

MCI Automatic Trace Metal Analyzer.
Reliable, Fast and Easy.

Utilizes ASV method to simultaneously measure concentrations of 5 different trace heavy metals. Ultra-high sensitivity and automatic sample feed/discharge measuring cell assures fast, precise results.
Reproducibility is 3-to-20%. Range: 0.1 PPB—50PPM.



AS-01 Trace Metal Analyzer

MITSUBISHI CHEMICAL INDUSTRIES LIMITED
Instruments Dept., Mitsubishi Bldg., 5-2, Marunouchi 2-chome, Chiyoda-ku, Tokyo, 100 Japan Telex: J24901 Cable Address: KASEICO TOKYO

CIRCLE 140 ON READER SERVICE CARD

before you buy another MINI-VIAL...



be sure to check our vials and closure systems brochure which features mini-vials and related accessories. A variety of other vials for lab use, sample preparation systems and Thread-Tite™ mini-vials for use with existing equipment are also shown.

Send for your free copy of our mini-vial brochure today!

Buy Mini-Vials direct from manufacturer & SAVE up to 30% Quantity discounts available.

RELIANCE GLASS WORKS, INC.
17 Gateway Road, Bensenville, IL 60106 (312) 766-1816

CIRCLE 183 ON READER SERVICE CARD

a counterweight, but the sphere was awkward to handle and too heavy for the microbalance. I then constructed a hollow, evacuated metal cylinder of stainless steel, light enough (17 g) to be weighed on a microbalance. Tracking the density of air with these devices as the temperature, barometric pressure, and humidity changed indicated that they give a density of air in agreement to better than 1 ppt with that calculated by Equation 3, not surprising inasmuch as they are calibrated using a density calculated by Equation 3.

One part per thousand in the density of air is almost good enough to make to the correction for buoyancy to the 1 ppm level, but in 1975 a paper (*18*) published by P. E. Pontius of NBS stated that the formula for calculating the density of air is incorrect. Equation 3 is based on the ideal gas laws, and the Pontius claim posed a completely new problem. The problem stated more simply is: Does moist air conform to the gas laws? As a check on this, I constructed a hollow, evacuated cylinder of stainless steel with flat ends (Figure 1). The end pieces are sealed into thin-walled tubing of stainless steel by electron beam welding, and the cylinder is finished in a specially designed cylindrical lapping block of adjustable diameter. The volume of this "absolute density cylinder" was determined by precise measurement of the length and diameter with an optical comparator and gauge blocks. The mass (in vacuum) was determined by still another invention, a "vacuum weighing bottle" (Figure 2). The weighing bottle is closed by a cap which bears an O-ring and carries a stainless steel valve, the sealing element of which is again an O-ring. The empty weighing bottle is first evacuated and weighed, then opened and the cylinder (or counterweight, or weights) inserted; the bottle is then again evacuated and weighed. The buoyancy of air on the weighing bottle is the same in both operations so that the increase in weight is the mass ("true mass" or "weight in vacuum") (Note 4). Two counterpoises, equal in weight in air to the cylinder, are shown in Figure 1. These are useful in the refined measurements leading to a check on the validity of Equation 3 and useful when the cylinder is used in routine work. The hollow counterpoise has the same surface area as the hollow cylinder and is used in studies of surface effects.

Work with these devices was first reported in the MS thesis of J. S. Gibson (Note 5), and work shortly to be reported will show that the density of air obtained by calculation from the temperature, barometric pressure, and relative humidity is reliable to 3–4

parts per 10 000, quite in contrast to the claim of Pontius.

A large version of the vacuum weighing bottle, large enough to accommodate a kilogram mass, is being used in a study of weights made of a specially selected stainless steel and subjected to surface treatment to make them easily yield up to mild vacuum gases adsorbed on the surface. Moisture on the surface of stainless steel was shown by Yoshimori and coworkers (*19*) to amount to almost 1 μg per cm^2, somewhat less than that calculated for a monomolecular layer; such films of moisture would be expected to vary with the relative humidity of the atmosphere and to increase relative to the mass on passing to smaller weights. In the current work we have constructed, polished, and treated a kilogram weight and the necessary smaller weights to make a subdivision down to the 1-g mass needed for analytical work, and are carrying out this dissemination of mass in the actual vacuum provided by the weighing bottle. During the past 25 years, a considerable volume of knowledge has accumulated about platinum surfaces, the formation of oxides which are relatively easily reduced, and of course, the solubility of gases in platinum has been long known. Platinum comes to constant weight reluctantly in a vacuum, and stainless steel appears to be a far more appropriate and satisfactory material for mass standards.

T. W. Richards once expressed the opinion that each push of the decimal point one place to the right increased the work required by 100 times. Experience in the present work leads me to a different estimate: to gain a half-order of magnitude at this level, that is, to reduce the combined systematic and random uncertainties in the faraday from 4.9 ppm to below 1 ppm is taking 1000 times as much work as that required in the preceding work. Richards himself once took a crack at the faraday, and I would like to believe that were he here now he would applaud the present effort but would probably be astonished that anyone would be foolish enough to attempt it.

References

(1) D. N. Craig, J. I. Hoffman, C. A. Law, and W. J. Hamer, *J. Res. Natl. Bur. Stand.*, **64A**, 381 (1960).
(2) W. F. Koch, W. C. Hoyle, and H. Diehl, *Talanta*, **22**, 717 (1975).
(3) W. F. Koch and H. Diehl, *ibid.*, **23**, 509 (1976).
(4) E. R. Cohen and B. N. Taylor, *J. Phys. Chem. Ref. Data*, **2**, 704 (1973).
(5) H. Diehl in "Atomic Masses and Fundamental Constants 5," J. H. Sanders and A. H. Wapstra, Eds., p 584, Plenum Press, New York-London, 1975.
(6) B. N. Taylor, *ibid.*, p 665.
(7) B. N. Taylor, *Metrologia*, **12**, 81 (1976).
(8) E. L. Eckfeld and E. W. Shaffer, Jr., *Anal. Chem.*, **37**, 1534 (1965).
(9) J. Knoeck and H. Diehl, *Talanta*, **16**, 181 (1969).
(10) J. Knoeck and H. Diehl, *ibid.*, p 567.
(11) F. R. Kroeger, C. A. Swenson, W. C. Hoyle, and H. Diehl, *ibid.*, **22**, 641 (1975).
(12) W. C. Hoyle, W. F. Koch, and H. Diehl, *ibid.*, p 649.
(13) W. F. Koch, D. P. Poe, and H. Diehl, *ibid.*, p 609.
(14) S. R. Palit, *Indian J. Phys.*, **45**, 575 (1971); *J. Sci. Ind. Res. (India)*, **31**, 435 (1972); *J. Ind. Chem. Soc.*, **60**, 636 (1974); *Chemistry*, **48**, 16 (1975).
(15) F. R. Kroeger and W. A. Rhinehart, *Rev. Sci. Instrum.*, **42**, 1532 (1971).
(16) NBS Time and Frequency Dissemination Services, S. L. Howe, Ed., p 9, NBS Special Publication 432, Washington, D.C., 1976.
(17) G. P. Baxter, *J. Am. Chem. Soc.*, **43**, 1317 (1921).
(18) P. E. Pontius, *Science*, **190**, 379 (1975).
(19) T. Yoshimori, S. Ishiwari, Y. Watanabe, T. Harada, and S. Yamada, *Trans. Jpn. Inst. Met.*, **14**, 396 (1973).

Notes

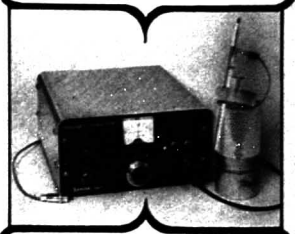
1. The physicists persist in using the term *mole* at this point in the definition. This is correct in the physical sense but often in electrochemistry, and more so in acid-base and oxidation-reduction chemistry, integral numbers other than one are involved and the term *gram-equivalent-weight* is preferable in chemistry. The history of our science and the fateful 50-year confusion of 1810–1860 are ample warnings that we as chemists must automatically by our terminology keep ourselves constantly aware of the distinction.

2. Craig's value for the faraday has undergone a number of "recalculations" to correct for: a) conversion of the table of atomic weight to the carbon-12 basis, b) a determination of the ratio of the isotopes of silver in the silver used, and c) changes in the definition of the ampere [see W. J. Hamer, *J. Res. Natl. Bur. Stand.*, **72A**, 435 (1968)]. For a critical review of the Craig work and a statistical, "least-squares" treatment of the Craig data, see B. N. Taylor, W. H. Parker, and D. N. Langenberg, *Rev. Mod. Phys.*, **41**, 403 (1969).

3. Richards dwelt at length on the insidious effect of water trapped within crystals and refused to work with materials which could not be fused before weighing; see T. W. Richards, "Determination of Atomic Weights: Methods Used in Precise Chemical Investigations" (Carnegie Institution of Washington, Publication No. 125, Washington, 1910), page 102. A more recent report along the same line is the study by Knoeck and Diehl (ref. *10*, page 191), who obtained photomicrographs of crystals of NBS 136b Potassium Dichromate showing water (as revealed by a meniscus) trapped in a closed cavity; the water in this "primary standard" amounts to about 250 ppm. An even more astonishing example is tris(hydroxymethyl)aminomethane in which the trapped solvent may amount to as much as 0.7%. How striking this is is shown in photomicrographs reproduced in the paper of W. F. Koch, D. L. Biggs, and H. Diehl, *Talanta*, **22**, 637 (1975), a paper fittingly entitled: "Tris(hydroxymethyl)-aminomethane, a Primary Standard?"

4. Mass, of course, is mass; basically, the terms *mass in vacuum, apparent mass, mass in air,* and *correction to mass in vacuum* are meaningless. Such terms appear in the literature and, judging from the his-

The Commercially Proven THERMO TITRATOR From SANDA



Titrates
50 Times Faster
Than Potentiometric
10 Times Faster
Than pH

Perfect for Research
due to direct heat curve and derivative capabilities.

Perfect for Quality Control
has one-button start and repeat function.

Provides
Instantaneous Response for Perfect Accuracy. Heat Curve, Derivative, and Automatic Cut-Off. Accurate, Automatic End-Point Detection. Sensitivity Variable from 0.001 to 5 Normal Solution.

Operates
Without Interference in Slurry, Color, Turbidity, or Non-Reactants using one universal probe.

Performs
15 of 21 Possible Functions
All 15 Possible Applications

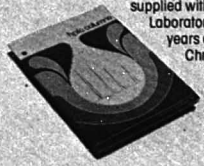
IT'S AMERICAN MADE

Call or write today for a free, sample titration of your solution.

SANDA, INC.
Manufacturers of Scientific Equipment
4343 East River Drive
Philadelphia, PA 19129
(215) 849-8100

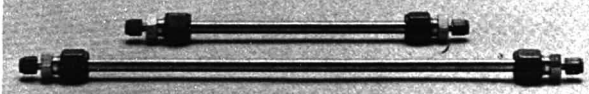
CIRCLE 190 ON READER SERVICE CARD

Now you can get pre-tested High Performance Liquid Chromatography Columns in three styles: Standard—five lengths from 5 to 50 cm and IDs from 2.1 to 20 mm...with more than 100 different packings; Economy—because of volume,these columns are offered at low cost for immediate delivery; and Custom-made—any packing, connection, length (to 100 cm) and ID (to 25 mm) to your specification. All pre-tested and supplied with test chromogram, report, and sample. Chrompack Laboratories are dedicated to manufacturing columns, with eight years experience in HPLC columns. Write for free catalog to Chrompack, P.O. Box 3, Middelburg, The Netherlands, or in the U.S. to P.O. Box 4131, Whittier, CA 90607.



Free Catalog

Pre-Tested HPLC Columns



Chrompack U.S.A. Inc.

CIRCLE 34 ON READER SERVICE CARD

SUB MICRON PARTICLE SIZE ANALYSIS DOWN TO 0.01 MICRON IT'S SIMPLE WITH A JOYCE-LOEBL DISC CENTRIFUGE 3

Benefit from the wealth of experience established in our application's laboratory in analysing a wide spectrum of particulate materials. The results are summarised in a free booklet 'APPLICATION REPORTS' covering the following major end-user groups:

- Polymer Emulsions
- Inks and Pigments
- Titanium Dioxide
- Magnetic Iron Oxide
- Carbon Black
- And many others

For your copy circle the reader enquiry card or write to:



JOYCE LOEBL
Marquisway, Team Valley
Gateshead NW11 0QW
England

JOYCE LOEBL

Vickers Instruments Inc.
100A Commerce Way
Woburn
Massachusetts 01801
U.S.A.

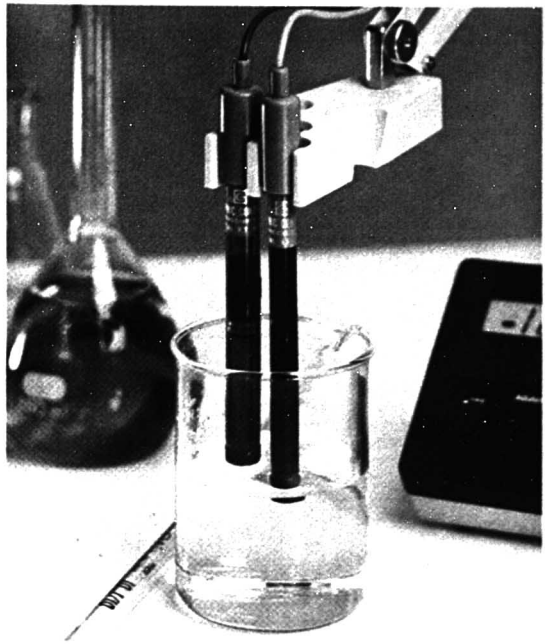
CIRCLE 97 ON READER SERVICE CARD

tory of science, it will take a generation or two to discard them. A start toward a more correct terminology and a convenient and definitive symbolism has been made; see next note.

5. J. S. Gibson, "Devices for the Rapid Determination of the Density of Air" (MS thesis, Iowa State University, Ames, Iowa, 1977). This thesis also contains a convenient symbolism and nomenclature for handling the various quantities in making a correction for buoyancy and in hydrostatic weighings. Such operations often involve numerous weighings under different conditions, and a too simple symbolism often results in confusion. The thesis also gives derivations of Equations 2 and 3 and an evaluation of the differential coefficients which enable a calculation of the accuracy needed in the various densities to secure a desired accuracy in a weighing. There is also given (Appendix II) a discussion of the current practices, in the calibration of weights, of the national physical laboratories and of the manufacturers of balances, of adopting arbitrary values for the densities of weights and air. There is also an explanation for the essentially trivial use of the terms *true mass* and *apparent mass* at the NBS in the calibration of weights.



Harvey Diehl is distinguished professor in sciences and humanities at Iowa State University. He received BS and PhD degrees from the University of Michigan. After serving briefly as an instructor first at Cornell and then at Purdue Universities, in 1939 he joined the chemistry faculty at Iowa State University as an assistant professor. He was promoted to professor in 1947 and to distinguished professor in 1965. Professor Diehl's principal interest has always been in teaching analytical chemistry to undergraduate and graduate students, and he regards his research work on organic analytical reagents and electrochemistry as distinctly secondary. In 1956 he was awarded the ACS Fisher Award in Analytical Chemistry, in 1961 the Iowa Award of the Iowa City Section of the ACS, and in 1966 the Anachem Award of the Association of Analytical Chemists. He has held various offices in the Division of Analytical Chemistry and in the Ames Section of the ACS.



We've lowered chloride detection to 10 parts per billion

Our new Ultra Sensitive Chloride Electrode responds to chloride in the 10 parts per billion range, without compromising selectivity. A range 25 times lower than can be measured with conventional chloride electrodes!

This revolutionary, new, solid-state electrode is a major break-through for industrial process applications demanding ultra-pure water, and for monitoring high purity water in steam boilers and conventional power generating stations. As such, it brings new sensitivity to direct chloride measurement in biological materials, foods, soils, insecticides, plating baths, potable water and wastewater . . . without resorting to pre-concentration steps and expensive, highly complicated techniques. This latest electrode development is just one example of how much we care about your need for improved electrode performance. We're on your side!

We also offer pH and ORP electrodes in conventional glass or break-proof polymer bodies, removable protective tips, renewable and porous Teflon junctions. More, we ship our electrodes in keep-fresh soaker bottles, ready for immediate use and for long shelf life. Should our electrode fail to operate properly, we've made it easy for you to return it. Just put it back in its own shipping carton, use our special "return" label, and mail. We'll ship a replacement within 24 hours.

For more information, see your local GC representative. Or contact Graphic Controls, Recording Chart Division, Box 1271, Buffalo, NY 14240.
Phone: 716/853-7500

We're on Your Side

GRAPHIC CONTROLS
Recording Chart Division

CIRCLE 88 ON READER SERVICE CARD



Pennies per Element.

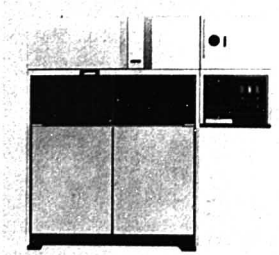


No-nonsense Plasma AtomComp™ 965 from Jarrell-Ash breaks price barrier in multi-element analysis.

At last: a plasma spectrometer for the modest budget. For the lab that wants the sensitivity of AA with the unique **simultaneous** capability of plasma.

Model 965. All our years of experience in computer-controlled direct-reading plasma emission spectrometers have gone into this new basic model. Only Jarrell-Ash could bring you **true plasma** instrumentation — with a price tag this low. Only Jarrell-Ash could bring you simultaneous analyses at a literal cost of pennies per element.

You can choose a 965 Plasma AtomComp to suit **your** specific needs: 20 channels, 30, you name it. You get high-speed DECwriter input/output system and dual floppy-disc storage as standard features. And a comprehensive selection of options. Like automated sample-introduction system.



Spectrum-shifter. "N+1" channel.

Thought you couldn't **afford** plasma? Think again. Send for literature on the 965 Plasma AtomComp today.

Jarrell-Ash Division
Fisher Scientific Company

590 Lincoln Street
Waltham, Massachusetts 02154
Phone (617) 890-4300

CIRCLE 124 ON READER SERVICE CARD

Janan M. Hayes
American River College
Sacramento, Calif. 95841

Licensing, Registration, and Certification: What Does It Mean to You as a Chemist?

Licensing, registration, and certification are periodically discussed as a means to ensure the quality and performance of chemists or chemists within certain specialities. Currently, the chemical community is taking a more active interest in these programs. One reason is the recent introduction of the American Institute of Chemists certification program. Also, the states of New Jersey, Ohio, and California are considering some types of mandatory licensing programs. Unfortunately, most chemists do not realize the differences between these types of programs and the ways in which they can apply to the individual chemist. Analytical chemists, in particular, should be concerned with these programs since most public issues that encourage governmental involvement are related to the reliability and accuracy of analytical results. Decisions of public health and safety organizations, such as EPA, FDA, and OSHA, are based on analytical results. Poor quality results by a few chemists can penalize the chemical community.

Before going into the specifics of currently suggested programs, let us examine just what is meant by each type of regulation of chemists. Certification is usually a voluntary program sponsored by a professional organization designed to certify the minimum competency of the individual. Certification is a form of peer recognition of ability and/or experience without legal status or governmental connection.

Registration is often similar in requirements to certification, but is sponsored by a governmental rather than professional organization. Frequently, examinations are required in addition to educational and experience requirements for registration. Although registration is usually not required by the state for the individual to function as a professional, those who are registered are assumed to have demonstrated a wider range of professionalism than those who have not elected to become registered.

Licensing, on the other hand, is a mandated regulation of the professional. Two types of licensing are commonly found: title acts, which permit the use of a licensed title, such as Professional Engineer; and practice acts, which permit an individual to practice a particular profession, such as the license required for physicians.

Differentiation between registration and licensing *is* difficult. For example, identical programs for the regulation of engineers is called licensing in one state and registration in another. The registration of chemists is currently limited to those in the clinical chemistry specialty. The only state now requiring mandatory licensing is Hawaii, which licenses those personnel performing analysis of pollutants affecting health and safety.

Many chemists are currently involved in the national certification program of the American Institute of Chemists. According to David A. H. Roethel, executive director of AIC, this program was established primarily to offer a form of peer recognition to those practitioners who demonstrate diligence in the maintenance of their professional competency through participation in continuing education and related development activities (*1*). Certification is based upon accumulation for three consecutive years of credits that are awarded for such activities as attending seminars, technical meetings, and college courses; for publications and technical paper presentations; and for individual activities such as journal reading, society participation, and community involvement related to professional experiences. Those successful in obtaining certification may use the initials C.P.C. (Certified Professional Chemist) and C.Ch.E. (Certified Chemical Engineer) to signify their certification by AIC and will be listed in a directory to be published each year.

A different type of voluntary certification is under consideration by the California-Nevada Section of the American Water Works Association. Much of the encouragement for governmental regulation of analytical chemists in California has come from chemists within the water–wastewater field. Because of the increasing level of technical competence needed in this field, combined with some state agency practices which have reduced requirements for hiring of workers in the field, the AWWA section is proposing a program to establish voluntary standards for workers at various levels within the industry. Many of these workers are chemists or have primary training in chemical sciences. The certification program recommends five levels of certification beginning with Junior Water Analyst, which requires only a high school diploma, one year experience in a qualified analytical laboratory, and successful completion of a test of the applicant's basic knowledge of laboratory skills, manipulations, math, and other nontheoretical matters such as safety, budgeting, and scheduling. Progress through higher levels of Assistant Water Analyst, Associate Water Analyst, Water Analyst, and Senior Water Analyst requires additional education and experience in water or wastewater laboratories. Higher levels of certification require additional testing of both basic knowledge and specialty knowledge plus oral examinations for Senior Water Analyst. The specialty tests can be selected from the areas of biology (plankton counting, benthic analyses, bioassay), microbiology (bacteriology, virology, mycology, etc.), general chemistry (sample collection, spectrophotometry, potentiometric titrimetry, etc.), instrumental inorganic chemistry (atomic absorption, polarography, flame photometry, etc.), instrumental organic chemistry (gas, liquid, thin-layer chromatography, etc.), and radiochemistry. It can be seen that this type of certification program involves a demonstration of competency that is not a part of the AIC certification program (*2*).

If the AWWA certification program is successful in California, state adoption will likely be encouraged. The program would then become a registration procedure with legal standing as a state verification of competency.

Assemblyman Bornheimer has introduced into the New Jersey legisla-

0003-2700/79/0351-333A$01.00/0
© 1979 American Chemical Society

ture a bill that would license the use of the terms *professional chemists, chemists,* and *chemical technicians* in that state. The licensing would be based upon educational and experience requirements and would involve an "appropriate examination" to be administered by a State Board of Chemists established by the act. This bill has not yet reached the committee level for consideration but if passed would provide penalties of $200 for a first offense and up to $500 for additional offenses in using the licensed categories (3).

Considered in Ohio but not introduced into its legislature is a bill that would, in similar manner, provide that "no person shall engage in or offer to engage in the practice of professional chemistry, or contact to offer such services, or use in connection with his name or otherwise assume, use or advertise any title or description tending to convey the impression that he is a professional chemist unless such a person is a (licensed) professional chemist" (4). In California, five separate bills have been introduced in the past 10 years to license analytical chemists. Both the bills in Ohio and in California apply mainly to those chemists who have contact with the public sector and are not mandated for those chemists who are involved in internal industrial functions.

The only current mandatory license practice act is that of the Republic of Philippines. This has been in force since 1952 and involves both academic and examination requirements for licensing. This is a general licensing act required of all chemists. The bill was enacted to recognize the practice of chemistry as a professional entity and to regulate it in accord with the needs of the Philippines. According to the current chairman of the Philippine Board of Chemistry, Remedios Abella Lim, the result of the licensing is that "the licensed chemist in his technical and social environments is more self-confident, more responsible, and more secure, professionally" (5).

Official ACS policy on these matters is summed in the following two statements:

The American Chemical Society endorses the licensure of those members of the clinical chemistry profession who direct or supervise chemical work in order to provide data for the purpose of prevention, diagnosis, prognosis, or the treatment of disease or otherwise assessing a medical condition.

The American Chemical Society endorses the registration of licensure of members of the chemical profession who are in responsible charge or supervision of chemical work involving analyses of air, water, food, drugs, or other items of concern to the general public.

As the licensing and/or registration of chemists working in areas affecting public health and safety come under scrutiny in the states, it is imperative that individual chemists express their views. We all have a stake in the outcome and want to be assured that qualifications for minimum competency are valid and realistic as they are mandated in the individual states.

References

(1) D.A.H. Roethel, letter to author, Apr. 18, 1978.
(2) "Progress Report of the Task Committee for Certification of Water Laboratory Personnel, California-Nevada Section, American Water Works Association, George Miller, Chairman, June 7, 1978.
(3) Assembly Bill No. 1541, State of New Jersey, Introduced June 26, 1978, by Assemblyman Bornheimer.
(4) Ohio State Senator John K. Mahoney, proposed bill for Licensure of Chemists in Ohio, 1977–78 Ohio Regular Session.
(5) R. A. Lim, *J. Chem. Educ.*, **53**, 787 (1976).



FRILLED NECK LIZARD
Chlamydosaurus
Kingii

Our Graphlok Ferrules are pretty tough customers.

Ferrules are ferrules, right?

Wrong! . . . SGE Graphlok* ferrules come on strong when you need them most.

In fact, a Graphlok ferrule is so good that, with care, you can use it over and over again. Because it can't fuse to metal or glass. Beautifully designed and a perfect companion for our glass lined stainless steel tubing (GLT*)

You'll like the way a Graphlok ferrule shapes up too. As soon as they're tightened they take up to the exact contours of the union.

You can forget the problem of flow under pressure and high temperatures because Graphlok ferrules are manufactured entirely without softener or filler. You won't experience any contamination problems either . . . thanks to their pure graphite composition.

The size range? From ¼" for packed columns to 0.8mm for WCOT columns. Larger or smaller ferrules and seals can also be made to your precise requirements.

Write for our "Accessories" catalogue.

Scientific Glass Engineering Pty.Ltd.

Head Office
Scientific Glass Engineering Pty. Ltd.,
111 Arden St., North Melbourne, Australia. 3051
Tel: (03) 329 6633

European Office
Scientific Glass Engineering (U.K.) Ltd.,
667 North Circular Road, London NW2 7AY.
Great Britain
Tel: 01 452 6244

U.S.A Office
Scientific Glass Engineering Inc.,
2800 Longhorn Blvd., Suite 104
Austin, Texas, 78758 U.S.A.
Tel: (512) 837 7190

SGE

*Trademarks of S.G.E.

If Union Carbide Corp., Schering Corporation, Baltimore Police Lab., Mobil Research and Development Corp.,* and many others have purchased and are using the GOW-MAC 750 FID Gas Chromatograph, why aren't you?



Is it because you weren't aware of all of its features:

- Excellent detectability, 10^{-12} g/sec hydrocarbon
- Solid state electrometer sensitivity 10^{-12} A, full scale
- Highly reproducible oven temperature control
- Rugged proportional temperature controller
- Detector, GOW-MAC's ultimate flame ionization design
- Easily accessible detector and column configuration
- Optional metal or glass column
- Compact size
- Maximum economy, basic unit $1735

The GOW-MAC 750 is used in research, analytical, and hospital laboratories throughout the world because of its performance and its simplicity. Its precision and sensitivity are equal to more expensive instruments.

Let us send you 750 information for your file. Complete specifications plus many applications. If you have a specific application, let our Applications Laboratory check it out for you.

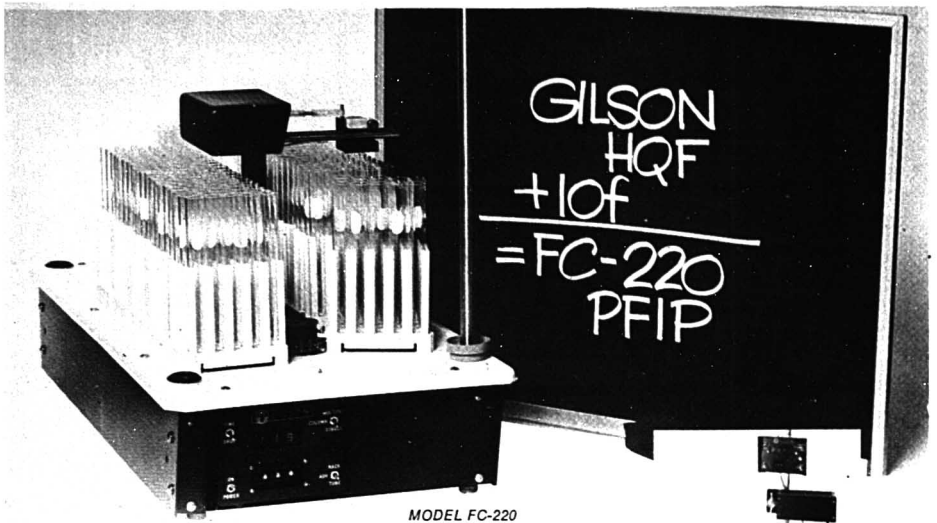
And, remember, the GOW-MAC 750 is unconditionally guaranteed.

Use the reader service number for more information.

*This does not constitute an endorsement, but merely reports the instrument's purchase and usage.

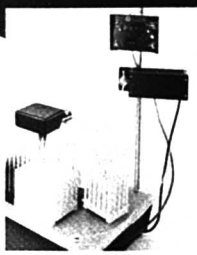
GOW-MAC INSTRUMENT CO.
P.O. Box 32; Bound Brook, NJ 08805 • Telephone: 201/560-0600
Shannon Free Airport, Co. Clare, Ireland • Telephone: 61632 • Telex: 6254

CIRCLE 86 ON READER SERVICE CARD



MODEL FC-220

Translated, that means you can buy this High-Quality Fractionator (GILSON's FC-220) PREFERRED FOR ITS PERFORMANCE— with the 10 important features listed below. Why pay more when you can get the best for less?



MODEL FC-220 WITH CONTROL BOX AND SHUT-OFF VALVE MOUNTED ON MAST

THE GILSON RACE TRACK FRACTIONATOR FOR LIQUID CHROMATOGRAPHY

Here are the COLD ROOM facts:

1. Reliable cold-room operation down to 0 degree Celsius. Includes self-contained heater, eliminating condensation problems. Components are selected to EXCEED requirements and will withstand hostile cold-room environment over extended use.

2. 220 test tubes (18x150 mm or 13x100 mm). Twenty-tube rack; block shape eliminates tipping of racks (separate rack carriers are not required).

3. Drop counting or time method of collection. Can be set from 0.1 minute to 100 minutes per tube, in 0.1-minute increments; or from one drop per tube to the liquid capacity, in one-drop increments.

4. Three-digit electronic display.

5. Optional flow-stop valve available.

6. Auxiliary power outlet is included for turning off accessory equipment after the last tube is filled.

7. Multiple-column collection available for 2, 3, 4 or 5 columns (with separate adapter).

8. Remote use of control unit is possible.

9. 220 tubes can be collected during unattended operation, or collection can be continued indefinitely without interruption by periodically removing filled racks and adding empty racks.

10. 21 U.S.A. Gilson sales and service locations —one-year warranty.

Size of the FC-220: 36 cm wide and 69 cm deep (14"x27"). **Weight:** 13 kg (28 lbs.)

GILSON

Write or phone

U.S.A. MANUFACTURING PLANT:

GILSON MEDICAL ELECTRONICS, INC.
P.O. BOX 27, MIDDLETON, WIS. 53562
Telephone 608/836-1551 • TELEX 26-5478

EUROPEAN MANUFACTURING PLANT:

GILSON MEDICAL ELECTRONICS (FRANCE) S.A.
69, 72 rue Gambetta • Boite Postale 5
VILLIERS-LE-BEL 95400 • ARNOUVILLE-LES-GONESSE, FRANCE
Telephone 990 54-41

CIRCLE 87 ON READER SERVICE CARD

1979 ACS National Meeting

April 1–6, 1979

Honolulu, Hawaii

Honolulu, "sheltered harbor" and the crossroads for trade and travel between East and West, will extend its warm alohas to the ACS/CSJ Chemical Congress, and stage possibly the largest chemical conference ever organized—attracting up to 8000 participants. Chemical societies from Australia, New Zealand, and Canada will join with the 177th ACS National Meeting and the 38th National Meeting of the Chemical Society of Japan to present 675 technical sessions consisting of nearly 5000 papers of which 1500 will be from the Japanese. As many as 74 technical sessions will be running concurrently. It appears at press time that most of the technical sessions will be presented in English. Twenty-nine of the 31 divisions of the ACS will meet as well as five committees. In addition to the technical sessions, professional and social activities are scheduled as usual. Two additional activities to note are the ACS/CSJ awards dinner on Monday evening, April 2, and the meeting of the ACS Council on Wednesday morning, April 4.

The Analytical Chemistry Division will hold 34 half-day sessions at which close to 268 papers will be presented; 104 of these papers will be Japanese. These sessions are composed of eight symposia of 14 sessions and 20 general sessions. The symposia topics are: the ACS award in analytical chemistry, ACS award in chromatography, Divisional instrumentation award, new developments in voltammetry and coulometry, microprobe techniques for elemental analysis, electrochemistry and spectroscopy in melts, new developments in thin-layer chromatography, and inorganic separations in analytical chemistry. Of these, the ACS award symposium in analytical chemistry and the symposium on new developments in voltammetry and coulometry seem to dominate the technical program of the Division with 32 and 18 presentations at four and three sessions, respectively. The general sessions will cover areas of spectroscopy, electroanalytical chemistry, atomic absorption and emission, liquid chromatography, GC–MS, and chelating agents.

The Division program will be highlighted by the presentation of the two ACS awards and the Divisional instrumentation award. The ACS Analytical Chemistry Award will be presented to Velmer A. Fassel of Iowa State University. His award address on simultaneous multielement determinations at all concentration levels will be delivered on Wednesday morning at the symposium dedicated to the award. The ACS Chromatography Award will be presented to Evan C. Horning of Baylor College of Medicine. Dr. Horning's award address will be presented on Monday morning at the symposium on bioanalytical systems based on chromatography and mass spectrometry. Finally, the Chemical Instrumentation Award, cosponsored by the Division of Analytical Chemistry and the Instrumentation Specialties Co., will be presented to John P. Walters of the University of Wisconsin-Madison. The award consists of a $2000 honorarium and a wall plaque. For more information on the award, see page 375 A. At the symposium dedicated to the



Waikiki Beach from Yacht Harbor to Diamond Head

award on Tuesday morning, Dr. Walters will speak on instrumentation for innovation in experimental atomic spectroscopy.

In addition to these programs, which are sponsored primarily by the Division of Analytical Chemistry, the Division will participate in two other symposia. A four-session symposium on recent advances in nuclear analytical methods is cosponsored by the Division of Nuclear Chemistry and Technology of ACS, the American Nuclear Society, and Isotopes and Radiation Division and Analytical Chemistry. The other symposium, two sessions on trace elements and hazardous compounds in fossil fuels, is sponsored primarily by the Division of Fuel Chemistry.

Other topics that are not necessarily related to the analytical chemistry discipline itself, but rather relevant to the entire chemical profession can also be found. A few of the symposia offered by other divisions include: analysis of food and beverages—liquid chromatographic techniques, by the Division of Agricultural & Food Chemistry; the monitoring of chemicals in the atmospheres of laboratories, by the Division of Chemical Health & Safety; developments in teaching energy-related problems—nonsolar conversions, by the Division of Chemical Education; computer-assisted data acquisition, control and interpretation, by the Division of Computers in Chemistry; contaminants and sediments—sampling and analytical, analysis of polar and high molecular weight compounds in water, and trace element analysis in hydrosphere, by the Division of Environmental Chemistry; international activities in professional relations, by the Division of Professional Relations; and concerns of consulting chemists and chemical engineers, by the Division of Small Chemical Businesses.

All sessions sponsored by the Analytical Division will be held in the Hilton Hawaiian Village (Ocean Tower). The symposia sponsored jointly with the Division of Nuclear Chemistry and Technology and the Division of Fuel Chemistry will be held in the Ilikai, Imperial Suite, and the Miramar, Kuhio Suite, respectively.

The Analytical Chemistry Division social hour and dinner will be held Tuesday, April 3 at 6 and 7 p.m., respectively, at the House of Hong (260A Lewers St.), and will not be subsidized by the Division. Tickets for the dinner can be purchased in advance (see *Chem. Eng. News*, Jan. 15, page 112) or at the meeting for $15.

The chemical exposition, held in the Mid-Pacific Convention Center of the Hilton Hawaiian Village, will be sponsored by ACS and the Hawaii Section. A special feature of this exposition will be the Japanese firms' participation.

Several ACS courses given in conjunction with and before the meeting will be of interest to analytical chemists. For more information, see page 376 A.

Preregistration forms and housing information are contained in *Chem. Eng. News*, Nov. 27, 1978, and Jan. 15, 1979. The complete technical program for the meeting appears in the Jan. 15 issue. The detailed technical program given below includes all the Analytical Division sessions and those cosponsored by the Division. Smoking and nonsmoking sections will be separated.

ANALYTICAL CHEMISTRY

MONDAY MORNING

SECTION A

Hilton Hawaiian Village (Ocean Tower), Gold Room (2nd Floor)

ACS Award in Chromatography Symposium: Bioanalytical Systems Based on Chromatography and Mass Spectrometry.

W. J. A. VandenHeuvel, N. Ikekawa, Presiding

9:00—Introductory Remarks.

9:05—**1.** *Award Address.* (ACS Award in Chromatography sponsored by SUPELCO, INC.) Contemporary Problems in Quantitative Analysis of Biologic Samples by Methods Based on Gas or Liquid Chromatography and Mass Spectrometry. **E. C. Horning.**

9:45—**2.** Profile Analysis of Vitamin D_3 Metabolites in Plasma by Gas Chromatography-Mass Spectrometry. **N. Ikekawa, M. Morisaki, S. Kidooka, Y. Tanaka, H. F. DeLuca.**

10:05—**3.** Cyclic Boronates as Derivatives of Unrivaled Versatility for GC-MS of Bifunctional Substrates. **C. J. W. Brooks.**

10:25—**4.** Separation and Determination of Unsulfated and Sulfated Bile Acids in Biological Fluids by High-Performance Liquid Chromatography. **T. Nambara, J. Goto, H. Kato.**

10:45—Intermission.

11:00—**5.** Therapeutic Drug Monitoring in the Clinical Laboratory. **A. Karmen, N. S. Longo.**

11:20—**6.** Microanalysis of Prostaglandins and Thromboxanes by Gas Chromatography-Mass Spectrometry. **H. Miyazaki, M. Ishibashi, K. Yamashita, Y. Nishikawa, M. Katori.**

11:40—**7.** Identification and Assay of Biologically Important Compounds by GLC-Related Methods. **W. J. A. VandenHeuvel.**

SECTION B

Hilton Hawaiian Village (Ocean Tower), Empire I (2nd Floor)

Symposium on New Development in Thin-Layer Chromatography

N. Suzuki, J. A. Vinson, Presiding

8:30—Introductory Remarks.

8:35—**8.** The Use of Mini-Thin Layer Chromatography for the Rapid Development of Solvent Systems for High Performance Liquid Chromatography. Separations of Poly(Ethylene Terephthalate) Oligomers. **W. R. Hudgins, Kurt Theurer.**

8:55—**9.** Preadsorbent Thin-Layer Chromatography—A New Era in TLC. **J. A. Vinson.**

9:15—**10.** Sintered Thin-Layer Chromatography. **T. Okumura.**

9:55—Intermission.

10:15—**11.** Fluorescence Enhancement in Thin-Layer Chromatography by Spraying Viscous Organic Solvents. **S. Uchiyama.**

10:35—**12.** The Search for Performance in TLC: Effect of Non-Conventional Development Methods. **T. Jupille.**

10:55—**13.** In Situ Determination of Drugs and Metabolites Using HPTLC-Plates with Concentrating Zones. **S. Ebel, E. Geitz, B. Missler.**

11:15—**14.** Separations Utilizing High Performance Radial Chromatography. **R. K. Vitek, D. M. Kent.**

11:35—**15.** Precision and Accuracy in Today's Instrumentalized TLC in Quantitative and Qualitative Analysis. **R. E. Kaiser.**

SECTION C

Hilton Hawaiian Village (Ocean Tower), Empire II (2nd Floor)

General: Electroanalytical Chemistry

A. R. Branfman, H. Kamada, Presiding

9:00—**16.** Immobilized Alcohol Oxidase in the Continuous Flow Determination of Blood Alcohol Using an Oxygen Electrode. **E. L. Gulberg, G. D. Christian.**

9:20—**17.** Redox Titration of Perchlorate in Nonaqueous Solutions. **C. Yoshimura.**

End cap for tight seal during storage.

1/16" "reverse nut" inlet/outlet, adaptable to virtually any chromatograph.

THE ANATOMY OF A QUALITY HPLC COLUMN

4 mm ID 316 stainless steel tubing with Lichromas interior finish.

Choice of packings for adsorption, reverse phase, ion exchange and exclusion chromatography.

Zero dead volume end fitting for minimum band spreading.

FROM BIO-RAD, OF COURSE!

You can have complete confidence in the performance of Bio-Rad's HPLC columns for the best of all possible reasons: we *guarantee* it. Specifically, we guarantee column efficiency, peak symmetry, and flow resistance. Furthermore, every Bio-Sil® column comes with a test chromatogram and a test solution sample so that you can verify performance yourself.

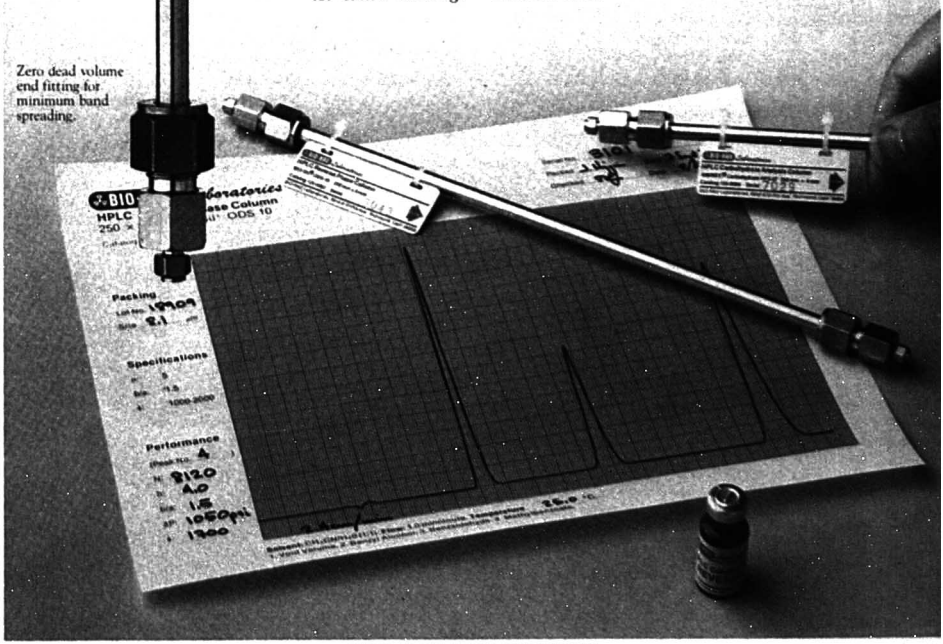
Bio-Rad offers a wide selection of columns — all competitively priced — and a wide choice of top quality packings including: • Bio-Sil HP-10 for adsorption • Bio-Sil ODS-10 for reverse phase • Bio-Sil GFC 100 for exclusion • Aminex® HP-C and Aminex A-9 for cation exchange • Aminex A-27 for anion exchange • A variety of custom packings for specific applications (HPX-87 and HPX-42 for carbohydrate analysis are two examples).

Request Bio-Rad Bulletin 1056 for details and our guide to HPLC column evaluation. Contact:

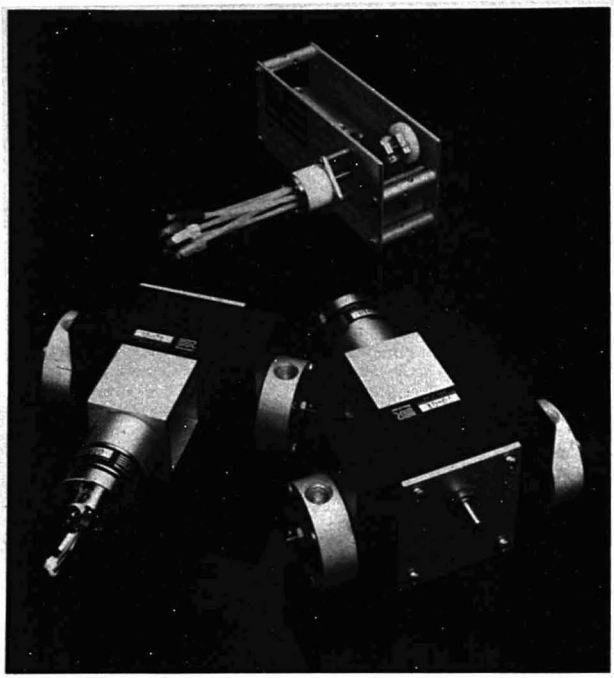
BIO-RAD *Laboratories*

2200 Wright Avenue
Richmond, CA 94804
Phone (415) 234-4130

Also in: Rockville Centre, N.Y.; Mississauga, Ontario; London; Milan; Munich; Vienna.



CIRCLE 22 ON READER SERVICE CARD



Just what you need to automate HPLC.

Inject samples. Switch columns. Select solvents. All automatically with Rheodyne valves.

Rheodyne's pneumatically-actuated valves enable you to introduce automatic stream control anywhere in your HPLC system. They work at pressures up to 7000 psi – offering many opportunities to save time and increase precision through automation.

Automatic sample injection. Done with Rheodyne Model 7010A, a pneumatically-actuated version of our popular loop-type injector. Excellent for use with an autosampler in routine analysis. Very helpful for injecting the same sample repeatedly in methods development. Removable sample loops in eight sizes from 10 μl to 2 ml insure that successive samples will be exactly the same volume.

Automatic column switching. Our 7000 Series valves will switch columns in and out of the stream to increase the speed of analysis. For example, two columns can be interfaced to analyze complex samples without employing gradient elution. Or a small column can be used to enrich and pre-fractionate a sample before switching the stream to an analytical column.

Automatic solvent selection. With Rheodyne's 5012A all-Teflon 6-position valve you can select any of six different solvents during automated methods development. Or automate many stepwise elution schemes of your own design.

Get the details now. Contact Rheodyne, Inc., 2809 Tenth St., Berkeley, California, 94710. Phone (415) 548-5374.

RHEODYNE

THE LC CONNECTION COMPANY

CIRCLE 184 ON READER SERVICE CARD

News

9:40—18. Application of Chemically Modified Electrodes to Organic Voltammetric Analysis. **R. P. Baldwin, J. F. Price, J. Siria.**

10:00—19. Pulse Polarographic Analysis for Carcinogenic Nitrosamine, N-Butyl-N-(4-Hydroxybutyl)-Nitrosamine. **K. Hasebe, S. Hikime, J. G. Osteryoung.**

10:20—Intermission.

10:30—20. Trace Ion Chromatography Using Coulometric Techniques. **J. E. Girard.**

10:50—21. Determination of Iodide Ion in Iodine by Potentiometric Titration with an Iodide-Selective Membrane Electrode. **J. Motonaka, Y. Nakabayashi, S. Ikeda, N. Tanaka.**

11:10—22. Determination of the Antineoplastic Agent, Indicine-N-Oxide (NSC 132139) in Biological Fluids by Differential Pulse Polarography. **A. R. Branfman, I. Bodek, M. McComish.**

11:30—23. Adsorption Behavior of Cytochrome C at the Mercury/Aqueous Solution Interface. **S. Sawada, M. Suzuki.**

11:50—24. Polarographic Estimation of Reactivities of ·OH Radical Produced in Fe-EDTA-H_2O_2 System. **H. Kaneko, K. Nozaki, T. Ozawa.**

SECTION D

Hilton Hawaiian Village (Ocean Tower), Beach Club I (2nd Floor)

General: Atomic Absorption and Emission

K. Matsumoto, J. D. Messman, Presiding

9:00—25. Application of High Resolution Continuum Source Atomic Absorption Spectrometry to the Analysis of Standard Reference Materials. **J. D. Messman, M. S. Epstein, T. C. Rains, I. L. Barnes, T. C. O'Haver.**

9:20—26. Vacuum UV Mercury Line Spectral Light Source. **Y. Akai, A. Honma.**

9:40—27. Wide Concentration Range Calibration Methods for Furnace Atomic Absorption. **J. A. Nichols, F. G. Dewalt, R. Woodriff.**

10:00—28. Determination of Metals in Minute Sample by Atomic Absorption and Emission Spectrometry with Discrete Nebulization Technique. **T. Uchida, I. Kojima, C. Iida.**

10:20—Intermission.

10:30—29. Condenser Assembly in Gaseous Hydride AAS Technique. **H. Kanai, R. Goo, H. Wakatsuki.**

10:50—30. Determination of Total Arsenic and Hydrolytic Arsenic in Biological Materials by Flameless

NEW & BEST-SELLING BOOKS from WILEY-INTERSCIENCE

QUANTITATIVE ANALYSIS OF ORGANIC MIXTURES Part 1: General Principles

T. S. Ma & Robert E. Lang

The first book to treat organic analysis from the viewpoint of mixtures, emphasizing the importance of knowing the influence of foreign matter in a determination. Covers general principles in handling organic materials intended for quantitative analyses, sample preparation, and the analysis of several components without separation.

approx. 295 pp. (1-55800-1) **April 1979** $19.50 (tent.)

PRINCIPLES OF INDUSTRIAL CHEMISTRY

Chris A. Clausen III & Guy C. Mattson

This book meets the need for a text in industrial chemistry at the senior or graduate level. It aims to complement the traditional training of the chemist making a change from the academic to the industrial world. Process Development is emphasized since it offers greatest opportunity to stress the correlation between classical and industrial chemistries.

312 pp. (1-02774-X) **1978** $18.95

ANALYTICAL LASER SPECTROSCOPY

Edited by Nicolo Omenetto

A collection of papers by outstanding international experts examining the techniques, applications, and future developments of analytical laser spectroscopy. Examines the physics underlying analytical implementation, covering fundamentals of the interaction of lasers with atoms and molecules.

approx. 560 pp. (1-65371-3) **1978** $34.95

ATOMIC ABSORPTION SPECTROSCOPY, 2nd Ed.

Morris Slavin

This new edition covers the latest methods and equipment for chemical analysis by atomic absorption spectroscopy. It differs from the previous edition in that it contains more emphasis on the chemistry of the atomic absorption technique, an expanded historical section, and a section devoted to the applications of the furnace as the volatizing medium of the sample. Provides all pertinent physical and chemical data on some 70 elements, from traces to major constituents, amenable to determination by atomic absorption. Data includes the most sensitive line, the lowest concentration, and the expected linear range for each element covered. 193 pp. (1-79652-2) **1978** $19.95

ORGANIC ELECTRONIC SPECTRAL DATA Vol. 14, 1972

Edited by John P. Phillips, Dallas Bates, Henry Feuer, & B. S. Thyagarajan

Continues the effort originally begun in 1956, to abstract and publish in formula order all of the ultraviolet-visible spectra of organic compounds in the journal literature. Vol. 14 contains spectra published in 1972 and includes the journal name, page number, and authors. 1,166 pp. (1-05076-8) **1978** $65.00

TRACE ELEMENT ANALYSIS OF GEOLOGICAL MATERIALS Vol. 51 in the Chemical Analysis Series of Monographs on Analytical Chemistry and Its Applications

R. D. Reeves & R. R. Brooks

This book covers the entire sequence of processes necessary in the analysis of geological materials for trace elements. It examines sampling techniques and physical and chemical methods of sample pretreatment, methods of chemical attack and of separation techniques, and elemental abundance data and standard rock materials.

421 pp. (1-71338-4) **1978** $27.50

TECHNIQUES OF CHEMISTRY, Vol. 14 Thin-Layer Chromatography, 2nd Ed.

Justus G. Kirchner

A thoroughly updated comprehensive treatise on TLC, covering techniques and applications to many types of organic and inorganic compounds.

1,137 pp. (1-93261-7) **1978** $60.00

PRACTICE OF THIN LAYER CHROMATOGRAPHY

Joseph C. Touchstone & Murrell F. Dobbins

"...practical, down-to-earth approach...highly recommended as a readable overview of TLC..."—*Analytical Chemistry*

All the basic techniques to practice TLC. Stresses skills needed to perform separation.

383 pp. (1-88042-6) **1978** $21.50

HANDBOOK OF ANALYTICAL DERIVATIZATION REACTIONS

Daniel R. Knapp

Brings together practical information previously available only in scattered sources. Includes an overview of analytical derivatization with a section on apparatus; analytical derivatization methods organized according to the sample to be derivatized; and a discussion of methods covering derivative type, reagent, sample type, reaction, and typical procedures.

approx. 1,136 pp. (1-03469-X) **April 1979** $29.50 (tent.)

DENSITOMETRY IN THIN LAYER CHROMATOGRAPHY Practice and Applications

Joseph C. Touchstone & Joseph Sherma

Here's a unique "how-to-do-it" guide to the instruments and methods for quantitation of materials separated on thin layer chromatograms *in situ* by densitometry. Includes a thorough discussion of Kubelka-Munk Theory.

768 pp. (1-88041-8) **Jan. 1979** $29.95

CHEMICAL ANALYSIS BY MICROWAVE ROTATIONAL SPECTROSCOPY Vol. 52 in the Chemical Analysis Series of Monographs on Analytical Chemistry and Its Applications

Ravi Varma & Lawrence W. Hrubesh

Representing the current state-of-the-art, this book provides details of basic theory and offers complete coverage of techniques. The authors present characteristics for qualitative and quantitative chemical analysis and include examples of actual applications. approx. 217 pp. (1-03916-0) **1978** $21.50

QUANTITATIVE ORGANIC ANALYSIS VIA FUNCTIONAL GROUPS, 4th Ed.

Sidney Siggia & J. Gordon Hanna

This book describes the methods for identifying and measuring the amounts of organic constituents present in materials—organic compounds either in the pure state or in complex mixtures. It uses the functional groups as the analytical handle for measuring the compounds being studied, and shows interrelationships between methods. approx. 880 pp. (1-03273-5) **Jan. 1979** $45.95

PHOTOMETRIC AND FLUOROMETRIC METHODS OF ANALYSIS Metals, Parts I & II

Foster Dee Snell

These two reference volumes condense all recently published information on photometric, spectrophotometric, colorimetric, and fluorometric methods of determination of metals. When used with appropriate instruments, they provide rapid and economical methods of determination of 57 common and uncommon metals, as well as rare earths. Each chapter is a quasi-monograph on the determination of one element with references to the original literature.

Two-Part Set: 2,192 pp. (1-81014-2) **1978** $160.00

PATTY'S INDUSTRIAL HYGIENE AND TOXICOLOGY, 3rd Revised Ed. Vol. 1: General Principles

Edited by George D. Clayton & Florence E. Clayton

The updated, revised, and expanded first volume of the classic reference on industrial hygiene originally compiled by Frank Patty. This new volume provides a complete guide to methods of evaluation, record keeping, and control, as well as historical background, and incorporates new topics, developments, and legislation. The scope of the book has been broadened to include agriculture, quality control, environmental pollution, and much more. Third printing in six months.

1,466 pp. (1-16046-6) **1978** $75.00

Still available: Industrial Hygiene and Toxicology, 2nd Edition, Vol. 2, Toxicology. **F. A. Patty.** 1963. (0-67188-2) $68.95

INTERPRETATION AND PROCESSING OF VIBRATIONAL SPECTRA

Milan Horák & Antonín Vítek

Summarizes rules and provides methodological hints for procedures in handling and interpreting vibrational spectra. Presents commonly used definitions, constants, conversion factors, relationships and schemes of computing procedures for numerical treatment of experimental data.

approx. 300 pp. (1-99504-5) **Feb. 1979** $38.00 (tent.)

Available at your bookstore or write to Nat Bodian, Dept. 092-A 3635.

WILEY-INTERSCIENCE
a division of John Wiley & Sons, Inc.
605 Third Avenue
New York, N.Y. 10016
In Canada: 22 Worcester Road, Rexdale, Ontario
Prices subject to change without notice. 092 A 3635-51

CIRCLE 238 ON READER SERVICE CARD

Atomic Absorption Spectrometry Using a Carbon Tube Atomizer. **M. Ishizaki, S. Ueno, N. Oyamada, K. Katsumura, M. Fujiki, S. Yamaguchi.**

11:10—**31.** Application of a Multi-Element Atomic Absorption Spectrometer to Biological Samples Using Graphite Furnace Atomization. **W. R. Wolf, J. M. Harnly, T. C. O'Haver.**

11:30—**32.** Atomic and Molecular Spectrochemical Analysis of Non-Metallic Elements Using Gas Generation Technique. **K. Matsumoto, M. Takahashi, H. Haraguchi, K. Fuwa.**

11:50—**33.** Anion Matrix Interferences in Constant Temperature and in Pulsed-Type Atomizers for AAS. **L. Hageman, J. A. Nichols, M. C. Verwolf, R. A. Woodriff.**

MONDAY AFTERNOON

SECTION A

Hilton Hawaiian Village (Ocean Tower), Gold Room (2nd Floor)

Symposium on Microprobe Techniques for Elemental Analysis.

G. H. Morrison, A. Mizuike, Presiding

2:00—**34.** Ion Microprobe Analysis. **G. H. Morrison.**

2:40—**35.** Electron Microprobe Analysis. **R. Shimizu.**

3:20—Intermission.

3:40—**36.** Microanalysis by Scanning Transmission Electron Microscope. **T. Komoda.**

4:20—**37.** The Laser Raman Microprobe: Instrumental Molecular Microanalysis of Solids. **K. F. J. Heinrich.**

SECTION B

Hilton Hawaiian Village (Ocean Tower), Empire I (2nd Floor)

General: Spectrophotometric

K. Ueno, Presiding

2:00—**38.** Selective Spectrophotometric Determination of Amines Using Thermochromism. **T. Sakai, N. Ishida.**

2:15—**39.** 1-Aryl 3-Methyl-4-acyl-5-Pyrazolones as Analytical Reagents. **M. Matsui, J. Tôei, S. Umtani, T. Shigematsu.**

2:30—**40.** Spectrophotometric Determination of Microamounts of Tungsten with Thiocyanate. **Y. Komiyama, Y. Hiratsuka.**

2:45—**41.** Spectrophotometric Determination of Iron(II) with 4-Hydroxy-2-Dimethylamino-5-Nitroso-6-Aminopyrimidine. **M. Tsuchiya.**

3:00—**42.** Spectrophotometric Determination of Zirconium in Ni-W-Zr Alloy. **M. Ezawa, A. Misumi.**

3:15—Intermission.

3:30—**43.** Spectrophotometric Determination of Metals by Adsorption of their Complexes on Naphthalene. **M. Satake, T. Fujinaga.**

3:45—**44.** Analysis of Ethylene Oxide-Propylene Oxide Polyethers by Nuclear Magnetic Resonance Spectroscopy. **M. Noshiro, Y. Akatsuka, Y. Jitsugiri, Y. Tamaki, S. Kozawa.**

4:00—**45.** Identification of Trace Phenols by Means of Resonance Raman Spectroscopy. **H. Nakamura, J. Itoh, K. Yoshimori, M. Takagi, K. Ueno.**

4:15—**46.** Determination of Trace Amounts of Some Phenylamide Pesticides in Water by Resonance Raman Spectrometry. **S. Higuchi, O. Aiko, S. Tanaka.**

4:30—**47.** Raman Circular Intensity Differential Spectra of Chiral Compounds with Related Structures. **H. Waki, S. Higuchi, S. Tanaka.**

SECTION C

Hilton Hawaiian Village (Ocean Tower), Empire II (2nd Floor)

General: Electroanalytical Chemistry

D. J. Curran, K. Ichise, Presiding

2:00—**48.** Analytical Application of the Adsorption of Nickel(II)-2,2'-Bipyridine Complex on the Hanging Mercury Drop Electrode. **H. Sawamoto.**

2:20—**49.** Reticulated Vitreous Carbon Electrodes as Voltammetric Flow-Through Detectors for Flow Injection Analysis. **D. J. Curran, A. N. Strohl.**

2:40—**50.** Simultaneous Microdetermination of Hydrazine and Hydroxylamine by Amperometric Titration. **S. Ikeda, H. Satake.**

3:00—**51.** Evaluation of Flow-Through Kel-F-Graphite Composition Electrodes as Detectors for Flow Injection Analysis. **D. J. Chesney, D. E. Weisshaar, J. L. Anderson, D. E. Tallman.**

3:20—Intermission.

3:30—**52.** Anodic Oxidation of N,N-Dimethyl Toluidines at a Platinum Electrode in Acetonitrile Solutions. **I. Taniguchi, H. Yamaguchi, K. Yasukouchi.**

3:50—**53.** Variable Temperature Electrochemistry on the Iron(III) Spin Equilibrium System $Fe[(X\text{-}sal)_2\text{-}trien]^+$. **K. M. Kadish, D. Schaeper, K. Das.**

4:10—**54.** Redox Potentiometric Titration of Selenic and Telluric Acids in Nonaqueous Solvents. **C. Yoshimura, K. Miyamoto.**

4:30—**55.** A Staircase Voltammetry Polarograph. **H. Hayashida, M. Son, M. Nishiyama.**

4:50—**56.** Potential Behaviors of Ion-Sensitive Field Effect Transistor in Electrolyte. **M. Okada, T. Inaguma, H. Matsushita.**

SECTION D

Hilton Hawaiian Village (Ocean Tower), Beach Club I (2nd Floor)

General: Atomic Absorption and Emission

W. MacCheran, K. Fuwa, Presiding

2:00—**57.** Determination of Trace Elements in Coal and Residual Fuel Oil by Atomic Absorption and Emission Spectrometry. **I. L. Barnes, J. D. Messman, T. J. Brady, T. C. Rains.**

2:20—**58.** Non-Dispersive Atomic Fluorescence Spectrometric Determination of Bismuth with Hydride Generation Technique. **T. Nakahara, S. Kobayashi, S. Musha.**

2:40—**59.** Determination of Antimony in Environmental Samples by a Semi-Automated Hydride Generation—Atomic Absorption Method. **P. N. Vijan.**

3:00—**60.** Determination of Chromium in Human Urine by Atomic Absorption Spectrometry with Heated Graphite Atomizer. **M. Kusumoto, H. J. Einbrodt.**

3:20—Intermission.

3:30—**61.** Determination of Selenium in Human Kidney Cortex Using Zeeman Effect Flameless Atomic Absorption Spectrometry. **K. H. Pearson, P. A. Pleban.**

3:50—**62.** Determination of Palladium by Atomic Absorption Spectrophotometry with the Solvent Extraction Using Potassium Xanthates as a Chelating Agent. **M. Aihara, M. Kiboku, K. Kirimoto.**

4:10—**63.** Flameless Atomic-Absorption Spectrophotometry of Copper by Introduction of Chelating Resin into Carbon Tube Atomizer. **A. Isozaki, N. Soeda, T. Okutani, S. Utsumi.**

4:30—**64.** Determination of Cadmium in Polished Rice by Atomic Absorption Spectrophotometry. **H. Narasaki.**

4:50—**65.** The Study of Sensitivity Enhancement of Aluminum with Nitrogen Compounds on an Oxygen Sandwiched Air-Acetylene Flame. **T. Kono.**

TUESDAY MORNING

SECTION A

Hilton Hawaiian Village (Ocean Tower), Gold Room (2nd Floor)

Polarography + Liquid Chromatography

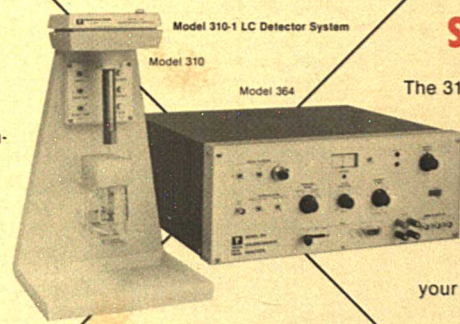
Now, get the benefits of these two powerful techniques by using our 310-1 Polarographic Detector System with your Liquid Chromatograph.

Versatility

Many different organic functional groups, anions, organometallics, and metals respond to the Model 310 polarographic LC detector. Application areas include: environmental, food, pharmaceuticals, cosmetics, pesticides, plastics and polymers, pulp, paper, and chemical industries.

Dynamic Range

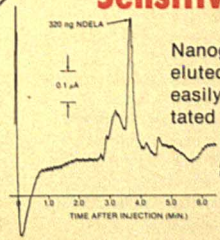
The peak height-concentration relationship remains linear over *several decades* of concentration with the Model 310.



Selectivity

The 310 selectivity is controlled by adjusting the applied potential and by choosing the optimum detection mode (sampled dc, normal pulse or differential pulse) for your particular application.

Sensitivity



DIRECT ANALYSIS OF SHAMPOO FOR N-NITROSODIETHANOLAMINE (NDELA). 1.0 g SHAMPOO IN 10 ml CONTAINING 32 ppm NDELA. INJECTION VOLUME 10 μL.

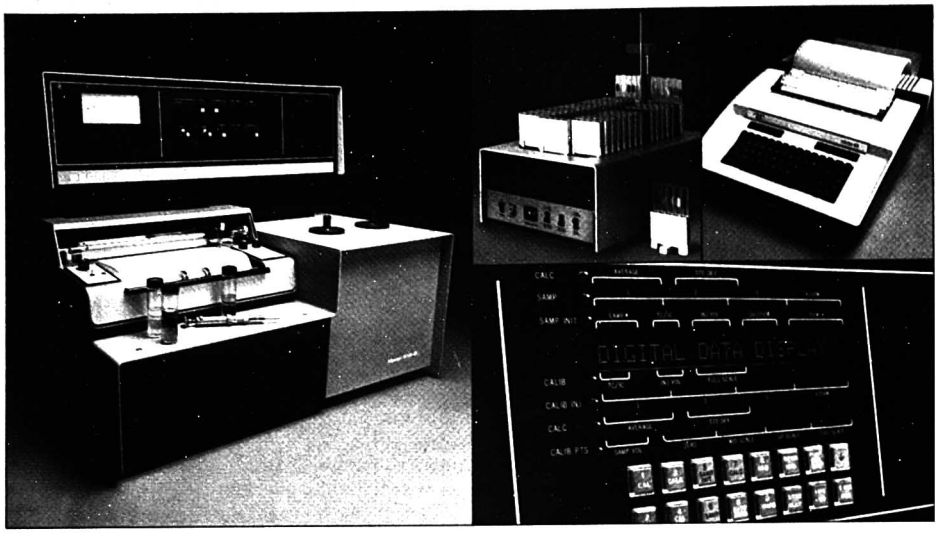
Nanogram levels of eluted substances are easily detected and quantitated with the Model 310.

EG&G PRINCETON APPLIED RESEARCH

P. O. BOX 2565 • PRINCETON, NJ 08540 • 609/452-2111

486

CIRCLE 171 ON READER SERVICE CARD FOR ADDITIONAL INFORMATION ONLY



BUY NOW. GROW LATER.

Beckman introduces microprocessor-controlled Total Organic Carbon Analyzer.

Here's the TOC Analyzer that meets your needs today and tomorrow.

Today. The 915-B provides 2-3 minute analysis in ranges of 0-1 ppm up to 0-4000 ppm with repeatability ±2% of full scale over 5 ppm; ±5% of full scale at 5 ppm and below. An integral microprocessor provides temperature control, over-temperature protection, temperature display and fast warm-up for the standard TC combustion furnace and the optional IC combustion furnace. Other features include high solids sample handling capacity, choice of IC removal methods and a simplified vertical sample injection system that reduces catalyst recharge time and frequency by up to 75%.

Tomorrow. Today's 915-B will grow with your needs, adding functional modules and a digital display for TOC and temperature readout. The microprocessor will be used for calibration, linearization, peak picking and averaging, scaling, autozero, channel correlation and service diagnostic checks.

The Beckman 915-B is successor to the 915—field-proven for more than 15 years. It incorporates the same precision and dependability demonstrated by the 915 in more than 2,000 installations worldwide. It makes possible new standards of accuracy and speed in such applications as measurement of wastewater effluents, detection of heat exchanger leaks, monitoring of evaporative processes, analysis of potable water supplies, and determination of waste treatment efficiency. For further information contact Process Instruments Division, Beckman Instruments, Inc., 2500 N. Harbor Boulevard, Fullerton, CA 92634.

BECKMAN®

CIRCLE 26 ON READER SERVICE CARD

Analytical Instrumentation Award Symposium.

D. M. Coleman, N. Tanaka, Presiding

8:30—Introductory Remarks.

8:35—66. New Perspectives on Chemical Instrumentation. **H. V. Malmstadt.**

8:55—67. Essential Criteria for Analytical Instrumentation in a Medical Analysis Laboratory. **M. A. Evenson.**

9:25—68. Laser Induced Thermal Effects: A New Resource for Chemical Analysis. **J. M. Harris, N. J. Dovichi.**

9:55—69. New Chemical Insights from Experiments Using Synchrotron Radiation. **J. W. Taylor.**

10:20—Intermission.

10:35—70. *Award Address.* (Sponsored by the Instrumentation Specialties Company). Instrumentation for Innovation in Experimental Atomic Spectroscopy. **J. P. Walters.**

11:05—71. Intensity Modulation of Spectral Lines by Current Pulse Synthesis in Quarter-Wave Spark Sources. **T. Uchida, S. Minami.**

11:35—72. Optical Emission Spectroscopic Instrumentation: Where Is It Going? **J. S. Beatty.**

SECTION B

Hilton Hawaiian Village (Ocean Tower), Beach Club I (2nd Floor)

Symposium on New Developments in Voltammetry and Coulometry: Voltammetry I.

J. Jordan, M. Senda, Presiding

9:00—Introductory Remarks.

9:10—73. Advances in Rotating Disk Electrode Voltammetry. **S. Bruckenstein.**

9:50—74. Window Sweep Chronopotentiometry—Theory, Instrumentation, and Simulation. **Y. Kato, N. Yoshida, K. Unoura, A. Yamada, N. Tanaka.**

10:10—75. A New Aspect of Theory and Application of the Catalytic Hydrogen Evolution Current (Brdicka Current) Produced by Proteins in the Presence of Cobalt Ion. **M. Senda, T. Ikeda, H. Kinoshita, K. Kano, Y. Yamane.**

10:30—Intermission.

10:50—76. Reverse Pulse Polarography. **J. Osteryoung, E. Kirowa-Eisner.**

11:10—77. Automated Pulse Polarographic Determination of Serum Glycoproteins in a Continuous-Flow System. **P. W. Alexander, M. H. Shah.**

11:30—78. Advances in Pulsed Voltammetric Methodology. **R. A. Osteryoung, J. H. Christie, J. O'Dea, J. A. Turner.**

SECTION C

Hilton Hawaiian Village (Ocean Tower), Empire II (2nd Floor)

General: Gas Chromatography, Mass Spectrometry

T. Kojima, S. P. Cram, Presiding

9:00—79. Super-Chrom: New GC Separation and Analysis Capabilities. **S. P. Cram, F. J. Yang, A. C. Brown, III.**

9:20—80. Correlation Between Activation Energy in Dissociative Electron Capture Reaction and Acidity Constant II. **M. Satouchi, T. Kojima.**

9:40—81. New Concepts of Thermionic Detection of Gas Chromatograph Effluents. **P. L. Patterson.**

10:00—82. Pyrolytic Sulfurization Gas Chromatography. VI. Improvement of the Apparatus. **T. Hara, K. Fujinaga, F. Okui.**

10:20—Intermission.

10:35—83. Capillary Gas Chromatography Sampling Without Splitting. **S. P. Cram, F. J. Yang.**

10:55—84. Pyrolytic Sulfurization Gas Chromatography. V. Simultaneous Determination of the Atomic Ratio Between C, H, O, and N in a Polymer. **T. Hara, K. Fujinaga, F. Okui.**

11:15—85. Fragmentation Patterns of GC Analytes in a Penning Ionization Reactor. **W. A. Aue, V. Paramasigamani.**

11:35—86. New Gas Chromatographic Detection of Nitric Oxide. **M. Tanaka, K. Funazo, T. Shono.**

SECTION D

Hilton Hawaiian Village (Ocean Tower), Empire I (2nd Floor)

General: Chelating Agents

K. Nagashima, R. Litman, Presiding

9:00—87. Partial Resolution of Optically Active $Cr(acac)_3$ and $Co(acac)_3$ by Salting-In-Effect with Metal Chelate Electrolytes. **Y. Yamamoto, E. Iwamoto, M. Yamamoto.**

9:20—88. A Study of the Extraction of Cadmium by Dithizone. **R. Litman, M. Gauthier.**

9:40—89. Extraction of Alkali Metal Picrates with Stereoisomers of Poly-and Bis(Crown Ether)s. **K. Kimura, H. Tamura, T. Tsuchida, T. Shono.**

10:00—90. Sulfonamides as Ligands. A New Class of Chelating Agents of Potential Utility in Inorganic and Analytical Chemistry. **K. Ueno, M. Takagi, T. Omori, S. Matsuo, S. Ide.**

10:20—Intermission.

10:35—91. Thermodynamic Aspects of Solvent Extraction of Tetraalkylammonium Iodide Ion Pairs. **E. Iwamoto, K. Ito, Y. Yamamoto.**

10:55—92. Influence of Temperature Upon Formation of Metal Halide Complexes in Nonaqueous Solvents. **Y. Sasaki, M. Takizawa, K. Umemoto, N. Matsuura.**

11:15—93. Kinetic Studies of Stripping of Bis(2,4-Pentanedionato)-Beryllium(II) in Liquid-Liquid Partition Systems. **H. Watarai, N. Suzuki.**

11:35—94. Solvent Extraction of Coordination-Unsaturated Chelate and Effect of Quaternary Ammonium Base. **S. Noriki, M. Nishimura.**

TUESDAY AFTERNOON

SECTION A

Hilton Hawaiian Village (Ocean Tower), Gold Room (2nd Floor)

General: Spectroscopy

G. E. Batley, B. I. Diamondstone, Presiding

2:00—95. Multielement Analysis of ICP Emission Spectrometry Using a Programmable Monochromator and a SIT Image Detector. **N. Furuta, H. Haraguchi, K. Fuwa.**

2:20—96. The Determination of Lithium by Resonance Ionization Spectroscopy. **J. P. Young, S. D. Kramer, M. G. Payne, G. S. Hurst.**

2:40—97. A Four Lines Method for Correction of Cationic Interference in Plasma Emission Spectroscopy. **K. Kitagawa, T. Takeuchi.**

3:00—98. Fourier Transform Ion Cyclotron Resonance Spectroscopy. **M. Comisarow, G. Parisod, J. Melka.**

3:20—Intermission.

3:35—99. A Study of Arsenic Speciation in Oysters. **B. I. Diamondstone, S. Hanamura.**

3:55—100. Determination of Selenium in Biological Materials and Foods by the Use of Instrumental Neutron Activation Analysis. **S. Hirai.**

4:15—101. Determination of the Organic Affinities of Trace Elements in Coal. **R. D. Smith, J. A. Campbell, K. K. Nielson.**

4:35—102. Neutron Activation and X-ray Fluorescence Analysis of Japanese Ancient Pottery, Sueki. **T. Mitsuji, Y. Maruo.**

6:00—*Divisional Social Hour.* House of Hong Restaurant, 260-A Lewers Street, Waikiki.

7:00—*Divisional Dinner.* House of Hong Restaurant, 260-A Lewers Street, Waikiki.

SECTION B

Hilton Hawaiian Village (Ocean Tower), Empire I (2nd Floor)

Symposium on New Developments in Voltammetry and Coulometry: Voltammetry II.

M. Senda, J. Jordan, Presiding

2:00—**103.** Chemical Modification of Carbon Electrodes. **M. Fujihira, Y. Fukuda, A. Tamura, T. Osa.**

2:40—**104.** Electrocatalysis and Chemically Modified Electrodes. **T. Kuwana.**

3:20—**105.** Chemically Modified Indium Oxide Electrodes and Their Applications to Chemical Analysis. **S. Suzuki, M. Karayama, S. Araki.**

3:40—Intermission.

4:00—**106.** 'State of the Art' of Voltammetry at Glassy Carbon Indicator Electrodes. **J. Jordan, D. G. Dube, M. Gross, G. Ritzler.**

4:20—**107.** Feature Extraction on the Electrode Process for Qualitative Electrochemical Analysis by Recent Digital Signal Processing Techniques. **M. Ichise, H. Yamagishi, H. Oe, H. Oishi, T. Kojima.**

4:40—**108.** On-Line Computerized FFT Faradaic Admittance Measurements: Recent Advances and Applications. **D. E. Smith, R. J. Schwall, J. C. Schaar, T. Matusinovic, J. Begemann.**

6:00—*Divisional Social Hour.* (see Section A for location).

7:00—*Divisional Dinner.* (see Section A for location).

SECTION C

Hilton Hawaiian Village (Ocean Tower), Empire II (2nd Floor)

General: Gas Chromatography, Mass Spectrometry

J. F. Parcher, S. Yanagisawa, Presiding

2:00—**109.** Characterization of By-Products from Oxidation and Pyrolysis of Raw Shale. **J. A. Campbell, D. M. Schoengold, W. C. Weimer.**

2:20—**110.** Determination of Hydrocarbons and Carbonyl Compounds in Auto Exhaust by Chemical Ionization Mass Spectrometry. **T. Kashiwagi, S. Daishima, Y. Iida.**

2:40—**111.** Quantitative Gas Chromatography/Mass Spectrometry. Analysis of Methylene Chloride in Rat Plasma by the Stable Isotope Dilution Technique. **A. R. Branfman, Y. Merrill, R. J. Bruni, C. Rogers, D. W. Yesair.**

3:00—**112.** An Approach to the Interpretation of Mass Spectra. **H. Nakashima, K. Okamoto.**

3:20—Intermission.

3:35—**113.** Mixed Bed Columns for Gas-Liquid Chromatography. **J. F. Parcher.**

3:55—**114.** Bio-Analytical Fractionation of Toxicants in Industrial Effluent Streams. **R. L. Garnas.**

4:15—**115.** Characterization of O-Trimethylsilyl Derivatives of D-Mono- and D-Disaccharides by Gas-Liquid Chromatography-Chemical-Ionization Mass Spectrometry with Ammonia as Reagent Gas. **T. Murata, S. Takahashi, T. Takeda, S. Onishi.**

4:35—**116.** Stable Isotope Dilution Technique for the Determination of Chromium in Biological Materials. **C. Veillon, B. E. Guthrie, W. R. Wolf.**

6:00—*Divisional Social Hour.* (see Section A for location).

7:00—*Divisional Dinner.* (see Section A for location).

SECTION D

Hilton Hawaiian Village (Ocean Tower), Beach Club I (2nd Floor)

General: Chelating Agents

M. Tanaka, Presiding

2:00—**117.** Preparation of Bead-Shaped Cellulosic Ion Exchangers. **Y. Motozato, K. Matsumoto, M. Hirato.**

2:20—**118.** Solvent Effects on Synergic Extraction of Europium Thenoyltrifluoroacetonate with Trioctyl Phosphine Oxide. **K. Akiba, M. Wada, T. Kanno.**

2:40—**119.** Sorption Behavior of Silver(I), Gold(III) and Palladium(II) on p-Dimethyl-amino-Benzylidenerhodanine Supported on Silica Gel. **K. Terada, K. Morimoto, T. Kiba.**

3:00—**120.** Extraction of Antimony and Bismuth with Pyrocatechol Violet and Tridodecylethylammonium Bromide. **Y. Shijo, K. Sakai, T. Mori, E. Tamura.**

3:20—Intermission.

3:30—**121.** Reaction of Heterocyclic Formazanes with Copper, Nickel and Zinc. **A. Uchiumi, A. Kawase.**

3:50—**122.** Formation of Zinc or Cadmium Oxinate in Suspended Solution of Lead Oxinate. **K. Takiyama, Y. Ishii, K. Ohoka.**

4:10—**123.** Precipitation Rate of Copper and Zinc Oxinates from Homogeneous Solution Containing 8-Acetoxyquinoline. **K. Takiyama, Y. Ishii, C. Inoue.**

4:30—**124.** Separation of Lanthanoids with Poly(Oxyethylene) Derivatives. **Y. Hirashima, Y. Moriwaki, J. Shiokawa.**

4:50—**125.** Extraction-Spectrophotometric Determination of Copper(II) with Sodium N,N-Dibutyldiselenocarbamate in Methylene Chloride. **T. Honjo.**

6:00—*Divisional Social Hour.* (see Section A for location).

7:00—*Divisional Dinner.* (see Section A for location).

WEDNESDAY MORNING

SECTION A

Hilton Hawaiian Village (Ocean Tower), Gold Room (2nd Floor)

ACS Award in Analytical Chemistry Symposium

P. N. Keliher, T. Takeuchi, Presiding

9:00—Introductory Remarks.

9:05—**126.** *Award Address.* (ACS Award in Analytical Chemistry, sponsored by Fisher Scientific Co.) Simultaneous Multielement Determinations at all Concentration Levels—the Renaissance of an Old Approach. **V. A. Fassell.**

9:55—**127.** Research on Multielement Analysis, Viewed from an Historical Perspective. **M. Margoshes.**

10:20—Intermission.

10:40—**128.** Continuous On-Line Multielement Analyzers for Elemental Analysis of Output Streams from Coal Gasifiers. **R. N. Kniseley.**

11:00—**129.** Laser Induced Photoacoustic Spectra of Rare Earth Ions in Aqueous Solution. **H. Kamada, T. Sawada, S. Oda.**

11:20—**130.** A Study of Peaks Generated During Graphite Furnace Atomic Absorption Analyses. **W. B. Barnett, M. M. Cooksey, L. P. Morgenthaler.**

11:40—**131.** Environmental Analytical Problems—A Challenge to Multielement Analysis. **C. H. Anderson.**

SECTION B

Hilton Hawaiian Village (Ocean Tower), Beach Club I (2nd Floor)

Symposium on New Developments in Voltammetry and Coulometry: Coulometry.

M. Senda, J. Jordan, Presiding

9:00—**132.** Coulopotentiographic Determination of Sub-ppb Level Copper and Lead in Sea Water. **T. Fujinaga, S. Okazaki.**

9:40—**133.** Coulometry and Voltammetry in Liquid SO_2. **L. A. Tinker, A. J. Bard.**

10:00—**134.** The Rapid Determination of the Apparent Value of n for Electrode Reactions by Coulometric Flow-Through Electrodes. **D. C. Johnson, B. G. Snider.**

PHI® ESCA/SAM

EXCELLENT ESCA PERFORMANCE... AND SCANNING AUGER TOO.



Physical Electronics has established a reputation as the leader in electron spectroscopy instrumentation. This is due, in large part, to a commitment to equipment advancement, as well as the belief that applications backup and interpretive aids are essential ingredients in an overall surface analysis capability. Recently, PHI introduced to the ESCA market a unique, multi-purpose instrument, the PHI Model 550, ESCA/SAM. One of the best ESCA instruments available today, it is backed up with applications support from our analytical laboratory along with a newly published Handbook of X-Ray Photoelectron Spectroscopy.

The Model 550 is, first and foremost, an ESCA system capable of solving a wide range of materials problems in the chemical process industry, as well as in other areas of materials technology. It offers the high energy resolution and high count rate capabilities required of the best ESCA systems. In addition, it offers optional state-of-the-art features such as automated ESCA depth-composition profiling, automatic quantitative analysis and angular resolution that make it unique in the field of ESCA instrumentation.

The outstanding ESCA performance of the Model 550 is supplemented by other important features. A scanning Auger microscopy capability adds rapid, high sensitivity, small area analysis. Ultrahigh vacuum ensures a reliable analysis. And a wide range of accessories dramatically increases the flexibility of the instrument. Presently-available accessories include a SIMS attachment, sample introduction system/reaction chamber, differential ion gun, interactive graphics terminal, and an ultraviolet light source.

Although a relative newcomer to the ESCA field, PHI has also developed the only comprehensive ESCA handbook designed with the ESCA user in mind. The result of years of experience by recognized experts in the field, the Handbook of X-Ray Photoelectron Spectroscopy contains a wealth of information including survey spectra for most elements, high resolution spectra for major peaks, charts relating binding energy to chemical matrix for most elements, and much more.

For further information on the most advanced instruments available, from the leader in electron spectroscopy instrumentation, write: Physical Electronics Industries, 6509 Flying Cloud Drive, Eden Prairie, MN, U.S.A., 55344, or call (612) 941-5540.

PERKIN-ELMER
Physical Electronics

CIRCLE 174 ON READER SERVICE CARD

10:20—135. The Use of the Faraday Constant as an International Standard and the Complexometric Coulometric Titration of Aluminum. **T. Yoshimori, T. Tanaka.**
10:40—Intermission.
11:00—136. Semi-integration in Electrochemistry. **K. B. Oldham.**
11:40—137. Semidifferential Electroanalysis and Its Application. **M. Goto, M. Kato, K. Ikenoya, D. Ishii.**

SECTION C

Hilton Hawaiian Village (Ocean Tower), Empire II (2nd Floor)

General: Liquid Chromatography

D. Ishii, W. E. May, Presiding

8:30—138. Development of a Trace Organics in Shale Oil Standard Reference Material: Analytical Methodology. **W. E. May, S. A. Wise, S. N. Chesler, L. R. Hilpert, J. M. Brown, F. R. Guenther, R. M. Parris, H. S. Hertz.**
8:50—139. Organic Conceptional Diagram as a Compass of Gas Liquid Chromatographic Analysis. **M. Omura, S. Sato, Y. Koda.**
9:10—140. Simultaneous Determination of Vitamins B_1, B_2, B_6 and Niacinamide in Multivitamin Preparations by Paired Ion Reversed Phase High Pressure Liquid Chromatography. **R. P. Kwok, R. Tabor, T. S. Pattison, F. C. Shaklee.**
9:30—141. HPLC of Carbohydrates Using Post-Labelling Method. **Y. Ishida, K. Okamoto, T. Kato, T. Kinoshita.**
9:50—142. HPLC Determination of Apomorphine and its O-Methyl Metabolites. **R. V. Smith, J. C. Glade, D. W. Humphrey.**
10:10—Intermission.
10:20—143. Determination of Benzalkonium Chloride by Reverse-Phase High Pressure Liquid Chromatography. **R. C. Meyer.**
10:40—144. Separation of Urushiol Diacetate Homologues by High Performance Liquid Chromatography. **Y. Yamauchi, R. Oshima, H. Mitsui, J. Kumanotani.**
11:00—145. Application of 4-Bromomethyl-7-Methoxy-2H-Benzo(b)Pyran-2-One to the Determination of Carboxylic Acids by HPLC with Fluorescent Detection. **G. L. Carlson, D. T. E. Belobaba.**
11:20—146. The Separation of Salicylic Acid and the Related Substances in Polymer Solution by HLC. **T. Saotome, Y. Ogasawara.**
11:40—147. Study of Acrylamide Gel Chromatography (VII). Spherical Gels of Polyacrylamide Polymerized with Acrylonitrile. **K. Suzuki, K. Nakazato, T. Takasaki.**

WEDNESDAY AFTERNOON

SECTION A

Hilton Hawaiian Village (Ocean Tower), Gold Room (2nd Floor)

ACS Award in Analytical Chemistry Symposium

K. Yasuda, A. T. Zander, Presiding

2:00—148. Multielement Analysis by Atomic Fluorescence Spectrometry—A Status Report. **J. D. Winefordner.**
2:30—149. Basic Excitation Processes and Spectrochemical Applications in Stable Spark Discharge Trains. **J. P. Walters, D. Ekimoff, R. J. Klueppel, T. Araki.**
2:50—150. Evaluation of Measurement Systems in Inductively Coupled Plasma Emission Spectrometry—Multichannel or Single Channel Detection. **H. Haraguchi, K. Fuwa.**
3:10—Intermission.
3:20—151. Multielement Analysis with an Atmospheric Pressure Nitrogen Afterglow Plasma. **A. P. D'Silva, V. A. Fassel.**
3:40—152. A Modular Analytical Data Management and Acquisition Network for an Inductively Coupled Argon Plasma Based Laboratory. **A. F. Ward.**
4:00—153. Evaluation of a Fiber-Optic Vidicon Spectrometer for Multielement Analyses. **K. W. Busch, B. Malloy.**
4:20—154. Direct Analysis of Alloys with ICAP Excitation of Spark Generated Alloys. **C. C. Wohlers.**
4:40—155. Applications of Atmospheric Pressure DC Argon Plasma and Microwave Helium Plasma Emission Spectroscopic Detectors in Chromatography. **R. M. Barnes, C. A. Poirier, B. D. Quimby, P. C. Uden.**
5:00—156. Multielement Detection of Trace Impurities in Silicon by Metastable Transfer Emission Spectrometry. **D. G. Sutton, L. Galvan, N. Cohen.**

SECTION B

Hilton Hawaiian Village (Ocean Tower), Beach Club I (2nd Floor)

Electrochemistry and Spectroscopy in Melts Symposium

G. Mamantov, S. Yoshizawa, Presiding

2:00—Introductory Remarks.
2:05—157. Oxide Ion Activity Measurements in Molten LiCl-KCl. **H. A. Laitinen, I. Hodara.**
2:25—158. Electrochemical Studies on Semiconductive Oxide Electrodes in Molten Salts. **I. Uchida, H. Urushibata, S. Toshima.**
2:50—159. Recent Electrochemical Studies of Lithium/Metal Sulfide Batteries. **D. R. Vissers, D. L. Barney, R. K. Steunenberg.**
3:15—160. Spectroscopical Study of Chemical Species Formed in the Fused Alkali Metal Halides—Iron Oxide System. **H. Kojima, Y. Kaneko.**
3:35—Intermission.
3:45—161. Study of Mass Transfer in a Molten Salt System, by the Use of Laser Interferometry. **Y. Ito, T. Murata, S. Yoshizawa.**
4:05—162. Electro-oxidation of Sulfur in Molten Chloroaluminates: Applications to a Rechargeable Molten Salt Battery. **G. Mamantov, R. Marassi, M. Matsunaga, K. Tanemoto, Y. Ogata, E. J. Frazer, J. P. Wiaux, V. E. Norvell, L. Klatt.**
4:30—163. Oxidation of Aromatic Hydrocarbons in a Room Temperature Molten Salt. **J. Robinson, R. J. Gale, R. A. Osteryoung.**
4:55—164. Reaction of NO with Molten Nitrates and Hydroxides. **S. Asakura, S. Yamano.**

SECTION C

Hilton Hawaiian Village (Ocean Tower), Empire II (2nd Floor)

General: Liquid Chromatography

Y. Nishikawa, P. J. Taylor, Presiding

2:00—165. Liquid Crystal Stationary Phases for HPLC. **P. J. Taylor, P. L. Sherman.**
2:20—166. Application of Packings for Aqueous High-Performance Gel Permeation Chromatography to Ion Exchange Chromatography. (II) Cation Exchange Chromatography. **M. Umino, H. Watanabe, M. Aiura.**
2:40—167. Selecting the Optimum Mobile Phase for HPLC with Fluorescence Detection. **P. Froehlich.**
3:00—168. Preparation of Monoglycerides by Direct Esterification and Determination of Reaction Products by Thin-Layer Chromatography. **K. Maruyana, C. Yonese.**
3:20—Intermission.
3:30—169. A New Rugged, Reliable, Simple Eluent Delivery System for Liquid Chromatography. **B. A. Bidlingmeyer.**
3:50—170. Study of Acrylamide Gel Chromatography (VIII). N-Hydroxymethylacrylamide Gel Crosslinked with Heat-Treatment. **K. Suzuki, K. Nakazato, Y. Watanabe, Y. Matumoto.**
4:10—171. A Beta Ray-Induced Luminescence Detector (BILD) for Liquid Chromatography. **E. A. Walters, W. H. Rahe.**

(Continued on page 357 A)

HEWLETT hp PACKARD

Tomorrow's Analytical Instruments Today

"The Future Is Now"

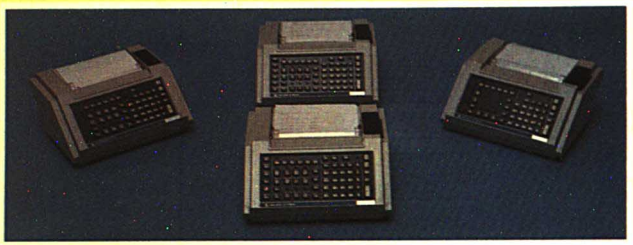
coming soon to
149 cities around the world–
"Journey into the Future"
exhibits and seminars



NEW HP 5880A GAS

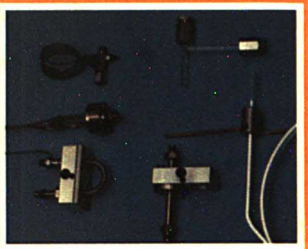
. . . tomorrow's gas ch

the most versatile and expandable gas ch



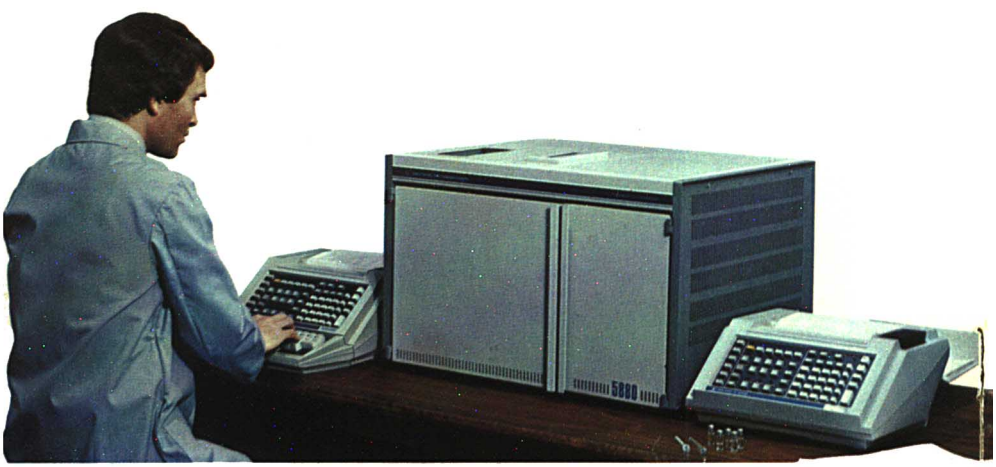
Unequalled EXPANDABILITY through four levels of friendly, functional keyboards for your needs . . . today and tomorrow

You can start with LEVEL 1, a simple, single-detector isothermal instrument with high-speed printer/plotter (35 characters per second) and retention time labeling. From there, you can upgrade through each level to a multi-detector, temperature programmed instrument with data handling and programming capabilities. Each level has numerous hardware and software options and can be upgraded to the next level without redundancy. An optional alpha/numeric keyboard provides report annotation, plus BASIC programming. A powerful HP cartridge tape unit allows off-line storage of information.



Accepts a wide range of optional accessories for extraordinary VERSATILITY

A wide range of all-glass accessories, cold trap and auxiliary oven, open up new application possibilities. In addition, six heated zones provide ample reserves for heated accessories such as transfer lines for sample collection, and catalyst tube for methanation of CO and CO_2 to improve minimum detectable limits.

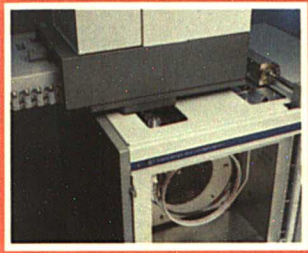




S CHROMATOGRAPH

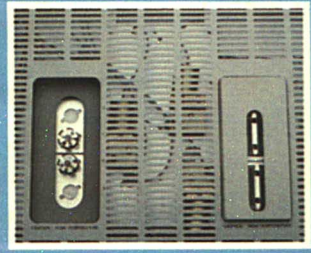
chromatograph today

hromatography system in the world today



Advanced AUTOMATION for easy operation

- The HP automatic sampler with cleverly designed injection-port-to-injection-port transport mechanism is keyboard controlled for automatic selection of all operating parameters.
- All GC functions are controllable through BASIC. New concepts in automation become feasible, including self-optimization of operating conditions.



Unmatched FLEXIBILITY with universal hardware mounting

This system permits simultaneous installation of glass capillary and conventional injection ports. Up to four single or two dual detectors can be accommodated. Choose from a wide range of detectors including new single-filament, inert TC Detector and FI Detector with auto-ignition. Up to four valves may be used in heated auxiliary zones between injection ports and detectors.



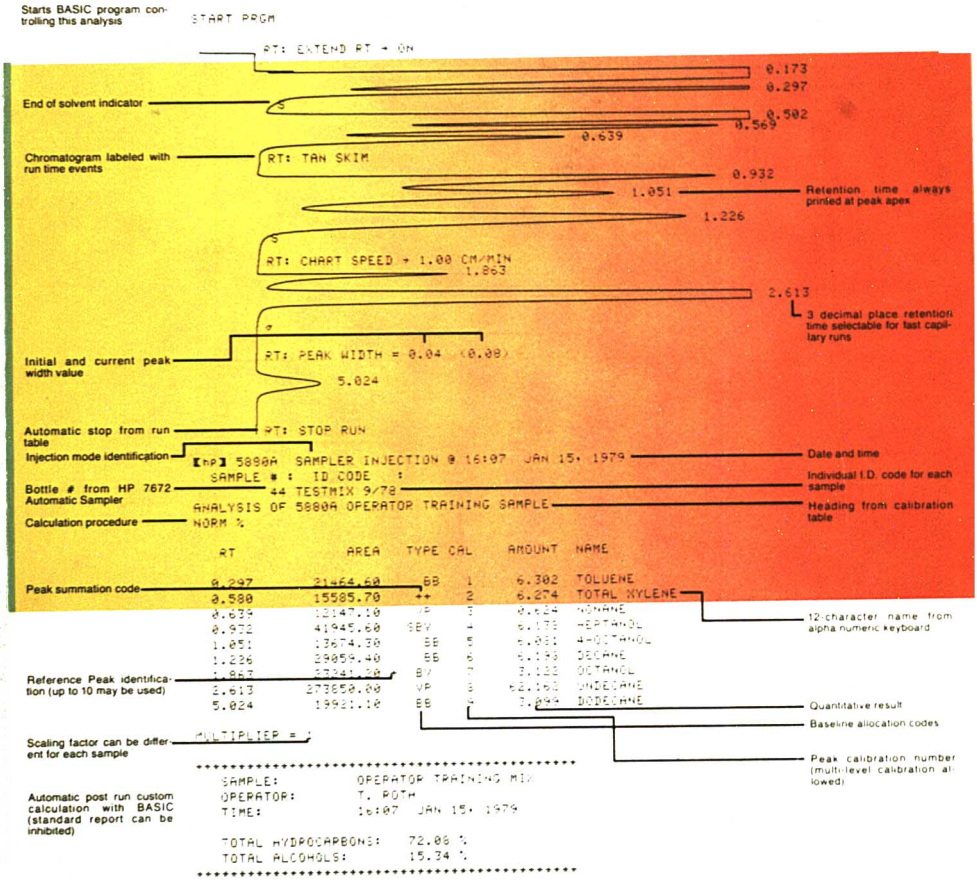
Brand new INTERFACING capabilities

- External connectors provide direct interfacing with HP 3350 Lab Automation Systems.
- The instrument's advanced design allows an additional conventional GC to use simultaneously all the data processing power of the HP 5880A, including BASIC.

the first and only microprocessor, keyboard-operated GC system with all these features . . .

- Multiple-channel capability with two printer/plotters
- Total instrument and sampler control through BASIC
- Two-channel, post run integrator and previously unavailable calibration procedures
- Large four column oven

only the new HP 5880A Gas Chromatograph gives you a chromatogram with so much information . . .



Here is an exciting new gas chromatography system, yet priced lower than other systems attempting to duplicate its capabilities.

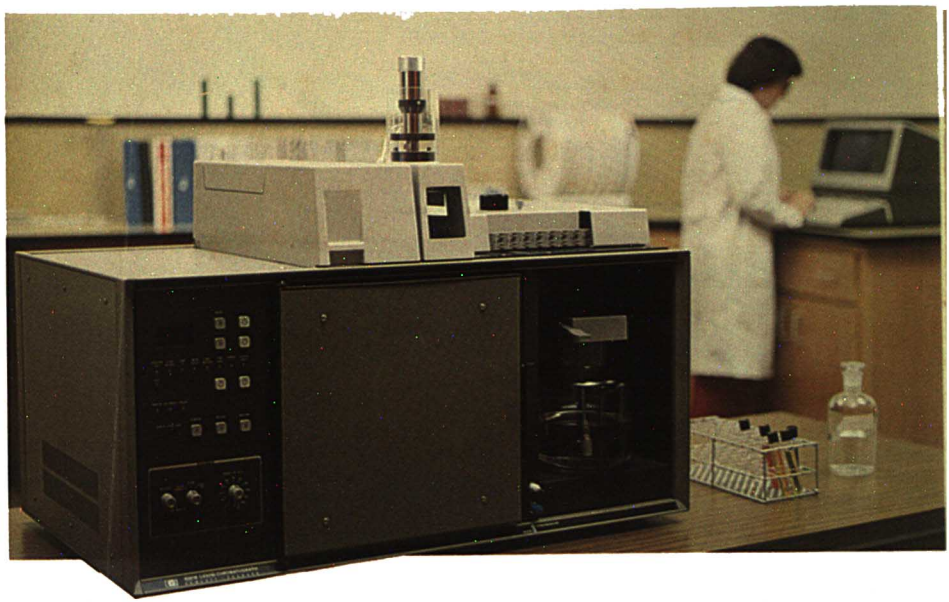
HEWLETT hp PACKARD



THE NEW HP 1081B LIQUID CHROMATOGRAPH

tomorrow's HPLC today

total 2-way communication for remote automated analyses



The HP 1081B has several modes of operation. It can be operated as a free-standing instrument, as a data source for an integrator or data acquisition system, or as an analyzing extension of a laboratory automation system.

Microprocessor control provides simplicity of operation in this isocratic liquid chromatograph. Only six keys are needed to adjust and inspect all of the processor-controlled functions, including operation of the optional 60 bottle sampling system.

The flow system uses a single head diaphragm pump with closed loop processor control. Actual and set flow rates, as well as all other processor-controlled functions, can be monitored on a three-digit numeric display.

Analytical procedures developed on the more sophisticated HP 1084B can be transferred to the HP 1081B and run with comparable precision. Features include:

- Optional variable volume sampler injects from 10 to 200 microliters at full column pressure and flow from up to 60 sample vials. No sample is wasted in flushing.
- Optional heated oven operates from ambient +5°C to 99°C.
- A highly sensitive fixed wavelength (254 nm) UV detector is available. Other detector types can be mounted.
- Up to ten 1081B's can be controlled by a single RS 232C interface.

HEWLETT hp PACKARD

LABORATORY AUTOMATION SYSTEMS

tomorrow's lab automation today

the system that expands to meet your growing need



HEWLETT-PACKARD offers a complete range of Lab Automation Systems and Reporting Integrators for today's laboratory—and tomorrow's.

Series 3350 Lab Automation Systems give you the friendly, flexible, trouble-free operation that you've come to expect from HP. Consider these other advantages:

- Long-term data and record storage
- Reintegration of peaks—eliminates costly, time-consuming reanalyses
- Compatibility with GPC and nonchromatographic equipment—such as AA, DSC and Autoanalyzers
- Expandability—adds capability, instruments and peripherals

For the smaller chromatographic lab, HP Reporting Integrators offer the right level of automation—printer/plotter or total instrument controller—at an attractive price.

Today and tomorrow, HP has the answer in lab automation.

HEWLETT hp PACKARD

Hewlett-Packard takes you on a

"Journey into the Future"

COMPUTER CONTROLLED GC/MS SYSTEMS

tomorrow's GC/MS systems today

new negative ion/CI feature greatly expands lab capability



New negative ion/chemical ionization feature now offered with the HP 5985B, pictured above, extends the sensitivity limits of this powerful system to low picogram range for appropriate compounds. This new option is especially applicable for biomedical compounds with fluorinated derivatives. HP GC/MS systems include:

HP 5992B Benchtop GC/MS with Automatic Tuning

This compact unit offers excellent performance at a budget price. Has friendly HP 9825A desktop computer for ease of use. Tunes itself automatically. Mass range to 800 amu. Software includes SIM and much more.

HP 5993B Desktop GC/MS with Disc-based Data System

A new middle-price combination . . . compact GC/MS of the HP 5992B and a powerful data system. Versatile software includes BATCH processing and much more. Mass range to 800 amu.

HP 5985B with Powerful Built-in Data System, Dual Source

This extraordinary system is one of the most powerful analytical tools for qualitative and quantitative measurements. Its dual source optimizes CI/EI results. Fully digital. Tunes itself to save time. Powerful software and libraries. Flexible GC/MS interface accommodates five different detectors. Hyperbolic quadrupole. Mass range to 1000 amu.

43722

For more information, call your local HP sales office or East (301) 948-6370 • Midwest (312) 255-9800 • South (404) 955-1500 • West (213) 877-1282. Or write, Hewlett-Packard, 1501 Page Mill Rd. Palo Alto, California 94304. **In Europe**, Hewlett-Packard S.A. 7, rue du Bois-du-lan, P.O. Box, CH-1217 Meyrin 2 Geneva, Switzerland. **In Japan**, Yokogawa-Hewlett-Packard Ltd., 29-21, Takaido-Higashi 3-chrome, Suginami-ku, Tokyo 168.

4:30—172. Liquid Chromatography of the Trace Amounts of Aldehydes by Thermal Reaction Tube. **Y. Suzuki, M. Maruyama.**
4:50—173. A New UV-Visible Multiwavelength Absorption Detector Applied to the Gel Chromatography of Metal-β-Diketonato Complexes. **K. Saitoh, N. Suzuki.**

SECTION D

Hilton Hawaiian Village (Ocean Tower), Empire I (2nd Floor)

General: Electroanalytical Chemistry

G. G. Guilbault, M. Goto, Presiding

2:00—174. Electrochemical Analysis of Enzyme Reactions. **G. G. Guilbault**
2:30—175. Determination of the Composition of Metal Complex Ions by Potential Sweep Voltammetry. **K. Ogura, Y. Fukusima, I. Aomizu.**
2:50—176. Voltammetric Immunoassay. **W. R. Heineman, H. B. Halsall, C. W. Anderson.**
3:10—177. Cathodic Stripping Voltammetric Determination of Sulfide and Organic Sulfur Compounds. **T. M. Florence.**
3:30—Intermission.
3:40—178. Characterization of Voltammetric Electrode Processes by Computerized Pattern Recognition. **S. P. Perone, D. R. Burgard, L. Kryger, R. A. DePalma, Q. V. Thomas, L. B. Sybrandt.**
4:10—179. Measurement of Chromium Speciation in Seawater by Electrodeposition on Graphite Tubes for Furnace Atomization. **G. E. Batley, J. P. Matousek.**
4:30—180. Voltammetric and Polarographic Studies on New Types of Neurotropic and Hypnotic Drugs. **J. M. Kauffman, G. J. Patriarche, J. C. Viré.**
4:50—181. On-Line High Precision Measurement of Ion Selective Electrodes. **Y. Umezawa, K. Sawatari, I. Uemasu, M. Nagata, Y. Imanishi, S. Fujiwara.**

THURSDAY MORNING

SECTION A

Hilton Hawaiian Village (Ocean Tower), Gold Room (2nd Floor)

ACS Award in Analytical Chemistry Symposium

A. T. Zander, H. Kawaguchi, Presiding

9:00—182. The Preparation of Absolute Mass Calibrated Particulate Filters for Multielement Quantitative Analyses by ICP-AES and XRF Spectroscopy. **E. L. DeKalb, K. W. Olson, V. A. Fassel.**
9:20—183. Excitation and Fragmentation in Reduced Pressure Electrical Discharges in Helium. **T. H. Risby.**
9:40—184. Application of Time Multiplex Multiple Slit Spectrometers and Diode Array Detectors to Multielement Atomic Measurements. **J. D. Ingle, Jr., M. A. Ryan, J. King.**
10:00—185. Sample Introduction for Multielement Analysis with the Inductively Coupled Plasma. **R. F. Browner, A. W. Boorn, J. W. Novak, J. H. Dillard.**
10:20—Intermission.
10:30—186. Multielement Analysis by Coherent Forward Scattering Atomic Spectroscopy. **M. Yamamoto, M. Ito, S. Murayama, K. Yasuda.**
11:00—187. Emission Profiles in the Inductively Coupled Plasma. **S. R. Koirtyohann, J. S. Jones, D. A. Yates.**
11:20—188. Aerosols, Aerodynamics, Atomic Analysis, and Associated Artifacts. **R. K. Skogerboe.**
11:40—189. Simultaneous Determination of Major, Minor, and Trace Elements in Powdered Materials by Direct-Reading Emission Spectrometry. **J. L. Seeley.**

SECTION B

Hilton Hawaiian Village (Ocean Tower), Beach Club I (2nd Floor)

Inorganic Separations in Analytical Chemistry Symposium

Y. Yamamoto, H. Freiser, Presiding

9:00—190. Effect of Hydration of Extractable Species on the Separation by Solvent Extraction. **T. Sekine.**
9:30—191. Factors Influencing the Selectivity in the Synergistic Extraction of Some Transition Metals. **H. Akaiwa.**
10:00—192. Enhancing Nuclear Analyses via Substoichiometric Separations. **J. Mitchell.**
10:30—193. Separation and Visual Photometric Determination of Alkali Metals Using Macrocyclic Polyethers. **M. Takagi, H. Nakamura, K. Ueno.**
11:00—194. Simultaneous Determination of Mercury and Cadmium in Biological Materials by Radiochemical Neutron Activation Analysis. **R. Greenberg.**
11:30—195. Separation of Trace Elements by Coprecipitation and Flotation. **A. Mizuike, M. Hiraide.**

SECTION C

Hilton Hawaiian Village (Ocean Tower), Empire II (2nd Floor)

General: Liquid Chromatography

Y. Suzuki, W. S. Hancock, Presiding

9:00—196. Electrocatalytic Detection of Cobalt in Liquid Chromatography. **Y. Takata, F. Mizuniwa, C. Maekoya.**
9:20—197. Correct Preparation of Ionic Mobile Phases for Microparticle Reversed Phase LC Columns. **F. M. Rabel, D. J. Popovich.**
9:40—198. Spectrophotometric-Catalytic Determination of Cobalt and Vanadium by Stopped Flow Technique. **K. Hirayama, N. Unohara.**
10:00—199. Separation and Determination of Trace Heavy Metals in Water by Solvent Extraction-High-Speed Liquid Chromatography. **M. Yamazaki, S. Ichinoki, R. Hamano.**
10:20—Intermission.
10:30—200. Flow Injection Analysis of Inorganic Polyphosphates. **Y. Hirai, N. Yoza, S. Ohashi.**
10:50—201. The Use of High Pressure Liquid Chromatography for the Analysis of Amino Acids, Peptides and Proteins. **W. S. Hancock, C. A. Bishop, H. T. W. Hearn.**
11:10—202. A Gel Chromatographic Study of the Interactions of Linear Polyphosphate Anions with Magnesium Ions. **T. Miyajima, T. Onaka, K. Kouchiyama, N. Yoza, S. Ohashi.**
11:30—203. High Pressure Liquid Chromatography of Lower Carboxylic Acids and Polyols. **Ting-Po I, A. R. Goulet, L. W. Blocker.**
11:50—204. New HPLC High-Speed Analytical System for Saccharides and Organic Acids. **I. Kaiho, S. Nakamura, T. Yamada, T. Hosogane.**

SECTION D

Hilton Hawaiian Village (Ocean Tower), Empire I (2nd Floor)

General: Electroanalytical Chemistry

Y. Masuda, J. L. Anderson, Presiding

9:00—205. Separation and Determination of Traces of Lead, Cadmium, Copper and Zinc from Pure Ferric Oxide Using Polarographic Techniques. **J. L. Vandenbalck, G. J. Patriarche.**
9:20—206. Chloride-Selective Electrodes Based on a Poly(Vinyl Chloride) Matrix Membrane and Their Application to Blood Serum Measurements. **H. Miyagi, H. Kawana, Y. Takata, W. Simon.**
9:40—207. Optimizing Reductive Electrochemical Detection in Liquid Chromatography. **W. A. MacCrehan, R. A. Durst.**
10:00—208. Micro Determinations of Drugs with Titanium(III), Chromium(II), Manganese(III), Ceri-

um(IV) and Silver(II) Electrogenerated. **G. J. Patriarche, M. Chateau-Gosselin, J. C. Viré, J. L. Vandenbalck.**

10:20—Intermission.

10:30—**209.** Automatic Determination of Glucose in Woody Polysaccharides with Enzyme Electrode. **T. Ishikawa, R. Tanaka, T. Sakaguchi.**

10:50—**210.** Four-Electrode Thin-Layer Flow-Through Cell for HPLC or Continuous-Flow Analysis. **S. G. Weber, W. C. Purdy.**

11:10—**211.** Application of Oscillographic Polarography(I) Lead(II)-Polyaminopolycarboxylato Complexes. **T. Matsuo, Y. Masuda, E. Sekido.**

11:30—**212.** Spectroelectrochemical Redox Investigations of Biocomponents Using a Circulating, Long Optical Path, Thin-Layer Electrochemistry Cell. **J. L. Anderson.**

11:50—**213.** Anodic Oxidation of o-Phenylenediamine at a Platinum Electrode in Acetonitrile Solutions. **H. Yamaguchi, I. Taniguchi, K. Yasukouchi.**

THURSDAY AFTERNOON

SECTION A

Hilton Hawaiian Village (Ocean Tower), Gold Room (2nd Floor)

ACS Award in Analytical Chemistry Symposium

K. Fuwa, P. N. Keliher, Presiding

2:00—**214.** Advances in Multielement Spectrometry with the Echelle Grating. **A. T. Zander, P. N. Keliher.**

2:20—**215.** Evaluation of Echelle Spectrometer with an Image Dissector for Simultaneous Multielement Determinations. **H. J. Pardue, H. L. Felkel.**

2:40—**216.** A High-Speed, Background-Corrected, Simultaneous, Multi-Element Atomic Absorption Spectrometer. **T. C. O'Haver, J. M. Harnly, W. R. Wolf.**

3:00—**217.** The Use of an Automatic, Multi-Element, DC Plasma, Echelle Grating Spectrometer in Industry. **H. Griffin.**

3:20—Intermission.

3:30—**218.** Application of a Programmable Monochromator with Repetitive Optical Scanner to Multielement ICP-Emission Spectrometry. **H. Kawaguchi, T. Ito, A. Mizuike.**

3:50—**219.** Design and Performance of a New, High-Efficiency Inductively Coupled Plasma Source. **R. N. Savage, G. M. Hieftje.**

4:20—**220.** New Sample Introduction Systems for Inductively Coupled Plasma Emission Spectroscopy. **G. Horlick.**

4:40—**221.** Simultaneous Multielement Trace Metal Analysis in Marine Sediments by DC Plasma Atomic Emission. **W. G. Cox, G. V. Cox, P. Wickramaratne.**

5:00—**222.** The Use of Specific Detectors for the Elimination of Interferences Using an ICAP. **A. F. Ward, L. F. Marciello.**

SECTION B

Hilton Hawaiian Village (Ocean Tower), Beach Club I (2nd Floor)

Inorganic Separations in Analytical Chemistry Symposium

H. Freiser, Y. Yamamoto, Presiding

2:00—**223.** Ion-Pair Extraction and Reversed-Phase Ion-Pair Partition Chromatography of 4-(2-Pyridylazo)-Resorcinolato Chelates and Its Derivatives. **T. Yotsuyanagi, H. Hoshino.**

2:30—**224.** Application of Bonded Chelating Groups to Trace Metal Extraction. **D. E. Leyden.**

3:00—**225.** Metal Ion Chelation Chromatography on Silica-Immobilized 8-Hydroxyquinoline. **J. R. Jezorek, H. Freiser.**

4:00—**226.** High-Resolution Gas and Liquid Chromatography of Inorganic Compounds. **P. C. Uden.**

4:30—**227.** Separation of Phosphorus Oxoacid Polymers by Liquid Column Chromatography. **S. Ohashi.**

SECTION C

Hilton Hawaiian Village (Ocean Tower), Empire II (2nd Floor)

General: Spectroscopy

S. Shibata, Presiding

2:00—**228.** Preconcentration of Trace Metals in Water Analysis for X-ray Fluorescence Spectroscopy—A Comparison Study. **D. E. Leyden, W. Wegscheider, W. B. Bodnar.**

2:20—**229.** Photoelectric Emission Spectral Analysis of Nickel-Base Superalloys with Fixed Time Integration Technique. **H. Okochi, K. Takahashi, S. Suzuki, E. Sudo.**

2:40—**230.** Analysis of Zhabotinski-Type Oscillatory Systems by Potentiometry, UV-VIS Spectroscopy, and X-ray Microanalysis Methods. **C. P. Keszthelyi, J. Soós, A. G. S. Jánossy, K. Kovacs.**

3:00—**231.** Determination of Gallium in Biological Tissue with Electron Microprobe Analyzer—Gallium Organic Compounds in Epoxy Resin as Standards for Microprobe Analysis. **K. Nakamura, M. Nakauchi, H. Orii.**

3:20—Intermission.

3:30—**232.** Successive Determination of Silicon and Nitrogen in Silicon Nitride Films. **M. Hayashi, E. Kitazume.**

3:50—**233.** Direct Quantitative X-ray Powder Diffractometry: Absorption Theory and Calculated Data. **S. Altree-Williams.**

4:10—**234.** Chemical Bonds and $K\beta_2/K\beta_1$, X-ray Intensity Ratios of Arsenic, Selenium, and Bromine. **T. Fukasawa, M. Iwatsuki.**

4:30—**235.** Estimation of Spectral Distribution of X-ray Tube for Quantitative X-ray Fluorescence Analysis. **M. Murata, H. Shibahara.**

SECTION D

Hilton Hawaiian Village (Ocean Tower), Empire I (2nd Floor)

General: Electroanalytical Chemistry

F. A. Schultz, T. Fujisawa, Presiding

2:00—**236.** Complementary Parameter Estimation: A Cyclic Voltammetric/Spectro-electrochemical Study of Porphyrin Reduction. **D. L. Langhus, G. S. Wilson.**

2:20—**237.** Determination of Tungstate in Interface layer of Oxide-Cathode. **Y. Hiratsuka, Y. Komiyama.**

2:40—**238.** Electroactive Polymer Films on Electrodes Deposited from Radiofrequency Plasma. **R. J. Nowak, F. A. Schultz, M. Umaña, R. Lam, R. W. Murray.**

3:00—**239.** Electrochemical Behavior of Glassy Carbons. **T. Fujisawa, T. Ogata, K. Oikawa, N. Tanaka.**

3:20—**240.** Polarographic Studies of Dilute Tungstate Solutions in HCl. **V. Thielmann.**

3:40—Intermission.

3:50—**241.** Behavior of an Ion-Selective Electrode for an Interferent in Flow Systems. **A. Jyo, N. Ishibashi.**

4:10—**242.** Hydrodynamic Modulation at a Vibrating Electrode. **K. W. Pratt, Jr., D. C. Johnson.**

4:30—**243.** Determination of Nitrogen Oxides and Sulfur Dioxide Absorbed into Iron(II) EDTA Solution by Voltammetry. **O. Hamamoto, K. Nozaki, and H. Kaneko.**

4:50—**244.** Biamperometric Determination of Glycerol and Triglycerides Using Open Tubular Carbon Electrodes in a Flow Stream. **A. S. Attiyat, G. D. Christian.**

FRIDAY MORNING

SECTION A

Hilton Hawaiian Village (Ocean Tower), Gold Room (2nd Floor)

General: Spectroscopy

S. Tanaka, J. E. Ingle, Jr., Presiding

Turner expands its spectrophotometer line!

For years, Turner spectrophotometers have been in a price/performance class by themselves. They still are. Now there's an expanded line of these sensibly-priced instruments from which to choose, including the Model 380 with digital display. Turner also offers a full range of accessories to enhance the convenience and utility of your spectrophotometer—everything from a concentration computer to far UV attachments. It's all part of a growing capability that satisfies a wide range of spectrophotometer requirements.

Compare our spectrophotometers to anyone else's and you'll agree that it's time to turn to Turner. All Turner spectrophotometers offer **resolution** of 9 nm, **stray light** less than 0.5%, **wavelength setting accuracy** of ±2 nm over the entire range, and a standard wavelength **range** of 320-710 nm.

For a convincing demonstration, contact your distributor or Turner Associates, 2524 Pulgas Avenue, Palo Alto, CA 94303. Telephone (415) 324-0077.

FREE catalog



Turn to

TURNER

. . . today

Model 380 with digital display, direct readout of concentration and linear absorbance. Price $1725.

Model 350 with large 7" meter. Price $940.

Model 330 with 4" meter. Price $780.



The spectrophotometer line that's kind to your bottom line



CIRCLE 207 ON READER SERVICE CARD

Other than headache, what are the symptoms of overexposure to mercury vapor?



There's a better alternative than learning the answer by first-hand experience

If you work with mercury, chances are you know the answer. Chances are you have a full work safety program. But does everyone in the program know that fatigue, irritability and inflammation of the gums are some of the other symptoms of chronic poisoning? Would everyone know if they were overexposed?

An integrated plan of information and detection is obviously a better alternative than first-hand experience of symptoms. And 3M has an inexpensive plan applicable to every size laboratory whether it involves one person, 50 or more.

Free Book



Working Safely With Mercury is the informational phase of the plan. It's a free 20-page booklet written by 3M as an objective overview for those who work with mercury and those responsible for health and safety.

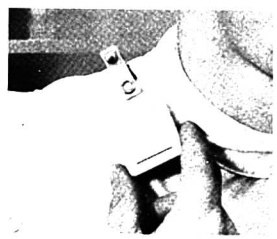
It's a concise presentation of the history, potential problems, methods of detection and protection, as well as current government recommendations for safe handling — even of small quantities.

The First Maintenance-free Mercury Vapor Monitor

Monitoring is a sure way to detect whether or not a person has been exposed to more than the government Threshold Limit Value (0.05 mg/m^3 in an 8 hour period).

The 3M Brand Mercury Vapor Monitor 3600 is the easy system. Nothing to assemble. No pumps. No maintenance. The lightweight badge-size monitor is simply clipped to the collar. Provides a precise measurement of personal exposure.

In comparison to a pump system, the 3600 is inexpensive enough so that monitors can be worn by everyone in the area of the mercury.



For analysis, you simply send the monitors to 3M. You'll receive a confidential report of Time Weighted Average concentrations for each monitor.

For your free copy of *Working Safely With Mercury* and detailed information about the maintenance-free 3600 monitor, write Occupational Health and Safety Products Div., 3M Company, P.O. Box 8327, Dept. FF1, St. Paul, MN 55113. In Canada contact 3M Canada Ltd., P.O. Box 5757, Terminal "A", London, Ontario, Canada N6A4T1 (519) 451-2500.

Additional copies of *Working Safely With Mercury* are available upon written request.

ANOTHER STEP TOWARDS BETTER OCCUPATIONAL HEALTH AND SAFETY

3M

CIRCLE 136 ON READER SERVICE CARD

9:00—245. Determination of Antigen and Antibody by Near Infrared Turbidimetry. **M. Sawai, T. Sudo, H. Okumura, S. Enomoto, S. Morita, S. Matsumoto.**

9:20—246. Instrumentation for Luminescence Kinetics-Based Measurements. **J. E. Ingle, Jr., M. A. Ryan, D. Marino.**

9:40—247. Difference Spectrofluorometry by Synchronous Excitation Method. **K. Ohkubo, M. Takada, R. Hira.**

10:00—248. The Fluorescence Properties of Metal Complexes of Aromatic Schiff Base and Their Use in Fluorometric Method. **K. Morishige, K. Hiraki, Y. Nishikawa.**

10:20—Intermission.

10:30—249. An Improved Fluorometric Method of Chlorophylls A, B and C. **Y. Onoue, K. Morishige, K. Hiraki, Y. Nishikawa.**

10:50—250. Determination of Trace Vanadium in Petroleum Products by Oxygen Flask Combustion-Catalytic Method. **T. Fukasawa, T. Yamane.**

11:10—251. Measurement of Hydrogen Distribution in Steel Sample by Tritium Autoradiography. **I. Taguchi.**

SECTION B

Hilton Hawaiian Village (Ocean Tower), Beach Club I (2nd Floor)

General: Liquid Chromatography

T. Shigematsu, J. W. Tolan, Presiding

9:00—252. Automated Measurement of Catecholamines in Urine, Plasma and Tissue Homogenates by High-Speed Liquid Chromatography with Fluorometric Reaction Detection. **K. Mori.**

9:15—253. Determination of the Avermectins in Plasma Using HPLC with Fluorescence Detection. **J. W. Tolan, P. Eskola, D. W. Fink, H. H. Mrozik, L. A. Zimmerman.**

9:30—254. HPLC of Peptides: Determination of Bovine Insulin. **A. Dinner, L. Lorenz.**

9:45—255. Direct-Coupling of FT-NMR to High Performance Liquid Chromatography. **E. Niki, N. Watanabe, H. Wakabayashi.**

10:00—256. Open-Tubular Microcapillary Liquid Chromatography Using Solid Adsorbents. **D. Ishii, T. Tsuda, T. Takeuchi, T. Nakanishi, K. Hibi.**

10:15—Intermission.

10:25—257. Colorimetric Determination of *N*-Substituted and *N*-Unsubstituted Nitroimidazoles. **D. W. Fink, A. Fox, J. W. Tolan.**

10:40—258. Thin-Layer Chromatography of Anions on DEAE-Cellulose in Hydrochloric Acid Media. **R. Kuroda, K. Oguma.**

10:55—259. Thin-Layer Chromatography of Carbohydrates on Silica Gel Sintered Plate. **H. Hirayama, K. Hiraki, Y. Nishikawa, T. Shigematsu.**

11:10—260. Application for Analytical Chemistry of Aluminum Anodic Oxide Films (I) Thin Layer Chromatography. **M. Yamada, I. Mita.**

SECTION C

Hilton Hawaiian Village (Ocean Tower), Empire II (2nd Floor)

General

M. Fujihira, G. W. C. Hung, Presiding

9:00—261. Studies of the Thermal Decomposition of Sephadex-Dextran Gels. **G. W. C. Hung.**

9:15—262. On Radiation Damage of Ion-Exchange Resin—Improvement of Measurement of Anion Exchange Capacity and Studies by Diffuse Reflectance Spectra. **T. Matsuura, H. Kurihara, T. Hashimoto, Y. Yamamoto.**

9:30—263. Application of Ion Chromatography to the Analyses of Anions in Radioactive Sludge Wastes and Silicate Glasses. **S. J. Johnson, M. J. Kupfer.**

9:45—264. Catalytic Determination of Ultratrace Amounts of Iron. **T. Kawashima, T. Onishi, M. Kamada, S. Nakano.**

10:00—265. Investigation of the Standardization of Chromium(III) Solution by the Prior Oxidation with Lead Dioxide Suspension. **T. Nagai, T. Matsuda, Y. Kouji.**

10:15—Intermission.

10:25—266. Molecular Weight Distributions of Some Metal Compounds in Anemia Blood. **M. Ishii, M. Tanikawa, T. Hobo, S. Suzuki.**

10:40—267. The Problems Concerning the Barium Borotartrate Method for the Gravimetric Determination of Boron. **K. Sugawara, K. Tanino.**

10:55—268. State Analysis of Nitrides and Oxides in Metals by a Vacuum Fusion-Kinetic Energy Ion Mass Analyzer. **M. Kanai, T. Kikuchi, K. Furuya, M. Tsuchiya.**

FUEL CHEMISTRY

WEDNESDAY MORNING

Miramar Hawaii, Kuhio Suite (5th Floor)

Symposium on Trace Elements and Hazardous Compounds in Fossil Fuels *Joint with Analytical Chemistry*

H. Schultz, Presiding

61 62 63

REAGENT-GRADE SOLVENTS

Users of Corco chromatographic, electronic and spectrophometric reagent-grade solvents know they can count on Corco for highest quality. Reliability. And delivery. In pints, gallons, five-gallons, or drums.

At Corco, we've been specialists in reagent-grade solvents since 1953—and have built our reputation on meeting the requirements and specifications of our customers, ACS and ASTM.

Corco can also provide reagent-grade acids, bases, and specialty chemicals.

Write or call regarding your specific solvent requirements and our complete solvent listing in Bulletin 10. Or circle the number.

CORCO

CORCO CHEMICAL CORPORATION

Manufacturers of

Reagent & Electronic Chemicals

Tyburn Road & Cedar Lane • Fairless Hills, Pa. 19030

(215) 295-5006

CIRCLE 33 ON READER SERVICE CARD

9:00—48. Intrabed Variation in and Geologic Controls on Element Concentrations in the Upper Freeport Coal. **C. B. Cecil, R. W. Stanton, S. D. Allshouse, R. B. Finkelman.**
9:25—49. Modes of Occurrence of Selected Trace Elements in the Upper Freeport Coal. **R. B. Finkelman, R. W. Stanton, C. B. Cecil, J. A. Minkin.**
9:50—50. Distribution of Trace Elements in Coal Macerals and Minerals: Determination by Electron Microprobe. **J. A. Minkin, E. C. T. Chao, C. L. Thompson.**
10:15—Intermission.
10:45—51. Rapid, Easy Multielement Analysis of Whole Coal via Slurry-Injection Atomic Absorption Spectrometry. **J. E. O'Reilly, D. G. Hicks.**
11:10—52. Precision on the Determination of Trace Elements in Coal. **M. Ihida, T. Ishii, R. Ohnishi.**
11:35—53. Trace Elements Variations in an Oil Shale Retorting Operation. **T. R. Wildeman, R. N. Heistand.**

WEDNESDAY AFTERNOON

Miramar Hawaii, Kuhio Suite (5th Floor)

Symposium on Trace Elements and Hazardous Compounds in Fossil Fuels (II) *Joint with Analytical Chemistry*

M. Ihida, Presiding

2:00—59. Aromatic Nitrogen Compounds in Fossil Fuels—A Potential Hazard? **C.-h. Ho, B. R. Clark, M. R. Guerin, C. Y. Ma, T. K. Rao.**
2:25—60. Micro-Analysis of Polynuclear Aromatic Hydrocarbons in Petroleum. **H. Matsushita.**
2:50—61. Trace Element Distributions in Coal Gasification Products. **D. W. Koppenaal, H. Schultz, R. G. Lett, F. R. Brown, H. B. Booher, E. A. Hattman, S. E. Manahan.**
3:15—Intermission.
3:45—62. Trace and Minor Element Associations with the Organic and Mineral Matter Phases of Coal as Related to Pyrolysis. **J. K. Kuhn, R. A. Cahill, R. H. Shiley, D. R. Dickerson.**
4:10—63. Chemical and Mineralogical Characterization of Coal Liquefaction Residues. **G. B. Dreher, S. J. Russell, R. R. Ruch.**
4:35—64. Development and Applications of Non-Dispersive X-Ray Sulfur Analyzer with Mechanisms for Nonlinear Approximation and for all Other Matrix Effect Corrections. **A. Masuko, F. Imai, T. Yamano.**

NUCLEAR CHEMISTRY AND TECHNOLOGY

WEDNESDAY MORNING

Ilikai, Imperial Suite (2nd Floor)

Symposium on Recent Advances in Nuclear Analytical Methods, I *Joint with American Nuclear Society, Isotopes and Radiation Division and Analytical Chemistry*

R. H. Filby, Y. Murakami, Organizers, Presiding

9:00—Introductory Remarks.
9:10—83. Neutron Activation Analysis Using Comparators of Different Resonance Integrals. **M. Koyama.**
9:50—84. Neutron Activation Analysis of Bullet-Lead Specimens in the Assassination of President Kennedy. **V. P. Guinn.**
10:15—85. Fissile Analysis in Hanford Waste Using Cf Multiplier/Delayed Neutron Counter System. **K. R. Shah.**
10:30—Intermission.
10:45—86. Parametric Counting—A New Era of Fast and Accurate Neutron Activation Analysis. **P. F. Schmidt, J. E. Riley.**
11:15—87. An Optimization/Prediction Method for Instrumental Neutron Activation Analysis. **V. P. Guinn, C. C. Perkins.**
11:30—88. A Technique for In-Situ Moisture Level Determinations in Relatively Inaccessible Matrices. **R. L. Brodzinski.**
11:45—89. Development of High Flux Fast Neutron Activation Analysis. **P. K. Hopke, R. Williams, R. A. Meyer.**

WEDNESDAY AFTERNOON

Ilikai, Imperial Suite (2nd Floor)

Symposium on Recent Advances in Nuclear Analytical Methods, II *Joint with American Nuclear Society, Isotopes and Radiation Division and Analytical Chemistry*

P. K. Hopke, H. Yamatera, Presiding

2:00—105. Recent Advances in Analysis Using Nuclear Track Techniques. **B. S. Carpenter.**
2:40—106. Determination of Plutonium Isotopic Ratios by Ge(Li) ν-Ray Spectrometry. **H. Baba, T. Suzuki, Y. Nakahara, H. Yagi, S. Okazaki.**
3:00—107. A Technique for the In-Situ Determination of Transuranic Elements in Relatively Inaccessible Locations. **R. L. Brodzinski.**
3:20—108. Activation of Nitrogen, Carbon and Metals by Photonuclear Reaction and Its Application to the Composition of High Temperature Materials. **K. Kaneko, E. Sakuma, Y. Kumashiro.**
3:40—Intermission.
3:55—109. Neutron-Capture Prompt Gamma-Ray Activation Analysis: A Versatile, Non-Destructive Analytical Technique. **M. P. Failey, D. L. Anderson, W. H. Zoller, G. E. Gordon.**
4:15—110. Calcium Balance Studies in Pituitary Dwarfism Using a Stable Isotope Tracer and Neutron Activation Analysis. **J. E. Gilmer, M. A. Kay, D. E. Troutner, C. A. Anast.**
4:35—111. A Hyperpure Germanium Well Detector for Low Energy Gamma and X-Ray. **J. E. Gilmer, A. F. Sill.**

THURSDAY MORNING

Ilikai, Imperial Suite (2nd Floor)

Symposium on Recent Advances in Nuclear Analytical Methods, III *Joint with American Nuclear Society, Isotopes and Radiation Division and Analytical Chemistry*

B. S. Carpenter, T. Kambara, Presiding

9:00—127. Recent Advances in Secondary Ion Mass Spectrometry. **C. A. Evans, Jr.**
9:40—128. Application of Mass Spectroscopy to Environmental Samples-Distribution of Copper, Cadmium and Thallium in Oceans. **M. Murozumi.**
10:20—129. Processes Affecting Plutonium Desorption from Carburized and Metallic Rhenium. **J. M. Kelley, D. M. Robertson.**
10:40—**Intermission.**
10:55—130. Development and Application of an In-Situ X-Ray Fluorescence Spectrometer for Underwater Sediment Analysis. **N. A. Wogman, K. K. Nielson.**
11:15—131. Particle Induced X-ray Emission Applied to Large Scale Atmosphere Aerosol Investigations. **A. C. D. Leslie, J. W. Nelson, J. W. Winchester.**
11:35—132. Analysis of Fissile Materials in Heterogeneous Matrices. **J. E. Fager, F. P. Brauer.**

THURSDAY AFTERNOON

Ilikai, Imperial Suite (2nd Floor)

Symposium on Recent Advances in Nuclear Analtyical Methods, IV *Joint with American Nuclear Society, Isotopes and Radiation Division and Analytical Chemistry*

N. A. Wogman, I. Fujiwara, Presiding

2:00—147. Substoichiometric Isotope Dilution Analysis. **K. Kudo.**
2:40—148. Electrodeposition of the Actinide Elements onto a Tantalum-Tungsten Cathode from an Ammonium Chloride Electrolyte. **K. W. Puphal.**
2:55—149. Substoichiometric Extractions of Molybdenum. **T. Shigematsu, K. Kudo.**
3:10—150. Determination of Strontium-89 and -90 in Soil With Total Sample Decomposition. **D. B. Martin.**
3:25—151. Simultaneous Determination Method of Radon and Thoron by Toluene Extraction-Liquid Scintillation Counter. **K. Horiuchi, Y. Murakami.**
3:40—Intermission
3:55—152. Redox Substoichiometric Isotope Dilution Analysis of Antimony in Metallic Zinc—A Comparison of Various Oxidants for Redox Substoichiometry. **T. Kambara, J. Suzuki, H. Yoshioka, Y. Watanabe.**
4:10—153. Application of the New Brunswick Laboratory (NBL) Potentiometric Method for Determining Uranium to Organic Extracts. **L. Z. Bodnar.**
4:25—154. Radiochemical Determination of Polonium-210 in Ores and Environmental Samples. **R. P. Bernabee, C. W. Sill.**
4:40—155. A Rapid Extraction Method for the Separation and Determination of Plutonium and Americium. **R. P. Bernabee, D. R. Percival, F. D. Hindman.**

FRIDAY MORNING

Ilikai, Imperial Suite (2nd Floor)

Symposium on Recent Advances in Nuclear Analytical Methods, V

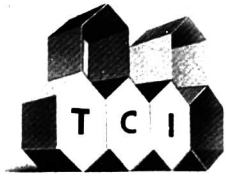
Joint with American Nuclear Society, Isotopes and Radiation Division and Analytical Chemistry

M. M. Williamson, M. Koyama, Presiding

9:00—171. Use of Muonic X-Rays for Chemical Analysis. **J. J. Reidy.**
9:45—172. Chemical Structure Effects on Sulfur Muonic Lyman Series X-Ray Patterns. **R. L. Hutson, J. D. Knight, J. J. Reidy, M. E. Schillaci, M. A. Yates-Williams.**
10:00—173. Negative Muon Capture in Alkali Halides and Alkaline Earth Sulfides. **M. E. Schillaci, J. D. Knight, C. J. Orth, R. A. Naumann.**
10:15—174. Isotopic Analysis of $^{239}PuO_2$ – $^{240}PuO_2$ Mixtures Using Muonic X-Rays. **R. L. Hutson, B. K. Barnes, D. A. Close, J. J. Ma-**

QUALITY! SELECTION! FAST DELIVERY!

All Yours From TCI—The Organic Reagent Specialist.



Organic Reagents
Fine Organic Chemicals
Rare Organic Chemicals
Custom Synthesis

Since 1922, TCI (Tokyo Kasei) has supplied leading chemical laboratories and industries worldwide with a broad selection of fine chemicals. Our current catalog includes over 10,000 different chemicals for every type of use. Virtually all orders are shipped within 12 hours of receipt. Five-gallon, 55-gallon and ton lots are available. Be sure of setting quality, selection and fast delivery. Buy TCI!

Write today for your free copy of the 750-page TCI Organic Chemicals Price List.

東京化成

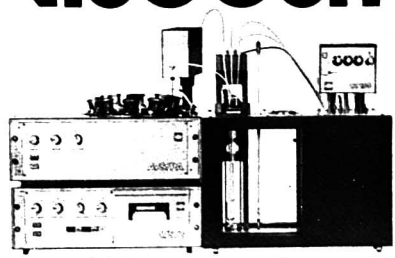
TCI **TOKYO KASEI KOGYO CO., LTD.**

(Tokyo Chemical Industry Co., Ltd.)

9-4, Nihonbashi-Honcho 3-chome, Chuo-ku, Tokyo, 103 Japan
Telex: 222-4719 ASACMN J Cable: ASACHEMCO TOKYO Tel: 241-0861

CIRCLE 206 ON READER SERVICE CARD

VISCOSITY



Automated Measuring Saves Lab Time.

If you measure viscosity with the capillary method, there's a SCHOTT AVS System for you. If you don't, maybe you should.
The fully automated AVS/PA will test up to 30 different samples without operator supervision. Select the program and let it go! Variable program capabilities include: number of rinses, number of repeat measurements, test temperature, sample temperature conditioning period, suction rates and more.
Standard-temperatures up to 150°C; High Temperature-up to 220°C. Measuring accuracy 0.1% with a range up to 30,000cSt.
Semi-Automated models also available. Building block concept allows expansion from basic unit to fully automated unit.

SCHOTT MAINZ JENA™ GLAS

SCHOTT JENA™ GLASWERK SCHOTT & GEN. INC

SEND FOR DESCRIPTIVE COLOR BROCHURE NOW!

11 EAST 26TH STREET, NEW YORK, N.Y. 10010 / (212) 679-8583

CIRCLE 188 ON READER SERVICE CARD

lanify, J. R. Phillips, M. E. Schillaci, M. A. Yates-Williams, J. J. Reidy.

10:30—Intermission.

10:45—175. Simultaneous Determination of Alpha-Emitting Nuclides of Radium Through Californium in Large Environmental and Biological Samples. **C. W. Sill, F. D. Hindman, J. I. Anderson.**

11:00—176. Simultaneous Determination of Uranium and Plutonium Isotopes in Soils by Single Alpha-Spectrometry. **T. Hashimoto, K. Taniguchi, H. Sugiyama, T. Sotobayashi.**

11:20—177. Development of a Beta Spectroscopy System for the Determination of Environmental Level Quantities of 89 and 90 Strontium. **J. T. Harvey.**

11:35—178. A Well Logging Technique for the In-Situ Determination of ^{90}Sr. **R. L. Brodzinski, H. L. Nielson.**

4th International Symposium on Column Liquid Chromatography

Boston, Mass.
May 7–10, 1979

Northeastern University and the Chromatography Forum of the Delaware Valley will sponsor the 4th International Symposium on Column Liquid Chromatography May 7–10, 1979, at the Park Plaza Hotel in Boston, Mass. The meeting is cosponsored by chromatography and other chemistry groups from Austria, German Federal Republic, Great Britain, France, Switzerland, and the Netherlands.

The symposium series was established in 1973 to provide a forum for the latest developments in column liquid chromatography. A total of 27 lectures and 41 poster presentations representing 14 countries will be given. The symposium volume will appear in the *Journal of Chromatography* after the meeting. In addition, an exposition of the latest instrumentation is included. All attendees are invited to a full social program consisting of a reception (May 7), an evening with the Boston Pops (May 8), and a New England Clambake at Plymouth, Mass. (May 9).

The program, registration form for the symposium, social program, tours, and hotel reservation form can be obtained from: Professor Barry L. Karger, Chairman, 4th International Symposium on Column Liquid Chromatography, Institute of Chemical Analysis, 341 Mugar Bldg., 360 Huntington Ave., Boston, Mass. 02115. All forms should be sent by April 1 to Dr. Karger. The detailed technical program follows.

Monday Morning, May 7

Session I

Considerations on Preparation and Operation of Very Efficient Liquid Chromatographic Columns. G. Guiochon, France

Studies of Open-Tubular Microcapillary Liquid Chromatography Using Soda–Lime Glass Columns Treated with Alkaline Solution. D. Ishii, T. Tsuda, T. Takeuchi, Japan

Potential Applications of Open Tubes in Liquid Chromatography. I. Halasz, Germany

Session II

Form of Theoretical Plate Height Equation from the Viewpoint of Practice in Column Liquid Chromatography. J.F.K. Huber, J. H. Quaadgras, A. Rizzi, Austria and The Netherlands

Sample Loading and Efficiency in Adsorption and Bonded Phase Liquid Chromatography. J. N. Done, UK

Monday Afternoon

Poster Session I

Trace Enrichment in HPLC Using Precolumn Technology; Application to Phthalates. H. V. Vliet, U.A.Th. Erinkman, R. W. Frei, The Netherlands

Resolution, Sensitivity, and Selectivity of HPLC Postcolumn Fluorometric Labeling Technique for Determination of Carbamate Insecticides. R. T. Krause, FDA

Interdependence of Pore Structure and Chain Length of Modifiers in Reversed Phase Chromatography. F. Eisenbeiss, K. F. Krebs, Germany

Reverse-Phase Chromatography of Organic Acids with Conductivity Detection. E. M. Thurman, U.S. Dept. of Interior

Upgrading HPLC with Fully Automated Sample Treatment. D. A. Burns, J. I. Fernandez, J. R. Grant, A. L. Pietrantonio, Technicon

Microcomputer-Controlled Low-Pressure Gradient System for HPLC. H.A.H. Billiet, P.D.M. Keehnen, H. C. van Dam, L. de Galan, The Netherlands

Purification of the Bacterial Ribosome and Its Subunits by Affinity Chromatography. F. Le Goffic, N. Moreau, S. Siegrist, S. Langrene, France

Poster Session II

HPLC and HPLC–MS Analysis of Organic Compounds in Water. B. Hidy, P. Mondron, R. Foltz, A. Graffeo, Battelle Columbus Laboratories

Liquid Chromatography Study of Nitrogen Transformation in Soils. C. Eon, France

HPLC Analysis of Polynuclear Aromatic Hydrocarbons in Environmental Water Samples. R. Reding, EPA

Retention Prediction in Surfactant HPLC. C. M. Riley, E. Tomlinson, T. M. Jefferies, UK

Extra Column Effects in High-Performance Liquid Chromatography. H. Colin, G. Guiochon, France

Approaches to Analysis of Polydisperse Dextran Products by High-Performance Gel Permeation Chromatography. J. N. Done, R. M. Alsop, UK

Liquid Chromatographic Determination of Tetracycline in Plasma and Urine Samples. S. Eksborg, H. Ehrsson, Sweden

HPLC of Synthetic Peptides: Selectivity, Derivation, and Comparison with Bioassay Results. H. K. Krummen, Switzerland

Tuesday Morning, May 8

Session I

Mobile Phase Effects in Reversed-Phase Chromatography. C. Horvath, W. Melander, J. Stoveken, Yale U

Reversed-Phase Ion-Pair Chromatography with Adsorbing and Complex-Forming Stationary Phases. K. G. Wahlund, G. Schill, Sweden

Study on Retention Mechanism in Reversed-Phase Ion-Pair Chromatography of Amines and Amino-Acids on Bonded Phases. R. S. Deelder, H.J.M. Linssen, The Netherlands

Session II

High-Performance Size Exclusion Chromatography of Colloids. J. J. Kirkland, Du Pont

BREAK THE GLASS HABIT



Nalgene® PMP Volumetric Flasks are as transparent as glass.



Nalgene® PMP Volumetric Flasks are just as clear as glass. PMP (polymethylpentene) construction gives them the clarity of glass without the breakability.

That makes Nalgene Volumetric Flasks safer than glass to use. When you drop one, it bounces instead of shattering. And the leakproof screw closure is easier to handle than a fragile penny head stopper.

Nalgene Volumetric Flasks are just as accurate as their glass equivalents, too. They're calibrated gravimetrically to guaranteed limits of error and individually marked. Unlike glass, Nalgene Labware is non-wetting, so these flasks deliver the amount of solution measured (TC = TD). Nothing is left on flask walls.

And because Nalgene Volumetric Flasks last longer than glass, you reduce replacement costs.

See for yourself why so many laboratories are breaking the glass habit with long-wearing Nalgene Labware.

And unbreakable Nalgene Labware lasts longer.

Nalgene® Graduated Cylinders are as accurate as glass.

Nalgene PMP Graduated Cylinders are as easy to use as glass cylinders. They're transparent and accurately calibrated. They meet the same federal specifications for accuracy established for glass.*

And because they're made of shatterproof polymethylpentene (PMP), they're safe and long lasting.

Our PMP cylinders can be used with acids, bases, and solvents. And they cost less than the leading glass cylinder.

See for yourself why so many laboratories are breaking the glass habit with long-wearing Nalgene Labware.

And unbreakable Nalgene Labware lasts longer.

*Federal Specification NNN-C-940

For a free Nalgene Cylinder, circle Reader Service Number 116 or return the coupon on the next page to Nalge.



Glass labware

Nalgene Labware

Nalgene® FEP Sep Funnels are as chemical resistant as glass.

Like glass, Nalgene* Sep Funnels of Teflon* FEP resist *any* chemical used in an extraction. But unlike glass, they won't break or crack, even when dropped, so you can reduce replacement costs. And both the screw cap on top and the stopcock at the bottom make these Nalgene Sep Funnels leakproof when they're shaken.

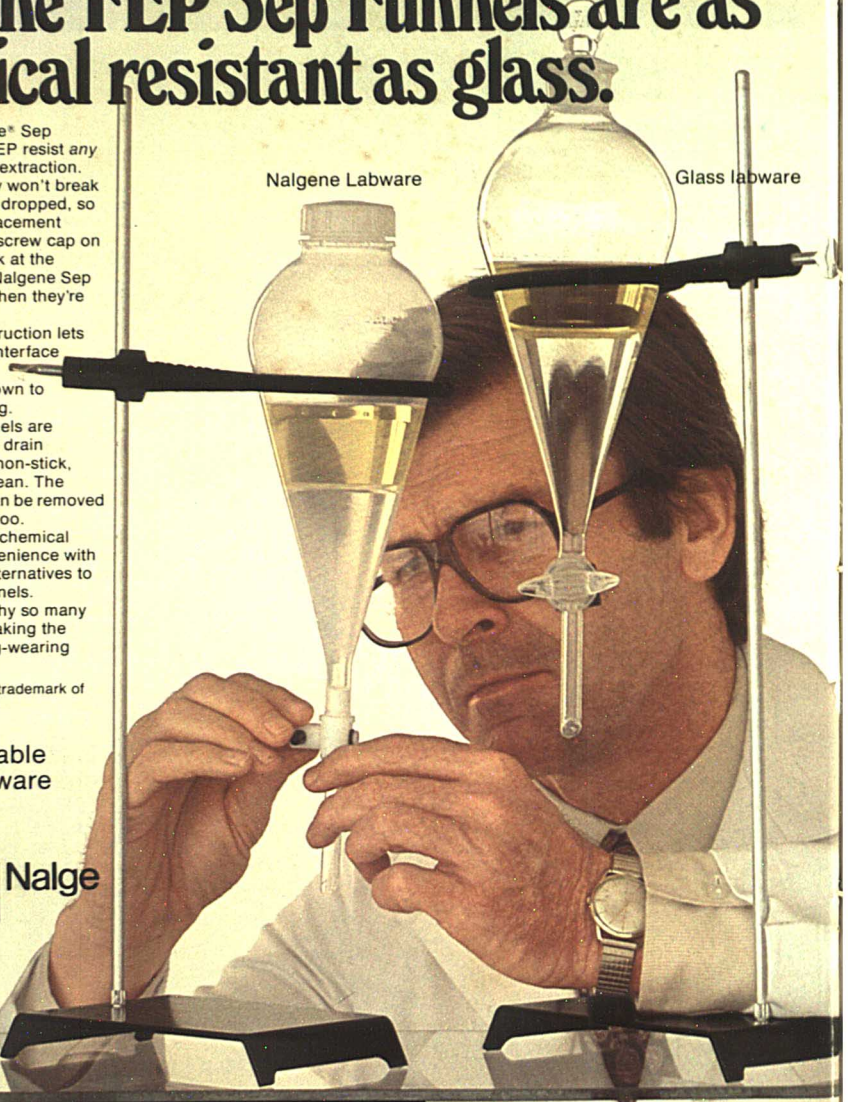
Teflon* FEP construction lets you see clearly the interface of even colorless liquids all the way down to the stopcock housing.

Nalgene Sep Funnels are non-wetting, so they drain completely. They're non-stick, so they're easy to clean. The stopcock housing can be removed for easier cleaning, too.

Get extraordinary chemical resistance and convenience with these economical alternatives to fragile glass sep funnels.

See for yourself why so many laboratories are breaking the glass habit with long-wearing Nalgene Labware.

*Teflon is a registered trademark of the Du Pont Company.



And unbreakable Nalgene Labware lasts longer.

SYBRON | Nalge

Nalge Company
Division of Sybron Corporation
Nalgene Labware Department
Box 365 / Rochester, N.Y. 14602

☐ Also send me the current Nalgene Labware catalog featuring over 250 products for professional use.

Name / Title _____

Company _____

Address _____

City _____ State _____ Zip _____

Get a free cylinder.

Put Nalgene* Labware to the test, and break the glass habit.

If you're not convinced that Nalgene Labware can do the job of glass in your lab, here's a chance to prove it to yourself. Just complete and mail the coupon, and we'll send you a Nalgene 100 ml, clear PMP Graduated Cylinder (a $4.90 value). Once you try it, we think you'll drop the glass counterpart you've used all along—and break the glass habit for good.

Circle Reader Service Number 116.

Mechanism of Band Dispersion in Exclusion Chromatography. J. H. Knox, F. McLennan, UK

Steric Field-Flow Fractionation: A New Tool for Separation of Particles 1–100 μm and Beyond. J. C. Giddings, M. N. Myers, J. W. Pav, T. T. Nguyen, K. D. Caldwell, U of Utah

Tuesday Afternoon

Poster Session I

Preparative and Analytical HPLC of Per-O-benzoylated Glycolipids. F. B. Jungalawa, H. Shea, S. J. Gross, D. Omen, R. H. McLeur, Eunice Kennedy Shriver Center for Mental Retardation and Center for Disease Control

Determination of 5-Aminolevulinic Acid and Porphobilinogen by High-Performance Liquid Chromatography. C. K. Lim, UK

Porous Pellicular Anion-Exchange Support for Proteins. A. Alpert, F. E. Pegnier, Purdue U

New Direct Liquid Inlet (DLI) Interface for LC/MS Coupling. P. Arpino, G. Guiochon, P. Krien, G. Devant, France

Combined Reversed-Phase and Normal-Phase High-Pressure Liquid Chromatography in Purification and Identification of 7,12-Dimethylbenz(a)anthracene Metabolites. M. W. Chou, S. K. Yang, Uniformed Services U of the Health Sciences

Analysis of Nonvolatile Organic Compounds in Water by High-Performance Liquid Chromatography. B. Crathorne, M. Fielding, C. D. Watts, UK

Influence of Organic Modifiers on Retention Behavior in Reversed-Phase Liquid Chromatography and Its Consequences for Gradient Elution. P. J. Schoenmakers, H.A.H. Billiet, R. Tijssen, L. de Galan, The Netherlands

Gradient Elution in Reversed-Phase Ion Pair Chromatography. I. J. Johansson, Sweden

Wednesday Morning, May 9

Session I

Influence of Structure on Resolution of Helicenes on Optically Active Supports. A. Balan, Y. H. Kim, A. Tishbee, E. Gil-Av, Israel

Broad Spectrum Resolution of Optical Isomers Using a Chiral HPLC Bonded Phase. W. H. Pirkle, D. W. House, U of Illinois

High-Performance Liquid Chromatography of Nucleotides and Nucleosides Using Metal Complexation. E. Grushka, F. K. Chow, State U of N.Y.

Session II

Principles of Selectivity in Reversed Phase Chromatography Using Metal Chelate Additives. Separation of Enantiomeric Pairs. W. Lindner, J. N. LePage, G. Davies, B. L. Karger, Northeastern U

Ligand-Exchange Chromatography of Recemates on Chiral Diamine Incorporated Resins. V. A. Davankov, A. A. Kurganov, USSR

Ligand-Exchange Chromatography of Enantiomer Amino Acids on Chiral Bonded Silica Gel and Amino Acids on Cu(II) Modified Silica Gel. A. Foucault, M. Caude, L. Oliveros, France

Wednesday Afternoon

Poster Session I

Nature of Polar Group Selectivity in Reversed-Phase Liquid Chromatography. P. J. Schoenmakers, N. Tanaka, B. L. Karger, Northeastern U

Chromatography of Xanthines on Ion-Exchange Resins. H. F. Walton, G. A. Eiceman, J. L. Otto, U of Colorado

Role of Temperature in Optimizing Throughput in Reverse-Phase Liquid Chromatography. J. R. Grant, J. W. Dolan, L. R. Snyder, Technicon Instruments Corp.

Application of Graphite Furnace Atomic Absorption Detector Automatically Coupled to HPLC for Speciation of Metal-Containing Macromolecules. E. J. Parks, F. E. Brinckman, W. R. Blair, NBS

Use of HPLC in Analysis of Biological Peptides. P. H. Corran, UK

HPLC of Biopolymers on Aqueous Compatible Rigid Organic Gels and Bonded Phase Silicas. S. R. Abbott, C. T. Wehr, R. M. Majors, Varian Instruments

Chelation, Ligand-Exchange, and Affinity Chromatography on Chitosan. R.A.A. Muzzarelli, Italy

High-Performance Liquid Chromatography of Peptides and Proteins on Chemically Bonded Hydrocarbonaceous Stationary Phases. M.J.W. Hearn, New Zealand

Separation of Small DNA and RNA Oligonucleotides by High-Performance Anion-Exchange Liquid Chromatography. M. Dizdaroglu, W. Hermes, Germany

Poster Session II

Combined Use of High-Efficiency Liquid Chromatography and High-Efficiency Capillary Gas Chromatography for Geochemical Examination of Crude Oils and Sediment Extracts. T. Doran, B. Hickmott, P.J.D. Park, D. V. Scammells, UK

High-Performance Liquid Chromatographic Study of Several Representative Polynuclear Aromatic Hydrocarbons and Their Oxidized Derivatives of Environmental Interest. F.S.C. Lee, Ford Motor Co.

Isotherm Linearity and Preparative Liquid Chromatography. A.W.J. deJong, J. C. Kraak, H. Poppe, The Netherlands

Isocratic vs. Binary Gradient Elution in Column Liquid Chromatography. J.F.K. Huber, I. Feher, Austria

Study of Nonlinear Elution in Preparative Liquid Chromatography. P. Gareil, L. Personnaz, J. P. Feraud, M. Caude, France

Characterization of Organic Porous Polymer Gels and ICP as a Selective Detector for Metal Complexes. T. Hanai, J. Hubert, G. Lussier, M. Bellavance, M. Lefebvre, Canada

Preparative Separation of Proteins and Enzymes in Mean Molecular Weight Range of 10 000 to 500 000 on Hydrophilic Surface-Modified Silica Packings. K. Unger, Germany

Liquid Chromatographic Determination of Amino Acids and Catecholamines in Biological Samples After Precolumn Derivatization. B. A. Persson, I. Carlsson, B. M. Eriksson, P. O. Lagerstrom, Sweden

What Performances Can be Expected from a Pressurized Pumping System in HPLC? C. L. Guillemin, France

Thursday Morning, May 10

Session I

Use of Microbore Columns in Separation of Biological Mixtures. R.P.W. Scott, P. Kucera, Hoffmann-La Roche

HPLC of Proteins. H. Engelhardt, D. Mathes, Germany

Protein-Stationary Phase Interaction in HPLC. R. A. Barford, B. J. Sliwinski, H. L. Rothbart, USDA

Session II

Weak Basic Dimethylamino-Modified Silica Ion Exchanger Applied to Separation of Oligonucleotides in Mean Molecular Weight Range of 500 to 5000. W. Jost, K. K. Unger, R. Lipecky, H. J. Gassen, Germany

Noncovalently Bonded Derivatives for Gel Permeation Chromatography. F. E. Regnier, K. M. Gooding, K. C. Lu, Purdue U

HPLC Separation and Identification of Hormonal Polypeptides and Proteins Secreted by Human Tumor Cells. E. C. Nice, M. J. O'Hare, UK

Thursday Afternoon

Session I

(Poster Sessions of Latest Results)

Session II

Coated Open Tubular Liquid Chromatography with Air Segmentation. Theory and Application for the Pretreatment of Samples Prior to Separation in Conventional HPLC. L. R. Snyder, N. Tanaka, J. W. Dolan, Technicon Instruments

HPLC Extraction Detector for Amines Based on Fluorescent Ion-Pair Formation. R. W. Frei, I. Honigberg, L. Feenstra, J. F. Lawrence, U.A.Th. Brinkman, The Netherlands

Solid Phase Reagent for Liquid Chromatographic Detection. J. Studebaker, IBM

Capabilities of On-Line Element-Specific Detection in HPLC Using Inductively Coupled Argon Plasma Emission Source Detector. C. H. Gast, J. C. Kraak, H. Poppe, F.J.M.J. Maessen, The Netherlands

9th Annual Symposium on Analytical Chemistry of Pollutants

Jekyll Island, Ga.
May 7–9, 1979

Jekyll Island, Gem of the Golden Isles located halfway between Savannah, Ga., and Jacksonville, Fla., will be the site of the 9th Annual Symposium on the Analytical Chemistry of Pollutants. The symposium is designed to bring together people concerned with the application of analytical chemistry to environmental problems. The first two symposia in this series were held at Halifax, Nova Scotia, Canada, in 1971 and 1972. The third symposium took place in Athens, Ga., in 1973 when the American Chemical Society, the U.S. Environmental Protection Agency, and the University of Georgia became sponsors. Their continued sponsorship has contributed significantly to the success of this symposium. With Basel, Switzerland, as the site for 1974, participation and sponsorship by the European scientific community promoted international communication. To continue this international exchange of ideas and experiences, the symposium now is held alternately in Europe and the United States. In 1975 the site was Jekyll Island, Ga., and in 1976, Vienna, Austria. After convening at Lake Lanier, Ga., in 1977, the symposium returned to Switzerland to Geneva in 1978.

This year's symposium will feature three plenary lectures that will represent diverse viewpoints concerning implementation of the 1976 Toxic Substances Control Act. The lectures will be given by Donna Roberts, director of Product Stewardship, Dow Chemical Co., Midland, Mich.; Robert H. Harris, Environmental Defense Fund and University of California, Berkeley, Calif.; and John B. Ritch, director, Office of Industry Assistance, Office of Toxic Substances, U.S. Environmental Protection Agency, Washington, D.C. Other invited speakers will present a balanced, relevant program concerning analysis of organic and inorganic environmental pollutants.

The focus of the technical program will be on identification and measurement of organic compounds, multielement analysis, and particulate analysis. The various analytical methods to be discussed for the identification of organic compounds will include LC, LC–MS, GC–MS, isotope dilution MS, ion microprobe analysis, photoacoustic spectroscopy, Raman spectroscopy, and methods based on luminescence. Analytical tools to be discussed for the analysis of particulates are the laser ion microprobe and surface techniques. There will also be a talk on the challenge of environmental analyses to multielement techniques. The pollutants to be discussed are particulates, organics, and priority pollutants.

To encourage maximum exchange of information, registration will be limited to 350 participants. Early preregistration is recommended. Preregistration and regular registration fees are $75 and $90, respectively. For more information, contact: Elaine McGarity, U.S. Environmental Protection Agency, Environmental Research Laboratory, College Station Rd., Athens, Ga. 30605 (404-546-3184).

Symposium on Advanced Analytical Concepts for the Clinical Laboratory

Oak Ridge, Tenn.
April 26–27, 1979

The symposium series on Advanced Analytical Concepts for the Clinical Laboratory is being continued under the sponsorship of the American Association for Clinical Chemistry and Oak Ridge National Laboratory, and will be supported by the Medical Products Division of Union Carbide Corp. The symposium will be held at Oak Ridge National Laboratory April 26–27, 1979.

The symposium series has been established as a forum for discussing recent developments in the application of advanced analytical concepts to clinical analysis. The technical program includes three sessions, Advanced Concepts, Analytical Systems, and Applications of Luminescence Analyses. In Advanced Concepts, theoretical considerations, component development, and computer applications will be covered. Analytical Systems will include the description and operational details of new systems or automated data analysis systems using advanced concepts. The highlight of the meeting, Luminescence Analyses, will cover papers on the basic concepts of bioluminescence and chemiluminescence analysis, particularly as they apply to the clinical laboratory, and on analytical techniques and instrumentation that will become useful in this area.

All attendees are invited to a social hour and dinner on Thursday evening, April 26. Proceedings of the symposium will be published as usual in a single issue of *Clinical Chemistry*. Attendance will be limited to 150, and registrants should make room reservations directly with local motels. Registration fee is $25. The technical program was not available at press time. Requests for information should be addressed to Charles D. Scott, Chairman, Oak Ridge National Laboratory, P.O. Box X, Oak Ridge, Tenn. 37830 (615-483-8611, ext. 3-1251).

HPLC News:

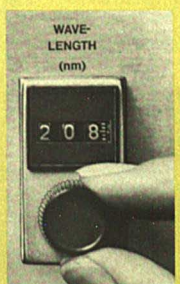
A variable UV detector with outstanding performance

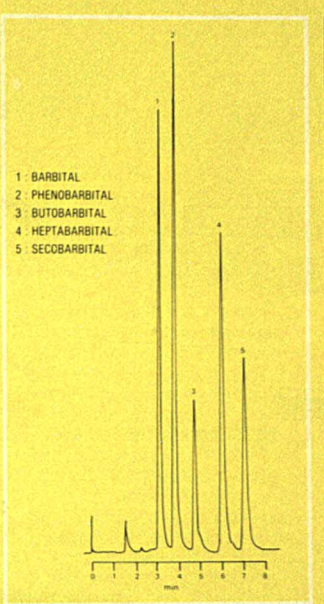
LDC's new SpectroMonitor III is all you have been asking for. Advanced optics give true dual beam operation for exceptional stability and low noise (1.5% peak to peak at 195 nm)

Sensitivity to 0.005 AUFS



Wavelength range 195 to 350 nm





Actual SpectroMonitor III chromatogram demonstrates low noise and exceptional stability.

LDC liquid chromatography

Easy inspection, with the cell and liquid connections easily removed from the front for inspection and servicing.



Price: $3290.

Write for brochure with complete technical data.

LABORATORY DATA CONTROL
Division of Milton Roy
P.O. Box 10235,
Riviera Beach, FL 33404
305/844-5241 telex 513479
European office:
Laboratory Data Control
Milton Roy House, High Street
Stone, Staffs., ST15 8AR England
Telephone 0785-83-3542 telex 36623



LDC

233

CIRCLE 130 ON READER SERVICE CARD

LIQUID CHROMATOGRAPHY



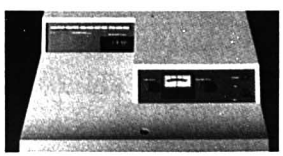
AT LAST. A SPECTROPHOTOMETRIC DETECTOR DESIGNED SPECIFICALLY FOR LC. THE SIMPLE, POWERFUL MODEL LC-75.

The new Perkin-Elmer Model LC-75 has a big edge over any UV detector you're presently using for liquid chromatography. It's the first of its kind to incorporate every LC requirement from the ground up.

We made it more powerful than earlier detectors. We made it smaller, so you can squeeze it into less bench space. We made it modular, to fit into our complete line of LC instruments and accessories, like the Autocontrol that multiplies its capabilities. And like all great ideas, we made it simple.

SIMPLE AND TROUBLE-FREE

It has a single power switch for both source and electronics. A single pushbutton range switch. Fine and coarse zero controls. And a variable wavelength select knob. That's all!



The Model LC-75 gives you pushbutton sensitivity selection in standard units. Its automatic order-filter change eliminates optical harmonics. Permanently calibrated, the instrument never needs service adjustments.

GREAT PERFORMANCE

You get dependable wavelength resettability to spectroscopic standards. Accurate reproduction of literature methods. And no time degradation in performance.

Performance is phenomenal. Trace analysis is excellent even with small samples, thanks to high-energy optics and a single light source for UV and visible ranges.

Quantitative capability is superior, providing the widest range of usable sample concentrations and reliable repeatability of results.

THE UNIQUE FLOW CELL

Sample degradation and heat effects are minimized because the monochromator *precedes* the flow cell – only the analytical wavelength passes through the sample.

The unique flow cell transmits all energy incident on it with standard 1 cm response. Result: total insensitivity to changes in solvent refractive index, temperature, flow rate, and laboratory environment. This high pressure cell minimizes interference from bubbles in the stream and permits use of multiple detectors in series.

AMAZING AUTOCONTROL

Adding the modular Model 75 Autocontrol unlocks the detector's tremendous spectroscopic power. Talk to its keyboard in simple language, and the Model 75 Autocontrol takes you through the most sophisticated chromatographic peak analyses step by step.



For example, it gives you quick, easy absorbance ratioing for positive peak identification and assurance of complete, adequate chromatography. At the push of a button, the scanning mode produces actual spectra which allow selection of optimum wavelengths for maximum sensitivity, and determination of the purity of component peaks.

Even at high sensitivity in the far UV, you can have background correction of mobile phase absorbance effects during gradient operation. You can even select optimum wavelengths for each portion of the chromatogram for single-run analysis of compounds with widely different spectral characteristics.

FIND OUT MORE

Get all the details on this radical new development in LC detection. Call your Perkin-Elmer representative now. Or write Perkin-Elmer Corporation, MS 12, Main Avenue, Norwalk, CT 06856.

PERKIN-ELMER

Expanding the world of analytical chemistry.

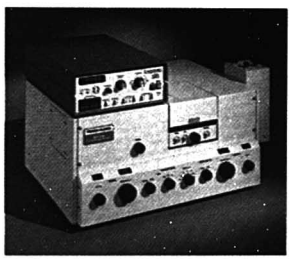
CIRCLE 166 ON READER SERVICE CARD

NOW–THE FIRST FULL FLUORESCENCE LINE WITH MICROPROCESSOR CONVENIENCE.

You won't find a more complete line of fluorescence spectrophotometers anywhere. These Perkin-Elmer "multiple choice" instruments range from research to routine in performance—with microprocessor control and a variety of accessories to stretch their capabilities.

MODEL MPF-44B
NOTHING BETTER
FOR RESEARCH

No other research-grade instrument matches it in sophistication, resolution, and sensitivity. It incorporates every advance gained through Perkin-Elmer's long experience. It's shown here with our DCSU-2 Differential Corrected



Spectra Unit, an ordinate microprocessor. This remarkable accessory enables you to perform spectra correction, subtraction, and polarization, and obtain first and second derivative curves of either corrected or uncorrected spectra.

MODEL 650-40
CONVENIENCE AND
CAPABILITY COMBINED

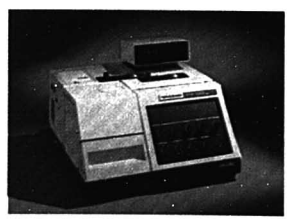
This is the abscissa-microprocessor-controlled member of the highly sensitive Perkin-Elmer 650



series—a medium priced line that offers many features found only in high priced units. The 650-40 operates with function keys and a numeric keyboard, includes automatic gain setting and auto zero, and gives you a digital display of fluorescence, wavelength, and other parameters. The Model 650-40/60 version has an ordinate microprocessor for such additional functions as spectra correction, CATing, rep scan, subtraction, and polarization.

MODEL 650-10
MORE SENSITIVITY
FOR THE DOLLAR

High-efficiency ruled concave grating monochromators and horizontal slit arrangements are combined in a proprietary optical design that gives this instrument extremely high sensitivity for a moderate price. Slit width is continuously adjustable down to 1.5 nm, another Perkin-Elmer exclusive that attains precision control of intensity and resolution you



won't find elsewhere except in high priced units. As little as 0.6 ml of sample is needed in the standard cell.

MODEL 3000
THE UNCOMMON UNIT
FOR ROUTINE WORK

Features like pushbutton operation and abscissa microcomputer control of scanning monochromators make the Model 3000 an exclusive Perkin-Elmer breakthrough in its class. You get excitation spectra quantum corrected automatically, and digital display of fluorescence values. The Model 3000 also has three pairs of wavelength memories (three for excitation and three for emission). A pulsed xenon source, together with ratio-recording electronics, provides excellent stability for long-term measurement.



Get all the facts on this remarkable selection of fluorescence instruments and accessories. For literature or a demonstration, phone (203) 762-6095. Or write Perkin-Elmer Corporation, MS-12, Main Avenue, Norwalk, CT 06856.

PERKIN-ELMER
Expanding the world of analytical chemistry.

CIRCLE 167 ON READER SERVICE CARD

Thermal Analysis Workshop

NBS, Gaithersburg, Md.
May 21–22, 1979

A workshop, sponsored by NBS and the University of Akron, will deal with recent advances and new interests in the field of thermoanalytical measurements at a two-day session May 21–22 at NBS in Gaithersburg, Md. Preliminary plans include topics on energy conservation in industrial processes, catalysts, environmental hazards, high-pressure thermal analysis, phase diagram studies, enthalpimetric measurements, and kinetics. A 2-hour contributed poster session is planned for Monday evening. Authors are requested to submit a 200-word abstract by April 30; notification of acceptance will be given by May 7.

The current list of topics and speakers includes current contributions of thermal analysis to the study of technological adsorbents, J. Rouquerol, France; thermal analysis in chemical processing, D. Dollimore, UK; recent instrumental developments, W. Wendlandt, University of Houston; phase studies in alloys, W. R. Bandi, U.S. Steel Research; thermal analysis in rubber industry, D. W. Brazier, Canada; studies on polymer ignition, B. Miller and J. R. Martin, Textile Research Institute; ceramic processes and energy conservation, W. R. Ott, Rutgers University; paper technology from Egyptian, Chinese, and Mayan cultures, H. G. Wiedemann, Switzerland; chemical complexes, P. Garn, University of Akron; enthalpimetric analysis, J. Jordan, J. D. Stutts, and W. J. Brattlie, Pennsylvania State University; and high-pressure thermogravimetry, N. C. Gardner, Case Western Reserve University.

For further information on the workshop, write to Oscar Menis, General Chairman, Chemistry Bldg. 222, Rm. B-326, NBS, Washington, D.C. 20234.

Chemical Instrumentation Award Nominations

The Chemical Instrumentation Award, sponsored by the Division of Analytical Chemistry and the Instrumentation Specialties Co., was established in 1976 to recognize and encourage achievement in the origination or improvement of analytical methods by instrumentation. A nominee must be a citizen of the U.S. or Canada and must have accomplished a practical and significant simplification of analytical procedures by means of instrumental techniques. Nominations for the 1980 award should be sent by May 1, 1979, to: Lynn L. Lewis, Chairman-Elect, Dept. 22, General Motors, Research Laboratories, Warren, Mich. 48090.

Small Business Research Proposals

NSF is seeking applied research proposals from small businesses on advanced concepts in 12 areas that have a high potential for public benefit and technological innovation, under a new program solicitation, "Small Business Innovation Research." The solicitation has been issued to provide an incentive for research on Federal objectives to also serve as a base for technological innovation in the private sector. Proposals for research on advanced concepts on any of the following topics will be considered: chemical threats to man and the environment; alternative biological sources of materials; human nutrition; science and technology to aid the physically handicapped; advanced production and manufacturing processes; measurement and advanced instrumentation; materials and processes; deep mineral resources; marine resources; plant productivity; reclamation of wastewater and sludges; and applied research project support, which includes high quality experimental or theoretical applied research on an important problem or opportunity that could have significant public benefit if the research were successful.

Forty to fifty awards are anticipated under the first of a three-phase program supported under NSF's Applied Science and Research Applications (ASRA) Directorate. Phase I proposals are limited to 20 pages for awards of up to $25 000 over a 6-month period. This phase is to determine the feasibility of the approach and the research capabilities of the small firm within these limits. Larger awards will be made for the principal research effort for those projects that appear most promising after the first phase. Both phases provide incentives for the small firm to use the research on ASRA objectives in phases I and II to pursue commercial objectives with private venture capital in phase III. Phase III private funding can be contingent upon the achievement of certain technical objectives in phase II. Patent rights to any inventions will be made available to the small firm subject to certain conditions, contingent upon phase III funds being invested by a third party in an amount at least equal to that requested from NSF for phase II.

High-risk innovation proposals for applied research on advanced concepts are desired from high technology, R&D and manufacturing firms with strong research capabilities in science or technology. The use of academic consultants also is encouraged. For research purposes, a small business must be profit-seeking with 1–500 employees in all affiliated firms.

Those interested in submitting proposals should request a copy of Program Solicitation 78-69, which defines the specific objectives and the format, from: Forms and Publications Office, Rm. 235, NSF, 1800 G St., N.W., Washington, D.C. 20550. The deadline for submission of proposals is April 1, 1979, for research efforts commencing in Oct. 1979.

Call for Papers

6th Annual Meeting of the Federation of Analytical Chemistry and Spectroscopy Societies (FACSS)
Philadelphia, Pa. Sept. 16–21. A previous call for papers announcement for this meeting was published in the Jan. issue, pages 52 A and 54 A. There have since been some changes made in the planned special symposia. The updated list includes special symposia in the following areas: plasma sources in analysis, forensic analysis, analytical chemistry in the steel industry, new developments in atomic absorption spectrometry, modern concepts in atomic absorption instrumentation, analytical application of optoacoustic spectrometry, gas and liquid chromatography, atomic fluorescence spectrometry, atomic emission spectrometry, drug analysis, MS, advancement in clinical instrumentation, recent advances in electrochemistry, clinical standards, trace analysis in biological fluids by atomic absorption spectrometry, high resolution ^{13}C-NMR spectroscopy of solids, IR, factors affecting spectrophotometric accuracy in clinical chemistry, advances in analytical chemistry and atomic spectroscopy in Canada, and hybrid methods using GC–LC–IR. Contributed papers are not restricted to symposia topics; original papers dealing with all phases of analytical chemistry may be contributed. Authors who wish to present papers must submit the title of presentation and a 50-word brief by April 15, 1979, to: P. D. LaFleur, Program Chairman FACSS-VI, A309, Chemistry, NBS, Washington, D.C. 20234 (301-921-2851). After receipt of title and brief, each author will be notified, and if the paper is accepted for pre-

sentation, the author will be asked to submit a 250-word abstract by July 1, 1979.

International Winter Conference 1980 on Developments in Atomic Plasma Spectrochemical Analyses

San Juan, Puerto Rico. Jan. 6–11, 1980. Papers describing original work on applications, fundamentals, and instrumentation development of atomic plasmas (inductively coupled plasma, dc plasma, and microwave induced plasma) in spectrochemical analyses are invited. Authors are requested to submit the title of their contribution and a 50–100-word preliminary abstract prior to June 1, 1979. Receipt of abstracts will be acknowledged, and authors of accepted papers will receive special typing instructions for submitting an extended abstract for the official conference book. Poster session papers will also be accepted. Submit abstracts or direct questions for further information to: Winter Conference 1980, ICP Information Newsletter, Chemistry, GRC Tower I, University of Massachusetts, Amherst, Mass. 01003. 413-545-2294

Symposium on Separation Science and Technology for Energy Applications

Gatlinburg, Tenn. Nov. 2, 1979. Sponsored by the DOE Office of Basic Energy Science and Oak Ridge National Laboratory, the symposium program is divided into five technical sessions: isotope separation, chromatographic processes, fluid-solid separations, solvent extraction, and membrane separations. A poster session will also be provided. Persons interested in presenting papers at the symposium should submit a 200–250-word abstract by June 15, 1979, to: A. P. Malinauskas, Oak Ridge National Laboratory, P.O. Box X, Oak Ridge, Tenn. 37830. Papers will be selected by July 15 and are due in a form suitable for publication at the time of presentation.

Meetings

- **Chromatography Workshop.** April 23–24. George Washington Motor Lodge, Fort Washington, Pa. *Contact: Frank van Lenten, E. I. du Pont de Nemours & Co., Jackson Labs, CD&P, Wilmington, Del. 19898*
- **American Society for Microbiology.** May 4–8. Los Angeles. *Contact: Richard Bray, 1913 I St., N.W., Washington, D.C. 20006*
- **25th International Instrumentation Symposium.** May 7–10. Anaheim, Calif. *Contact: Instrument Society of America, Test Measurement Div., 11009 Prospect N.E., Albuquerque, N.M. 87112*
- **Workshop on Thermal Analysis.** May 21–22. Gaithersburg, Md. *Contact: Oscar Menis, B326 Chemistry Bldg., NBS, Washington, D.C. 20234. 301-921-2175*
- **5th Annual National Meeting of the Clinical Radioassay Society.** May 22–25. Washington, D.C. *Contact: 5th CRS Meeting, Box 119, Fairfax, Va. 22030*
- **27th Annual Conference on Mass Spectrometry and Allied Topics.** June 3–8. Seattle, Wash. *Contact: H. M. Fales, Bldg. 10, Rm. 7N322, National Institutes of Health, Bethesda, Md. 20014*
- **National Conference on Synchrotron Radiation Instrumentation.** June 4–6. Gaithersburg, Md. *Contact: David Ederer, A251 Physics Bldg., NBS, Washington, D.C. 20234. 301-921-2301*
- **Third European Congress of Clinical Chemistry.** July 3–8. Brighton, UK. *Contact: P.J.N. Howarth, Dept. of Chemical Pathology, Guys Hospital Medical School, London SE1 9RT, UK*
- **National Conference on Weights and Measures.** July 22–27. Portland, Ore. *Contact: Harold Wollin, A211 Metrology Bldg., NBS, Washington, D.C. 20234. 301-921-3677*
- **International Conference on Liquid Scintillation Counting: Recent Applications and Development.** Aug. 21–24. University of California at San Francisco. *Contact: C. T. Peng, School of Pharmacy, University of California, San Francisco, Calif. 94143*
- **3rd Annual Arnold O. Beckman Conference.** Oct. 2–5. Colorado Springs, Colo. *Contact: Michele Tuttle, Meeting Coordinator, AACC, 1725 K St., N.W., Washington, D.C. 20006*
- **Instrument Society of America Conference & Exhibit.** Oct. 22–25. O'Hare Exposition Center, Chicago. *Contact: ISA, 400 Stanwix St., Pittsburgh, Pa. 15222*
- **ACS 31st Southeastern Regional Meeting.** Oct. 24–26. Roanoke, Va. *Contact: J. Wolfe, Virginia Polytechnic Institute and State University, Blacksburg, Va. 24060*
- **Society of Forensic Toxicologists Annual Meeting.** Oct. 31–Nov. 2. Williamsburg, Va. *Contact: R. V. Blanke, Medical College of Virginia, MCV Station, Box 696, Richmond, Va. 23298*
- **American Nuclear Society Conference on "Measurement Technology for Safeguards and Materials Control."** Nov. 26–29. Kiawah Island, Charleston, S.C. *Contact: Tom Canada, Los Alamos Scientific Lab, MS-540, Los Alamos, N.M. 87544*

Short Courses

ACS Courses. For more information, contact: Department of Educational Activities, American Chemical Society, 1155 Sixteenth St., N.W., Washington, D.C. 20036. 202-872-4508

Gas Chromatography, Theory and Practice

Blacksburg, Va. Sept. 24–27. H. M. McNair. $425, ACS members; $485, nonmembers

Microprocessors and Minicomputers—Interfacing and Applications

Blacksburg, Va. June 10–15, Sept. 23–28, Dec. 9–14. R. E. Dessy and the Chemistry Dept. Instrument and Design Group of VPI&SU. $455, ACS members; $515, nonmembers

Flavor Research Workshop

Honolulu, Hawaii (ACS/CSJ Chemical Conference). Mar. 29–30. Roy Teranishi, R. A. Flath, and J. Sugisawa. $200, ACS members; $240, nonmembers

Planning for Safe Laboratory Handling of Highly Toxic Chemicals

Honolulu, Hawaii (ACS/CSJ Chemical Conference), Mar. 30–Apr. 1; Washington, D.C. (178th ACS National Meeting), Sept. 7–9. N. V. Steere and Maurice Golden. $295, ACS members; $340, nonmembers

Modern Techniques in Gas Chromatography

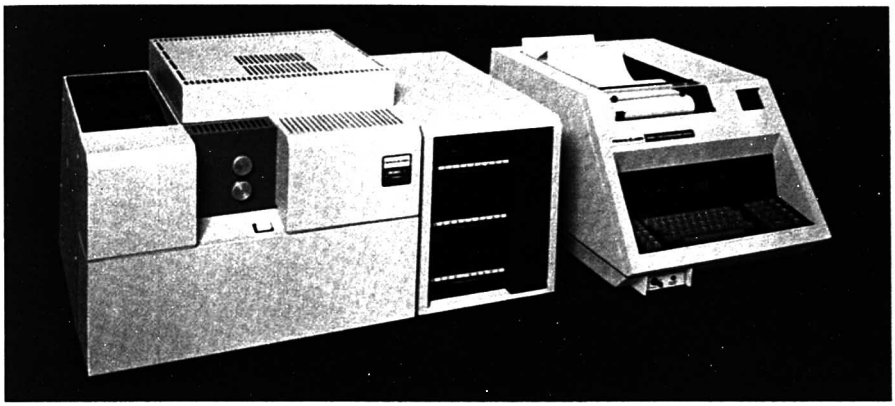
Honolulu, Hawaii (ACS/CSJ Chemical Conference). Mar. 31–Apr. 1. H. M. McNair and S. P. Cram. $225, ACS members; $265, nonmembers

Solving Problems with Modern Liquid Chromatography

Honolulu, Hawaii (ACS/CSJ Chemical Conference). Mar. 31–Apr. 1. J. J. Kirkland and L. R. Snyder. $245, ACS members; $290, nonmembers

Maintaining and Troubleshooting Chromatography Systems Workshop

PERKIN-ELMER'S SIGMA GC SERIES– MORE THAN EVER, YOUR SOUNDEST CHOICE.



Two years ago, we introduced our SIGMA gas chromatography concept. Today it has proved itself as the most advanced, common-sense move of its kind.

Because the SIGMA series gives you a unified set of instruments to match your applications and budget. Plus options. Plus accessories. Plus a microprocessor-controlled data handling unit that serves them all. And they've all demonstrated their capabilities fully, from the most sophisticated at the top of the line to the routine-use instrument that still shares the basic advantages of the whole series.

THE FULL LINE

The SIGMA 1 leads off. It combines one or more gas chromatographs with integral microprocessor control and multi-channel data handling. The internal printer/plotter gives the chromatogram, analytical conditions, and quantitative results.

The SIGMA 2 is a multi-detector, microprocessor-controlled instrument that combines versatility with operating ease. You set the analytical parameters on a keyboard that instructs you in the setup routine.

SIGMA 3 gas chromatographs are modestly priced but exceptionally versatile single or dual channel temperature programmed instruments. They may be equipped with an extremely wide choice of detectors. A simple numerical keyboard sets parameters and the microprocessor checks that no "impossible" values are entered.

SIGMA 4 instruments are excellent for routine applications. They are dedicated isothermal units offering the same detectors, injectors, and ovens as their more expensive counterparts.

MORE ACCESSORIES

Even the list of SIGMA accessories is longer now, widening the SIGMA capabilities for handling your applications. There's the new HS-6 headspace sampler, especially useful for environmental analysis, simple in operation and low in cost. Others include an automatic gas analyzer for refinery gases, the MS-1 automatic syringe for pushbutton injection and the AS-100 automatic sampler which injects up to 100 samples automatically. These new accessories join a long list of standard accessories including gas sampling valves, a pyrolysis injector, the MS-41 solid injector, spectroscopic detectors and a complete line of packed and capillary glass and metal columns.

JOIN THE PARADE

Don't let more time pass before you start to enjoy the benefits of the most significant advance in GC today. Get the details now. Talk to your Perkin-Elmer representative. Or write Perkin-Elmer Corporation, MS-12, Main Avenue, Norwalk, CT 06856.

PERKIN-ELMER

Expanding the world of analytical chemistry.

CIRCLE 168 ON READER SERVICE CARD



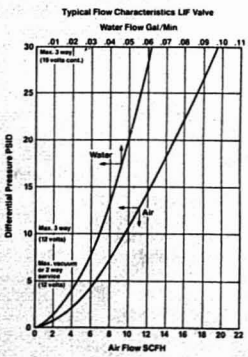
Small wonder.
(shown actual size)

The Lee Interface Fluidic miniature solenoid valve from Lee.

Designed to flow clean air, water, or other noncorrosive fluids, the miniature LIF offers some very big benefits:

- ☐ Low power consumption – 270 mW at 12V DC
- ☐ Fast response – 3mS (air)
- ☐ Stainless steel or brass construction
- ☐ Extended life – 200,000,000 cycles (air)
- ☐ Quiet switching
- ☐ Small internal volume – 0.006 in^3
- ☐ Pressures up to 30 PSI

And the kind of quality construction Lee is famous for. The perfect miniature valve for medical/analytical equipment. Textile machinery. Automatic processing equipment. And many other applications where compact design, consistent performance, and superior reliability are critical considerations.



The LIF Valve. It's from Lee. Small wonder.

For more information write to The Lee Company, 2 Pettipaug Road, Westbrook, Connecticut 06498. (203) 399-6281/ Telex 963-491.

Lee. Helping in small ways.

LEE

CIRCLE 127 ON READER SERVICE CARD

News

Boston, May 5–6; Philadelphia (ASTM E-19 Meeting), Oct. 20–21. J. Q. Walker, M. T. Jackson, and M.P.T. Bradley. $250, ACS members; $300, nonmembers

Federal Regulations in the Chemical Industry
Chicago, May 18–19; Washington, D.C. (178th ACS National Meeting), Sept. 8–9. G. S. Dominguez. $225, ACS members; $265, nonmembers

Toxicology for Chemists
Chicago. May 22–24. Morris Joselow. $485, ACS members; $555, nonmembers

Safety and Health for Academic Chemistry Laboratories
Chicago. June 2–3. N. V. Steere. $130, ACS members and nonmembers

Liquid Chromatography, Theory and Practice
Blacksburg, Va. June 4–7, Dec. 10–13. H. M. McNair. $450, ACS members; $510, nonmembers

Multinuclear NMR Spectroscopy
Los Angeles, June 7–9; Tallahassee, Fla., June 14–16. G. C. Levy. $295, ACS members; $340, nonmembers

Atomic Absorption Spectroscopy
Atlanta. June 14–15. Samuel Koirtyohann, Michael Epstein, and Theodore Rains. $245, ACS members; $290, nonmembers

Design and Analysis of Industrial Experiments
Atlanta, June 14–16; Philadelphia (FACSS Meeting), Sept. 14–16. John Hromi. $295, ACS members; $340, nonmembers

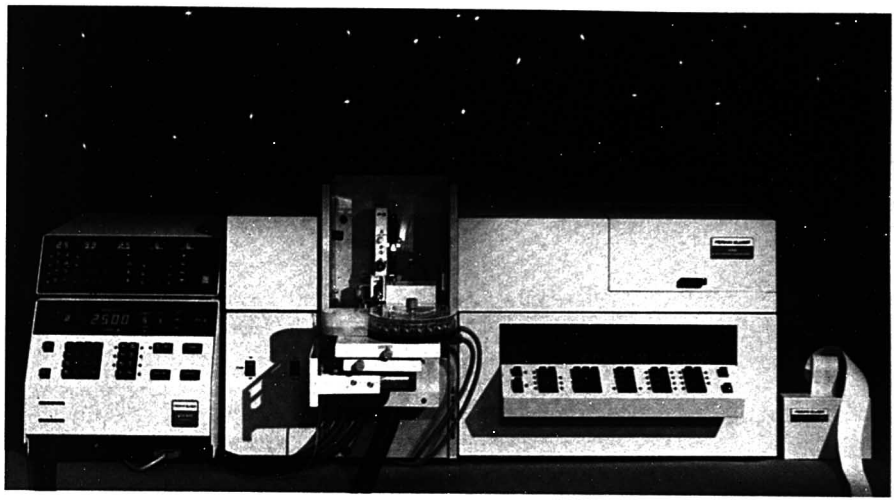
Carbon-13 NMR Spectroscopy
Washington, D.C. (178th ACS National Meeting). Sept. 7–9. G. C. Levy and Paul Ellis. $295, ACS members; $340, nonmembers

Effective Writing for Scientists and Engineers
Washington, D.C. (178th ACS National Meeting). Sept. 7–9. Henrietta Tichy and Sylvia Fourdrinier. $295, ACS members; $340, nonmembers

High-Performance Management
Washington, D.C. (178th ACS National Meeting). Sept. 8–9. J. H. Morrison. $225, ACS members; $265, nonmembers

High-Pressure Liquid Chromatography Apparatus Workshop
Philadelphia (FACSS Meeting). Sept.

MEET THE AA NIGHT SHIFT.



Load up this Perkin-Elmer atomic absorption system for flameless analysis, insert the proper magnetic card, and press the START button when you leave at night. Enjoy your evening. In the morning, you can pick up the results —a determination of six elements at trace levels in 35 samples— made with no supervision at all.

The spectrophotometer is our *Model 5000*, the world's only automated multi-element sequential AA instrument. It has every function under microcomputer control. Its memory will store all the analytical conditions you enter for up to six elements and select them automatically.

NEW FURNACE, NEW AUTO SAMPLER.

The *HGA-500* graphite furnace also has microcomputer control and stores six analytical programs with up to nine different steps. It's so versatile, you can choose optimal analytical conditions for any sample matrix. You can program temperature, ramp, and hold times in each step and select an alternate gas to optimize matrix destruction.

Our new microcomputer-controlled *AS-40* auto sampler can pipet from 5 to 99 μl of 35 samples into the graphite furnace. It can perform analyses by the standard additions method automatically, and you don't even need to prepare a set of dilutions for each sample. The AS-40 can also inject a reagent into the furnace for matrix modification automatically.

FLAME ANALYSIS BY DAY.

During the night, analyses proceed without flames or flammable gases. By day, your Model 5000 will be available for flame analyses. Automatically, it will process 50 samples for six elements in as little as 30 minutes. With its automatic flame and flameless capabilities, the Model 5000 gives you two days' work in one day's time.

Get details on everything this remarkable Perkin-Elmer AA system can do, day or night, whether you're present or not. Contact our nearest representative. Or write Perkin-Elmer Corporation, MS-12, Main Avenue, Norwalk, CT 06856.

PERKIN-ELMER

Expanding the world of analytical chemistry.

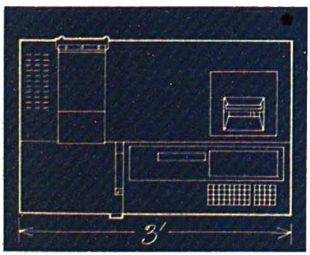
CIRCLE 169 ON READER SERVICE CARD



Now when you think powerful IR analysis, think compact.*

Presenting the Beckman Microlab™ 620 MX Computing Infrared Spectrophotometer. An incredibly powerful and versatile analytical instrument designed in a uniquely compact and easy-to-operate configuration.

There is nothing else like it. Packed into its three-foot frame is the analytical horsepower of a mainframe external computer, floppy disk data storage center, and totally preprogrammed and interfaced software systems.



Besides drastically reducing space requirements, the Microlab 620 also slashes cost, lab work time and training requirements.

The more you use the Microlab, the more powerful it becomes. It can analyze, code and store a virtually unlimited number of spectra for qualitative comparison. It does sample identification without the need for separation. Plus, the Microlab memorizes and recalls at the push of a button a virtually unlimited number of quantitative protocols.

No matter what your area of analysis or range of applications, the Microlab's spectral library can be personalized to meet your lab's needs.

The Microlab also features multiple data output, fully automatic operation, repetitive scan and a whole lot more.

So if you think unlimited analytical capability requires unlimited space, money and time, think again. Then call your local Beckman representative for the full story on the Microlab 620 MX. Or write: Scientific Instruments Division, Beckman Instruments, Inc., P.O. Box C-19600, Irvine, CA 92713.

Innovation in IR since 1940

BECKMAN

CIRCLE 27 ON READER SERVICE CARD

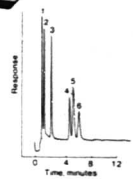
Nitrosamine Analysis

The importance of nitrosamine analysis is well known. Present methods call for a large capital investment for this analysis. For under $9,000, Tracor offers a quick, accurate and precise nitrosamine determination of subnanogram levels by chromatography.

Gas Chromatography



The Tracor 560 Gas Chromatograph equipped with the new HALL® 700A Electrolytic Conductivity Detector will detect subnanogram levels of nitrosamines selectively in the nitrogen mode. The Tracor 560/700A combination is small and compact and incorporates modern digital electronics. Not only does the Tracor 560/700A detect nitrosamine at the subnanogram level, but it also is capable of providing selective detection of halogenated and sulfur containing compounds to the same degree of accuracy and precision.



CONDITIONS

Instrument	Tracor 560/ HALL® 700A
Column	5%C-20M 80/100 Chromosorb W-HP
Column Temp.	130°C
Carrier	He at 25ml/min
Reactor	800°C
Reaction Gas	H_2 at 70ml/min
Solvent	50% n-Propanol
Attenuation	100 x 2
Sample	1ng each

No.	Peak Identity
1	N-nitrosodimethylamine
2	N-nitrosodiethylamine
3	N-nitrosodipropylamine
4	N-nitrosodibutylamine
5	N-nitrosopiperidine
6	N-nitrosopyrrolidine

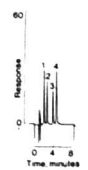
CIRCLE 204 ON READER SERVICE CARD

Liquid Chromatography



The Tracor Model 900-965 Liquid Chromatograph also enables selective detection of nitrosamines using the Tracor 950 pump, 970A Variable Wavelength Detector and the new Tracor 965 Photo-conductivity Detector. In the 965 detector the weak nitrosamine bond is readily photodegraded to form a highly conductive species which is detected by the differential conductivity cell.

CIRCLE 205 ON READER SERVICE CARD

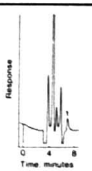


CONDITIONS

Instrument	Tracor 965*
Column	Spherisorb ODS 5µm 4.6 mm x 25 cm
Solvent	ACN:MeOH:H_2O 15:10:75
Flow	1.5ml/min
Temp.	Ambient
Attenuation	10 x 50
Source	254nm Mercury Lamp
Sample	10 ng each

*Patent Pending

No.	Peak Identity
1	N-Nitrosodimethylamine
2	1-Nitrosopyrrolidine
3	N-Nitrosodiethylamine
4	1-Nitrosopiperidine



CONDITIONS

Instrument	Tracor 950/965
Column	Zorbax CN 5µ 4.6mm x 25cm
Solvent	ISO/IPA:MeOH
Flow	85cc/min
Temp.	Ambient
Attenuation	1 x 5
Sample	1ng each
Source	254nm Hg lamp
Sample	155 pg

No.	Peak Identity
1	Diethanolnitrosamine



CONDITIONS

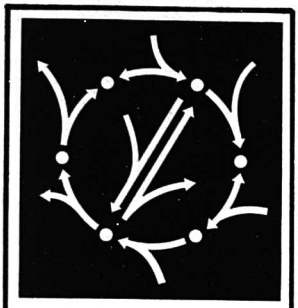
Instrument	Tracor 965*
Column	Spherisorb ODS 5 µm 4.6 mm x 25 cm
Solvent	ACN:MeOH:H_2O 65/10/25
Flow	1.5 ml/min
Temp.	Ambient
Attenuation	10 x 50
Source	254 nm Mercury Lamp
Sample	5 ng each

*Patent Pending

No.	Peak Identity
1	N-Nitrosodipropylamine
2	N-Nitrosodibutylamine
3	N-Nitrosodicyclohexylamine

Tracor Instruments

Tracor, Inc. 6500 Tracor Lane Austin, Texas 78721 Telephone 512:926 2800 TELEX 77-6414



Drug Metabolism Concepts

ACS Symposium Series No. 44

Donald M. Jerina, *Editor*
The National Institutes of Health

A symposium co-sponsored by the Division of Medicinal Chemistry and the Division of Analytical Chemistry of the American Chemical Society.

Eight chapters present in-depth research reports on the role of enzyme systems, especially cytochrome P-450, in drug activation and detoxification. This timely study on drug metabolic pathways is vital because of the possibilities of toxic or carcinogenic intermediates caused by the action of enzymes on drugs and anesthetics.

CONTENTS

Cytochrome P-450 in Oxygen Activation for Drug Metabolism • Synthetic Models for the Reaction Stages of Cytochrome P-450 • Isolation of Mutliple Forms of Liver Microsomal Cytochrome P-450 • Resolution of Multiple Forms of Rabbit Liver Cytochrome P-450 • Enantiomeric Selectivity and Perturbation of Product Ratios as Methods for Studying the Multiplicity of Microsomal Enzymes • Purified Cytochrome P-448 and Epoxide Hydrase in the Activation and Detoxification of Benzo[a]pyrene • In vitro Reactions of the Diastereomeric 9,10-Epoxides of (+) and (−)-*trans*-7,8-Dihydroxy-7,8-dihydrobenzo[a]pyrene with Polyguanylic Acid • Metabolic Activation in Chemical-Induced Tissue Injury

196 pages (1977) clothbound $15.50
LC 77-2279 ISBN 0-8412-0370-9

SIS/American Chemical Society
1155 16th St., N.W./Wash., D.C. 20036

Please send _____ copies of *SS 44 Drug Metabolism Concepts* at $15.50 per copy.

☐ Check enclosed for $ _____. ☐ Bill me. Postpaid in U.S. and Canada, plus 40 cents elsewhere.

Name

Address

City State Zip

News

15–16. D. H. Freeman. $250, ACS members; $300, nonmembers

Laboratory Automation: Micro-, Mini-, or Midicomputers?
Philadelphia (FACSS Meeting). Sept. 15–16. R. E. Dessy and the Chemistry Dept. Instrument and Design Group of VPI&SU. $225, ACS members; $265, nonmembers

Gas Chromatography
Los Angeles. Mar. 19–21. $225. *Contact:* C. D. West, Dept. of Chemistry, Occidental College, Los Angeles, Calif. 90041. 213-259-2762

Advances in Polymer Synthesis, Modification, and Characterization
State University of New York. June 4–8. J. P. Kennedy. *Contact:* Angelos V. Patsis, Chairman, Dept. of Chemistry, State University of New York at New Paltz, New Paltz, N.Y. 12562. 914-257-2175

Atomic Absorption
Los Angeles. June 11–13. $225. *Contact:* C. D. West, Dept. of Chemistry, Occidental College, Los Angeles, Calif. 90041. 213-259-2762

Liquid Chromatography
Los Angeles. June 18–20. $225. *Contact:* C. D. West, Dept. of Chemistry, Occidental College, Los Angeles, Calif. 90041. 213-259-2762

Scanning Electron Microscopy and X-Ray Microanalysis
Bethlehem, Pa. June 25–29. J. I. Goldstein. $495. *Contact:* J. I. Goldstein, Metallurgy and Materials Engineering Dept., Whitaker Lab No. 5, Lehigh University, Bethlehem, Pa. 18105. 215-691-7000, ext. 672

Design and Analysis of Scientific Experiments
MIT. June 25–30. Harold Freeman and Paul Berger. *Contact:* Director of the Summer Session, Rm. E19-356, Massachusetts Institute of Technology, Cambridge, Mass. 02139

Applied Molecular Spectroscopy: Infrared, Raman, and Ultraviolet
Arizona State University. July 23–27. $300. *Contact:* Jacob Fuchs, Director, Modern Industrial Spectroscopy, Dept. of Chemistry, Arizona State University, Tempe, Ariz. 85281

Interpretation of Gas Chromatographic Mass Spectrometric Data: Environmental Applications
MIT. Aug. 6–10. R. A. Hites. *Contact:* Director of the Summer Session, Rm. E19-356, Massachusetts Institute of Technology, Cambridge, Mass. 02139

Modern Industrial Spectroscopy
Arizona State University. Aug. 6–17. $600. *Contact:* Jacob Fuchs, Director, Modern Industrial Spectroscopy, Dept. of Chemistry, Arizona State University, Tempe, Ariz. 85281

For Your Information

An air monitoring instrumentation training seminar will be jointly offered by EPA and Beckman Instruments to government agencies and private industries within the southern states March 13–16 at the Russell Research Center in Athens, Ga. Theory, operation, calibration, and maintenance of EPA-designated Beckman air monitors for SO_2, O_3, CO, and NO_2 will be discussed. For further information, interested government agencies should call Jerry Burger, EPA, at 404-546-3197; private industries are asked to contact Larry Swink, Beckman Instruments, Inc., Norcross, Ga., or call 404-449-9009.

Scott Specialty Gases, a division of Scott Environmental Technology, Inc., is offering its Collaborative Cross Reference Services for gas analysis. Gases checked for quality control include: methane, propane, butane, carbon monoxide, carbon dioxide, oxygen, benzene, and nitric oxide. The subscriber analyzes the sample, reports the results back to Scott who compares all results, and provides statistical data showing the interlaboratory comparisons to each subscriber. For more information, contact: Sally R. Michener, Scott Specialty Gases, Rte. 611, Plumsteadville, Pa. 18949, or call 215-766-8861.

Gelman Instrument Co., a multinational firm manufacturing health, filtration, and environmental products, has officially announced a new name, **Gelman Sciences, Inc.** The new name reflects the expanded growth and progress of the company's products range.

Information Handling Services of Denver, Colo., is offering a computer-indexed information retrieval system of major U.S. industrial manufacturers' products called Master Catalog. For more information, contact: Information Handling Services, 15 Inverness Way East, Englewood, Colo. 80150.

Selection guide to

Swagelok® QUICK-CONNECTS

. . . the easy way to add versatility to your gas and fluid systems

- Reliable, leak-free service with vacuum or pressure
- Fast operation—no twisting
- Combinations of body and stem assemblies to suit your system requirements
- 360° swivel action
- Pressure ratings to 10,000 psi
- Brass and 316SS in sizes from 1/16" to 1" tubing or pipe connections
- Available from local distributor stocks

CRAWFORD FITTING COMPANY

29500 Solon Road, Solon, Ohio 44139
Crawford Fittings (Canada), Ltd., Ontario

MINIATURE "QM" SERIES

Finger-tip operation, low dead space, 1/16" male and female NPT, 1/16" and 1/8" tube connections.



STEMS









BODIES



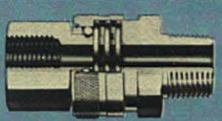




Patented

FULL FLOW "QF" SERIES

No orifice restrictions, 1/4" to 1" male and female pipe ends or tube connections.



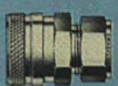
STEMS







BODIES







Patented

STANDARD "QC" SERIES

All stems available in single end or double end shut off, 1/8" to 1/2" sizes.



STEMS















BODIES













Patented

ACCESSORIES Special devices are available to prevent damage or contamination in the disconnected position.







"KEYED QC" SERIES

"Keyed" and color coded *(positive mechanical lockout system)* to prevent unmatched stems and bodies from coupling, eliminating accidental mixing of gases and fluids in multi-line systems. Eight different "Keys" available.



Patented

© 1978 Markad Service Co. / all rights reserved C-51

CIRCLE 32 ON READER SERVICE CARD



TAKING THE WRAPS OFF A NEW SERIES OF GILFORD RESEARCH INSTRUMENTATION PACKAGES.

For you who were waiting, NOW is that "better time."

In a day when everything except the dollar is going up, you have the opportunity to acquire a complete Gilford system at yesterday's prices. Eight Gilford Research Instrumentation Packages with dozens of applications and a performance-to-price ratio that translates to real value in today's economy.

An example? Our Wavelength Scanning/Kinetic System, at a price that was good last year, and which is even a better bargain today. The ideal instrumentation package for the researcher who recognizes the value of high sensitivity and a 3A range in enzyme kinetics, and who also requires high-resolution wavelength scanning.

You get the same performance/value in all the new Gilford Research Instrumentation Packages. There are two systems for wavelength scanning, others for kinetic assays. Yet another for automatic sample processing with an aspirating cuvette. And a system for scanning 20cm gels, as well as one which uses precise thermoelectric heating and cooling for DNA thermal denaturation - renaturation assays of exceptional quality.

Find out how these systems can benefit your research. Our instrumentation packages make it convenient. And accurate. And reliable. Our prices make it a pleasure.

Gilford Research Spectrophotometers:
Every job easier, every result more accurate.

CIRCLE 85 ON READER SERVICE CARD

gilford® INSTRUMENT

Oberlin, Ohio 44074
(216) 774-1041 Telex: 98-0456
Paris (Evry 91), France
Düsseldorf, W. Germany
Teddington, Middx., England





CIRCLE 96 ON READER SERVICE CARD

DO YOUR OWN THING with the

SPEX

FLUOROLOG/FLUOROCOMP

SPECTROFLUOROMETER SYSTEMS FOR FRONTIER RESEARCH

VERSATILE

. . large, removable compartment for all samples
. . interchangeable sources and detectors
. . modular and updatable

RELIABLE

. . two SPEX DOUBLEMATE monochromators reject stray light, maximize S/N
. . the unequalled response of photon counting

DIGITAL

. . the accuracy of box-car integration
. . interfaced for data processing and programmed control

SPEX INDUSTRIES, INC.
P.O. BOX 798 METUCHEN, N.J. 08840 (201) 549-7144

CIRCLE 191 ON READER SERVICE CARD

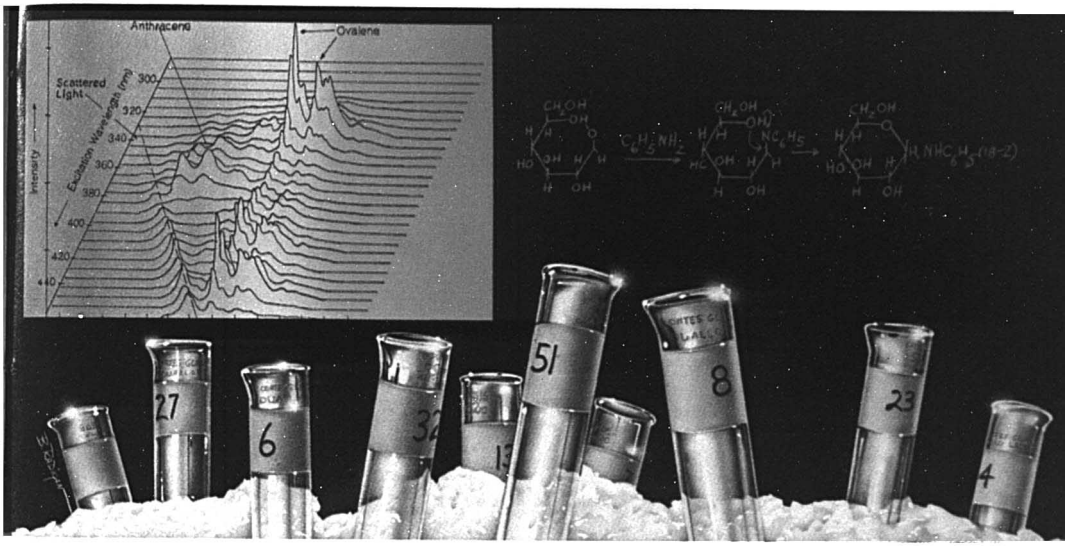
YOUR "READER SURVEY" VIEWS ARE VITAL

Analytical Chemistry occasionally presents a Reader Survey section that provides you with an opportunity to indicate your interests and activities. Your answers help us in planning editorial material that will be useful to you in your work.

To express your Reader Survey views, simply circle your answers on one of these adjacent reply cards and drop it in the mail. No postage is required.

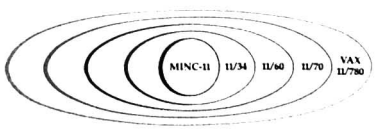


Total lab automation: Only Digital can help you every step of the way.



Big chemical labs have big computer requirements. And small requirements, and everything in between. Which is precisely why so many of them count on Digital as they plan their automation.

Digital is the only computer company with a complete line of compatible systems that spans the range from small interactive MINC-11's, which can be literally rolled from bench to bench, right up to powerful PDP-11/70's and VAX-11/780's for large scale computation and data base management.



The DECLAB Family Computers For The Laboratory.

You can choose Digital systems for the little jobs like data acquisition, and the big jobs like simulation and analysis. And with Digital's uniquely compatible software and advanced networking capability, these systems can be hooked to each other and even to the control systems in your processing plants to make your computer dollars work harder at every step.

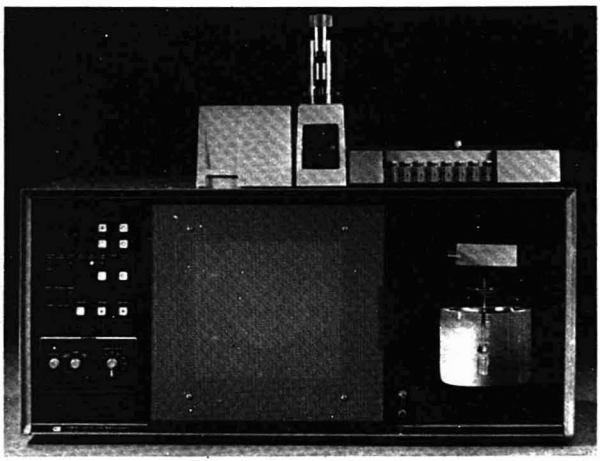
Call your local Digital sales office and find out why the largest chemical companies in the world choose Digital. Or write Digital Equipment Corporation, Laboratory Data Products, MR2-4/M16, One Iron Way, Marlborough, Massachusetts 01752. European headquarters: 12, av. des Morgines, 1213 Petit-Lancy/Geneva. In Canada: Digital Equipment of Canada, Ltd.

See us at booth 1017-1020 at the Pittsburgh Conference. March 5 through March 8.

digital

CIRCLE 48 ON READER SERVICE CARD

New Products



HP 1081B liquid chromatograph, designed for industrial control, incorporates many of the components used in the HP 1084A microprocessor-based liquid chromatograph. The components include pump, injector, column, detector, solvent reservoir, and microprocessor. The chromatograph's solvent flow system is based on a single-head reciprocating diaphragm pump that is adjusted automatically until the desired flow rate is reached. Samples are detected with an optional UV detector that has a fixed wavelength of 254 nm. Other detectors can be accommodated. The 1081B offers a choice of either a 6-port valve injector or a variable-volume injector which injects preset sample volumes between 10–200 μL. An optional automatic sampling system can analyze batches of up to 60 samples in sequence or in replicate. Price is under $8000. Hewlett-Packard **402**

Pumping System for HPLC

Model 750 solvent delivery system is a dual-piston reciprocating design that incorporates a hypercompensated cam and electronic flow multiplexing synchronization to achieve typical flow precision better than ±0.50% at flows from 0 to 20 mL/min and pressures to 6000 psi. The absence of pulse dampeners provides a reduction in total system volume. Micromeritics Instrument Corp. **413**

UV Monitor

Uvicord S UV monitor can monitor at 206, 254, and 280 nm simultaneously at two sensitivities ranging from 0.005 to 2 AUFS. The temperature-stabilized nonelectrode gas discharge lamp, rated at 3 W and guaranteed for 6000 h, gives higher intensity at 206 nm than deuterium lamps. The performance of the monitor is unaffected by temperature over the range 0–30 °C. Price is $2295. LKB Instruments Inc. **414**

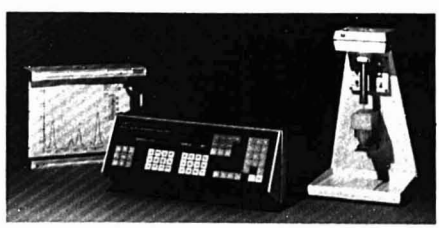
ICP Plasma Spectrometer

Model 1160 inductively coupled argon plasma AtomComp spectrometer operates by a PDP-11/34-based spectrochemical controller system. User controls entire analysis through an LA36 DEC writer, and results are printed out directly in concentration. Maximum memory is 128K MOS; standard system is configured at 32K. A variety of available options include multipoint automatic background correction, variable wavelength channel, spectrum scanning, storage and retrieval, and statistics. Jarrell-Ash Division, Fisher Scientific Co. **411**

Data System for IR Spectrometers

SP 2080 data conversion unit offers coaddition of spectra improving the signal-to-noise ratio, spectral subtraction removing unwanted components of a spectra, storage of a sequence of commands with associated parameter changes for later use as a single command, and a program for printing the peak position and transmittance for all absorption bands above a defined level. The data conversion unit communicates between the SP 2000 or SP 4000 IR spectrometers and a Hewlett-Packard desk-top "conversational" calculator. The collection and replotting of data are controlled by the calculator, and the company's software enables commands/parameters to be entered on the calculator's standard typewriter keyboard using conversational English. Pye Unicam Ltd., Cambridge, England **418**

For more information on listed items, circle the appropriate numbers on one of our Readers' Service Cards



Model 384-1 polarographic analyzer system incorporates a 40-character alphanumeric display for communication with the user, a floppy disk for software, curve and method storage and recall, a touch panel for operating controls, a static mercury drop electrode for both polarography and stripping voltammetry, and a digital plotter. The instrument is fully autoranging over the sensitivity range 10 nA to 1000 μA full scale. As many as nine different peaks can be accommodated in each scan, and sample peaks are quantitated by use of an automatic calculation routine incorporating the best polynomial fit to 1, 2, or 3 standards. Princeton Applied Research Corp. **406**

Flight cancelled.



When the stars come out in Mexico, and other parts of Latin America, hordes of vampire bats do also. These bats (Desmodus rotundus) have been attacking cattle, bleeding them and acting as dangerous vectors of paralytic rabies.

The cattle ranchers, suffering losses of $350 million a year in meat and milk production, saw their livelihoods at stake. And while Count Dracula may have been kept in his place by a wooden stake, the ranchers needed a better solution.

The U.S. Agency for International Development (AID) funded U.S. Fish and Wildlife Service scientists who devised a control method. An anticoagulant solution, diphenadione, based on a Kodak intermediate, was developed by a chemical firm. It is smeared on vampire bats after they are trapped in nets. The bats, grooming each other, ingest it and die as they live—by bleeding. The purpose is not to eradicate the species, but to control them. Since other bat species do not associate with vampire bats, this method selectively controls only Desmodus rotundus, and only in those areas where they pose a threat to domestic livestock and human needs.

It's just one of the many creative uses of chemistry we've seen since 1918, when Kodak founded America's first industrial research laboratory to supply laboratories with organic chemicals.

Through a nationwide network of dealers, you can meet an enormous range of challenges with a choice of thousands of Kodak lab chemicals—available whenever and wherever needed. Just call your dealer for a fast response.

To learn more about the cancelled flight of vampires, write: Dept. 412L, Eastman Organic Chemicals, Eastman Kodak Company, Rochester, NY 14650.

For the creative chemist.

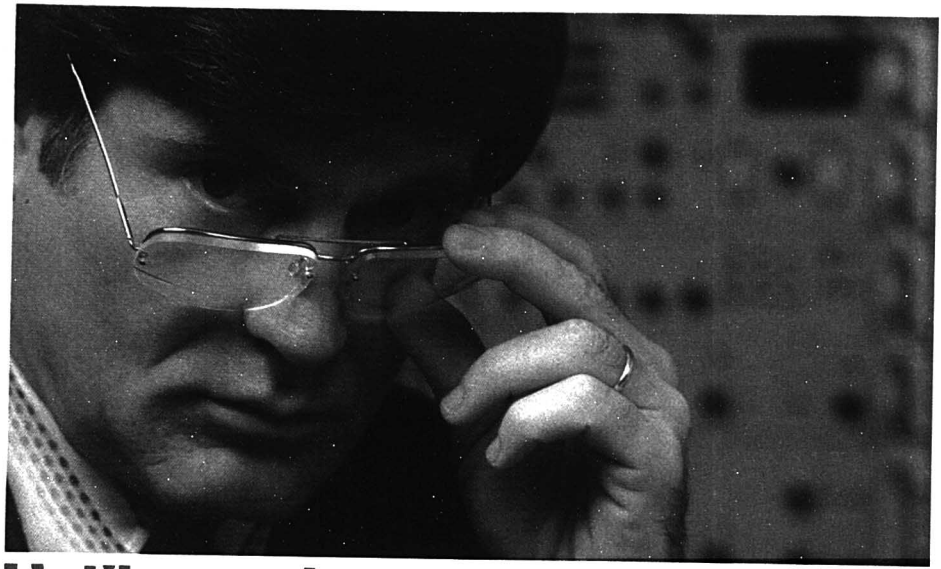
Kodak

Dealers handling EASTMAN Organic Chemicals: American Scientific & Chemical; Bioclinical Laboratories; Brand-Nu Laboratories, Inc.; Bryant Laboratory, Inc.; CAMX Scientific; Custom Chemical Laboratories, Inc.; Fisher Scientific; GAC Laboratories, Inc.; Labproducts, Inc.; Midland Scientific, Inc.; North-Strong, Inc.; Preiser Scientific; Sargent-Welch; Scientific Products; Scientific & Industrial Sales & Service, Inc.; VWR Scientific Inc.; Ward's Natural Science Establishment, Inc.

CIRCLE 63 ON READER SERVICE CARD

* Eastman Kodak Company, 1978

We can't really show off Inficon's versatile surface analysis system.



Until you show up with a sample for comparative analysis.

The best way to demonstrate Inficon's LHS-10 surface analysis system is by direct application. So bring in any vacuum compatible sample—give us two weeks' notice, please—and we'll analyze it.

And we'll prove ours is the simplest, most cost-effective system for your surface analyses.

Whatever your analytical problem, the LHS-10 will help you obtain more complete surface characterizations, correlate data faster, and reach firmer experimental conclusions.

LHS-10's universal analysis chamber allows customizing to your exact needs—whether it's catalyst efficiency testing, elemental or quantitative analysis, trace detection, depth profiling, or chemical fingerprinting.

You can have ESCA (XPS), UPS, AES, SAM, SIMS, ISS modules now, or add any later at minimal cost. Even add a computer system for simultaneous instrument operation and data manipulation.

No matter what techniques you select for present or future use, all can be employed on the same sample area—without specimen manipulation—for rapid sample analysis.

For now, let the other surface analysis companies first demonstrate their capabilities—then let Inficon give you proof positive of the LHS-10's superior performance, versatility and simplicity.

Write or call today. We'd like to see you and your sample soon.

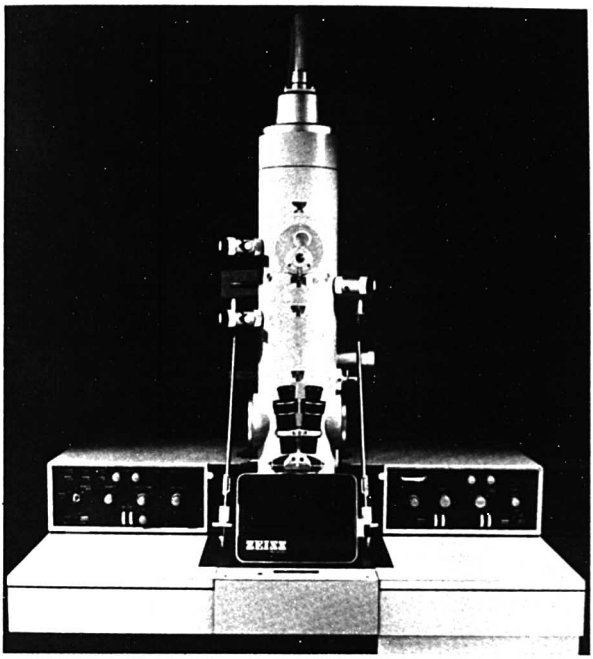
We also offer contract surface analysis and assistance with special problems.



The plexiglas model of our universal chamber clearly shows our versatile analysis techniques.

INFICON
LEYBOLD-HERAEUS
6500 Fly Road, East Syracuse, New York 13057
315/437-0377 ■ TWX 710 541-0594

CIRCLE 89 ON READER SERVICE CARD



EM 109 electron microscope covers a magnification range from a low 150X to 400 000X with a resolution of 3.44 Å. It operates on accelerating voltages of 50 and 80 kV and has a double condenser system as well as a 4-lens imaging system. The electron microscope offers Trans-Fiber photography, a camera system totally outside the vacuum, which includes a high-resolution fiber plate coated with a polycrystal fluorescent screen; Micro-Dose focusing, an automatic focusing system for maximum specimen protection, which allows the specimen area to be selected at low intensity; and the Ion-Getter-Pumping vacuum system, which provides ultraclean specimen conditions. Model EM 109R is offered with a simplified pump system but with the same electron optical features as the EM 109. Carl Zeiss, Inc. **405**

Fluorescence Decay Time Spectrometer

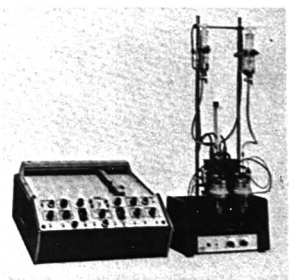
EI 199 fluorescence decay time spectrometer consists of three subsystems available separately or as an integrated system—the nanosecond spectrometer, digital data acquisition, and a data processing microcomputer. Based on the PDP 11/01 microcomputer with dual floppy discs and 32K bytes of main memory, the spectrometry software package includes display of spectra, relative quantum yield calculation, spectral response correction, peak detection, spectrum differentiation and multiple region of interest integration for time-resolved and fluorescence spectrometry. The nanosecond spectrometer subsystem consists of thyratron-gated flash lamp and control electronics, vacuum pump and gas handling system, excitation and fluorescence monochromator, sample chamber, matched wide aperture coupling optics, and high-gain photomultiplier detector. The data acquisition subsystem, which includes a 1024 multichannel analyzer with CRT display, measures decay times using signals from synchronization and main photomultipliers. The data processing microcomputer, based on the DEC PDP 11/03, is supplied with a complete library, MCA communication software, the DEC RT-11 package, and a Fortran IV compiler. Boston Electronics Corp. **412**

Data Acquisition System

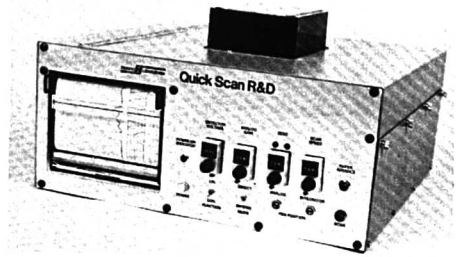
FI 7252C data acquisition system with data reduction capability contains 10 low-level inputs for thermocouples, RTD, strain gages or any millivolt signal, a 5½-digit full-function DMM with a reading rate of 12 samples/s, a scanner/mainframe with capacity for 13 extra input/output cards, 80-column 320-character/s printer, and a computer. The computer features a 9-in. CRT that can display sixteen 64-character lines and/or bar graphs and quasi-graphics, a 42K BASIC interpreter ROM, 8K RAM (expandable to 32K), and a 89K minidiskette (expandable to 178K). Price is $15 200. FI Electronics **410**

Balances

Three electronic balances, Models 300, 1500, and 1500D, feature a stability indicator, a red "g" next to the weight readout that lights up to signal when the display is steady. The model designations indicate the weight capacities in grams; the 1500D has a dual-range capability to switch from a 1500 × 0.1 g range to 150 × 0.01 g range. Tare measurements go to the full limit of the balance's capacity by subtraction. Optional BCD outputs permit interfacing with printers, calculators, and computers. Basic prices of the models are $1195, $1395, and $1595, respectively. Ohaus Scale Corp. **415**



Model 472 multipolarographic analyzer, fitted with a sequencer to perform automatic stripping voltammetry, provides front panel control over the scanning mode allowing the selection from ramp, triangle, pulsed ramp, and pulsed triangle. Other panel controls include preset electrolysis delay selectable from 0 to 300 s, initial and sweep amplitude voltages accurate to 1 mV within the range ±5 V, and current range preset from 10 nA to 10 mA. Model 472 includes a X-Y recorder that supplies 100 mV f.s. for the Y-axis and the same scanning voltage supplied to the polarographic cell for the X-axis. Model 472 W/R is offered without the recorder. ECO Inc. **403**



Quick Scan R&D densitometer is capable of scanning cellulose acetate, acrylamide gels and tubes, agarose, starch gels, TLC plates (up to 20 × 20 cm), and X-ray diffraction patterns. Features include scanning capabilities throughout the visible range as well as 254 and 280 nm; variable focus high-resolution optics; fluorescent scanning with excitation at 254, 280, or broad band at 360 nm; measurement of fluorescent quenching; and three manually changeable slits with option of any size up to 1 cm. Helena Laboratories **404**

MS Leak Detector

Model 936-40 helium mass spectrometer leak detector requires no liquid nitrogen, handles high gas loads, and measures gross leaks without the need for throttling. Helium can be detected to at least the mid 10^{-10} atm mL/s range when the system is used with a 5-CFM mechanical pump. Response time for helium is 2 s. Price is $6690. Varian **416**

Balance Accessory

GC 301 application input device, available as a plug-in attachment for the company's top-loading series balances, programs a balance for counting small parts, determines weight changes in percent and in grams, determines net totals, and enters negative reference values for serial weighings to zero. Price is $225. Mettler Instrument Corp. **419**

Fluorine Compounds

Brochure lists over 200 fluorine compounds including fluorinating reagents, ion implantation gases, Fluorographite polymers, fluorosilvers, epoxy catalysts, and fluorine compounds with catalytic applications. Ozark-Mahoning Co. **442**



EDAX 9100 energy-dispersive X-ray analysis system comprises a lithium drifted silicon detector that fits to the microscope column, a multichannel analyzer to process and store pulses from the excited sample, a computer for data processing and system control, a VDU input/output device, and a dual floppy disc drive for program and data storage. The analyzer can interface with any type of scanning or transmission microscope or microprobe to provide fast simultaneous identification or measurement of the elements present in a sample. Notable features include a centralized interlocking bus structure and the dynastatic display in which spectral peaks are automatically maintained at constant height on the video screen while the digital scale indicator increases with measuring time. N.V. Philips Gloeilampenfabrieken, Eindhoven, The Netherlands **401**

Strip Chart Recorder

Series 4900 strip chart recorders offer 280 chart speeds ranging from 0 to 40 in./min or per hour and 1–100 cm/min or per hour and 14 calibrated input sensitivity ranges with overlapping variable control. The recorders use a noncontacting rotary capacitance transducer as the feedback or rebalance element for pen positioning. Accuracy is ±0.25%, and linearity is ±0.2% of full scale. Houston Instrument Division, Bausch & Lomb **420**

Reagent System for Water Analysis

SpectroKit portable reagent systems are modular and come complete with chemicals, instructions, and hardware for the test to be performed. Chemistry is precalibrated, and scale overlays and standard curves are provided for the company's Mini 20 and Spectronic 20 spectrophotometers. Cross-contamination between tests is avoided by supplying separate reaction vessels, cuvettes, and captive spoons with each kit. Bausch & Lomb **446**

pH Meter

Model 750 pH/ion meter features infinite slope correction and temperature compensation. All operating parameters are entered from a calculator-type keyboard; pH, mV, solution temperature, and concentration are displayed on a 5-digit LED. Ion concentrations are directly determined or by incremental addition or subtraction of either sample or standard. Fisher Scientific Co. **421**

Fluorescence-Yielding Substrate for Phosphatases

Flavone-3-diphosphate triammonium salt is a stable and sensitive enzyme substrate for acid and alkaline phosphatase. The enzymatic cleavage of the diphosphate group liberates 3-hydroxyflavone, which can be assayed by direct absorption at 410 nm or fluorometrically at 510 nm. Chemical Dynamics Corp. **444**

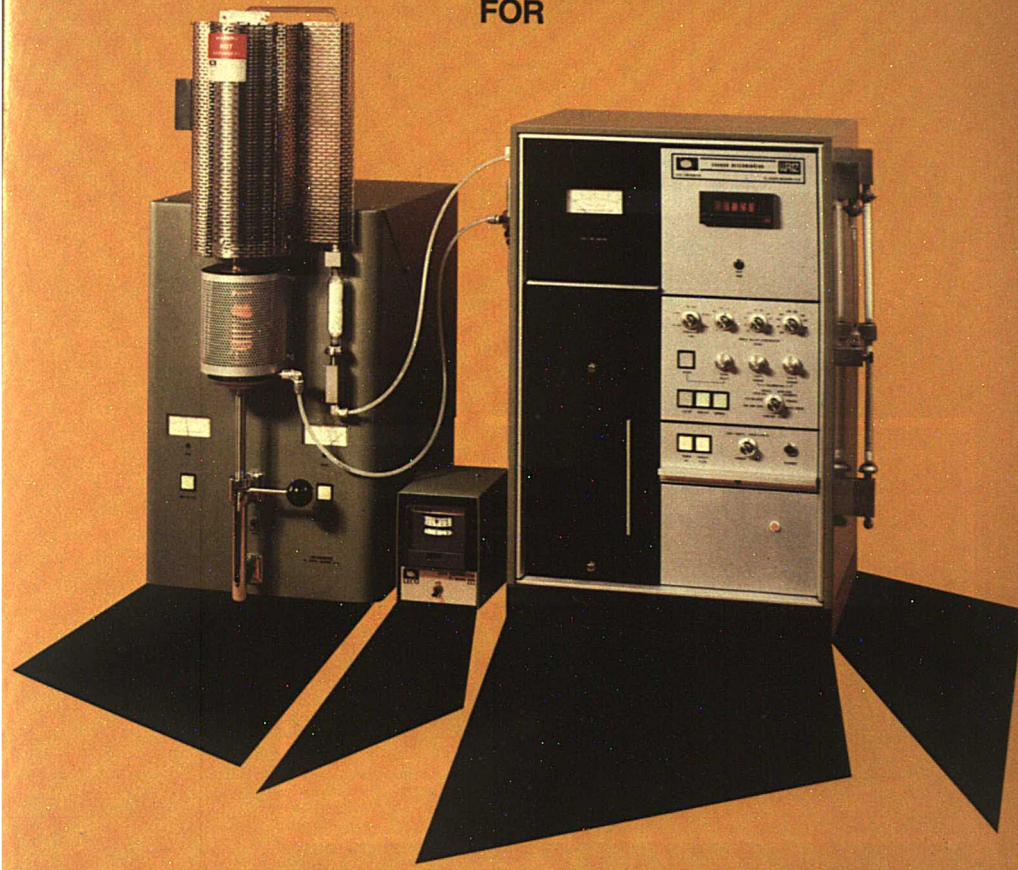
Chemicals

Ninhydrin Reagent Kit

Ready-Nin contains an instrument-ready bottle of premixed methyl cellosolve/sodium acetate buffer and packages of premeasured ninhydrin and stannous chloride. Beckman Instruments, Inc. **443**

For more information on listed items, circle the appropriate numbers on one of our Readers' Service Cards

LECO® DC-12 DUO CARB DETERMINATOR FOR



Organic & Inorganic Carbon in Organic Materials such as:

- Shales
- Soil
- Limestone

Contact LECO Today!

LECO CORPORATION 3000 Lakeview Ave. St. Joseph, MI 49085, U.S.A. Phone: (616) 983-5531

LECO®

CIRCLE 125 ON READER SERVICE CARD

Each one is an original.

The new Sargent-Welch Series 6 UV/VIS spectrophotometers are designed to outperform. Because each one has an original blazed holographic grating—not a replica—for the highest optical performance. Reduces stray light to less than 0.02% at 220 nm.

There's no best way to present data. So we offer both meter scale and digital display models. All present unambiguous results in transmission, absorbance or concentration.

Color-coded controls and indicators for source and detector make these instruments the easiest to use. Wavelength is quickly set, digitally displayed. Other controls are simple, too.

Measures up more ways!
Wide wavelength range—UV/VIS from 195 to 1000 nm; VIS from 325 to 1000 nm—and accessory options make these spectrophotometers suitable for any laboratory. The sample compartment has a universal cell holder for macro- and microcells. Accessories include a rapid-sampling autocell, manual or automatic cell changers, special data systems and more.

Keeps working harder, longer.
Every Series 6 single beam spectrophotometer is built to take heavy use in stride. Monochromators are sealed against dust, corrosion; mirrors and gratings have a hard, protective silica coating. All components are performance-proven for more reliability, less downtime.



Apart from the ordinary... yet sensibly priced. The kind of instrumentation you've come to expect from Sargent-Welch.

To see an original Series 6, contact your Sargent-Welch representative today!

SARGENT-WELCH SCIENTIFIC CO.

7300 NORTH LINDER AVENUE. P.O. BOX 1026. SKOKIE, ILLINOIS 60077

We're instrumental in your laboratory!

CIRCLE 195 ON READER SERVICE CARD

Anaheim, Baton Rouge, Birmingham, Cincinnati, Cleveland, Dallas, Denver, Detroit, Skokie, Springfield, NJ, Washington, D.C.

© 1979 Sargent-Welch Scientific Company

NEW!

CUSTOM PACKED HPLC COLUMNS



OUR HPLC COLUMNS ARE INDIVIDUALLY TESTED BY COMPUTER & ARE SUPPLIED WITH A SAMPLE OF THE TEST MIXTURE & THE ACTUAL CHROMATOGRAM....

ALL THIS AND YOU SAVE $ TOO!

WRITE FOR OUR LATEST CATALOG..

ALLTECH ASSOCIATES

202 CAMPUS DR./ARLINGTON HEIGHTS, ILLINOIS 60004
312/392-2670

CIRCLE 4 ON READER SERVICE CARD



PRA's high intensity pulsed light sources.

The PRA 610 microsecond pulsed light sources offer maximum versatility for applications requiring high ultraviolet intensities.

- Discharge energy per pulse to 100 joules
- Repetition rate 1 to 100 pps
- Spectral range 200 nm to 1200 nm with peak intensities in UV
- Various pulse widths 1.5-50 μ sec.
- Non magnetic lens aperture for ESR/NMR applications
- Carefully designed for minimized RFI

PRA manufactures pulsed light sources with a variety of pulse widths and discharge energies and has people with broad experience in optical systems design to advise you.

PRA **Photochemical Research Associates Inc.**
45 Meg Drive, London, Ontario
Canada N6E 2V2
(519) 686-2950 Telex 064-7597

CIRCLE 170 ON READER SERVICE CARD

Algorithms for Chemical Computations



This multidisciplinary collection of state-of-the-art papers assesses significant developments in algorithms for several important areas of chemistry and pinpoints places where currently available algorithms are inadequate.

ACS Symposium Series No. 46

Ralph E. Christoffersen, *Editor, The University of Kansas*

A symposium sponsored by the Division of Computers in Chemistry of the American Chemical Society.

Leading experts not only evaluate the tremendous opportunities for progress in chemical research that algorithms provide but also analyze the substantial difficulties that algorithms may present.

CONTENTS

Graph Algorithms in Chemical Computation • Algorithm Design in Computational Quantum Chemistry • Rational Selection of Algorithms for Molecular Scattering Calculations • Molecular Dynamics and Transition State Theory • Newer Computing Techniques for Molecular Structure Studies by X-ray Crystallography • Algorithms in the Computer Handling of Chemical Information

151 pages (1977) Clothbound $12.75
LC 77-5030 ISBN 0-8412-0371-7

SIS/American Chemical Society
1155 16th St., N.W./Wash., D.C. 20036

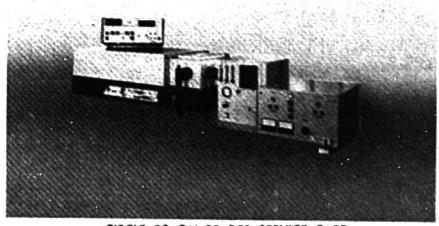
SEQUENTIAL PLASMA SPECTROANALYZER

Better than AA, the JY-38 high resolution spectroanalyzer, using an Inductively Coupled Plasma, offers unequaled speed, sensitivity and accuracy. Most elements, including B and P, can be analyzed in such materials as metals, alloys, coal, oils, rare earths, soils, ores, water pollutants, pharmaceuticals and biologicals.

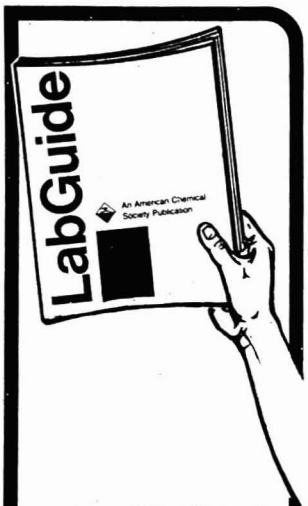
Advantages include holographic gratings permitting high accuracy. Repeatability in excess of 1%, dynamic range of 10^5 down to nanogram/ml. Send today for the details on the JY-38 and our JY-48 Simultaneous Spectroanalyzer.

Instruments SA, Inc., J-Y Optical Systems Division, 173 Essex Avenue, Metuchen, N.J. 08840. (201) 494-8660. Telex 844-516. In Europe, Jobin Yvon, Division d'Instruments SA, 16-18 Rue du Canal, 91160 Longjumeau, France. Tel. 909.34.93 Telex JOBYVON 842-692882.

JOBIN YVON **Instruments SA, Inc.**
J-Y Optical Systems Division



CIRCLE 90 ON READER SERVICE CARD



MOST USED

...because it's most useful.

The annual ACS **LabGuide** is the definitive directory to scientific instruments, equipment, chemicals, services, books, trade names, manufacturers and their sales offices.

It leads all others in editorial pages, in advertising pages, and in reader usage: **more than 70,000 inquiries every year.**

Manufacturers' Literature

Photoionization Detector. Applications of the high-temperature photoionization detector in gas chromatography are described. Analytical data including column conditions, sample size, and detection limits are included. Characteristics of the detector, principle of operation, its response to a wide range of organic and inorganic compounds, and electrometer/power supply characteristics are also given. 12 pp. HNU Systems, Inc. **450**

Cellosize Hydroxyethyl Cellulose (HEC). Cellosize HEC is used to thicken, suspend, bind, emulsify, form films, stabilize, disperse, retain water, or provide protective colloid action. A booklet discusses the chemistry of Cellosize HEC, properties, viscosity grades, toxicology, solubility, solution properties, the effect of enzymatic action and preservatives, and many other topics. 38 pp. Union Carbide Corp. **451**

Spectromatic System. The instrument is detailed in bulletin no. 515. It consists of a spectrometer, a thermal flow cell, pump unit, and the system controller. The instrument covers the 325–650-nm range with ±2-nm accuracy, and photometric accuracy is ±0.2% T. Fisher Scientific Co. **452**

Chemist-Analyst. Volume 67, no. 3 of the company's publication features a Nobel Laureate interview with G. T. Seaborg, the institution of a Nobel Laureate Signature award, subnanogram detection of amino acids, organic liquid adsorbent, and improvement of the GC assay procedure for organic solvents. 7 pp. J. T. Baker Chemical Co. **453**

Varian Instrument Applications. Volume 12, no. 3 features a routine sampler accessory for Model 219 UV/VIS spectrometer, discussion of Model XL-200 superconducting NMR spectrometer, an article on the "greenhouse effect" of fertilizers with gas chromatography, applications of a microprocessor-based liquid chromatograph (Model 5020), and a column conditioning article. 15 pp. Varian **454**

Optimize HPLC Analysis. Application note (Pub. #5953-0025), "Run Programming and Wavelength Programming Significantly Improve HPLC Lab Efficiency," describes how to develop and optimize an analysis with an HP 1084 series liquid chromatograph. The separation of anticonvulsant drugs is used to illustrate the automation method. 6 pp. Hewlett-Packard Co. **465**

Catalogs

Supplies for Ultraviolet Spectrophotometers. Catalog 7695 provides background information on UV cells and discusses the complete line of the company's UV cells and supplies. 23 pp. Beckman **468**

Chemicals and Materials. The 79–80 catalog of research chemicals and materials includes inorganic, organic, and organometallic chemicals; ultrapure chemicals; pure metals and alloys; catalysts; deuterated NMR solvents; and safety equipment. Technical data such as assay, molecular weight, and other physical constants are also featured. Alfa Division, Ventron Corp. **469**

Polymers. Catalog no. 781 lists over 400 polymers along with physical data and solubility information. 16 pp. Scientific Polymer Products, Inc. **470**

Supplies. The January 1979 laboratory supplies catalog includes spectrometer aids, TLC, radiation detectors, disposables, dispensers, and safety equipment. 120 pp. Interex Corp. **471**

Audiovisual Guide. More than 65 audiovisual cassette programs that include AA, HPLC, pH control of industrial streams, principles of RIA, RIA data reduction and quality control, and basics in pH measurements are available in bulletin no. 5613, "New Dimensions Audio-Visual Guide—II." Described also in the catalog is a broad line of reference books such as "The Dictionary of Scientific and Technical Terms," and publications pertaining to chemistry, medicine, and OSHA. 24 pp. Beckman Instruments, Inc. **485**

Optical Cells. Catalog no. L-209 covers optical cells for spectrophotometers, fluorimeters, and general spectrochemical instrumentation. Cells are available in optical, special optical and borosilicate glass, and standard IR and UV grade quartz. Tintometer **486**

For more information on listed items, circle the appropriate numbers on one of our Readers' Service Cards

FOOD ENGINEERING

Principles and Selected Applications

By MARCEL LONCIN and RICHARD LARRY MERSON

CHAPTER HEADINGS: Operations of the Food Industry. Measurement, Dimensions, Units. Equations Related to the Transfer of Mass, Heat and Momentum. Solution of the Transfer Equations. Determination of Transfer Coefficients. Equilibrium Between Phases. Evolution of Driving Forces. Mechanical Operations. Applied Biochemical Kinetics. Cleaning, Disinfection, and Rinsing. Optimization.

1979, about 476 pp., $44.00
ISBN: 0-12-454550-5

COMPUTERS IN MASS SPECTROMETRY

Edited by J. R. CHAPMAN

Mass spectrometry has been, perhaps more than any other analytical technique, affected by the impact of computer methods, and has, in its turn, made greater demands on these methods. This new exposition of the subject starts by covering the growth of the analytical techniques and describing the instrumentation available in both the mass spectrometer and computer fields. The first half of the book deals with the processes by which data is acquired and treated, how the raw data is converted to mass and intensity data, and how this data is reduced for more intelligible presentation. The second half is devoted to the options available in the use of mass spectroscopic data. A comprehensive discussion of methods for comparing a spectrum with a library of reference spectra for identification allows the prospective user to assess the merits and particular relevance of each method. The final chapter discusses the application of mass spectrometer computer techniques in the currently important area of quantitative analysis.

1978, about 217 pp., $20.25
ISBN: 0-12-168750-3

FLAVOR OF FOODS AND BEVERAGES

Chemistry and Technology

Edited by GEORGE CHARALAMBOUS and GEORGE E. INGLETT

CONTENTS: *C. E. Eriksson*, Flavor Modification. *I. Flament et al.*, New Developments in Meat Aroma Research. *G. A. M. van den Ouweland and L. Schutte*, Flavor Problems in the Application of Soy Protein Materials as Meat Substitutes. *R. F. Heinze et al.*, Flavoring Vegetable Protein Meat Analogs. *E. Voudouris et al.*, Flavor Development of White and Provincial Greek Bread for Rural Breadmaking Process. *J. Adda et al.*, Some Recent Advances in the Knowledge of Cheese Flavor. *D. Reymond and W. Rostagno*, Flavor Aspects of Chocolate. *W. Grab et al.*, Cocoa Substitution. *L. N. Ferguson et al.*, Biomolecular Studies of a Class of Sweet Compounds. *C. E. Inglett*, Intense Sweetness of Natural Origin. *F. Z. Saleeb and J. G. Pickup*, Flavor Interactions with Food Ingredients From Headspace Analysis Measurements. *G. A. M. van den Ouweland et al.*, Occurrence of Amadori and Heyns Rearrangement Products in Processed Food and Their Role in Flavor Formation. *R. Treisl et al.*, Formation of Lactones and Tertenoids by Microorganisms. *J. P. Casier et al.*, The Chemistry of the Black Caramel Colour Substances of Several Human Foods. *J. Bricout and J. Koziet*, Characterization of Synthetic Substances in Food Flavors by Isotopic Analysis. *M. M. Hussein and D. A. M. Mackay*, Analysis of Air Odorants in the Environment of a Confections Manufacturing Plant. *J. C. Boudreau*, Cat and Human Taste Responses to L-a-Amino Acid Solutions. *Montedoro G.*, Aroma Analysis of Virgin Olive Oil by Head Space (Volatiles) and Extraction (Polyphenols) Techniques *J. Alberola and L. J. Izquierdo*, The Volatile Fraction of Orange Juice. Methods for Extraction and Study of Composition. *T. Yamanishi*, The Aroma of Various Teas. *M. Moll et al.*, Relationship between Physical and Chemical Analysis and Taste Testing Results with Beers. *P. Jounela-Eriksson*, The Aroma Composition of Distilled Beverages and Perceived Aroma of Whiskey. *P. Ribereau-Gayon*, Wine Flavor. *S. van Straten et al.*, Alteration in a Wine Distillage During Aging. *Rapp et al.*, Possibilities of Characterizating Wine Quality and Vine Varieties by Means of Capillary Chromatography.

1978, 424 pp., $26.00 ISBN: 0-12-169060-1

Send payment with order and save postage and handling charge.

Prices are subject to change without notice.

Academic Press, Inc.

A Subsidiary of Harcourt Brace Jovanovich, Publishers
111 FIFTH AVENUE, NEW YORK, N.Y. 10003
24-28 OVAL ROAD, LONDON NW1 7DX

CIRCLE 2 ON READER SERVICE CARD

Solve Your Materials Problems 6 Ways

More R&D and QC labs use Micromeritics proven, precision instruments to measure physical properties of material than those of any other manufacturer in the world. These measurements include:

1 **Automatic particle size distribution** gives rapid analysis from 100 to 0.1 μm diameter.

2 **Manual and automatic physical adsorption** for B.E.T. surface area from 0.001m^2/g up; adsorption and desorption isotherms; pore structure (volume, size and shape) from 600 to 20Å diameter.

3 **Manual and automatic chemisorption** measures active material availability; percent metal dispersion.

4 **Mercury porosimetry** measures pore structure (volume, size and shape) from 354 to 0.0035μm diameter; density, surface area and average particle size.

5 **Manual and automatic density** determines absolute volume to ± 0.02cc.

6 **Electorophoretic mass-transport analysis** to study flocculation and dispersion; particle-liquid systems behavior; zeta potential.

We also invite you to use our complete Materials Analysis Laboratory Services. Let us show you how to solve your material problems. Call or write Micromeritics Instrument Corporation, 5680 Goshen Springs Road, Norcross, Georgia 30093. (404) 448-8282. Telex: 70-7450.

micromeritics®

CIRCLE 144 ON READER SERVICE CARD



Physical Basis of NMR Spectra

Proton and Carbon-13 NMR Spectroscopy: An Integrated Approach. R. J. Abraham and P. Loftus. xiii + 230 pages. Heyden & Son Inc., 247 S. 41st St., Philadelphia, Pa. 19104. 1978. $13.50

Reviewed by Robert J. Highet, NIH, National Heart, Lung and Blood Institute, Bethesda, Md. 20014

The current proliferation of Fourier transform NMR spectrometers has the happy consequence that organic and analytical chemists can expect to use both proton and carbon-13 NMR spectra in the characterization of organic compounds and the analysis of mixtures. It follows that students of chemistry must acquire a working knowledge of both types of spectra and of the instruments that produce them. The book addresses this problem and does it very well.

Within 200 pages of text the authors provide a lucid account of the physical basis of NMR spectra, their interpretation, and the instruments used. Although mathematical derivations are limited to the most fundamental relations, the concise presentation does not sacrifice accurate statement. Chemical shift and spin-spin properties of both proton and carbon-13 nuclei are treated simultaneously or, where appropriate, alternately. There is a brief but valuable description of sample handling, and in a chapter comprising only a tenth of the text, there is a description of the principles and problems of Fourier transform spectrometers. The difficulties encountered in quantitative analysis and such advanced techniques as double-resonance experiments, lanthanide shift reagents and spin-lattice relaxation measurements are briefly treated, followed by a stimulating chapter on applications of NMR spectra. A set of 25 elementary problems and a somewhat scanty index complete the book.

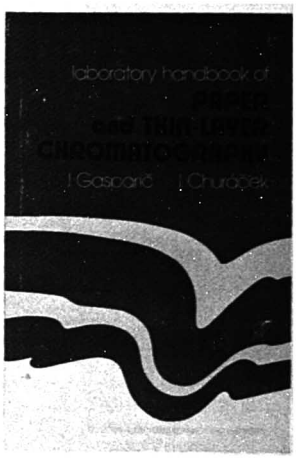
It is difficult to fault the choice of subjects in a work that has so successfully achieved a concise presentation. Perhaps homonuclear Overhauser effects and the use of zero-filling might have been mentioned. More frequent reference to original publications would have been welcome, but the secondary sources listed after each chapter provide the guide necessary. It is indeed a pleasure to read a work almost totally free of typographical errors. The work can be enthusiastically recommended to beginners in NMR.

Laboratory Handbook of Paper and Thin-Layer Chromatography. J. Gasparic and J. Churacek. 362 pages. John Wiley & Sons, Inc., 605 Third Ave., New York, N.Y. 10016. 1978. $42.50

Reviewed by Robert L. Clements, USDA SEA AR, Soft Wheat Quality Laboratory, Ohio Agricultural R&D Center, Wooster, Ohio 44691

For many of us who have come to depend on TLC, paper chromatography seems little more than a nostalgic reminder of the past. However, paper chromatography is alive and well and is sometimes a method of necessity, if not of choice. The two methods have much in common, and it is logical to consider them together. The authors, however, have undertaken a tremendous task in attempting to distill the vast literature into this small volume. Obviously, they have had to be highly selective, and therefore intimately familiar with the field.

This book differs from most similar monographs in that it is not oriented toward biochemistry, but rather approaches the subject in terms of basic organic chemistry (although the authors outline typical methods for isolating specific classes of biological materials). The first part ("Principles") is an excellent summation of prevailing tools and techniques. It also includes a section on the relation of chromatographic behavior to chemical structure. "Applications" (234 pages) is tightly organized into 26 classes of compounds, many of which are divided into subheadings (e.g., *N*-heterocyclic compounds are broken down into 11 types). This organization is augmented by an extensive subject index and a separate index of compounds chromatographed (about 2000 entries). An Appendix lists 88 detecting agents, keyed to the text by number. Unfortunately, the list gives formulations only, but the text can be consulted via the index to determine uses and specificities. Additional detecting agents are noted in the text. Useful derivatives and their preparations are also discussed. Wherever

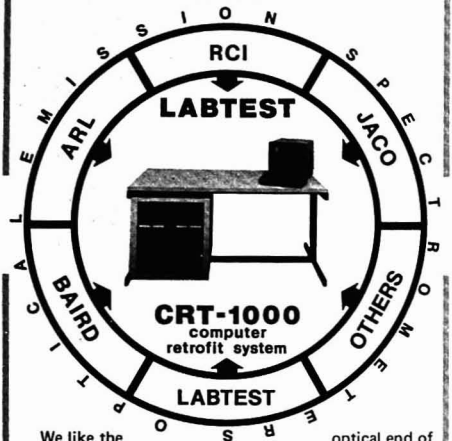


possible, the authors relate migration behavior to chemical structure, and stress conditions that are "the result of logical considerations based on knowledge of the substance chromatographed and the chromatographic process." This approach should appeal to the synthetic organic chemist and others who may be confronted with unique separation and isolation problems. The book includes many specific hints and precautions, all too often learned only through experience.

A breakdown of the 362 pages shows about 75 pages of tables (mainly R_f values) and 35 pages of references (about half of which appear to be in English). Most citations are pre-1970, although references as recent as 1977 were noted. The text is minimal and very concise and unambiguous. The translation seems excellent, although occasional awkward phrases and "unusual" words (e.g., *involatile*) appear.

It is not easy to criticize this book, but if a fault must be found, it is the necessarily selective nature of the references. The experienced chromatographer will undoubtedly find favorite innovations and reviews missing. Above all, the book is a "Laboratory Handbook", conceived as a convenient reference and guide for the bench chemist. It should be useful to the or-

MODERNIZE YOUR OLD SPECTROMETER



We like the optical end of OLD spectrometers made by ARL, Baird, JACO, RCI, and others. By-and-large they are still doing a good optical job. But technological advances have obsoleted their readout equipment. And modern laboratory demands have outpaced their capability. To solve this problem we designed the CRT-1000 Data Acquisition and Readout System. It is a highly reliable microprocessor controlled data acquisition, spectrometer control, and readout system designed specifically for use with optical emission spectrometers. IT WILL BRING YOUR SPECTROMETER UP TO CURRENT TECHNICAL STANDARDS FOR ABOUT 1/3 THE COST OF A COMPLETE NEW SYSTEM. The CRT-1000 will satisfy your existing readout requirements and provide additional features such as video display and/or hard copy printout of percent concentration, interelement corrections, averaging, automatic standardization, daily logging, and many other features. And you don't need a computer programmer to run it.

Over 100 major corporations have selected Labtest computer products and Labtest software. And Labtest computer installations have already logged hundreds of thousands of hours of field operation.

If reliability, low maintenance, flexibility, speed, and freedom from operator error are important in YOUR laboratory—modernization of your existing spectrometer system with the CRT-1000 may be the answer to your needs. Call us collect today to discuss your application. Ask for the Retrofit Project Manager.

LABTEST

EQUIPMENT

COMPANY

11828 La Grange Avenue, Los Angeles, CA 90025
Telephone (213) 478-2518 478-1610

subsidiary SYSTRON DONNER corporation

CIRCLE 128 ON READER SERVICE CARD

Books

ganic chemist or to the biochemist who needs a supplement to more specialized literature. The book probably will be of less value to the worker with a limited background in organic chemistry. It should be a worthwhile addition to the chemistry library, where it will be in constant demand as a convenient no-nonsense source.

New Books

An Introduction to Microscopy by Means of Light, Electrons, X-Rays, or Ultrasound. T. G. Rochow and E. G. Rochow. xvi + 367 pages. Plenum Publishing Corp., 227 West 17th St., New York, N.Y. 10011. 1978. $29.50

This book deals with all aspects of microscopy, both classical optical microscopy and the extension of microscopical concepts and procedures to the use of electrons, ions, X-rays, and ultrasonic waves for studying biological, mineral, and synthetic materials. Each instrument is considered in detail with diagrams to explain its operation; the performance of the microscope is evaluated in terms of resolution, contrast, depth of field, and magnification.

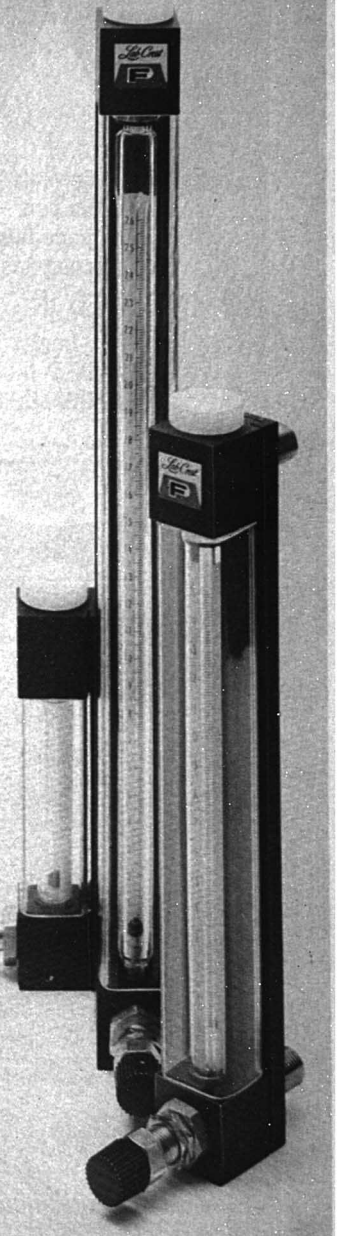
Introduction to X-Ray Spectrometric Analysis. Eugene P. Bertin. xiv + 485 pages. Plenum Publishing Corp., 227 West 17th St., New York, N.Y. 10011. 1978. $23.50

The book emphasizes X-ray fluorescence spectrometry for chemical analysis, particularly as applied on standard commercial wavelength-dispersive instruments. The principles underlying instrumentation, methods, and techniques are given in elementary, rather than mathematical, descriptive terms. Much of the text and many of the figures and tables are taken from the author's previous book, "Principles and Practice of X-Ray Spectrometric Analysis"; however, much new material has been added.

CRC Handbook of Chemistry and Physics, 59th ed. Robert C. Weast, Ed. 2512 pages. CRC Press Inc., 2255 Palm Beach Lakes Blvd., West Palm Beach, Fla. 33409. 1978. $44.95

The 59th edition includes an updated 55-page section of chemical elements, a table of lattice energies, an updated bond strength table featuring the addition of 80 diatomic molecules, 133 pages of tables of line spectra for 96 elements, and transition probability tables for atomic and ionic species. Also given is information on the limits of human exposure to toxic and hazardous substances.

Lab-Crest® Low-Flow Rotameters



The New Performance Leader . . . By All Standards

Now you can get all the features and options that make a great low-flow rotameter, combined in one and the same instrument. Built by the industry's most experienced team of control engineers and glass craftsmen, the new Lab-Crest Low-Flow Rotameter features a unique precision valve that provides linear control throughout the range of flows . . . a new low-flow tube with ⅛-inch float that operates reliably in industrial environments . . . plus all the time-tested features that have made Fischer & Porter rotameters the standard of comparison since the birth of the industry:

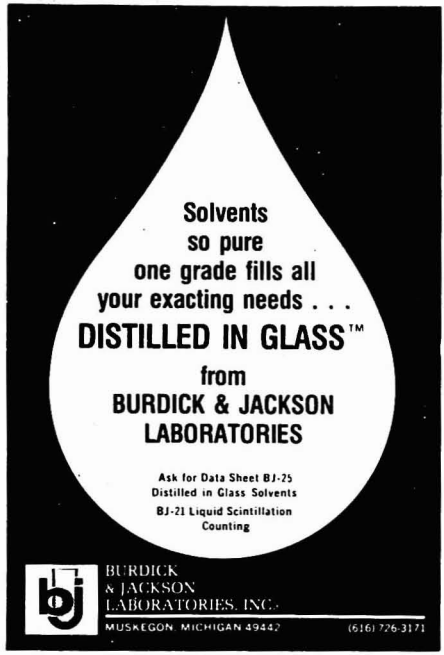
- **Convenience.** Quick-release metering tubes with Viton cup seals are easily interchanged without tools.
- **Rangeability.** Eight interchangeable tubes provide a choice of flow ranges from 50 cc/min to 148 SCFH (air).
- **Accuracy.** Instantaneous readings are repeatable within ±¼%, a direct result of F&P's unsurpassed experience.
- **Visibility.** Ceramic scale with white background is easy to read, permanently fused into the borosilicate glass surface.
- **Versatility.** Choice of meter bodies with 3, 6 or 10-inch scale for in-line or panel-mounting . . . or with tripod mount.
- **Controllability.** Precision sixteen-turn valve with interchangeable stems and sleeves provides linear control at all flow rates, as well as positive shut-off; low-cost valve also available for less sensitive applications.
- **Corrosion Resistance.** Standard aluminum end fittings are also available with interchangeable brass or stainless steel inserts; stainless steel standard on models with precision valve.

More than ever, it makes sense to call us for all your rotameter needs, whether you are looking for OEM quantities or just one of a kind. We have the right type and the right options to meet your requirements exactly.

Call (215) 674-6000 and ask for Lab-Crest Scientific Division. Fischer & Porter Company, County Line Road, Warminster, Pa. 18974.

LAB-CREST SCIENTIFIC
A DIVISION OF FISCHER & PORTER

CIRCLE 78 ON READER SERVICE CARD



CIRCLE 23 ON READER SERVICE CARD



Books

Archaeological Chemistry II. Giles F. Carter, Ed. 389 pages. American Chemical Society, 1155 16th St., N.W., Washington, D.C. 20036. 1978. $46

This book is number 171 in the Advances in Chemistry Series based on a symposium at the 174th Meeting of the ACS in Chicago, Ill., Aug. 31–Sept. 1, 1977. The 20 chapters are organized around the classification of the materials analyzed—organic materials, ceramics, and metals—along with five introductory chapters on overall perspectives and general techniques. Among the techniques are radiocarbon dating, spark source MS, X-ray radiography, trace element analysis, amino acid analysis, AA, and lead isotope analysis.

Continuing Series

Advances in Infrared and Raman Spectroscopy, Vol. 5. R.J.H. Clark and R. E. Hester, Eds. xvii + 405 pages. Heyden & Son Inc., 247 S. 41st St., Philadelphia, Pa. 19104. 1978. $48

Volume five presents articles on the following: high-resolution infrared spectroscopy with tunable lasers; vibrational spectra of carbon monoxide chemisorbed on the surfaces of metal catalysts—a suggested scheme of interpretation; vibrational spectroscopy of water; resonance Raman spectroscopy of nucleic acids; recent advances in microwave spectroscopy; and mean amplitudes of vibration for organic molecules. The literature is surveyed through 1977.

ASTM Publications

The following is available from the American Society for Testing and Materials, 1916 Race St., Philadelphia, Pa. 19103 (USA, Canada, and Mexico add 3% shipping charges. Other countries add 5%.)

Part 41 of Annual Book of ASTM Standards. 1004 pages. 1978. $30

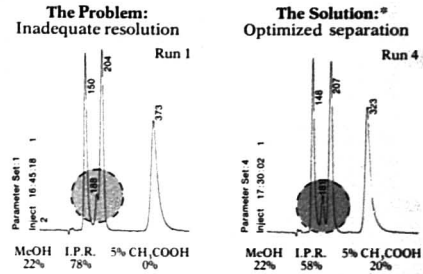
Part 41 contains 127 standards of which 21% are new, revised, or changed in status since 1977 and 63 are approved as American National Standards. New standards include specifications for laboratory weights and precision mass standards; thermal analysis; apparatus for testing—lab balances, filtration materials, glassware lab apparatus, microchemical apparatus; statistical methods; occupational health and safety aspects of materials; and many others.

Specify Spectra-Physics For Creative Chromatography.

Superior performance for the same price.

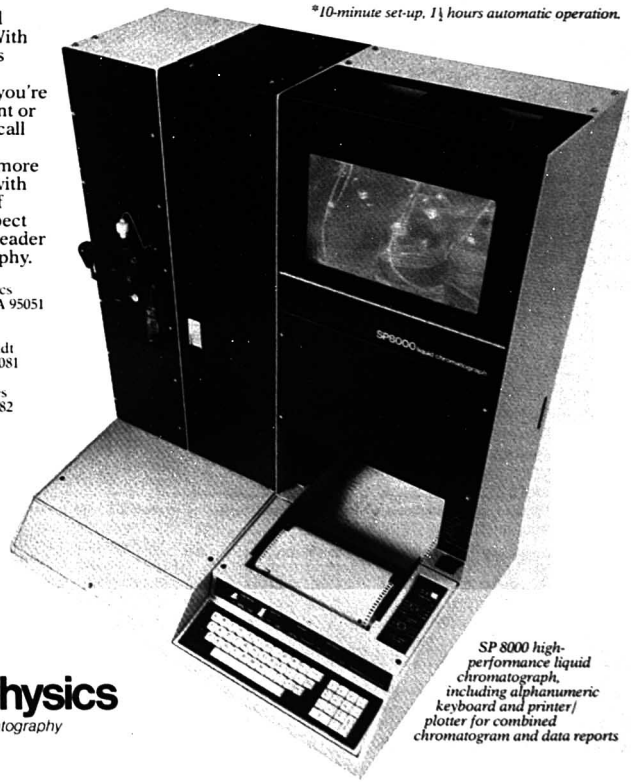
Why be content with a multiple-pump, limited-capability HPLC gradient system when for the same price you can get the microprocessor-automated SP 8000 chromatograph? With its three-solvent mixing it is more flexible than any conventional LC, whether you're doing methods development or routine analysis. Give us a call or drop a line. We'd like to show you how you can do more creative chromatography with our SP 8000, It's the kind of advanced system you'd expect from Spectra-Physics, the leader in automated chromatography.

USA headquarters: Spectra-Physics
2905 Stender Way, Santa Clara, CA 95051
European headquarters:
Spectra-Physics GmbH
Alsfelder Strasse 12, 6100 Darmstadt
West Germany, Telephone: 6151/7081
TELEX: 419471
Or call one of our regional US sales offices: Midwest (Ill.): (312) 956-0882
Mid-Atlantic (Md.): (301) 345-7333
East (N.J.): (201) 981-0390
South (Tex.): (713) 688-9886
West (Calif.): (408) 249-0105



The ternary solvent system of the SP 8000 automatically varied the ion pairing reagent independently of the methanol concentration. (Ask for Application Brief CAX-005 on water-soluble vitamins to get more details.)

**10-minute set-up, 1¼ hours automatic operation.*

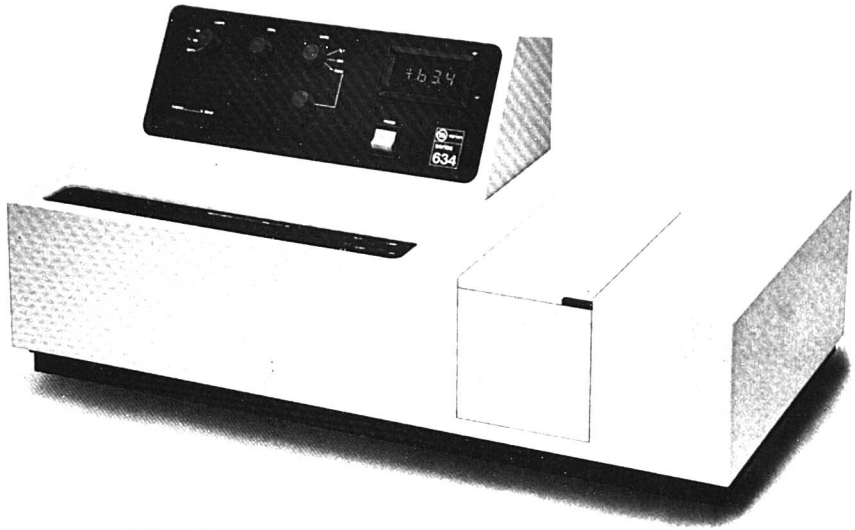


SP 8000 high-performance liquid chromatograph, including alphanumeric keyboard and printer/plotter for combined chromatogram and data reports

Spectra-Physics
Innovators in Chromatography

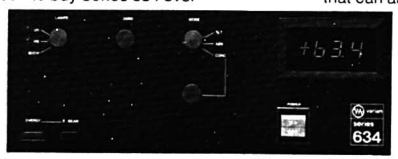
CIRCLE 193 ON READER SERVICE CARD

Varian UV-Vis spectrophotometers for every need.



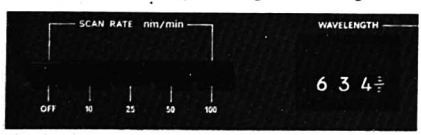
Choose Varian's UV-Vis spectrophotometer ...join thousands of happy users.

The Series 634 Spectrophotometers offer outstanding value in low-priced instruments. Take a look at their versatility. Thousands have chosen to buy Series 634 over all competitors.



Digital readout. This is standard on both instruments for all three operating modes: absorbance, transmission, and concentration. And there's automatic decimal positioning in the absorbance and %T modes.

Versatile wavelength ranges. Series 634 covers the 190 to 900-nm range—unsurpassed in low-priced instruments. Choose the model that fits your needs and budget. *All* Series 634 spectrophotometers measure up to 900 nm so you can do those important analyses at higher wavelengths.



Choice of wavelength scanning. Both manual and automatic scanning are available. Automatic scanning is simple with pushbutton selection of four speeds. Automatic scanning is standard on the Model 634S and an integral part of the instrument.

Recorder compatibility. Unlike some spectrophotometers, Series 634 is compatible with standard laboratory recorders that can also be used with other instruments. You're not locked in to a one-use recorder, an important feature for the budget-limited lab. And when it comes to a fine, all-round recorder to do best by your Series 634, Varian has that, too.

Sample compartment versatility. The key is size. The extra large compartment lets you handle a wide range of sample accessories of different sizes and shapes. Three sided access plus a large beam separation make it easy to use. With Series 634 you can measure many samples that other low-priced instruments can't handle.



These are just a few highlights of this versatile, low-priced spectrophotometer. We haven't even touched on its outstanding performance, so you'll want to know more.

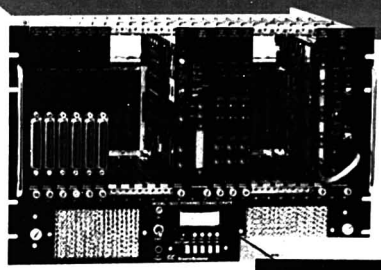
Circle **220** for a Series 634 data package.

Circle **221** if you'd like to see a representative.

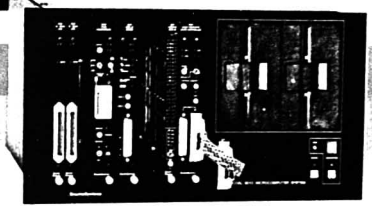
varian

Varian Instrument Division, 611 Hansen Way, Box D-070, Palo Alto, California 94303

from KineticSystems



microcomputer-controlled



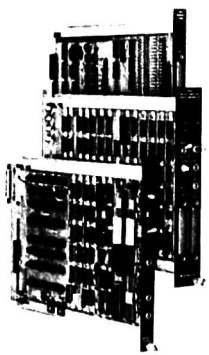
CAMAC systems

Whatever your application, you can choose from a variety of microcomputer-controlled systems utilizing the CAMAC (ANSI/IEEE-583) computer interface standard.

Each of these systems can provide data acquisition, automated monitoring and control for scientific or industrial laboratory automation and industrial process control. CAMAC systems give you a proven flexible system design, limitless expansion capabilities, a choice of standard I/O modules, computer independence, high-speed access of remote points, and powerful distributed control.

AVAILABLE SYSTEMS INCLUDE:

- Disk development systems with Assembler, extended XYBASIC, and FORTH programming languages
- ROM development systems with extended XYBASIC
- Stand-alone systems programmed in Assembler, extended XYBASIC, or FORTH
- Up to 62 development and stand-alone systems interconnected by the CAMAC serial highway (IEEE 595)



A KineticSystems CAMAC Microcomputer system offers you great flexibility. You can put the system together yourself, module by module, and write your own control software using XYBASIC, FORTH, or 8080 Assembler. Or we can supply you a complete system package, with hardware and software tailored to your needs.

NOTE THESE FEATURES

Hardware

- more than 100 types of CAMAC I/O modules from which to choose
- convenient terminals for field wiring
- CAMAC minicrate has 12 slots, self-contained power supplies, and up to two minifloppy disk drives
- 32K memory expansion module (optional)
- up to 32K bytes of memory with CPU
- programmable real-time clock
- DMA controller
- hardware arithmetic (optional)
- 8085 CPU

Software

- extended XYBASIC - lets you program in BASIC and execute CAMAC I/O commands in a very natural and straightforward way
- FORTH - an interpretive language and operating system in one, designed with simplicity and effectiveness in mind
- Macro Assembler
- Editor

Please contact us for additional information

the CAMAC people

KineticSystems Corporation

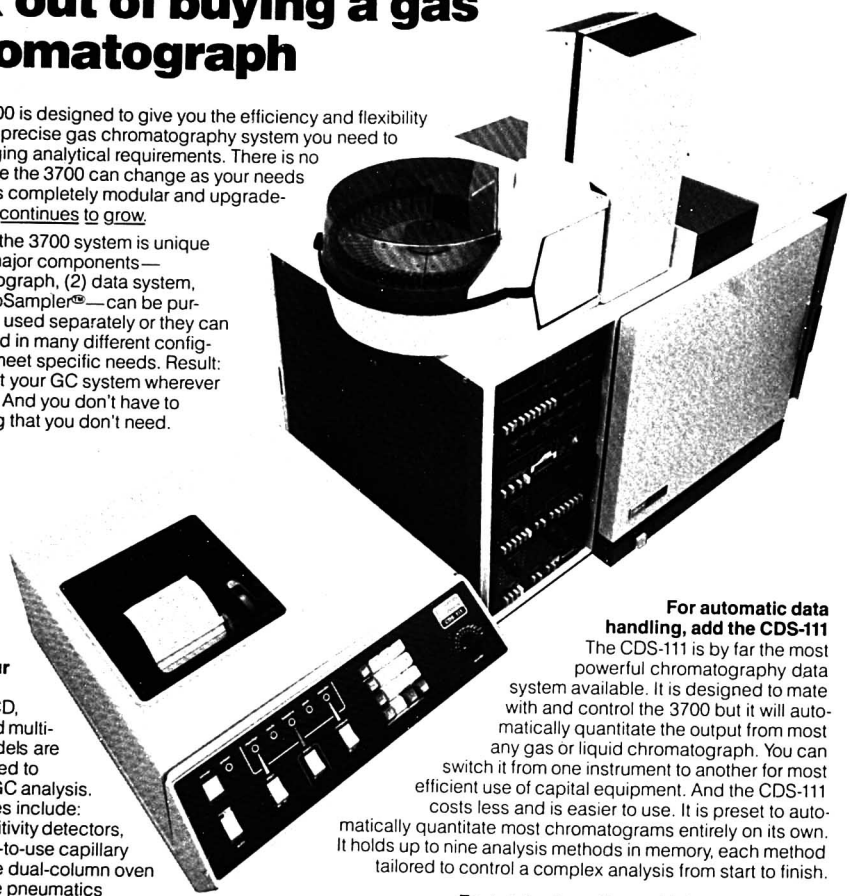
11 Maryknoll Drive, Dept. AC39 • Lockport, Illinois 60441 • (815) 838 0005
6 Chemin de Tavernay, Dept. AC39 • 1218 Geneva, Switzerland • (022) 98 44 45

CIRCLE 152 ON READER SERVICE CARD

How Varian's 3700 series takes the risk out of buying a gas chromatograph

Varian's 3700 is designed to give you the efficiency and flexibility to build the precise gas chromatography system you need to meet changing analytical requirements. There is no risk because the 3700 can change as your needs change. It is completely modular and upgradeable, and it continues to grow.

In addition, the 3700 system is unique in that the major components—(1) chromatograph, (2) data system, and (3) AutoSampler®—can be purchased and used separately or they can be combined in many different configurations to meet specific needs. Result: You can start your GC system wherever you want to. And you don't have to buy anything that you don't need.



Choose a 3700 for your application
TCD, FID, ECD, FPD, TSD and multi-detector models are offered tailored to handle any GC analysis. Major features include: highest sensitivity detectors, the first easy-to-use capillary system, large dual-column oven and separate pneumatics compartment for versatility and convenience. You can begin with a basic dual-column unit and add capability as you need it. Or you can start right now with the world's most powerful and fully automatic GC system by combining the 3700 with the CDS-111 data system and the 8000 AutoSampler.

For automatic data handling, add the CDS-111
The CDS-111 is by far the most powerful chromatography data system available. It is designed to mate with and control the 3700 but it will automatically quantitate the output from most any gas or liquid chromatograph. You can switch it from one instrument to another for most efficient use of capital equipment. And the CDS-111 costs less and is easier to use. It is preset to automatically quantitate most chromatograms entirely on its own. It holds up to nine analysis methods in memory, each method tailored to control a complex analysis from start to finish.

For total automation, add the AutoSampler
The reliable, proven Model 8000 AutoSampler obtains injection reproducibility that sets the standard for automatic gas chromatography. Sample cross contamination is virtually eliminated. It will handle up to 60 samples in a single unattended run. Model 8000 can be used with any gas chromatograph. Or it can be microproccesor controlled by the CDS-111 in a completely automatic fail-safe system with the Model 3700 Gas Chromatograph.

Let us help you select a gas chromatography system that will meet your changing analytical needs.

varian

For detailed information circle the indicated **Reader Service Numbers: 226** CDS-111 Chromatography Data System, **227** Model 8000 AutoSampler, **228** Model 3700 Gas Chromatographs, **229** Model 3711 Automatic Gas Chromatographs, **230** Have a representative call.

Editors' Column

Clinical Reference System: Voluntary or Enforced?

"Will the clinical laboratory field be legislated into conformity, or will it stave off this unwelcome possibility through vigorous, voluntary self-regulation?" This is the motto of an organization dedicated to the self-regulation of clinical laboratory performance through voluntary consensus standards. The activities of this 11-year-old organization, the National Committee for Clinical Laboratory Standards (NCCLS), are perhaps familiar to some, particularly those in the field of clinical chemistry. One recent activity being conducted under the aegis of NCCLS in the development of a National Reference System in Clinical Chemistry deserves some special attention, not only because of the traditional role of the analytical chemist in the practices of the clinical laboratory, but also because of the far-reaching implications of such self-policing efforts in today's regulatory climate.

The origin of the activity can be traced to the 1977 Conference on a National Understanding for the Development of Reference Materials and Methods for Clinical Chemistry. The conference was hosted by the Center for Disease Control (CDC) in joint sponsorship with FDA, NBS, and seven other cosponsoring professional and industrial associations. What is significant here is the initiation of the conference by the three government agencies deeply involved in the development of reference materials and methods with the realization that the complexity of their task required the active participation of the private sector. Each of the participating organizations was asked to prepare its own "position paper" specifically addressed to seven major areas of concern to the conduct of clinical chemistry:

- Analytical goals and quality requirements of a national reference system
- Organizational components of a national reference system
- Reference materials
- Biological reference materials
- Definitive methods
- Reference methods
- Provisional reference principles.

The position papers were submitted to CDC and were compiled into a study package for distribution to the participants prior to the conference. When the conference convened in Atlanta in late fall of 1977, after more than a year of planning, a panel was designated for each of the above areas to conduct discussions based on the position papers. After the conference, each panel prepared a list of recommendations that were distributed to all attendees.

The consensus evolving out of this conference was that the development of a National Reference System in Clinical Chemistry would be much more effective if the overall efforts were coordinated through a voluntary consensus organization like NCCLS. Subsequently, NCCLS was asked and agreed to undertake the management of such a national reference system. In fact, this organization is already involved in the development of standards for all clinical laboratory operations. NCCLS sees this as part of its broad objective to establish voluntary consensus standards for all phases of clinical laboratory performance essential to the delivery of good health care. In view of the critical role this organization promises to play in the development of voluntary consensus standards, a brief look at its organization and its standard development process is necessary.

Founded in 1968, NCCLS is a nonprofit association that derives its membership from all three sectors of the clinical laboratory field: the professions (American Chemical Society included), government agencies, and manufacturers. Membership is limited to organizations. As of May 1978, it had 97 organizational members, each of which appoints a delegate and an alternate who attend general meetings, circulate proposed and tentative standards to their colleagues for review, vote on approved standards, and elect officers and directors. The actual responsibility for preparing standards falls to 10 area committees, each with responsibility in a specific area and each with several subcommittees. The consensus process by which a proposed method or material drafted by the subcommittee is finally adopted as a standard typically takes two to three years. The working mechanism is similar to that of other organizations concerned with standards, such as ASTM, AOAC, and ANSI. The consensus mechanism, a long and tedious but nevertheless clearly defined process, is designed to achieve acceptance by all parties and to assure widespread use once adopted. Currently, there are

Varian announces training courses in gas chromatography

Schedule for April, May and September 1979:

Basic Gas Chromatography
April 10–12, Chicago, IL
May 9–11, Florham Park, NJ
September 5–7, Palo Alto, CA
Lecture & Lab, 3 days, $225
Lecture only, 2 days, $155

Automatic Gas Chromatography*
April 18–20, Chicago, IL
May 16–18, Florham Park, NJ
September 12–14, Palo Alto, CA
Lecture & Lab, 3 days, $200

Glass Capillary Gas Chromatography
May 14–15, Florham Park, NJ
Lecture & Lab, 2 days, $225

Maintenance of the Gas Chromatograph
April 16–17, Chicago, IL
September 10–11, Palo Alto, CA
Lecture & Lab, 2 days, $225

To enroll in Chicago and Palo Alto courses, please contact the Varian Instrument Division Training Department, 2700 Mitchell Drive, Walnut Creek, CA 94598. Telephone (415) 939-2400, ext. 225. Enroll in Florham Park courses at Varian Instrument Division Training Department, 25 Hanover Road, Florham Park, NJ 07932; Telephone (201) 822-3700.

varian

*One tuition-free course per Model 37111 purchase.

CIRCLE 231 ON READER SERVICE CARD

in various stages of adoption about 30 standard methods and materials available from the Headquarters of NCCLS, 711 E. Lancaster Ave., Villanova, Pa. 19085 (212-525-2435).

As a first step toward its commitment to act as a vehicle for development of the reference system in clinical chemistry, NCCLS has established a Council on the National Reference System in Clinical Chemistry. The Council, chaired by Roy N. Barnett of Yale University School of Medicine, is composed of 12 members representing governmental, professional, and industrial sectors. Following its establishment in the summer of 1978, the Council has held four meetings at various locations. The NCCLS' proposal to establish the Council was endorsed by the unanimous agreement of the clinical chemistry organizations gathered at the 1977 Atlanta meeting; therefore, the Council derives its clear mandate from that consensus. However, the precise role the Council is to play in carrying out that mandate is less clearly defined and is still evolving. At one of its recent meetings at NBS in Washington, D.C., the chairman saw the function of the Council as a liaison designed to facilitate effective communication between the scientific groups in the government, industry, and professions. As such, any recommendations or guidelines formulated by the Council should deal only with broad issues and provide the fundamental guiding principles for the Area Committee on Clinical Chemistry, which operates within the NCCLS organization.

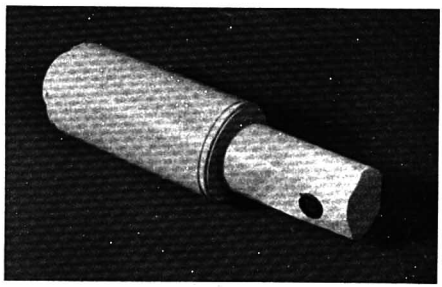
In this role, for instance, the Council has completed the drafts of two documents: "Guidelines for the Development of Certified Reference Materials for Use in Clinical Chemistry" and "Guidelines for the Development of Definitive Methods for Use in Clinical Chemistry". These drafts are to be transmitted to the NCCLS board of directors with the recommendation that they be distributed to the NCCLS membership for comment. Once these guidelines are adopted, they are to serve two purposes: (a) to provide guidance for those interested in developing reference methods and materials for use in the clinical laboratory and (b) to serve as a primary document for those entrusted within the NCCLS with the review of proposed NCCLS certified reference methods and materials, prior to formal acceptance.

Another significant accomplishment of the Council includes a report compiled by one of its members, Desmond Burke, which identifies 25 priority clinical chemistry analytes. The report constitutes a recommendation of priority as determined by the frequency of use, the usefulness to the clinician, and the need for reference materials and methods. A specific report covering this study, which will include additional recommendations of the Council, will be available soon from the NCCLS headquarters.

In recognition of these and other activities that are aimed ultimately at achieving quality clinical laboratory performance without regulation, NBS, FDA, and CDC have recently issued a joint statement of support. In their statement, the three government agencies recognize the limitations of the resources available from each major sector—professions, government, and industry—each acting separately. The statement stresses that the most efficient, cost-effective means of developing needed standards is to first set priorities and then to have all three sectors work together in a well-managed consensus mechanism.

Barbara Cassatt

Machlett's New Dual-Target Spectroscopy Tubes



Improved direct replacement for GE/DIANO EA-75

- **DTS — 75A for Air-Helium Spectrometer**
- **DTS — 75V for Vacuum Spectrometer**

Increased cooling has been designed into the anode structure of these beryllium window x-ray tubes that are rated for operation up to 75 kVp.

Tungsten and chromium targets are standard. Other combinations can be provided on special order.

The standard 0.010" (0.25 mm) Be window can be replaced with 0.005" (0.125 mm) for long wavelength radiation on special order.

For data sheets, prices and deliveries contact:

Product Manager, Industrial X-ray
The Machlett Laboratories, Inc.
1063 Hope Street
Stamford, Conn. 06907
Tel: 203-348-7511 TWX: 710-474-1744

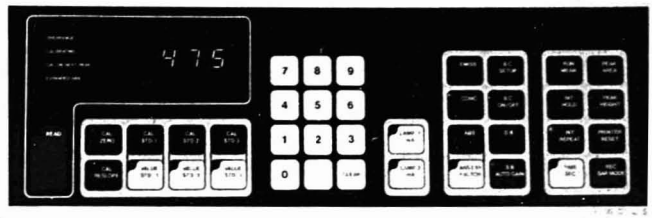
MACHLETT **The Machlett Laboratories, Incorporated**

A Raytheon Company

CIRCLE 186 ON READER SERVICE CARD

New from Varian... Low cost, microcomputerized AA-475 and AA-275

The pacesetters in atomic absorption



Routine AA analysis has never been this easy, this sensitive, this economical. The AA-475 and AA-275 fully exploit their powerful 8-bit, 10K microcomputers to give you high quality data quickly and simply.

The AA-475 and AA-275 are designed with the novice operator in mind. Prompts on the interactive instrument panel provide step-by-step guidance through set-up and calibration procedures. Operator errors are identified and flagged. Ten vital flame functions are monitored continuously for programmed ignition and safe shutdown.

Computerized signal processing gives you reliable data every time. Varian's unique Rational Method allows rapid, accurate calibration, with a reslope function for recalibration against a single standard. The running mean mode simplifies data collection.

Totally versatile, the AA-475 and AA-275 adapt readily to your requirements. Select from the single beam AA-275 or the double beam AA-475. Customize your system with powerful Varian AA accessories such as the CRA-90 carbon rod atomizer, automatic sample changers for flame and furnace, and programmable calculators. The new M-65 Vapor Generation Accessory greatly simplifies hydride analyses, bringing new levels of convenience and throughput.

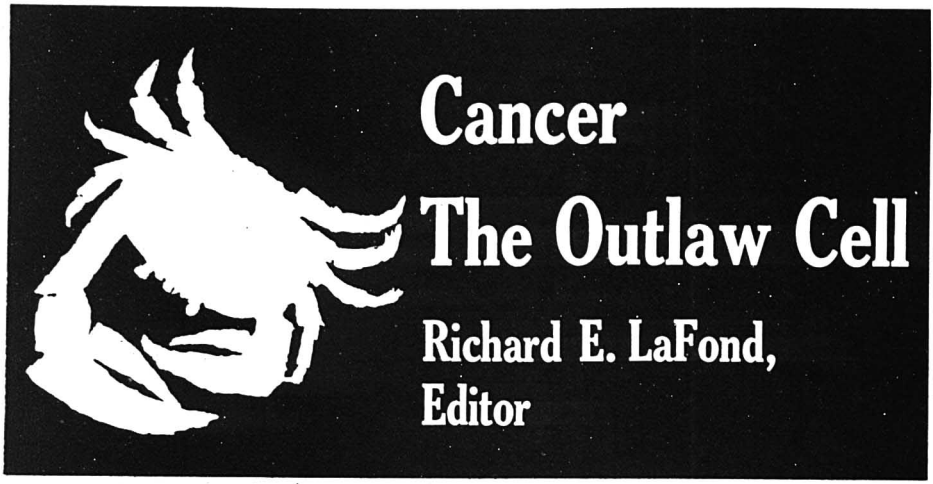
There is no compromise in performance. The low cost AA-475 and AA-275 provide a sensitivity level that matches or exceeds that of competitive models at twice the price.

Find out more about the AA-475 and AA-275 today. Circle **235** for product literature. Circle **236** if you wish a representative to call. Or write: Varian Associates, Inc., 611 Hansen Way, D-070-2, Palo Alto, CA 94303.

SEE US AT THE PITTSBURGH CONFERENCE.

varian





An estimated 390,000 Americans will die of cancer this year alone and one out of every four will develop some form of this dread disease within their lifetime.

Statistics such as these show the need for a book that will explain our current state of the art in cancer research using simple, straightforward, non-medical language. *Cancer — The Outlaw Cell* successfully fulfills this need by making the latest advances in cancer research available to the general public in a clear, non-technical style that can be read and understood by both the professional scientist and non-scientist.

Written by leading experts at the forefront of their specialties and profusely illustrated in color, this collection of articles covers the great strides that have been made in understanding the causes of cancer, how this disease is spread, cancer as a biochemical problem, and non-surgical modes of therapy.

CONTENTS

Cancer — An Overview, *Henry C. Pitot*
Tumor Growth and Spread, *Isaiah J. Fidler and Margaret L. Kripke*
Control of Cell Growth in Cancer, *Arthur B. Pardee and David S. Schneider*
Cancer as a Problem in Development, *Armin C. Braun*
Puzzling Role of Cell Surfaces, *David I. Meyer and Max M. Burger*
Cancer-Causing Chemicals, *Elizabeth K. Weisburger*
Cancer-Causing Radiation, *Robert L. Ullrich, J. Michael Holland and John B. Storer*
Cancer and Viruses, *Arnold J. Levine*
RNA Tumor Viruses, *Robert D. Cardiff*
Herpesviruses — A Link in the Cancer Chain, *Ariel C. Hollinshead and William A. Knaus*
Cancer and The Immune Response, *John L. Fahey*
Immunotherapy of Human Cancer, *Larry A. Schafer and Evan M. Hersh*
Radiation Therapy, *Diana F. Nelson and Philip Rubin*
Chemotherapy of Cancer, *Joseph H. Burchenal and Joan R. Burchenal*

192 pages (1978) clothbound $15.00
LC 78-2100 ISBN 0-8412-0405-5

192 pages (1978) paperback $8.50
LC 78-2100 ISBN 0-8412-0431-4

SIS/American Chemical Society/1155 16th St., N.W./Wash., D.C. 20036

Please send _____ copies of *Cancer—The Outlaw Cell.*

☐ cloth $15.00 (ACK 0405-5) ☐ paper $8.50 (ACK 0431-4) ☐ Check enclosed for $_____. ☐ Bill me.
Postpaid in U.S. and Canada, plus 75 cents elsewhere.

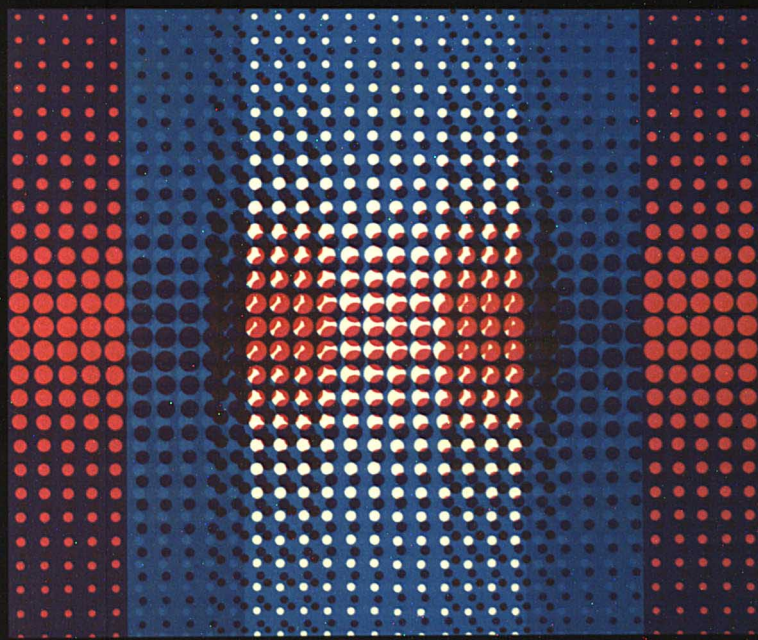
Name _____

Address _____

City _____ State _____ Zip _____

Spectrophotometry moves into the future

In the continually changing world of analytical chemistry, new and more detailed applications demand an ever increasing range of technologically sophisticated instruments.
The new Pye Unicam range of Spectrophotometers combine the latest developments in electronic and optical engineering with tried and tested analytical techniques to take *your* spectrophotometry into the future...



PHILIPS

Pye Unicam

A SCIENTIFIC INSTRUMENT COMPANY OF PHILIPS



New in UV/visible Spectrophotometry: the first totally holographic range.

Pye Unicam have many spectroscopic 'firsts' to their credit and now we introduce two more technological breakthroughs, pioneered in our own laboratories, which will leave other UV/visible spectrophotometers in our shade. Our complete range now benefits from the increased performance of **master, blazed holographic gratings** and the durability conferred by **silica coated optics**.

SP6 Series

- ☐ Improved performance
- ☐ Improved construction
- ☐ Visible or UV/visible range
- ☐ Meter or digital display
- ☐ Colour-coded controls
- ☐ Automatic drift compensation

This highly popular range of single beam spectrophotometers is now relaunched with major improvements in performance, features and construction. The SP6 is available as four low-cost models with choice of visible or UV/visible ranges and meter or digital display. Simplicity of design and colour-coded controls allow the instruments to be used with speed and precision even by inexperienced operators. Their proven high reliability and rugged construction make the SP6 the perfect 'workhorse' instrument for any laboratory, as thousands of satisfied operators around the world can testify. **Circle No. 100**





SP8-100 and SP8-150

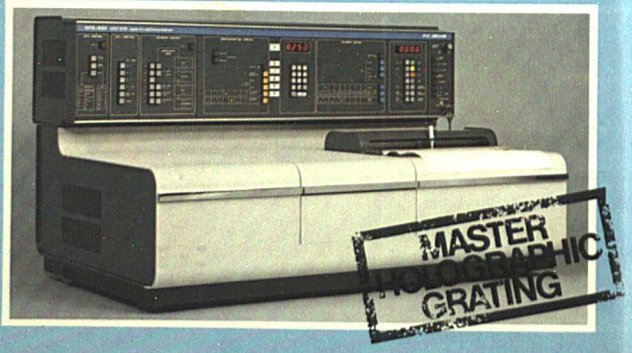
- ☐ Double beam scanning
- ☐ High performance
- ☐ Synchroscan recording principle
- ☐ Flexible, modular design
- ☐ Vast accessory range

The SP8-100 has rapidly established itself as a truly versatile UV/visible scanning spectrophotometer with very simple operation. As part of our policy of continuous product improvement, it is now offered with higher guaranteed performance and the SP8-150 is added to the range with an extended wavelength range and even better specification. **Circle No. 101**

SP8-200 and SP8-250

- ☐ Research performance
- ☐ Single or double monochromator
- ☐ Microprocessor control
- ☐ Keyboard operation
- ☐ Complete remote control facilities
- ☐ 185-950nm range

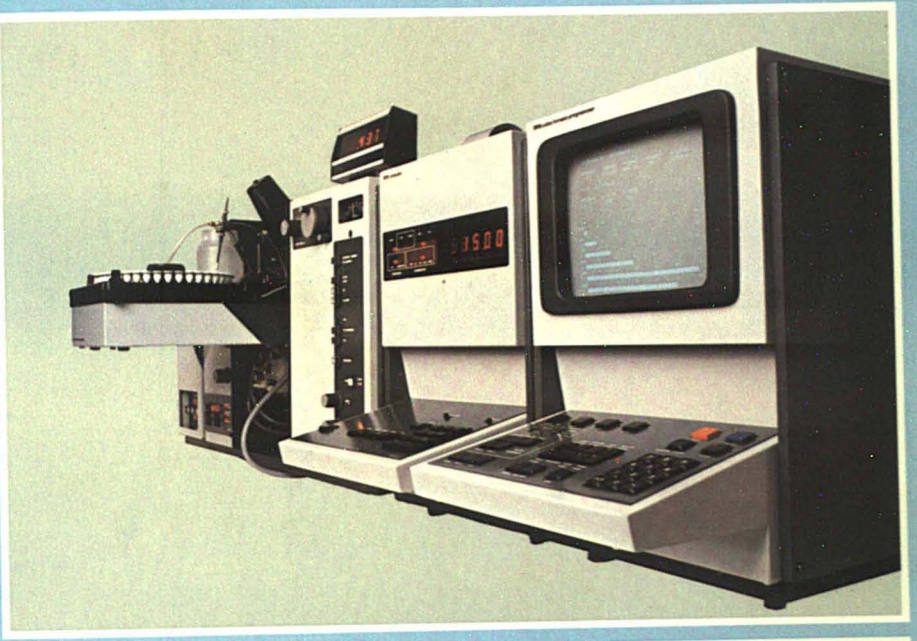
When the SP8-200 was announced, we challenged that its performance could only be significantly bettered by double monochromator instruments. That's still true, but with the introduction of the SP8-250 and its double, master holographic monochromator, there's no need to look beyond the Pye Unicam range for the ultimate in low stray light levels. Both instruments have the full range of slitwidths, scan speeds, chart expansions and other facilities expected of research performance spectrophotometers. **Circle No. 102**

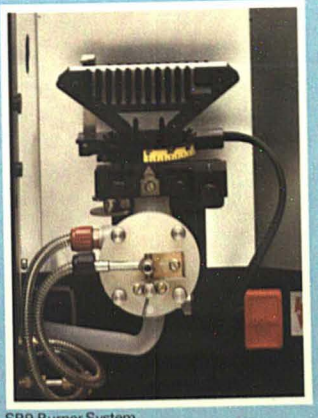


New in AA Spectrophotometry: System SP9. The instrument choice for your analytical needs.

SPECTROPHOTOMETRY MOVES INTO THE FUTURE

Flame or flameless, System SP9 offers a unique choice of advanced systems capable of handling any Atomic Absorption analysis.





SP9 Burner System

SP9 Computer

The power and flexibility of the **microprocessor** applied to AAS data handling. Calibration using up to 5 standards in fixed or variable ratios plus running mean and full statistics capability.

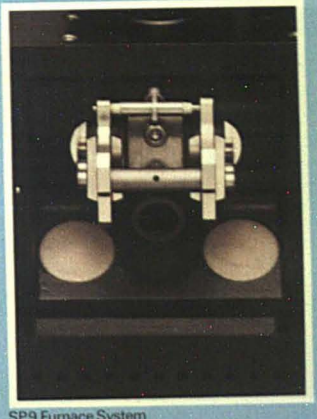
SP9 Video Furnace

Unique video display of all parameters and current status. Temperature feedback control, ramping, gas stop programmable for each of 6 phases and EAROM storage of 10 full furnace programs. Built-in autosampler controls with unique standard additions program.

Automation

Unattended automatic operation and improved precision via the world's most flexible flame and flameless autosamplers.

Circle No. 103



SP9 Furnace System

Atomic Absorption Spectrophotometry

SP2900 Double Beam Atomic Absorption Spectrophotometer

Range 190 – 852 nm

The SP2900 provides an ideal combination of precision, sensitivity and good detection limits. In addition to a 4 lamp magazine, large sample compartment and advanced burner design, unique readout facilities are offered including peak height and peak area measurement, and a peak timer.

The unparalleled simultaneous background correction system enables 1.5A of background to be corrected to an accuracy of better than 1%.

When combined with the Pye Unicam Data Centre the SP2900 provides fully automatic data processing facilities.

Circle No.104

Infrared Spectrophotometry

SP2000/4000 Infrared Spectrophotometer

Range 200 – 4000 cm^{-1} (SP 2000)
400 – 4000 cm^{-1} (SP 4000)

Capable of the most demanding applications in the infrared region, the SP2000/4000 features include 6 slit programs, 12 chart and scanning speeds, 9 time constants, 7 different wavenumber expansions and up to x20 transmission expansion, calibrated back-off, chart synchronisation, superimposed and sequential scanning with visual display of all operating modes. Air drier, sample changer, a full range of sample handling accessories and a comprehensive data system are available.

Circle No.114

Automatic Chemistry

AC1 Automatic Chemistry Unit

The AC1 performs the functions of sample dilution, addition of three further reagents, mixing, incubation and transfer of the processed solution to a UV/visible Spectrophotometer for measurement at speeds of up to 240 samples/hr. The fully variable sample and reagent volumes, incubation times and temperatures permit the total automation of many spectrophotometric analyses. The data is corrected for sample or reagent blanks and is printed in concentration or enzyme units together with rack and tube number. Systems based on the AC1 will prove invaluable in fields as diverse as clinical chemistry, water management, foodstuffs and pharmaceuticals.

Circle No.115

Gas Chromatography

GCD

A low cost range of dedicated chromatographs offering a choice of Flame Ionization, Thermal Conductivity or Electron Capture detectors. Other features include separately heated injection ports and detectors with recorder readout of temperature. A dual flame ionization instrument is available with isothermal or temperature programmed automatic door column oven.

Series 204

A complete range of analytical gas chromatographs – modular in design to provide optimum flexibility coupled with outstanding performance. Choice of five detectors (FID, TCD, ECD, FPD, ND) which may be used singly or in any dual combination. Updating or extension is simple via the wide range of accessories and modules.

The wide range of accessories available for use with both GCD and Series 204 instruments includes full capillary facilities, multi-dimensional unit, digital flow controllers and automatic injector. **Circle No.116**

Liquid Chromatography

LC-XP Series

A new range of instruments for HPLC which can provide the system to suit your requirements from quality control to complex research studies. The LC-XP Series contains both isocratic and gradient elution liquid chromatographs which, while modular in design, have been conceived as fully integrated systems. This means that if your requirements change your system can be updated at minimum expense.

Circle No.117

Industrial Chromatography

Series 604 Process Chromatography

The Series 604 Process Chromatograph is an advanced, low cost on-stream composition analyser for the chemical, petroleum and natural gas industries. It has been designed to provide single stream, single component analysis at a price well below that normally associated with chromatographs, while retaining the flexibility to perform multi-stream analysis when required. In addition the 604 has low installation costs, is simple to operate and maintain and represents a significant breakthrough in performance/cost index.

Circle No.118

For further information on all Pye Unicam products, please write to Pye Unicam direct, or contact your local Philips Analytical office: **Australia** Philips Industries SIED Ltd., 25-27 Paul Street, North Ryde, N.S.W. Telephone 888 8222. **Austria** Österreichische Philips Industrie GmbH, A1230 Wien, Parttartgasse 32, Breitenfurterstr. 219 Telephone 0 22/8 31501. **Belgium** M.B.L.E. SA, 80 Rue des Deux Gares, Brussels 7. Telephone 5230000. **Canada** Canadian Laboratory Supplies, 80 Jutland Road, Toronto, Ontario M8Z 2H4. Telephone 416 252 5151. **Denmark** Philips Elektronic Systemer A/S, Afdeling for Industrie og Forskning, Strandlodsvej 4, DK-2300 Copenhagen S. Telephone Copenhagen 2222. **Eire** P. J. Brennan & Co. Ltd., 26 Fosters Avenue, Mount Merrion, Dublin. Telephone 886844. **Finland** Oy Philips AB, Industrial and Scientific Equipment, SF-02700 Kauniainen. Telephone Helsinki 517271. **France** Philips Industrie SA, 105 Rue de Paris, 93002 Bobigny. Telephone Paris 830 1111. **Holland** Philips Nederland BV, Boschdijk 525, Eindhoven. Telephone Eindhoven 7. **Italy** Philips SpA, Via le Elvezia 2, 20052 Monza. Telephone 36140. **Norway** Norsk Aktieselskap Philips, Industrie og Forskning, Essendropsgaten 5, Oslo 3. Telephone 463890. **New Zealand** Philips Electrical Industries of NZ Ltd., P.O. Box 2097, 181 Wakefield Street, Wellington. Telephone 3339. **Portugal** Philips Portuguesa SARL, Av. Eng. Duarte Pacheco 6, Lisbon 1. Telephone 693121. **Spain** Philips Iberica SAE, Martinez Villergas 2, Madrid 27. Telephone 404 22 00. **Sweden** Svenska AB Philips, Fack 102 50, Stockholm 27. Telephone 6350000. **Switzerland** Philips AG, Abt. Industrie und Forschnung, Allmendstrasse 140, Postfach, CH-8027 Zürich. Telephone 442211. **South Africa** South African Philips Pty. Ltd., P.O. Box 7703, Johannesburg 2000. Telephone 240531. **USA** Sargent-Welch Scientific Company, 7300 North Linder Avenue, Skokie, Illinois 60077. Telephone (312) 677 0600. **West Germany** Philips GmbH, Unternehmensbereich Elektronik für Wissenschaft und Industrie, 35 Kassel-B, Miramstr. 87. Telephone 0561 5011.

7060.05.3010.11

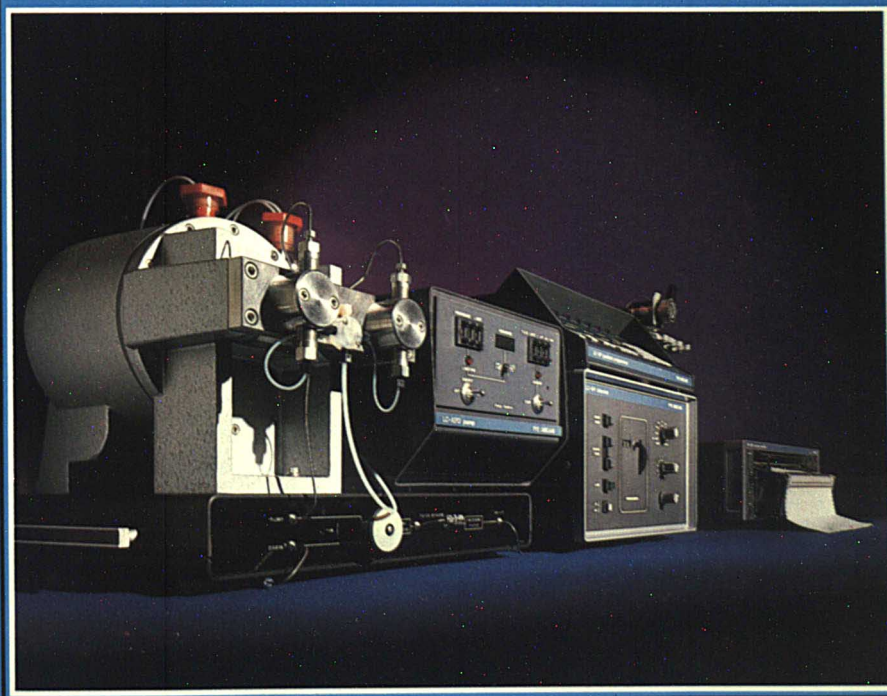
PHILIPS

Pye Unicam Ltd

York Street Cambridge CB1 2PX England
Telephone (0223) 58866 · Telex 817331

LC-XP Series: you choose the system.

Pye Unicam's wide selection of modular instruments helps you to put together precisely the right system for your particular application. No need to purchase a large and expensive unit; save by selecting and building up a modular system according to your requirements.
You need a simple isocratic instrument? A high performance gradient elution system? A degree of automation? We have them all, and more. A highly reliable pump. A gradient elution system with a unique storage facility (programme the system, switch off at any time and, on your return, switch back into the programme again). A choice of detectors, UV and fluorescence, recorders and many accessories. All with Pye Unicam's usual high specification and performance.
Learn more about our modular LC systems by writing to us at the address overleaf or using the reader service card.



PHILIPS

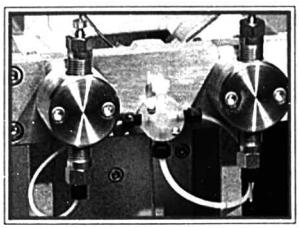
Pye Unicam

A SCIENTIFIC INSTRUMENT COMPANY OF PHILIPS

LC-XP Series combines systems capability with modular flexibility

Advanced microprocessor logic makes the LC-XP Gradient Programmer the most sophisticated device yet for gradient applications. A simple keyboard can be used to enter up to nine gradient segments, each of which can be programmed in linear or exponential fashion. The programmer will store up to ten complete programmes in non-volatile memory and provides an electrical output to remote devices at the end of each gradient segment.

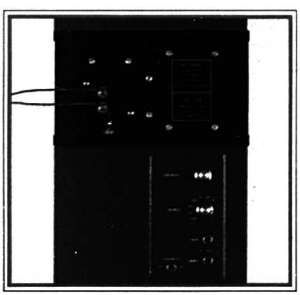
The LC-XPD Pump has been designed for use in all branches of liquid chromatography – no matter how demanding the application. It offers electronically corrected, pulseless flow metering from 0.03 to 10.0 ml./min. at pressures up to 700 bar. Digital selection of flow-rates and pressure limits ensures high reproducibility and rapid setting of conditions.





The LC-UV variable wavelength UV detector has unique reference compensated optics which combine the high energy throughput of a single beam system with the stability of a genuine double beam instrument. The most sensitive absorbance range of 0.005 A enables the chromatographer to make full use of the outstanding performance capability.





The highly sensitive and specific LC-FL fluorescence detector is particularly useful for trace analysis applications. Excitation and emission wavelengths are accurately defined by means of the twin filter optical system and bandwidths can be optimised for the compounds of interest. LC-FL is equally suitable for the detection of naturally fluorescing compounds or fluorescent derivatives.

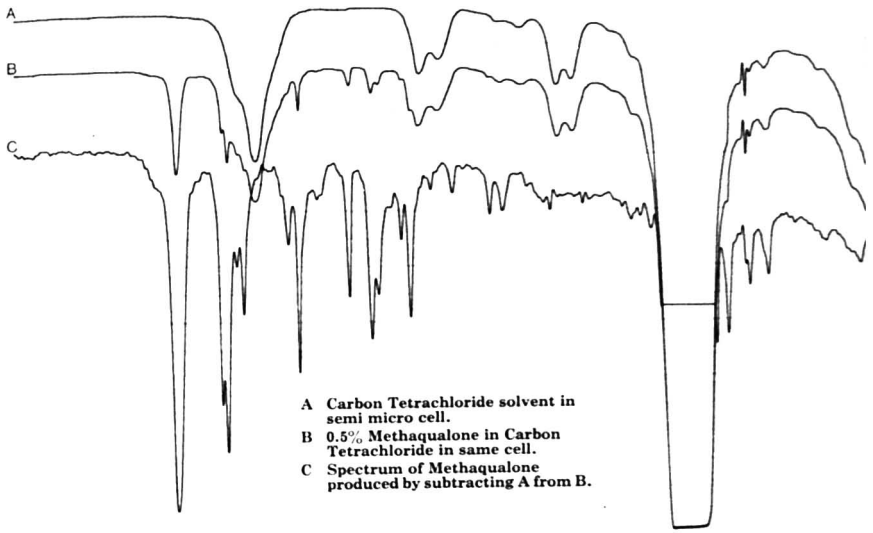
Reader Reply No 119

Pye Unicam Ltd
York Street Cambridge CB1 2PX England
Telephone (0223) 58866 · Telex 817331

Printed in England by Lund Humphries 1/79
7042 05 3143 11

An Infrared Spectrophotometer Data System

with mini computer performance at calculator cost



A Carbon Tetrachloride solvent in semi micro cell.
B 0.5% Methaqualone in Carbon Tetrachloride in same cell.
C Spectrum of Methaqualone produced by subtracting A from B.

The established and proven Pye Unicam SP2000/4000 infrared spectrophotometers can now be coupled to a data system offering significant advantages:

* Removal by spectral subtraction of spectra of unwanted components in a sample (shown in the simple example above).
* Co-addition of spectra to improve final signal-to-noise ratio.
* Storage of commands with associated parameter changes for use as a single command.
* A program for printing the peak position and transmittance for all absorption bands above a defined limit.
* Storage of up to 40 full range spectra per cassette.
* Self diagnostic programs provided.

The basic system comprises an interface and a HP9825A calculator, to which a VDU may be added. The calculator provides a 32 character LED display of commands, a printer for hard copy of commands and parameters and a tape cassette drive. The software allows commands and parameters to be typed on the standard typewriter keyboard in conversational English language.

For further details of how the Pye Unicam Data System can extend the capabilities of the SP2000/4000, write now to the address below or use the reader reply service card.

Pye Unicam

A SCIENTIFIC INSTRUMENT COMPANY OF PHILIPS
York Street Cambridge CB1 2PX England
Telephone (0223) 58866 Telex 817331

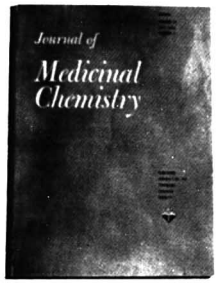
CIRCLE 99 ON READER SERVICE CARD



IT'S GOOD FOR YOU!

Journal of Medicinal Chemistry

Chemists, pharmacologists, research physicians . . . keep up with developments in the design and synthesis of novel medicinal agents . . . the correlation of molecular structure with biological activity . . . and studies on the relationship between chemical constitution, distribution and metabolism of drugs, with this authoritative monthly journal.



The Journal, publishing approximately 400 papers a year, is one of the fastest growing journals in its field.

Subscribe now — and learn why the *Journal of Medicinal Chemistry* is the *prescription of choice* for those who like to stay current in this fast-moving field.

CALL TOLL FREE New Orders (800) 638-2000 / MD Only (301) 949-1551 or mail the coupon below.

Journal of Medicinal Chemistry 1979
American Chemical Society
1155 Sixteenth Street, N.W.
Washington, D.C. 20036

YES, I would like to receive JOURNAL OF MEDICINAL CHEMISTRY at the one-year rate checked below:

	U.S.	Foreign Countries**
ACS Member, One-Year Rate*	☐ $21.00	☐ $27.00
Nonmember	☐ $84.00	☐ $90.00

Payment enclosed. ☐ Bill me. ☐ Bill company. ☐

Name _____

Organization _____ Title _____

☐ Home
Address ☐ Business _____

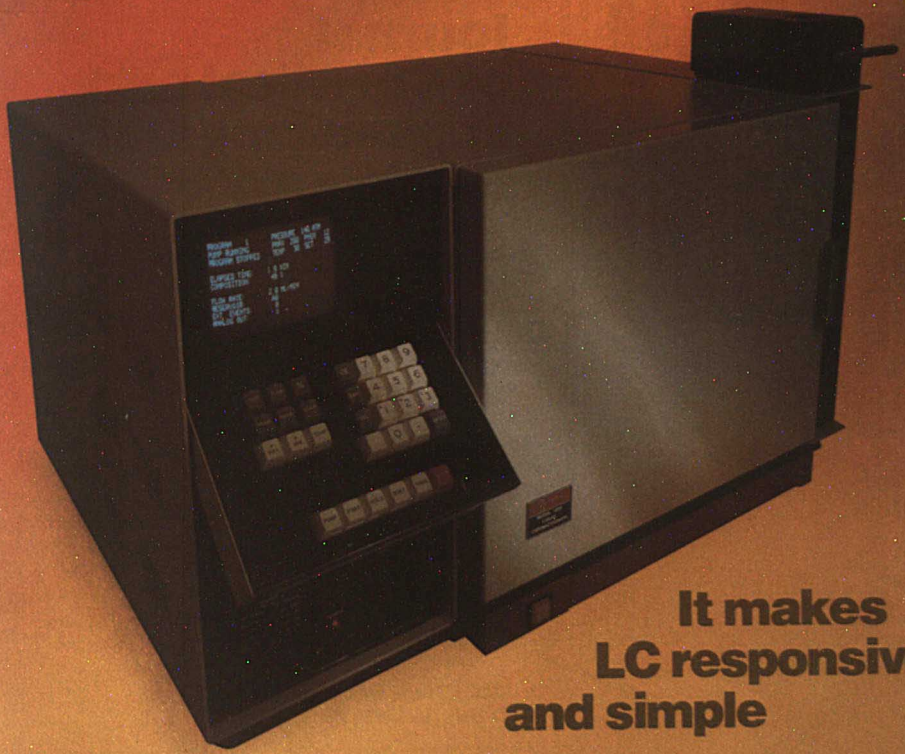
City _____ State _____ Zip _____

Journal subscriptions start January 1979

**Note: Subscriptions at ACS member rates are for personal use only.*

***Payment must be made in U.S. currency, by international money order, UNESCO coupons, U.S. bank draft, or order through your book dealer.* 0034L

INTRODUCING
the Varian 5000 family of liquid chromatographs



It makes LC responsive and simple

The Varian 5000 Series is a family of powerful microcomputer-CRT-based liquid chromatographs that make LC easy for anyone.

It makes tough separations seem simple. The helpful CRT continuously displays *all* instrument conditions. Tells you everything you need to know, right now. Responds to you. Helps you build programs. Prompts and leads you. Makes LC easier than ever before.

It comes with full support. With your Model 5000 you receive a commitment from Varian to provide strong, continuing support—training, service and applications assistance—that will assure successful solution of your liquid chromatography problems.

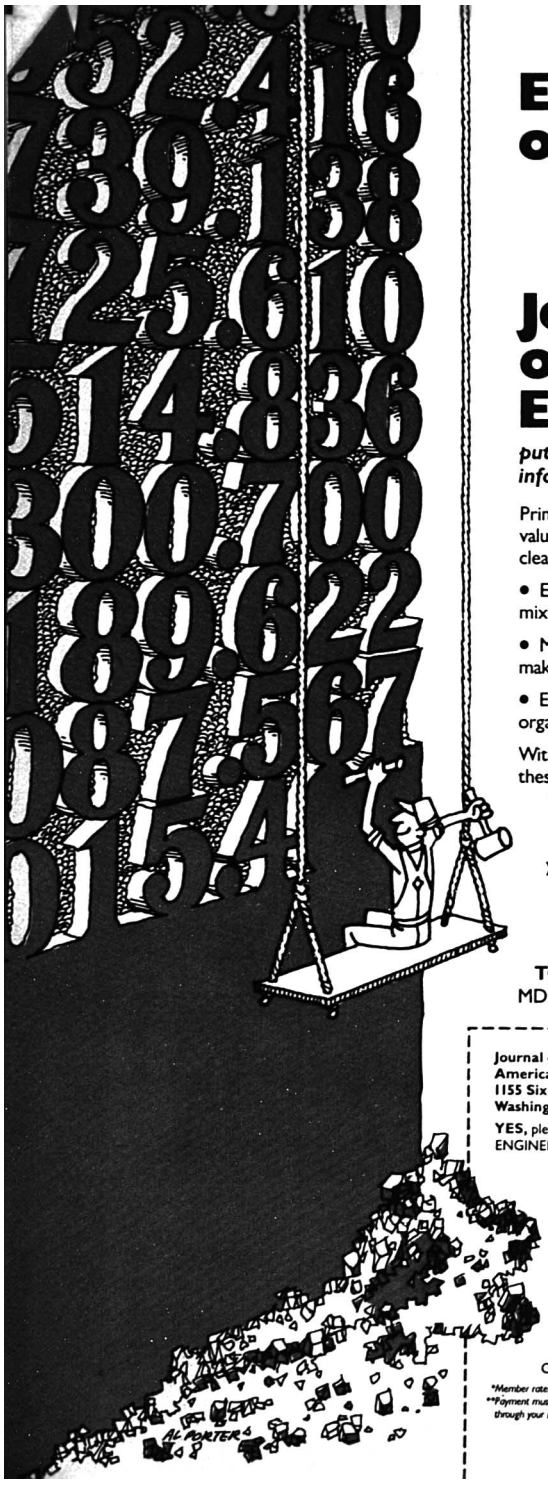
Price/performance. There are six basic models in the 5000 Series: from simple isocratic to completely automatic gradient systems. Each is designed to offer unbeatable price/performance; to provide a new level of LC capability at system prices lower than most LC components.

Upward expandability. 5000 Series chromatographs are upward expandable and offer many options. You can configure a 5000 that is exactly right for your laboratory. Later, as your needs change, you can add whatever new capability you require.

For full details on a 5000 that may be exactly right for you, circle Reader Service Number 222.

To have a Varian representative contact you, circle Reader Service Number 223.

varian



Experimental data of lasting value

Journal of Chemical and Engineering Data

puts precise, reliable, useful technical information at your fingertips

Primarily concerned with the presentation of data of lasting value, this authoritative quarterly journal covers several clearly defined areas:

- Experimental data relating to pure compounds or mixtures covering a range of states
- Manuscripts based on published experimental information making tangible contributions through their presentations
- Experimental data that aid in identifying or utilizing new organic or inorganic compounds.

With your professional activities or interests dependent on these vital fields, the JOURNAL OF CHEMICAL AND ENGINEERING DATA will prove an important research and reference tool, since the information it covers is carefully selected for its value both now and in the years ahead.

Use the coupon below or the toll-free number to enter your subscription now — and keep current today and *tomorrow!*

TOLL FREE: New Orders: (800) 638-2000
MD Only: (301) 949-1551

Journal of Chemical and Engineering Data **1979**
American Chemical Society
1155 Sixteenth Street, N.W.
Washington, D.C. 20036

YES, please enter my one-year subscription to JOURNAL OF CHEMICAL AND ENGINEERING DATA as follows:

	U.S.	*Foreign***
ACS Member*	☐ $20.00	☐ $23.00
Nonmembers	☐ $80.00	☐ $83.00

☐ Payment enclosed. (Payable to American Chemical Society)

☐ Bill me. ☐ Bill company.

Name _____

Title _____

Organization _____

Address _____

City, State, Zip _____

*Member rates are for personal use only
**Payment must be made in U.S. currency, by international money order, UNESCO coupons, U.S. bank draft, or order through your book dealer

Journal subscriptions start January 1979.
0034L

Announcing:

Finnigan Series 1020 Automated GC/MS

Now the power of GC/MS analysis is within reach of every laboratory.



- Significantly lower initial cost
- Simplified, automated operation
- Fast sample throughput
- Highest qualitative and quantitative performance
- Reduced maintenance and operating costs

The need for a GC/MS system suitable for routine, simplified, general purpose analyses has led to the Finnigan 1020. A number of design innovations, based on our years of experience in GC/MS and in data system technology, make the Finnigan 1020 suitable for modern laboratories which need the performance of GC/MS analysis but which have been reluctant to use it.

A powerful set of data acquisition, data processing and system control software is included with the instrument. The operator need not be an instrument expert however, because of the 1020's unique method of automatic program selection. Maximum analysis throughput is achieved because the system can acquire and process data simultaneously; that is, perform both foreground and background computer operation.

Data collected on the disc cartridge can be further processed on any Incos data system such as that incorporated in the Finnigan 4000 Series. This capability makes the Series 1020 an ideal workhorse partner for the 4000 in laboratories already equipped with the more comprehensive Finnigan instrument.

If your laboratory requires the power of GC/MS analysis, let Finnigan—the GC/MS people—show you how the 1020 Series can meet your needs more easily and inexpensively than ever before. It'll pay for itself many times over.

finnigan
Instruments
A DIVISION OF FINNIGAN CORPORATION
845 WEST MAUDE AVENUE
SUNNYVALE, CALIFORNIA 94086
(408) 732-0940

©Finnigan Instruments, 1979

CIRCLE 75 ON READER SERVICE CARD

Laser Raman Molecular Microprobe (MOLE)

P. Dhamelincourt and F. Wallart
Laboratoire de Spectrochemie Infrarouge et Raman, C.N.R.S., Université de Lille, B.P. 36, 59650 Villeneuve d'Ascq, France

M. Leclercq and A. T. N'Guyen
I.S.A. Nord
35 rue Inkermann
59000 Lille, France

D. O. Landon
I.S.A. Inc.
173 Essex Avenue
Metuchen, N.J. 08840

This new microanalysis technique for detecting, identifying, and obtaining the distribution of the different components of an heterogeneous sample is similar to electron or ion microprobe methods. However, an important advantage is the ability to study samples in air, under a controlled atmosphere, or even inside transparent media rather than just in a vacuum

Most microanalysis physical methods are based on atomic properties and only indirectly provide information on how atoms link together to form polyatomic structures. This is the case for electron or ion microprobe methods, which are based on the analysis of electron X-rays or secondary ions emitted by samples under electron or ion beam impact. These methods often fail to yield information on chemical bonds and conformation of molecules.

In the laser molecular microprobe (*1, 2*), photons generated by a laser are used to excite the sample and cause the emission of Raman lines of different components. By use of these Raman lines, each component can be detected, identified, and then located by forming a micrographic image that gives the "map" of its distribution in the sample. This is the principle of the nondestructive microanalytical method described here.

Instrument Description

The basic instrument (*3–6*) combines a conventional optical microscope (with bright and dark field illumination), an optical filter possessing a very low stray light level, and a multichannel and/or monochannel detection system. This configuration gives a very versatile instrument because it permits different modes of operation without disturbing the sample. A block diagram of the instrument is shown in Figure 1.

A laser (argon, krypton, dye laser, etc.) is the monochromatic source of light used for irradiating the sample.

A conventional optical microscope provides an illuminatory stage and forms part of the imaging system. The sample under study is placed on the microscope stage. All modes of observation available in a standard optical microscope are available in the instrument; therefore, the samples can be studied in air, liquid, or transparent media.

A double monochromator spectrometer with two concave aberration corrected gratings is the central part of the instrument. This device permits spectral separation of the chosen spectral line, which corresponds to a particular vibrational mode, and it transmits good images in a wide spectral range without changing components.

The detection system is composed of two separate assemblies. One, which has a photomultiplier, records the spectrum on a chart recorder. The other has a three-stage image intensifier, a TV-type detector, and a visualization system that displays micrographic images. A computer and disc or tape memory can be attached to the system for information processing and storage. Figure 2 gives the optical scheme of the instrument.

Modes of Operation

The two modes of operation currently used depend on the type of irradiation of the sample.

Punctual Illumination with Monochannel or Multichannel Detection. By use of the bright field illumination system of the microscope, the same objective (50×, NA, 0.85–100×, N/A, 0.90) focuses the laser beam into a spot on the component of the sample to be identified and collects the scattered light. In this case, the top aperture of the objective, the grating surfaces, the sample, and entrance slit are simultaneously optically aligned by the transfer optic. To obtain the Raman spectrum, the optical filter can function as a Raman spectrometer when the detector is a photomultiplier followed by an amplifier and a chart recorder, or as a Raman spectrograph when the detector is an intensifier phototube, followed by a low-level TV camera (SIT or SEC tube).

Global Illumination and Imaging System. Selecting, in the Raman spectrum, radiation characterizing one particular component forms a micro-

0003-2700/79/0351-414A$01.00/0
© 1979 American Chemical Society

graphic image that gives the distribution of this component. The aperture of the microscope objective (O) (Figure 2) is optically aligned with the three slits (O_1, O_2, O_3) of the optical filter. The image (S_1) of the sample (S) given by the objective is formed on the gratings (S_2, S_3) and goes through the aperture of the exit slit (O_3) to the photocathode of the intensifier tube (S_4). A rotating laser beam feeding the objective annular illuminator (dark field illuminator) homogeneously illuminates the sample and suppresses the "speckle noise" of the images. The spatial resolution of the images is about 1 μm.

The Spectral Mode. In the *monochannel spectral mode* classical Raman spectra can be recorded of the entire sample or of a specific portion selected to identify positively the nature of that portion.

In the *multichannel spectral mode* the Raman spectra can be observed in spectrographic form on an oscilloscope in real time in up to 100-cm^{-1} segments. This mode is particularly useful for monitoring the evolution of a sample.

The Imaging Mode. To locate one of the components of the sample, an image of the surface obtained from a characteristic line of this component can be directly observed on the TV monitor screen. This allows "mapping" the distribution of a given substance in a heterogeneous sample.

Some Applications of the Laser Raman Microprobe

To show the many possibilities opened by the laser Raman microprobe, we now present some examples of applications of the instrument.

Geochemistry and Geophysics. The first example is a fragment of a natural stone of celestine (collection of the Faculty of Science of Lille, France). The stone has been cut and roughly polished to make it approximately plane. By examination under an optical microscope (dark field illumination by reflected white light), an area comprising crystal inclusion is selected.

In the monochannel spectral mode, using punctual illumination (spot diameter: 2 μm), we obtain a characteristic Raman spectrum for each of the two areas of interest (Figures 3 and 4).

In the multichannel spectral mode, using global illumination, we isolate the 473-cm^{-1} wavelength characteristic of sulfur, and the image is observed at this wavelength in the imaging mode (Figure 5). Similarly, the 1000-cm^{-1} wavelength characteristic of $SrSO_4$ is isolated, and the image is observed at this wavelength (Figure 6).

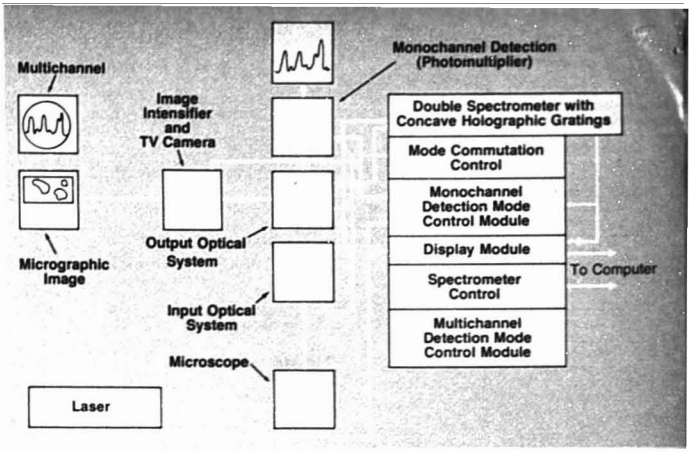


Figure 1. Block diagram of laser Raman microprobe

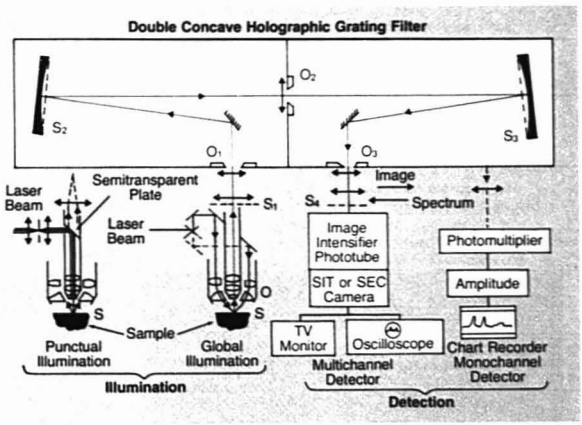


Figure 2. Optical scheme of instrument

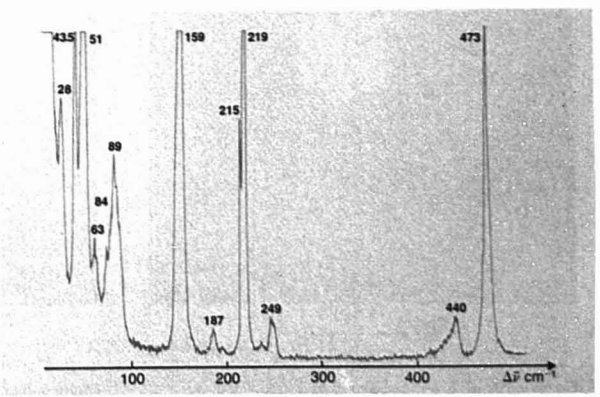


Figure 3. Raman spectrum of Celestine crystal inclusion: sulfur

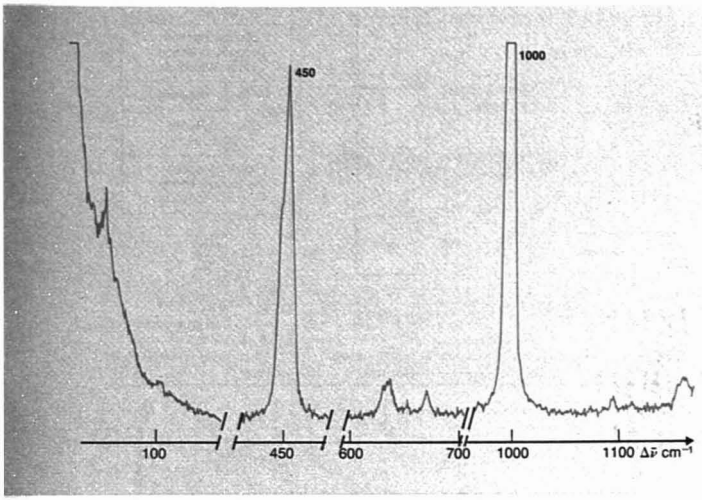


Figure 4. Raman spectrum of area around same inclusion: Strontium sulfate

When the image at the characteristic line of $SrSO_4$ is observed, the sulfur is no longer obvious but its trace is still visible. The sulfur crystal in the plane of the surface is thin and therefore transparent to the radiation emitted by $SrSO_4$. Further impurities at the surface appear as dark spots on the micrographic image. Fluid inclusions can also be directly analyzed (7) provided that the matrix is sufficiently transparent to the laser beam and scattered light.

Archeology and Gemnology. Knowing the exact nature of a stone object without taking a sample (even a microscopic one) would be greatly beneficial in any museum of art and archeology. With the laser Raman microprobe, it is possible to identify directly the nature of the stone.

Examining the precise location of a small area of the stone can prevent contact with fluorescent impurities, which are often present in natural materials and which, in most cases, prevent the recording of Raman spectra with a classical Raman spectrometer.

Figure 7 shows the comparison between Raman spectra obtained from

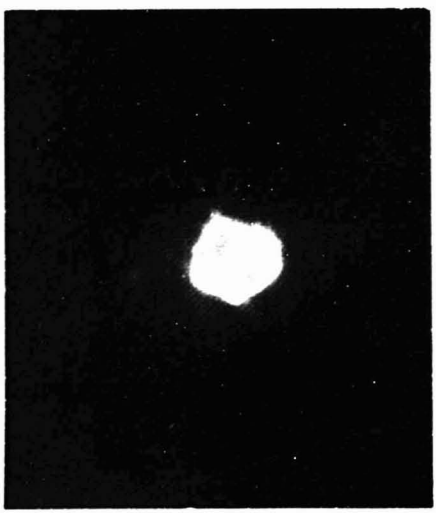


Figure 5. Raman image of sulfur inclusion obtained with 473-cm^{-1} line

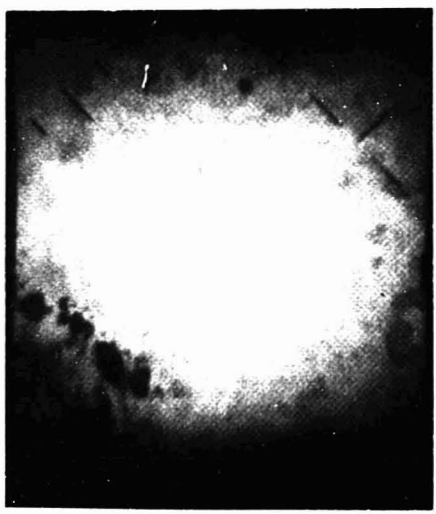


Figure 6. Raman image of same area obtained with 1000-cm^{-1} characteristic line of sulfate

a precious Chinese vase and from a sample of serpentine (*8*).

Another important application is the determination of authenticity and geographical origins of gems by identifying in situ the solid inclusions present in precious stones.

Investigation of Defects in Industrial Materials. The formation of bubble-like inclusions is a problem currently encountered in the commercial production of glass. The in situ analysis of bubble content aids in properly selecting materials and process parameters which will inhibit their formation.

Figure 8 represents one example of the investigation of solid deposits on the wall of a bubble inside a sample of industrial glass (in collaboration with the Inorganic Chemistry Laboratory E.N.S.C. Strasbourg, France). Spectra a, b, and c represent sulfur, polysulfide, and sulfate of sodium, respectively. Each deposit can be imaged by use of a characteristic Raman line.

Pollution Analysis. This new nondestructive analytical tool is also perfectly suited to the study and identification of urban and industrial dusts. Figure 9 shows the results obtained from dust collected on a highway. The two broad maxima near 1400 and 1600 cm^{-1} (Figure 9c) are often observed on the spectra of air particulate dust. They can be attributed to degraded organic compounds or soot coating (*9*).

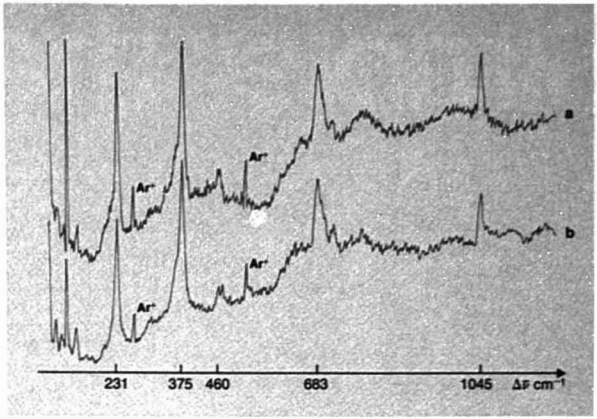


Figure 7. Raman spectra obtained from a) precious Chinese vase, b) specimen of serpentine

Industrial Quality Control. In the industrial field, it is very important to control the quality of manufactured products. Local defects in synthetic films or fibers impair their clarity and can cause rending. The compounds responsible for these defects can be identified with MOLE (molecular optics laser examiner) by simply recording in situ the Raman spectra of the defects. Generally, the defects are caused by atmospheric dusts, local differences of crystallinity, degraded areas, or local concentration of copolymers.

These studies are useful for quality control of semiconductors and integrated circuits. Figure 10 shows the spectra of different parts of an integrated circuit and the pollutants discovered on its surface. The major pollutant found was lead acetate mixed with organic compounds.

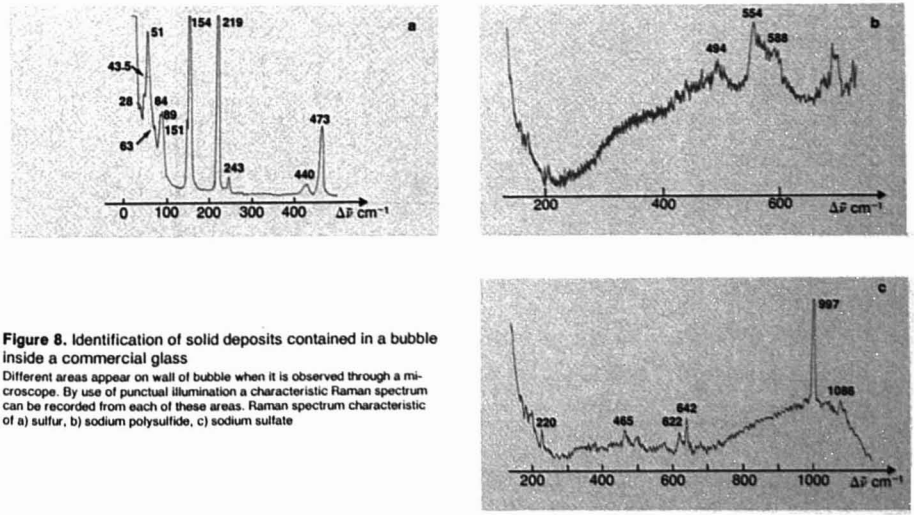


Figure 8. Identification of solid deposits contained in a bubble inside a commercial glass

Different areas appear on wall of bubble when it is observed through a microscope. By use of punctual illumination a characteristic Raman spectrum can be recorded from each of these areas. Raman spectrum characteristic of a) sulfur, b) sodium polysulfide, c) sodium sulfate

Simpler than AA!



Faster, and more versatile too. That's ICP (Inductively Coupled Plasma), the most advanced method of elemental analysis available. Better than Atomic Absorption because it's simpler. And the best ICP's available are from ARL. That's saying a lot. But then ARL's complete line of ICP's do a lot. Here's what we mean:

- **Faster**—Simultaneous multi-element analysis—up to 60 elements at once and 3000 determinations per hour means speed and efficiency unavailable with AA.
- **Increased Versatility**—For changing requirements you select the elements of interest at any time with ARL's ICP. What could be simpler?
- **Greater Sensitivity**—Superior to flame AA across the periodic table. Up to a million times more sensitive than flame AA for rare earths and refractory elements. You get boron at 5 ng/ml, and sulfur at 40 ng/ml among others.
- **More Reliable**—Simple, yet solid, ARL design requires fewer instrument settings to adjust, less sample preparation and therefore, less chance for error. *Greater accuracy!*

So whatever your analytical task—water quality, soils, foods, pharmaceuticals, petroleum, biological, or geological—use ICP. And when you do, choose ARL, the first to introduce a commercial ICP system, and the company whose sole business is spectrochemistry. We've got a network of manufacturing plants, sales and service engineers and technical support specialists on six continents ready to serve you.

We're ARL. The company whose ICP makes solutions... Simpler!
Ask us to show you how.

ARL
a division of BAUSCH & LOMB

USA	9545 Wentworth St., Sunland, California 91040
FRANCE	78320 Le Mesnil Saint-Denis
AUSTRIA	Rudolfinergasse 2, A-1190 Wien
AUSTRALIA	P.O. Box 426, Brookvale NSW 2100
CANADA	P.O. Box 147, Mississauga, Ontario L4T 3B5
SUISSE	En Vallaire, 1024 Ecublens
GB	Wingate Road, Luton, Bedfordshire
BRD	Konigstrasse 5, D-4000 Dusseldorf
SVERIGE	Rasundavagen 101, S-17103 Solna
RSA	P.O. Box 557, 1620 Kempton Park

CIRCLE 3 ON READER SERVICE CARD

MOLECULAR SPECTROSCOPY ON A MICROSCOPIC SCALE

The MOLE — Molecular Microprobe Microscope Optical Laser Examiner — represents an innovative technique in spectroscopic analysis.

MOLE can identify molecular components, can map their distribution in microscopic samples, and can monitor in real time their physio-chemical changes.

Samples down to one micron can be studied non-destructively under ambient conditions without special preparation.

The MOLE provides three options for experimental analysis:

- A microscopic Raman or fluorescence spectrum
- A microscopic Raman image on a video system
- A real-time spectrographic display on a vidicon system

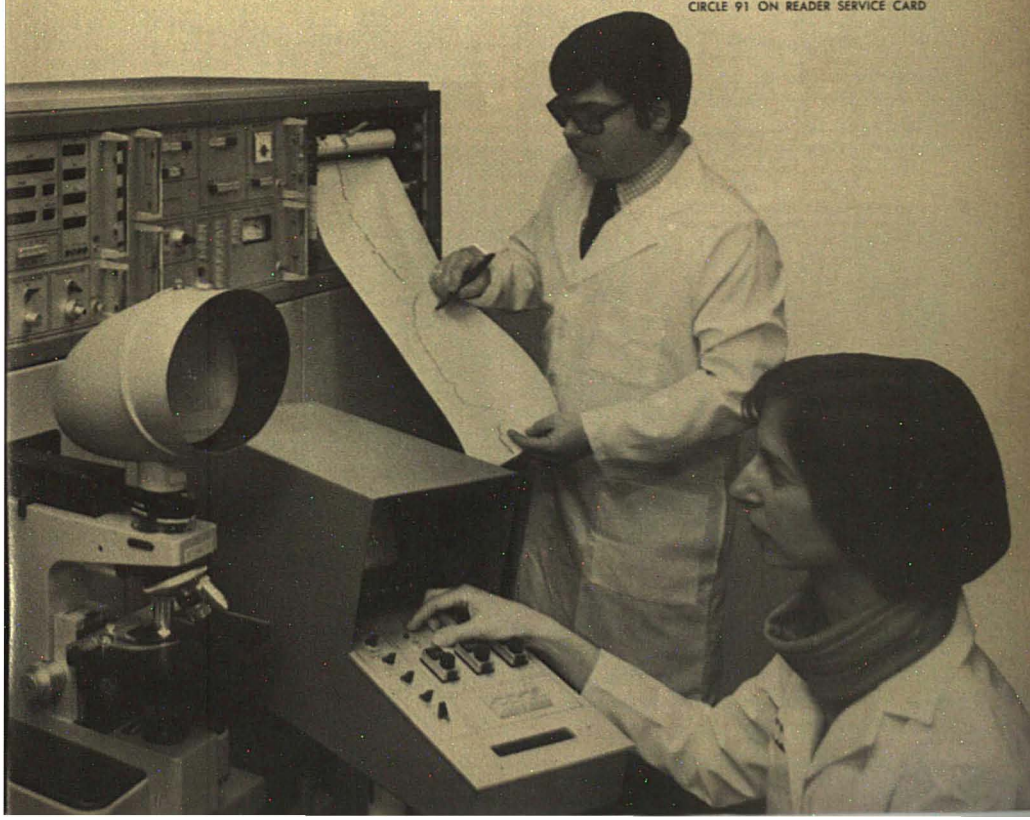
In the past year we have solved a number of problems for clients in such fields as geology, plastics, microelectronics, fibers and pollution studies.

Instruments SA has three molecular spectroscopy laboratories in operation. Each is staffed by outstanding spectroscopists, who would be pleased to consider your requirements in strict confidence. If you would like to discuss your application or receive more information about the MOLE, please call or write today.

Instruments SA, Inc., J-Y Optical Systems Division, 173 Essex Avenue, Metuchen, N.J. 08840. (201) 494-8660. Telex 844-516. In Europe, Jobin Yvon, Division d'Instruments SA, 16-18 Rue du Canal, 91160 Longumeau, France, Tel. 909.34.93 Telex JOBYVON 842-692882.

JOBIN YVON Instruments SA, Inc.
J-Y Optical Systems Division

CIRCLE 91 ON READER SERVICE CARD



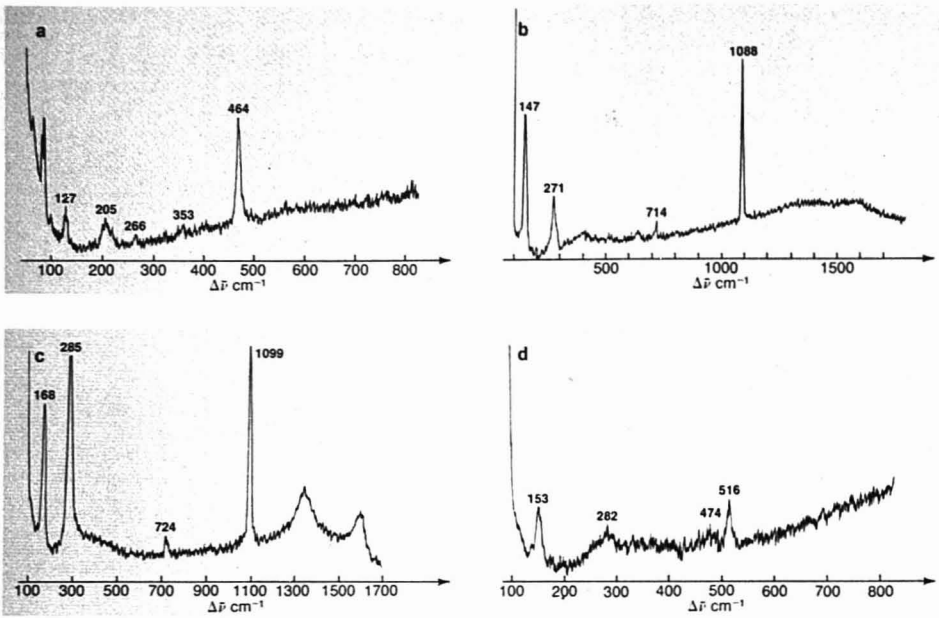


Figure 9. Raman spectra of some particles (2–10 μ in size) removed from surface of a collection filter placed near a highway
Raman spectrum of a) quartz particle (α-SiO_2), b) calcite particle ($CaCO_3$), c) Dolomite particle [$CaMg(CO_3)_2$], d) Feldspar particle (Orthoclase)

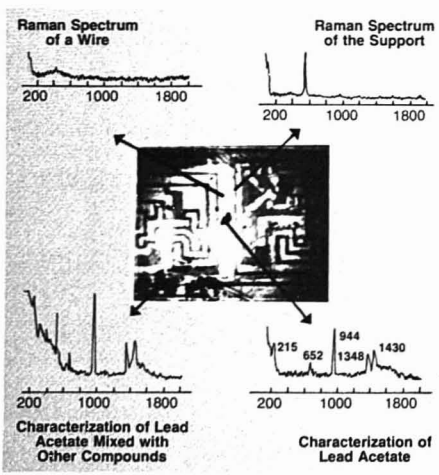


Figure 10. Analysis of pollutants found at surface of a commercial integrated circuit



Figure 11. Micrographic image (×300) of part of an histological section of *Blatella germanica L*

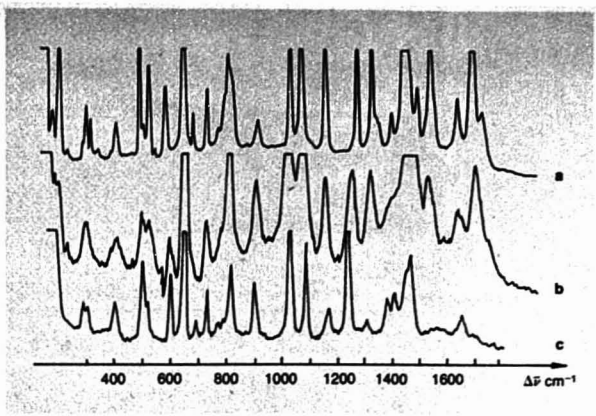


Figure 12. Raman spectra obtained from a) commercial sample of uric acid (particle ~5 μ in size), b) fat body spherocrystal (~5 μ in diameter), c) commercial sample of potassium urate (particle ~5 μ in size)

Biology. Important information unattainable by electron or ion microprobe can be obtained on biological samples. For example, Figure 11 shows spherocrystals (*10*) (1–12 μ) of fat body of *Blatella germanica L.* (*Insecta Dictyoptera*). Fat body can be roughly considered as the liver of invertebrates, and puric catabolism is important. The samples are histological sections of fixed and paraffin-embedded material. Traditional methods of study have given the following results (*10, 11*): biochemistry, uric acid; X-ray, amorphous structure; and Castaing microprobe, abundant K and small quantities of Ca and P. Figure 12 represents the spectra obtained from reference materials (uric acid, potassium urate) and fat body spherocrystals. A comparison between these spectra shows that fat body is mainly composed of uric acid with a small amount of potassium urate.

Conclusions

The purpose of the results presented here is simply to show the widespread interest in this new microanalytical technique.

Several other fields will be investigated, and studies are already in progress (i.e., corrosion, and photochemical and electrochemical reactions). We expect the laser Raman microprobe to find application in laboratories using such microprobe techniques as Auger (AES), low-energy electron diffraction (LEED), X-ray photoelectron spectroscopy (ESCA), secondary ion mass spectrometry (SIMS), and electron microscopy. The high-energy intensity required in some of these techniques and sample treatment prevent their use on delicate samples. The Raman microprobe probably provides the only approach to surface analysis on living materials. In addition, the instrument performs nondestructive analysis in various media (air, controlled atmosphere or liquid) for small quantities of sample down to a few picograms.

The versatility of this new instrument should greatly facilitate microanalysis and structural determination, and complement other techniques.

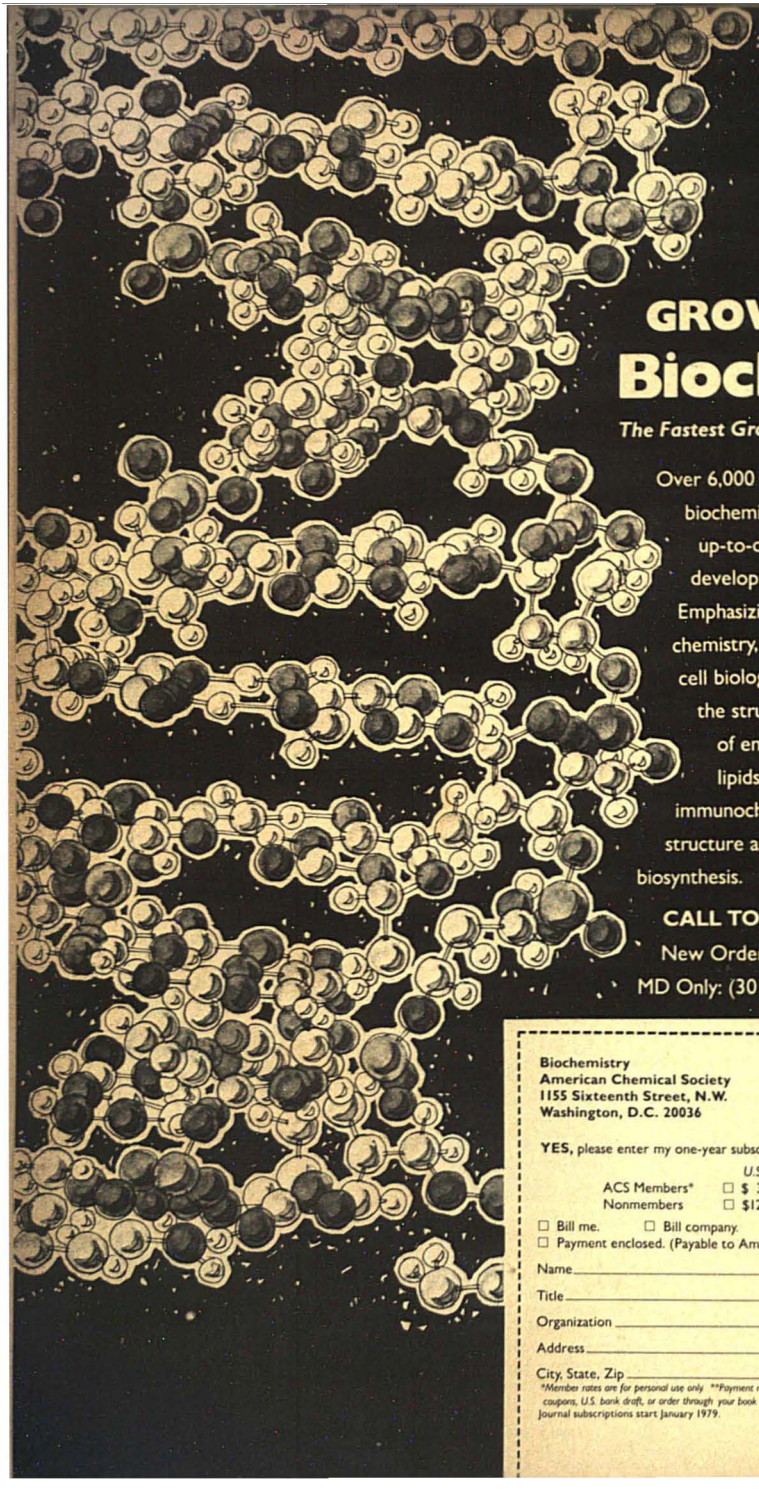


From left to right: P. Dhamelincourt has played a major role in the conception and realization of the molecular microprobe. He specializes in micro Raman spectroscopy. M. Leclercq was in charge of the Mole Laboratory at Lirinord Division Instrument S.A. He is now technical manager at D.I.L.O.R. (rue des Bois Blancs à Lille, France). A. T. N'Guyen worked in the Mole Laboratory at Lirinord Division Instrument S.A. He is now in charge of the Application Laboratory at D.I.L.O.R. F. Wallart is assistant professor at the University of Lille. He specializes in Raman spectroscopy and instrumentation. D. O. Landon (not shown) is manager of research and development at Instruments S.A., Metuchen, N.J. His interests include optical spectroscopy and instrument design.

References

(1) M. Delhaye and P. Dhamelincourt, *J. Raman Spectrosc.*, **3**, 33 (1975).
(2) G. J. Rosasco, E. S. Etz, and W. A. Cassatt, *Appl. Spectrosc.*, **29**, 396 (1975); in Proc. of the Fifth Int. Conf. on Raman Spectroscopy, E. O. Schmid et al., Freiburg, Germany, Sept. 2–8, 1976.
(3) M. Delhaye, P. Dhamelincourt, and Y. Moschetto, U.S. Patent 4,030,827 (1977).
(4) M. Delhaye, P. Dhamelincourt, and E. Da Silva, French Patent ANVAR 762 1539 (1976).
(5) P. Dhamelincourt and P. Bisson, *Microsc. Acta*, **79**, 267 (1977).
(6) P. Dhamelincourt, "Lasers in Chemistry," Elsevier, Amsterdam, The Netherlands, 1977.
(7) G. J. Rosasco, E. Roedder, and J. H. Simmons, *Science*, **190**, 557 (1975).
(8) P. Dhamelincourt and H. J. Schubnel, *Rev. Gemnol.*, **52**, 11 (1977).
(9) E. S. Etz and G. J. Rosasco, "Environmental Analysis," Academic Press, New York, N.Y., 1977.
(10) C. Ballan-Du Francais, doctoral thesis, Paris, France, 1975.
(11) C. Ballan-Du Francais, *Cellule*, **70**, 317 (1974).

This study financially supported by C.N.R.S., University of Lille, the Direction Générale de la Recherche Scientifique, and the Agence Nationale pour la valorisation de la Recherche of France.



GROW WITH Biochemistry

The Fastest Growing Journal in Its Field

Over 6,000 pages a year of current biochemical research keep subscribers up-to-date in all recognized and developing areas of the fast-moving field. Emphasizing the close relationship between chemistry, biochemistry, and molecular and cell biology, this timely biweekly covers the structure, function, and metabolism of enzymes, proteins, carbohydrates, lipids, nucleic acids, as well as immunochemistry, genetics, membrane structure and function and protein biosynthesis.

CALL TOLL FREE:

New Orders: (800) 638-2000

MD Only: (301) 949-1551

Biochemistry **1979**
American Chemical Society
1155 Sixteenth Street, N.W.
Washington, D.C. 20036

YES, please enter my one-year subscription to BIOCHEMISTRY as indicated:

	U.S.	*Foreign***
ACS Members*	☐ $ 32.00	☐ $ 44.00
Nonmembers	☐ $128.00	☐ $140.00

☐ Bill me. ☐ Bill company.
☐ Payment enclosed. (Payable to American Chemical Society.)

Name _____

Title _____

Organization _____

Address _____

City, State, Zip _____

*Member rates are for personal use only **Payment must be made in U.S. Currency, by international money order, UNESCO coupons, U.S. bank draft, or order through your book dealer
Journal subscriptions start January 1979.

0034L

polarimetry simplified

the autopol® series by rudolph research

Only two controls are needed to operate the Autopol, power and reset, all other functions are completely automatic. Rudolph's automatic polarimeters and saccharimeters offer wide range, high precision design and construction at a reasonable price.

Send for more information today. Call or write Rudolph Research, 40 Pier Lane, Fairfield, N.J. 07006 201/227-6810.



RUDOLPH RESEARCH
the Polarimetry experts

CIRCLE 185 ON READER SERVICE CARD

total sulfur measured below 1 PPM, up to 100% in....

☑ gases!
☑ liquids!
☑ solids!



It's the Houston Atlas Model 856/825R-d Total Sulfur Analyzer

For true versatility and accuracy, the Houston Atlas Model 856/825R-d has it! Plus reliability. And effective control. It routinely measures sulfur without interference in just 6-minutes time. Response is linear, with direct input to the recorder, making possible the elimination of complicated calculations. Effortless operation is achieved without need for technical personnel.

Actual applications by major laboratories have already proved the reliability and usefulness of the Model 856/825R-d.

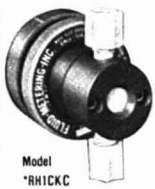
Write right now for details, or call 713/462-6116. Houston Atlas, Inc., 9441 Baythorne Drive, Houston, Texas 77041.

HOUSTON ATLAS, INC.

CIRCLE 94 ON READER SERVICE CARD

FMI METERING PUMPS

The FMI LAB PUMP line of valveless, variable metering pumps is available from stock at catalog prices. Models are available with maximum flow rates as low as microliters per minute or as high as one liter per minute at pressures to 200 PSIG. A wide variety of pump head materials offer superb chemical resistance. New items include: RYTON* liners, miniature panel mount pumps, and water flush gland option for use with problem fluids.



Model *RHICKC

*This model has a variable displacement of 0.01 to 0.1 ml/revolution
Price $250.00

FMI FLUID METERING, INC. SINCE 1959
P.O. BOX 507, OYSTER BAY, N.Y. 11771 • (516) 922-6050

CIRCLE 77 ON READER SERVICE CARD

TEFLON® PFA THREADED VIALS, BOTTLES & JAR CONTAINERS

For difficult-to-handle solutions and exacting specimen preservation problems



- STERILIZE/HEAT TO +500° F
- UNBREAKABLE TO -320° F
- CHEMICALLY RESISTANT
- INERT
- NONSTICK
- TRANSLUCENT

15 SIZES IN STOCK: 5cc THROUGH 1 LITER WITH SPECIAL ADAPTATION FOR FLUID TRANSFER

NEW: FILTER HOLDERS & MEMBRANES, SYRINGE CAP CONTAINERS, CORROSION CELLS, ADDITIONAL CLOSURE SIZES ALL IN TEFLON

* DUPONT TM

SAVILLEX CORP. (612) 938-7727
5325 HWY. 101 MINNETONKA, MINN 55343

CIRCLE 194 ON READER SERVICE CARD

LABORATORY SERVICE CENTER

Aluminon • ε-Amino-n-caproic Acid • DL & L-Aspartic Acids • Aurin
Benzamide • 2,7-Diaminofluorene • 3,3-Dimethylglutaric Acid • Dulcitol
Ethanesulfonic Acid • Hydroxylamine HCl & Sulfate • Iodobenzene
Neocuproine & HCl • 4-(p-Nitrobenzyl)pyridine • o-Nitrophenylacetic Acid
Orcein • Orcinol • Potassium & Sodium m-Periodates • Pyruvic Acid
Reinecke Salt • Salicin • Silver & Sodium Diethyldithiocarbamates
Sodium Tetraphenylboron • Suberic Acid • Tetramethylcyclobutanedione
Thymolphthalein • Triphenylmethane • Triphenyl Phosphine • o-Vanillin

Write for our Products List of over 3000 chemicals

Tel: 516-273-0900 TWX: 510-227-6230

EASTERN CHEMICAL
Division of GUARDIAN CHEMICAL CORP.
BOX 2500 K
HAUPPAUGE, N. Y. 11787

environmental & material analysis
■ Water, waste water, sewage ■ Industrial hygiene
■ Precious metal fire assay ■ Microbiology ■ GC IR
■ Spectrographic analysis ■ Metals, ores, chemicals
princeton testing laboratory
Princeton Svc. Ctr.
U.S. Hwy 1, Box 310R
Princeton, N.J. 08540
(609) 452-9050

SOLVENTS—Highest Purity
Call or write for prices.
Pollard & Co. Box 7131 Wilmington, DE 19803
Phone: 302-656-0060

Laboratory Service Center (Equipment, Materials, Services, Instruments for Leasing), Maximum space — 4 inches per advertisement. Column width, 2-3/16"; two-column width, 4-9/16". Artwork accepted. No combination of directory rates with ROP advertising. Rates based on number of inches used within 12 months from date of first insertion. Per inch: 1" — $69; 12" — $68; 24" — $65; 36" — $64; 48" — $63.

CALL OR WRITE BARBARA AUFDERHEIDE

ANALYTICAL CHEMISTRY
25 Sylvan Road, So.
Westport, Ct. 06880
203-226-7131

USE LABORATORY SERVICE CENTER

INDEX TO ADVERTISERS IN THIS ISSUE

CIRCLE INQUIRY NO.	ADVERTISERS	PAGE NO.
2	*Academic Press — Flamm Advertising	397A
4	*Alltech Associates — Chromad	395A
1	*Altex Scientific, Inc. — Oliver Smith Advertising, Inc.	307A
3	*Applied Research Laboratory — Illustrated Design Services	418A
18	J. T. Baker Chemical Company — Naimark & Barba, Inc.	315A
24	Barnstead — Marketing Dimensions, Inc.	IFC
26	*Beckman Instruments, Inc. — Ayer Jorgensen MacDonald	344A
xxx	Beckman Instruments, Inc. — Bernard Hodes Advertising, Inc.	402A
27	*Beckman Instruments SID — Ayer Jorgensen MacDonald	380A
22	*Bio-Rad Laboratories — Fred Schott & Associates	339A
20	*Brinkmann Instruments, Inc. — Blatt Advertising, Inc.	OBC
21	*Buchler Instruments — Jud Jaffe Advertising	322A
23	*Burdick & Jackson Laboratories, Inc. — Studio 5 Advertising	402A
34	Chrompack — Mealer & Emerson, Advertising	330A
33	Corco Chemical Corporation — Sit/Com	361A
32	*Crawford Fitting Company — Falls Advertising Company	383A
46, 48	Digital Equipment Corporation — Creamer, Trowbridge, Case & Basford, Inc.	323A, 387A
50-57	Dionex — Fred Schott & Associates	327A
63	*Eastman Kodak Company — Rumrill-Hoyt, Inc.	389A
75	*Finnigan Instruments — Robert Pease & Company Advertising	413A
78	Fischer & Porter Company — Furlong Promotions, Inc.	401A
77	Fluid Metering, Inc. — Arnold H. Nachman Associates	423A
85	*Gilford Instrument Laboratories, Inc. — Oberlin Industrial Advertising	384A
87	*Gilson Medical Electronics, Inc. — Fred Schott & Associates	336A
86	*Gow-Mac Instruments — Kenyon Hoag Associates	335A
88	Graphic Controls Corporation — Conklin, Labs & Bebee, Inc.	331A
96	*Hamilton Company — Mealer & Emerson Advertising	385A, 386A
xxx	*Hewlett-Packard — Benn Associates, Inc.	349A-356A
94	Houston Atlas — Harold Siegel Consultants	423A
89	Inficon — Paul, John & Lee, Inc. Advertising	390A
90, 91	*Instruments SA, Inc., J-Y Optical Systems Div. — Kathy Wyatt & Associates Advertising	395A, 419A
124	*Jarrell-Ash Div., Fisher Scientific Co. — Tech-Ad Associates	332A
98	*Johns-Manville — Frye-Sills Advertising	312A-313A
97	Joyce-Loebl — S. & M. E. Winship	330A
152	KineticSystems Corporation — Lockport Business Ads	405A
123	*Kontes — The Aitkin Kynett Co., Inc.	426A

INDEX TO ADVERTISERS IN THIS ISSUE

CIRCLE INQUIRY NO.	ADVERTISERS	PAGE NO.
129	*Labindustries Fred Schott & Associates	320A
126, 130	Lab Data Control Kelleher, Bamberger, Terry Advertising	321A, 371A
128	Labtest Equipment Company Clarke Advertising	400A
125	LECO Corporation LECOM	393A
127	The Lee Company Keiler & McKinlay Advertising	378A
136	3M Occupational Health & Safety Products Kamstra Communications, Inc.	360A
137–138, 145–151	*Matheson Kenyon Hoag Associates	310A, 311A
142–144	*Micromeritics Adgraphics	316A–317A, 398A
140	*Mitsubishi Chemical Industries Ltd. Global Advertising Co., Ltd.	328A
116	*Naige Labware Hutchins/Y & R	365A–368A
156	*Orion Research OBC Advertising	305A
166–169	*Perkin-Elmer Corporation Marquardt & Roche, Inc. Adv.	372A–373A, 374A, 377A, 379A
170	Photochemical Research Associates Quantum Communications	395A
173	Photovolt Corporation Michel-Cather Inc.	301A
174	*Physical Electronics Visual-Media Inc.	347A
171, 172	*Princeton Applied Research Corporation. The Message Center	325A, 343A
99–104, 114–119	**Pye Unicam Ltd.	410B–410E, 410F–410G, 410H
186	Raytheon Medical Electronics James A. Ford Advertising	408A
183	Reliance Glass Company MG Creative Arts	328A
184	*Rheodyne Bonfield Associates Advertising	340A
185	*Rudolph Research Kathy Wyatt & Associates	423A
190	Sanda, Inc. Ferguson Advertising	329A
195	*Sargent-Welch Scientific Company Polytech Advertising	394A
194	Savillex Corporation T. Russell Agency	423A
192	*Schleicher & Schuell, Inc. Jarman, Spitzer & Felix, Inc.	309A
188	Schott & Gen., Inc. Bloom-Zagoren, Inc. Advertising	363A
187	*Scientific Glass Engineering Arden Advertising Agency	334A
189	Shimadzu Seisakusho Ltd. General Advertising Agency, Inc.	324A
193	*Spectra Physics Paul Pease Advertising, Inc.	403A
191	SPEX Industries Seymour Nussenbaum	385A
206	Tokyo Kasei Kogyo Co., Ltd. Global Advertising Co., Ltd.	363A
204–205	*Tracor Analytical Instruments Aim Advertising Agency	381A
207	Turner Associates Fred Schott & Associates	359A
220–223, 226–231, 235–236	*Varian Moran, Lanig & Duncan Advertising	404A, 406A, 407A, 409A, 411A
240–242	*Waters Associates Marketing Dimensions, Inc.	314A
239	*Whatman, Inc. J. S. Lanza & Associates	302A
238	*John Wiley & Sons, Inc. 605 Advertising Group	341A

** See ad in ACS Laboratory Guide*

*** Company so marked has advertisement in Foreign Regional edition only.*

Advertising Management for the American Chemical Society Publications

CENTCOM, LTD.

Thomas N. J. Koerwer, President; James A. Byrne, Vice President; Clay S. Holden, Vice President; Benjamin W. Jones, Vice President; Robert L. Voepel, Vice President; 25 Sylvan Rd. South, Westport, Connecticut 06880 (Area Code 203) 226-7131

ADVERTISING SALES MANAGER
James A. Byrne

SALES REPRESENTATIVES

Atlanta, GA . . . Robert E. Kelchner, CENTCOM, Ltd. Telephone: 203-226-7131

Boston, MA . . . Don Davis, CENTCOM, LTD. Telephone 203-226-7131

Chicago . . . John W. McGuire, CENTCOM, LTD., 540 Frontage Rd., Northfield, Ill. 60093, 312-441-6383.

Cleveland . . . Bruce E. Poorman, CENTCOM, LTD., 17 Church St., Berea, Ohio 44017, 216-234-1333.

Houston . . . Robert LaPointe, CENTCOM, LTD., 415-781-3430

Denver . . . Clay S. Holden, CENTCOM LTD., 213-325-1903

Los Angeles 90045 . . . Clay S. Holden, CENTCOM, LTD., Newton Pacific Center, 3142 Pacific Coast Highway, Suite 200, Torrance, CA 90505, 213-325-1903

New York 10017 . . . Don Davis, Richard L. Going, CENTCOM LTD., 60 East 42nd St., 212-972-9660

Philadelphia . . . Richard L. Going, CENTCOM LTD., GSB Building, Suite 510 1 Belmont Avenue Bala Cynwyd, Pa. 19004. Telephone: 215-667-9666

San Francisco, CA . . . Robert E. LaPointe, CENTCOM, Ltd., Suite 303, 211 Sutter Street, San Francisco, CA 94108. Telephone: 415-781-3430

Westport, CT . . . Robert E. Kelchner, CENTCOM, Ltd., 25 Sylvan Rd. South, Westport, Ct. 06880. Telephone: 203-226-7131.

United Kingdom
Reading, England . . . Malcolm Thiele, Technomedia Ltd., Wood Cottage, Shurlock Row, Reading RG10 OQE. Telephone: 073-581-302
Manchester, England . . . Jill E. Loney, Technomedia Ltd., 216 Longhurst Lane, Mellor, Stockport SK6 5PW. Telephone: 061-427-5660

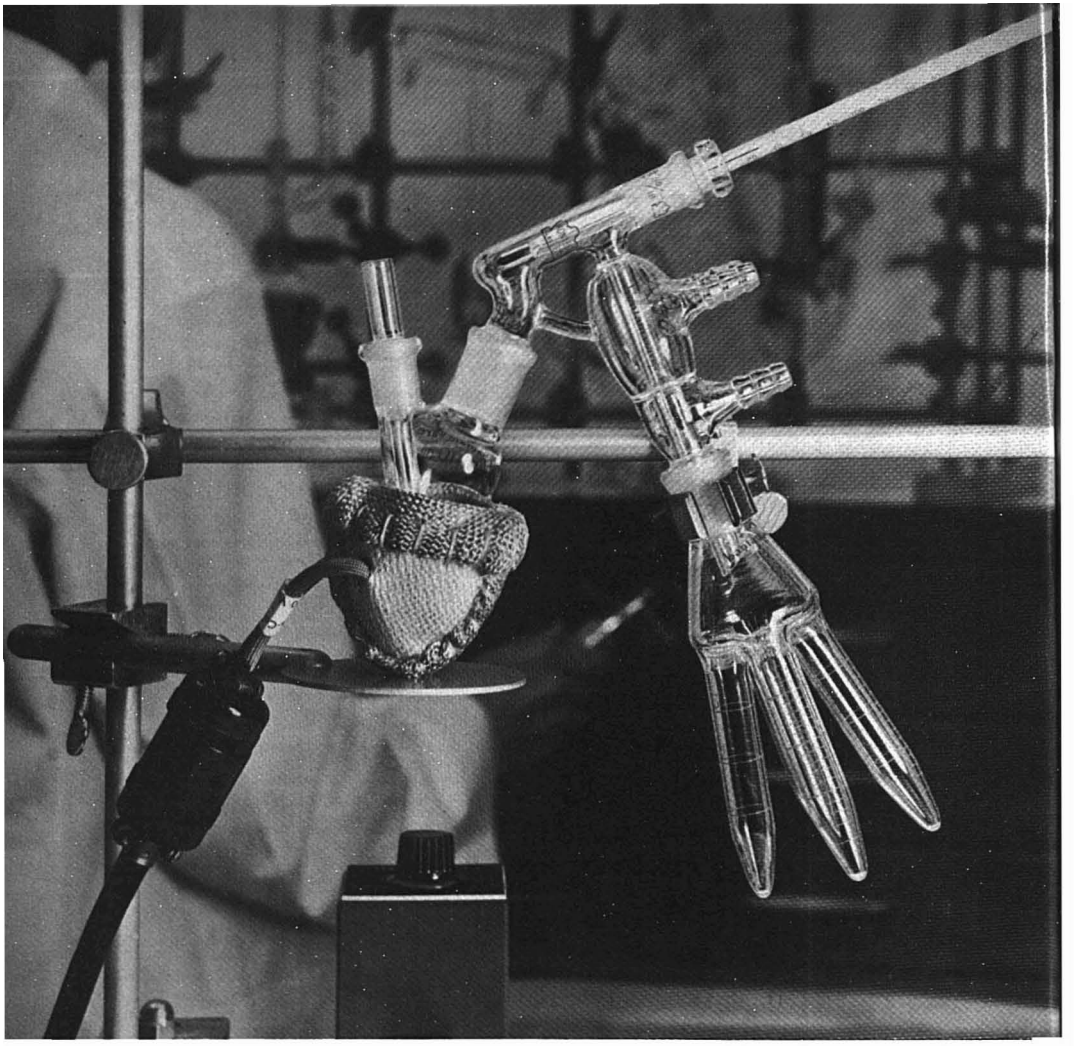
Tokyo, Japan . . . Haruo Moribayashi, International Media Representatives Ltd., 2-29 Toranomon, 1-Chome Minato-ku Tokyo 105 Japan, Telephone: 502-0656

Continental Europe . . . Andre Jamar, Rue Mallar 1, 4800 Verviers, Belgium, Telephone: (087) 22-53-85, Telex #49263

PRODUCTION DEPARTMENT

Production Director
Joseph P. Stenza

Advertising Production Manager
Barbara Aufderheide



The Case of the Meandering ML's

In the vicinity of many research laboratories, small organic solutions are being mysteriously lost, daily. They are placed in small flasks, heated, and then... they vanish. Chemists patiently wait for their meandering ml's to show up. Sometimes a few straggle into fraction cutters, but most of them escape. The M.O. is always the same. Our job ... find them.

Acting on a tip from Dr. Raymond Firestone at Merck & Co., Rahway, we went to work on our K-284800 Bantam-ware Short Path Fractionator.

Make the column about an inch long and let the thermometer bulb and stem serve as a packing, he said. Construct the condenser and vacuum connection in two inches, total length. Use only one joint on the fraction cutter but design it so that pipettes can be inserted to the bottom of any of the four receivers. Then, tilt the whole assembly so that drops fall from the drip tip ₹ 14/20 joint into one of the four receivers without unnecessary wetting. But nothing is vertically aligned, we pleaded. I know, he said. In desperation, we tried it.

We're happy to report that most of the meandering ml's now show up as product. The case is closed.

Sequel: K-284800 has been added to the line because it fits in with the whole Bantam-ware concept. Very compact, low hold-up... functional.

Bantam-ware Kits and hundreds of individual pieces are described in Catalog BW-20. Contact your Kontes man or write:

KONTES
Vineland, N.J. 08360

Exclusive Distributors: **KONTES OF ILLINOIS,** Evanston, Illinois • **KONTES OF CALIFORNIA,** San Leandro, California
KONTES (U.K.) LTD., Carnforth, England

CIRCLE 123 ON READER SERVICE CARD

WHY WAIT



A MONTH . . . OR MORE . . . FOR THAT ROUTED COPY OF ANALYTICAL CHEMISTRY TO REACH YOUR DESK?

For only $16.00 a year . . . ($12.00 if you're a member of A.C.S.) . . . you can own your very own subscription.

Why use a worn-out copy or wait until it comes to rest in the library? You can have your own copy to clip, to read at leisure, and to add to your personal file of vital information.

You'll receive FOURTEEN information-packed issues including THE ANNUAL LABORATORY GUIDE TO INSTRUMENTS, EQUIPMENT, AND CHEMICALS and the special APRIL ANNUAL REVIEWS.

All you have to do is fill in the order form below. We'll do the rest!

Please send me ANALYTICAL CHEMISTRY at the following subscription rate:

	U.S.	Canada	All Other Countries
ACS Members*			
1-Year	☐ **$12.00**	☐ **$21.00**	☐ **$21.00**
3-Years	☐ **$30.00**	☐ **$57.00**	☐ **$57.00**
Nonmembers			
1-Year	☐ **$16.00**	☐ **$25.00**	☐ **$33.00**
3-Years	☐ **$42.00**	☐ **$69.00**	☐ **$89.00**

Name _____

Address _____

City _____ State/Country _____ Zip _____

Your Company _____ Nature of Company's Business _____

☐ Bill company ☐ Bill me for $_____ ☐ Payment enclosed in the amount of $_____

Note: Subscriptions at ACS Member Rates are for personal use only.
Please allow 60 days for your first copy to be mailed.

1 0586C

Please send me ANALYTICAL CHEMISTRY at the following subscription rate:

	U.S.	Canada	All Other Countries
ACS Members*			
1-Year	☐ **$12.00**	☐ **$21.00**	☐ **$21.00**
3-Years	☐ **$30.00**	☐ **$57.00**	☐ **$57.00**
Nonmembers			
1-Year	☐ **$16.00**	☐ **$25.00**	☐ **$33.00**
3-Years	☐ **$42.00**	☐ **$69.00**	☐ **$89.00**

Name _____

Address _____

City _____ State/Country _____ Zip _____

Your Company _____ Nature of Company's Business _____

☐ Bill company ☐ Bill me for $_____ ☐ Payment enclosed in the amount of $_____

Note: Subscriptions at ACS Member Rates are for personal use only.
Please allow 60 days for your first copy to be mailed.

1 0586C



NO POSTAGE
NECESSARY
IF MAILED
IN THE
UNITED STATES

BUSINESS REPLY CARD

FIRST CLASS PERMIT NO. 10094 WASHINGTON, D.C.

POSTAGE WILL BE PAID BY ADDRESSEE

AMERICAN CHEMICAL SOCIETY
Attn: Gayle Hebron
1155 Sixteenth Street, N.W.
Washington, D. C. 20036



NO POSTAGE
NECESSARY
IF MAILED
IN THE
UNITED STATES

BUSINESS REPLY CARD

FIRST CLASS PERMIT NO. 10094 WASHINGTON, D.C.

POSTAGE WILL BE PAID BY ADDRESSEE

AMERICAN CHEMICAL SOCIETY
Attn: Gayle Hebron
1155 Sixteenth Street, N.W.
Washington, D. C. 20036

analytical chemistry

Editor: **Herbert A. Laitinen**

EDITORIAL HEADQUARTERS
1155 Sixteenth St., N.W.
Washington, D.C. 20036
Phone: 202-872-4570 Teletype: 710-8220151

Managing Editor: Josephine M. Petruzzi
Associate Editors: Andrew A. Husovsky, Barbara Cassatt
Associate Editor, Easton: Elizabeth R. Rufe
Editorial Assistant: Andre D'Arcangelo
Associate Editor, editing: Nancy J. Oddenino
Production Manager: Leroy L. Corcoran
Art Director: John V. Sinnett
Designer: Alan Kahan

Advisory Board: L. S. Birks, Peter Carr, David Firestone, Kurt F. J. Heinrich, Philip F. Kane, Barry L. Karger, J. Jack Kirkland, Marvin Margoshes, Robert S. McDonald, James W. Mitchell, Royce W. Murray, Harry L. Pardue, Garry A. Rechnitz, Walter Slavin, John P. Walters

Instrumentation Advisory Panel: Gary D. Christian, Catherine Fenselau, Gary M. Hieftje, Tomas Hirschfeld, Peter T. Kissinger, C. David Miller, Carter L. Olson, Sidney L. Phillips, Thomas H. Ridgway

Regulations, Analytical Division Ad Hoc Committee: Robert A. Libby (Chairman), Warren B. Crummett, William T. Donaldson, Donald T. Sawyer

Contributing Editor: Claude A. Lucchesi
Department of Chemistry, Northwestern University, Evanston, Ill. 60201

Published by the
AMERICAN CHEMICAL SOCIETY
1155 16th Street, N.W.
Washington, D.C. 20036

Books and Journals Division
Director: D. H. Michael Bowen
Journals: Charles R. Bertsch
Magazine and Production: Bacil Guiley
Research and Development: Seldon W. Terrant
Circulation Development: Marion Gurfein

Manuscript requirements are published in the January 1979 issue, page 171. Manuscripts for publication (4 copies) should be submitted to ANALYTICAL CHEMISTRY at the ACS Washington address.

The American Chemical Society and its editors assume no responsibility for the statements and opinions advanced by contributors. Views expressed in the editorials are those of the editors and do not necessarily represent the official position of the American Chemical Society.

Does the Ph.D. Degree Serve the Needs of Industry?

From time to time, there are suggestions that the Ph.D. degree, which by its nature is a research degree, does not best serve the careers of all of its recipients. Some years ago, there were proposals that college teachers would be better trained for their profession by a degree that would be less research-oriented. In a similar way, it is sometimes argued that training in pure research is not the best background for a career in industrial chemistry. At the Fifth Biennial Conference on Chemical Education, described in a series of reports in the January 1979 *Journal of Chemical Education*, this issue was discussed at some length.

If the final career goals of each student could be set forth immediately upon entry into graduate school, it would be relatively simple to prescribe the best educational path for each. The fact is that many, if not most, entering graduate students are uncertain about their final goals, and that many change their minds along the way. After all, the final choice depends upon available jobs as well as qualifications and interests of the candidates. All things considered, we should first examine the Ph.D. program for flexibility before deciding that it is inadequate to meet a variety of needs.

There is a great deal more in common among small colleges, Ph.D. granting universities, governmental laboratories, and industrial laboratories than there are differences among them with regard to their needs for scientists with the qualities that are developed in graduate school. The ability to plan, execute, interpret, and report research is valuable far beyond the bounds of pure research. Searches for information, formulation of plans, logical deductions, organization of facts, oral and written presentations are all important aspects of the professional lives of all chemists, and all play an intimate part in the Ph.D. program.

To be sure, one occasionally hears criticisims that pure research is poor preparation for the rough and tumble practice of industrial science. The abilities most often found wanting appear to be those concerned with economic realities, large scale production problems, communication skills, and planning and organizational skills. Some of these already form a part of the Ph.D. program, and others could be emphasized, if desired, by adding one or two courses. Such a modification appears preferable to launching an entirely new degree program to meet the needs of industry. Many of these needs are so specific in terms of company goals that they can be met only by experience, so industry must inevitably finish the job of training. Academic institutions can best serve science and technology by stressing those fundamentals of knowledge and skill which have the broadest importance to the total field rather than to any of its parts.



Chronopotentiometry with Programmed Current

Li Hang Chow[1] and Galen W. Ewing*

Department of Chemistry, Seton Hall University, South Orange, New Jersey 07079

An instrument has been constructed for chronopotentiometry with current that varies as any selected power of time, t^q, where q can lie anywhere between 0.2 and 5.0. The ambiguity due to charging current is minimized by an initial brief operation at constant current. The determination of reducible species alone or in the presence of other species can be carried out to concentrations as low as 2.5×10^{-5} M. Relative standard deviations are of the order of 1% at 5×10^{-4} M.

Although constant-current electrolysis (as in chronopotentiometry) has been practiced for nearly 100 years (*1*, *2*), its potential as an analytical tool was pointed out by Gierst and Juliard (*3*) only in 1953, and brought to the general attention of analytical chemists through the work of Delahay (*4*, *5*), Reilley (*6*), and their respective co-workers in 1955. It appeared to these authors that chronopotentiometry would develop into a highly sensitive analytical tool; Reilley (*6*) mentioned 5×10^{-5} M as a probable lower attainable concentration limit. Since then, however, most electroanalytical chemists have taken a much dimmer view, seeing no advantage and many disadvantages to the method; see for example, Lingane (*7*).

The objections to chronopotentiometry have stemmed largely from the inherent difficulty in distinguishing between the component of the current responsible for chemical effects (the faradaic current) and that utilized in charging the double-layer capacitance.

This dilemma has been attacked by several means. The first of these consists of some type of graphical correction of the observed voltage–time curve to allow for the effect of the charging current. The several attempts in this direction have been summarized previously (*7–9*); the most successful is the method of Laity and McIntyre (*10*).

The second method requires the use of two duplicate electrolysis cells, one containing the supporting electrolyte alone, to act as a reference. The sample cell is connected conventionally to an operational amplifier acting as a galvanostat, while the reference cell is controlled by a potentiostat which forces the reference electrodes in the two cells to the same potential, while both working electrodes are maintained at virtual ground. The current passing through the reference cell is converted to a corresponding voltage and summed with the constant current as normally fed to the sample cell. The result is that the faradaic current is held constant to a good approximation. This method was introduced by Shults et al. (*11*) and modernized by Bos and Van Dalen (*8*).

This procedure has two drawbacks: the possibility of instability and resulting oscillation due to the inherent positive feedback, and the questionable validity, particularly in the presence of adsorption, of the implicit assumption that the capacitance of the double layer is independent of the presence of the electroactive material (*7*).

Another approach to the problem depends on the fact that the rate of double-layer charging is a function of the derivative dE/dt. The potential of the working electrode increases rapidly at both the beginning and the end of the transition period; hence, it is primarily in these regions that the charging current is important. A plot of the derivative against time gives, for a single electroactive species, a curve with two well-defined maxima.

Takemori et al. (*12*) employed an ac modulation technique, analogous to ac polarography, which was shown mathematically to produce a voltage proportional to dE/dt. These authors estimated the transition time by measuring the time between maxima. Iwamoto (*13*) and Peters and Burden (*14*) achieved a similar result by electronic differentiation of the dc potential. The coordinates of the intermediate minimum are shown (*14*) to be functionally related to the transition time, and a measurement of this quantity is essentially unaffected by charging current. Sturrock and co-authors (*15–18*) have modernized this treatment by providing positive feedback to add to the applied current a signal proportional to the derivative, so that the current impressed upon the system constitutes faradaic current only.

The chief disadvantage to analog differentiation lies in the inherent degradation of the signal-to-noise ratio, a defect not found in the ac modulation technique. The latter, however, has not to our knowledge been pursued further than the paper cited (*12*).

Advantages of Programmed Current. Since the double-layer charging is independent of the faradaic current, its importance is much less when the faradaic current is relatively large. As pointed out above, the charging current depends on the time derivative of the potential, and this is greatest at both the start and the close of the transition period. The rise at the end of this period can thus be made less significant by the application of current programmed to increase as some positive power of time. However, this also enhances the charging effect at the start, when the current is rising from zero (*19*).

Programmed current alters the functional relation of the transition time τ as related to bulk concentration C. If the faradaic current I_F is forced to follow the relation

$$I_F(t) = bt^q \tag{1}$$

in which b is a constant, it can be shown by means of a mathematical treatment analogous to that of Oldham (*20*), presented in Appendix A of this paper (Equation 23, for $p = 0$), that the governing relation is

$$\tau^{(q+1/2)} = kC \tag{2}$$

where k is another constant. The calculated transition times

Table I. Relation between Concentration and Transition Time for Various Exponents of Time[a]

q	τ (s), $C = 10^{-3}$ M	C (M), $\tau = 100$ s
0	100	10^{-5}
1/2	10	10^{-4}
1	4.7	10^{-3}
3/2	3.2	10^{-2}
2	2.5	10^{-1}
5/2	2.2	10^{0}

[a] Calculated from Equation 2, assuming $k = 10^6$ mol·dm^{-3}·s$^{(q+1/2)}$.

[1] Present address, Warner-Lambert Co., Morris Plains, N.J. 07950.

0003-2700/79/0351-0322$01.00/0 © 1979 American Chemical Society

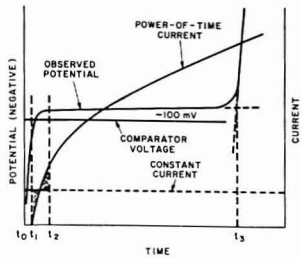


Figure 1. Time sequencing diagram, showing both potential of the reference electrode and cell current as functions of time. The comparator flips at t_1; switching from constant to varying current occurs at t_2. Transition time is given by $t_3 - t_1$. The instrumental constants must be chosen to make the two shaded segments equal in area

for a series of q values are given in Table I, together with values of concentration that will give a constant transition time, $\tau = 100$ s. Hence, if a method were available to permit selection of q at will, a wide range of concentrations could be measured on a convenient time scale. It should be noted that with constant-current chronopotentiometry at an electrode of constant area, a similar selection of suitable transition times can be made only by altering the current level, which permits far less accessible range.

To remove substances that are more easily reduced than the species of interest, a number of workers (*8, 19, 21, 22*) have utilized a potentiostat to hold the potential of the working electrode at a point slightly positive of the potential where the desired species begins to be reduced at a significant rate. The potentiostat is disconnected at the instant of application of the (constant) electrolysis current. This procedure, however, results in the passage of a finite amount of current at a level not related to the subsequent constant current.

Switched Current. We propose that, instead of a pre-electrolysis at constant potential, a constant *current* be passed through the cell for a period of time Δt short compared to τ, followed by current increasing as a positive power of time. The cell must be switched electronically from constant to increasing current at the instant at which the quantity of electricity passed at the constant rate is exactly equal to the quantity that would have been passed by the increasing current starting from zero, assuming only faradaic current to be present. This will have the effect of almost completely eliminating interference due to charging current at both the start of the transition period, where the potential will assume its plateau value very quickly, and at the end, where the current will have increased to the point where the charging current is effectively swamped out.

The time relations involved will be clarified by reference to Figure 1. At zero time, the electrodes are switched to a source of constant current (typically a few tens of microamperes). This current continues to flow until (at time t_1) the potential becomes negative enough to start reduction of the species of interest, at which preselected potential a voltage comparator trips a relay, accomplishing two things: it starts the recording of voltage as a function of time, and it turns on a generator of the desired power of time, though this does not yet control the cell current. At time t_2, the constant current is terminated and replaced by the time varying current. Electrolysis then continues until the voltage rises abruptly at the end of the transition period. The transition time is the interval $t_3 - t_1$, where t_3 is established by the intersection of tangents (*10*).

In the work described in this paper, the exponent of time, q, is selected as $^1/_2$ because, as has been shown by previous workers (*23, 24*), if the current varies with the square root of time, the transition time of one species becomes independent of the presence of other reducible species, a major convenience.

INSTRUMENTATION

We now describe an instrument designed to implement power-of-time chronopotentiometry with constant-current preelectrolysis.

The chronopotentiometer (25) consists of three segments: (1) conventional circuitry for driving the electrochemical cell at constant current, (2) circuitry for driving the cell at a selectable power of time, and (3) timing circuits for semi-automatic changeover from constant current to the selected power.

The power-of-time circuit is based on the multifunction module, type 433J (Analog Devices). This is a logarithmic multiplier-divider capable of producing an output potential

$$E_o \propto Y(Z/X)^m \tag{3}$$

where X, Y, and Z are analog inputs. The exponent m is continuously variable from 0.2 to 5.0 via a resistive network (*26*). For our purposes, the 433J is fed a linear ramp (generated by analog integration at amplifier A-1, Figure 2) through the Z-input (i.e., $Z \propto t$), both X and Y are given fixed potentials, and the exponent is set at $^1/_2$, so that

$$E_o = Kt^{1/2} \tag{4}$$

where K is an adjustable constant with the units of $V \cdot s^{-1/2}$. The voltage output of the 433J is inverted by amplifier A-2 if a reductive process is to be studied, and fed to the control amplifier A-3.

The sequencing circuitry operates in the following manner. Prior to $t = t_o$, the power supply (not shown) is ON, switch S-3 is in the position shown, both relays are unenergized, FET-switch Q-2 is ON (but no current is flowing through it), Q-3 is OFF, and the output of comparator A-5 is high (+5 V). At $t = t_o$, when S-3 is reversed manually, nominally constant current starts to flow through Q-1 and Q-2 to the cell, and the recorder starts. The potential of the reference electrode increases rapidly until (at $t = t_1$) it fires the comparator A-5, which has several simultaneous effects: it fires the monostable (74121) thereby energizing relay L-2 so that constant current flows to the cell without going through the poorly-defined channel resistances of the FET-switches, and it closes Q-3 so that the power-of-time voltage starts to be generated, even though it cannot yet result in a cell current. This state of things continues until the pulse from the monostable has expired (several seconds) at which time ($t = t_2$) the relay relaxes and the current switches from constant to power-of-time. This is allowed to continue until the recorder trace rises abruptly, when S-3 is opened by hand to stop the experiment (except that if more than one reducible species is present, the current may be allowed to continue as needed).

The necessary constant current for a selected switching time ($t_2 - t_1$) is calculated as follows: Equation 1 is written twice, with the exponent $q = 0$ for the constant case and $^1/_2$ for the ramp:

$$I_{\text{constant}} = b_o t^0 = b_o \tag{5}$$

$$I_{\text{SqRt}} = b_{1/2} t^{1/2} \tag{6}$$

The surface concentrations for the two cases are shown by Murray and Reilley (27) to be, respectively,

$$C(0,t) = C - \frac{2b_o t^{1/2}}{nFAD^{1/2}\pi^{1/2}} \tag{7}$$

$$C(0,t) = C - \frac{b_{1/2}\pi^{1/2}t}{2nFAD^{1/2}} \tag{8}$$

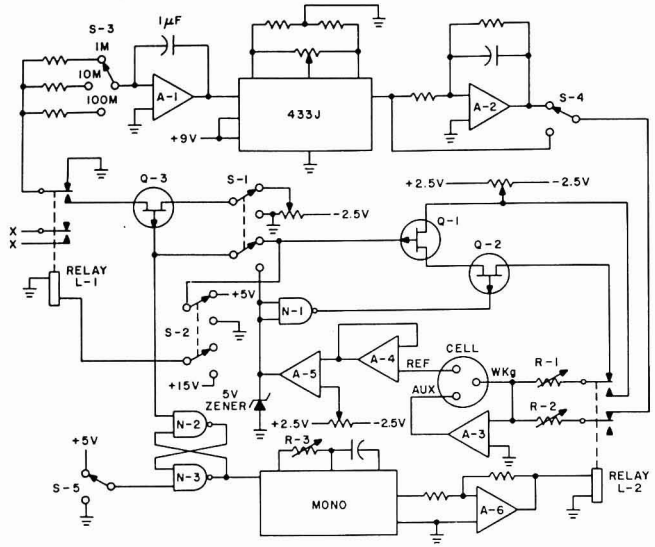


Figure 2. Schematic of power-of-time amperostat. FET switches Q-1, 2, 3 are segments of AD-7511 (Analog Devices) analog switch. Operational amplifiers A-1 and A-3 are FET-input types; all others are 741. The monostable is 74121; N-1, 2, 3 are 7400. Power supplies are conventional. The points marked x,x connect to a remote start switch on the $x-y$ recorder

Table II. Transition Time as a Function of Switching Time[a]

	switching time, s		
	2.0	3.0	5.0
	constant current, μA		
run	44.5	54.4	70.3
1	16.40	16.04	16.36
2	16.20	15.72	15.88
3	16.36	15.84	15.88
4	16.20	15.96	15.92
5	16.00	16.24	15.92
6	16.16	16.12	15.92
mean	16.22	15.99	15.98
std. dev., σ	0.13	0.17	0.17
rel. std. dev., %	0.80	1.1	1.1

[a] Solution: 1.00×10^{-3} M Pb^{2+} in 0.5 M KNO_3. Electrode: Mercury pool, 0.99-cm diameter. $b_{1/2}$: 40 $\mu A \cdot s^{-1/2}$.

Since the switch-over is to take place at the moment when $C(0,t)$ is the same as calculated either way, Equations 7 and 8 can be equated and solved for b_o, and hence the constant current becomes

$$I_{\text{constant}} = b_o = \frac{\pi}{4} b_{1/2}(t_2 - t_1)^{1/2} \qquad (9)$$

So, for a known $b_{1/2}$ and a selected switching time, the required constant current can be determined and dialed into the apparatus at R-1.

Function Generation. For settings of the exponent m between 0.4 and 2.5, the output voltage from the 433J function generator was found to be in error by an average of only 0.32% (relative) with a spread from 0.00 to 0.72, which compared rather well with the manufacturer's specification of ±0.3%.

Table III. Reproducibility of Transition Times[a]

	concentration, M	
run	5.00×10^{-4}	10.00×10^{-4}
1	5.36 s	10.76 s
2	5.36	10.76
3	5.36	10.92
4	5.40	10.80
5	5.40	10.80
6	5.40	10.68
7	5.48	10.68
8	5.44	10.76
9	5.52	10.76
10	5.52	10.76
11		10.76
12		10.68
13		10.84
14		10.88
15		10.84
16		10.80
17		10.80
18		10.72
mean	5.42	10.78
std. dev., σ	0.06	0.07
rel. std. dev., %	1.11	0.65

[a] Solution: TlCl in 0.1 M KCl. Electrode: Mercury pool, 0.99-cm diameter. $b_{1/2}$: 40 $\mu A \cdot s^{-1/2}$; b_o: 44.5 μA. Switching time: 2.0 s.

The measured error includes any nonlinearity in the integrator circuit.

Transition-Time Constancy. Ideally, the measured transition time should be independent of the selected switching time over a fair range. To test this relation, experiments were made with millimolar lead solutions, as summarized in Table II. The 2-second time was selected for routine use. In another test (Table III), the transition times

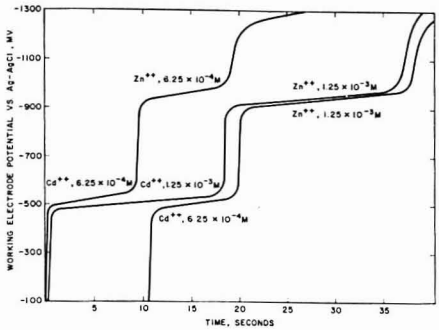


Figure 3. Square-root-of-time current chronopotentiograms of cadmium and zinc in 0.5 M KNO_3. β_0 = 44.5 μA; $\beta_{1/2}$ = 40 μA; switching time = 2 s

were measured on two concentrations of thallous chloride. The linearity is seen to be valid within the limits of experimental error.

Transition Times in a Multicomponent System. A typical series of chronopotentiograms, reproduced in Figure 3, shows the expected direct additivity of transition times, as well as the proportionality with concentration. The transition time in each curve is measured from the time (t_1) at which the potential is 150 mV below the plateau to the time (t_3) defined by the intersection of the plateau with the subsequent rise, both extrapolated. It should be noted that the rising portions of the curves are much closer to vertical than in previous methods (see, for example, Figure 8 of ref. 7).

Sensitivity. Many experiments were performed with $b_{1/2}$ (Equation 6) taken as 40.0 $\mu A \cdot s^{-1/2}$, which was satisfactory for concentrations down to about 5×10^{-4} M. For more dilute solutions, the transition time is too short to measure accurately, and a smaller current must be chosen. With $b_{1/2}$ = 3.0 $\mu A \cdot s^{-1/2}$, concentrations down to about 2.5×10^{-5} M could be measured with adequate precision. Figure 4 shows a curve for 5.00×10^{-5} M Cd^{+2} in KNO_3, with $b_{1/2}$ = 3.0. Note that at this low current, a time of about 10 s was required to charge the double layer to the point where the comparator flipped (t_1). The dashed curve shows that cadmium in the supporting electrolyte could not have been greater than about 1×10^{-6} M.

In this paper, we have explored experimentally only the utility of current varying as the square root of time. The apparatus, however, can be used with equal ease to produce other powers of time, and some of these will be described in further publications.

APPENDIX A

Oldham (*20*) has presented equations for chronopotentiometry (among other procedures) under conditions where the area of the electrode surface can be varied as a function of time, but he does not treat in detail the equally significant case providing for programming the current. He has shown that the concentration of an electroreducible species at the surface of an electrode under conditions of semi-infinite diffusion control can be predicted from the very general equation,

$$C(0,t) = \frac{I(t)}{nFkA(t)} \exp\left[\frac{\alpha nF}{RT}\Delta E\right] + [C - C(0,t)] \exp\left[\frac{nF}{RT}\Delta E\right] \quad (10)$$

(symbols are identified in Appendix B).

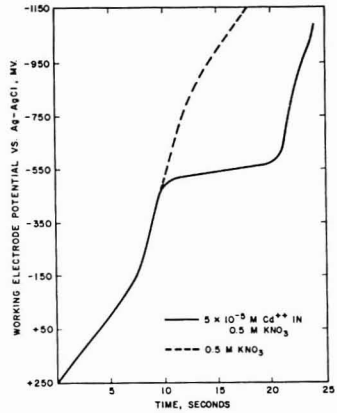


Figure 4. Square-root-of-time current chronopotentiogram of cadmium in 0.5 M KNO_3. Conditions as in Figure 3

In Oldham's treatment, the current I is allowed to vary independently only linearly with time. This can be generalized by means of two modulating relations:

$$A(t) = at^p \quad (11)$$

and

$$I(t) = bt^q \quad (12)$$

Following Oldham, we can now introduce new variables as follows:

$$Y \equiv \left[\frac{k^{(4p+2)}}{(2p+1)^{(2p+1)}D^{(2p+1)}}\right] t^{(2p+1)} \equiv Gt^{(2p+1)} \quad (13)$$

$$\iota(Y) \equiv \left[\frac{bk^{(2p-1)}}{naFC(2p+1)^pD^p}\right] t^q \equiv Ht^q \quad (14)$$

$$\epsilon(Y) \equiv \exp\left[\frac{nF}{RT}\Delta E\right] \quad (15)$$

where Y replaces the independent variable t, $\iota(Y)$ replaces the current $I(t)$, and $\epsilon(Y)$ replaces the rationalized potential $\Delta E(t)$. G and H merely stand in for the awkward time-invariant multipliers. Using Oldham's procedure, we can show that Equation 10 can be replaced by the following relation in which the symbol $L\{\ldots\}$ indicates Laplace transformation with respect to the variable Y:

$$L\left\{\frac{Y^{[-p/(2p+1)]}\iota(Y)\epsilon^a(Y) + \epsilon(Y)}{1 + \epsilon(Y)}\right\} = \frac{1}{s} - \frac{1}{\sqrt{s}} L\{Y^{[-2p/(2p+1)]}\iota(Y)\} \quad (16)$$

The Reversible Case. For this case, Equation 16 simplifies to

$$L\left\{\frac{\epsilon(Y)}{1 + \epsilon(Y)}\right\} = \frac{1}{s} - \frac{1}{\sqrt{s}} L\{Y^{[-2p/(2p+1)]}\iota(Y)\} \quad (17)$$

Substituting from Equation 13 and 14 and performing the

indicated Laplace transformation gives:

$$L\left\{\frac{\epsilon(Y)}{1+\epsilon(Y)}\right\} = \frac{1}{s} - \frac{1}{\sqrt{s}}\, HG^{[-q/(2p+1)]}\, \Gamma\left(\frac{q+1}{2p+1}\right) \frac{1}{s^{[(q+1)/(2p+1)]}} \quad (18)$$

By combining terms and taking the inverse transforms, we obtain:

$$\frac{\epsilon(Y)}{1+\epsilon(Y)} = 1 - HG^{[-q/(2p+1)]} \frac{\Gamma\left(\frac{q+1}{2p+1}\right)}{\Gamma\left(\frac{2p+2q+3}{4p+2}\right)} \cdot Y^{[(2q-2p+1)/(4p+2)]} \quad (19)$$

This, when solved for $\epsilon(Y)$ and converted back to the original variables, gives

$$\Delta E = \frac{RT}{nF} \ln\left(nFCD^{1/2}Qt^{-z} - 1\right) \quad (20)$$

in which Q represents the numerical constants:

$$Q \equiv \frac{a}{b} \cdot \frac{\Gamma\left(\frac{2p+2q+3}{4p+2}\right)}{\Gamma\left(\frac{q+1}{2p+1}\right)} \cdot (2p+1)^{1/2} \quad (21)$$

and

$$z \equiv q - p + 1/2 \quad (22)$$

It must be noted that although the electrolysis current does not appear explicitly in Equation 20, it is nevertheless involved through its equivalent bt^q (Equation 12).

The next step is to derive a general expression for the transition time, τ, defined as the time required for the concentration of the electroactive substance at the electrode surface to decrease from its initial value, C, to zero. This is the time at which the logarithmic term of Equation 20 becomes zero, so that

$$\tau^z = nFCD^{1/2}Q = KC \quad (23)$$

Substitution of this value into Equation 20 gives:

$$\Delta E = \frac{RT}{nF} \ln\left(\frac{\tau^z - t^z}{t^z}\right) \quad (24)$$

Note that for conventional chronopotentiometry, where $p = q = 0$, Equation 24 becomes the well-known Karaoglanoff relation (*28*), and Equation 23 is the Sand equation (*2*),

$$\tau = \frac{\pi n^2 a^2 F^2 C^2 D}{4I^2} \quad (25)$$

The Irreversible Case. If the system is irreversible, Equation 16 reduces to

$$L\{Y^{[-p/(2p+1)]}\iota(Y)\epsilon^{\alpha}(Y)\} = \frac{1}{s} - \frac{1}{\sqrt{s}} L[\iota(Y)\, Y^{[-2p/(2p+1)]}] \quad (26)$$

Table IV. Selected Parameters

q	p	z	$(2^{1/z} - 1)$	notes
0	0	1/2	3.	constant current
1/2	0	1	1.	sq. rt. of time
1	0	3/2	0.587	linear ramp
3/2	3/2	1/2	3.	(DME)

Treating this equation by a similar sequence of steps to that used for the reversible case leads to

$$\Delta E = \frac{RT}{\alpha nF} \ln\left[\frac{a}{b} nFCkt^{(1/2 - z)} - \frac{\Gamma\left(\frac{q+1}{2p+1}\right)}{\Gamma\left(\frac{2p+2q+3}{4p+2}\right)} \cdot \frac{kt^{1/2}}{(2p+1)^{1/2}D^{1/2}}\right] \quad (27)$$

Taking the logarithmic argument as zero and solving for t (which is replaced by τ), gives an expression identical with that of Equation 23.

Equation 23 can be used to predict the relative values of the transition times for successive reductions taking place in a multicomponent system. As pointed out by Delahay and Mamantov (*4*) and by Reilley, Everett, and Johns (*6*), at the conclusion of the transition time associated with the more easily reduced species, the potential jumps to a more negative value where a second species begins to be reduced, but the oxidized form of the first species continues to diffuse to the electrode and be reduced, so that the impressed current is split between the two components. The authors cited were concerned only with constant current, but their conclusions can be generalized as follows:

From Equation 23, taking τ_1 as the transition time for component 1,

$$\frac{\tau_1^z}{n_1 C_1 D_1^{1/2}} = FQ = \text{constant for any value of } z \quad (28)$$

This constant, FQ, can also be equated to the difference between the combined transition times of two components and that of the first alone:

$$\frac{(\tau_1 + \tau_2)^z - \tau_1^z}{n_2 C_2 D_2^{1/2}} = FQ \quad (29)$$

Hence these two can be set equal. If we simplify by assuming the two species to be equal with respect to n, C, and D, then

$$\tau_1^z = (\tau_1 + \tau_2)^z - \tau_1^z \quad (30)$$

from which,

$$\tau_2 = (2^{1/z} - 1)\tau_1 \quad (31)$$

In Table IV are listed values of $(2^{1/z} - 1)$ for various z corresponding to potentially interesting physical situations. The value for $q = p = 0$ is identical to that given by the previous authors (*4*, *6*); that for $q = 1/2$, $p = 0$ agrees with the predictions of Murray and Reilley (*27*) for current varying as the square root of time; the value for $q = 1$, $p = 0$ corresponds to Oldham's Equation 53 (*24*). The last entry is predicted for chronopotentiometry at the dropping mercury electrode under conditions that give constant current density.

APPENDIX B

a	Electrode area at unit time
$A(t)$	Electrode area at time t
b	Electrolysis current at unit time

C	Bulk concentration of active species
$C(0,t)$	Concentration of active species at surface of electrode at time t
D	Diffusion coefficient of active species
E_o	Voltage output from 433J function generator
ΔE	Potential of electrode at time t, minus a reference potential
F	Faraday's constant
G	Numerical constant defined in Equation 13
H	Numerical constant defined in Equation 14
$I(t)$	Electrolysis current at time t
I_F	Faradaic current
k	Reference rate constant corresponding to the selected reference potential; a constant
K	A constant
$L[\ldots]$	Laplace operator with respect to Y
m	Exponent of time
n	Number of electrons transferred per ion
p	Power of time by which electrode area increases
q	Power of time by which the current increases
Q	Numerical constant defined in Equation 21
R	Universal gas constant
s	Dummy variable of Laplace transformation
t	Time; for subscripts, see Figure 2
T	Kelvin temperature
X, Y, Z	Variables used to describe action of 433J
z	$q - p + 1/2$
α	Cathodic transfer coefficient
$\epsilon(Y)$	Dimensionless analog of potential, defined in Equation 15
$\iota(Y)$	Dimensionless analog of current, defined in Equation 14
τ	Transition time

LITERATURE CITED

(1) H. F. Weber, *Wied. Ann.*, **7**, 536 (1879).
(2) H. J. S. Sand, *Phil. Mag.*, **1**, 45 (1901).
(3) L. Gierst and A. Juliard, *J. Phys. Chem.*, **57**, 701 (1953).
(4) P. Delahay and G. Mamantov, *Anal. Chem.*, **27**, 478 (1955).
(5) P. Delahay, "New Instrumental Methods in Electrochemistry", Interscience, New York, 1954, Chap. 8.
(6) C. N. Reilley, G. W. Everett, and R. H. Johns, *Anal. Chem.*, **27**, 483 (1955).
(7) P. J. Lingane, *Crit. Rev. Anal. Chem.*, **1**, 587 (1971).
(8) P. Bos and E. Van Dalen, *J. Electroanal. Chem.*, **45**, 165 (1973).
(9) M. L. Olmstead and R. S. Nicholson, *J. Phys. Chem.*, **72**, 1650 (1968).
(10) R. W. Laity and J. D. E. McIntyre, *J. Am. Chem. Soc.*, **87**, 3806 (1965).
(11) W. D. Shults, F. E. Haga, T. R. Mueller, and H. C. Jones, *Anal. Chem.*, **37**, 1415 (1965).
(12) Y. Takemori, T. Kambara, M. Senda, and I. Tachi, *J. Phys. Chem.*, **61**, 968 (1957).
(13) R. T. Iwamoto, *Anal. Chem.*, **31**, 1062 (1959).
(14) D. G. Peters and S. L. Burden, *Anal. Chem.*, **38**, 530 (1966).
(15) P. E. Sturrock, J. L. Hughes, B. Vandreuil, G. E. O'Brien, and R. H. Gibson, *J. Electrochem. Soc.*, **122**, 1195 (1975).
(16) P. E. Sturrock, B. Vandreuil, and R. H. Gibson, *J. Electrochem. Soc.*, **122**, 1311 (1975).
(17) P. E. Sturrock and R. H. Gibson, *J. Electrochem. Soc.*, **123**, 629 (1976).
(18) R. H. Gibson and P. E. Sturrock, *J. Electrochem. Soc.*, **123**, 1170 (1976).
(19) R. W. Murray, *Anal. Chem.*, **35**, 1784 (1963).
(20) K. B. Oldham, *Anal. Chem.*, **41**, 936 (1969).
(21) H. Hurwitz and L. Gierst, *J. Electroanal. Chem.*, **2**, 128 (1961).
(22) F. Jović and I. Kontusić, *J. Electroanal. Chem.*, **50**, 269 (1974).
(23) M. Senda, *Rev. Polarogr.*, **4**, 89 (1965).
(24) T. Kambara and I. Tachi, *J. Phys. Chem.*, **61**, 1405 (1957).
(25) L. H. Chow, Ph.D. Dissertation, Seton Hall University, South Orange, N.J., 1977.
(26) G. W. Ewing, *Analog Dialogue*, **8**(1), 19 (1974).
(27) R. W. Murray and C. N. Reilley, *J. Electroanal. Chem.*, **3**, 64 (1962).
(28) Z. Karaoglanoff, *Z. Elektrochem.*, **12**, 5 (1906).

RECEIVED for review October 6, 1978. Accepted December 4, 1978. One of us (L.H.C.) was supported by a grant from the State of New Jersey under the Independent Colleges and Universities Utilization Act of 1972. Presented in part at the 29th Pittsburgh Conference on Analytical Chemistry and Applied Spectroscopy, Cleveland, Ohio, February 28, 1978.

Experimental Evaluation of Recursive Estimation Applied to Linear Sweep Anodic Stripping Voltammetry for Real Time Analysis

Paul F. Seelig[1] and Henry N. Blount*

Brown Chemical Laboratory, The University of Delaware, Newark, Delaware 19711

The recursive estimation technique known as the Kalman filter has been experimentally verified for linear sweep anodic stripping voltammetry (LSASV) at hanging mercury drop (HMDE) and thin film mercury (TFME) electrodes. Synthetic lead samples were employed for a critical comparison between this real time recursive estimation technique and traditional nonreal time digital filtering techniques. The recursive technique generally returned concentration estimates which were of greater precision than the other digital methods for LSASV at an HMDE and of comparable precision for LSASV at a TFME. The limits of detection for these techniques (0.4 ppb) were found to be governed by the exogenous background concentration of the analyte rather than the technique per se.

[1] Present address: Department of Chemistry, Reiss Science Center, Georgetown University, Washington, D.C. 20057.

Recent advances in digital hardware which permit more comprehensive data analysis and experimental control are being incorporated into chemical instrumentation. As hardware costs drop and expertise with these new devices increases, more sophisticated and "intelligent" microprocessors are appearing as integral parts of new instruments (*1–7*). Such systems become increasingly capable of executing complex algorithms designed to extract analytically significant information from the output of the transducers.

Paralleling these hardware developments have been substantial improvements in numerical methods of data analysis. The classification of data and identification of subsets by methods such as factor analysis (*8–12*), principal components (*13*), and pattern recognition (*14–16*) have been demonstrated. Smoothing of data (*17–19*) has been shown to be advantageous in many situations (*20, 21*), although caution must be exercised to maintain the information content of the signal. Transforms

0003-2700/79/0351-0327$01.00/0 © 1979 American Chemical Society

of data by Fourier or Hadamard methods have been used in various applications of filtering (*22–24*), computing derivatives (*25, 26*), and pattern recognition (*27, 28*).

The integration of the computer into instrumentation affords the possibility of real time data processing for more efficient analysis as well as real time control. The extent to which these real time attributes can be realized is largely determined by the nature of the computational algorithm employed. Traditionally, the analysis has been carried out by some ex post facto method such as multiple regression. Such methods afford the optimal analytical result, but with the forfeiture of real time control capabilities. Various "pseudo-real time" techniques are available (*17–21*) wherein estimates of the analytical parameters of interest are provided during the course of the experiment, but with a delay of several observation intervals. These methods sacrifice some degree of optimality of result, but with a concomitant gain in control capability. Recently, an algorithm for the real time analysis of data, the Kalman filter, has been described (*29*). This recursive technique has been shown to return precise and accurate estimates of the analytical parameters of interest over a broad range of signal-to-noise ratios. The real time character of this method minimizes the overall analysis time and maximizes real time control capabilities.

The thrust of this present work is twofold: first, to present an experimental evaluation of the Kalman filter as applied to the analysis of trace metal analytes by linear sweep anodic stripping voltammetry (LSASV) and second, to critically compare the analytical results from LSASV experiments obtained through the use of real time, pseudo-real time, and nonreal time analysis algorithms.

EXPERIMENTAL

Apparatus. The instrument employed for the linear sweep anodic stripping voltammetric experiments was a Princeton Applied Research Corporation Model 174A polarographic analyzer (PAR174A). This instrument utilizes a conventional three-electrode configuration and does not provide a means for ohmic drop compensation. Standard operational amplifier and digital timing circuits were used to couple the PAR174A to an analog-to-digital system which was designed and built in-house and has been described elsewhere (*30*). Control of the PAR174A and processing of the digital representations of the analog current and potential transients were affected using a NOVA1200 computer (Data General Corporation) configured as previously described (*29*). Software was written in standard ANSI FORTRAN IV, with the data acquisition subroutines being written in assembly language, compatible with Data General DOS FORTRAN IV.

The electrochemical cell bodies and glass probes were made of borosilicate glass and the cell tops fabricated from Teflon. A saturated calomel electrode (SCE) served as the reference and was separated from the solution by a saturated lithium perchlorate salt bridge with a Vycor plug used for the junction. The ohmic drop between working and reference electrodes was determined by ac conductance measurements and found to be 77 Ω. The auxiliary electrode was a platinum spiral approximately 1.0 cm in length and 2.0 mm in diameter. All potentials are reported relative to the SCE. All measurements were carried out at 25.0 ± 0.5 °C.

The magnetic stirrer was made from a 300-rpm Bodine sychronous motor. For all experimental measurements, the electrochemical cell was positioned on a vibration free table (Serva-Bench, Block Engineering) to minimize undesired convective mass transport.

Reagents and Materials. Water used for solution preparation was deionized by passage through a high capacity mixed-bed resin column (Barnstead D0803) and distilled in a well leached glass still.

Lithium perchlorate (Alfa Products) used for the supporting electrolyte was purified in the manner previously described (*31*). One-liter quantities of 0.100 M lithium perchlorate in 0.100% nitric acid (Ultrex, J. T. Baker Chemical Co.) and 1.00 M lithium perchlorate in 1.00% nitric acid were prepared from this material and further purified by gross electrolysis for 24 h over a mercury pool electrode maintained at −900 mV.

Stock lead standards, 10.00 g/L lead, were prepared by dissolving 1.598 g lead nitrate in distilled water and diluting to 100 mL with 0.10 M lithium perchlorate solution. Standards containing less than 1.00 ppm lead were prepared daily and the 1.00 ppm lead standard was prepared weekly.

Mercuric nitrate solutions were prepared from triply distilled mercury (Bethlehem) which was further purified by a method described elsewhere (*32*).

Quarter-inch diameter spectroscopic grade carbon rods (National Carbon), used for the thin-film mercury electrode (TFME), were wax impregnated with paraffin (Gulfwax).

Nitrogen (Linde), used for deoxygenation of the analyte solutions, was first bubbled through a vanadous chloride solution (*33, 34*) for oxygen removal and then through two stages of supporting electrolyte solution before being introduced into the electrochemical cell.

Electrode Preparation and Characterization. *Hanging Mercury Drop Electrode (HMDE).* Mercury drops, formed at the tip of a DME capillary, were transferred to a mercury plated platinum tip electrode (Sargent S-29314-40 transfer apparatus). The mercury drop radius was determined to be 0.0479 (±0.0005) cm by drop mass measurements. For good reproducibility of the electrochemical response, it was necessary to clean the mercury from the tip with concentrated nitric acid and to redeposit the mercury prior to daily experimentation.

Thin Film Mercury Electrode (TFME). Graphite rods, ca. 2.0 cm in length, were immersed in hot paraffin and degassed with a water aspirator vacuum until all venting of gas from the rod had ceased (ca. 15 min). After withdrawing the rod from the paraffin, it was cut into 0.65-cm segments to expose the graphite surface which was then polished using Crocus cloth (Norton No. 1507-3) and then filter paper (Whatman No. 1) until the surface exhibited a mirror finish. The rod was attached to a glass tube (6.0 mm) using Teflon heat shrink tubing (0.65 cm). The shrinkage of the tubing and the excess paraffin on the outside of the graphite rod were found to form an air-tight seal. Mercury was used to make contact to the top of the graphite rod.

For characterization, mercury films were deposited onto the wax impregnated graphite electrode under potentiostatic conditions (750 mV) for 300 s from a mercuric nitrate solution, either 4.0×10^{-5} M or 8.0×10^{-5} M. The quantity of mercury deposited was determined coulometrically and calculations of film thickness were based on the assumption of uniform coverage.

Procedure. All glassware was leached with 10% nitric acid solution for 24 h and then triply rinsed with 10% nitric acid and distilled water immediately before use.

Linear Sweep Voltammetry (LSV) at HMDE. The standard lead solutions were prepared by diluting the appropriate quantity of 1.00 ppm stock lead solutions to 100 mL using the 0.100 M lithium perchlorate (pH = 1.7 ± 0.2). After introducing the sample into the cell, a stream of nitrogen was bubbled through the solution for deoxygenation for 300 s after which the nitrogen was directed over the top of the solution. For the stripping analysis trials, the lead was deposited into the drop under stirred conditions for 300 s at a potential of −750 mV. The stirrer was then turned off and the solution allowed to come to rest for 20 s whereupon a potential sweep from −750 mV to 0 mV at the desired scan rate was initiated by the computer. The current and potential responses were digitized by the computer every 2.0 mV of the sweep and the data saved for later analysis. For nonstripping trials, the solution was allowed to come to rest for 20 s after which the potential was scanned from 0 mV to −750 mV at the desired rate.

LSV at TFME. The standard lead solutions were prepared by diluting 0.50 mL of 10.0 mM mercuric nitrate solution and the appropriate amount (0.0500–0.400 mL) of 1.00 ppm stock lead solution to 100 mL with 0.100 M lithium perchlorate (pH = 1.8 ± 0.2). The lead standards and the tap water analytes were analyzed in an identical manner. Ten milliliters of the sample were placed in the cell and deoxygenated for 300 s after which the nitrogen was directed over the top of the solution. Under stirred conditions, codeposition of the mercury and lead at −750 mV was carried out, after which the stirrer was turned off and the solution allowed to come to rest for 20 s. The computer then initiated the potential sweep from −750 mV to 0 mV at 100 mV/s

Table I. Accuracy and Precision of LSV Models at Various Potential Sweep Rates

	LSV at plane electrode[a]		LSV at HMDE[b]		LSASV at HMDE[c]	
sweep rate, mV/s	concentration reported, M × 10^3	% RSD[d]	concentration reported, M × 10^4	% RSD	concentration reported, M × 10^6	% RSD
500	0.989	0.2	4.44	0.6	[e]	
200	1.01	0.4	4.49	0.4	8.63	1.2
100	1.00	0.6	4.55	0.6	8.66	2.3
50	0.992	1.1	4.54	0.3	8.67	1.3
20	0.974	1.3	4.47	0.5	9.02	1.4
10	[e]		4.45	0.8	9.76	2.2
5	[e]		4.38	2.1	10.32	4.7

[a] Concentration taken was 1.00 × 10^{-3} M DPA. Concentration reported is the average for four trials. [b] Concentration taken was 4.83 × 10^{-4} M lead. Concentration reported is the average of five trials. [c] Concentration in the HMDE was for a 300 s deposition from a 2.41 × 10^{-7} M lead sample. Concentration reported is the average of four trials. [d] Percent relative standard deviation. [e] Not determined.

and acquired a current and a potential data point every 2.0 mV during the potential sweep. These data were saved for later analysis. After each trial, the mercury film was stripped off at +750 mV before the next trial was run.

Computational Algorithms. For the analysis of the experimental data the *general* current model employed was

$$i = f(C,E) + \mu E + \beta \quad (1)$$

where i (μA) is the total current, $f(C,E)$ is the appropriate faradaic current model which is dependent on the concentration (C) and the potential (E), μ (μA/mV) is the constant background slope, and β (μA) is the current offset or intercept at the start of the potential sweep. This background model assumes C_{dl} (capacitance of the double layer) to be constant over the potential range of the experiment.

Nonreal Time (NRT) Analysis. For the ex post facto analysis of the data, a standard multiple regression algorithm was employed (*35*). This method, which assures the minimization of the squared residuals between the model and the raw data, computed estimates of the concentration, background slope, and the background intercept. This computational algorithm carried out a stepwise search along the potential axis for the global minimum of the squared error for a given current–potential transient.

Pseudo-Real Time (PRT) Analysis. For these techniques, the raw data were first corrected by subtracting the linear background, then either not smoothed or smoothed by one of four algorithms: five-point moving average, cubic spline (*36*), five-point grouping, or seven-point quartic quintic (*18*). Subsequent determinations of the concentration were based both on the peak faradaic current and the integral of the faradaic current over the potential sweep. In the former case, the peak faradaic current was determined both by absolute peak picking (APRT) wherein the entire data set was sequentially searched for the maximum current and by derivative peak picking (DPRT) in which the derivative of the current–potential transient was computed using a nine-point quadratic algorithm (*18*). For the estimate of the maximum current, the maximum value and two data points on each side of the peak were averaged together. In the latter case, the transient was integrated (IPRT) using the trapezoidal method (*37*).

Real Time (RT) Analysis. The two-measurement, five-state Kalman filter was essentially the same as previously described (*29*). The error covariances matrix computation was modified to ensure the matrix remaining symmetric positive definite and was carried out using

$$P_i = (I - K_iH_i)M_i(I - K_iH_i)^T + K_iR_iK_i^T \quad (2)$$

where the subscript i is the time increment, P is the a posteriori state error covariance matrix, M is the a priori state error covariance matrix, R is the measurement variance matrix, K is the filter gain, H_i is the observation model relating the states to the measurements, I is the identity matrix, and the superscript T indicates transposition. Other commonly used notation is given in Appendix I. While the computation of the error covariances, using this form, proceeds more slowly than that given earlier (reference 29, Equation 11), round-off error is diminished.

The initial state estimates provided to the filter were computed from the first five data points acquired. The estimate of the background intercept was the first data point, the background slope was estimated from the first five data points, and the concentration estimate arose from considerations of the estimated background intercept and slope together with the faradaic current model. The rapid convergence of the filter from greatly erroneous initial estimates (*29*) indicated that more stringent algorithms for the computation of the initial states would not have a significant effect on the final estimate of the concentration.

Input from the operator provided the value of the initial covariance for state and measurement errors. The error covariances are an indication of the confidence placed in the initial estimates and for these cases the variances were made large, 10^4 or greater for the concentration, slope, and intercept and 10^2 for the initial potential and the potential sweep rate. For the concentration, slope, and intercept, this variance indicates that the initial estimate falls within a range of ±100 mol/L, μA/mV, or μA (depending on which state is being considered), and for the initial potential and rate of potential sweep the estimate is within ±10 mV or mV/s. The measurement variances for the current and the potential were both set to one indicating the electrode potential noise as being ±1 mV and the current noise as being ±1 μA.

RESULTS AND DISCUSSION

Models. The accuracy of the models was investigated for a wide range of potential sweep rates with the data being analyzed by NRT multiple regression. All models used for these trials were computed for a potential range of ±150 mV with respect to the $E°$. The effects that errors in the model $E°$ and errors in the radius or area of the electrode have on the concentration reported were determined using synthetic data which was free of any measurement noise. These errors in concentration were found to be deterministic, representing nominal values, and additional perturbation by measurement noise caused the overall error to increase.

Plane and Spherical Electrodes, Semi-infinite Diffusion. The general faradaic current response for these models is composed of two contributions, the plane component, i_p, and the spherical component, i_s as given by (*38*)

$$i = i_p + i_s \quad (3)$$

where the individual current components are given in Appendix II, Equations 1–6. Equation 3, as written, is for the linear sweep voltammetric (LSV) nonstripping model and conversion to the LSV stripping model requires only that the sign on the spherical component be changed (*39*).

LSV at Plane Electrode. The plane electrode model was verified for the one-electron oxidation of 9,10-diphenylanthracene (DPA) at a plane, shielded platinum electrode over a wide range of potential sweep rates. The computed concentration of DPA based on a comparison of theoretical and experimental current responses for various sweep rates is shown in Table I. The higher reported variance at the slower sweep rates is attributable to the decreased current response.

Table II. Effect of E° Error on Reported Concentration Computed by Multiple Regression Analysis[a]

E° bias, mV	LSV (plane electrode),[b] % error[f]	LSV (HMDE),[c] % error	LSASV (HMDE),[d] % error	LSASV (TFME),[e] % error
30	−6.6	−65.6	−51.5	−50.1
20	−0.6	−34.9	−17.1	−25.6
10	1.6	−10.5	−0.4	−6.9
0	0.0	0.0	0.0	0.0
−10	−5.1	−2.7	−14.1	−6.2
−20	−13.7	−22.2	−40.0	−26.0
−30	−25.3	−59.1	−71.3	−50.5

[a] Faradaic current models are given in Appendix II. [b] Model parameters are: $n = 1$, $D_R = 1.35 \times 10^{-4}$ cm²/s, $\nu = 0.100$ V/s, $E^* = -0.200$ V vs. E°, $E^\circ = 0.0$ V. [c] Model parameters are: $n = 2$, $D_o = 0.98 \times 10^{-5}$ cm²/s, $\nu = -0.100$ V/s, $E^* = 0.100$ V vs. E°, $E^\circ = 0.0$ V, and $r_o = 0.076$ cm. [d] Model parameters are: $n = 2$, $D_R = 1.39 \times 10^{-5}$ cm²/s, $\nu = 0.100$ V/s, $E^* = -0.100$ V vs. E°, $E^\circ = 0.0$ V, and $r_o = 0.1056$ cm. [e] Model parameters are: $n = 2$, $D_R = 1.39 \times 10^{-5}$ cm²/s, $D_o = 0.98 \times 10^{-5}$ cm²/s, $\nu = 0.100$ V/s, $l = 30$ μm, $E^* = -0.200$ V vs. E°, and $E^\circ = 0.0$ V. [f] Error reported is the absolute percent error from the true concentration.

For the plane electrode, errors made in the estimate of the electrode area are transformed to errors in the reported concentration such that a ±5.0% error in the electrode area will result in a ∓5.0% error in the reported concentration. Errors resulting from uncertainty in the E° of the model are shown in Table II. For this one-electron process, the error associated with a cathodic bias of the model results in a more severe error in the reported concentration because of the rapidly changing current response in the leading edge of the faradaic signal.

LSV at HMDE. The LSV spherical electrode model was characterized over a wide range of potential sweep rates for the two-electron reduction of lead at an HMDE. The results are shown in Table I and again the lower current levels for the slower sweep rates give rise to the observed decrease in precision.

The dependence of the concentration error on the electrode radius error is twofold with inaccuracies arising from errors in the estimate of the electrode area and from errors in the estimate of the spherical component of the current for the model. Erroneous area estimates affect both the plane and spherical components of the current in a linear fashion such that ±5.0% deviations in the area give rise to ∓5.0% errors in the concentration. The electrode area exhibits a quadratic dependence on the electrode radius so that radius errors will result in area errors which are asymmetrically distributed about the correct area, with a positive radius error creating a greater area error. For the electrode radius of 0.0479 cm used in this investigation a +5.0% radius error yields an area error of +10.0% whereas a −5.0% radius error yields a −9.8% area error.

At high rates of potential sweep, the contribution of the spherical term to the total current is decreased; thus, as the potential sweep rate increases, concentration errors arising from electrode radius inaccuracies diminish. The percentage of the peak current which is due to the spherical term is illustrated in Figure 1. Perturbation of the spherical current component by electrode radius errors gives rise to concentration errors which are asymmetrically distributed about the true concentration. Thus, a +5.0% error in the electrode radius used in this work affords an error of +4.8% in the spherical term and a −5.0% error in the electrode radius yields an error of −5.3% in the spherical current term.

Errors in the concentration estimates resulting from errors in the E° can occur because of the requirement that the electrochemical model accurately represent the dynamics of the system. The effects that model E° errors have on the reported concentration are shown in Table II. The narrower peak for this two-electron process is responsible for the error in the reported concentration which is seen to be greater than that noted for the one-electron process. Because this is a

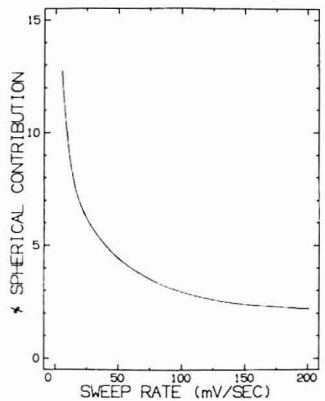


Figure 1. Percentage of spherical contribution to the total peak current for LSV at HMDE. Modeling parameters are $n = 2$, $r_0 = 0.0603$ cm, $A = 1.0$ cm², $D_0 = 0.98 \times 10^{-5}$ cm²/s, $T = 298$ K, $E^* = -0.100$ V vs. E°, $E^\circ = 0.0$ V, and $C_0^* = 1.0$ M

reduction process, the error is more pronounced on the positive side of the E°, which again is attributable to the sharply rising leading edge of the faradaic current response.

LSASV at HMDE. The LSASV spherical electrode model was investigated over a wide range of potential sweep rates for the stripping of lead from an HMDE. Although the same deposition time and stirring rate were employed for each analysis, no attempt was made to determine the quantity of lead actually deposited into the mercury drop other than by the voltammetric response. The concentrations computed for reduced lead in the mercury drop are shown in Table I. The lessened precision at the lower sweep rates is attributable to the decrease in the current response. There is good agreement among the reported concentrations across the range of sweep rates.

The effects that electrode radius errors have on the reported concentration parallel those effects observed for the nonstripping case at a spherical electrode. The only change from the nonstripping case is that the sign for the spherical term is negated resulting in a partial cancellation of the errors arising from the plane and spherical components of the current. For this two-electron oxidation process, the magnitudes of the concentration errors arising from uncertainty in the model E°, shown in Table II, are similar to the two-electron reduction process, although the greater concentration errors now occur for cathodic bias of the E°. Overall, the

Table III. Effect of Physical Perturbations on Mercury Coverage of a WIGE[a]

perturbation	% mercury lost
none	0
electrode lifted from a stirred solution (500 rpm)	7
electrode lifted from a quite solution	20
deposition with stirring and N_2 bubbling	34
after deposition, N_2 bubbled and solution stirred for 200 s	56

[a] Mercury deposition from a stirred solution of 0.050 mM mercuric nitrate was carried out for 300 s at −0.750 V vs. SCE.

precision of LSASV is less than LSV because of the uncertainty introduced in the deposition step. Based upon the two linear sweep cases investigated, LSASV and LSV, it can be estimated that a relative error of 1.5% is introduced by the deposition process prior to onset of potential sweep.

LSASV at TFME. Verification of this thin film model (Appendix II, Equations 7–13) first involved characterization of the electrode surface. Coulometric characterization of the mercury deposition process indicated that 1.42 (±0.04) × 10^{-8} mol of mercury (surface coverage of 4.5 × 10^{-8} mol/cm^2) were deposited during a 300-s controlled potential electrolysis from a solution of 0.050 mM mercuric nitrate. Assumption of a uniform thin film affords an electrode thickness of 7.0 × 10^{-7} cm which is comparable to that reported by Florence (*40*) for deposition under similar conditions. Previous investigators (*41–44*) have reported that the wax impregnated graphite electrode (WIGE) gives rise to a globular form of mercury on the surface rather than a uniform thin film. The evolution of hydrogen at the surface of the electrode at a potential of −750 mV indicated that the graphite was indeed exposed to the solution since hydrogen overpotential on mercury is in excess of −1.0 V under these conditions.

Other investigators (*41*, *44*) have noted increased residual current at the TFME with increased age of the mercury film. This has been explained (*44*) as the coalescing of the mercury into hemispheres on the electrode surface to give exposed graphite which contributes to the residual current. Perone (*43*) noted that exposure of a thick mercury film (1–10 μm) to air for moderate lengths of time rendered the electrode unusable, presumably because of the increase in the residual current. Clem (*41*) noted that high concentrations of mercuric ion present during the deposition process resulted in poor reproducibility because tiny mercury droplets which were being deposited were also being swept off the surface of the electrode. In this work, difficulties similar to those reported by Clem were encountered with preformed mercury films (i.e., those not prepared by codeposition with the analyte) in that poor reproducibility was observed in the current response using the same TFME in different solutions of the same concentration. Results of determination of the mercury on the graphite surface following physical perturbation during deposition and before the strip-off are shown in Table III. On these graphite surfaces, the film was unstable to even the mildest physical abuse and for this reason mercury films were generated by in situ deposition.

The effects which thin-film electrode area errors have on the reported concentration are the same as in the plane electrode case. These area errors are linearly transformed, so that a ±5.0% error in the electrode area will result in a ∓5.0% error in the reported concentration. The errors introduced by uncertainty in the model $E°$, shown in Table II, are symmetrical about the $E°$ of the system. For such errors, the deviation of the reported concentration from the true value is more severe than that for the HMDE cases because of the more sharply peaked faradaic response.

From the estimated electrode thickness the peak width at half height, $b_{1/2}$, is expected to be 38 mV (*45*). Recently Pinchin and Newham (*46*) found $b_{1/2}$ values of 48 to 51 mV for the current response at a WIGE in the analysis for lead. In this present work, $b_{1/2}$ values were observed to be between 50 and 55 mV which has been shown by DeVries (*45*) to be indicative of an electrode thickness of 25 to 30 μm. As pointed out by DeVries (*47*), the theoretical peak current decreases both as the uncompensated resistance increases and as the film thickness increases. Concomitant with the decreasing peak current, a broadening of the peak occurs. The discrepancy of the theoretical and experimental $b_{1/2}$ values observed in this work is most probably due to the incomplete coverage of the graphite surface by the mercury. As noted by Matson (*44*), broadening of the peak and decrease in the peak current is coupled to an increased exposure of the graphite to the solution. For the analysis of the data from the LSASV experiments at a TFME, an electrode thickness of 30 μm was determined by minimizing the error between the model and the experimental data with respect to the electrode thickness.

Evaluation of Kalman Filter Performance Using Synthetic Samples. The observation dynamics of a system can be formalized as

$$z_i = H_i x_i + v_i \tag{4}$$

where at time i, v_i is the measurement uncertainty and H_i expresses the functional relationship of the states, x_i, to the observations, z_i. The state processes in the time domain are a continuum and the relationship from one time period, i, to the next time period, $i + 1$, is given by

$$x_{i+1} = \Phi_i x_i + w_i \tag{5}$$

where Φ_i is the state transition matrix, w_i is additive state uncertainty. If the measurement noise is assumed to be zero mean white Gaussian of known variance, R_i, and uncorrelated with the state uncertainty, w_i, which has known variance, then minimization of the state error covariances gives rise to the Kalman filter (*29*). Such state error covariances are given by

$$P_i = E[(\hat{x}_i - x_i)(\hat{x}_i - x_i)^T] \tag{6}$$

where $\hat{x}_i$ is the estimate of the states (viz., concentration, background slope, background intercept, potential sweep rate, and potential) and x_i is the true value of the states.

The performance of the Kalman filter was evaluated under controlled conditions for the determination of lead in aqueous synthetic samples. For confidence to be placed in the results computed by the Kalman filter, it is imperative that the convergence of the states to invariant values and the accuracy of these values be demonstrated. The criteria which were established to test the convergence of this Kalman filter were designed such that evaluation of both the operational aspects of this filter, as well as the accuracy of the measurement and state models, could be carried out. These three criteria were:

1. Monotonically decreasing diagonal elements of the error covariance matrix, P.
2. Convergence of the states (concentration, background slope, background intercept, and potential sweep rate) to invariant values.
3. Convergence of the innovation sequence

$$v_i = z_i - H_i \hat{x}_i \tag{7}$$

to values uniformly distributed about a zero mean.

If the Kalman filter algorithm operates properly, then criteria one and two will be met. However, the fact that criteria one and two have been satisfied is insufficient to

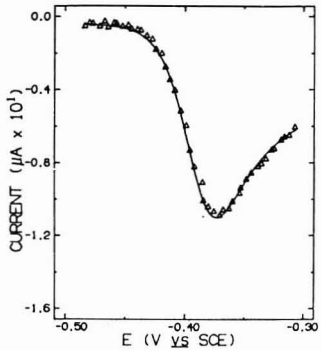


Figure 2. Experimental current response (Δ) with model current overlayed (—) for the LSASV (HMDE) determination of a 4.0 ppb lead standard. Deposition time for this trial was 300 s. Model parameters are: $n = 2$, $T = 298$ K, $D_R = 1.39 \times 10^{-5}$ cm²/s, $\nu = 0.100$ V/s, $E^* = -0.100$ V vs. E^o, $E^o = -0.388$ V, $C_R^* = 1.28 \times 10^{-5}$ M, $r_o = 0.0479$ cm, and $A = 0.0288$ cm²

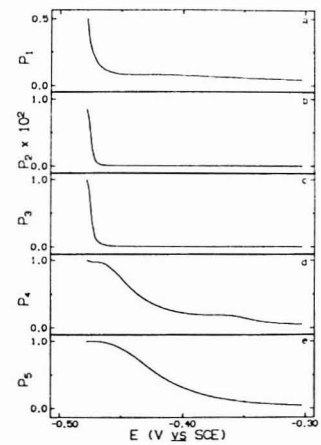


Figure 3. Kalman filter computed state variances for the LSASV (HMDE) trial shown in Figure 2. Initial value for all state variances (diagonal elements of P) and measurement variances was 1.00. The state variances shown are (a) potential (mV²), (b) concentration (M²), (c) background slope (μA/mV)², (d) background intercept (μA²), and (e) potential sweep rate (mV/s)²

demonstrate that the filter has converged to the true values of the states. Divergence of the computed state estimates from the true state values occurs primarily because either the computed error covariances, P, become artificially small relative to the true error covariances or there are inaccuracies in the measurement (H) or state (Φ) models. By fulfillment of the requirements of criterion three, not only is the possibility of divergence eliminated, but also the accuracy of the state estimates with respect to the models is assured.

The convergence of the Kalman filter for a single LSASV determination at an HMDE, shown in Figure 2, was evaluated by application of the three criteria described above. The LSASV trial is for the determination of a 4.0 ppb lead sample and overlayed on this experimental data is the model employed for the Kalman filter analysis. For the analysis of this

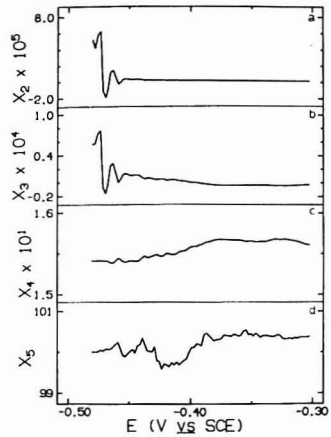


Figure 4. Kalman filter computed state estimates for the LSASV (HMDE) trial shown in Figure 2. The initial estimates of the concentration were computed using the algorithm discussed in the text and were $x_1 = 0.480$ V vs SCE, $x_2 = 5.16 \times 10^{-4}$ M, $x_3 = 5.64 \times 10^{-4}$ μA/mV, $x_4 = 1.54 \times 10^{-1}$ μA, and $x_5 = 100$ mV/s. The states shown are (a) concentration (M), (b) background slope (μA/mV), (c) background intercept (μA), and (d) potential sweep rate (mV/s)

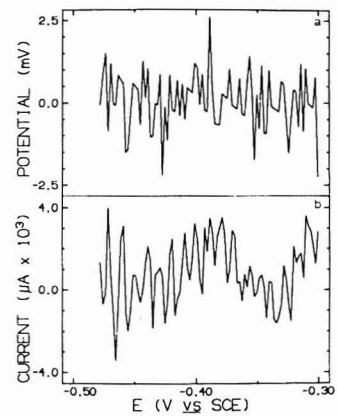


Figure 5. Potential innovation (a) and current innovation (b) sequences for the LSASV (HMDE) trial shown in Figure 2, variances in Figure 3, and states estimates in Figure 4

trial, the initial error covariances and measurement variances were all set equal to one. As pointed out in a previous paper (*29*), increases in the initial state error covariances give rise to increases in the rate of convergence of the states to the true values. This is due to the greater confidence placed in the data relative to that placed in the initial state estimates. Figure 3 shows the convergence of the diagonal elements of the error covariance matrix, P, during the potential sweep. It can be seen that these covarianes are monotonically decreasing, thereby fulfilling the requirements of criterion one. Figure 4 shows the convergence of the state estimates with respect to the potential of the current measurements. For the states (concentration, background slope, background intercept, and potential sweep rate), an invariant estimate is achieved

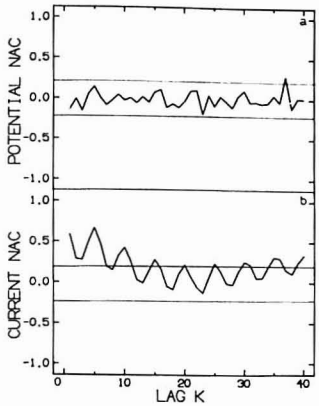


Figure 6. Potential (a) and current (b) normalized autocorrelation coefficient sequences for the LSASV (HMDE) innovation sequences shown in Figure 5. The solid horizontal lines are the 95% confidence interval computed as given in the text (Equations 8 and 9)

very quickly, indicating fulfillment of criterion two. The minor variations in the estimates of the background intercept and slope arise from the assumption of a linear background for the measurement model. Figure 5 shows the innovation sequences for the potential and current measurements for this trial. The potential measurement innovation sequence is normally distributed about a zero mean. This distribution, which satisfies criterion three, is indicative of convergence and the high accuracy resulting from the potential measurement model and potential state dynamics. The current measurement innovation sequence shows minor trending due to the simplifying assumptions made for the background models. From Figures 3, 4, and 5 it can be seen that for this LSASV trial, shown in Figure 2, the Kalman filter converges according to the first and second criteria. The potential innovation sequence is indicative of convergence, but the simplifying assumptions made in the current background model result in the slight trending of the current innovation sequence.

The performance of the filter was further evaluated by examination of the autocorrelation of the innovation sequence. A biased estimator of the autocorrelation coefficients, C_k, at various lag times, k, is given by (*48*)

$$\hat{C}_k = (1.0/N) \sum_{i=k}^{N} v_i v_{k-i}^{\mathrm{T}} \tag{8}$$

where N is the total number of data points and v_i is the innovation sequence at time i. The normalized autocorrelation coefficients (NAC), $\hat{\rho}_k$,

$$\hat{\rho}_k = \hat{C}_k / \hat{C}_0 \tag{9}$$

can range from +1.00 to −1.00 and provide a measure of the correlation of the innovation sequence at some time i to the innovations at some later time $i + k$. For the innovation sequences in Figures 5a and 5b, the NAC are shown in Figures 6a and 6b. The NAC for a finite white noise sequence have a normal distribution centered about a zero mean with the 95% confidence interval for the coefficients given by $\pm 1.96/N^{1/2}$ (*48*). If less than 5.0% of the coefficients fall outside this confidence interval, then the innovation sequence is taken to reflect white noise and the filter is performing optimally. The NAC for the potential innovations, shown in Figure 5a, exhibit optimal behavior with only 2.5% of the coefficients outside the 95% confidence limits. Twenty percent of the

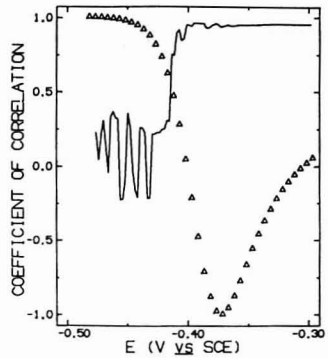


Figure 7. Coefficients of correlation (—) of concentration taken with Kalman filter estimate of the concentration at each measurement potential for LSASV (HMDE). Faradaic current model (Δ) used for the analysis is overlayed. Model parameters are: $r_0 = 0.0603$ cm and $A = 0.0457$ cm^2; all other model parameters are identical with those given in Figure 2

NAC for the current innovation sequence are outside the 95% confidence range which is indicative of a nonoptimal Kalman filter for the current measurements. Again the non-ideality of the behavior is due to the simplifying assumption of a linear background. A prominent feature of the current innovations NAC sequence is the periodicity, which is attributable to the 60-Hz interference that is not obvious in the measured current response (see Figure 2).

The current–potential data for a series of LSASV trials over a range of concentrations from 0.5 to 4.0 ppb lead were analyzed by the Kalman filter. For each trial, the Kalman filter computed an estimated concentration for each current observation along the potential axis. These results were similar to those seen in Figure 4a. At each measurement potential, these Kalman filter estimates of the concentrations were regressed with respect to the concentrations taken. The correlation coefficients for this series of regressions is shown in Figure 7 as a function of the measurement potential. Overlayed on this figure is the faradaic current model used for the analysis of the data. It can be seen that the Kalman filter estimate of the concentration becomes highly correlated with the analytical concentration well in advance of the maximum amplitude of the analog signal from which quantitative measurements are traditionally made.

Analysis of Synthetic Analytes. The data from LSASV experiments at the TFME and HMDE were analyzed by three basic approaches: nonreal time, pseudo-real time, and real time algorithms. As discussed in a previous section, the NRT and RT algorithms utilized the complete current potential transient to compute an estimate of the concentration. The PRT and DPRT algorithms utilized the magnitude of the peak faradaic current response and the IPRT analysis relied on the integral of the current as a concentration related parameter. In the ensuing discussion the three basic approaches, NRT, RT, and PRT analysis, will be critically compared. The various PRT algorithms will first be evaluated, and then the NRT and RT algorithms will be evaluated together because both employ the same model for the analysis. The NRT multiple regression algorithm provides a numerically equivalent cross check of the results for the RT Kalman filter. The PRT algorithms will then be compared to the NRT and RT algorithms with respect to the fidelity of the results, complexity of algorithm development, tractability of operation, and control capabilities.

Table IV. Comparison of Nonreal Time, Pseudo-Real Time and Real Time Computational Algorithms for Linear Sweep Anodic Stripping Voltammetric Analysis at an HMDE

	concentration reported[a]											
	pseudo-real time analysis methods										nonreal time analysis	real time analysis
	absolute peak picking					derivative peak picking						
concentration taken, M × 10^9	no smoothing	5-point grouping	5-point moving average	7-point quintic	cubic spline	no smoothing	5-point grouping	5-point moving average	7-point quintic	cubic spline	multiple regression	Kalman filter
19.3	22.2	22.2	22.1	22.0	22.0	22.2	22.1	22.0	22.2	22.1	22.1	22.2
RSD[b]	9.6	10.9	9.1	9.7	9.6	10.1	17.2	10.0	10.1	10.0	4.0	4.2
14.5	10.4	10.2	10.3	10.4	10.4	10.4	9.7	10.3	10.4	10.4	10.8	10.6
RSD	6.9	9.8	7.4	7.1	7.1	9.2	21.3	7.6	9.1	9.0	4.6	4.6
9.65	9.9	9.7	9.9	10.0	10.0	9.7	10.3	10.0	9.7	9.8	9.8	9.8
RSD	18.1	19.6	18.3	17.5	18.4	17.5	19.4	18.0	18.1	18.1	9.1	9.6
4.83	4.7	5.0	4.7	4.6	4.6	4.7	5.7	4.7	4.7	4.7	3.6	3.7
RSD	18.3	24.7	19.0	18.6	18.2	18.4	30.2	20.0	18.2	18.2	5.6	5.5
2.41	4.1	4.3	4.1	4.1	4.1	4.1	4.4	4.1	4.1	4.1	3.9	4.0
RSD	30.5	36.6	30.2	30.5	30.5	33.8	46.4	31.3	31.5	33.0	2.6	2.5

[a] Concentrations reported are based on the average of three trials. Potential sweep rates for these trials was 0.100 V/s and a current data point was acquired every 2.0 mV. [b] Relative standard deviations expressed in percent.

LSASV at HMDE. The results of the LSASV analysis at an HMDE for lead standards are shown in Table IV. Generally the APRT algorithms afford results which are comparable to each other in both precision and reported concentration, with the five-point grouping algorithm being the primary exception. The precision of the results reported by the DPRT algorithms was generally poorer than the precision of the APRT algorithms, although the reported concentrations were comparable. IPRT algorithms were not evaluated in this context because the long tailing of this type of data does not lend itself to valid integration over a range of experimental conditions. The results computed by NRT and RT algorithms were comparable to each other in both precision and reported concentration. For these analyses, the correlation between NRT and RT reported concentrations was 0.99 or greater. These two approaches, NRT and RT analysis, returned concentration estimates which were, in general, significantly more precise than the PRT analysis methods.

LSASV at TFME. The results of the LSASV analysis at a TFME for lead standards are shown in Table V. Again the results determined using the APRT algorithms were comparable to each other, except for the five-point group smoothing which again exhibited poorer precision. DPRT algorithms returned concentration estimates which were similar in value and precision to the PRT algorithms. The IPRT algorithms returned concentration estimates which were of comparable value to the DPRT and APRT algorithms, but of greater precision. The precision observed for the IPRT analysis of data smoothed by the five-point group algorithm was greater than the precision of either APRT or DPRT analysis with smoothing by five-point grouping. This is because the loss in data density from the grouping makes location of the peak more difficult and consequently introduces more error. The estimated concentrations for the NRT and RT analyses were comparable in both concentration estimate and precision. For these analyses, the correlation between NRT and RT reported concentrations was 0.99 or greater. The NRT multiple regression and RT Kalman filter estimates of the concentration were generally comparable to the APRT and DPRT algorithms, the only exception being the poorer precision of the smoothing by five-point grouping. The IPRT algorithms returned concentration estimates which agreed well with the APRT, DPRT, NRT, and RT algorithms and did so with generally increased precision.

Comparison of Operational Aspect of Numerical Algorithms. In addition to the evaluation of these algorithms using the accuracy and precision of the computed results, other aspects such as developmental complexities, operational tractability, and control capabilities must be considered. The developmental complexities are threefold: the experience required to utilize the algorithm, the difficulties in encoding the algorithm, and the time required for full implementation. Of the three basic approaches, RT, PRT, and NRT, the PRT methods require the least experience and time for implementation, and have fewer developmental problems than either the NRT or RT methods. Both NRT and RT methods are similar in developmental complexity. The tractability of an algorithm refers to the stability and time required for execution of the algorithm. All three techniques are computationally stable. Although divergence of computed estimates from the true values is possible for any of these methods, proper design of the algorithm eliminates these problems. PRT methods require the least computer time for execution. NRT methods utilize more execution time than the PRT methods, but less time than that for the RT approach. The control capabilities of the algorithms refer to those attributes which afford real-time computer feedback to the system based on the dynamic response of the signal. While some real-time control can be accomplished using PRT algorithms, feedback based on the analytical information for the system cannot occur until after the maximum amplitude of the signal. For NRT methods, control feedback is predicated on completion of the trial, whereas RT techniques, which are designed for control, afford feedback to the system subsequent to each observation.

Reproducibility and Limit of Detection. Using the optimized NRT multiple regression technique, an analysis of the variance of the reported concentrations was carried out for the LSASV data at an HMDE to determine the precision of the analysis technique and the reproducibility of the solution preparation. The RSD for repetitive analysis of the same 0.4 ppb lead standard was found to be 6.0%. The RSD for the repetitive analysis on four independent 0.4 ppb lead standards was 15.0%. From error propagation considerations, it is estimated that the maximum RSD introduced by volume errors in the dilutions is 2.8%. If it is assumed that the analysis errors and the dilution errors are additive, then the RSD which could be expected across samples of the same concentration is estimated to be 8.8% in contrast to the 15.0% observed. Considering the concentration of the lead, 0.4 ppb, this magnitude of unexplained error, 6.2%, suggests that 4.8×10^{-11} mol of lead contamination was introduced from ex-

Table V. Comparison of Nonreal Time, Pseudo-Real Time, and Real Time Computational Algorithms for Linear Sweep Anodic Stripping Voltammetric Analysis at a TFME

concentration reported[a]																
	pseudo-real time analysis methods													nonreal time analysis	real time analysis	
	absolute peak picking				derivative peak picking				trapezoidal integration							
concentration taken, $M \times 10^9$	no smoothing	5-point grouping	5-point moving average	7-point quintic	cubic spline	no smoothing	5-point grouping	5-point moving average	7-point quintic	cubic spline	no smoothing	5-point grouping	5-point moving average	7-point quintic	cubic spline	multiple regression	Kalman filter
19.3	17.0	10.5	16.8	16.5	17.0	17.3	c	16.9	16.8	17.2	18.0	17.5	18.1	18.0	18.0	17.3	17.3
RSD[b]	6.7	8.8	8.8	9.6	6.9	7.1		8.4	9.7	7.2	6.8	3.8	9.0	10.8	6.7	3.8	4.3
14.5	16.6	16.7	16.7	16.9	16.6	16.4	33.8	16.6	16.7	16.4	15.6	16.1	15.6	15.7	15.6	16.4	16.4
RSD	4.2	4.3	4.3	4.4	4.2	4.2	16.3	4.6	4.3	4.2	3.1	3.7	1.7	2.5	3.5	4.8	3.6
9.65	10.5	10.6	10.6	10.7	10.5	10.4	15.7	10.6	10.6	10.1	10.4	10.3	10.2	10.1	10.4	10.3	10.1
RSD	3.5	3.4	3.4	3.5	3.4	4.2	18.2	3.4	3.6	3.6	2.2	4.2	1.5	2.4	2.2	4.1	4.5
4.83	4.2	4.2	4.2	4.2	4.2	4.3	1.8	4.2	4.3	4.3	3.9	4.3	4.2	4.2	3.9	4.4	4.3
RSD	5.9	6.0	6.0	6.2	5.8	6.6	25.2	5.6	6.6	6.5	3.4	6.7	3.7	4.8	3.3	6.1	5.5
2.41	2.9	2.8	2.8	2.8	2.9	2.8	c	2.9	2.7	2.8	2.9	2.8	3.0	3.0	2.9	2.9	3.0
RSD	5.4	5.3	5.3	5.5	5.5	3.7		5.1	3.8	3.7	3.5	2.8	1.9	1.3	3.7	2.3	2.3

[a] Concentrations reported are the average of three trials. Potential sweep rate for these trials was 0.100 V/s with current data being acquired every 2.0 mV. [b] Relative standard deviation expressed in percent. [c] Concentration reported was negative.

ogenous sources such as glassware, pipets, or dust in the air (*49*).

From the error associated with the intercept of the calibration plot, the limit of detection for LSASV at an HMDE is 0.4 ppb lead. From repetitive analyses of the 0.4 ppb lead analyte and backgrounds run on the same day, the estimate of the limit of detection based on twice the standard deviation of the background is 0.3 ppb lead. From these results, it is clear that the lower limit of detection is determined by the background lead concentration rather than the precision of the technique.

SUMMARY AND CONCLUSIONS

The thrust of this work was to evaluate the Kalman filter and critically compare the relative merits of real time, pseudo-real time, and nonreal time algorithms for analyzing data resulting from linear sweep anodic stripping voltammetric analysis at an HMDE and a TFME.

The model current–voltage transients for LSV at a plane electrode were found to agree well with the experimental data over the range of sweep rates investigated. For the LSV and LSASV model at a spherical electrode, there was good agreement among the calculated concentrations over the range of potential sweep rates. The model for TFME showed slight deviations from the experimental current response. Other investigators using essentially identical experimental conditions (*40*, *50*), but with different electrode substrates (e.g., glassy carbon or silver), have demonstrated agreement of stripping peak shapes with the model of DeVries (*45*). For the WIGE, Pinchin et al. (*46*) observed deviation of the experimental waveforms from theory, while others have shown agreement (*44*). This present work indicates that on a WIGE the peak shapes cannot be accurately estimated from the film thickness not only because of uncertainty regarding the physical form of the mercury on the surface and incompleteness of the mercury coverage of the graphite, but also because of possible alteration of peak shape by uncompensated resistance.

The Kalman filter was evaluated by the convergence of the states and the accuracy of the computed concentrations for LSASV experiments at the HMDE using synthetic water samples. The convergence of the states to invariant values and the covariances to small values was rapid even though system modeling errors were made apparent by the current innovation sequence. It should be noted that, even in the presence of correlated noise (60 Hz), there was still rapid convergence to accurate estimates of the states. The optimal NRT multiple regression analysis was employed as a cross check for the Kalman filter results because both the NRT and RT analysis methods utilized the same faradaic and nonfaradaic current models. The coefficients of correlation of the concentrations reported for the optimal NRT multiple regression method with the concentrations reported by Kalman filter analysis were always 0.99 or greater. The rapid convergence of the states and the accuracy of the results computed by the Kalman filter were further demonstrated by the high degrees of correlation between the analytical concentration and the concentration estimated at each measurement potential. This high correlation was established well in advance of the maximum amplitude of the faradaic signal, thus demonstrating greater capabilities for dynamic control than are possible with PRT or NRT methods.

The synthetic analyte studies indicate that the RT and NRT analysis methods return results which have higher precision than the PRT analysis methods. It is noteworthy that the smoothing algorithm which yielded the most precise results was the five-point moving average. This is because the frequency cutoff for this filter (*51*, *52*) is considerably lower than for the other smoothing filters, except for grouping. The

grouping algorithm reduces the data density significantly and, because of this, the difficulty in locating the peak is increased and the precision is decreased. This coupling of the filter frequency response with the precision of the results suggests that more accurate and precise results could be obtained using the PRT analysis if the filter employed had an even lower cutoff frequency than that of the five-point moving average.

As expected with the PRT analysis methods, the concentrations computed for the TFME trials were more precise than those reported by the HMDE analysis because of the magnitude of the current response. The sharpness of the peak for the TFME analysis lends itself well to the location of the peak by derivative methods.

APPENDIX I. RECURSIVE ESTIMATION NOMENCLATURE

For the representation and discussion of equations referring to the Kalman filter, the following notation holds:

(1) Lower case English letters represent vectors or scalars.

(2) Upper case English and Greek letters define matrices; the corresponding use of lower case letters signifies the scalar representation of the matrix.

(3) The expectation value of x, $E(x)$, is given by

$$E(x) = \int_{-\infty}^{\infty} x\hat{p}(x)dx$$

where $\hat{p}(x)$ is the probability density function of x.

(4) Superscript −1 indicates matrix inversion.

(5) Superscript T indicates matrix transposition.

(6) Vector quantities, x, expressed as $\hat{x}$, signify a posteriori information, while those quantities expressed as $\bar{x}$ signify a priori information.

APPENDIX II. MODELS

The faradaic current at a plane electrode for semi-infinite linear diffusion conditions is given by (*38*)

$$i_p = nFAC^*\sqrt{\frac{Da}{\pi}}\left(2\sqrt{p}/\theta + 1/2\int_0^P \sqrt{z}\frac{\tanh[(\ln\theta - p + z)/2]}{\cosh^2[(\ln\theta - p + z)/2]}dz\right) \quad \text{(A-1)}$$

for $\theta \gg 1$ and the faradaic contribution for electrode sphericity is (*38*)

$$i_s = nFAC^*D/r_0[1/(1 + \theta\exp(-at))] \quad \text{(A-2)}$$

where

$$z = a(t - \tau) \quad \text{(A-3)}$$

$$\theta = \exp[(nF/RT)(E^* - E^0)] \quad \text{(A-4)}$$

$$a = nF\nu/RT \quad \text{(A-5)}$$

$$pa = (nF/RT)(E^* - E) \quad \text{(A-6)}$$

and C^* is the concentration of the electroactive species and the significance of the other electrochemical notation is summarized below.

The faradaic current response for the thin-film electrode is given by (*45*)

$$q_i = [(3/4)C_R^*(\pi D_R/\xi)^{1/2}(1 - \exp[-ja\xi]) - [1 + \exp[-ja\xi](D_R/D_0)^{1/2}/\theta']S_1 - (3/2)S_2]/[(3/2)(A_1 - B_1) + 1 + \exp[-ja\xi](D_R/D_0)^{1/2}/\theta'] \quad \text{(A-7)}$$

where

$$S_1 = -q_{j-1} + \sum_{k=1}^{j-1}(q_k - q_{k-1})[(j - k + 1)^{3/2} - (j - k)^{3/2}] \quad \text{(A-8)}$$

$$S_2 = q_{j-1}B_1 + \sum_{k=1}^{j-1}[(q_k - q_{k-1})(j - k) + q_k]A_{j-k+1} - (q_k - q_{k-1})B_{j-k+1}] \quad \text{(A-9)}$$

$$A_u = a_u - a_{u-1};\ B_u = b_u - b_{u-1} \quad \text{(A-10)}$$

$$b_u = (2/3)\sum_{i=1}^{\infty}[u^{3/2}\exp[-i^2l^2/\xi D_R u] - (i^2l^2/\xi D_R)a_{u,i}] \quad \text{(A-11)}$$

$$a_u = \sum_{i=1}^{\infty}a_{u,i} = \sum_{i=1}^{\infty}[2u^{1/2}\exp[-i^2l^2/\xi D_R u] - 2(\pi i^2l^2/\xi D_R)^{1/2}\mathrm{erfc}[i^2l^2/\xi D_R u]] \quad \text{(A-12)}$$

$$\theta' = (f_R'/f_0')\exp[(nF/RT)(E^* - E^0)] \quad \text{(A-13)}$$

ξ is the time interval (seconds) on the potential axis between computed currents, u is a positive integer, a is defined by Equation A-5, C_R^* is the concentration of the reduced form of the electroactive species in the mercury film and the significance of the other common electrochemical notation is summarized below.

For equations pertaining to the models of the electrochemical systems, the following notation holds:

i = current (amperes)
n = equivalents/mol
A = electrode area (cm^2)
D = diffusion coefficient (cm^2/s)
ν = sweep rate (V/s)
F = 96 485 coulombs/equivalent
R = 8.3143 V-coulomb/deg-mol
π = 3.14159
r_0 = radius of HMDE (cm)
t = time (s)
f' = activity coefficient (M^{-1})
l = thickness of TFME (cm)
q = i/nFA
E^0 = standard electrode potential (V)
E^* = initial sweep potential (V)
E = electrode potential (V)

LITERATURE CITED

(1) R. E. Dessy, P. J. Vuuren, and J. A. Titus, *Anal. Chem.*, **46**, 917A (1974).
(2) R. E. Dessy, J. A. Titus, and P. J. Vuuren, *Anal. Chem.*, **46**, 1055A (1974).
(3) L. P. Morgenthaler and T. J. Poulos, *Am. Lab.*, **8** (8), 37 (1976).
(4) J. A. Keenan and P. F. Cox, *Am. Lab.*, **9** (2), 55 (1977).
(5) D. L. Wallace and A. C. Brown III, *Am. Lab.*, **9** (1), 67 (1977).
(6) W. A. Wolstenholme and J. N. Gerber, *Am. Lab.*, **9** (2), 69 (1977).
(7) M. Tarter, *Am. Lab.*, **9** (10), 89 (1977).
(8) D. L. Duewer, B. R. Kowalski, and J. L. Fasching, *Anal. Chem.*, **48**, 2002 (1976).
(9) G. L. Ritter, S. R. Lowry, T. L. Isenhour, and C. L. Wilkins, *Anal. Chem.*, **48**, 591 (1976).
(10) E. R. Malinowski, *Anal. Chem.*, **49**, 606 (1977).
(11) E. R. Malinowski, *Anal. Chem.*, **49**, 612 (1977).
(12) E. R. Malinowski and M. McCue, *Anal. Chem.*, **49**, 284 (1977).
(13) R. N. Carey, S. Wold, and J. O. Westgard, *Anal. Chem.*, **47**, 1824 (1975).
(14) T. F. Lam, C. L. Wilkins, T. R. Brunner, L. J. Soltzberg, and S. L. Kaberline, *Anal. Chem.*, **48**, 1768 (1976).
(15) G. M. Pesyna, R. Venkataraghavan, H. E. Dayringer, and F. W. McLafferty, *Anal. Chem.*, **48**, 1362 (1976).
(16) J. S. Mattson, C. S. Mattson, M. J. Spencer, and F. W. Spencer, *Anal. Chem.*, **49**, 500 (1977).
(17) D. E. Aspnes, *Anal. Chem.*, **47**, 1181 (1975).
(18) A. Savitsky and M. J. E. Golay, *Anal. Chem.*, **36**, 1627 (1964).
(19) J. Steinier, Y. Termonia, and J. Deltour, *Anal. Chem.*, **44**, 1906 (1972).
(20) C. G. Enke and T. A. Nieman, *Anal. Chem.*, **48**, 705A (1976).
(21) H. E. Keller and R. A. Osteryoung, *Anal. Chem.*, **43**, 342 (1971).
(22) K. R. Betty and G. Horlick, *Appl. Spectrosc.*, **30**, 23 (1976).
(23) C. A. Bush, *Anal. Chem.*, **46**, 890 (1974).
(24) J. W. Hayes, D. E. Glover, D. E. Smith, and M. W. Overton, *Anal. Chem.*, **45**, 277 (1973).
(25) R. deLevie, S. Sarangapani, P. Czekaj, and G. Benke, *Anal. Chem.*, **50**, 110 (1978).

(26) G. Horlick, *Anal. Chem.*, **44**, 943 (1972).
(27) T. R. Brunner, R. C. Williams, C. L. Wilkins, and P. J. McCombie, *Anal. Chem.*, **46**, 1798 (1974).
(28) P. C. Jurs, *Anal. Chem.*, **43**, 1812 (1971).
(29) P. F. Seelig and H. N. Blount, *Anal. Chem.*, **48**, 252 (1976).
(30) J. F. Evans, Ph.D. Dissertation, University of Delaware, Newark, Del., 1977.
(31) D. T. Shang and H. N. Blount, *J. Electroanal. Chem.*, **54**, 305 (1974).
(32) G. C. Whitnack and R. Sasselli, *Anal. Chim. Acta*, **47**, 267 (1969).
(33) Princeton Applied Research Corporation Application Note, AN-108.
(34) L. Meites, "Polarographic Techniques", John Wiley and Sons, New York, 1965, p 89.
(35) W. W. Cooley and P. R. Lohnes, "Multivariate Data Analysis", John Wiley and Sons, New York, 1971.
(36) B. Carnahan, H. A. Luther, and J. O. Wilkes, "Applied Numerical Methods", John Wiley and Sons, New York, 1969.
(37) M. Abrahmowitz and I. A. Stegun, Ed., "Handbook of Mathematical Functions", National Bureau of Standards Applied Mathematics Series, No. 55, U.S. Government Printing Office, Washington, D.C., 1964.
(38) W. H. Reinmuth, *J. Am. Chem. Soc.*, **79**, 6358 (1957).
(39) W. H. Reinmuth, *Anal. Chem.*, **33**, 185 (1961).
(40) T. M. Florence, *J. Electroanal. Chem.*, **27**, 273 (1970).
(41) R. G. Clem, G. Litton, and L. D. Ornelas, *Anal. Chem.*, **45**, 1306 (1973).
(42) W. R. Matson, D. K. Roe, and D. E. Carritt, *Anal. Chem.*, **37**, 1594 (1965).
(43) S. P. Perone and K. K. Davenport, *J. Electroanal. Chem.*, **12**, 269 (1966).
(44) W. R. Matson, Ph.D. Dissertation, Massachusetts Institue of Technology, Cambridge, Mass., 1968.
(45) W. T. DeVries, *J. Electroanal. Chem.*, **9**, 448 (1965).
(46) M. J. Pinchin and J. Newham, *Anal. Chim. Acta*, **90**, 91 (1977).
(47) W. T. DeVries and E. van Dalen, *J. Electroanal. Chem.*, **12**, 9 (1966).
(48) R. K. Mehra, *IEEE Trans. Auto. Control*, **15**, 175 (1970).
(49) R. A. Hofstader, O. I. Milner, and J. H. Runnels, Ed., "Analysis of Petroleum for Trace Metals", *Adv. Chem. Ser.*, **No. 156**, 1976.
(50) Z. Stojek and Z. Kublick, *J. Electroanal. Chem.*, **77**, 205 (1977).
(51) K. R. Betty and G. Horlick, *Anal. Chem.*, **49**, 351 (1977).
(52) K. Steiglitz "An Introduction to Discrete Systems", John Wiley and Sons, New York, 1974, p 50.

RECEIVED for review August 2, 1978. Accepted November 3, 1978.

Correction for Background Current in Differential Pulse, Alternating Current, and Related Polarographic Techniques in the Determination of Low Concentrations with Computerized Instrumentation

A. M. Bond*[1] and B. S. Grabaric[2]

Department of Inorganic Chemistry, University of Melbourne, Parkville, 3052, Victoria, Australia

Modern electroanalytical techniques, such as differential pulse and alternating current polarography, can be used to accurately determine concentrations of electroactive species at 10^{-7} M concentration levels, or below, provided the background current can be corrected for. Using computerized instrumentation, a quadratic least squares fit of data removed from the faradaic peak current of interest is shown to provide a general method of predicting the base line over all of the required potential range. Since no theoretical assumptions are involved in the calculation, contributions from residual oxygen levels or other trace impurities are included in the background prediction and correction procedure, and the method is applicable to a wide range of techniques and conditions. Results are presented for the determination of cadmium in the 10^{-6} to 10^{-8} M concentration range in 1 M NaCl, and data at these very low concentration levels are generally found to be superior to those obtained by storing a polarogram of the blank in memory and subsequently subtracting the result from test solutions.

As an analytical technique, direct current polarography suffers from the disadvantage of having a relatively unfavorable faradaic to charging current ratio (*1–3*). Consequently, modern polarographic techniques such as differential pulse polarography, phase-selective alternating current polarography (fundamental and second harmonic), linear sweep voltammetry, and other techniques which substantially discriminate against the charging current are becoming widely used as alternatives to the direct current method (*4, 5*). However, despite the improved sensitivity offered by these more modern polarographic methods, the fact remains that it is still the background or residual current, rather than an unfavorable signal to noise ratio, which ultimately determines the limit of detection available with these techniques.

With direct current polarography, the charging current or background current in general is approximately a linear function of potential. This approximation is certainly an excellent one over the small potential range occupied by a sigmoidal shaped direct current wave. Indeed, many commercially available polarographs provide an analog circuit, using the linear approximation, to compensate for the charging or background current and accurate measurement of limiting current is facilitated by this method. More recently, the advent of instrumentation using laboratory computers has become common (*5, 6*). With data obtained in digital format, correction for the background current can be made by storing the data obtained on a blank, if available, and mathematically subtracting the result from the test solution made up in the same matrix. Alternatively, a mathematical algorithm to represent the background currents may be constructed from data obtained at potentials removed from the faradaic current. An extrapolation to the potentials of interest where the faradaic current is present and subtraction of calculated values thereby enables the purely faradaic current to be calculated. This latter procedure has been exploited in direct current and normal pulse polarography with considerable success (*7*) and with alternating current techniques assuming the background current is purely capacitive (*8*). The former approach is, in fact, equivalent to the dual cell or subtractive method of polarography available in analog instrumentation (*1*) and the second is akin to the linear compensating analog electronic circuit available with direct current polarographic instrumentation. However, both methods are implemented far more successfully with computerized instrumentation than with purely conventional instrumentation.

[1] Present address, Deakin University, Division of Chemical and Physical Sciences, Waurn Ponds, Victoria, 3217, Australia.
[2] On leave from the Department of Inorganic Chemistry, Faculty of Technology, University of Zagreb, Zagreb, Yugoslavia, 1975–1977.

0003-2700/79/0351-0337$01.00/0 © 1979 American Chemical Society

Of particular relevance to the present study is the work of Perone et al. (*9, 10*) who have described in detail the use of on-line interactive data processing procedures and presented examples in the area of linear sweep and cyclic voltammetry at a dropping mercury electrode (*10*). Even at the relatively high (compared to our work) concentration level of 10^{-6} M these authors report considerable difficulty in correcting for the blank using the analog dual cell or subtractive method because of problems in adequately matching the dual cells. The computerized subtractive method of recording the blank in an initial experiment and subtracting the result from subsequent experiments could, however, be carried out conveniently and accurately. At the concentration levels well below 10^{-6} M that we wished to examine, this result indicates computerized approaches will almost be mandatory and indeed this is our experience as subsequent results will demonstrate.

With differential pulse, alternating current, and other modern polarographic techniques, the background current cannot be approximated by a linear function of potential as is the case with direct current polarography, so that mathematical correction for charging current is not straightforward. Furthermore, because the techniques are so sensitive, with concentrations of many species in the 10^{-7} to 10^{-8} M range producing measurable responses, the apparent background current in the real analytical situation is unlikely to be void of a faradaic component from an "impurity". For example, oxygen at variable, but trace, levels can represent a significant component of the background when trying to determine concentration of other species below 10^{-7} M. Thus, the obvious approach of recording the polarogram at a blank and storing the data in memory for subsequent subtraction from test solutions is not as reproducible and reliable as it may appear to be in principle, when determining species near the limit of detection with modern polarographic methods. Other terms such as electrode area growth during the course of current measurement may also contribute to the background current (*11*). The correction for background current, which is a prerequisite for accurate analysis at trace levels via polarographic methods, therefore represents a non-trivial problem which needs to be solved to take full advantage of the capabilities of modern instrumentation.

In view of the fact that correction for background current is a problem always confronted when working near the limit of detection with the extremely sensitive modern polarographic techniques, we thought it might be useful to describe a general approach to the problem of correction for background current that we have developed for use with on-line computerized polarographic instrumentation. This is the purpose of the present communication. The technique uses a quadratic least-squares fit of the data at potentials removed from the faradaic current and, unlike most previous methods, it is applied directly to the solution being measured without making any assumptions about the nature or theory pertaining to the background current. Numerical background fitting techniques have been successfully employed in other areas of analytical chemistry, for example, mass spectrometry (*9*) and chromatography (*9, 12–14*). Thus, despite the fact that such techniques do not appear to have been employed in the polarographic area, available data from these other studies imply that such an approach will be successful.

Measurement on the reduction of cadmium in chloride media in the 10^{-6} to 10^{-8} M concentration range are presented to demonstrate the fidelity of the method. This reduction process has been considered because it represents a difficult situation for the following two reasons. Firstly, the reduction process occurs near the electrocapillary maximum where the shape of the double-layer capacitance changes rapidly as a function of potential and is, therefore, not as easily defined as at more negative or more positive potentials. Secondly, oxygen is reduced over the same potential range making the shape and magnitude of the residual current critically dependent on the oxygen concentration present in solution.

EXPERIMENTAL

All chemicals used were of analytical grade purity. Solutions were thermostated at 22 ± 1 °C and degassed with argon or nitrogen prior to recording a polarogram.

All polarograms were obtained using a conventional three-electrode configuration. The reference electrode was Ag/AgCl (1 M NaCl) and the auxiliary electrode was platinum wire.

The electrochemical instrumentation consisted of a PAR Model 174 Polarographic Analyzer (Princeton Applied Research Corporation, Princeton, N.J.) interfaced to a PDP 11/10 minicomputer (Digital Equipment Corporation, Marlborough, Mass.) used in conjunction with a CAPS-11 operating system.

The computer was equipped with a DR-11 general purpose interface which could be used to provide the logic and buffer register necessary for program controlled parallel transfers of 16-bit data between the PDP-11 system and the Polarographic Analyzer. This interface also includes status and control bits that could be controlled by either the program or the external device for command, monitoring, and interrupt functions. A TA-11 Cassette System Interface was used to load programs and for the input/output of data.

Sampling of the current output from the Polarographic Analyzer was performed using an AR-11 real time analog sub-system which included a 16-channel, 10-bit A/D converter with sample and hold, a programmable real time clock with one external input and a display control with two 10-bit D/A converters. Sampled data as well as any transformed data were displayed on either a Tektronix D13 Storage Oscilloscope or on an X–Y recorder.

A program operating the Polarographic Analyzer, acquiring data, evaluating data, and displaying data was written in BASIC language using system sub-routines written in PAL-11 assembly language.

The program for background correction was written in BASIC language and is a quadratic least-squares fit of an equation of the type $I = A(E - E^*)^2 + B$ where A, E^* and B are constants, I is the current, and E the applied potential. The computer controlled system, background correction, and data reduction form an interactive system. Thus the operator can specify which data points the quadratic least-squares fit is applied to. Having defined the background from a least squares fit of chosen data points, prediction of the background current, I, for all values of $(E - E^*)$ can be made. This result is stored in memory and the result subtracted from subsequent experiments. Replicate scans can be made for averaging of data; however, all data presented in this paper was based on a single scan of the potential. Peak heights and peak positions are calculated via a quadratic least-squares fit of data located near the peak. Listings of all programs are available on request to the authors.

Pulse polarographic measurements were performed with the aid of modifications to the commercially available instrument described elsewhere (*15, 16*). A PAR Model 129 two-phase/vector lock-in-amplifier using an Optimation Inc. Model RCD-10 sinewave oscillator to provide the input and reference signals was used to obtain phase-selective and total alternating current polarographic measurements. The ac circuitry and polarograph were interfaced with PAR accessory Model 174/50.

RESULTS AND DISCUSSION

In recording a polarogram of a species to be determined by differential pulse or an alternating current technique, a potential range sufficient to cover the peak shaped faradaic current response plus the background base-line current on either side of the peak is required. From the profile of the base-line current at potentials removed from the faradaic current, it is necessary to predict what the base line would have been at the peak position and possibly other potentials on the wave. Subtraction of the predicted base-line current should lead to the purely faradaic current response required for analytical or theoretical purposes.

Table I. Comparison of Two Different Methods of Background Correction for a 1×10^{-6} M Solution of Cadmium in 1 M NaCl[a]

	data corrected by quadratic least-squares fit or background[b]		data corrected by subtraction of background[b]	
run no.	peak height, nA	peak position, V vs. Ag/AgCl	peak height, nA	peak position, V vs. Ag/AgCl
1	81.6	−0.6344	80.9	−0.6345
2	82.3	−0.6350	82.0	−0.6348
3	80.6	−0.6352	83.2	−0.6358
4	81.2	−0.6349	81.6	−0.6342
5	83.0	−0.6340	82.0	−0.6351
6	81.6	−0.6342	82.0	−0.6342
7	82.5	−0.6346	81.6	−0.6358
8	83.1	−0.6355	80.8	−0.6341
9	80.8	−0.6360	83.4	−0.6349
10	83.0	−0.6347	80.2	−0.6342
average	82.0 ± 0.8	−0.6349 ± 0.0005	81.8 ± 0.8	−0.6348 ± 0.0005

[a] Differential pulse polarography. Drop time = 5.0 s. Pulse amplitude = −25 mV, Temperature = 22 °C. [b] Solutions degassed with argon for 30 min prior to recording a polarogram.

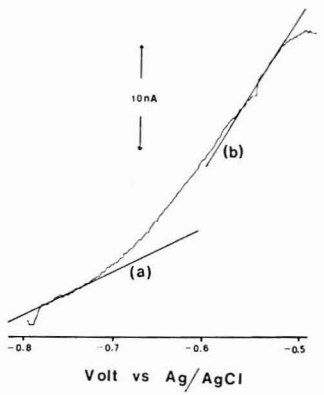


Figure 1. Differential pulse polarogram of 1 M NaCl. Pulse amplitude = −25 mV, drop time = 1.0 s. (a) and (b) linear extrapolations from data obtained at potentials removed from where cadmium electrode process would occur

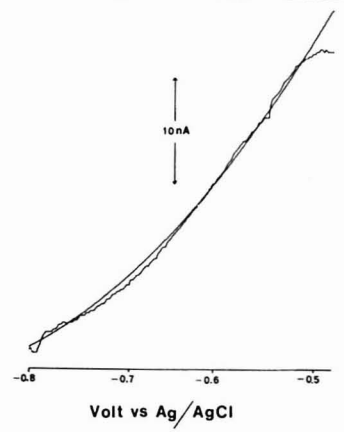


Figure 2. Differential pulse polarogram of 1 M NaCl and a computerized quadratic least-squares fit of data. Pulse amplitude = −25 mV, drop time = 1.0 s

Figure 1 shows the background current recorded by differential pulse polarography on a 1 M NaCl solution at a drop time of 1.0 s over the potential range required for the determination of cadmium. The magnitude of the currents being measured is small, and some noise is present in the response. However, it is clear that the background current cannot successfully be approximated by a straight line. Furthermore, as shown in Figure 1, a linear extrapolation from either extremity of the data range, as required in the real situation, would lead to a poor prediction of the base line in the middle of the data range where the peak due to reduction of cadmium would be observed.

In Figure 2, a computer plot of a quadratic least-squares fit to all of the data presented in Figure 1 is given. Obviously, the computer implemented approximation of the background current to a parabola is far superior to the linear one usually employed in manual graphical interpolations.

Figure 3 shows the determination of 10^{-6} M cadmium in 1 M NaCl using the quadratic least-squares fit to correct for the charging current. In Figure 3a, the raw data are shown with a drop time of 1.0 s and pulse amplitude of −25 mV. A quadratic least-squares fit made from data obtained at both extremities of the data range provides the curve shown in Figure 3b. Subtraction of curve 3b from raw data in Figure 3a produces the corrected differential pulse curve shown in Figure 3c. In the corrected curve, current values near the foot of both sides of the peak are close to zero and shape analysis and peak position of the observed wave is essentially identical to that obtained at higher concentrations when the base-line problem is unimportant.

From the corrected curve, a quadratic least-squares fit of data enables peak location to be made with a reproducibility of ±1 mV at the 10^{-6} M level under the conditions presented in Figure 3. The peak height is reproducible to ±2% under the same conditions and both peak position and height agree within the limit of experimental error to values obtained via subtraction of background current obtained from a blank obtained as in Figure 1, providing care is taken to completely remove oxygen from both test and blank solutions when using the latter approach (see later). Representative data at the 10^{-6} M concentration level are presented in Table I.

Some options available in the computer program enabling the final data shown in Figure 3c to be obtained should be mentioned. Importantly, in establishing which data to employ in constructing the quadratic least-squares fit, complete flexibility is available and any number of data points may be used as specified by the operator. In Figure 3, the initial points on the most positive potential side of the peak, where the scan is commenced, were not included in the calculation because

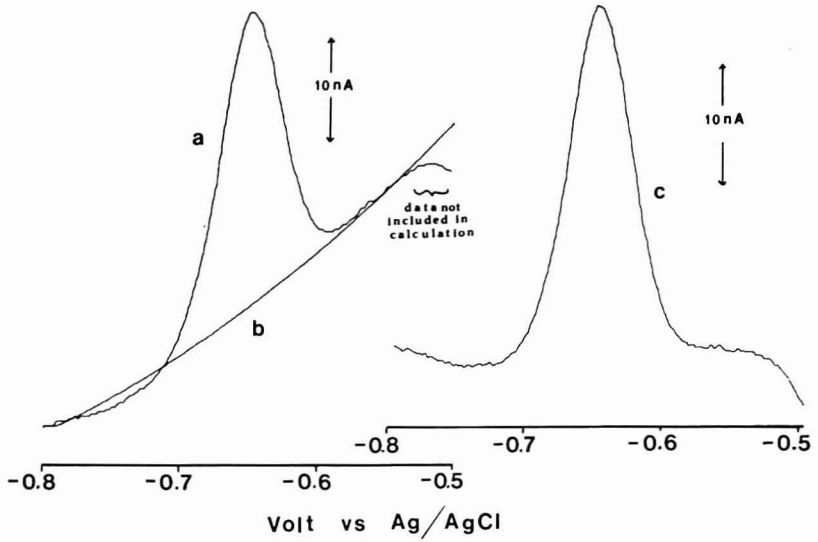


Figure 3. Differential pulse polarogram of 1×10^{-6} M cadmium in 1 M NaCl. Pulse amplitude = −25 mV, drop time = 1.0 s. (a) Raw data. (b) Background current calculated by quadratic least-squares fit. (c) Final data from which peak height and position are calculated.

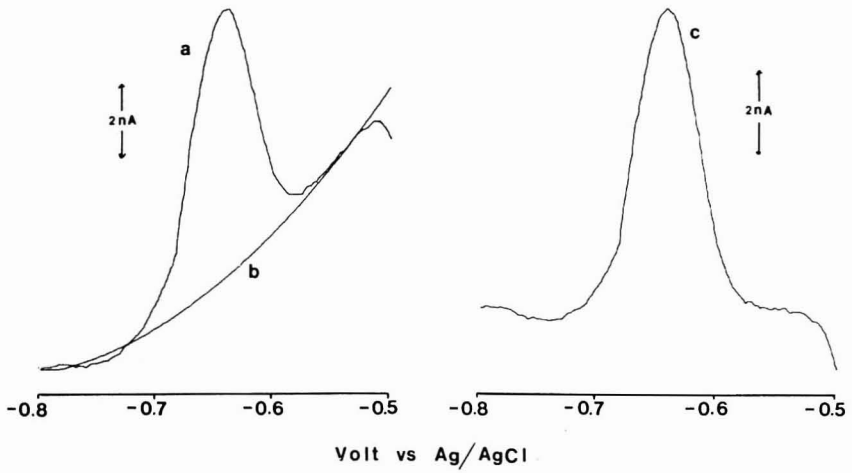


Figure 4. Differential pulse polarogram of 1×10^{-7} M cadmium in 1 M NaCl. Pulse amplitude = −25 mV, drop time = 5.0 s. (a) Raw data. (b) Background current calculated by quadratic least-squares fit. (c) Final data from which peak height and position are calculated.

they are clearly not relevant to defining the base line at the peak. This is shown on Figure 3a. The first few data points obtained commonly had to be rejected with differential pulse measurements because of instrumental distortion associated with them. Data points resulting from a bad drop could also be rejected from the quadratic least-squares fit to obtain the background.

The problem of the background current obviously becomes more severe at lower concentrations and, at least with differential pulse polarography, it is critically governed by the drop time, with the most favorable faradaic to charging current ratio being obtained at longer drop times. Thus, to determine concentrations in the 10^{-7} to 10^{-8} M concentration range by differential pulse polarography, a drop time of 5 to 10 s needs to be employed, rather than the 1.0 s shown in Figure 3. Shorter drop times are more suitable for higher concentrations, with the trade-off, of course, being the concomitant increase in scan time required to obtain the data when using long drop times, vs. sensitivity.

Figure 4 shows the determination of 10^{-7} M cadmium in 1 M NaCl using a drop time of 5.0 s and a pulse amplitude of −25 mV. While the background current is of considerable

Table II. Comparison of Two Different Methods of Background Correction for a 1×10^{-7} M Solution of Cadmium in 1 M NaCl with Variable Degassing Time[a]

	data corrected by quadratic least-squares fit of background		data corrected by subtraction of background[c]	
degassing time,[b] min	peak height, nA	peak position, V vs. Ag/AgCl	peak height, nA	peak position, V vs. Ag/AgCl
5	8.0	−0.6352	12.3	−0.6382
5	8.2	−0.6371	6.4	−0.6322
5	8.4	−0.6364	5.8	−0.6341
15	8.0	−0.6368	6.8	−0.6362
15	8.2	−0.6340	10.2	−0.6384
15	8.2	−0.6351	10.0	−0.6396
30	8.3	−0.6346	10.6	−0.6384
30	8.2	−0.6359	9.8	−0.6384
30	8.2	−0.6356	8.2	−0.6362

[a] Differential Pulse Polarography. Drop time = 5.0 s, pulse amplitude = −25 mV, temperature = 22 °C. [b] Argon. [c] Background recorded after same time as test solution.

magnitude, the final curve after correction is eminently suitable for analytical work. A reproducibility of peak position of ±2 mV and peak height of ±3% was obtained with the above conditions. A limit of detection of 10^{-8} M is obtained with the present computerized instrumentation, at long drop time with differential pulse polarography, and plots of peak height vs. concentration are linear within the limit of experimental error over the concentration range of 10^{-6} to 10^{-8} M as predicted theoretically. We therefore conclude that the quadratic least-squares fit to obtain the base line is extremely successful in differential pulse polarography.

When working at the 10^{-7} to 10^{-8} M concentration range, the base line is critically dependent on the presence of trace amounts of oxygen. In our hands, approximately half an hour's degassing with argon on both the blank and test solution was necessary to provide reproducible data when using the background correction method of recording a blank and subtracting the result from subsequent solutions containing trace amounts of cadmium in the same media. Furthermore, because long drop times and slow scan rates are required to determine low concentration, the problem of maintaining oxygen-free conditions while recording a polarogram is a non-trivial problem and, at the 10^{-7} level, results with a reproducibility of better than ±5% are very difficult to obtain with this correction method. Additionally, such a process inherently contributes noise to the measured response and it is very time consuming. By contrast, when the base line is calculated from a quadratic least-squares fit, variable oxygen levels and the presence of other trace impurities are essentially accounted for in the calculations and, provided products of the oxygen electrode process do not cause interference with the electrode species being determined, extreme care to completely eliminate oxygen is not required. Data obtained under various conditions at the 10^{-7} M level are provided in Table II and the superiority of the quadratic least-squares method is clearly obvious. We have therefore reached the conclusion that, despite the inherently more complex mathematics involved in the use of the quadratic least-squares fit, results are substantially superior to a simple background subtraction procedure because of the complete generality of the method.

While the above discussion is presented with respect to differential pulse polarography, the same approach has been tested with alternating current polarography (phase-selective fundamental and second harmonic), as well as with differential pulse and alternating current anodic stripping and normal voltammetry at the dropping mercury and stationary electrodes. Results are equally as impressive with these techniques as for differential pulse polarography, so the widespread applicability of the background correction problem can be appreciated. Overall, we therefore believe the approach to be both versatile and extremely useful. In particular, area growth terms which can cause difficulties when undertaking fast sweep alternating current or differential pulse voltammetric measurements at a dropping mercury electrode are accounted for (*16*, *17*) in situations where species to be determined appear as shoulders on another faradaic wave; for example, with species reduced or oxidized near the solvent limit, the quadratic least-squares fit is also successful in correcting the data for this kind of faradaic interference.

LITERATURE CITED

(1) H. Schmidt and H. Von Stackelberg, "Modern Polarographic Methods", Academic Press, New York/London, 1963.
(2) L. Meites, "Polarographic Techniques", 2nd ed., Interscience, New York/London/Sydney, 1965.
(3) J. Heyrovsky and J. Kuta, "Principles of Polarography", Academic Press, New York, 1966.
(4) J. B. Flato, *Anal. Chem.*, **44** (11), 75A (1972).
(5) A. M. Bond, "Modern Polarographic Methods in Analytical Chemistry", Marcel Dekker, New York, in press.
(6) "Computers in Chemistry and Instrumentation", J. S. Mattson, H. D. MacDonald, Jr., and H. B. Mark, Jr., Ed., M. Dekker, New York, 1972.
(7) A. M. Bond and B. S. Grabaric, *Anal. Chim. Acta*, **101**, 309 (1978).
(8) R. J. Schwall, A. M. Bond, R. J. Loyd, J. G. Larsen, and D. E. Smith, *Anal. Chem.*, **49**, 1797 (1977) and references cited therein.
(9) J. W. Frazer, L. R. Carlson, A. M. Kray, M. R. Bertoglio, and S. P. Perone, *Anal. Chem.*, **43**, 1479 (1971).
(10) S. P. Perone, J. W. Frazer, and A. Kray, *Anal. Chem.*, **43**, 1485 (1971).
(11) J. H. Christie and R. A. Osteryoung, *J. Electroanal. Chem.*, **49**, 301 (1974).
(12) F. Baumann, E. Herlicksa, A. C. Brown, and J. Blesch, *J. Chromatogr. Sci.*, **7**, 680 (1969).
(13) F. Baumann, A. C. Brown, and M. B. Mitchell, *J. Chromatogr. Sci.*, **8**, 20 (1970).
(14) H. A. Hancock, Jr., L. A. Dahm, and J. F. Muldoon, *J. Chromatogr. Sci.*, **8**, 57 (1970).
(15) A. M. Bond and R. J. O'Halloran, *J. Electroanal. Chem.*, **68**, 257 (1976).
(16) H. Blutsein and A. M. Bond, *Anal. Chem.*, **48**, 242 (1976).
(17) A. M. Bond and B. S. Grabaric, *Anal. Chem.*, **51**, 126 (1979).

RECEIVED for review March 9, 1978. Accepted December 4, 1978. The financial assistance of the Australian Research Grants Committee in support of this work is gratefully acknowledged. B.S.G. also wishes to express his appreciation to the University of Melbourne for providing a Post-Doctoral Research Grant.

Potentiometric Stripping Analysis in Non-Deaerated Samples

Daniel Jagner

Department of Analytical Chemistry, University of Göteborg, Fack, S-402 20 Göteborg, Sweden

Potentiometric stripping analysis is based on the potentiostatic pre-concentration of analytes in a mercury film and the subsequent registration on a xt-recorder of the resulting redox titration curve obtained when the potentiostatic circuitry is disconnected. In the present study, it is shown that zinc, thallium, cadmium, lead, bismuth, and copper can be analyzed in acid solution using dissolved oxygen, in equilibrium with air, as oxidant. For analyte concentrations above approximately 25 μg/L potentiometric stripping analysis in non-deaerated samples is more rapid than analysis in deaerated samples using mercury(II) as oxidant.

In potentiometric stripping analysis (*1*), analytes are pre-concentrated in a mercury film (plated) by potentiostatic reduction and amalgamation. The potentiostat is then disconnected and the reduced analytes are oxidized by a suitable oxidizing agent. The redox titration curve thus obtained is registered on a high input impedance recorder or on a pH meter. The time elapse between two consecutive equivalence points is taken as a measure of the sample concentration of the particular analyte oxidized in this interval, the analyte being identified by the redox potential. As in anodic stripping voltammetry, the technique is restricted to elements forming reversible amalgams. The instrumentation is, however, much less complicated. In a previous paper (*1*), the use of ppm concentrations of mercury(II) as oxidant in potentiometric stripping analysis has been described. In order to ensure that mercury(II) was the predominant oxidant in the sample, dissolved oxygen was removed by bubbling nitrogen gas through the sample for 20 min previous to the commencement of the analysis. In samples containing relatively high concentrations of metal analytes where short plating times could be used, the deaeration process was the most time-consuming part of the analysis. Consequently, it seemed advantageous to investigate whether or not dissolved oxygen could be used as an oxidant in potentiometric stripping analysis.

The oxidation of dilute amalgams by dissolved oxygen has been studied in detail by Pelletier, Buffle, and Monnier using a hanging mercury drop electrode (*2, 3*). Although the purpose of their work was to investigate whether or not this reaction could be exploited for the analysis of traces of dissolved oxygen, some of their findings are applicable to the present study. The authors conclude that the rate of the reaction

$$\mathrm{M(Hg)} + \frac{n}{2p}\,\mathrm{O_2(l)} \rightarrow \mathrm{M}(n) + \frac{n}{p}\,\mathrm{O}(-p)$$

where $p = 1$ (H_2O_2) or $p = 2$ (H_2O), depending on the metal M, is controlled by the diffusion rate of dissolved oxygen or amalgamated metals. Consequently, the oxidation rate depends on the concentration of dissolved oxygen and amalgamated metal.

EXPERIMENTAL

Chemicals. All chemicals used except mercury(II) nitrate were of Suprapure grade.

Instrumentation. A semi-automatic Potentiometric Stripping Controller (Radiometer prototype) equipped with a three-electrode potentiostat and a timer/switcher unit was used in all experiments. The controller could be programmed to yield plating times between 1 and 64 min. Immediately before the commencement of the stripping, i.e., disconnection of the potentiostat, the paper feed of the recorder (Radiometer REC 61 Servograph, amplifier REA 105/120) was automatically started and was terminated after a programmed fraction of the plating time.

Electrodes. A platinum foil (Radiometer P 101) was used as counter electrode and a saturated calomel electrode (Radiometer K 4040) was used as reference electrode. The working electrode was a glassy carbon electrode (Radiometer F 3500).

Electrochemical Cell. A titration assembly (Radiometer TTA 60) was used as electrochemical cell. The three electrodes could be screwed into the lid of the titration vessel. The sample was agitated by a constant rate mechanical stirrer (Radiometer TTA 60).

Analytical Procedures. During the pre-concentration of metal analytes by means of potentiostatic reduction and amalgamation, the glassy carbon working electrode must be coated with a mercury film which is thick enough to dissolve all metals reduced. This can be achieved either in situ by adding mercury(II) ions to the sample prior to analysis or by pre-coating the working electrode with mercury in a separate solution. If the latter procedure is used, as in the experiments below, mercury(II) ions need not, of course, be added to the sample. The procedure is, however, more elaborate than in-situ mercury coating.

In the in-situ procedure, the working electrode is first polished with 3-μm diamond paste for 30–60 s. It is then cleaned carefully with acetone to remove polishing lubricant. The electrodes are screwed tightly into the lid of the sample vessel. After acidification of the sample with hydrochloric acid, 10–50 mg/L of mercury(II) is added and sample stirring is started. The plating potential is adjusted to −0.95 V vs. SCE and the plating time to 1 min. A minimum of four plating/stripping cycles, each cycle comprising 60 s of plating and 15 s of stripping, are then performed automatically. Immediately after completion of the last plating/stripping cycle, the plating potential and the plating time are adjusted to the values to be used during the subsequent analysis and the potentiometric stripping controller is initiated. It is advisable to minimize the time during which the mercury-coated working electrode is exposed to the mercury(II)-containing sample in the absence of a reducing potential applied to the electrode. A couple of minutes of such exposure may result in the formation of calomel on the electrode surface, according to the reaction

$$\mathrm{Hg} + \mathrm{Hg(II)} + 2\mathrm{Cl^-} \rightarrow \mathrm{Hg_2Cl_2(s)}$$

which will decrease the sensitivity.

Separate pre-coating of mercury can be carried out in a solution containing approximately 40 mg/L of mercury(II) and 0.5 M hydrochloric acid. After introducing this solution into the sample vessel, the stirring is initiated and the plating potential and time are adjusted to 1 min and −0.95 V vs. SCE, respectively. A minimum of four plating/stripping cycles is then performed automatically. After completion of the last cycle, the solution is removed and the working electrode is carefully cleaned with distilled water in order to remove mercury(II) ions. If not removed, these ions may cause formation of calomel on the electrode surface. The pre-coated electrode, which can be used for the analysis of several samples, should be stored either dry or in distilled water.

Irrespective of the mercury pre-coating method employed, the analytical results are evaluated either by standard addition by using a calibration curve or by the use of an internal standard.

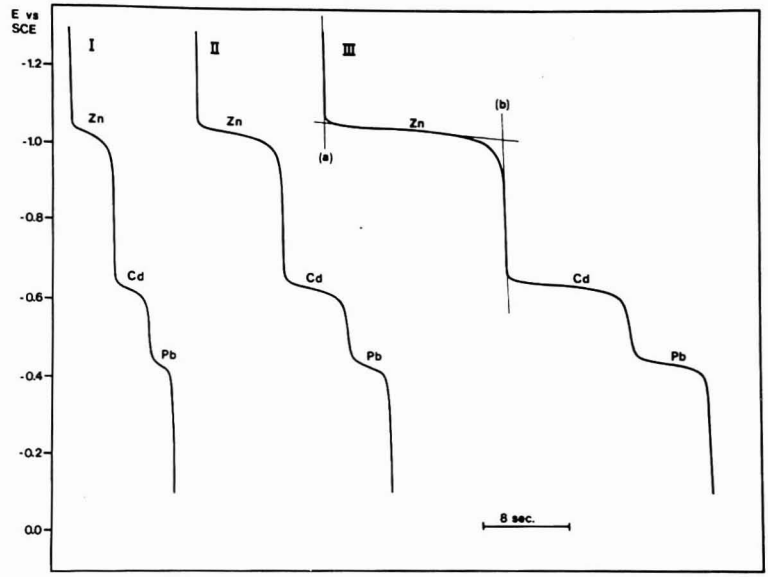


Figure 1. Potentiometric stripping analysis in a non-deaerated sample containing 0.005 M hydrochloric acid. Plating at −1.30 V for 16 min. Zinc, cadmium, and lead concentrations 200, 400, and 800 μg/L in curves I, II, and III, respectively. The distance between points (a) and (b) on curve III is taken as the analytical signal for zinc

RESULTS AND DISCUSSION

Determination of Zinc, Cadmium, and Lead. To 40 mL of a sample containing 0.005 M hydrochloric acid, 200 μg/L of zinc(II), cadmium(II), and lead(II) was added. The sample was plated for 16 min at −1.30 V and the potentiometric stripping curve registered. The procedure was repeated for zinc(II), cadmium(II), and lead(II) concentrations of 400 and 800 μg/L, respectively. The potentiometric stripping curves are shown in Figure 1 and the linear relationship between concentration and stripping signal is shown in Figure 2.

Determination of Copper and Bismuth. A sample, 40 mL, containing 200 μg/L of copper and bismuth in 1 M hydrochloric acid was plated at −0.75 V for 8 min. After the registration of the potentiometric stripping curve, the copper and bismuth concentrations were increased stepwise to 400, 800, and 1600 μg/L. The potentiometric stripping signals registered after each increment increased linearly with increasing concentration. The potentiometric stripping curves for 200 and 400 μg/L are shown in Figure 3.

pH Dependence. During reductive pre-concentration of the trace analytes in oxygen-containing samples, a pH gradient is built up close to the electrode. The pH at the electrode surface is higher than that in the bulk of the sample. This may cause hydrolysis of the metal ions close to the electrode surface and thus decrease the sensitivity. The extent of hydrolysis depends on the particular metal ion analyzed, on the sample pH, and, more important, on the buffering capacity.

To investigate the pH effect on potentiometric stripping analysis in non-deaerated samples, 40 mL of 0.1 M sodium chloride solution containing 100 μg/L of cadmium, copper, and lead was acidified by stepwise addition of hydrochloric acid to give total concentrations of 0.0005, 0.005, 0.05, and 0.5 M. The potentiometric stripping curves registered after each increment of acid did not differ significantly. When the

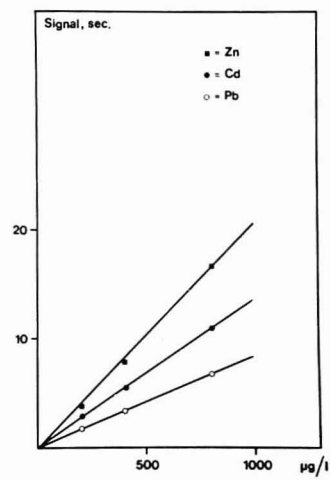


Figure 2. Calibration curve obtained by potentiometric stripping analysis in non-deaerated solution. Plating for 16 minutes at −1.30 V (cf. Figure 1)

experiment was repeated without the addition of acid, the resulting potentiometric stripping curve showed a pronounced decrease in sensitivity.

Further experiments with pH variations revealed that the optimum pH range for potentiometric stripping analysis in non-deaerated solution is 0–3.5 for cadmium, lead, thallium, and copper, 2–4 for zinc and gallium, and 0–0.5 for bismuth.

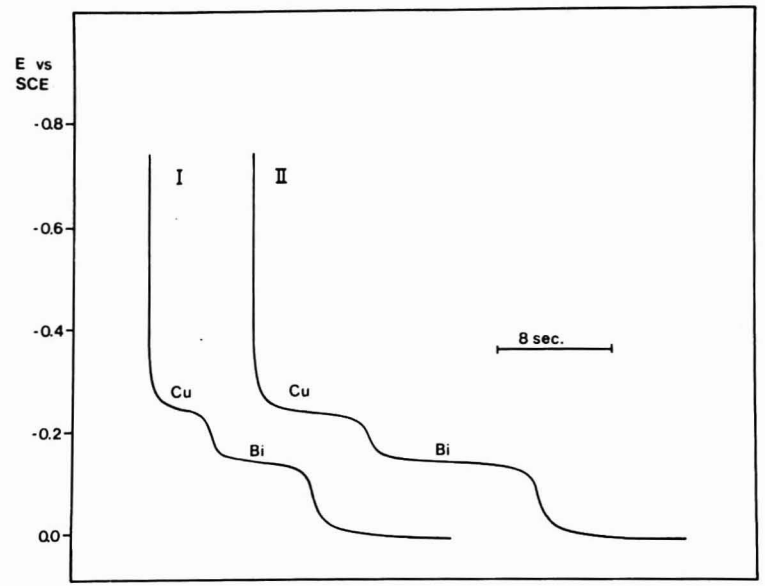


Figure 3. Potentiometric stripping analysis in a non-deaerated sample containing 1 M hydrochloric acid and 200 (curve I) or 400 (curve II) μg/L of copper and bismuth. Plating for 8 min at −0.75 V

The pH is preferably adjusted by means of hydrochloric acid and sodium acetate.

Comparison between Dissolved Oxygen and Mercury(II) as Oxidant. To compare the oxidation rate in a sample saturated with dissolved oxygen and the oxidation rate in a deaerated sample containing small concentrations of mercury(II) as the major oxidant, 40 mL of a 0.01 M hydrochloric acid solution containing 400 μg/L of cadmium(II), lead(II), and copper(II) was plated at −0.95 V for 4 min. The potentiometric stripping curve was registered and the same plating/stripping cycle was repeated twice. Two ppm of mercury(II) nitrate was then added to the sample and a stream of nitrogen was passed above the sample surface. The potentiometric stripping controller was programmed to register automatically the potentiometric stripping curves obtained during consecutive 4-min plating/stripping cycles. The increase in potentiometric stripping signal due to the decrease in oxygen concentration is shown in Figure 4.

As seen from Figure 4, deaeration by passing nitrogen above the sample surface is rather a slow process. After approximately 50 min of nitrogen purge, mercury(II) ions are the predominant oxidants in the sample and a steady signal is obtained. It is also apparent from Figure 4 that the oxidation rates for lead and cadmium are approximately 25 times higher in a solution saturated with dissolved oxygen than in a deaerated sample containing 2 ppm of mercury(II). For copper, the oxidation rate is only approximately 12 times higher. Oxidation of lead and cadmium by oxygen is a two-electron process while oxidation of copper is a one-electron process.

Temperature Dependence. Temperature variations affect the diffusion rates of metal ions, amalgamated metals, and dissolved oxygen, and the saturation concentration of dissolved oxygen. Consequently, temperature changes influence both the mass transport rate during plating and the rate of oxidative stripping. To determine the effect of temperature variations on the potentiometric stripping signals in non-deaerated samples, 40 mL of a 0.1 M hydrochloric acid solution containing 400 μg/L of cadmium(II), lead(II), and copper(II) was thermostated at 15 °C for 2 h. The temperature was then increased stepwise up to 35 °C and a 8-min plating/stripping cycle was initiated after each increase in temperature. The relative changes with temperature in the potentiometric stripping signals were measured.

The cadmium signal proved to be more sensitive to changes in temperature than the copper and lead signals. The relative increase in the cadmium signal was 0.04 $°C^{-1}$ in the temperature range investigated, the corresponding values for lead and copper being 0.015 $°C^{-1}$ and −0.005 $°C^{-1}$, respectively.

Accuracy. The accuracy was tested by means of calibration plots. Linear relationships through the origin were obtained for zinc, cadmium, thallium, lead, copper, and bismuth in the concentration range tested, 50–1000 μg/L.

Precision. The precision was estimated from 15 repetitive plating/stripping cycles in a sample containing 200 μg/L of zinc, cadmium, and lead in 0.05 M hydrochloric acid. The temperature was held at 23.2 ± 0.4 °C. The relative standard deviations were 0.04 for cadmium and 0.02 for lead and zinc. The same experiment was repeated in a 1 M hydrochloric acid solution containing 200 μg/L of copper and bismuth. The relative standard deviations were 0.03 and 0.02 for copper and bismuth, respectively.

Detection Limit. The detection limits in potentiometric stripping analysis cannot be defined uniquely since they decrease linearly with plating time. In practice, plating times of more than 1 h are seldom employed. To estimate the detection limits for such a plating time, a 0.01 M hydrochloric acid solution at −0.95 V for 64 min prior to stripping was used. The potentiometric stripping curve registered is shown in Figure 5.

Assuming a resolution of the xt-recorder of 0.1 s, the detection limits for cadmium, lead, and copper, plated for 64

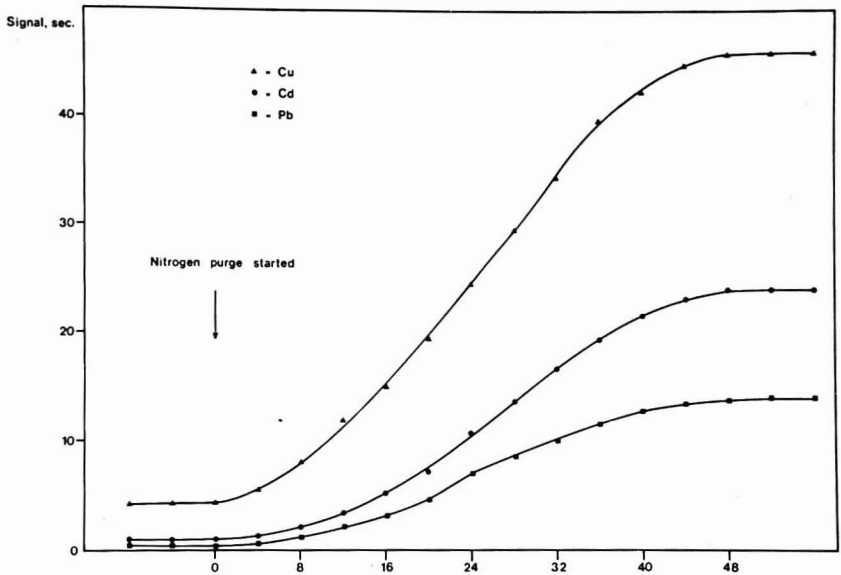


Figure 4. Increase in potentiometric stripping signal during sample deaeration with a stream of nitrogen above the sample surface. Repetitive plating for 4 min at −0.95 V prior to each stripping. Sample contains 0.01 M hydrochloric acid and 400 μg/L of cadmium(II), lead(II), and copper(II); 2 ppm of mercury(II) was added immediately before the commencement of nitrogen purging

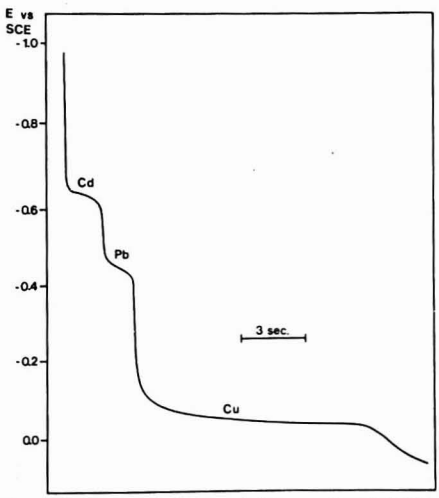


Figure 5. Potentiometric stripping analysis in a non-deaerated sample of 0.01 M hydrochloric acid containing 40 μg/L of cadmium, lead, and copper. Plating for 64 min at −0.95 V

min, were estimated to be 2.5, 2.5, and 1.0 μg/L, respectively. The lower detection limit for copper is due to the one-electron process in the oxidation with dissolved oxygen.

CONCLUSION

It has been shown that dissolved oxygen can be used as oxidizing agent in acid samples for all elements normally analyzed by potentiometric stripping analysis. The major advantage of this technique, compared to oxidation with mercury(II), is that time-consuming deaeration is not necessary. The risk of contamination by the inert gas or by mercury ions added to the sample is also eliminated. Oxidation by dissolved oxygen can be particularly advantageous when performing potentiometric stripping analysis in a continuous mode.

The main drawback of oxygen oxidation is the high concentration of oxygen present in a sample in equilibrium with air. This means that the oxidation rate is very rapid and the potentiometric stripping plateaus may be difficult to detect on a normal xt-recorder if the sample concentration of analytes is low or if short plating times are exploited. For analyte concentrations above 20–50 μg/L, depending on the elements analyzed, potentiometric stripping analysis is more rapid and accurate in non-deaerated samples than in deaerated samples containing 2–4 mg/L of mercury(II).

The precision of potentiometric stripping analysis in oxygen-containing solutions is slightly less than that in deaerated samples. This is due to the higher temperature sensitivity. The precision can be improved by avoiding sample temperature variations of more than ±0.5 °C during analysis.

LITERATURE CITED

(1) D. Jagner, *Anal. Chem.*, **50**, 1924 (1978).
(2) M. Pelletier, J. Buffle, and D. Monnier, *Chimica*, **25**, 61 (1971).
(3) J. Buffle, M. Pelletier, and D. Monnier, *J. Electroanal. Chem.*, **43**, 185 (1973).

RECEIVED for review September 19, 1978. Accepted November 17, 1978.

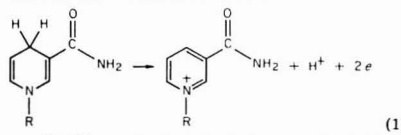
Optimization of the Analytical Oxidation of Dihydronicotinamide Adenine Dinucleotide at Carbon and Platinum Electrodes

Jacques Moiroux[1] and Philip J. Elving*

Department of Chemistry, University of Michigan, Ann Arbor, Michigan 48109

Much of the difficulty associated with the voltammetric determination of NADH at carbon electrodes (glassy carbon and pyrolytic graphite) can be eliminated by first covering the electrode surface with adsorbed electrochemically generated NAD^+. Such an electrode can be repeatedly used for NADH measurement without the necessity for pretreatment. At the millimolar NADH level, analytically satisfactory results can be obtained by simply comparing the test solution current at one potential on the limiting current plateau for the RDE with the background solution current at the same potential; a comparably simple procedure can also be used at the micromolar level. Results obtained at rotating and stationary glassy carbon, pyrolytic graphite, and platinum electrodes are compared.

A previous paper (*1*) summarized past studies on the electrochemical two-electron (2*e*) oxidation at carbon and platinum electrodes in aqueous media of dihydronicotinamide adenine dinucleotide (NADH) to yield the corresponding nicotinamide (NAD^+), indicated the analytical chemical interest in this reaction, and described the effect of experimental conditions and variables in producing a prewave or prepeak as a result of the adsorption on the electrode of NAD^+ produced in the oxidation. The latter phenomenon can result in overlapping voltammetric waves or peaks due to the presence of both the adsorption-controlled and diffusion-controlled processes, which is analytically disadvantageous. The electrochemical reaction involved is



NADH NAD^+ (adsorbed or nonadsorbed) (1)

where R represents adenosine diphosphoribose (ADPR). NAD^+ exhibits an aromatic pyridinium ring whereas NADH does not. The adsorption of NAD^+ on carbon is likely to be related to the presence of this aromatic structure.

The present paper describes the development of procedures for the voltammetric oxidation of NADH, which avoid the overlapping waves by suppressing the current due to the production of adsorbed molecules of NAD^+ during the NADH oxidation, which minimize the preparation procedure for electrodes sufficiently reproducible to be used for analysis, and which simplify the analytical procedure by allowing the use of current measurement at a single potential.

Emphasis was placed on the use of the glassy carbon electrode (GCE) previously designated as GC-2 (*1*), on which the adsorption of NAD^+ is less than at the pyrolytic graphite electrode (PGE) and the other type of GCE (GC-1) examined (*1*), although the utility of both the PGE and GC-1 electrode was also examined, as was that of a platinum electrode. All of the electrodes were used in a disk configuration, stationary and/or rotating.

EXPERIMENTAL

Materials. 1,4-Dihydronicotinamide adenine dinucleotide (NADH) and nicotinamide adenine dinucleotide (NAD^+) (P-L Biochemical ChromatoPure grade) were used as received. Reagent grade chemicals were obtained from J. T. Baker Chemical Co., except for 2-amino-2-methyl-1,3-propanediol (Tris) from Sigma, and tetraethylammonium chloride from Eastman.

Electrodes. The working glassy carbon electrodes (GCE) used were those previously designated as GC-1 and GC-2 (*1*); GC-1 was made from material supplied by the Tokai Electrode Manufacturing Company of Tokyo and GC-2 was made from a Vitrecarb rod furnished by Fluorocarbon Process Systems Division of Anaheim, Calif.; their areas were 0.230 cm^2 for GC-1 and 0.254 cm^2 for GC-2. The working pyrolytic graphite electrode (PGE) was also previously described (*1*) (area = 0.383 cm^2).

For the working platinum electrode, a platinum wire (1-mm diameter; 10-mm length) was sealed into 6-mm o.d. glass tubing; the tubing and wire were ground flush to each other on a rotating 600-mesh SiC paper disk. Electrical connection was made by dipping a nickel wire into a mercury pool contained above the platinum. The effective electrode area, determined by measurement of the anodic ferrocyanide cyclic voltammetric peak (n = 1; $D = 6.32 \times 10^{-6}$ cm^2 s^{-1}; ref *2*) was 0.0090 ± 0.0002 cm^2.

The reference electrode was an aqueous saturated calomel electrode, to which all potentials cited are referred. The counter electrode was a platinum gauze.

Apparatus. Electrochemical measurements were made with a Princeton Applied Research 170 multipurpose instrument and a three-compartment water-jacketed cell (*3*), whose counter and reference electrode compartments were filled with the background solution and whose temperature was 25 °C. For cyclic voltammetry, a Tektronix 5103N cathode ray oscilloscope with suitable modules and cameras was used. A Sargent synchronous motor (10 revolutions per second) was used to rotate the electrodes.

Procedures. Unless otherwise indicated, these were identical to those previously described (*1*).

Electrode Pretreatment. A working electrode designated as *pretreated* or *clean* is one which has been both conditioned and pretreated before the experiment by the Blaedel and Jenkins (*4*) procedure: the electrode is conditioned (15 sweeps from 1.50 to −1.50 V at scan rate (v) = 0.1 V s^{-1}), and pretreated (1.50 V for 2 min; −1.50 V for 2 min; repeated twice) in the background solution. Following pretreatment, background cyclic voltammograms (0.00 to 0.75 V; v = 2 mV s^{-1}) are recorded at the rotating disk electrode (RDE) until successive cycles yielded superposable curves; NADH solution is then added. The electrode, held at the initial potential of 0 V, is rotated for 2 min before recording each voltammetric curve. No electrode pretreatment is necessary between measurements on the same NADH solution. Between experiments on different NADH solutions, the electrode is rinsed with distilled water, wiped with a paper tissue, and stored while immersed in distilled water.

In order to prepare a *covered* electrode, i.e., one coated with adsorbed NAD^+ (cf. subsequent discussion), the electrode, held at 0.75 V, is rotated in a 1 mM NADH solution (pH 7 buffer) for 1 h. Such an electrode can be used repeatedly, if treated as subsequently described in the section on Oxidation at a Covered GCE, by rinsing it with distilled water between experiments and by storing it in air when not in use.

Each new electrode is first conditioned and pretreated, and then used either as a clean electrode or one covered with adsorbed NAD^+.

[1] Permanent address: Ecole Normale Superieure de l'Enseignement Technique, 94230 Cachan, France.

0003-2700/79/0351-0346$01.00/0 © 1979 American Chemical Society

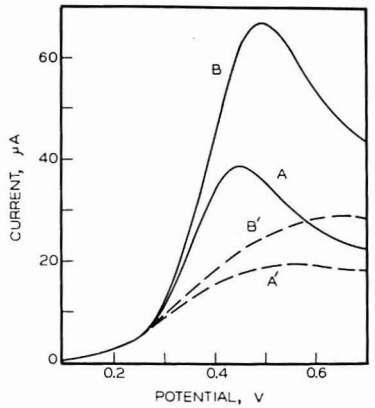


Figure 1. Voltammetric curves for NADH at the stationary GCE, recorded after electrode pretreatment and corrected for background current. Solution composition: 0.8 mM NADH; 2 mM NAD^+; 0.25 M Na_2SO_4; 0.05 M phosphate buffer. (A) pH 9.0; $v = 0.1$ V s^{-1}. (B) pH 9.0; $v = 0.4$ V s^{-1}. (A′) pH 6.3; $v = 0.1$ V s^{-1}. (B′) pH 6.3; $v = 0.4$ V s^{-1}

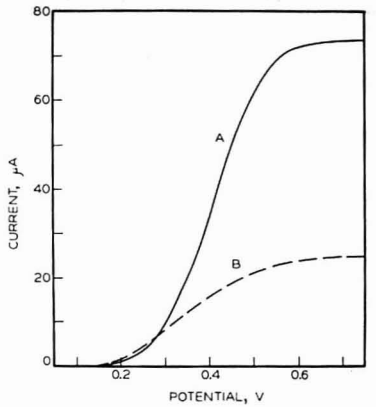


Figure 2. Voltammetric curves at $v = 2$ mV s^{-1} for NADH at the rotating GCE (10 rps), recorded after electrode pretreatment and corrected for background current. Solution composition: 1 mM NADH; 2 mM NAD^+; 0.25 M Na_2SO_4; 0.05 M phosphate buffer. (A) pH ≥ 7.0. (B) pH 6.3

RESULTS AND DISCUSSION

Oxidation at a Clean GCE. *Background, pH, and Time Dependencies.* On addition of 0.15 M Et_4N^+ to a 1 mM NADH solution (background: 0.25 M Na_2SO_4 or 0.5 M KCl; pH 7.0, 0.05 M phosphate or Tris buffer), the adsorption-controlled process is still partially apparent. On addition of 2 mM NAD^+ in place of Et_4N^+, derivative pulse polarography at the rotated GCE does not show an adsorption-controlled peak; on stationary GCE voltammetry, such a peak becomes apparent only when v exceeds 20 V s^{-1}.

1. *Sulfate Effect.* The shape and height of the voltammetric peak recorded after electrode pretreatment are strongly dependent upon pH and v (Figure 1) for a background of Na_2SO_4 plus phosphate or Tris buffer; the RDE wave-height also depends on pH (Figure 2). No anodic current due to NADH oxidation is seen below pH 6.0 under those conditions; this result excludes the assumption of acid hydrolysis of NADH since the latter reaction is too slow at pH 6 (*5*, *6*) to cause all of the NADH to disappear in less than the 5 min needed for recording a RDE voltammogram.

With KCl as supporting electrolyte (other experimental conditions being unchanged), voltammetric curves identical to A and B of Figure 1 and A of Figure 2 are recorded between pH 5 and 9.5, i.e., the curves are pH-independent whereas they are strongly pH-dependent when Na_2SO_4 is used. This result excludes involvement of NADH in a bulk solution reaction since such an inhibitory reaction between NADH and sulfate anions is unlikely. Furthermore, curves recorded with a covered electrode are unaffected by the presence of Na_2SO_4 even at pH below 7.

The behavior observed in sulfate background with a clean electrode is probably due to surface phenomena, e.g., specific adsorption of sulfate on graphite electrodes with resultant swelling of the graphite (*7–9*). This sulfate effect indicates the sensitivity of the electrochemical behavior of NADH to phenomena which may affect the electrode surface.

2. *Time Effect.* On continuously repeated cyclic scanning (0 to 0.8 V) at the RDE, $E_{1/2}$ slowly shifts positively while the limiting current (i_l) remains practically constant (Figure 3). The magnitude of the $E_{1/2}$ shift decreases with each new cycle; after ca. 2 h, the curve reaches a steady-state shape (S in Figure 3; the difference in i_l between curves 1 and S corresponds to NADH electrolyzed during the 2 h. Curve S can also be obtained by holding the RDE at 0.75 V for 30 min. Such an $E_{1/2}$ shift, which can be observed with any solution containing 1 mM NADH, 2 mM NAD^+, 0.5 M KCl, and 0.05 M phosphate or Tris buffer, occurs at the same slow rate between pH 5 and 9.5, as well as when Na_2SO_4 replaces KCl and the pH exceeds 7. With Na_2SO_4 at pH less than 7, a curve similar to B of Figure 2 is initially recorded; $E_{1/2}$ shifts positively with time (repeated cycles or RDE held at 0.75 V) but i_l increases; however, the rate of the $E_{1/2}$ shift is very slow and decreases strongly when pH decreases. If NAD^+ is not initially present (KCl or Na_2SO_4 as electrolyte), a longer time is needed to reach the steady state.

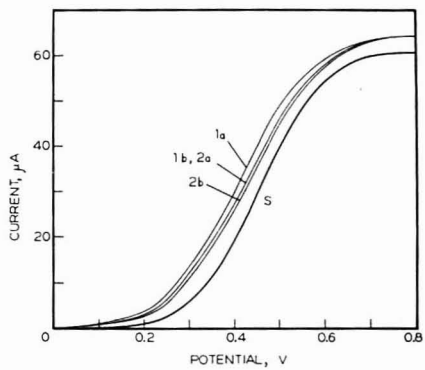


Figure 3. Effect of time on voltammetric curves at $v = 2$ mV s^{-1} for NADH at the rotating GCE (10 rps), corrected for background current. Solution composition: 0.85 mM NADH; 2 mM NAD^+; 0.5 M KCl; 0.05 M Tris buffer; pH 7.1. Number indicates the chronological order of the cycle; a indicates a scan with increasingly positive potential and b with decreasing potential; S identifies the steady-state pattern obtained after ca. 2 h (with forward and back scans)

A similar shift can be observed at a stationary electrode for v considerably higher than at the RDE, e.g., Figure 4. When Na_2SO_4 is used, a curve similar to B′ of Figure 1 is initially

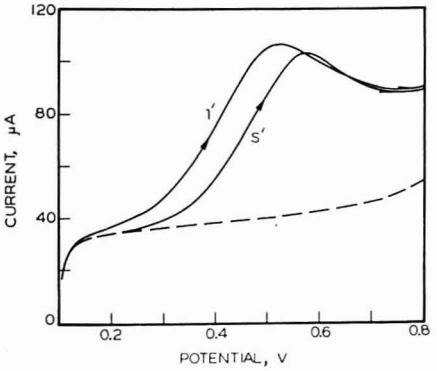


Figure 4. Effect of time on voltammetric curves at $v = 0.4$ V s^{-1} for NADH at the stationary GCE. Solution composition: 0.75 mM NADH; 2 mM NAD^+; 0.5 M KCl; 0.05 M phosphate buffer; pH 5.6. The dashed line is for the background solution alone (NAD^+ present); the initial curve is marked 1′; the steady state curve is S′; arrowheads indicate the direction of the scan. The difference in peak heights between curves 1′ and S′ corresponds to the bulk NADH concentration decrease due to electrolysis

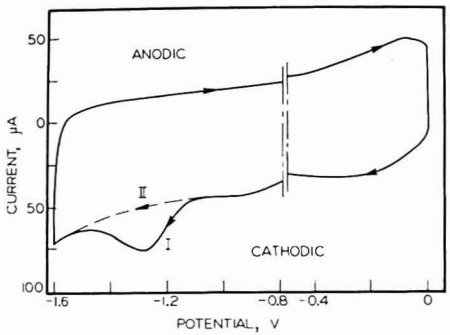


Figure 5. Cyclic voltammograms at $v = 1$ V s^{-1} for (I) a GCE covered with adsorbed NAD^+ (span of 0.0 to −1.6 V; solid line) and (II) a pretreated GCE in the same background solution (broken line, which is not shown where it overlaps with the solid line). Solution composition: 0.5 M KCl; 0.05 M phosphate buffer; pH 9.0. Preparation and previous treatment of the electrodes are described in the text. Arrowheads indicate the direction of the scan.

recorded at pH less than 9 and a longer time is required to reach the steady state than when the pH exceeds 9 or KCl is used. In the latter cases, curve S′ is recorded after the RDE electrode has been held at 0.75 V for 0.5 h; it takes longer (1 h) if NAD^+ is not initially present.

Nature of Electrode Coverage. When steady state curves like S′ of Figure 4 are recorded, the most probable phenomenon, which may have occurred, is saturation coverage of the electrode surface with adsorbed electrogenerated NAD^+ molecules.

Presence of rather strongly adsorbed NAD^+ on the electrode was confirmed as follows. After an hour rotation at 0.75 V in 1 mM NADH solution (KCl; phosphate buffer; pH 9.0), the electrode was removed, rinsed with distilled water, and immersed in a new deoxygenated background solution; the voltammogram then recorded at the stationary electrode (Figure 5; curve I) shows a peak at a potential corresponding to the reduction of NAD^+ (*6*); in a cyclic experiment, only background current is recorded during the second scan (curve II), i.e., the curve I peak can only be due to reduction of NAD^+ adsorbed at the electrode surface. The peak height increases linearly with v as expected for reduction of an adsorbed species.

The adsorbed NAD^+ is reduced and desorbed at potential more negative than −1.3 V since curves similar to 1a in Figure 3 and 1′ in Figure 4 are recorded if the initial potential is more negative than −1.3 V. Thus, it is possible to clean the electrode surface of adsorbed NAD^+ by the Blaedel and Jenkins (*4, 10*) pretreatment of alternatingly applying potentials of −1.5 and +1.5 V. It is also safe to assume that, when steady state voltammetry was used to study the oxidation of NADH at the rotated GCE (*4, 10*), the procedure actually allowed for slow coverage of the electrode surface with adsorbed NAD^+.

Oxidation at a Covered GCE. When an electrode is covered with adsorbed NAD^+, i.e., it gives steady-state voltammetric curves, it is not necessary to pretreat it again to obtain reproducible results; it suffices to hold the electrode at 0.75 V between voltammograms, to rinse it with distilled water and to store it exposed to air when not in use. In use, the only requirements are to rotate the electrode, held at 0 V, for 2 min before recording each voltammetric curve, and not to expose it to potentials more negative than −0.5 V.

A covered electrode should not be held in the range of −0.5 to 0.3 V for longer than a few minutes in order to minimize the slow desorption of NAD^+. Exposure of the electrode to an NADH solution at potentials, at which the latter is oxidized, reforms the adsorbed NAD^+ layer.

Optimum Procedures and Their Analytical Applicability. With a covered electrode, curve S of Figure 3 is obtained on the first scan at the RDE for a background of 0.5 M KCl or 0.25 M Na_2SO_4, 0.05 M Tris or phosphate buffer at pH between 5 and 9.5, and NAD^+ initially added or not. Characteristics of the wave are given in Table I.

The i and E reproducibilities over a micromolar NADH concentration range at two different GCE are summarized in

Table I. Oxidation of NADH at Glassy Carbon, Pyrolytic Graphite, and Platinum Electrodes

Voltammetry at the RDE (10 rps; $v = 2$ mV s^{-1})[a]

electrode	$E_{1/2}$, mV	i_l/ac, μA/cm² mM	$dE/d(\log[i/(i_l - i)])$, mV
GCE[b,c]	450 ± 10[e]	295 ± 3	160 ± 5
PGE[b,d]	520 ± 10	300 ± 3	167 ± 2
PE[d]	510 ± 10	290 ± 10	137 ± 4

Voltammetry at the Stationary Electrode ($v = 0.05$ V s^{-1})[a]

electrode	E_p, mV	$i_p/ac v^{1/2}$, μA/cm² mM V$^{1/2}$ s$^{-1/2}$
GCE[b,c]	475 ± 10	493 ± 8
PGE[b,d]	560 ± 15	490 ± 10
PE[d]	550 ± 20	420 ± 20[f]

[a] Currents are corrected for background currents. NADH concentration = 1 mM. [b] Electrode covered with adsorbed NAD^+. [c] Background: 0.5 M KCl or 0.25 M K_2SO_4; 0.05 M Tris or phosphate buffer; pH ≥ 7. Data given are the mean and standard deviation for 10 experiments. [d] Background: 0.5 M KCl; 0.05 M Tris buffer; pH 7.1. Data given are the mean and standard deviation for 5 experiments. [e] Independent of NADH concentration between 0.5 and 2 mM. [f] Diffusion-controlled current function, calculated on basis that $i_p/ac v^{1/2} = 602 \times 0.496 \times 10^3 \times n(\beta n_a)^{1/2} D^{1/2}$ (ref. 11) with $\beta n_a = 0.43$ and $D = 2 \times 10^{-6}$ cm² s^{-1}, is 560.

Table II. Reproducibility of Current and Potential Characteristics for Oxidation of NADH at the Micromolar Level at Glassy Carbon Rotating Disk Electrodes[a]

concn, μM	i_l,[c] μA	i_l/ac, μA/cm² mM	Δi_l,[d] μA	Δi_l/ac, μA/cm² mM	$E_{1/2}$, mV	slope⁻¹, mV	βn_a[e]
			GC-1 Electrode[b]				
4.9	0.31 ± 0.01	275 ± 10	0.31 ± 0.01	275 ± 10	350 ± 17	210 ± 10	0.28 ± 0.01
9.8	0.63 ± 0.02	280 ± 9	0.62 ± 0.02	275 ± 9	361 ± 16	202 ± 9	0.29 ± 0.01
33.5	2.22 ± 0.05	288 ± 7	2.10 ± 0.05	273 ± 7	373 ± 13	198 ± 8	0.30 ± 0.01
90.0	6.2 ± 0.1	300 ± 5	6.0 ± 0.1	290 ± 5	385 ± 10	193 ± 6	0.31 ± 0.01
			GC-2 Electrode[b]				
4.9	0.33 ± 0.01	265 ± 8	0.32 ± 0.01	257 ± 8	368 ± 17	232 ± 10	0.25 ± 0.01
9.8	0.67 ± 0.02	270 ± 8	0.67 ± 0.02	270 ± 8	375 ± 14	224 ± 9	0.26 ± 0.01
33.5	2.34 ± 0.04	275 ± 5	2.32 ± 0.04	273 ± 5	391 ± 12	219 ± 7	0.27 ± 0.01
90.0	6.6 ± 0.1	295 ± 5	6.6 ± 0.1	289 ± 5	410 ± 10	202 ± 4	0.29 ± 0.01

[a] Background solution: 0.5 M KCl; 0.05 M Tris buffer; pH 7.1. Polarization rate, $v = 2$ mV s⁻¹. Rotation speed =10 rps. Data given represent the mean and standard deviation for 3 experiments for each concentration at each electrode. [b] Covered electrodes (cf. text). Electrode areas: GC-1, 0.230 cm²; GC-2, 0.254 cm². [c] Corrected for background current. [d] Difference between test and background solution currents at 0.6 V. [e] β is the transfer coefficient for the heterogeneous electron-transfer and n_a is the number of electrons involved in the potential-determining step so that $dE/d\{\log [i/(i_l - i)]\} = 2.3\ RT/\beta n_a F$.

Table III. Reproducibility of Background Current at 0.6 V for the Same Covered Electrode in Different Background Solutions of the Same Composition[a]

date	number of solutions examined	electrode used	background current range, μA	background current mean, μA	background current std. dev., μA
July 13, 1978	8	GC-2	1.70-2.90[b]	2.0	±0.2
July 14, 1978	4	GC-2	2.00-2.70	2.3	±0.2
July 18, 1978	7	GC-1	0.65-1.05[c]	0.75	±0.10
July 19, 1978	5	GC-1	0.60-0.90[d]	0.66	±0.09

[a] Same composition, polarization rate, and rotation speed as in Table II. [b] Seven of the solutions were in the range of 1.70-2.00. [c] Six of the solutions were in the range of 0.65-0.80. [d] Four of the solutions were in the range of 0.60-0.65.

Table II and Figure 6. The procedure was as follows: the electrode, held at 0.0 V, was rotated for 2 min in the background solution; the background curve was recorded; NADH solution was then added; the electrode was again held at 0.0 V for 2 min; a voltammetric curve was again recorded.

It is clear from Figure 7 that correction for background current is essential; however, it is also evident (Table II) that applying this correction at a single potential on the i_l plateau, e.g., by taking the difference in current readings at 0.6 V between background and test solutions, is sufficient for quantitative analysis. The simplicity and speed of analysis introduced by such single-point measurement on each sample is obvious, especially when a single background measurement can be used for a number of test solutions.

The latter is always possible in the NADH millimolar range; the standard deviation in background current magnitude at 0.6 V is only 0.2% of the current intensity in the presence of NADH at the same potential with the GC-2 electrode, and 0.1 % with the GC-1 (cf. Tables I and III). The following procedure can be used: (a) insert background solution in the cell, immerse RDE and hold it for 2 min at 0.0 V, rapidly switch the potential to 0.7 V (0.7 V is better than 0.6 V since $E_{1/2}$ is more positive than at the micromolar level) and read the current; (b) remove background solution, rinse electrode, insert first test solution in the cell, immerse RDE and hold it for 2 min at 0.0 V, rapidly switch to 0.7 V and read the current; (c) repeat b for each subsequent test solution.

Use of this procedure at the micromolar level could decrease accuracy and precision since the uncertainty in background current at 0.6 V may amount to 65% of Δi_l for 4.9 μM NADH with the GC-2 electrode (35% with GC-1), but only to 3.5% for 90 μM NADH (1.5% with GC-1), (cf. Tables II and III). At 4.9 μM NADH, the speed of analysis may be greatly improved with only a small loss in accuracy and precision by using the following procedure: insert background solution in the cell; immerse RDE and hold it for 2 min at 0.0 V; rapidly switch to 0.6 V and read the current; switch potential back to 0.0 V, add NADH sample solution and hold electrode for 2 min at 0.0 V; rapidly switch to 0.6 V and read the current. Three different measurements on 4.9 μM NADH solution gave $\Delta i_l = 0.32 \pm 0.015$ μA at both GCE.

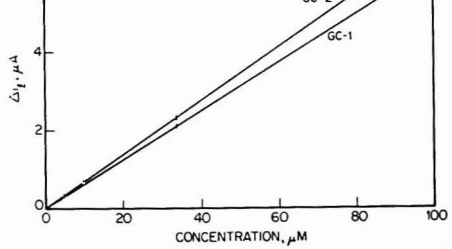


Figure 6. Variation of the net limiting current (Δi_l) with NADH concentration (c). Experimental conditions and definition of Δi_l are given in Table II

Most of the uncertainty in the measurements described comes from the time-decay and degree of nonreproducibility of the background current when the RDE is held at a given potential. Holding the RDE at 0.0 V for 2 min before each measurement allows for background current stabilization at the initial potential and its satisfactory reproducibility.

$E_{1/2}$ becomes more positive and the wave slope increases with increasing NADH concentration (Table II). This is

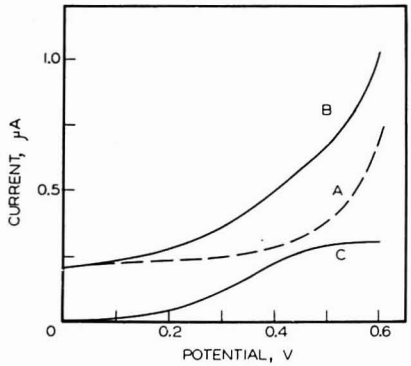


Figure 7. Voltammetric curves at $v = 2$ mV s^{-1} for 4.9 μM NADH at the rotating GC-1 electrode (10 rps), covered with adsorbed NAD^+. Background: 0.5 M KCl; 0.05 M Tris; pH 7.1. (A) Background; (B) 4.9 μM NADH; (C) curve B corrected for background current

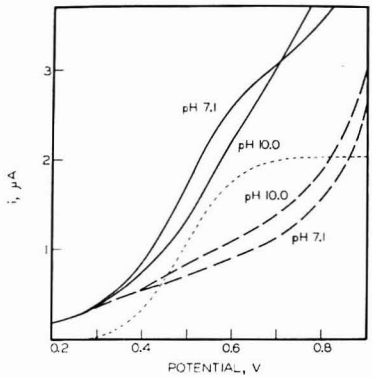


Figure 8. Voltammetric curves at $v = 2$ mV s^{-1} for NADH at a rotating platinum disk electrode (10 rps). Solution composition: 0.8 mM NADH; 0.5 M KCl; 0.05 M Tris buffer at pH 7.1 or 0.05 M phosphate buffer at pH 10.0; pH indicated on the curves. Background: broken lines; test solutions: solid lines; NADH curve at pH 7.1 corrected for background current: dashed line

essentially due to the decreased relative importance of the preceding drawn-out current increase, e.g., between 0.1 and 0.3 V on Figure 7.

Oxidation at a PGE. To examine further the effect of the electrode nature, the oxidation of NADH was investigated briefly at the pyrolytic graphite electrode (PGE) and more extensively at the platinum electrode (PE).

Results obtained with the PGE are generally similar to those described for the GCE with some noticeable differences. To obtain an electrode surface so covered with adsorbed NAD^+ that a steady-state wave is reached at the RDE and that no adsorption-controlled process appears on derivative pulse polarography or stationary electrode sweep voltammetry (v up to 50 V s^{-1}), the rotating PGE had to be held at 0.75 V for 4 h in 1 mM NADH compared to 1 h for the GCE.

Characteristics of PGE voltammetric curves are given in Table I. $E_{1/2}$ and E_p values show that NADH is somewhat more difficult to oxidize at the PGE than at the GCE; however, there is good concordance in respect to i_l/ac and $i_p/acv^{1/2}$, and RDE wave slopes.

Oxidation at a Platinum Electrode. No pretreatment is needed to obtain reproducible voltammetric curves when the PE is rotated for 2 min at 0.0 V before each scan. No adsorption-controlled process appears on normal or derivative pulse polarography at the RDE or sweep voltammetry at the stationary PE. No fouling of the electrode was observed.

As with carbon electrodes, when the pH exceeds 7, the results are the same for Tris and phosphate buffers, and KCl or Na_2SO_4 as supporting electrolyte.

At pH 7.1, a well defined wave, when corrected for background, is obtained at the RDE (Figure 8; Table I); $E_{1/2}$ is close to that for the PGE, i_l/ac agrees well with those at the GCE and PGE, but the slope is greater. This greater slope may be related to the apparent non-adsorption of NAD^+ on the PE. The greater adsorption of NAD^+ on carbon than platinum is likely to be related to the presence of residual aromatic structure in the carbon electrode.

$E_{1/2}$ values reported for different NADH concentrations in different backgrounds at pH 7.5 to 8.2 vary between 0.56 and 0.75 V (*10, 12–14*); in all cases, the voltammetric curves were described as badly defined, but no attempts were made to correct for background current. Without such correction, our curves are also badly defined (Figure 8) and a more positive $E_{1/2}$ may be incorrectly evaluated. However, this does not totally account for the difference in $E_{1/2}$, at least, between our results and those of Haas (*13*) which are the most detailed.

The current-function for the peak at the stationary PE never reaches the value corresponding to a purely diffusion-controlled process (Table I), even at v as slow as 0.01 V s^{-1}. With KCl as supporting electrolyte between pH 6 and 8 or Na_2SO_4 at pH above 7, the results ($E_{1/2}$, i_l/ac, and wave slope at the RDE; E_p and $i_p/acv^{1/2}$ at the stationary PE) do not change appreciably.

Below pH 7 in sulfate background, i_l at the RDE decreases as pH decreases but to a lesser extent than at the GCE, e.g., i_l at pH 6.0 is two-thirds of that at pH 7.0, $E_{1/2}$ is 40 mV more positive and the wave slope increases by 10 mV. Above pH 8, the wave becomes less well defined as pH increases, e.g., the curve obtained at pH 10 (Figure 8). Compared to pH 7, $E_{1/2}$ is 90 mV more positive and the slope increases by 35 mV at pH 10 in both KCl and Na_2SO_4 backgrounds. This $E_{1/2}$ increase corresponds to the $\Delta E_{1/2}/\Delta$pH ratio of about +30 mV/pH previously reported (*12, 14*) and is rather surprising, as was pointed out by Leduc (*14*), since the ratio is expected to have a zero or negative value for the grossly irreversible process (*15*),

$$NADH \rightarrow NAD^+ + H^+ + 2e \qquad (2)$$

LITERATURE CITED

(1) J. Moiroux and P. J. Elving, *Anal. Chem.*, **50**, 1096 (1978).
(2) M. Von Stackelberg, M. Pilgram, and V. Toome, *Z. Elektrochem.*, **57**, 342 (1953).
(3) D. A. Hall and P. J. Elving, *Anal. Chim. Acta*, **39**, 141 (1967).
(4) W. J. Blaedel and R. A. Jenkins, *Anal. Chem.*, **46**, 1952 (1974).
(5) S. G. A. Alivisatos, F. Unger, and G. J. Abraham, *Biochemistry*, **4**, 2612 (1965).
(6) R. D. Braun, K. S. V. Santhanam, and P. J. Elving, *J. Am. Chem. Soc.*, **97**, 2591 (1975).
(7) H. H. Heller, *Trans. Electrochem. Soc.*, **87**, 501 (1945).
(8) B. Wallen and G. Wranglen, *Electrochim. Acta*, **10**, 43 (1965).
(9) M. M. Fliskii, I. E. Veselovskaya, and R. V. Dzhagatspanyan, *Zh. Prikl. Khim. (Leningrad)*, **33**, 1901 (1960).
(10) W. J. Blaedel and R. A. Jenkins, *Anal. Chem.*, **47**, 1337 (1975).
(11) R. S. Nicholson and I. Shain, *Anal. Chem.*, **36**, 706 (1964).
(12) M. Aizawa, R. N. Coughlin, and M. Charles, *Biochim. Biophys. Acta*, **385**, 362 (1975).
(13) R. G. Haas, Ph.D. Thesis, The University of Wisconsin, 1970.
(14) P. Leduc, These de Doctorat d'Etat, Universite Pierre et Marie Curie, Paris, France, 1976.
(15) M. Heyrovsky and S. Vavrika, *J. Electroanal. Chem.*, **36**, 223 (1972).

RECEIVED for review September 15, 1978. Accepted December 13, 1978. The authors thank the National Science Foundation, which helped support the work described.

Neutral Carrier Sodium Ion-Selective Microelectrode for Intracellular Studies

R. A. Steiner, M. Oehme, D. Ammann, and W. Simon*

Department of Organic Chemistry, Swiss Federal Institute of Technology, Universitätstr. 16, CH-8092 Zürich, Switzerland

Na^+-selective microelectrodes based on new, synthetic, electrically neutral ion carriers are described. The selectivities in respect to K^+ and Mg^{2+} are adequate for intracellular measurements of Na^+ ion activities $\geq$ 10 mM at ionic backgrounds of 100 mM K^+, 2 mM Mg^{2+}, and 10^{-7} M Ca^{2+}. Electrodes with tip diameters of around 1 μm have an electrical resistance of about 10^{10} Ω and a 90% response time as specified by the IUPAC recommendation of $\leq$5 s.

Microelectrodes with tip diameters of about 1 μm may be used for the potentiometric measurement of intracellular ion activities (*1–3*). Although Na^+-selective glasses have been described (*4*) which have a sufficiently high selectivity with respect to K^+ for intracellular studies, the corresponding microelectrodes have not found wide acceptance in practice (*3*). The most attractive glasses of the type NAS_{11-18} (*4*) possess elevated glass transition temperatures and therefore give rise to vexing technical problems in the preparation of microelectrodes (*1*). They commonly have an active membrane of around 10-μm length. In connection with the penetration into cells, this introduces uncertainties which are minimized by using recessed-tip glass microelectrodes (*5*), which, however, suffer from disadvantages like the volume of the recess (*5*), the possibility of tip blockage (*5*), and a rather sluggish response (*5*) which might partly be a consequence of the possible contamination of the glass surface by proteins (see also (*6*)). Since the hydration of the glass seems to be essential for the electrode response, a repeated reactivation of the glass is necessary (*5*).

Microelectrodes based on liquid ion exchangers sidestep these drawbacks (*7, 8*). For the measurement of intracellular Na^+ activities, an exchanger based on the antibiotic monensin has been suggested (*8*). Since intracellular ion concentrations are around 200 mM and 10 mM for K^+ and Na^+, respectively, the Na^+/K^+ selectivity of 13 claimed for this electrode (*8*) ($K_{NaK}^{Pot} = 0.08$) is meagre: in the extreme case presented, the interference by K^+ introduces an error in the Na^+ determination of more than 100%. Similarly, the high intracellular Mg^{2+} concentration is a serious source of interference.

Recently Na^+-selective neutral carriers have been developed which induce a K^+ discrimination in PVC–liquid membrane electrodes (*9*) comparable to Na^+-selective glass membrane electrodes. Here we report on the use of this and a similar ligand as ion-selective components in microelectrodes of high Na^+-selectivity.

EXPERIMENTAL

Electrode System. Cells of the type

$$\underbrace{\text{Hg; } Hg_2Cl_2,\ KCl(\text{std.})\|1\ M\ CH_3COOLi\|\text{sample solution}\|}_{\text{external macro reference electrode}}$$

$$\underbrace{\text{membrane}\|0.01\ M\ NaCl,\ AgCl;\ Ag}_{\text{ion-selective microelectrode}}$$

have been used. The external reference electrode was a double junction calomel electrode Philips R11.

Ion-Selective Microelectrodes. Glass micropipets were drawn from double-barreled Pyrex glass tubing (W. Krannich KG, D-34 Göttingen, BRD; 80 mol % SiO_2, 2% Al_2O_3, 13% B_2O_3, 1% K_2O, 3% Na_2O, 1% Fe_2O_3). They were filled using a modification of the technique described by Lux and Neher (*10*). The two channels of the microelectrodes contained 0.01 M NaCl and 0.01 M KCl respectively. The inner wall of the NaCl channel was made hydrophobic by silanization with a solution (5% w/w) of dichlorodimethylsilane in CCl_4. A solution of 10% w/w of the neutral carrier in *o*-nitrophenyloctyl ether (*o*-NPOE) (with or without 0.5% w/w of sodium tetraphenyl borate (NaTPB) in the case of ligand 1) was introduced into the tip of the NaCl channel up to a height of 200 μm. For the characterization of the electrode properties, the reference channel (KCl) of the double barreled electrode was not used (see above); instead an external macro reference electrode was used.

EMF Measurements. The EMF measurements were performed at 20 °C using a digital voltmeter model F 223-A (W-P Instruments Inc., New Haven, Conn.). The operational amplifier had an input impedance of 10^{15} Ω, an input capacitance of 1 pF, and capacity neutralization. It was located directly on top of the electrode. With a source resistance of 10^{11} Ω, the response time (to within 1% of final value) is according to the manufacturer's specifications about 0.4 s (evidently response to 90% (*11*) is faster). The electrode assembly and other high impedance components were located inside a faraday cage.

Reagents. All solutions were made from doubly distilled water and salts of the highest purity available. The synthesis of ligand 1 is described in detail in (*9*). Ligand 2 was prepared by a similar procedure.

Selectivity Factors, Electrode Response. Selectivity factors were obtained by the separate solution method (SSM, 0.1 M metal-chloride solutions), following the IUPAC recommendations (*11*). The activity coefficients used are described in detail in (*12, 13*).

RESULTS AND DISCUSSION

Among the Na^+-selective components suitable for liquid membrane electrodes, the neutral carriers 1 and 2 (Figure 1) are the most attractive ones with respect to selectivity (*13*). In Table I, selectivities of microelectrodes based on these ligands are compared with those of other Na^+-selective electrode systems. Except for Li^+, ligand 1 exhibits higher selectivities than ligand 2. Therefore only electrodes with ligand 1 have been studied in greater detail. To reduce the electrical resistance of the microelectrode, sodium tetraphenyl borate was added to the ion-selective liquid as described earlier for other systems (*15–17*). As expected, there is some loss in selectivity with respect to divalent cations (*18*). Since the pivotal Na^+/K^+-selectivity is not affected, and simultaneously a reduction in resistance from 2×10^{11} Ω to 10^{10} Ω is obtained by adding sodium tetraphenyl borate, this type of electrode is the most attractive for practical applications. A linear regression over the response function of such an electrode assembly over the range 10^{-1} to 10^{-3} M NaCl yields a slope of 53.0 ± 2.5 mV (s.d.; $N = 3$) theoretical: 58.2 mV at 20 °C; see Figure 2).

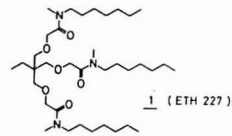
Based on the selectivity factors given in Table I, the electrode response (EMF vs. log a_{Na}) presented in Figure 3 was calculated using the Nicolsky formalism (*11*). Assuming

0003-2700/79/0351-0351$01.00/0 © 1979 American Chemical Society

Table I. Selectivity Factors log K_{NaM}^{Pot} for Different Na^+ Microelectrodes

		log K_{NaM}^{Pot} for M^{z+}									
electrode based on	method	Li^+	K^+	Rb^+	Cs^+	Mg^{2+}	Ca^{2+}	Sr^{2+}	Ba^{2+}	H^+	acetylcholine$^+$
ligand 1 (ETH 227) without TPB^-	SSM[a] 0.1 M	0.4	−1.7	−2.0	−2.2	−2.7	−0.7	−1.1	−1.3	−0.9	
ligand 1 (ETH 227) with TPB^-	SSM 0.1 M	0.4	−1.7 −2.3[d]	−1.6	−1.8	−2.4	0.2	−0.2	−0.4	−0.8	−1.8
ligand 2 (ETH 237) without TPB^-	SSM 0.1 M	0.2	−1.1	−1.4	−1.6	−1.9	−0.1	−1.0	−0.9	−0.1	
monensin (8)	FIM[b] 1 M[e]		−1.1			−0.8	−2.2			−1.1	
Na-glass[c] (NAS_{11-18}) (4)	?	−3.0	−3.0	−4.3	−3.0	−4.3				3.0	

[a] SSM: Separate solution method (11). [b] FIM: Fixed interference method (11). [c] Typical values for a Na^+-glass macroelectrode (see (14)). [d] Value adjusted to the Na^+ response; background electrolyte considered (see Figure 3). [e] Experience with various electrode systems (24) shows that the SSM (0.1 M) consistently gives too conservative estimates for the selectivity factors as compared to the FIM (1 M).



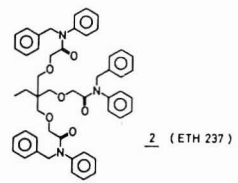


Figure 1. Na^+-selective neutral carriers

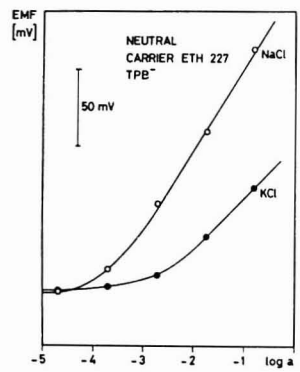


Figure 2. EMF response of the Na^+-microelectrode cell assembly (based on ligand 1) to aqueous solutions of the chlorides of Na^+ and K^+. All measured EMF values were corrected by the Henderson formalism (12) before plotting and regression analysis

a representative intracellular fluid containing 200 mM K^+, 2.0 mM Mg^{2+}, 0.01 mM Ca^{2+}, varying the amount of Na^+ makes obvious that the neutral carrier electrode shows a detection limit (indicated by arrows (11)) which is by about an order of magnitude lower than the one of the monensin based microelectrode. An analysis of the Nicolsky equation

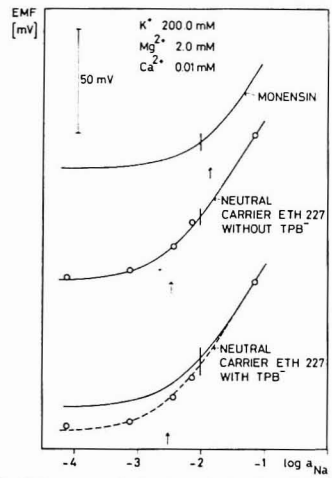


Figure 3. EMF response of microelectrodes to changing Na^+ activities at constant ionic background. Solid curves: response computed using selectivity data of Table I and actual slopes of the electrode response (monensin: see (8); neutral carrier 1: see Figure 2). Dashed curve: response computed using selectivity data of Table I and a value K_{NaK}^{Pot} of 5×10^{-3} found to best fit the experimental results. Dots: experimental values. An arrow indicates the detection limit (11) and a vertical bar represents the physiological Na^+ activity

indicates that the detection limit of the monensin based sensor is given mainly by the interference of K^+ and Mg^{2+} whereas the neutral carrier electrode suffers almost exclusively from K^+ interference. In contrast to the monensin based electrode, where the detection limit is slightly above the physiological Na^+ activity (10^{-2} M, vertical bar in Figure 3), the neutral carrier electrode does make intracellular Na^+ activities accessible. This is all the more true if the intracellular K^+ concentration becomes smaller, as is observed in several living cells (19–21).

Whereas the classical Na^+ selective glass electrodes exhibit a preference of H_3O^+ over Na^+ by a factor of about 10^3 (Table I), the neutral carrier systems discriminate H_3O^+ with respect to Na^+. Therefore pH changes of the sample solution in the range of pH 2 to pH 10 do not heavily influence the EMF if the concentration of Na^+ is kept constant either at 10^{-1} M (±1 mV (2 < pH < 10)) or 10^{-2} M (±5 mV (2 < pH < 10)). Therefore pH changes over the physiological range will not

interfere with the Na^+ determination.

The 90% rise time of the electrode obtained by adding 1 mL of 1 M solution of NaCl to 50 mL of a 10^{-3} M NaCl is about 5 s, significantly longer than the rise time of the electronic equipment with a source resistance of 10^{11} Ω. The double barreled electrodes (tip diameter 2 μm) described here have a resistance of about 10^{10} Ω. Since the speed of mixing in the sample solution after the stepwise addition of NaCl solution is rather critical, the actual response time of the sensor will be considerably smaller than indicated. Indeed, 90% response times of 0.2 s were reported for the same electrode (*22*).

The lifetime of the microelectrode in contact with aqueous electrolytes is several weeks and the drift is ≤1 mV/day.

The microelectrode described here is designed for intracellular use. A first series of intracellular measurements has been successfully conducted (*22*); in analogy to observations on other microelectrodes based on electrically neutral carriers (*13*), no interference due to the presence of proteins was detected. Since the extracellular ion activities differ sharply from the intracellular ones, extracellular measurements with this electrode are prone to interference due to the rather poor Na^+/Ca^{2+}-selectivity. It is a fair assumption that a useful Na^+ microelectrode on the basis of electrically neutral ligands can be developed for extracellular work, inasmuch as corresponding macroelectrodes with K_{NaCa}^{Pot} as low as 10^{-3} have been described (*9*, *23*). Because of their small selectivity with respect to K^+ ($K_{NaK}^{Pot} = 5 \times 10^{-1}$ (*9*, *23*)), their application will be limited to extracellular environments. The same might hold for the monensin-based electrode (see Table I (*8*)).

LITERATURE CITED

(1) M. Lavallée, O. F. Schanne, and N. C. Hebert, Ed., "Glass microelectrodes", Wiley & Sons, Inc., New York, London, Sydney, Toronto, 1969.
(2) H. J. Berman and N. C. Hebert, Ed., "Ion Selective Microelectrodes", Plenum Press, New York, London, 1974.
(3) M. Kessler, L. C. Clark, Jr., D. W. Lübbers, I. A. Silver, and W. Simon, Ed., "Ion and Enzyme Electrodes in Biology and Medicine", Urban and Schwarzenberg, Munich, Berlin, Vienna, 1976.
(4) G. Eisenman, Ed., "Glass Electrodes for Hydrogen and Other Cations", M. Dekker Inc., New York, 1967.
(5) R. C. Thomas, in ref. 3, p 141.
(6) R. N. Khuri, in ref. 3, p 123.
(7) J. L. Walker, Jr., *Anal. Chem.*, **43** (3), 89A (1971).
(8) R. P. Craig and C. Nicholson, *Science*, **194**, 725 (1976).
(9) M. Güggi, M. Oehme, E. Pretsch, and W. Simon, *Helv. Chim. Acta*, **58**, 2417 (1976).
(10) H. D. Lux and E. Neher, *Exp. Brain Res.*, **17**, 190 (1973).
(11) G. G. Guilbault, R. A. Durst, M. S. Frant, H. Freiser, E. H. Hansen, T. S. Light, E. Pungor, G. Rechnitz, N. M. Rice, T. J. Rohm, W. Simon, and J. D. R. Thomas, "IUPAC Information Bulletin, No. 1", 1978, p 70.
(12) P. C. Meier, D. Ammann, H. F. Osswald, and W. Simon, *Med. Progr. Technol.*, **5**, 1 (1977).
(13) P. C. Meier, D. Ammann, W. E. Morf, and W. Simon, in "Medical and Biological Applications of Electrochemical Devices", J. Koryta, Ed., John Wiley & Sons, Ltd., Chichester, 1978 (in press).
(14) K. Cammann, "Das Arbeiten mit ionenselektiven Elektroden", Springer Verlag, Berlin, Heidelberg, New York, 1977.
(15) M. Oehme and W. Simon, *Anal. Chim. Acta*, **86**, 21 (1976).
(16) M. Oehme, M. Kessler, and W. Simon, *Chimia*, **30**, 204 (1976).
(17) R. C. Thomas, W. Simon, and M. Oehme, *Nature (London)*, **258**, 754 (1975).
(18) W. E. Morf and W. Simon, in "Ion-Selective Electrodes in Analytical Chemistry", H. Freiser, Ed., Plenum Publishing Co., New York, 1978 (in press).
(19) T. Zeuthen, *J. Membr. Biol.*, **39**, 185 (1978).
(20) J. A. Coles and M. Tsacopoulos, *J. Physiol.*, **270**, 12P (1977).
(21) S. W. de Laat, W. Wouters, M. M. Marques da Silva Pimenta Guarda, and M. A. de Silva Guarda, *Exp. Cell Res.*, **91**, 15 (1975).
(22) S. Levy, Experimental Ophthalmology Laboratory, Geneva, Switzerland, private communication, 1978.
(23) D. Ammann, R. Bissig, Z. Cimerman, U. Fiedler, M. Güggi, W. E. Morf, M. Oehme, H. Osswald, E. Pretsch, and W. Simon, in ref. 3, p 22.
(24) W. Simon, D. Ammann, M. Oehme, and W. E. Morf, *Ann. N.Y. Acad. Sci.*, **307**, 52 (1978).

RECEIVED for review August 28, 1978. Accepted November 9, 1978.

Reticulated Vitreous Carbon Flow-Through Electrodes

A. N. Strohl and D. J. Curran*

Department of Chemistry, GRC Tower I, University of Massachusetts, Amherst, Massachusetts 01003

Flow-through electrodes have been fabricated from Reticulated Vitreous Carbon (RVC). This material has low electrical resistance, large surface area, and a physically continuous structure. The resistance to solution flow is low and flow rates up to 25 mL/min were easily attained. Solutions in the concentration range 1 to 1000 μM produced currents from about 1 to 1000 μA, respectively, using flow rates from 0.5 to 25 mL/min. Current–voltage curves were generated using these electrodes. At constant potential, the analyte solution was pumped through the electrode at a constant rate, thereby generating a steady-state current. The linearity and slope of calibration curves (steady-state current vs. concentration) were found to depend on flow rate. Higher sensitivities were obtained at higher flow rates and coulometric conversions occurred at the lowest flow rates. Ferricyanide ion and ascorbic acid were used as test systems, and ascorbic acid in vitamin C tablets was determined with results that were in excellent agreement with a titrimetric check method.

Electrodes based on various forms of carbon have received increasing attention in recent years for use in flowing streams. In general, three configurations have been used which are described by the position of the electrode in relation to the flowing stream: flow-by, where the electrode surface is parallel to the direction of flow; flow-onto, where the surface is normal to the direction of flow; and flow-through. Pungor and co-workers have developed a silicone rubber based graphite flow-by electrode (*1–3*) and have summarized earlier work. The same electrode has been used for turbulent hydrodynamic voltammetry in a flow-onto mode (*4–6*). Carbon paste flow-by electrodes have been used by Kissinger and others in electrochemical cells for liquid chromatography detectors (*7*). Curran and co-workers (*8*) have used a pair of carbon-wax electrodes for the same purpose.

Two types of flow-through electrodes can be distinguished, depending upon whether the electrode is simply a hollow cylinder or is a porous matrix of some sort through which the solution flows. With respect to the former, the work of Blaedel with tubular electrodes should be mentioned (*9*). An excellent discussion of the latter is found in the paper by Johnson and Larochelle where a packed electrode is used as a coulometric detector for liquid chromatography (*10*). Various forms of porous matrix flow-through carbon electrodes have been used previously. A review of electrolytic chromatography by Fujinaga and Kihara (*11*) describes the work of these authors with columns containing glassy carbon grains, which served as the electrode material. Crushed graphite was used in a short column electrode by Blaedel and Strohl (*12*). Finely divided

0003-2700/79/0351-0353$01.00/0 © 1979 American Chemical Society

graphite chips or flakes were used by Bennion and Newman to construct a porous flow-through cathode for the removal of copper in a flowing stream (*13*). Ostrovidov made porous carbon electrodes by hot pressing techniques using a polyethylene binder (*14*). These electrodes had significant resistance to flow, and a considerable pressure (0.2–0.3 atm) was required to produce a flow rate of 0.2 mL/min. In later work, porous carbon electrodes were formed from blocks of commercial pyrographite, which were used for the determination of dichromate and ferric ions (*15, 16*). The electrodes were cylinders 0.9 cm in diameter and 1–2 cm long. No information on their physical properties was provided. It is stated that the lowest concentration of Fe(III) which could be determined was 7 ppb (*16*).

We report here on the use of Reticulated Vitreous Carbon, RVC (trademark) as an electrode material for studies in flowing streams. It is available from Chemotronics International, Inc., Ann Arbor, Mich. The only previous reports of its use as an electrode are that of Norvell and Mamantov (*17*) who used a thin slice of RVC as an optically transparent electrode, and that of Butcher, Chambers, and Pagni who used a stationary RVC anode for the coulometric electrolysis of uranocene in THF (*18*). Tentorio and Casolo-Ginelli have reported a study of the mass transfer characteristics of a reticulated copper electrode made by electroless deposition of copper on polyurethane foams (*19*). In the present work, current–voltage curves were obtained with electrodes of very large surface area using the reduction of ferricyanide and the oxidation of ascorbic acid as examples. Determinations by steady-state voltammetry were investigated and the conditions necessary to achieve coulometric conversion are presented. Ascorbic acid was determined in vitamin C tablets.

EXPERIMENTAL

Chemicals. All chemicals were reagent grade. Ascorbic acid and potassium ferricyanide were dried at 110 °C for 1 h. Distilled water was redistilled from alkaline permanganate.

Solutions. Stock solutions of ascorbic acid and potassium ferricyanide were several millimolar. Boiled distilled water containing 0.5 g/L $Na_2EDTA{\cdot}2H_2O$ was used in preparation of all ascorbic acid solutions to prevent chemical oxidation (*20*).

Iodate was used to assay the ascorbic acid stock solution. The hydroquinone method of Simon and Zyka (*21*) was used to potentiometrically analyze the ferricyanide stock solution. Dilutions for electrochemical analyses were made with supporting electrolyte which was a 0.025 M phosphate buffer (pH 6.82), 0.1 M in potassium chloride.

Vitamin C tablets were obtained from commercial sources and the stock solutions were approximately 3 mM in ascorbic acid. Assays and dilutions followed the treatment for ascorbic acid.

Equipment. Either a Princeton Applied Research Corp. Model 170 Electrochemical System or a PAR 173/376 System with a Houston Model 2000 Omnigraphic X-Y Recorder was used. A Hewlett-Packard Model 3439A Digital Voltmeter or a Textronix DM 501 Digital Multimeter was available for digital readouts of currents. Most current–voltage curves were obtained without the use of positive feedback IR compensation. A Cole-Parmer Masterflex Console Pump with a 7013 pump head maintained constant flow through the RVC Electrode. The flow rate was checked volumetrically. Silicone rubber tubing, 0.8-mm i.d., was used for all fluid connections. A Perkin-Elmer Model 202 Spectrophotometer was used.

Electrode Construction. RVC-A, a high conductivity form of RVC, obtained from Chemotronics International, Inc., Ann Arbor, Mich., was used for all experiments. Figure 1 shows the electrode construction. A cylinder (A) cut from a RVC-A block with a cork borer and a piece of glass tubing (D) were encased in heat-shrink plastic tubing (B). A spectrochemical grade graphite rod sidearm (C) was fitted through the plastic tubing to make a press-fit electrical contact with the RVC cylinder. All joints and any possible locations for leaks were sealed and strengthened by a glass outer shell filled with epoxy cement (E). The electrode used for all determinations except the ferricyanide

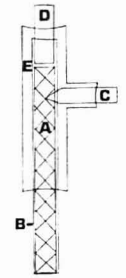


Figure 1. RVC Electrode. (A) RVC cylinder, (B) heat-shrink tubing, (C) graphite rod sidearm, (D) glass tube, (E) glass and epoxy support

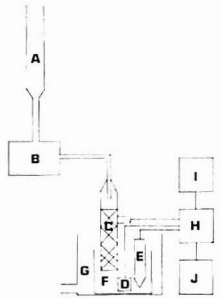


Figure 2. Schematic diagram of equipment for steady-state electrolysis. (A) Analyte reservoir, (B) pump, (C) RVC electrode, (D) platinum electrode, (E) SCE reference electrode, (F) downstream reservoir, (G) runover collector, (H) potentiostat, (I) recorder, (J) digital voltmeter

work was 1.0 cm in diameter and 10.8 cm long, having a calculated volume of 7.8 mL and an electrode surface area of 515 cm^2. The electrode used for ferricyanide determinations was 0.5 cm in diameter and 10.8 cm long, having a calculated volume of 1.9 mL and a surface area of 125 cm^2. The resistance of these electrodes measured end-to-end in air was 11.0 and 16.3 Ω for the 7.8- and 1.9-mL volume electrodes, respectively. For the larger electrode, the resistance between the graphite rod and one end of the RVC was 12.4 Ω and 5.2 Ω to the other end. Similar resistances for the smaller electrode were 12.9 and 5.4 Ω. These numbers demonstrate that the contact resistance between the graphite rod and the RVC is no more than a few ohms. The major contributor to any electrode resistance effects is the electrolyte resistance which was about 700 Ω for the 7.8-mL electrode.

Electrode Operation. The solution to be analyzed passed from the analyte reservoir (A) (Figure 2) through the pump (B) to the upper portion of the electrode (C). A layer of solution was kept over the top of the electrode to ensure that it was totally filled with liquid. This was initially back-pumped from the down-stream reservoir. Thus the entire surface area of the electrode could be available. The other end of the electrode dipped into the downstream reservoir (F) containing Pt counter and SCE reference electrodes (D and E). During analysis, the pumped solution flowed through the electrode into the downstream reservoir and overflowed from it into the runover collector (G), so a constant volume of liquid was maintained in the downstream reservoir. In the amperometric mode each solution was pumped through the electrode until a current plateau was achieved. Before the next solution was introduced for analysis, the analyte solution reservoir and pump system were washed and flushed with several milliliters of the test solution. At fast flow rates, it was necessary to turn off the pump to add wash and sample solutions. During all analyses the potentiostat (H) applied a constant potential to the RVC electrode, and the currents were monitored by recorder and digital readout (I and J).

Table I. Physical Properties—Nominal Values,[a] RVC-A-100

bulk void volume	90%
pores per linear inch	100
surface area (cm^2/cm^3)	66
bulk resistivity (ohm-cm)	0.23

[a] Bulletin 176R2k, Chemotronics International, Inc., Ann Arbor, Mich. 48104.

Table II. RVC Anodic Limiting Reaction[a]

phosphate buffer, pH 7	DME, i_d (μA) at E, -1.2 V
air sat'd	5.7
O_2 removed	0.2
21-h electrolysis,[b] RVC at 0.8 V	0.8
O_2 removed	0.2
19-h electrolysis,[b] RVC at 1.0 V	5.5

[a] Potentials vs. SCE. [b] Under N_2.

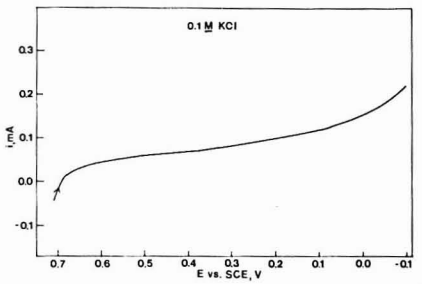


Figure 3. Background current–voltage curve. Electrolyte 0.1 M KCl; electrode volume, 7.8 mL; flow rate, 8 mL/min; scan rate, 2 mV/s

RESULTS AND DISCUSSION

Table I lists physical properties of the RVC-A material. The low bulk resistivity and high surface area are attractive properties for a flow-through electrode. In contrast to materials used in packed or fluidized bed electrodes, RCV is mechanically continuous and therefore does not rely on physical packing for electrical contact throughout the matrix. In addition, the pressure drop across the material is extremely small in a flowing stream. Both gravity flow and high flow rate systems are easily implemented. Except for the time required for epoxy cement to harden, electrodes (Figure 1) can be fabricated in less than one hour.

Electrode Potential Limits. Figure 3 shows a residual current–voltage curve obtained in 0.1 M KCl. The background current in this scan contains a charging component which, of course, can be reduced considerably if data points are obtained manually at fixed potentials. The anodic limit is determined by the process responsible for the rise in current in the vicinity of 0.7 V.

Experiments conducted in a pH 7 phosphate buffer without any chloride ion present showed that oxygen was produced anodically. The oxygen limiting current at −1.2 V vs. SCE was monitored with a DME after prolonged electrolysis at the RVC anode. Results are shown in Table II. Very little oxygen is produced at 0.8 V, but more substantial amounts are produced at 1.0 V. Oxygen is generated at a considerable overpotential. The anodic limit was examined in solutions of various acidities in the absence of chloride ion and it shifted in the positive direction with increasing acidity as would be predicted by the oxygen reaction. The cathodic limiting reaction depends on the solution pH. There does not appear to be a substantial hydrogen overpotential, and further work in this area will be reported.

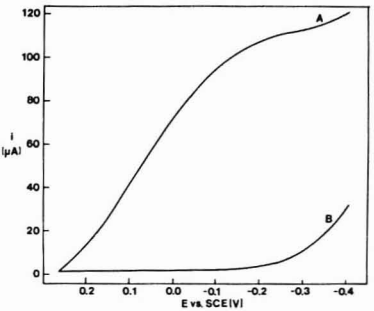


Figure 4. Current–voltage curve of 7.8×10^{-5} M potassium ferricyanide. Electrode volume, 7.8 mL; flow rate, 0.83 mL/min; scan rate, 1 mV/s; no IR compensation. Electrolyte; 0.1 M KCl, 0.025 M phosphate buffer (pH 6.82). (A) Scan uncorrected for background, (B) scan of background

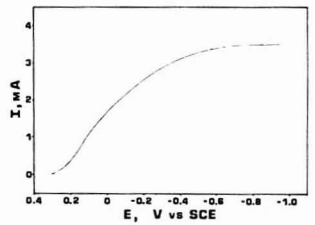


Figure 5. Current–voltage curve of 1.6×10^{-3} M potassium ferricyanide corrected for background. Flow rate, 8.0 mL/min; scan rate, 2 mV/s; positive feedback IR compensation used; supporting electrolyte: 0.1 M KCl, 0.025 M phosphate buffer (pH 6.82)

The Ferricyanide–Ferrocyanide Test System. Figure 4 shows a current–voltage curve for the reduction of ferricyanide (curve A) along with the residual current curve (B). Because of the large surface area of the electrode and convective mass transport, a large current signal is produced with fairly dilute solutions. If the background (curve B) is subtracted from curve A shown in Figure 4, the corrected curve shows a maximum. Similarly, maxima are shown by the current–voltage curves in Figure 8 for the ascorbic acid system. Fujinaga and Kihara have developed equations for the current–voltage curve in packed column electrodes (*11*). Their results predict a peak current with fast scan rates and slow flow rates and a limiting current plateau with slow scan rates and fast flow rates. On this basis, our curves should not show peaks. The cell geometry is far from ideal and all of these curves were generated without the use of positive feedback IR compensation. Figure 5 shows a current–voltage curve for 1.6 mM ferricyanide which is corrected for background current and where both the background curve and the total current curve were obtained using IR compensation. If no IR compensation is used or the compensation control is incorrectly set, apparent maxima are obtained for corrected curves when the background current is changing rapidly. It was particularly troublesome to make the IR compensation adjustment correctly for concentrations in the 10-μM concentration region since the divider ratio for the compensation potentiometer is very small. Expansion of the resolution of the voltage divider would improve this situation. Further evidence was obtained which demonstrated that the maxima are only apparent. A current–voltage curve for 1.6 mM ferricyanide was generated under conditions where the cor-

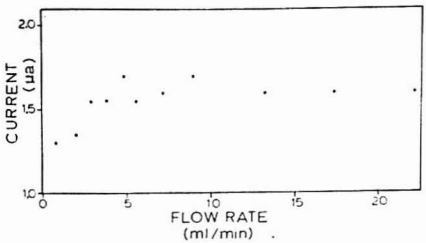


Figure 6. Background current as a function of flow rate. Solution; 0.1 M KCl, 0.025 M phosphate buffer (pH 6.82), potential, −0.2 V vs. SCE; electrode volume, 1.9 mL

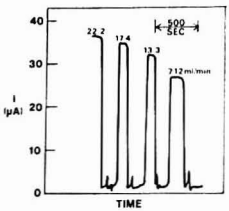


Figure 7. Tracing of the recorder readout of steady-state current as a function of flow rate. Solution: 3.9×10^{-6} M ferricyanide; potential, −0.2 V vs. SCE; electrode volume, 1.9 mL

rected curve showed a maxima at about −0.50 V. Holding the potential constant at this value, the effluent from the electrode was collected, being careful to avoid diluting it downstream. This experiment was then repeated at −1.05 V where the current was apparently lower than at the maximum. Analysis of the two effluent solutions by spectrophotometry at 420 nm (only ferricyanide absorbs at this wavelength) showed that the absorbance of ferricyanide was lower by about 0.14 absorbance unit in the solution obtained at −0.5 V, as would be expected for a current–voltage curve showing a slightly rising plateau. Ferricyanide ion is thermodynamically capable of reaction with hydrogen gas but no evidence could be found spectrophotometrically that this reaction occurs when the gas is bubbled into a solution of ferricyanide. The conclusion is that these maxima are apparent and arise from uncompensated IR drop.

From Figure 4, a control potential of −0.2 V vs. SCE was chosen for further experiments. It was of interest to determine the background current at this potential as a function of the flow rate, and the results are shown in Figure 6. On the whole, the background current is independent of flow rate, a result similar to that found by Jordan and co-worker for a conical microelectrode in flowing streams (22). Above 3 mL/min, the scatter in the data is probably experimental error; while below 3 mL/min, it appears that the background current is somewhat lower. If we assume a representative background current of 1.60 μA, the background current density is 13 nA/cm^2 based on the manufacturer's area specifications.

Actual recorder tracings of steady-state currents with 3.9 μM ferricyanide are shown in Figure 7 for a series of flow rates. Initially the analyte reservoir was filled with supporting electrolyte which was used as a wash solution. During the wash, the flow rate was adjusted and back-pumping was used to refill the electrode if necessary. The small perturbations in the base line are due to changing the flow rate, momentarily turning the pump off, or back-pumping. On addition of ferricyanide, a steady-state current was achieved in less than 60 s. For purposes of this figure, supporting electrolyte was

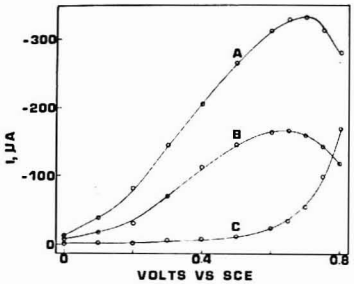


Figure 8. Current–voltage curves of ascorbic acid. Electrode volume 7.8 mL; flow rate, 8 mL/min; no IR compensation. (A) 1.6×10^{-5} M, corrected for background; (B) 0.8×10^{-5} M, corrected for background; (C) background, 0.1 M KCl, 0.25 M phosphate buffer (pH 6.82)

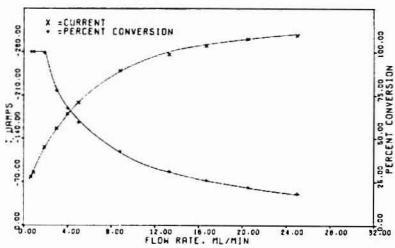


Figure 9. Current output and percent conversion of ascorbic acid as a function of flow rate. Solution 2.08×10^{-5} M ascorbic acid; potential, 0.4 V vs. SCE; electrode volume, 7.8 mL, electrolyte: 0.1 M KCl, 0.025 M phosphate buffer (pH 6.82) (x) current, (+) percent conversion

added between each analysis run. However, when constructing a working curve at a constant flow rate, the wash solution can also be the next standard solution to be determined.

Ascorbic Acid System. Figure 8 shows current–voltage curves for the oxidation of ascorbic acid. The steady-state current at each data point was obtained at constant flow and potential. Curve A is that of 16 μM ascorbic acid corrected for the background current (curve C) and curve B is the corrected curve for 8 μM ascorbic acid. In contrast to current–voltage curves generated at microelectrodes, these curves involve a substantial change in the bulk concentration of the electroactive species. For example, for curve B, we calculate that 84% of the ascorbic acid is oxidized at the steady-state at 0.6 V based on the flow rate, the electrode volume, and the magnitude of the current. Similarly, for the ferricyanide curve shown in Figure 4, the percent conversion is about 100% at a potential of −0.26 V. Steady-state currents are achieved because of the continual replenishment of the electrode by the flowing stream. The shape of the current–voltage curve is irreversible and the curve is shifted anodically along the voltage axis with increasing concentration as shown in Figure 8. The influence of flow rate for 2.08×10^{-5} M ascorbic acid is shown in Figure 9. As the flow rate increases, the current rises rapidly at first, but then more slowly. On the one hand, increasing flow tends to shift the curve anodically. However, because the residence time in the electrode is shorter at higher flow rates, the percent conversion decreases as is shown in Figure 9, and the amount reacted is smaller.

Working curves for the ascorbic acid system are shown in Figure 10 for three different flow rates. Each data point was corrected for the background current. Curves A and B were obtained at a control potential of 0.6 V vs. SCE which was chosen on the basis of the current–voltage curves shown in

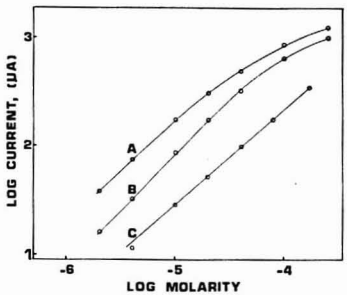


Figure 10. Calibration curves for ascorbic acid. Electrode volume, 7.8 mL; electrolyte: 0.1 M KCl, 0.025 M phosphate buffer (pH 6.82). (A) 8.4 mL/min, 0.6 V; (B) 4.0 mL/min, 0.6 V, (C) 0.7 mL/min, 0.4 V

Table III. Determination of Vitamin C in Tablets

source	M x 10^3	M x 10^3
X	2.84[a]	2.83[b]
Y	2.86	2.87
Z	2.78	2.78

[a] Titration method. [b] RVC method, sample diluted 1:1000.

Figure 8. The curvature shown by the working curves is due mainly to the shift of the current–voltage curve with concentration and flow rate. At the lower flow rate, the curve is linear to a higher concentration. These curves are most useful in the linear portion, and very large currents are obtained for concentrations in the micromolar region. While the utility of curves A and B is clear, their basis is empirical. At a given flow rate, F_r, the maximum possible steady-state current would correspond to complete conversion of the electroactive material. Curves A and B do not achieve this maximum current, and thereby the maximum slope, because the flow rates are too high. Curve C illustrates a case where 100% conversion has been achieved. The slope of curve C is 2.16 A/μM, and is in satisfactory agreement with the theoretical slope of 2.30 A/μM calculated from Faraday's law. Thus, it is possible to achieve working curves linear out to higher concentrations by working at low flow rates to obtain 100% conversion. However, maximum sensitivity is obtained at higher flow rates. For example, the slope of curve A in the linear region is 22 μA/μM. It is probably better to use higher flow rates for more dilute solutions.

The utility of the electrode in the analysis of real samples is illustrated by the determination of ascorbic acid in vitamin C tablets. The work was done early in the study and a control potential of 0.4 V vs. SCE was used. A calibration curve was constructed at a flow rate of about 7 mL/min. Vitamin C tablets were dissolved in deaerated aqueous buffer containing EDTA as a preservative. Dilutions were made so that the concentrations used for determination were in the linear region of the working curve. The results are compared in Table III with those obtained by the KIO_3 titration method. The agreement is excellent. The solutions determined with the flow-through electrode were 1000 times more dilute than those determined by titration. However, even with EDTA present, micromolar ascorbic acid solutions were not stable on standing. This problem was minimized by using the standard and unknown solutions as promptly as possible.

ACKNOWLEDGMENT

The authors thank L. Rubin and the Princeton Applied Research Corporation for the loan of a 173/376 Electrochemical System.

LITERATURE CITED

(1) E. Pungor, Zs. Fehér, and G. Nagy, *Anal. Chim. Acta*, **51**, 417 (1970).
(2) G. Nagy, Zs. Fehér, and E. Pungor, *Anal. Chim. Acta*, **52**, 47 (1970).
(3) Zs. Fehér and E. Pungor, *Anal. Chim. Acta*, **71**, 425 (1974).
(4) M. Varadi and E. Pungor, *Anal. Chim. Acta*, **80**, 31 (1975).
(5) M. Varadi, M. Gratzl, and E. Pungor, *Anal. Chim. Acta*, **83**, 1 (1976).
(6) M. Varadi, and E. Pungor, *Anal. Chim. Acta*, **84**, 351 (1977).
(7) P. T. Kissinger, *Anal. Chem.*, **49**, 447A (1977).
(8) R. J. Fenn, S. Siggia, and D. J. Curran, *Anal. Chem.*, **50**, 1067 (1978).
(9) W. J. Blaedel and G. W. Schieffer, *Anal. Chem.*, **46**, 1564 (1974).
(10) D. C. Johnson and J. Larochelle, *Talanta*, **20**, 959 (1973).
(11) T. Fujinaga and S. Kihara, *Crit. Rev. Anal. Chem.*, **7**, 223 (1977).
(12) W. J. Blaedel and J. H. Strohl, *Anal. Chem.*, **36**, 1245 (1964).
(13) D. N. Bennion and J. Newman, *J. Appl. Electrochem.*, **2**, 113 (1972).
(14) E. A. Ostrovidov, *Russ. J. Prakt. Chem.*, **43**, 1502 (1970).
(15) E. A. Ostrovidov and P. F. Veselovskii, *Zavod. Lab.*, **40**, 1247 (1974).
(16) E. A. Ostrovidov and P. F. Veselovskii, *Russ. J. Anal. Chem.*, **30**, 156 (1975).
(17) V. E. Norvell and G. Mamantov, *Anal. Chem.*, **49**, 1470 (1977).
(18) J. A. Butcher, Jr., J. Q. Chambers, and R. M. Pagni, *J. Am. Chem. Soc.*, **100**, 1012 (1978).
(19) A. Tentorio and U. Casolo-Ginelli, *J. Appl. Electrochem.*, **8**, 195 (1978).
(20) L. Erdey and G. Svehla, "Ascorbinometric Titrations", Akadémiai Kaldó, Budapest, 1972, pp 21–31.
(21) V. Simon and J. Zýka, *Collect. Czech. Chem. Commun.*, **21**, 327 (1956).
(22) J. Jordan, R. A. Javick, and W. E. Ranz, *J. Am. Chem. Soc.*, **80**, 3846 (1958).

RECEIVED for review September 29, 1978. Accepted December 11, 1978. Presented in part at the 29th Pittsburgh Conference on Analytical Chemistry and Applied Spectroscopy, Cleveland, Ohio, February 1978.

Introduction of Functional Groups onto Carbon Electrodes via Treatment with Radio-Frequency Plasmas

John F. Evans[1] and Theodore Kuwana*

Department of Chemistry, The Ohio State University, 140 West 18th Avenue, Columbus, Ohio 43210

Radio-frequency, inductively coupled, non-equilibrium plasmas of oxygen and ammonia were found to be a rapid and contaminant-free method by which functional groups could be introduced onto the surface of carbon (pyrolytic graphite and glassy carbon) electrodes. These functional groups provide sites for further attachment of molecules/ions employing conventional chemical reactions. Evidence is presented which suggests the formation of a variety of functional groups using the radio-frequency method and that the species in the plasma discharges were capable of modifying basal as well as edge plane surfaces. Substrate modification appeared to be confined to the surface region without causing structural damage or any adverse electrochemical response. Attempts to brominate pyrolytic graphite using a hydrogen bromide plasma were not successful.

The modification of conductive and semiconductive electrode surfaces via the attachment of chiral (*1–3*), electroactive (*4–31*), and photosensitive (*32, 33*) species has become a very active area of research. Attachment of modifier has generally been accomplished by (1) irreversible adsorption of the modifier onto the electrode material (*8, 10, 14, 28–30, 33–38*) or (2) covalent bonding of the modifier to functional groups extant on the electrode surface (*1–7, 9, 11–13, 16–27, 31, 32*). Surface preparation has been of utmost importance in obtaining high surface coverage of modifier via a highly stable interaction (be it physical or chemical in nature). In the case of the covalent attachment mode, this surface preparation must yield a high surface coverage of functional groups as linkage precursors.

Often the electrode material of choice will not possess the requisite functional groups for covalent attachment at a sufficient site density to ensure a high surface coverage of the chemically bonded modifier. In some case, this drawback may be overcome by selection of a different physical form of a given material on which higher surface coverage of the desired functionalities may occur naturally (e.g., microcrystalline graphite composites vs. pyrolytic graphite). In the case of graphitic materials, this selection could be a compromise to the electrochemical properties (e.g., edge vs. basal planes; edge planes bearing more functional groups per unit area but also having high charging currents and memory effects). Therefore, it becomes necessary to investigate methods by which one may introduce the functional groups necessary for covalent modification without sacrificing the desirable properties of the electrode.

Several approaches may be taken to introduce oxygen-containing functional groups onto the surface of graphite electrodes. For example, condensed phase reactions employing chemical oxidants such as permanganate or dichromate (*21*), thermally accelerated gas phase oxidation (*1, 2*), or treatment with a non-equilibrium (*39, 40*) oxygen plasma (*15*) have been reported. Although the coverage of oxygen functionalities on conductive carbon may be increased by the use of strong condensed phase oxidants, such treatments generally are unsuitable by virtue of contamination arising from retention of the reduced form of the oxidant on the surface (*21*). On the other hand, the success of thermally induced gas phase oxidations depends markedly on the crystal orientation at the surface of graphitic carbon (*2*). We have previously investigated the use of reactive, non-equilibrium oxygen plasmas as a means of introducing oxygen-containing functional groups onto the surfaces of isotropic pyrolytic graphite (PG) with promising results (*15*). This treatment has been shown to lead to incorporation of such groups in a rapid, contaminant-free fashion. Since our earlier report, Anson et al. (*24, 25*) have used a non-equilibrium plasma of argon to generate reactive sites on graphite, and Cadman et al. (*41*) have fluorinated graphite using a microwave discharge of SF_6.

A more detailed investigation is reported here of plasma-induced formation of functional groups on various conductive carbon electrodes, including PG, the basal plane of highly ordered pyrolytic graphite (HOPG), and glassy carbon (GC). The reactive plasma employed for modification of these carbon surfaces include oxygen, ammonia, and hydrogen bromide gases. The physical (roughening and "surface damage") and chemical (surface functional group formation) consequences of the plasma treatments were investigated by cyclic voltammetry, capacitance measurements, and X-ray photoelectron spectroscopy (XPS). The results indicated that the coverage of oxygen- or nitrogen-containing functional groups was enhanced by the use of oxygen and ammonia discharges. The increase of halogenated sites was minimal in the case of hydrogen bromide.

EXPERIMENTAL

Materials. Isotropic, vapor deposited pyrolytic graphite (PG) coated disks (0.375 in. diameter × 0.125 in. thickness) were obtained from Ultra Carbon Corporation (Bay City, Mich.). Prior to any characterization or plasma treatment, these electrodes were extracted for 24 h in a Soxhlet apparatus using anhydrous methanol. Highly ordered pyrolytic graphite (HOPG) was obtained from Union Carbide Corporation (Parma, Ohio). Generally, pieces were cut from sheets such that basal planes were ca. 0.75 in. × 0.75 in. Thickness varied when these pieces were cleaved to expose a fresh basal plane surface. After cleaving, these electrodes were extracted similarly to that described for PG. Glassy carbon (GC-30) was obtained from Tokai Electrode Manufacturing Co., Ltd. (Tokyo, Japan) in the form of sheets 0.12 in. thick. These were cut to give electrodes ca. 0.75 in. × 0.75 in. Surfaces were polished using successively finer silicon carbide paper (to number 600) followed by polishing with alumina (1.0 μm, then 0.5 μm). These electrodes were rinsed with methanol between polishing steps and finally, ultrasonically cleaned (2–3 min, methanol) and extracted overnight (Soxhlet apparatus, methanol). This final step was found to be essential to remove alumina imbedded during the polishing steps. After ultrasonic cleaning, no aluminum was detectable by XPS.

All electrochemical characterizations were carried out in Sorensen's buffer (0.1 M glycine + 0.1 M NaCl) at pH 2.50. Deionized, triply distilled water was used throughout. Gases used

[1] Present address, Department of Chemistry, Smith and Kolthoff Halls, University of Minnesota, 207 Pleasant Street, S.E., Minneapolis, Minn. 55455.

0003-2700/79/0351-0358$01.00/0 © 1979 American Chemical Society

Table I. Effects of Oxygen Plasma Treatment of PG Found via XPS Analysis

sample	length of exposure, min[a]	C(1s) binding energy[b] before	C(1s) binding energy[b] after	O(1s) binding energy[b] before	O(1s) binding energy[b] after	O/C elemental ratio[c] before	O/C elemental ratio[c] after
1	2	284.3 (1.20)[d]	284.3 (1.15)	532.7 (2.70)	532.6 (2.60)	0.023	0.156
2	5	284.3 (1.10)	284.3 (1.15)	532.3 (2.70)	532.9 (2.75)	0.024	0.168
3	10	284.3 (1.10)	284.3 (1.15)	532.5 (2.80)	532.5 (2.50)	0.028	0.159
4	20	284.3 (1.10)	284.3 (1.10)	532.3 (2.80)	532.6 (2.65)	0.039	0.160
5	30	284.3 (1.05)	284.3 (1.15)	532.3 (2.60)	532.4 (3.00)	0.023	0.158
av 1–5		284.3 (1.11 ± 0.05)	284.3 (1.14 ± 0.02)	532.4 ± 0.2 (2.72 ± 0.08)	532.7 ± 0.2 (2.67 ± 0.19)	0.027 ± 0.007	0.160 ± 0.005

[a] Oxygen plasma treatment at 150 mTorr. [b] All binding energies referenced to C(1s) of graphite (284.3 eV). [c] Corrected for cross section, see Experimental. [d] Parentheses contain FWHM, eV.

in the plasma discharges were obtained from Matheson Gas Products (East Rutherford, N.J.) and were the following grades: ammonia, anhydrous (99.99%); argon, high purity (99.995%); hydrogen bromide (99.8%); and oxygen, ultra high purity (99.95%). All other chemicals were reagent grade or equivalent.

Apparatus. Electrochemical equipment and the two-compartment Lucite cell have been described previously (*13, 15*). The cell was modified slightly to accommodate the HOPG and GC electrodes. For the capacitance measurements, the method employed was that described by Gileadi (*42*). These measurements were made using a 300-Hz triangular waveform perturbation of 50-mV amplitude. After each reading was recorded, the working electrode was biased to a new value, and the current waveform was allowed to come to a steady state before recording the new capacitive current. The experimentally observed capacitance values were calibrated by use of a standard capacitor. IR compensation was used as required (*42*). Electrode areas reported are the geometrically measured areas. All potentials are referenced to the Ag/AgCl couple (1.00 M KCl).

Scanning electron microscopy (SEM) examination of surfaces was carried out using a Cambridge mode S4-10 Stereoscan. XPS analyses were obtained using a Physical Electronics Industries, Inc. (Eden Prairie, Minn.) model 548 electron spectrometer. All spectra were taken at a base pressure of 5×10^{-9} Torr in the sample chamber. Low resolution spectra were recorded at 100-eV pass energy. High resolution spectra at 25-eV pass energy were signal averaged through the use of a Data General Corporation (Southboro, Mass.) NOVA 800 minicomputer to which the electron spectrometer was interfaced. Elemental ratios were determined by measurement of peak areas at high resolution, and then were corrected for elemental photoelectron cross-section differences using the empirical parameters reported by Wagner (*43*). The aforementioned integrations were carried out using the stored spectra by fitting a base line via linear least squares to the base line on either side of the high resolution peak, and then summing the data for each digitized point, corrected according to the best fit base line. The $4f_{7/2}$ line of clean gold (83.8 eV) was used as an energy calibration for all XPS spectra. As such, a secondary standard, C(1s) for graphite (284.3 eV) was established.

The plasma system was constructed of glass and stainless steel. The RF oscillator/power supply was the same as described previously (*15*) but the plasma apparatus was modified so that two gases could be mixed before entering the discharge region as shown in Figure 1. Before each plasma experiment, the vessel and substrate support were cleaned by a 300-mTorr discharge of argon for 0.5 h. Also, samples to be treated were vacuum dried in the plasma apparatus at ambient temperature until the pressure reached the system base pressure of $1–2 \times 10^{-2}$ Torr.

RESULTS AND DISCUSSION

Oxygen Plasma Treatment of PG. The structural and chemical changes to PG surfaces resulting from RF oxygen plasma treatments were evaluated using SEM, XPS, and electrochemical methods. Table I summarizes the electron spectroscopic results with respect to elemental ratios of O/C found, the peak binding energies and full width at half maxima (FWHM) of the C(1s) and O(1s) bands, for specific samples

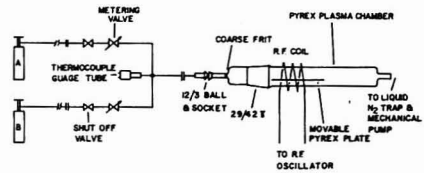


Figure 1. Block diagram of plasma reaction vessel used for treatment of conductive carbons. Substrates were centered in the coil during plasma treatments

exposed to the oxygen RF plasma for various lengths of time. No elements other than oxygen and carbon were detected in the XPS spectra either before or after plasma treatment.

The most striking feature of these results is that a relatively short exposure time (2 min) results in the "saturation" of the PG surface with oxygen-containing carbon groups. Although oxygen plasma treatment would be expected to render the carbon surface more hydrophilic, we believe that the majority of surface oxygen content observed by XPS results from the oxygen-containing functional groups rather than adsorbed water which might be retained under ultrahigh vacuum conditions. Since there is a substantial removal of surface material during the discharge (cf. the scanning electron micrographs of ref. *15*), a steady-state condition is apparently established rapidly in which the rate of incorporation of oxygen species becomes equivalent to the rate of removal of carbon oxides (presumably as CO and CO_2) at the surface. Further support of this steady state hypothesis is found in the electrochemical behavior of oxygen plasmolyzed PG (vide post).

The identity of the oxygen-containing functional groups is not easily inferred from the high resolution XPS data. The peak binding energies and FWHMs of the C(1s) and O(1s) bands after plasmolysis are statistically indistinguishable from those of the untreated samples (Table I). Most importantly, the O/C ratio increased ca. 6-fold after plasma treatment (see last column, Table I) and indicated the enhancement of oxygen functional group coverage. As may be seen from curves A and B of Figure 2, the effect of the increase in O/C elemental ratio on the C(1s) band is quite subtle. One can note, however, that the presence of high binding energy shoulders on the C(1s) peak is more pronounced in the case of the plasmolyzed samples. Curve fitting was not attempted for accurate determination of the binding energies and intensities of the surface oxide components because of complications caused by the loss structure (asymmetry) on the high binding energy side of the C(1s) band (*46*), inherent to graphitic carbon. Rather, chemical modification studies (*13*) and electrochemical characterizations (*15*) of the plasmolyzed surfaces have shown the introduction of at least two types of

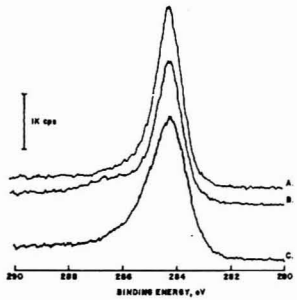


Figure 2. Effect of oxygen plasma and argon ion bombardment treatments on the C(1s) band of PG: (A) extracted only; (B) exposed to oxygen plasma for 5 min at 150 mTorr; (C) bombarded with 2-keV argon ions until O(1s) band not detected

oxygen-containing functionalities, carboxyl and quinone/hydroquinone-like groups.

If quantitative statements regarding functional group incorporation are to be meaningful, it is important to assess the extent of surface damage and roughening which result from RF treatment. Extent of damage is determined on a relative basis by comparison of the C(1s) band of oxygen plasmolyzed PG (Figure 2, curve B) with that of PG subjected to sputter etching with high energy (2 keV) positive argon ions (Figure 2, curve C). The ion bombarded PG surface shows a very much broadened C(1s) band (*46*) indicating severe lattice damage caused by the impact of the high velocity argon ions as their energy is dissipated in the surface and near-surface regions. Since such broadening is not found for the plasmolyzed PG samples, we conclude that the O_2 plasma treatment results in negligible damage to the near-surface lattice structure.

To determine the extent to which the PG surface is roughened (i.e., increased surface area), the capacitance was measured for several O_2 plasma treated electrodes. Capacitance as a function of potential is shown in Figure 3, in which a plasmolyzed PG electrode is compared to a control (extracted only). Assuming that the minimum observed capacitance at −0.6 V vs. Ag/AgCl is a valid indication of the double-layer capacitance, one finds that the capacitance rapidly increases to a maximum, constant value with respect to treatment time (Table II). This is consistent with the steady-state model for the plasma–surface reaction. It should be noted that the measured increase in electrode area, assuming proportionality

Table II. Effect of Oxygen Plasma Treatment on the Capacitance[a] of PG Electrodes

sample[b]	length of exposure, min	C_{obsd} at −0.6 V	C_{obsd} at +0.3 V	C_{dl} at +0.3 V	C_f at +0.3 V
1	2	6.4	12.5	8.6	3.9
2	5	6.1	15.0	8.2	6.8
3	10	6.6	14.1	8.7	5.5
4	20	6.1	15.5	8.6	7.0
av 1–4		6.3 (±0.2)[c]	14.3 (±1.3)	8.5 (±0.2)	5.8 (±1.4)
6[d]	0	2.7	3.3	3.0	0.3

[a] All determinations carried out in pH 2.5 aqueous glycine buffer using a 300-Hz triangle waveform of 50 mV peak-to-peak amplitude. All capacitance values are in $\mu F/cm^2$ (geometric). [b] Same samples as those appearing in Table I. Capacitance studies were carried out after post-plasma XPS analysis. [c] Parentheses contain one standard dev. [d] Control, extracted with methanol only.

between increase in capacitance with increase in area, is a factor of 2.3 while increase of O/C elemental ratio is at least a factor of 5.9 (the latter neglects any shadowing effects in the XPS determination). Thus, the oxygen plasma treatment not only increases the surface area of the electrode, but, more importantly, increases the site density of oxygen-containing functional groups by at least a factor of 2.5.

The capacitance maximum at +0.3 V vs. Ag/AgCl may be taken as a sum of the double layer capacitance, C_{dl}, and a pseudocapacitance, C_f, arising from the interconversion of the quinone/hydroquinone-like groups on the PG surface:

$$C_{obsd} = C_{dl} + C_f \quad (1)$$

By extrapolation of the capacitance curves from both sides of the maximum, a value of C_{dl} at the potential of the capacitance maximum may be estimated. A value of C_f (Table II) is obtained by difference. The validity of this approach is upheld by the relatively good agreement between the increase in the estimated value of C_{dl} at +0.3 V (× 2.3) and that found at the minimum in the capacitance curve (at −0.6 V) resulting from O_2 plasma treatment. Since the pseudocapacitance arising from an electroactive surface species is linearly related to the surface coverage of that species (*14*), we may calculate that at steady state (>2-min exposure to oxygen plasma), there is a 7-fold increase (normalized to surface area) in the surface coverage of the electroactive functional group. The fact that the relative increase observed attains a *limiting value* further supports the conclusion that

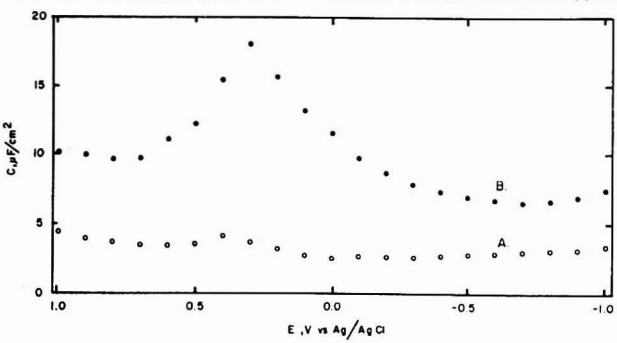


Figure 3. Effect of oxygen plasma treatments on the apparent capacitance of PG electrodes; (A) extracted only; (B) oxygen plasma treated for 20 min at 150 mTorr. All determinations carried out in pH 2.50 glycine buffer using a 300-Hz triangular waveform of 50-mV amplitude

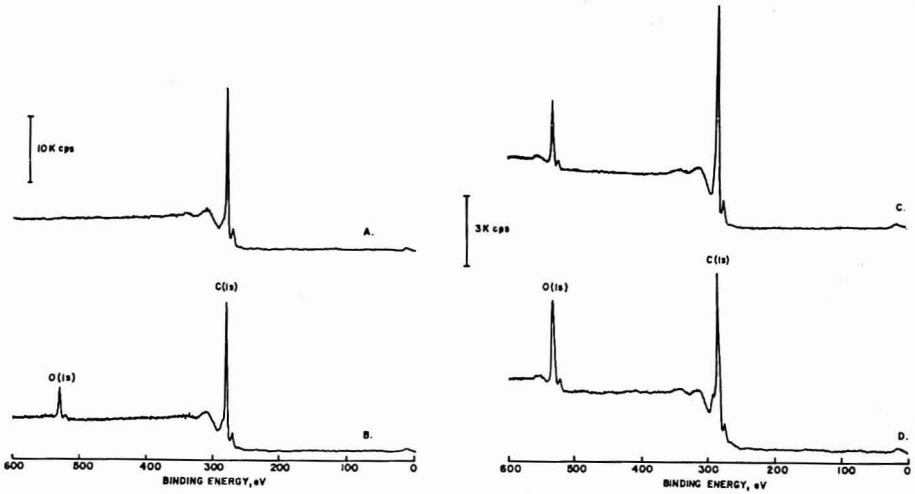


Figure 4. Low resolution XPS spectra of HOPG basal plane and GC electrode: (A) HOPG before and (B) after oxygen plasma treatment at 150 mTorr for 15 min, (C) GC before and (D) after oxygen plasma treatment at 150 mTorr for 5 min

the plasma interaction with the PG surface is at steady state within 2 min.

Since the electroactive functional group introduced during plamolysis appears to be one of the thermodynamically and/or kinetically favored plasma–surface reaction products, it is appropriate to discuss the surface electrochemistry associated with this species which we have previously assigned to quinone/hydroquinone (*15*) in more detail.

The cyclic voltammetric peak potential for the anodic process was found to be quite reproducible [+0.366 (±0.002 V) at 50 mV/s in pH 2.50 glycine buffer] regardless of the extent of oxygen plasma exposure received prior to electrochemical characterization (0 to 20 min). At a scan rate of 50 mV/s the peak separation for the surface redox processes indicated some measure of irreversibility (ΔE_p = 36 mV), the peak separation becoming greater with increasing scan rate. Both the anodic and cathodic peak potentials were found to shift to the same extent as scan rate was varied. On the other hand, differential pulse polarography gave results indicative of reversible behavior of the electroactive surface species when the polarograms were recorded under conditions of 1 mV/s sweep rate, 25-mV pulse amplitude, and 2-Hz frequency. For both anodic (0.0 to +1.0 V) and cathodic (+1.0 to 0.0 V) sweeps, the maximum current response was found at a potential of +0.340 (±0.002) V in pH 2.50 glycine. This behavior is exemplary of the relative insensitivity of the differential pulse polarographic method to irreversible electron transfer processes compared to the linear sweep techniques (compare ref. *44* and *45*).

The stability of the electroactive functionality is extremely high. No loss in peak current was observed during an experiment in which an electrode was cycled over 150 times between the limits of 0.0 and +0.8 V at a scan rate of 50 mV/s. (solution pH 2.5, glycine buffer).

Oxygen Plasma Treatment of Highly Ordered Pyrolytic Graphite Basal Plane. There are many reports in the literature supporting the concept that the oxygen-containing functional groups are confined to the edge planes of graphite (*46–51*). There are several mechanisms by which the ratio of edge to basal plane surface area may be increased. One could involve preferential electrophilic attack of the reactive plasma components (nascent oxygen and ozone) on the edge planes, giving more sites. Another would involve attack of reactive components at both edge and basal planes resulting in new edge plane regions.

The observation of basal plane attack by oxygen on graphitic materials which were exposed to fast particle irradiation has been reported by Hennig et al. (*52*). It is therefore of interest to examine the possibility of basal plane attack in a non-equilibrium or "cold" oxygen plasma. For this purpose synthetic "single crystal" HOPG was cleaved and the basal plane exposed to the O_2 plasma under conditions similar to those employed for treatment of PG. No discernible change in surface topography after plasma treatment for 1.5 h was seen compared to SEM taken before treatment. However, the electron spectroscopic analyses and electrochemical characterization of O_2 plasma treated HOPG were markedly different from those observed for untreated samples.

The XPS spectra of HOPG basal planes before and after plasmolysis are shown in Figure 4. As can be seen the freshly cleaved and extracted HOPG basal plane shows no detectable oxygen. After oxygen plasmolysis, a substantial oxygen signal is noted, although the elemental O/C ratio (corrected for photoionization cross section) is less than that found for similarly treated PG (0.102 vs. 0.160). For the plasma treated HOPG basal plane, the observed elemental ratio is in good agreement with that reported by Evans and Thomas (*46*) who bombarded such samples with high energy argon ions and subsequently reacted them with oxygen to yield monolayer coverage of oxygen-containing functional groups. The difference in the O/C ratios is, therefore, most likely a consequence of increased roughness for the PG surface.

The high resolution XPS data in the C(1s) region are not markedly different for the plasmolyzed HOPG vs. the untreated sample. As in the case of PG, there are subtle differences such as small higher binding energy signals on the plasma treated sample. There are no statistically significant changes in either the peak binding energy or the FWHM.

The electrochemical response of HOPG subjected to oxygen plasma treatment is dramatically different from that observed on the untreated surfaces as seen in Figure 5. The cyclic voltammogram of untreated HOPG is virtually featureless in

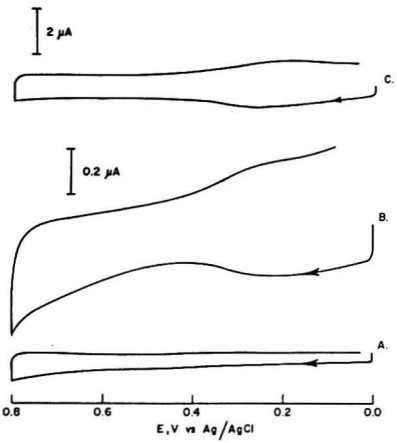


Figure 5. Cyclic voltammetric behavior of HOPG basal plane and GC electrodes: (A) HOPG before and (B) after oxygen plasma treatment (15 min at 150 mTorr), and (C) GC after oxygen plasma treatment (5 min at 150 mTorr). GC cyclic voltammetry was identical to trace C before plasma exposure. Solution conditions: pH 2.50 glycine buffer, sweep rate: 50 mV/s, electrode area: 0.52 cm^2

the voltage region 0.0 to +0.8 V. After plasmolysis, the charging current is increased by an order of magnitude and a reversible surface couple is seen at ca. +0.25 V. In this case, it is difficult to define the reasons for such a large change in the electrode capacity. It certainly may not be attributed solely to a change in actual electrode area, and most probably reflects the change from a hydrophobic surface (untreated basal plane) to a hydrophilic surface (after plasma treatment).

From the above, there is every indication that the oxygen plasma does indeed alter the basal planes of graphitic materials. It would seem, however, that by comparison of SEM micrographs of the surface topography changes of HOPG basal plane to that found for isotropic PG, reaction at the edge planes of PG (in terms of erosion of surface material) occurs at a much higher rate than at the basal planes of this material (PG).

Oxygen Plasma Treatment of Glassy Carbon (GC). For completeness, the effects of oxygen plasma treatment on glassy carbon were briefly examined. Although no physical damage in terms of increased roughness could be ascertained from SEM examination of a polished GC surface before and after plasma exposure, comparison of the low resolution XPS spectra (Figure 4) shows incorporation of oxygen-containing species.

The low resolution XPS spectrum of GC following polishing and methanol extraction shows a much higher O/C elemental ratio than found on the other unplasmolyzed conductive carbons examined (0.141 for GC compared to 0.027 for PG and nil for HOPG basal plane). Following oxygen plasma treatment, the O/C ratio increases (to 0.221 for the example given in Figure 4). Unlike the former cases (PG and HOPG), there are noticeable changes in the high resolution C(1s) and O(1s) bands (aside from changes in area ratios).

In Figure 6, the high resolution XPS spectra in the C(1s) region are shown for GC. Small bands in the 285–288 eV binding energy region are present, although the binding energy of the most intense peak is at 284.3 eV. After plasma treatment, a new peak is seen at higher binding energy (292.6 eV). Although this peak is of low intensity, it was unobservable on all other types of carbon. This band is not readily

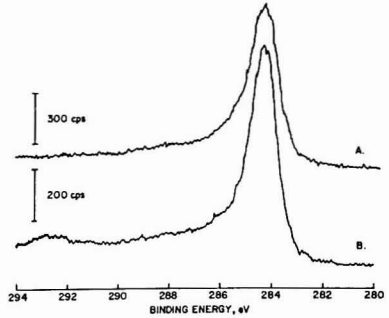


Figure 6. High resolution XPS spectra of GC in the C(1s) region: (A) before and (B) after oxygen plasma treatment at 150 mTorr for 5 min

assignable to any oxygen-containing funcionality by comparison to binding energy shifts available from the literature. Indeed, the chemical shift is of the magnitude observed for $-CF_3$ functional groups (8.7 eV) which have been introduced onto HOPG basal planes by the action of SF_6 plasmas (*41*). If this peak is the result of a surface oxygen-containing group, it suggests that the carbon atoms from which it arises are in a very extraordinary bonding environment. Another possible explanation is that this is a charge shift attributable to carbon–oxygen functionalities in regions where the surface conductivity has been lowered because of structural modification induced by the oxygen plasma. Such an effect would be expected to manifest itself in the electrochemical behavior of the plasma treated surface, yet this was not the case (vide post). Yet another explanation would entail assignment of this peak to a shake-up, possibly involving a paramagnetic species (surface free radical) introduced during the plasma treatment. Further work must be carried out to properly assign this band.

The high resolution spectrum of the O(1s) region also exhibits a uniqueness which is a consequence of the oxygen plasma treatment. Not only is the O(1s) peak significantly broadened following plasma exposure (from 2.85 to 3.05 eV FWHM), but it is also shifted to higher binding energy (531.6 to 532.1 eV). We are presently unable to explain the chemical significance of this shift.

The cyclic voltammetric behavior of a GC electrode before and after oxygen plasma treatment is shown in Figure 5. While there are features present which indicate the presence of reversible, electroactive surface species, the plasma exposure does not change the electrochemical response, either with respect to the faradaic surface process at ca. +0.25 V or to the double-layer capacitance.

Ammonia Plasma Treatment of Pyrolytic Graphite. Given the success of the oxygen plasma treatments, the technique was evaluated for the introduction of nitrogen containing functionalities on PG and HOPG basal plane using ammonia as the discharge gas. Such an approach was suggested by the work of Hollahan et al. (*53*) in which it was reported that plasmas of ammonia or nitrogen/hydrogen mixtures intereacted with various polymers to yield surface amino groups. Because of the multitude of free radical species (*53, 54*) arising from such discharges (e.g., NH_2·, NH·, N·, H·) it was anticipated that the ammonia plasma modification of pyrolytic graphite would be more complex than the oxygen case. It could not be assumed that all of the surface nitrogen content would be synthetically useful groups, such as =NH and $-NH_2$. Consequently, four aspects of the ammonia plasma treatment of pyrolytic carbon were evaluated. These were: (1) the NH_3 pressure dependence for which maximal

Table III. Summary of the Conditions Employed for Argon and Oxygen Plasma Treatment of PG Preceding Ammonia Plasma Exposure

sample	plasma treatment sequence	steps in the procedure[a]
6	O_2/Ar/NH_3	1. O_2 plasma treatment: 5 min at 150 mTorr 2. Ar plasma treatment: 10 min at 300 mTorr 3. NH_3 plasma treatment: 5 min at 2 Torr 4. NH_3 equilibration: 5 min at 2 Torr
7	O_2/Ar[b]	1–2
8	O_2/NH_3	1, 3–4
9	Ar/NH_3	2, 3–4

[a] Between plasma treatment, the excitation was turned off and the discharge vessel was evacuated to system base pressure (10 mTorr) before admission of next discharge gas, with the exception of experiments in which the NH_3 plasma treatment followed Ar plasma treatment. In these cases (samples 6 and 9), the discharge was left on and Ar flow remained on as the total pressure was increased to 2 Torr by the admission of NH_3, after which Ar flow was gradually reduced and NH_3 flow increased to maintain a total pressure of 2 Torr throughout until only NH_3 was being fed to the discharge. The time required for gas changeover was ca. 1 min. [b] This sample was included as a control for sample 6.

coverage of nitrogen-containing groups would be obtained; (2) the effect of oxygen and argon plasma pretreatments on the extent of introducing these functional groups; (3) the relative surface coverages of various functionalities; and (4) whether or not the components of an ammonia plasma would react with the HOPG basal plane.

Initial experiments using PG substrates involved variations in ammonia pressure during the discharge with the same exposure time and post-discharge handling as in the case of the O_2 plasmas. It was observed that as the ammonia pressure was decreased, the light emitted from the plasma increasingly resembled that observed for nitrogen plasmas (red color) suggesting a predominance of atomic nitrogen in the plasma. In accordance with this, preliminary experiments with ammonia discharges on PG showed that a higher coverage of nitrogen-containing functional groups could be obtained with higher pressure discharges (2 Torr NH_3). Not only were low pressure discharges less effective but at these pressures (0.2 Torr NH_3), an increase in surface oxygen content was found in comparison to that observed on PG prior to ammonia plasma exposure. It was concluded that in the N_2-like plasmas (0.2 Torr), the nitrogen radicals (atomic nitrogen) were less effective in addition reactions with the graphitic surface than were species such as NH· and NH_2· which were expected to be present at higher concentrations in the higher pressure ammonia plasmas (2 Torr). The increase in oxygen content resulting from the low pressure ammonia discharges probably reflects the effectiveness of the N_2-like plasma in generating long-lived surface free radical sites which ultimately react with oxygen and/or water during transfer of samples from the plasma chamber to the XPS spectrometer (cf. ref. *23* and *24*). An alternative explanation for the observed trend in oxygen content with discharge pressure would be that a higher relative partial pressure of oxygen is present in the ammonia discharge at lower pressures because of leakage. As such, atomic oxygen may effectively compete with nitrogen-containing free radicals for surface addition sites.

To evaluate whether or not oxygen functional groups can be removed or displaced by either argon or ammonia plasmas to produce a higher coverage of nitrogen groups, a series of

Table IV. XPS Analyses of PG Samples Treated According to Steps Listed in Table III

sample	binding energies, eV	peak FWHM, eV	O/C elemental ratio[a]	N/C elemental ratio[a]	N/O elemental ratio[a]
6	C(1s) = 284.3	1.17	0.051	0.089	1.74
	N(1s) = 399.0	2.70			
	O(1s) = 532.3	3.20			
7	C(1s) = 284.3	1.20	0.10	---	---
	O(1s) = 532.8	2.60			
8	C(1s) = 284.3	1.15	0.044	0.057	1.31
	N(1s) = 399.1	2.65			
	O(1s) = 532.3	2.90			
9	C(1s) = 284.3	1.15	0.043	0.106	2.48
	N(1s) = 399.5	2.70			
	O(1s) = 532.4	2.70			

[a] Corrected for elemental cross section, see Experimental.

experiments were undertaken in which PG samples were exposed first to an argon or oxygen plasma followed by a high pressure (2 Torr) NH_3 plasma. The XPS results of O/C, N/C, and N/O elemental ratios for electrode samples, 6 to 9, as treated by steps listed in Table III are tabulated in Table IV.

The main conclusion to be drawn from these data is that the removal of oxygen functional groups on the surface is difficult and such groups cannot be completely eliminated. However, treatment with an inert gas such as argon is effective in promoting the introduction of nitrogen-containing groups during subsequent NH_3 plasmas (see N/O elemental ratio for samples 6 and 9). Although there is an increase in the N/O ratio when PG is reacted first in an oxygen plasma followed by ammonia (cf. samples 8, Table IV), this increase may be the consequence of the O_2 plasma providing a larger area of exposed edge planes at which the constituents of the NH_3 plasma react more readily.

The binding energy data reported in Table IV do not provide much insight into the identity of the nitrogen groups on the carbon surface. There appears to be no significant coverage by species in which oxygen and nitrogen are bonded to one another. Nitro and nitroso groups if present would show N(1s) peaks at substantially higher binding energies, ca. 402–405 eV (*55*, *56*). The high resolution spectra are equally uninformative although the broadness of the O(1s) and N(1s) peaks reflects the presence of several different types of groups.

To ascertain the relative concentrations of basic (synthetically useful) and nonbasic nitrogen groups introduced onto PG by the NH_3 plasma, several samples were treated and subsequently equilibrated with gaseous HBr. In these experiments, evaluation of additional plasma parameters was sought, i.e., the stabilization of basic surface groups via HBr salt formation (*57*), the reproducibility of NH_3 plasma treatment in general, and the relative percentage of nitrogen groups which were readily hydrolyzable (e.g., imine and amide groups).

Table V summarizes the results. The invariance of the XPS elemental ratios for samples 11 to 14 indicates that relatively good reproducibility could be attained for the gaseous HBr equilibration. More importantly, the average Br/N elemental ratio of 0.62 (±0.12) suggests that a considerable fraction of the nitrogen-containing groups was not sufficiently basic to form HBr salts (such as nitriles, see ref. *58*). The nitrogens that do form HBr salts are presumed to be groups such as imines, amides, or amines. It should be noted that high resolution spectra of the N(1s) band of HBr equilibrated samples was considerably broadened (FWHM = 3.40 eV) compared to the unequilibrated samples (FWHM = 2.70 eV, Table IV) as would be expected from HBr surface salt formation. However, no unique band was resolved which could

Table V. Evaluation of Ammonia Plasma Treatment of PG Involving Subsequent Equilibration with Gas Phase Hydrogen Bromide[a]

sample	O/C elemental ratio[b]	N/C elemental ratio[b]	Br/C elemental ratio[b]	N/O elemental ratio[b]	Br/N elemental ratio[b]
10[c]	0.047	---	---		---
11	0.035	0.044	0.035	1.26	0.80
12	0.046	0.071	0.041	1.54	0.58
13	0.045	0.069	0.038	1.53	0.55
14	0.047	0.071	0.040	1.51	0.56
av 11-14	0.043 (±0.006)[d]	0.064 (±0.013)	0.039 (±0.003)	1.46 (±0.13)	0.62 (±0.12)
11, washed[e]	0.052	0.019	---	0.58	---

[a] NH_3 plasma treatment for 5 min at 2 Torr, followed by equilibration with NH_3 for 5 min at 2 Torr, followed by evaluation to base pressure (10 mTorr) and equilibration with HBr for 5 min at 3 Torr. [b] From XPS analysis, corrected for cross section (see Experimental). [c] Control; treated exactly the same as samples 11-14 with exception of NH_3 plasma treatment (see footnote *a*). [d] Parentheses contain 1 standard dev. [e] Sample 11 was subsequently washed in triply distilled water for 0.5 h, dried in vacuo (ambient temperature, 10 mTorr) re-analyzed via XPS.

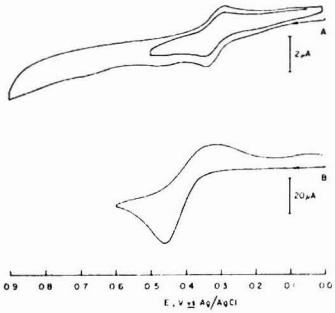


Figure 7. Cyclic voltammetric behavior of (A) ammonia plasma treated PG (sample 9, Table III) in pH 2.50 glycine buffer and (B) untreated PG in 0.4 mM *p*-phenylenediamine in pH 2.50 glycine buffer. Sweep rate was 50 mV/s and electrode area was 0.52 cm^2 in both cases

Table VI. Effects of Ammonia Plasma Treatment on the Basal Plane of HOPG[a]

sample	length of exposure, min	O/C elemental ratio[b]	N/C elemental ratio[b]	N/O elemental ratio[b]
A[c]	0	nil	nil	---
B	2	0.008	nil	---
C	5	0.025	0.082	3.28
D	10	0.018	0.047	2.61
E	20	0.021	0.045	2.14

[a] NH_3 plasma treatment at 2 Torr for the indicated time period, followed by equilibration with NH_3 for 5 min at 2 Torr. [b] From XPS analysis, corrected for cross section (see Experimental). [c] Control, no plasma treatment, only equilibration with NH_3.

be assigned to protonated nitrogen. For sample 11, which was hydrolyzed following initial XPS analysis and then reanalyzed, some conclusions may be drawn regarding the relative coverage of nitrogen groups which are readily hydrolyzable vs. those which are not. Assuming quantitative reaction of such groups with HBr (57), one may assume that the Br/N ratio of 0.80 indicates that ca. 80% of the N has formed HBr salt leaving ca. 20% of the N(1s) signal assignable to surface nitriles. Of the original nitrogen content of 0.044 N/C, 0.019 N/C remains following hydrolysis. Those nitrogen groups lost or transformed during hydrolysis are presumed to be imines and amides, each of which would be hydrolyzed to a group containing an additional oxygen atom (quinones and carboxylic acids, respectively). Therefore, an increase in the O/C ratio after hydrolysis is expected and is observed (Table V). The nitrogen lost during hydrolysis indicates that 57% of the original nitrogen-containing functional groups are imines and amides, and by difference 23% of the original surface nitrogen content is attributable to unhydrolyzable, basic functionalities—amines. In summary, of the nitrogen-containing functional groups introduced by the ammonia plasma, approximately 80% are synthetically useful (amines, imines, and amides), although only a third of these are stable toward hydrolysis. The electrochemical response of PG electrodes treated with ammonia plasmas (Figure 7, curve A) is dominated by the surface electrochemistry seen for the oxygen plasma treated surfaces. There are subtle differences which are most noticeable on the first anodic scan: a broad wave at ca. +0.2 V and a better defined wave with a peak potential of +0.47 V, both of which are diminished on the subsequent scan and absent by the third. The nature of the surface species giving rise to the low potential wave is unknown. The process of +0.47 V could be a *p*-phenylenediamine-like species by analogy to the aqueous electrochemistry of this molecule at unmodified PG (Figure 7, curve B). The reaction of such a surface species by an EC process (hydrolysis of the oxidized form) would be expected to be relatively rapid (59) and therefore the loss of the wave at +0.47 V is not surprising.

Ammonia Plasma Treatment of HOPG. It was of interest to determine whether or not the ammonia plasma was capable of modifying HOPG as had been found in the case of the oxygen plasma. A series of experiments was carried out using higher pressure (2 Torr) ammonia discharges on freshly cleaved/methanol extracted, HOPG basal plane. Plasma exposure times were varied as indicated in Table VI. It should be noted that the N/C ratios found from these treatments are approximately the same as found on the isotropic pyrolytic material; yet in all cases oxygen was also found in the XPS spectra. The binding energies of the N(1s) and O(1s) bands were 398.8 and 531.5 eV, respectively, with corresponding FWHMs of 2.60 and 2.70 eV. Compared to the results found on ammonia plasma treated PG, these bands are slightly narrower and of lower binding energy, although probably not significantly so. There is no reason to believe that the oxygen- and nitrogen-containing functionalities on ammonia plasma treated HOPG basal plane are different from those found on PG.

Reaction of Hydrogen Bromide Plasmas with PG. Preliminary experiments were undertaken in attempts to brominate PG surfaces. A brominated carbon surface would be an advantageous precursor to reactions with organometallic intermediates such as organolithium and Grignards for attachment of terminal reactants. However, HBr plasmas under various pressures were rather ineffective and XPS analysis indicated that the extent of bromination was minimal (only trace Br detected). Experiments are underway with other

gaseous reactants in the plasma in attempts to yield high coverage of surface halogenation.

CONCLUSIONS

RF plasmas provide a means of conveniently introducing oxygen and nitrogen functional groups rapidly and cleanly on various carbon surfaces. Steady-state concentration of the groups is attained due to two competing effects; that is, the removal of surface atoms or fragments by etching reactions and addition reactions between reactive sites and the reactant species in the plasmas. Thus, surface area roughening occurs to varying extents depending on the reactant species, gas pressure, and particular carbon material.

The structural damage to the near surface region is minimal (as evidenced by the retention of narrow FWHM of C(1s) bands) by comparison to argon ion bombardment with subsequent molecular oxygen or oxygen plasma treatment (*46*). Such observations are important if the modified carbon surfaces are to be used for electrochemical purposes. For PG, there is an increase in synthetically useful oxygen-containing groups, notably carboxyl and hydroxyl groups. The primary species generated in the oxygen plasma may be atomic oxygen although the excited states of oxygen and ground state ozone cannot be ruled out. The mechanism of oxygen group incorporation may be the electrophilic attack of oxygen free radicals at graphitic sites. It should be noted, in addition, that RF discharges are excellent sources of broadband electromagnetic radiation and that radiative energy transfer to the surface may be an important factor. It seems, however, that with respect to the *surface* of the substrates being studied, direct energy transfer and addition of plasma components to the surface might be expected to be relatively more important than processes involving radiative excitation of surface structures, by analogy to the recent work of Clark and Dilks (*60*) on plasma treatment of polymeric materials.

With respect to the NH_3 plasmas, the presence of substantial oxygen in all of the treated samples, as indicated by XPS analysis, makes it difficult to ascertain whether or not the components of the NH_3 plasma reacted directly with carbon. In fact, oxygen is detected at shorter exposure times (sample B, Table VI) than those required for the formation of detectable surface nitrogen. Unfortunately, because samples are exposed to atmospheric oxygen during transfer from the plasma chamber to the XPS spectrometer, the possibility of oxygen incorporation during sample transit cannot be eliminated. Another possibility, although less likely, is that surface imino groups were hydrolyzed by water (in the atmosphere) during transfer and resulted in the incorporation of oxygen. Regardless of the mechanism, nitrogen groups introduced by RF treatment under the present conditions always resulted in some oxygen functionalities on the carbon surface.

The versatility of RF plasmas for introducing a variety of surface functional groups and their respective optimization needs to be further explored. A further consideration is that plasmas may be effective in abstracting atomic species from surfaces (*39*, *40*) and that the surface free radical sites formed are sufficiently long lived to be synthetically useful. Such a mechanism may explain why the argon pretreatment was effective in the NH_3 plasma (see sample 9, Tables III and IV) as well as the amine surface on carbon generated by Oyama and Anson (*24*, *25*). We believe that the present RF approach, because of its rapidity and convenience, will provide means of surface modification of great utility for electrochemical as well as chromatographic purposes.

ACKNOWLEDGMENT

The authors are indebted to W. A. Moore and the Union Carbide Company for the kind gift of HOPG samples.

LITERATURE CITED

(1) B. F. Watkins, J. R. Behling, E. Kariv, and L. L. Miller, *J. Am. Chem. Soc.*, **97**, 3459 (1975).
(2) B. E. Firth, L. L. Miller, M. Mitani, T. Rogers, J. Lennox, and R. W. Murray, *J. Am. Chem. Soc.*, **98**, 8271 (1976).
(3) B. E. Firth and L. L. Miller, *J. Am. Chem. Soc.*, **98**, 8272 (1976).
(4) C. M. Elliot and R. W. Murray, *Anal. Chem.*, **48**, 1247 (1976).
(5) P. R. Moses and R. W. Murray, *J. Am. Chem. Soc.*, **98**, 7435 (1976).
(6) R. J. Burt, G. J. Leigh, and C. J. Pickett, *J. Chem. Soc., Chem. Commun.*, 940 (1976).
(7) M. Fujihira, T. Matsue, and T. Osa, *Chem. Lett.*, 875 (1976).
(8) A. P. Brown, C. Koval, and F. C. Anson, *J. Electroanal. Chem.*, **72**, 379, (1976).
(9) P. R. Moses and R. W. Murray, *J. Electroanal. Chem.*, **77**, 393 (1977).
(10) D. G. Davis and R. W. Murray, *Anal. Chem.*, **49**, 194 (1977).
(11) J. R. Lenhard and R. W. Murray, *J. Electroanal. Chem.*, **78**, 195 (1977).
(12) J. C. Lennox and R. W. Murray, *J. Electroanal. Chem.*, **78**, 395 (1977).
(13) J. F. Evans, T. Kuwana, M. T. Henne, and G. P. Royer, *J. Electroanal. Chem.*, **80**, 409 (1977).
(14) A. P. Brown and F. C. Anson, *Anal. Chem.*, **49**, 1589 (1977).
(15) J. F. Evans and T. Kuwana, *Anal. Chem.*, **49**, 1633 (1977).
(16) S. Mazur, T. Matusinovic, and K. Cammann, *J. Am. Chem. Soc.*, **99**, 3888 (1977).
(17) A. W. C. Lin, P. Yeh, A. M. Yacynych, and T. Kuwana, *J. Electroanal. Chem.*, **84**, 411 (1977).
(18) M. Fujihira, T. Osa, and A. Tamura, *Chem. Lett.*, 361 (1977).
(19) G. J. Leigh and C. J. Pickett, *J. Chem. Soc., Dalton Trans.*, 1797 (1977).
(20) C. A. Koval and F. C. Anson, *Anal. Chem.*, **50**, 223 (1978).
(21) A. M. Yacynych and T. Kuwana, *Anal. Chem.*, **50**, 640 (1978).
(22) A. F. Diaz and K. K. Kanazawa, *J. Electroanal. Chem.*, **86**, 441 (1978).
(23) M. S. Wrighton, R. G. Austin, A. B. Bocarsly, J. M. Bolts, O. Haas, K. D. Legg, L. Nadjo, and M. C. Palazzotto, *J. Electroanal. Chem.*, **87**, 429 (1978).
(24) N. Oyama, A. P. Brown, and F. C. Anson, *J. Electroanal. Chem.*, **87**, 435 (1978).
(25) N. Oyama and F. C. Anson, *J. Electroanal. Chem.*, in press.
(26) A. Diaz and M. Genies; A. Diaz, F. A. Orozco Rosales, and K. K. Kanazawa, IBM Research Labs, San Jose, Calif., private communications, 1978.
(27) D. C. S. Tse and T. Kuwana, *Anal. Chem.*, **50**, 1315 (1978).
(28) L. L. Miller and M. R. Van de Mark, *J. Am. Chem. Soc.*, **100**, 639 (1978); *ibid.*, p. 3223.
(29) A. Merz and A. J. Bard, *J. Am. Chem. Soc.*, **100**, 3222 (1978).
(30) F. Kaufman, Abstracts, IUPAC meeting, Tokyo, Japan, September 1977.
(31) M. Fujihira, N. Ohishi, and T. Osa, *Nature (London)*, **268**, 226 (1977).
(32) M. Fujihira and T. Osa, *Nature (London)*, **264**, 349 (1976).
(33) D. D. Hawn and N. R. Armstrong; N. R. Armstrong and R. Shepard, Michigan State University, East Lansing, Mich., private communications, 1978.
(34) R. F. Lane and A. T. Hubbard, *J. Phys. Chem.*, **77**, 1401 (1973).
(35) R. F. Lane and A. T. Hubbard, *J. Phys. Chem.*, **77**, 1411 (1973).
(36) H. L. Landrum, R. T. Salmon, and F. M. Hawkridge, *J. Am. Chem. Soc.*, **99**, 3154 (1978).
(37) J. C. Stargardt, F. M. Hawkridge, and H. L. Landrum, *Anal. Chem.*, **50**, 930 (1978).
(38) H. Tachikawa and L. R. Faulkner, *J. Am. Chem. Soc.*, **100**, 4379 (1978).
(39) J. R. Hollahan and A. T. Bell, Ed., "Techniques and Applications of Plasma Chemistry", John Wiley & Sons, New York, 1974.
(40) Mitchel Shen, Ed., "Plasma Chemistry of Polymers", Marcel Dekker, New York, 1976.
(41) P. Cadman, J. D. Scott, and J. M. Thomas, *Carbon*, **15**, 75 (1977).
(42) M. Babai, N. Tshernikovski, and E. Gileadi, *J. Electrochem. Soc.*, **119**, 1018 (1972).
(43) C. D. Wagner, *Anal. Chem.*, **44**, 1051 (1972).
(44) R. S. Nicholson, *Anal. Chem.*, **37**, 1351 (1965).
(45) R. L. Birke, *Anal. Chem.*, **50**, 1489 (1978).
(46) S. Evans and J. M. Thomas, *Proc. R. Soc., London, Ser. A*, **353**, 103 (1977).
(47) J. P. Randin and E. Yeager, *J. Electroanal. Chem.*, **58**, 313 (1975).
(48) J. P. Randin and E. Yeager, *J. Electroanal. Chem.*, **36**, 257 (1972).
(49) J. M. Thomas, E. L. Evans, M. Barber, and P. Swift, *Trans. Faraday Soc.*, **67**, 1875 (1971).
(50) M. Barber, E. L. Evans, and J. M. Thomas, *Chem. Phys. Lett.*, **18**, 423 (1973).
(51) B. D. Epstein, E. Dalle-Molle, and J. S. Mattson, *Carbon*, **9**, 609 (1971).
(52) G. R. Hennig, G. J. Dienes, and W. Kosiba, *Proc. Second Int. Conf. Peaceful Uses of Atomic Energy*, **7**, 301, (1958).
(53) J. R. Hollahan, B. B. Stafford, R. D. Falb, and S. T. Payne, *J. Appl. Polymer Sci.*, **13**, 807 (1969).
(54) J. C. Devins and M. Burton, *J. Am. Chem. Soc.*, **76**, 2618 (1953).
(55) E. Sokolowski, C. Nordling, and K. Siegbahn, *Phys. Rev.*, **110**, 776 (1958).
(56) G. C. Allan and P. M. Tucker, *J. Chem. Soc., Dalton Trans.*, 470 (1973).
(57) J. Hlavay and G. G. Guilbault, *Anal. Chem.*, **50**, 965 (1978).
(58) H. Yasuda, H. C. Marsh, S. Brandt, and C. N. Reilley, *J. Polymer Sci., Polymer Chem. Ed.*, **15**, 991 (1977).
(59) R. N. Adams, "Electrochemistry at Solid Electrodes", Marcel Dekker, New York, 1969, pp 356–360.
(60) D. T. Clark and A. Dilks, *J. Polymer Sci.*, **15**, 2321 (1977).

RECEIVED for review August 23, 1978. Accepted November 29, 1978. The support provided by NSF (Grants CHE76-81591 and CHE76-04911 and the U.S. Public Health Service (Grant GM19181) is hereby gratefully acknowledged.

Metal-Ion Chelation Chromatography on Silica-Immobilized 8-Hydroxyquinoline

John R. Jezorek[1] and Henry Freiser*

Department of Chemistry, University of Arizona, Tucson, Arizona 85721

A chromatographically useful packing is prepared by immobilizing 8-hydroxyquinoline on Porasil. This material, whose capacity is about 50 μequiv/g, behaves with an efficiency of about 0.2–0.5 mm/theoretical plate but is capable of separating such similar metal ions as Co–Ni, Cd–Pb–Zn, and La–Gd–Yb at trace levels employing both isocratic and continuous gradient elution. On a fundamental level, the relationship between solution chelate stability and chromatographic behavior is described.

Although chromatographic techniques have been widely used for the separation and identification of organic compounds, they have been somewhat less extensively employed for metal analysis (*1*, *2*).

To be sure, excellent metal ion separations have been achieved using ion exchange (*3*, *4*) but with conventional resins selectivity factors are relatively low. Reverse phase extraction chromatography (*5*, *6*) makes use of more selective metal ion extractants, but like all liquid–liquid chromatographic techniques, this faces the often severe problem of bleeding of the stationary phase (*7*, *8*). This problem can be solved generally by chemical bonding of suitable moieties to solid substrates (*9–11*). Hence, chemically bonded chelating agents on suitable chromatographic supports would seem to be an appropriate medium for several ion separations. Recently several such materials have been described. Corning Glass has produced 8-hydroxyquinoline (oxine) and ethylenediaminetriacetic acid on Controlled Pore Glass (CPG) and Bio-Rad offers Chelex 100, imminodiacetic acid on a polystyrene–divinylbenzene copolymer.

Dimethylglyoxime (*12*), ferroin-type chelating agents (*13*), hexylthioglycolate (*14*), alkylamines, and thiocarbamates (*15*, *16*), 8-amino- (*17*) and 8-hydroxyquinolines (*18–20*), have all been immobilized on various substrates.

The major use of these interesting new materials has been in the preconcentration of trace levels of metal ions from dilute aqueous samples or for relatively simply separations of pairs of metal ions having widely disparate chelate formation constants by step gradient techniques (*21*, *22*). The behavior of these new materials under truly chromatographic conditions (both isocratic and continuous gradient elution) has not yet been explored. This is the major objective of the work reported here.

We have selected oxine (HOx) because this reagent is well characterized. Over 60 metal ions react with oxine to form complexes whose aqueous phase formation constants range from about $10^4(Ba^{2+})$ to $10^{38}(Fe^{3+})$. Several types of metal oxinates are known: the simple MOx_n for coordinatively saturated metal ions (i.e., those whose coordination number is twice their electrovalence), and adduct chelates $MOx_n \cdot \alpha HOx$ for coordinatively unsaturated metal ions. In this study we are concerned with the characterization of immobilized oxine and its chromatographic use in separating a number of divalent and trivalent metal ions. A particular point of interest is the relation of the aqueous phase oxine chemistry to the chromatographic behavior of the immobilized reagent.

[1] On leave during the 1977–78 academic year from the Department of Chemistry, University of North Carolina at Greensboro, Greensboro, N.C. 27412.

EXPERIMENTAL

Apparatus. The chromatographic system is shown schematically in Figure 1. Everything within the large square is part of the Spectra Physics (Santa Clara, Calif. 95051) 3500B liquid chromatograph. Eluent from reservoir A and/or B is sent to the 1.2-mL mixing chamber of pump A and/or B, and thence to the injection valve, a Valco Instruments (Houston, Texas 77024) Model CV-6-UHPa-N60, equipped with a 10-μL sample loop. Column effluent is sent to a Plexiglas mixing "Y", 2.5 cm diameter × 1.5 cm high, with 1.8-mm channels bored to accept $^1/_4$-28 Cheminert-type plastic fittings. Indicating solution is brought to the mixing "Y" by a peristaltic pump (Gilson Minipuls II, Gilson Medical Electronics, Inc., Middleton, Wis. 53562), using standard PVC pump tubing equipped with $^1/_4$-28 Cheminert-type end fittings (Laboratory Data Control, Riviera Beach, Fla., 33404).

The column effluent–indicator mixture then goes to a Schoeffel Instruments (Westwood, N.J. 07675) Model 770, dual beam UV-visible spectrophotometric detector. All tubing from the end of the column to the detector is 0.8-mm i.d. Teflon, equipped with Cheminert or Altex Scientific (Berkeley, Calif. 94715) $^1/_4$-28 fittings. Mixing coils about 1 m long were provided downstream from the peristaltic pump and mixing "Y". These were constructed from 0.8-mm i.d. Teflon tubing wrapped around a plastic cylinder, and immersed in a dish of water at ambient temperature. The mixing coils were employed to smooth out the pulses from the peristaltic pump and to ensure complete mixing of the indicator–column effluent streams. The water bath helped to smooth temperature gradient-caused spectrophotometric noise. Both stainless steel and glass columns were used. The stainless steel was a standard $^1/_4$ in. tube, 25 cm × 3.2 mm i.d. and the glass was 6-mm o.d., 25 cm × 4 mm i.d., equipped with standard $^1/_4$ in. stainless steel end fittings and Teflon ferrules or rubber O-rings. Before packing, the glass columns were treated sequentially with 6 M HNO_3, dilute EDTA solution, water, and oven dried. This was followed by rinsing with dichlorodimethylsilane for several minutes, baking at 85 °C in an oven, and water rinsing. All columns were dry packed.

Spectrophotometric data were taken on either a Cary 14 (Varian Instruments, Palo Alto, Calif. 94304) or Beckman DB (Beckman Instruments, Inc., Irvine, Calif. 92713) recording device or a Guilford Instrument Co (Oberlin, Ohio 44074) Model 2400 single-beam spectrophotometer.

Reagents and Solutions. Unless otherwise noted, all chemicals were analytical reagent grade quality, and were used as received. Various purifications of water were performed, from distilled–deionized to distilled–triply deionized–distilled (dd^3d). The quality of the latter was found to be about the same as that which was redistilled from a Corning Megapure Still (Corning Glass Works, Corning, N.Y. 14830). The dd^3d water was made by taking the house-distilled water, passing it rapidly through a Crystalab Deeminizer cartridge (Crystalab, Hartford, Conn. 06106) letting it drip slowly through a second cartridge, and finally through a 25 cm × 25 mm bed of Dowex 50W-X8 cation exchange resin. This was then distilled from an all-glass apparatus which had been washed with 1:1 HNO_3.

The Corning 8-hydroxyquinoline (GPG-550), 300–600 μm, was obtained from Pierce Chemical Co. (Rockford, Ill. 61105). Porous silica, 37–74 μm, (Porasil B) was purchased from Waters Associates (Framingham, Mass. 01710). 4-(2-Pyridylazo)resorcinol (PAR) was obtained from Eastman Organic Chemicals (Rochester, N.Y. 14650) and used as received. Triethylamine (Eastman), technical grade, was used as received, as was the γ-aminopropyltriethoxy

0003-2700/79/0351-0366$01.00/0 © 1979 American Chemical Society

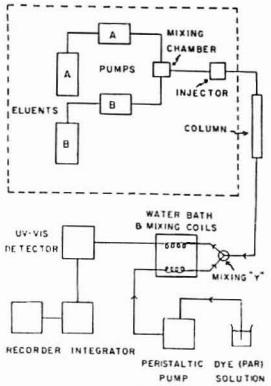


Figure 1. Schematic diagram of chromatograph and detection system. (--- indicates SP3500B liquid chromatograph)

silane (PCR Inc., Gainesville, Fla. 32602). 8-Hydroxyquinoline was recrystallized several times from ligroin.

Porasil–8OHQ was prepared using Hill's procedure (*18*). Some difficulty was encountered while reducing the $-NO_2$ group to $-NH_2$ with sodium dithionite. Apparently some elemental sulfur formed, which had to be washed out with carbon disulfide and ethanol. It should be noted that this procedure yields a phenylazo-8-hydroxyquinoline (see below).

Metal ion sample solutions were generally from 1 to 5×10^{-4} M. (~10–50 ppm) in metal perchlorate (G. F. Smith Chemical Co., Columbus, Ohio 43223). Gadolinium and ytterbium solutions were made from the chloride salts, lanthanum from the nitrate.

PAR solutions were generally about 3×10^{-5}M in PAR (6.4 mg PAR per liter), 0.5 M in NH_4Cl, to which 30 mL of 1×10^{-3} M ZnEDTA reagent had been added, as well as sufficient concentrated NH_3 to obtain pH 11. PAR solutions at pH 9 (0.05 M NH_4^+/NH_3 buffer) did not contain ZnEDTA. Chromatographic studies of the lanthanides solutions utilized 3×10^{-4} M PAR solutions which were 0.1 M in THAM (tris(hydroxymethyl)-aminomethane) and brought to pH 7 with HCl.

ZnEDTA reagent was prepared by adding from a buret an equivalent amount of zinc perchlorate to a 10^{-2} M EDTA solution. Both solutions were standardized using Eriochrome Black T indicator in the usual way (*23*).

All solution and water containers were soaked overnight in 1:1 H_2O–HNO_3, rinsed, and soaked overnight again in a dilute EDTA wash solution at about pH 8–9. These were periodically rinsed again with the HNO_3 wash solution before being finally rinsed with water. Most solutions were stored in polyethylene bottles to minimize contamination.

Capacity Values. Capacities of controlled pore glass- or Porasil-immobilized oxine were determined by adding a known excess of 10^{-2} M copper(II) nitrate solution to a known weight of the chelating substrate, shaking for 30 min, decanting or filtering to separate the solid from the liquid phase, washing the substrate, combining all filtrate portions and washings, and titrating the residual copper(II) with 10^{-2} M EDTA using murexide indicator (*23*). The amount of excess Cu(II) was subtracted from the total used to obtain the amount absorbed.

The capacity of the material in a column was determined by first flushing the column with 0.1 M HNO_3, followed by water. Then a 10-mL portion of 10^{-2} M copper(II) nitrate was passed through the column using the peristaltic pump. Excess Cu(II) was flushed off the column with water. The effluent containing the excess Cu(II) was titrated with EDTA as noted above for bulk capacity studies.

The amount of Cu(II) adsorbed was also determined by stripping the metal from the column with about 15 mL of 0.1 M HNO_3, neutralizing with 1 M NH_3, and titrating the Cu(II) in this eluate with EDTA as above. The average of two runs, using capacity calculated from titration both of unabsorbed Cu(II) and that of the Cu(II) eluate from the saturated column, was used for the column capacity value (Table I).

Table I. Characteristics of Immobilized Oxine Columns[a]

	Corning CPG–8OHQ	Porasil–8OHQ
particle size, μM[b]	300–600	37–75
surface area, M^2/g[b]	70	140–230
pore diameter, A[b]	550	150
weight of packing in column, g	1.10	1.54
column void volume, mL	1.12	2.30
bonded oxine, μequiv/g	30[b]	54,
	22	49[c]
surface coverage, oxine groups per 10^4 A^2	18	18[d]
column capacity, μequiv oxine	24	83

[a] Column dimensions, 250 × 4 mm i.d. [b] Manufacturer's values. [c] Column capacity after 40 days. [d] Based on an average area of 185 M^2/g.

In all these measurements, it was assumed that the stoichiometry of the bonded copper complex was 1:1. This assumption was confirmed by a potentiometric titration of a gram of the Porasil–8OHQ in a solution containing 102.3 μmol HCl with 0.0153 M NaOH. From the observed end point at 3.36 mL, the capacity of 51.6 μmol/g was calculated. The capacity values listed in the Table are those found from the copper determination, which we think are more reliable. Values of the pK_a of the immobilized 8-hydroxyquinoline obtained from the potentiometric titration, 3.3 and 6.2, are in reasonable agreement with those observed by Takamoto et al, (*24*), making allowances for the solvent medium difference.

Distribution Coefficients. To about 200 mg (≈10 μequiv) of dried Porasil–8OHQ in a screw-cap vial, 0.50 mL of 10^{-2} M Cd(II) or Ni(II) solution, the appropriate amount of pH 1 or pH 2 HNO_3, and water to bring the volume to 10 mL were added. To obtain pH values above 4, dropwise addition of 0.1 M NH_3 was used. No acid or base was added to the pH 3.6 Cd(II) sample. The mixture was shaken for about 30 min, allowed to settle, and a portion taken for pH measurement. The solid was separated from the liquid by filtration using a fritted-glass funnel, and washed with water. All filtrate portions and washings were combined and titrated with 10^{-3} M EDTA using Eriochrome Black T indicator after pH adjustment to 9 or 10 with NH_4^+/NH_3 buffer for Cd(II); or an excess of 10^{-3} M EDTA added, and back titration performed with 10^{-3} M Zn(II) at pH 10 for Ni(II) studies.

General Conditions. The chromatography columns were periodically flushed with 1 M $HClO_4$ or 0.1 M HNO_3 to remove any noneluted metal contaminants such as copper(II), iron(III), chromium(III). The 1 M $HClO_4$ was pumped directly through the columns using the peristaltic pump to minimize corrosion of the LC pump and tubing. Before injecting any sample, the column was first conditioned with 15–20 mL of the eluent to be used or eluent component if gradient elution was employed. The detector was disconnected from the column during conditioning, which was normally conducted at a flow rate of 2 mL/min. Most chromatographic runs were performed at 1 mL/min flow rate. PAR indicator was mixed at 1 mL/min with the column effluent, giving an overall 2 mL/min flow rate through the spectrophotometric detector. The detector was set at 510 nm for most studies, as this appeared to be the optimum setting when several metals were being investigated (*25*). The indicator solution was 3×10^{-5} M in PAR and ZnEDTA, NH_3/NH_4Cl buffered at pH 11. Samples were 10 μL, 5×10^{-4} M in each metal.

Chromatographic Peak Measurements. Base lines were approximated as carefully as possible and peak heights (H) and widths at $H/2$ ($W_{1/2}$) were measured. Areas were calculated as $H \times W^{1/2}$. Peak widths, W_b, were calculated as $1.7 \times W_{1/2}$. Peak areas and widths were normalized to those obtained under conditions for which the sample was eluted at or near the column void volume.

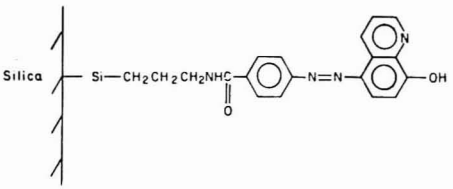
Void Volumes. The overall void volume was obtained by observing the base-line change on switching eluent from water to 0.1 M HNO_3, or vice-versa. Void volume of system tubing, mixing coil, etc., was obtained by injecting a metal ion and

observing its retention time with the column removed from the system. Column void volume was the difference in these two values.

Metal Ion Detection. The metal ions were detected spectrophotometrically by post-column blending of the eluate with a PAR or $Zn(PAR)_2$-EDTA system described elsewhere (25).

RESULTS AND DISCUSSION

Characteristics of Immobilized Oxine Columns. The characteristics of the Corning CPG-8OHQ and the Porasil-8OHQ are compared in Table I. The major differences in the surface areas and the amounts of oxine bonded to the surfaces are reconciled by essentially the same surface density of oxine groups ($\sim 18/10^4$ Å^2). As mentioned above, the immobilized ligand incorporated in both these materials is actually the phenylazo-8-hydroxyquinoline shown below.



The efficiency of the Corning column proved to be extremely low. The only separation which could be effected were between metals having widely different oxine chelate stability constants, so that at a particular eluent pH, one metal would be washed off the column while the other would not move at all. Separations of which the Porasil-8OHQ column was easily capable, such as Cd from Zn, or Cd from Pb (vide infra) produced only single, at best, somewhat unsymmetrical peaks on the Corning column. Probably the large and wide-ranging size of the CPG particles (300–600 μM) contributed to poor metal ion-stationary phase interaction. Further, as can be seen in Table I, the larger surface area of the Porasil-8OHQ resulted in about three times as many oxine groups in an equivalent volume of stationary phase, despite the fact that the coverage per unit area is about the same for the two materials. These observations led us to abandom any further attempts to use the CPG-8OHQ for chromatographic purposes.

The capacity of the Porasil-8OHQ column was checked after about 3 months. During that time, the column was in use for a total of 300 h. The rest of the time, it was stored with water on the column, at about pH 3–5. Whenever it was washed with 1 M $HClO_4$ to remove all adsorbed metal ions, a slightly orange effluent resulted, indicating some degradation of the material: yet the capacity of the column dropped only to 49 μequiv/g compared to about 54 μequiv/g when new, an 8% decrease. As it was found that sufficiently good column cleaning was obtained with 0.1 M HNO_3, which produced little or no column degradation, use of the 1 M HNO_3 was abandoned except for occasional thorough column washing, e.g., if column capacity was to be determined.

Chromatographic Behavior of Porasil-8OHQ. A simple criterion serves to distinguish "column washing" and true chromatographic behavior. In the former, the metal ion is washed through with the eluent, because, at the pH employed, it has little or no tendency to be bound by oxine, and its distribution coefficient, D, therefore is very low. D is obtained from the equation

$$V_r = V_m + DV_s \quad (1)$$

where V_r is the retention volume, V_m and V_s the volumes of the mobile and stationary phases, respectively. As a result, small retention volumes and peak widths, W, will be observed. Chromatographic behavior will occur when the D value becomes appreciable. This follows from a sufficient rise in eluent pH as may be seen from the equation

$$M^{n+} + HOx(\text{bound}) \overset{K_1}{\rightleftharpoons} M\text{-}Ox(\text{bound}) + H^+ \quad (2)$$

which is similar to the homogeneous reaction equilibrium

$$M^{n+} + HOx \overset{K_{PD}}{\rightleftharpoons} MOx^{(n-1)+} + H^+ \quad (3)$$

The extent of reaction 3 is described by the proton displacement constant, K_{PD}, which is equal to the product of the ligand dissociation constant, K_a, and the 1:1 metal chelate formation constant, β_1. Thus

$$K_{PD} = \frac{[MOx][H^+]}{[M^{n+}][HOx]} = K_a \beta_1 \quad (4)$$

Although the exchange constant K_1 of Equation 2 cannot be directly compared with K_{PD} because of the different standard states for bound oxine and bound chelate from those for the corresponding dissolved species, one might nevertheless expect values of K_1 and K_{PD} to parallel one another from metal to metal. Similarly, the value of the metal distribution ratio, D_1 as derived from Equation 1

$$D = \frac{[M\text{-}Ox(\text{bound})]}{[M^{n+}]} = K_1 \frac{[HOx](\text{bound})}{[H^+]} \quad (5)$$

varies with K_1 and hence with β_1, the formation constant of $MOx^{(n-1)+}$. Equation 5 also predicts that log D should increase linearly with pH at a slope of unity, since the concentration of the bound oxine is invariant in a particular batch of stationary phase.

The column behavior of Cd(II), Zn(II), Co(II), and Ni(II) is summarized in Figure 2, where the retention volume and peak width are plotted as a function of eluent pH. At low pH values, D will be small (Equation 5) and $V_R \simeq V_m$. Since the metal ion under these conditions is simply "washed through" the column with little or no interaction, the peak width will also remain small and essentially constant. The small and essentially constant V_R and W values are seen at the lower pH ranges in each case.

At a higher pH, characteristic for each metal ion (Equation 5), the D values become appreciable, V_R increases, and the process becomes truly chromatographic. This may be more clearly seen from Figure 3, in which the ratio V_R/W_B which measures column efficiently (since the number of theoretical plates is proportional to the square of this ratio) is plotted as a function of D. The high values of the ratio at $D \sim 1.5$, further evidence the "wash-through" aspect of the low pH runs. The rise in peak width accompanying increasing V_R seen in Figure 2 is expected from chromatographic theory, since column efficiency should be fairly constant. This is borne out by the near convergence of the curves in Figure 3 of the Cd, Zn and Co ions at higher D values. The column efficiencies we observe are surprisingly small in view of the relatively good separations obtained (vide infra), being of the order of 50–100 plates. The outstanding exception to the general behavior of the other metal ions is Ni(II), as may be seen from both Figures 2 and 3. From the latter, it is obvious that as D_{Ni} becomes appreciable, a very broad band is observed. This is undoubtedly due to the relatively slow rates of Ni(II) substitution reactions and, while chromatographically most undesirable, might be used as the basis for evaluating the kinetics of the Ni(II)–oxine chelate formation and dissociation.

Values of D, free from possible complications arising from kinetic factors, can be obtained by batch equilibrations. As seen in Table II column and batch D values for Cd(II), whose substitution reactions are very rapid, agree very well. The

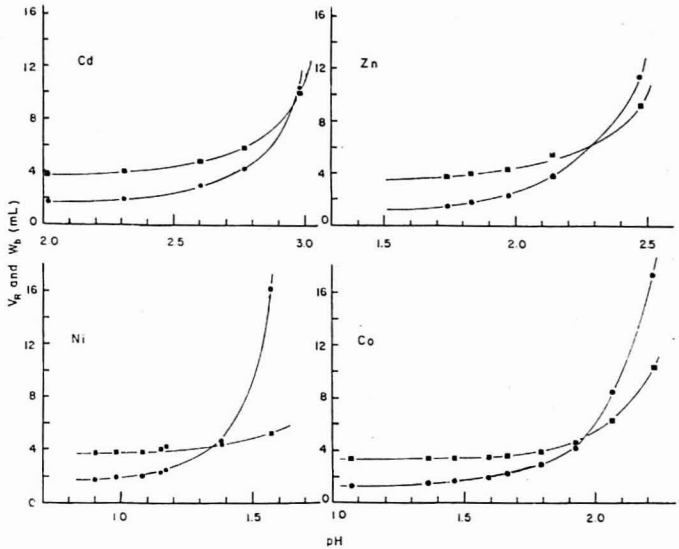


Figure 2. Retention volume (V_R) and peak base width (W_b) as a function of pH for Cd, Zn, Co, and Ni using HNO_3 eluent. ■ = V_R, ● = W_b

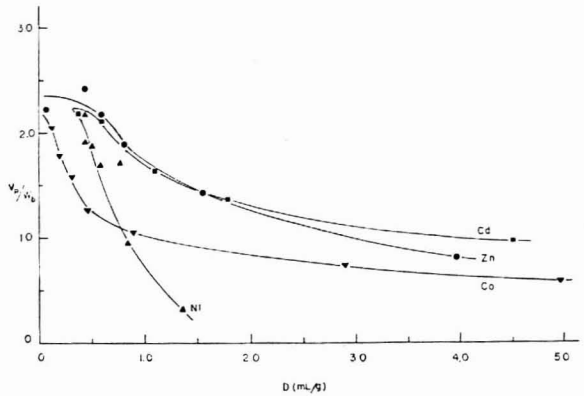


Figure 3. Ratio of retention volume to peak base width. (V_R/W_b) vs. D for Cd, Zn, Co, and Ni. ■ = Cd, ● = Zn, ▼ = Co, ▲ = Ni

Table II. Comparison of Metal Ion Distribution Ratios

		D, mL/g	
	pH	batch[a]	column
Cadmium(II)	2.31	0.5	0.6
	2.60	1.0	1.1
	2.77	1.8	1.8
	2.98	5.5	4.5
Nickel(II)	0.97	0.9	0.4
	1.17	1.5	0.8
	1.38	3.8	0.8
	1.57	6.5	1.4

[a] Obtained under 2:1 mole ratio of immobilized oxine to metal.

significantly lower D values for Ni(II) obtained from column behavior than by batch indicates that for the slow Ni(II) ion reaction, a greater driving force (i.e., higher pH) is needed on the column than that required under true equilibrium conditions to get a particular D value.

In Figure 4, the variation of log D for Cd(II) with pH is seen to be linear, having a slope of 1.01 ± 0.04, indicating that the metal:immobilized oxine complex is 1:1 in accord with Equation 2. This is compatible with the 25–30 Å separation between neighboring oxines on the silica surface, estimated from the surface loading of 18 oxine groups in 10^4 Å^2 (Table I). This would seem to hold for the other metals as well, with the exception of cobalt which exhibits a high, and as yet inexplicable, slope.

Gradient Elution Chromatography. As may be seen from the values for V_R and W for Cd(II), efficient isocratic chromatography is limited to a range of D values that are fairly low. For Cd(II), a V_R of 5 mL, just over the total system void

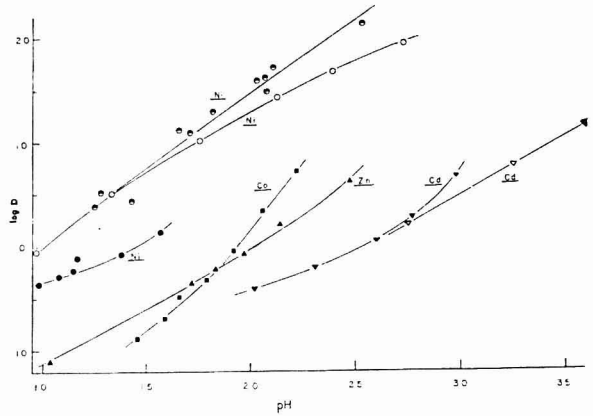


Figure 4. Log D vs. pH for Cd, Zn, Co, and Ni from both column and batch studies. ● = Ni column; ○ = Ni batch, 2 oxine:1 Ni; ◓ = Ni batch, 10 oxine:1 Ni; ■ = Co column; ▲ = Zn column; ▼ = Cd column; ▽ = Cd batch, 2 oxine:1 Cd

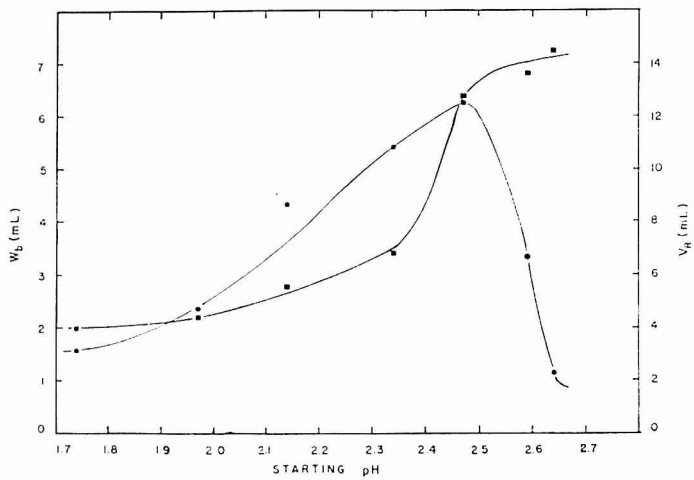


Figure 5. Retention volume (V_R) and peak base width (W_b) vs. pH at start of linear 15-min gradient for Zn. Eluent A = H_2O, B = pH 1 HNO_3; pH at end of gradient = 1.58; ● = W_b, ■ = V_R

volume of about 4 mL is observed at pH 2.55, which corresponds to a D of 0.6 mL/g. At pH 2.98, a V_R of about 10 mL is obtained, corresponding to a D of 4 mL/g. Just above this pH value, the V_R and W_b curves cross, and peaks become too diffuse to be of any value for chromatographic purposes. It appears, therefore, that one is limited to D values between 1 and 4 in order to perform isocratic elutions with this column material.

This is a rather severe restriction for pH dependent metal ion separations, because operation within these limits for one metal ion may place other metal ions in a mixture out of the optimum D range. Some peaks may not emerge at all if D is too large, much above 4, or may come out at the void volume if D is much below unity, or severely overlap with other peaks if the D values of a pair are too close. The obvious answer to the problem of peak overlap and elution volumes that are either too large or too small (the "general elution problem") (*26*) is to operate under gradient elution conditions, either step-wise, or better, with continuous change of pH. Values of both V_R and W_b for Zn(II) and Cd(II) were obtained under various continuous gradient conditions. Shown in Figure 5 are the results for Zn(II) from a series of runs using a 15-min gradient, linear in volumes of mixing of H_2O and HNO_3. Values of V_R and W_b are plotted as a function of the pH at the start of the gradient, at which point the sample was injected. The pH at the end of the gradient was the same for all runs, and set so that D was near 0 for the metal in question. It might be noted that those peaks which came out at about the void volume were not affected by the gradient, as the mixing of eluents in the mixing chamber causes a lag of about 5 to 6 mL in response at the column head. Similar results were obtained with Cd(II).

For both Cd(II) and Zn(II), V_R undergoes a rapid increase in the intermediate pH regions, then levels off somewhat as

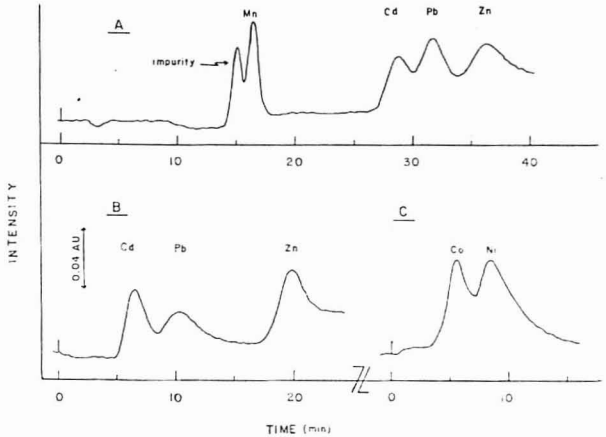


Figure 6. Gradient elution chromatograms of some metal-ion mixtures. (a) Eluent A = H_2O, B = pH 2 HNO_3; 30 min, slightly concave gradient (No. 4 on SP3500B), H_2O–60% B (pH 2.2). (b) Eluent A = H_2O, B = pH 2 HNO_3; 15 min, No 4 gradient, 20–100% B (pH 2.7–2.0). (c) Eluent A = H_2O, B = pH 1 HNO_3; 30 min, highly convex gradient (No. 8), 25–100% B (pH 1.6–1.0)

the starting pH gets higher. On the other hand, W_b for both metals goes through a maximum, then falls back to values as small or smaller than those obtained at more highly acidic starting pH values. Three "regions" or responses can be identified here. When the pH at the start of the gradient is such that the distribution coefficient, D, is low (below 1), the peak comes off at or near the void volume; it is essentially "washed down" the column immediately upon injection. At the other extreme, when the starting pH is such that D is high, the metal sample goes onto the column as a narrow band, and does not begin to move until the D value gets much lower. For Cd(II), for example, at starting pH of 3.7, D is about 17, so that the metal remains on the stationary phase and does not move or spread out appreciably. Because the gradient is linear with respect to volume, it is not linear in pH, but rather convex in shape. This means that the pH and, hence, the D value decreases rather sharply during the latter part of the run. Therefore, the peak does not have a chance to spread out but rapidly traverses the column in a narrow band. Inasmuch as the band did not move appreciably until D became very small, i.e., near the end of the gradient, however, large V_R values are obtained. For the gradient for which the starting pH was 3.7, W_b was about 3.2 mL but V_R about 24 mL. This is also an example of a peak being rapidly washed off the column (once the D value is made very low), but because V_R is large, it can be termed "late wash". Because the peak is rapidly eluted from the column under these "late wash" conditions, and moves at the system flow rate, the V_R curve tends to flatten out as more rapid peak movement is obtained at the end of the gradient compared to the intermediate situation discussed below.

For both Zn(II) and Cd(II), the maximum in the W_b vs. starting pH curve occurs at the pH where the isocratic V_R and W_b curves crossed (Figure 2) and at D values of about 3 and 4, respectively. Beyond the maximm in W_b, D is greater than 4, and "late wash" conditions exist so that narrow peaks are again obtained.

Between these two extremes of early and late "washing", the true chromatographic region occurs, because the D values are in the optimum intermediate range discussed above. The peak begins to move slowly immediately upon injection and continues to move during the entire run; whereas at higher initial pH values where D is large, movement occurs only during the last part of gradient run. Therefore, at these intermediate D values, for example from 1 to about 6 mL/g, more extensive band spreading occurs. The maximum peak width appears to occur when D at the beginning of the gradient run is near 4 mL/g; i.e., when about 80% of the metal is on the stationary phase and 20% off, as seen above. These results are for the linear volume, convex pH gradient used, and would be expected to take other forms for other gradient shapes and times. Nevertheless, it is clear from the above results that conditions can be tailored with the easily acquired knowledge of D values to maximize separation conditions for a mixture of metal ions so that minimum peak width and retention times are obtained. During any given gradient elution run for a metal ion mixture, some of the ions will likely be in an "early wash" situation, others in a "late wash", and others in the intermediate chromatography region. With the knowledge of D values, which can be estimated from chelate stability constant values, assuming rapid kinetics of formation and dissociation, reasonable estimates of the column selectivity for a given separation can be made.

Analytical Applications. In Figures 6–9 are shown some examples of typical separations of metals using the Porasil-8OHQ column. In Figure 6A, the separation of Mn(II), Cd(II), Pb(II), and Zn(II) is shown using the H_2O–pH 2 HNO_3 eluent pair. Column conditioning with water resulted in the scavenging by the column of some impurity which is the first peak off during the gradient run. This peak is believed to be Ca(II) since inclusion of Mg(II) in this sample produced an unsymmetrical peak at this position (not shown). It should be noted that, because of a higher level of impurities in the acid eluent, the base line rises beneath the Cd–Pb–Zn triad, but that nearly base-line resolution of the Pb–Zn pair is realized. The initial impurity peak was eliminated (Figure 6B) by conditioning the column and beginning the run at a weakly acid pH, 2.7, causing the impurity to be flushed through. In this example base-line resolution of the Pb–Zn pair is observed and good resolution for the usually difficult to separate Cd–Pb pair. A 15-min gradient was used here rather than the 30-min one used in Figure 6A. In Figure 6C is shown the Co–Ni pair using the H_2O–pH 1 HNO_3 eluent system. These two ions proved to be difficult to separate

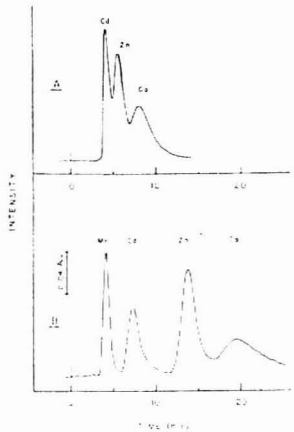


Figure 7. Chromatograms of some metal-ion mixtures using the 0.01 M Na_2 SO_4–0.01M $NaHSO_4$ eluent system, pH about 6.2 and 2.2, respectively. (a) Isocratic usng 100% B, $NaHSO_4$. (b) 15 min, slightly convex gradient (No. 6), 50–100% B (pH 2.6–2.2)

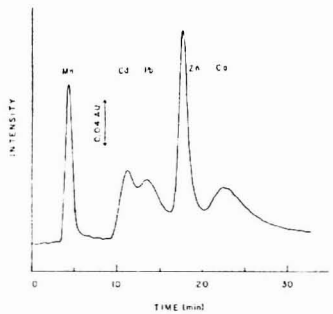


Figure 8. Gradient elution of metal-ion mixture using the 0.01 M Na_2 SO_4–0.01 M $NaHSO_4$ system (eluents A and B); 15 min, slightly convex (No. 6) gradient, 30–100% B (pH 2.8–2.2)

because of the very slow Ni(II) kinetics. Although base-line separation was not obtained, an adequate resolution was obtained by conditioning the column at pH 1.6 and using a highly convex gradient to pH 1.0.

In Figure 7A is shown the isocratic separation of a Cd–Zn–Co mixture using $NaHSO_4$ eluent (0.01 M, pH 2.1). The same three metals with Mn(II) added are shown in Figure 7B using the Na_2SO_4–$NaHSO_4$ eluent pair (Na_2SO_4, 6.01 M, pH 6.2) using a slightly concave gradient from 50 to 100% B. This pH range is about 2.6–2.2. The distinct improvement in Cd–Zn separation results from the higher initial pH placing Cd in the "chromatographic", but Zn in the "late wash" D regions. Lead(II) was added, and this mixture chromatographed using the same gradient except from 30–100% B, (pH range 2.8–2.2)(Figure 8). As was found in the isocratic results, elution with the SO_4^{2-}/HSO_4^{-1} buffer yielded somewhat sharper peaks than using H_2O–HNO_3. This may be a result of the slight complexing power of the SO_4^{2-} for the metal ions, setting up a competition with the 8OHQ.

Based on the log D vs. pH results for Cd(II), it appears that 1:1 metal complexes form with the Porasil-8OHQ. The order of β_1 values for the 1:1 metal complexes of 8-hydroxy-(5-

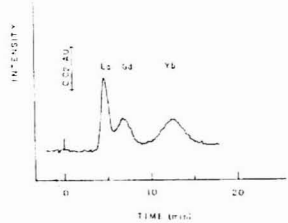


Figure 9. Separation of some lanthanides using HNO_3 eluent. Eluent A = H_2O, B = pH 3 HNO_3; flow rate = 0.52 mL min^{-1}, 3 × 10^{-4} M PAR, pH 7.1 THAM–HCl buffered, 15-min linear gradient, 50–100% B (pH 3.5–3.0)

phenylazo)quinoline (essentially the same as the immobilized species which results from the synthesis used in this study) in 50% H_2O–dioxane media is Mn < Cd < Pb ~ Zn < Co < Ni, as determined by Takamoto et al. (*24*). Their data imply that Pb(II) and Zn(II) would be unresolvable (if there were no kinetic differences), whereas we were able to easily separate them. Otherwise, the order of elution we obtained experimentally follows exactly the order of homogeneous solution β_1 values. It should be pointed out, however, that the method of calculating the β values leads to only approximate figures, and more exact calculations might produce a value for Zn(II) different from that for Pb(II), as our chromatographic data imply.

As an illustration of how effective the column is for lanthanide separations, we observed base-line separation of Gd(III) and Yb(III) and nearly so for La(III) and Gd(III). This separation utilized the H_2O–pH_3 HNO_3 eluent pair and a linear 15-min gradient from 50–100% B (pH 3.5 to 3.0) (Figure 9). Although no phenylazo oxine data for lanthanides exist, the order of elution follows that of the aqueous stability constants for oxine itself.

CONCLUSIONS

The work reported here demonstrates that immobilized chelating agents such as oxine can be successfully used for trace level metal separations and, provided that the particle size of the silica substrate is sufficiently small, can be highly selective. Column behavior can be predicted from solution chelate formation constants. In those cases where metal chelation kinetics is slow in solution, the nature and extent of deviations in chromatographic behavior can also be explained.

With the Porasil-8OHQ, reasonably good separations of several metal ions were obtained using gradient elution over relatively narrow pH ranges. This was the case even though the size of the packing material was somewhat large compared to that used in much modern high performance liquid chromatography, and the capacity of extent of coverage of the silica was low compared to what is obtainable under optimum synthetic conditions. It is to be expected that a much improved number of plates are possible with reduced size and higher capacity of the solid substrate.

The advantages of silica immobilized chelating agents as substrates for metal ion chromatography are several when compared to the efficient but nonselective ion-exchange resins and the selective but experimentally tedious liquid–liquid extraction chromatographic methods. The bleeding of stationary phase from a liquid–liquid system not only may result in appreciable capacity changes from run to run but can also cause loss of extracted metal ions and interfere in detection of sample peaks. Nor are the organic resins used for ion exchange immune from contamination of the eluate by organic moieties leached from the resin beads.

The fact that mild eluting conditions are sufficient to remove the metal ions from the Porasil-8OHQ column is an added plus compared to previous techniques. Should the metal ion need to be recovered after elution from the column, only dilute acid conditions are present, ~0.1 M, so that purification is not difficult. In most ion-exchange techniques, selectivity is obtained through the addition of complexing agents to the eluent (*27, 28*), which must be removed in any purification scheme for the eluted ions; or very strong (several molar) acid conditions are used for elution which also complicate post-column metal purification. Thus, the good stability and likelihood of higher capacity and efficiency of silica immobilized chelating agents offer great promise for metal ion chelation chromatography, and work is underway in our laboratories to demonstrate this.

LITERATURE CITED

(1) G. Nickless, *Adv. Chromatogr.*, **7**, 121–159 (1968).
(2) J. Michal, "Inorganic Chromatographic Analysis", Van Nostrand-Reinhold, New York, 1970.
(3) F. Helfferich, *Adv. Chromatogr.*, **1**, 3–60 (1965).
(4) H. F. Walton, Ed., "Ion-Exchange Chromatography", Dowden, Hutchinson and Ross, Stroudsburg, Pa., 1976.
(5) T. Braun and G. Ghersini, Ed., "Extraction Chromatography", Elsevier, New York, 1975.
(6) E. Cerrai and G. Ghersini, *Adv. Chromatogr.*, **9**, 3–189 (1970).
(7) F. Helfferich, *Adv. Chromatogr.*, **1**, 77–81 (1965).
(8) J. R. Parrish, *Anal. Chem.*, **49**, 1189 (1977).
(9) E. Grushka and E. J. Kikta, *Anal. Chem.*, **49**, 1005A (1977).
(10) I. Sebestian and I. Halasz, *Adv. Chromatogr.*, **14**, 347 (1977).
(11) E. Grushka, "Bonded Stationary Phases in Chromatography", Ann Arbor Science Publishers, Ann Arbor Mich., 1974.
(12) D. W. Lee and M. Halmann, *Anal. Chem.*, **48**, 2214 (1976).
(13) J. L. Lundgren and A. A. Schilt, *Anal. Chem.*, **49**, 974 (1977).
(14) E. M. Moyers and J. S. Fritz, *Anal. Chem.*, **48**, 1117 (1976).
(15) D. E. Leyden and G. H. Luttrell, *Anal. Chem.*, **47**, 1612 (1975).
(16) D. E. Leyden, G. H. Luttrell, A. E. Sloan, and N. J. DeAngelis, *Anal. Chim. Acta*, **84**, 97 (1976).
(17) I. I. Antokolskaya, G. V. Myaesoedova, L. I. Bolshakova, and O. P. Shvoeva, *J. Chromatogr.*, **102**, 287 (1974).
(18) J. M. Hill, *J. Chromatogr.*, **76**, 455 (1973).
(19) K. F. Sugawara, H. H. Weetall, and G. D. Schucker, *Anal. Chem.*, **46**, 489 (1974).
(20) Z. Slovak, S. Slovakova, and M. Smrz, *Anal. Chim. Acta*, **75**, 127 (1975).
(21) M. M. Guedes da Mota, F. G. Roemer, and B. Griepink, *Fresnius Z. Anal. Chem.*, **287**, 19 (1977).
(22) J. R. Parrish, *Lab. Pract.*, **24**, 399 (1975).
(23) G. Schwarzenbach and H. Flaschka, "Complexometric Titrations", Methuen, London, 1969.
(24) S. Takamoto, Q. Fernando, and H. Freiser, *Anal. Chem.*, **37**, 1249 (1965).
(25) J. R. Jezorek and H. Freiser, *Anal. Chem.*, following paper in this issue.
(26) L. R. Snyder, "Principles of Adsorption Chromatography", Marcel Dekker, New York, 1968, pp 21–22.
(27) M. D. Arguello and J. S. Fritz, *Anal. Chem.*, **49**, 1595 (1977)
(28) J. S. Fritz and J. N. Story, *Anal. Chem.*, **46**, 825 (1974).

RECEIVED for review August 24, 1978. Accepted November 9, 1978. This work was conducted with the financial assistance of the U.S. Department of Energy.

4-(Pyridylazo)resorcinol-Based Continuous Detection System for Trace Levels of Metal Ions

John R. Jezorek[1] and Henry Freiser*

Department of Chemistry, University of Arizona, Tucson, Arizona 85721

A sensitive continuous metal ion detection system based on the use of PAR–ZnEDTA has been developed and characterized. Sensitivities of the order of 0.1 to 1.0 nmol, which represents a thousand-fold improvement over previously reported systems, were observed for 13 metal ions. The system has been employed in a liquid chromatographic separation study.

In the course of our liquid chromatographic study of metal ions using immobilized chelating agents (*1*), we considered it desirable to develop a spectrophotometric detection scheme. Inasmuch as the metal ions themselves are not highly colored, the scheme would have to involve mixing the eluate with a suitable chromophore. We investigated a number of metallochromic indicators, and finally settled on 4-(2-pyridylazo)resorcinol (PAR) as the optimum choice. Fritz and coworkers (*2, 3*) had previously used this reagent and also found it to be superior to other dyes they studied. PAR forms water-soluble complexes with a larger number of metal ions than any other commonly available indicator. These complexes have large molar absorptivities (~10^4) (*4*) at about 500 nm and hence exhibit high sensitivity for photometric detection.

[1]On leave during the 1977–78 academic year from the Department of Chemistry, University of North Carolina at Greensboro, Greensboro, N.C. 27412.

Although PAR has been extensively used as a reagent for spectrophotometric analysis of metal ions (*4*) and, as noted above, in several chromatographic studies, apparently no formal investigation or characterization of its use in a chromatographic context has been published. We wish to report here our findings on the stability of various types of PAR solutions, its suitability as an indicator for various metal ions, and some difficulties encountered due to metal ion contamination of chromatographic elements.

EXPERIMENTAL

The liquid chromatography apparatus, detection hardware, and immobilized-oxine support have been described elsewhere (*1*).

The water used for PAR and metal-ion solutions was house distilled and deionized, or was obtained from a Corning Megapure still (Corning Glass Works, Corning, N.Y. 14830). The preparation of water used for elution solvents has been previously discussed (*1*). PAR was used as received from Eastman Organic Chemicals (Rochester, N.Y. 14650). Metal-ion solutions were prepared from the analytical reagent grade perchlorate salts (G. F. Smith Chemical Co., Columbus, Ohio 43223) except for lanthanum(III) which was the 99.99% pure nitrate salt from MC & B (The Matheson Co., East Rutherford, N.J.). PAR solutions at pH 9 and 11 were 0.05 M in NH_4Cl, to which enough concentrated NH_3 was added to obtain the desired pH (pH meter). In addition the pH 11 PAR solutions were equimolar in ZnEDTA. PAR solutions at pH 7 were 0.1 M in Tham (tris(hydroxymethylamino)methane), with HCl added to reach the desired pH value.

ZnEDTA reagent was prepared by mixing equivalent amounts of standardized zinc perchlorate and 10^{-2} M EDTA solutions. All

0003-2700/79/0351-0373$01.00/0 © 1979 American Chemical Society

other reagents were analytical reagent grade, obtained from Departmental supplies, and used as received.

RESULTS AND DISCUSSION

PAR Solution Stability. We found that storage of approximately 3×10^{-5} M PAR solutions either in the light or in glass bottles caused deterioration overnight so that little or no detector response was obtained upon injection of a metal sample. This situation did not occur if plastic containers were used and the solutions stored in the dark. Attempts to prepare 10^{-4} M, or higher, unbuffered PAR stock solutions for subsequent dilution resulted also in significant overnight deterioration, whether stored in glass or plastic, as evidenced by a 50% decrease overnight in the absorbance at 411 nm (λ_{max} for PAR), and the appearance of a new band at 340 nm. A 10^{-5} M solution prepared independently or immediately diluted from the above stock reagent after preparation, and buffered at pH 9, showed good stability over several days. A 10^{-4} M stock solution buffered with NH_4^+/NH_3 at pH 9 was found to be more stable than the unbuffered stock; and that buffered at pH 11 even more so. These solutions could be kept for several days without significant deterioration.

Tham buffered PAR solutions, 10^{-4} M or higher, were found to be adsorbed on the walls of the plastic container after a day or so. This was also true of pH 9 solutions at 5×10^{-4} M and higher, but not at pH 11 at any concentration studied.

The PAR–ZnEDTA reagent buffered with NH_4^+/NH_3 at pH 11 (discussed below) was found to deteriorate rapidly if glass-bottle storage was employed. A drop in absorbance at 411 nm from 0.88 to 0.62 for a 3×10^{-5} M solution occurred in 2 days, and an increase in absorbance from 0.01 to 0.12 occurred at about 495 nm. It is likely that either PAR or ZnEDTA abstracted metal ions from the glass, in the former case forming PAR–metal complexes or, in the latter, releasing Zn(II) from the $Zn(PAR)_2$ complex which absorbs at 495 nm. However, when these PAR–ZnEDTA solutions were stored in clean plastic containers, there was no change in either the absorbance or chromatographic response for up to 5 weeks, at which time we halted our monitoring of the solutions.

Even though λ_{max} for PAR is 411 nm, there was some residual absorbance at the monitoring wavelength, 510 nm, due to some contaminant metal–PAR complexes and to the high-pH PAR band (λ_{max} 500 nm) from its dianion (*4*). This, along with the fact that two liquid streams were being mixed using peristaltic pump pressure for one stream led to some detector noise at higher sensitivities. Use of two 1-m mixing coils helped to reduce the noise significantly at the 0.4, 0.2, and 0.1 AUFS settings commonly used. It is of interest that use of acid eluents (0.1 M e.g.) resulted in less noise than if solutions closer to neutral were used. This may be a result of better mixing of the two eluent streams due to the heat released in neutralization of the acid by the pH 9 or 11 NH_4^+/NH_3 PAR solutions.

Metal–PAR Chromatographic Interactions. Metal-ion sample solutions were typically from $1\text{–}5 \times 10^{-4}$ M, (~10–50 ppm) while the PAR detector solution was about 3×10^{-5} M. For an injection of 10 μL of 5×10^{-4} M metal, which spreads out into a volume of 1 mL (the narrowest chromatographic peak obtained) or more at the detector, the chromophore concentration was present at about a 100-fold excess over the metal. Indeed, as expected, we found no increase in peak size for 10 ppm Zn solution or increasing the indicator concentration 10-fold, to 3×10^{-4} M.

Because previous work by Munshi and De (*5*) recommended a pH between 6 and 7 for rare-earth analysis using PAR, and because of the ease of hydroxide precipitation ($K_{sp} \approx 10^{-21}$) (*6*) we decided to use pH 7, Tham-buffered PAR solutions for initial lanthanide work. Subsequent studies with La(III), however, revealed that the optimum detector response with PAR occurs at pH 9. This is in agreement with the report that the rare earth–PAR molar absorptivities increase as pH increases (*4*). Even though La(III) normally precipitates as the hydroxide at pH 8 or higher, reaction with PAR apparently is sufficiently rapid, even up to pH 11, to prevent or minimize hydroxide-complex formation. It should be noted that a somewhat more concentrated PAR solution (1×10^{-4} M PAR) is necessary to get a detector response of the same magnitude as with transition metals, possibly because of the necessity of overcoming hydroxide complex formation.

Table I. Relative Responses for Some Metals with PAR and PAR–ZnEDTA[a]

metal[a]	peak height, in PAR	peak height, in PAR–ZnEDTA	metal	peak height, in PAR	peak height, in PAR–ZnEDTA
Ca^{2+}	0.1	2.5	Zn^{2+}	3.0	2.1
Mg^{2+}	0.1	1.8	Ni^{2+}	3.0	2.3
Sr^{2+}	0.2	2.4	Cu^{2+}	1.7	1.6
Ba^{2+}	0.1	3.2	Co^{2+}	2.0	2.0
Pb^{2+}	0.3	1.2	Al^{3+}	0.7	0.2
Mn^{2+}	0.3	2.1	Fe^{3+}	1.5	0.2
La^{3+}	(see text)		Hg^{2+}	4	0.8

[a] Detector at 510 nm 0.4 AUFS; (PAR–ZnEDTA) and (PAR) ≈ 3×10^{-5} M (Metal ≈ 10^{-4} M dummy column, 10 μL metal (≈10^{-4} M) injected; dummy column.

As the alkaline earths, Mn(II), Pb(II), and other metals which we wanted to study chromatographically did not give a suitable response with the PAR indicator solution, we decided to use the PAR–ZnEDTA system described by Fritz and Arguello (*7*). Typically we prepared this reagent to be about 3×10^{-4} M in both PAR and ZnEDTA.

The detection of the alkaline earth metals and others which do not react with PAR alone depends on the displacement of Zn from the ZnEDTA complex and its subsequent coordination with PAR. For example,

$$Ca + 2PAR + ZnEDTA \rightleftharpoons CaEDTA + Zn(PAR)_2 \quad (1)$$

The overall reaction is composed of three simpler ones.

$$Ca + EDTA \rightleftharpoons CaEDTA \quad \log K = 10.7 \quad (2)$$

$$Zn + PAR \rightleftharpoons Zn(PAR)_2 \quad \log K = 23.5 \quad (4) \quad (3)$$

$$Zn + EDTA \rightleftharpoons ZnEDTA \quad \log K = 16.5 \quad (4)$$

$$K'_{overall} = \frac{K'_{CaEDTA} K_{ZnPAR_2}}{K''_{ZnEDTA}} = 10^{25.6} \quad (5)$$

since $\log K'_{CaEDTA}$ at pH 11 = 10.6, and $\log K''_{ZnEDTA}$ at pH 11 and ~0.5 M NH_3 = 8.5.

Under NH_4/NH_3 buffer conditions at pH 11, this displacement reaction is quite rapid, and good response was found for all the metals tested [except, as discussed below, for Fe(III), Hg(II), and Al(III)]. If these metals are of interest, rather than the alkaline earths, Mn(II), and Pb(II), then PAR by itself at pH 9 would probably be the better choice.

In Table I are compared relative responses for some metals with PAR and PAR–ZnEDTA.

It is not known why Mn(II) and Pb(II) gave such small responses with PAR alone, but for these and a number of other ions, significant improvement in sensitivity was realized with the PAR–ZnEDTA system. However, as seen in Table I, Fe(III), Al(III), and Hg(II) could not be detected at the pH 11 conditions used with the PAR–ZnEDTA. Presumably, rapid formation of the metal oxides in these cases prevented formation of the metal–PAR complex.

The chromatographic detector characteristics of the PAR–ZnEDTA system were further investigated by preparing a calibration curve with Cd(II) from 1×10^{-3} to 1×10^{-5} M. The Porasil-oxine column previously described (*1*) was used

in the isocratic mode, elution of the Cd peak being effected with pH 2.7 HNO_3. Except for the 1×10^{-5} M Cd solution, when it was reduced to 0.75×10^{-5} M to minimize detector noise, the PAR–ZnEDTA concentration was 3×10^{-5} M. Both peak height and area were examined as a function of Cd concentration, and straight line response was obtained for each over the entire concentration range studied. The linear-regression equations were $H = 1.037 \times 10^4$ [Cd] + 0.1859 and $A = 1.825 \times 10^4$ [Cd] + 0.2803 for peak height and area, respectively, with correlation coefficients of 0.9987 and 0.9990, where [Cd] is from $1–100 \times 10^{-5}$ M.

It should be noted that a 5×10^{-5} M Cd solution, for which a significant response was easily obtained, represents an approximately 1000-fold reduction in amount of metal ion over that used in previous published studies.

Contamination Problems. As a rule, in any method for trace analysis, much time will be spent wrestling with contaminated reagents, cleaning glassware, etc. This investigation was no exception, and we would like to comment briefly on some of our experiences. As we have earlier shown (*1*), the Porasil–oxine column material is a fairly efficient substrate for separating metal ions in a sample mixture. This was a mixed blessing, however, in that the column material also is a good scavenger for trace impurities in eluent solvents. When the column is conditioned with eluent at a particular pH prior to sample injection, any metal impurities in the eluent which can complex with the oxine at that pH will be retained. These impurities may cause insignificant interference with sample peaks upon subsequent elution of the column.

The PAR or PAR–ZnEDTA metallochromic indicator was chosen for the detector system in this chromatographic work because of its sensitivity. It also provides a convenient and sensitive test for reagent contamination. Singly ionized PAR (pH 5.5) has an absorption maximum at 411 nm (our value) as mentioned earlier and doubly ionized PAR (pK 12.3) at about 490–500 nm (*4*). Using a solution of PAR–ZnEDTA (pH 11, 3×10^{-5} M) and diluting it in half with the solvents or solutions in question allows trace contaminants to be easily seen. If the diluting medium is totally pure, dilution should yield an absorbance, A_d, one-half that of the original PAR solution, A_o. If metal contaminants are present in significant amounts, A_d at 510 nm will be greater than one-half A_o, because of the contribution at 510 nm of the metal–PAR complexes. A drop in absorbance at 411 nm will also be noted as there is less free PAR present when some is complexed by the contaminants. It should also be noted that an increase in acidity (lower pH) causes the free PAR band at 411 nm to increase and the 500-nm band to decrease because of a shift in the $PAR^{-1} \rightleftharpoons PAR^{-2}$ equilibrium to the left. Data for some reagents are presented in Table II.

Looking particularly at the $A_{d,510}$ values, it can be seen that even with rather extensive precautions such as doubly distilling and triply deionizing, cleaning all glass and plasticware with 1:1 HNO_3 and EDTA, contamination is still present. For completely pure diluents, the $A_{d,510}$ values should be 0.114 and 0.117 AU for Table II (a) and (b), respectively. The redistilled Corning water appears to be the most pure. Of the solutions tested, the 1 M Na_2SO_4 can be seen to be highly contaminated; the 0.01 M Na_2SO_4 and $NaHSO_4$ somewhat contaminated, although ion-exchange treatment helped considerably, as shown for the 0.01 M Na_2SO_4. Contamination of the pH 1 HNO_3 is masked in that $A_{d,510}$ decreases and the $A_{d,411}$ increases because of the shift in the $PAR^{-2} \rightleftharpoons PAR^{-1}$ equilibrium due to the lower pH after dilution.

No attempt was made to positively identify these contaminants. However, about 700 mL of dd^3 water was run through a column of immobilized ozine, the metal contaminants collected by eluting with 1 M HCl, and atomic absorbance analysis for Cu(II) made. A value of about 5 ppb was obtained. So, we are really dealing with rather small amounts of contaminants which are magnified by being scavenged by the immobilized 8OHQ during column conditioning.

Table II. Dilution in Half of a 3×10^{-5} M PAR–ZnEDTA Solution by Selected Reagents

(a) $A_{o,411} = 1.041$; $A_{o,510} = 0.228$

diluting solution	absorbance, A_d, nm 411	510
dd^3 H_2O[a]	0.499	0.155
dd^{3}d H_2O[b]	0.519	0.130
Corning H_2O[c]	0.506	1.128
pH 2 $HClO_4$ in dd^3 H_2O	0.483	0.172
pH 2 HNO_3 in dd^{3}d H_2O	0.505	0.137

(b) $A_{o,411} = 1.002$; $A_{o,510} = 0.233$

redistilled Corning H_2O	0.495	0.129
1 M Na_2SO_4	0.300	0.391
0.01 M Na_2SO_4, dil. from above	0.476	0.146
0.01 M Na_2SO_4, after ion-exchange treatment[d]	0.497	0.138
0.01 M $NaHSO_4$	0.476	0.146
pH 1 HNO_3	0.515	0.100
pH 1 HNO_3, same as above except pumped through the liquid chromatograph	0.426	0.199

[a] House distilled, triply deionized. [b] "a" followed by distillation. [c] From Corning Megapure still. [d] 25-cm column of Dowex 50W-X8, on SO_4^{2-} cycle.

Blank elutions run after conditioning the column with about 20 mL of water normally produced peaks at two locations on the blank chromatogram if the column was eluted with pH 1 or 2 acid. Usually a single peak came out early in the run and this is believed to be Ca(II) or a Ca(II)–Mg(II) mixture.

One or more later peaks are probably various transition metals which came from the water, reagents, glassware, and/or the stainless steel of the liquid chromatograph itself. The size of the first peak increases as the volume of water (solvent A) used to condition the column increases. The size of the second peak is independent of the volume of conditioning solvent, implying that it originates primarily from impurities already in the acid eluent (solvent B) or produced on passage through the LC System. That the latter is a major source of contamination, especially where acidic eluents are involved, can be seen from the data for pH 1 HNO_3 in Table II(b). Even thought the pH drop of the PAR–ZnEDTA upon dilution counteracts the effect of metal contaminants upon dilution, $A_{d,510}$ for the HNO_3 which was passed through the LC System shows that the extent of contamination has increased dramatically upon traversing the LC (pump, tubing injection valve, etc.). No matter how pure the aqueous reagents are, they will cause corrosion of the stainless steel during passage through the LC and become more or less contaminated themselves.

Interference by alkaline earths can be avoided by conditioning the column at a slightly acid pH (for example, 3 or below) which prevents their retention. However, there is really no good way to completely eliminate contamination from stainless steel corrosion, and at best what one obtains is a base line which rises during a gradient run due to the increased extent of metal contamination in the more acidic solution used to elute the column. If the gradient is a sharp one, however, that is, there exists a rapid pH rise during a gradient so that a more or less diffuse pH "front" obtains somewhere in the column, and because the contaminants in the acid "pile up" at the edge of this "front", a peak will emerge simultaneously with the base-line rise. The same situation is seen if a column

conditioned with water or a solution rather more basic than solvent B is eluted isocratically with solvent B. If one of the sample peaks is found at this position, interference will, of course, occur. Corrosion of the stainless steel appears to be a limiting factor in trace metal analysis by HPLC, given the equipment available at this time. What is needed besides very pure reagents and solutions is an all-Teflon system or at least one where the amount of stainless steel is severely limited (*8*).

The detection system described here is ideally suited for use in conjunction with an HPLC investigation involving a wide variety of polyvalent metal ions. We have found it more than adequate for use in applying chemically bonded chelating agents as immobile phases (*1*), but it should be readily adaptable for ion exchange and liquid–liquid reverse phase partition separations as well.

LITERATURE CITED

(1) J. R. Jezorek and Henry Freiser, *Anal. Chem.*, preceding paper in this issue.
(2) K. Kawazu and J. S. Fritz, *J. Chromatogr.*, **77**, 397 (1973).
(3) J. S. Fritz and J. N. Stary, *Anal. Chem.*, **46**, 825 (1974).
(4) S. Shibata, in "Chelates in Analytical Chemistry", H. Flaschka and A. J. Barnard, Ed., Vol. 4, Marcel Dekker, New York, 1972, pp 116–165.
(5) K. N. Munshi and A. K. De, *Anal. Chem.*, **36**, 2003 (1964).
(6) L. G. Sillen and A. E. Martell, Ed., "Stability Constants of Metal-Ion Complexes", Suppl. No. 1, Special Pub. No. 25, The Chemical Society, London, 1971.
(7) M. D. Arguello and J. S. Fritz, *Anal. Chem.*, **49**, 1595 (1977).
(8) W. A. MacCrehan, R. A. Durst, and J. M. Bellama, *Anal. Lett.*, **10**, 1175 (1977).

RECEIVED for review August 24, 1978. Accepted November 9, 1978. This work was conducted with the financial assistance of the U.S. Department of Energy.

Lead, Cadmium, and Zinc Bis(diethyldithiocarbamate) and Diethyldithiocarbamic Acid as Reagents for Liquid–Liquid Extraction

Sixto Bajo* and Armin Wyttenbach

Swiss Federal Institute for Reactor Research, 5303 Würenlingen, Switzerland

The extraction constants of $Pb(DDC)_2$, $Cd(DDC)_2$, and $Zn(DDC)_2$—where DDC is used to denote the diethyldithiocarbamate anion—were determined for the system $H_2O/CHCl_3$; log K_{ex} was found to be 7.94 ± 0.09, 5.77 ± 0.05, and 2.39 ± 0.02. Solutions of $Cd(DDC)_2$ and $Zn(DDC)_2$ in $CHCl_3$ were shown to be stable for at least 40 days. When solutions of $Cd(DDC)_2$, $Zn(DDC)_2$, or HDDC as reagents in $CHCl_3$ were used to extract acid aqueous solutions, their titer deteriorated as a function of pH and time; however, this deterioration is much less rapid than the destruction of a solution of NaDDC. The title compounds therefore can be considered suitable reagents for extractions from acid aqueous solutions.

Extraction of metals as their diethyldithiocarbamates (the anion $(C_2H_5)_2NCS_2^-$ will in the following be denoted as DDC) is becoming more and more popular. The reagent is traditionally introduced into the aqueous phase as NaDDC or into the organic phase as $NH_2(C_2H_5)$DDC. Substitution of these reagents by metal diethyldithiocarbamates (dissolved in an organic diluent) results in an improved stability in contact with acid aqueous solutions and in an increased specificity of the extraction. Examples for the application of metal dithiocarbamates as reagents can be found in many publications (*1–11*).

Selectivity of these extractions is governed by the extraction constants of the reagents (*1*), which unfortunately are not well known for the practically important system $CHCl_3/H_2O$. Furthermore, safe application of these reagents requires some knowledge about the stability of their titer.

The present work was undertaken in order to contribute to the knowledge of metal dithiocarbamates as reagents by determining the extraction constants of $Pb(DDC)_2$, $Cd(DDC)_2$, and $Zn(DDC)_2$ and by measuring the stability of their solutions (as well as of HDDC) in $CHCl_3$ alone and in contact with various acids. Both points are prerequisites to the appropriate use of these reagents.

EXPERIMENTAL

Extractions. Extractions were done in 250-mL separatory funnels at room temperature (21 °C) on a shaking machine with a capacity of 6 cm and a frequency of 6.6 s^{-1}. The phases were then separated by decantation.

Reagents. The solid products $Pb(DDC)_2$, $Cd(DDC)_2$, and $Zn(DDC)_2$ were prepared as described before (*1*). They were weighed to prepare solutions in $CHCl_3$ of known content, which were stored in dark bottles. Solutions of HDDC in $CHCl_3$ were prepared by shaking equal volumes of $Zn(DDC)_2/CHCl_3$ solutions and 2 M HCl for 30 s.

Determination of the Extraction Constants. Solutions of the different metal diethyldithiocarbamates in $CHCl_3$ (30 mL) were shaken with aqueous solutions of $HClO_4$ (100 mL). The concentration of the $M(DDC)_2$ as well as the acidity was varied within the limits given in Table I, whereas the concentration of ClO_4^- in the aqueous phase was kept constant at 1 M with $NaClO_4$. The concentration of the metals in the organic phase both before and after the experiment was determined by evaporating and wet ashing aliquots which were then analyzed by complexometry (Zn, Cd) or by atomic absorption (Pb).

Control of the Titer of Solutions of $Cd(DDC)_2$, $Zn(DDC)_2$, and HDDC in $CHCl_3$. The variation of the titer with time was checked by periodically extracting a radioactive aqueous metal solution (100 mL) with aliquots of the organic solutions (30 mL) under conditions that were substoichiometric with respect to the reagent. The activity extracted was measured and taken to be proportional to the titer. The following systems were used: (a) for $Cd(DDC)_2$ and $Zn(DDC)_2$ in $CHCl_3$: Hg^{2+} (^{203}Hg) in 1 M HCl, extraction time was 2 min; (b) for HDDC in $CHCl_3$: Cu^{2+} (^{64}Cu) in 0.1 M $HClO_4$, and Zn^{2+} (^{65}Zn) in a citrate buffer of pH 5, extraction time was 4 min.

Control of the Titer of Organic Solutions in Contact with Acid Aqueous Solutions. Aliquots of the organic solutions (30 mL) were shaken for various times with 100 mL HNO_3, $HClO_4$, HCl, or H_2SO_4 of different concentrations. Thereafter an excess of Cu^{2+} (^{64}Cu) was added to the aqueous phase and shaking was

0003-2700/79/0351-0376$01.00/0 © 1979 American Chemical Society

Table I. Extraction Constants for $Zn(DDC)_2$, $Cd(DDC)_2$, and $Pb(DDC)_2$ for the System $H_2O/CHCl_3$

metal	range of $[H^+]$ used	range of initial concentration C used	range of F found	no. of determinations	$\log K_{ex}$ this work	$\log K_{ex}$ literature values
Zn^{2+}	0.01–0.06	$(1.7–5.2) \times 10^{-3}$	0.24–0.60	7	2.39 ± 0.02	2.2 (*13*), 2.3 ± 0.2 (*14*)
Cd^{2+}	0.1–1.0	$(1.1–1.8) \times 10^{-3}$	0.42–0.85	11	5.77 ± 0.05	5.6 (*8*), 5.4 (*13*), 5.50 ± 0.05 (*14*)
Pb^{2+}	0.1–1.0	$(0.2–1.6) \times 10^{-3}$	0.51–0.96	10	7.94 ± 0.09	7.0 (*13*), 5.0 ± 0.1 (*14*)

continued for another 4 min. The activity extracted was taken to be proportional to the titer.

Counting was done with a well-type NaI(Tl) crystal, taking care of counter dead-time, background, and radioactive decay as usual.

RESULTS AND DISCUSSION

Extraction Constants. The extraction of a metal from the aqueous phase into an organic phase (subscript org) as well as the reverse process can be described by

$$M^{n+} + HDDC_{org} \rightleftharpoons M(DDC)_{n,org} + nH^+ \quad (1)$$

The equilibrium constant for this process is called the extraction constant K_{ex} (for the given organic phase) and can be written as

$$K_{ex} = \frac{[M(DDC)_n]_{org}\,[H^+]^n}{[M^{n+}]\,[HDDC]^n_{org}} \quad (2)$$

The determination of the extraction constant is usually done under conditions of a large excess of extractant (*12*). Our approach is different in that the total concentration of extractant is exactly stoichiometric to the total concentration of the metal. With the assumptions (which are fulfilled in our case) that $M(DDC)_n$ is the only extracted complex, that M^{n+} exists in the aqueous phase only as aquo ion and that $(HDDC)_{org} >> (HDDC)_{aq} + (DDC)_{aq}$, the following relations hold at equilibrium:

$$[M(DDC)_n]_{org} = F \times C \quad (3)$$

where C is the original concentration of $M(DDC)_n$ in the organic phase and F the fraction of the metal staying in the organic phase at equilibrium. For stoichiometric reasons it follows that

$$[HDDC]_{org} = n\{C - [M(DDC]_n)_{org}\} = nC(1 - F) \quad (4)$$

$$[M^{n+}] = \{C - [M(DDC]_n)_{org}\} \times \frac{V_{org}}{V} = C(1 - F)\,\frac{V_{org}}{V} \quad (5)$$

Substituting Equations 3, 4, and 5 into Equation 2 gives:

$$K_{ex} = \frac{F}{n^n C^n (1 - F)^{n+1}} \times \frac{V}{V_{org}} \times [H^+]^n \quad (6)$$

where V and V_{org} are the volumes of the aqueous and of the organic phase.

It can be seen from Equation 6 that under the conditions of stoichiometry as used here, K_{ex} can be calculated from a determination of F and $[H^+]$ alone. There is no need to introduce other constants (as e.g. the acid dissociation constant or the distribution constant of the reagent) or to add auxiliary complexants into the aqueous phase. Although this procedure is limited to a certain range of K_{ex}, we think that apart from the cases studied here it could also be applied to $In(DDC)_3$ and Tl(DDC) or to other types of chelates.

Extraction times used in these experiments were 0.5 min for Cd and Pb, and 4 min for Zn. It was assured that these times were long enough to reach equilibrium and not long enough to allow for a noticeable destruction of the reagent (see later).

The results are given in Table I. The individual determinations of $\log K_{ex}$ for every element show a relative standard deviation of approximately 1%; this can be taken to indicate the internal consistency of the results. Agreement with literature values is fair for Zn and Cd, but only moderate for Pb. For this latter element, the same authors (*13*, *14*) have published two very different values.

Stability of Solutions of $Zn(DDC)_2$ and $Cd(DDC)_2$ in $CHCl_3$. Both reagents were studied at concentrations of 5×10^{-3} M, 5×10^{-4} M, and 5×10^{-5} M for a period of 40 days. No deterioration of their titer exceeding the experimental accuracy of 2% was found. These reagents therefore seem to be perfectly stable up to 40 days.

These findings are at variance with the statement that $Zn(DDC)_2$ (10^{-6} M in $CHCl_3$) looses 10% of its titer within 4 days, and that more dilute solutions are even less stable (*15*); it is suspected that in these cases the apparent instability is due to the quality of NaDDC or to the method used for the preparation of the $Zn(DDC)_2$.

Stability of Solutions of HDDC in $CHCl_3$. The solutions studied were 3×10^{-4} M and showed a decrease in their titer which followed a complicated pattern. They were stable for 6 to 7 min, then deteriorated with an apparent half-life of 7 min to a value that was approximately 12% of the original value; this residual titer then stayed constant from 60 to 220 min. Experiments in which the titer was determined by extraction of Cu^{2+} or of Zn^{2+} showed identical results. In separate experiments the variation of the absorbance of the organic phase with time was measured at 350 nm, the wavelength given by Bode (*16*) for HDDC; this variation paralleled the change in the titer. It seems thus reasonable to attribute the residual titer to HDDC and not to some stable decomposition product.

In order to verify if the observed decomposition might be due to traces of HCl in the organic phase originating from the preparation of the HDDC, solutions of HDDC in $CHCl_3$ were washed with a buffer of pH 4 immediately after their preparation. However their behavior was identical to the unwashed solutions.

Stability of Solutions of HDDC, $Zn(DDC)_2$, and $Cd(DDC)_2$ in $CHCl_3$ That Are Being Shaken with Acid Aqueous Solutions. All solutions showed a decrease of their titer which followed first-order kinetics: the apparent half-lives are given in Table II.

Joris et al. (*17*, *18*) showed that aqueous solutions of HDDC decompose according to

$$-\frac{d([HDDC] + [DDC^-])}{dt} = k'([HDDC] + [DDC^-]) = k[HDDC] \quad (7)$$

where k (the true rate constant) is 0.1 s^{-1}. The apparent rate constant k' is in general pH-dependent, but in the region used in our work (pH 0–3) can be considered constant and equal to k.

Equation 7 can also be used to describe the deterioration of the titer of a two-phase system if it is assumed that (i) the decomposition of HDDC in the aqueous phase is the only reaction leading to a deterioration of the titer; (ii) the establishment of the equilibrium between the two phases given by Equation 2 (which involves transportation of $Me(DDC)_n$ and HDDC across the phase boundary as well as dissociation and formation of $Me(DDC)_n$ and of HDDC) is very fast with

Table II. Decomposition of Solutions of HDDC (3.4×10^{-3} M), $Zn(DDC)_2$ (1.7×10^{-3} M), and $Cd(DDC)_2$ (1.7×10^{-3} M in $CHCl_3$ While They Are Shaken with Acid Aqueous Solutions[a]

compound	molarity of acid	HNO_3	$HClO_4$	HCl	H_2SO_4
HDDC	1.0		52 (81)		
	0.10		71 (81)		
	0.010		70 (81)		
	0.0010		68 (81)		
$Zn(DDC)_2$	1.0	41	57 (81)	74	90
	0.10	88	82 (87)	99	99
	0.01	229	245 (186)	237	240
$Cd(DDC)_2$	1.0		83 (139)	78	
	0.10		479 (500)	346	
	0.010		(2200)	1525	

[a] Values given are half-lifes in minutes for the rate of destruction of the reagent. Values in parentheses were calculated according to Equation 8.

respect to the destruction of HDDC.

Assumption (i) is sustained by the observed stability of $Zn(DDC)_2$ and $Cd(DDC)_2$ in the organic phase alone.

If we denote with Q the sum of all forms of DDC in the two-phase system, it follows that

$$\frac{Q_t}{Q_{t=0}} = \exp\left(-k'\alpha \frac{V}{V_{org}} \times t\right) \quad (8)$$

where k' is the apparent rate constant as used in Equation 7, and α is the ratio of the concentrations of all forms of DDC in the aqueous phase to all forms of DDC in the organic phase:

$$\alpha = \frac{[HDDC] + [DDC^-]}{[HDDC]_{org} + n[M(DDC)_n]_{org}} \quad (9)$$

α can be calculated with the aid of K_{ex}, the partition coefficient p_{HDDC} (2360 for $CHCl_3/H_2O$ (*19*)) and the acid dissociation constant K_{HDDC} (4.47×10^{-4} (*20*)). Its value depends on the pH of the aqueous solution.

The half-lives as calculated from Equation 8 are given in Table II. The agreement with the experimental data is fair, thus lending support to the assumptions made in deriving Equation 8. It can be seen that, under otherwise identical conditions, the stability of a given $M(DDC)_n$ against acid decomposition increases with K_{ex}; it is therefore to be expected that solutions of $Pb(DDC)_2$—which have not been tested in this work—are even more stable than those of $Cd(DDC)_2$.

The observed stability of solutions of HDDC in $CHCl_3$ that are shaken with aqueous acid solutions is hard to understand. Although the observed half-life is consistent with the mechanism used above for $M(DDC)_n$, we have found much shorter half-lives for organic solutions that are not shaken with aqueous solutions. For the time being we cannot advance any explanation for this apparent contradiction.

The experimental results given in Table II show that the half-life for the decomposition of organic solutions of metal diethyldithiocarbamates in contact with acids is of the order of hours. This contrasts favorably with the half-life of about 10 s for NaDDC dissolved in acid aqueous solutions (*17*, *18*) and avoids many difficulties arising from the fast decomposition of NaDDC.

LITERATURE CITED

(1) A. Wyttenbach and S. Bajo, *Anal. Chem.*, **47**, 1813 (1975).
(2) S. Bajo and A. Wyttenbach, *Anal. Chem.*, **48**, 902 (1976).
(3) J. Kučera, *Radiochem. Radioanal. Lett.*, **24**, 215 (1976).
(4) P. A. Schubiger and O. Müller, *Radiochem. Radioanal. Lett.*, **24**, 353 (1976).
(5) P. A. Schubiger, O. Müller, and W. Gentner, *J. Radioanal. Chem.*, **39**, 99 (1977).
(6) J. M. Lo, J. C. Wei, and S. J. Yeh, *Anal. Chem.*, **49**, 1146 (1977).
(7) J. M. Lo, J. C. Wei, and S. J. Yeh, *Anal. Chim. Acta*, **93**, 301 (1977).
(8) S. Bajo and A. Wyttenbach, *Anal. Chem.*, **49**, 158 (1977).
(9) S. Bajo and A. Wyttenbach, *Anal. Chem.*, **49**, 1771 (1977).
(10) S. Bajo and A. Wyttenbach, "Extraction liquide–liquide de l'arsenic, de l'antimoine, du sélénium et du tellure par le diéthyldithiocarbamate de zinc", EIR-Report No. 336, Swiss Federal Institute for Reactor Research, Würenlingen, March 1978.
(11) E. Pernicka, P. A. Schubiger, and O. Müller, *Analyst (London)*, **103**, 475 (1978).
(12) J. Stary and K. Kratzer, *Anal. Chim. Acta*, **40**, 93 (1968).
(13) P. C. A. Ooms, U. A. Th. Brinkman, and H. A. Das, "Separation of metal ions from an aqueous solution by displacement reactions in liquid–liquid extraction systems", ECN-Report No. 77-018, Stichting Energieonderzoek Centrum Nederland, Petten, December 1976.
(14) P. C. A. Ooms, U. A. Th. Brinkman, and H. A. Das, *Radiochem. Radioanal. Lett.*, **31**, 317 (1977).
(15) D. A. Beardsley, G. B. Briscoe, J. Ruzicka, and M. Williams, *Talanta*, **14**, 879 (1967).
(16) H. Bode, *Fresenius Z. Anal. Chem.*, **142**, 414 (1954).
(17) K. I. Aspila, V. S. Sastri, and C. L. Chakrabarti, *Talanta*, **16**, 1099 (1969).
(18) S. J. Joris, K. I. Aspila, and C. L. Chakrabarti, *Anal. Chem.*, **41**, 1441 (1969).
(19) H. Bode and F. Neumann, *Fresenius Z. Anal. Chem.*, **169**, 410 (1959).
(20) H. Bode and K. J. Tusche, *Fresenius Z. Anal. Chem.*, **157**, 414 (1957).

RECEIVED for review May 8, 1978. Accepted November 10, 1978.

Fluidic Logic Element Sample Switch for Correlation Chromatography

Raymond Annino*

Department of Chemistry, Canisius College, Buffalo, New York 14208

Marie-France Gonnord and Georges Guiochon

Ecole Polytechnique, Laboratoire de Chimie Analytique Physique, Route de Saclay, 91128 Palaiseau Cedex, France

A gas stream switch has been fabricated from two bistable fluidic amplifiers. In contrast to the usual application of Coanda wall attachment devices which must operate into fairly low impedences, this system has been used as a gas chromatographic sample switch at column head pressures of 800 mbars. As demonstrated in this report, the ability of this switch to reproducibly inject varying amounts of sample on command makes it ideally suited for correlation chromatography. Further efforts are being directed to developing a switch which will work at higher pressures for use with high speed packed column chromatography, and also which will provide smaller sample widths at faster switching speeds for capillary column applications of correlation chromatography.

The use of correlation chromatography as a means of increasing signal to noise ratios has been suggested by a number of investigators (*1, 2*). The origin of a number of difficulties which have been experienced with this technique has been established and some basic guidelines for the effective use of correlation chromatography have been published (*3, 4*).

This previous work has been concerned primarily with the theoretical basis for the idea with some but not a great deal of supporting experimental data. One of the difficulties in obtaining laboratory evidence has been due to the lack of a suitable sampling valve for the chromatograph which would not only have the required switching speed but also a lifetime comparable to the commonly used single injection devices. These requirements have been difficult to meet. The duty cycle of a correlation chromatography sample valve is usually 500 to 1000 times greater than experienced in the normal mode of operation, and switching speeds must be at least twice as fast as required for a comparable high speed injection procedure.

Our experience (*5–7*) as well as that of Cram and his coworkers (*8, 9*) with fluidic wall attachment devices has shown that they can be readily adapted to act as chromatographic injection valves. The advantages of these fluidic elements are that by virtue of their fast switching speeds they can deliver very small samples and, as they have no moving parts to wear, their lifetimes appear to be extremely long.

This report is preliminary and describes our progress in the development of a suitable correlation chromatography injection system utilizing fluidic elements.

THEORY

In correlation chromatography, the sample or carrier gas is alternately injected into the chromatograph at the command of a pseudo random binary sequence (PRBS). There may be as many as 1000 injections made during the period of a retention time. This produces an output signal consisting of a number of overlapping peaks. Because of the special properties of the PRBS, it is quite simple to unscramble this output and obtain a chromatographic signal which theoretically has an increased signal to noise ratio over the normal single injection chromatogram.

The theory underlying this operation has been published as has a discussion of the mathematical operations involved in obtaining the correlogram from the output (*1, 3*).

Basically, an array of output signal values is memorized from the present time to one PRBS code period in the past. A single point on the correlogram is generated by multiplying each one of these values with the corresponding point of the PRBS (either +1 or −1), summing these products and dividing by the total number of values. The next correlogram point is generated in the same manner after the PRBS is shifted one time unit. The process continues until one full code unit has been shifted through the experimental array.

The correlogram is then presented as a plot of each of these correlation points vs. the time shift of the code which produced it. The above operation is a particularly simple task to accomplish electronically and thus the procedure would appear to offer increased detectability at a minimum cost. The only basic hardware modification that must be considered is the sample valve.

The principal component of the sample injection system used in this research is the fluidic logic gate shown schematically in Figure 1. If the flow into the device is maintained in the turbulent region, the stream entering at S will attach itself to a wall at the junction of O_1 and O_2. A pressure signal (usually 10%–30% P_s) momentarily applied to a command port (C_1 or C_2) will cause the stream to switch to a channel opposite the active command port and remain in this position until a pressure pulse is applied to the opposite command port. Vents V_1 and V_2 are provided to ensure sufficient volume flow and consequently proper stream switching even if ports O_1 and O_2 are blocked.

Cram and his co-workers have published excellent papers describing various possible configuration of these devices as chromatographic logic and sampling systems, and the reader is referred to these reports for a more detailed presentation (*8, 9*).

EXPERIMENTAL

The correlation chromatograph is shown schematically in Figure 2. The sample valve consists of two bistable fluidic logic elements (Corning 191454) and a control circuitry to switch carrier gas or sample gas into the column on command from the pseudo random switching code generated by the computer (HP21MX-30).

A detail view of the logic gate housing and connections is shown in Figure 3. The sample valve consists of two previously described (*5*) single impulse units modified to work into packed columns and connected to each other through a check valve. Also, the original monostable amplifiers have been replaced with bistable amplifiers. Carrier gas is directed to the column and sample is diverted to O_1 (sample) by momentarily activating electrovalve 4. Similarly, sample is directed to the column and carrier diverted to O_1 (carrier) by momentarily activating electrovalve 4′.

The various adjustments which must be made when initially setting up the apparatus can be generalized in terms of the

0003-2700/79/0351-0379$01.00/0 © 1979 American Chemical Society

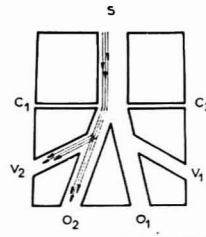


Figure 1. Schematic representation of a bistable fluidic amplifier showing the supply gas attached to the wall of the O_2 leg and splitting its flow between O_2 and the vent, V_2. S = Inlet for supply gas (carrier gas or sample gas), C_1 and C_2 = control or command ports, V_1 and V_2 = vents, O_1 and O_2 = exits

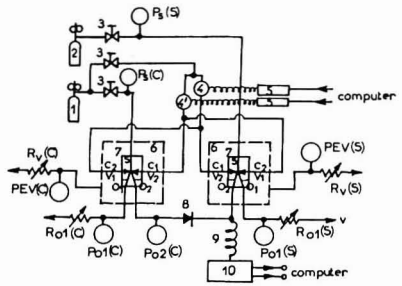


Figure 2. Schematic diagram of correlation chromatograph. (1) Pressurized carrier gas source (nitrogen), (2) Pressurized sample source, (3) Pressure regulators, (4) and (4′) Electrovalves (Clippard Minimatic EV-3), (5) Drivers for electrovalves, (6) Housings for fluidic gates, (7) Bistable fluidic amplifiers (Corning 191454), (8) Check valve, (9) Analytical column (3 ft × $^1/_8$ inch o.d., 17.8% bis(2-ethoxyethyl)sebacate on 80/100 mesh Chromosorb P), (10) FID detector (Varian 02-001953-00)

requirements for the chromatographic column and the sample switch. Usually some known column inlet pressure is necessary to obtain the desired flow rate. Also the fluidic amplifiers used in this research will have a pressure drop of 800–1000 mbars if they are operated in the turbulent flow region. Finally, since one or the other of the two fluidic elements is always connected to the column, the total column flow of gas is available through either of the two fluidic devices.

The procedure adopted in this research for apparatus setup involved connecting the carrier gas and increasing the input pressure, P_s(carrier), to the fluidic amplifier while adjusting the vent restrictor, R_v(carrier), until the desired column's input pressure, P_{cv}, was obtained, and in addition, P_s was 800–1000 mbars greater than P_{cv}. Electrovalves 4 and 4′ were activated while watching for a pressure change to O_1 (carrier) to determine if indeed the stream was switching. The restrictor R_{O1}(C) was adjusted so that when carrier gas was exiting through O_1, the pressure P_{O1}(C) was the same as the pressure, P_{O2}(C) when carrier was exiting through O_2(C). The command pressure, P_c, was usually set at 10–30% P_s.

The process was repeated with the sample, but, in addition, the FID output was monitored for sharp sample signal profiles and the absence of base-line upsets upon switching from sample to carrier and back.

Pseudo-random code sequences were computer generated using the algorithms previously discussed (3). These command signals were then transmitted to the electronic drivers which powered the electrovalves. Sample widths were limited to 50 ms or greater as the result of the combined time constants of the drivers, electrovalves, and the dead volume of the connecting tubing.

Data acquisition was accomplished synchronously with a Hewlett-Packard 21-MX30 minicomputer equipped with a 12-bit Analog-Digital interface subsystem operated with an external

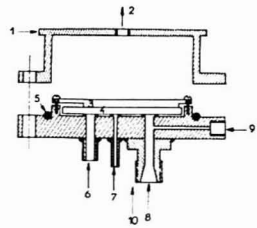


Figure 3. Section of the fluidic gate housing not drawn to scale but illustrating the construction and location of the various elements of the system. (1) Pressure housing. The logic gate vents into this chamber, (2) Connection for restricter R_v and pressure gauge, P_{cv}, (3) Holder for logic gate, (4) Logic gate, bistable fluidic amplifier, (5) Rubber O-rings, (6) Gas entrance. This may be carrier gas or sample gas depending on the application, (7) Command port. One is positioned behind the other, (8) Swagelok fitting. A $^1/_8$-inch o.d. column with ends notched so that it can be mounted against the fluidic gate, fits into this connection if the logic gate is powered by sample gas. If this is the carrier gas gate, connection is made between this point and the check valve input to the sample side of the system, (9) In the sample gas powered gate, the check valve is mounted here and carrier gas enters this port. In the carrier gas gate housing the pressure gauge, P_{O2} is mounted at this point, (10) The exit for O1 is located behind 8 and is constructed in a manner similar to that shown for 7

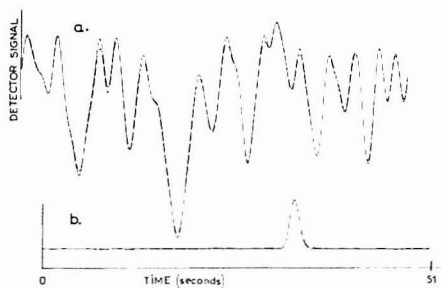


Figure 4. Reproducibility of sampling system. (a) Solid line = predicted output for multiple 100-ms injections commanded by a 511 PRBS using the experimentally determined 100-ms pulse response of the system as the basis for the construction. Dotted line = experimental detector response to multiple 100-ms injections commanded by a 511 RPBS. (b) Solid line = correlogram calculated from the predicted detector response shown in a. Dotted line = correlogram calculated from the experimental detector output shown in a. Sample = methane doped air, Carrier gas = nitrogen.

pacer at 1 kHz. To simplify programing, all data were acquired and stored on magnetic tape and correlations were performed at a later time and then presented on a Hewlett-Packard 9872 A plotter.

For test purposes, methane doped air and 50-ppm concentrations of ethane, propane in nitrogen were used as samples and nitrogen was used as the carrier gas.

To determine the reproducibility under the high speed conditions of correlation chromatography, the following method was used.

A single sample was injected within a predetermined time interval and the resulting chromatographic signal was recorded and memorized. This peak profile was then used as the impulse response of the system for the particular sample pulse width. A synthetic detector signal was constructed using this impulse response as the building block. The number and spacing of these pulses was determined by a pseudo-random binary sequence. Using this same binary code as the pattern for actual sample inputs, an experimental curve was then generated and compared to the synthetic curve for accuracy of correspondence. An example of such a comparison is shown in Figure 4 for a 100-ms unit code.

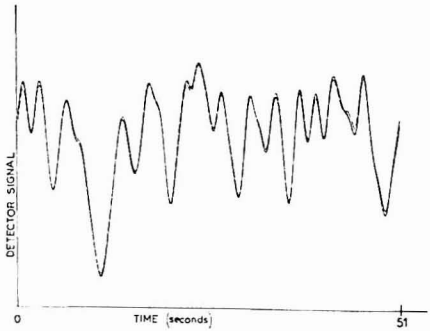


Figure 5. Stability of sampling system over extended periods of time. Experimental detector output measured over three periods of a 511 PRBS. Unit code width = 100 ms. Length of abscissa is equal to one PRBS period

Acceptable results were also obtained for 50-ms unit codes. The stability of the sample over longer periods of time is illustrated in Figure 5.

RESULTS AND DISCUSSION

In view of our suggestion that correlation chromatography is possible with an unmodified chromatograph provided that a sufficiently rapid sample valve is available (*3*), the stream switching arrangement depicted in Figure 1 seems unduly complicated. Indeed, preliminary experiments were conducted in this laboratory with a single bistable fluidic switch injecting small amounts of sample into the carrier gas. These efforts met with little success. The correlogram showed little or no relationship to single impulse chromatograms. On reflection, the reasons for this became quite obvious.

Consider that during the length of a correlation chromatography experiment, the pseudo-random code requests sample injection for 50% of the time. Thus, the detector base-line signal is really one for sample continuously present in the detector at a concentration level of 50% of its original value. The output is then developed about this elevated base line.

The retention time of the peaks is governed by the value of the equilibrium constant under these conditions and, although it may not be exactly the same as that obtained under normal single impulse chromatography conditions, the system will behave linearly as long as the concentration difference between the two streams is not too large (*4*, *10*), i.e., for trace analysis or difference chromatography. Thus retention time shift which may have been due to this effect was not the source of the problem we experienced in the analysis of the 50-ppm hydrocarbon mixtures used for test purposes.

The absolute value of the FID elevated base-line signal, however, depends directly on the number of ionizable components entering the flame per second (coulombs/second = amperes) and thus is no longer flow insensitive as with pure carrier gas. With the fluidic switch single injection procedure, sample is injected in addition to the carrier gas flowing into the column. The accompanying flow changes which caused changes in base-line signal and possibly flow related retention time shifts destroyed the linearity of the system and thus made correlation impossible.

It should be noted at this time that this problem is also expected to occur with the normal sample loop type injectors unless great care is exercised in balancing the sample loop pressure to the column head pressure.

The stream switch shown in Figures 2 and 3 was developed to eliminate these difficulties.

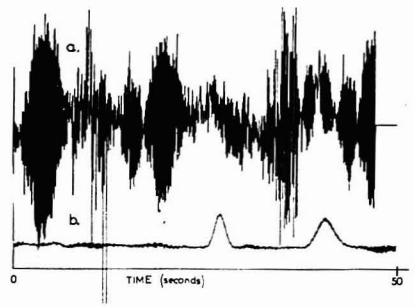


Figure 6. Comparison of a single injection chromatogram with a correlogram run under the same conditions. Carrier gas = nitrogen. Sample = 50-ppm concentrations of ethane and propane in nitrogen. (a) Chromatogram obtained from a single 50-ms injection of sample. (b) Correlogram obtained from multiple 50-ms injections using a PRBS of 1023

On examination, the configuration shown in Figure 2 reveals only one check valve. The reason for this is not obvious. One would expect that another one is needed to prevent the carrier gas from shorting out through the sample logic gate. However, it was found that the addition of another check valve in the O_2 leg of the sample gate destroyed the sharp sample profiles which were obtained in its absence and also increased the minimum sample width which could be reproducibly injected into the column. This problem persisted even with a physically close coupled configuration of the two logic gates.

It was also noted that P_s(carrier) and P_{ev}(carrier) had to be operated at higher pressures than P_s(sample) and P_{ev}(sample) to avoid the base-line shifts which occurred when switching from sample to carrier gas. In addition sharp increases in P_{ev}(sample) were observed when carrier gas was switched into the column.

These observations are consistent with the supposition that when the carrier gas was switched into the column, some of its flow is diverted back up through the sample logic gate while the rest flows into the column. The interesting consequence of this phenomenon is that apparently the diverted carrier gas flow washes all remainder of sample from the connecting tubing and logic gate leg so that when sample is again switched to the column leg, a sharp profile is presented to the column. In absence of this washout, sample remains in the connecting tubing and is mixed with some of the carrier gas. The next sample injection forces this diluted sample plus pure sample into the column. This leads in some cases to what appears to be a double injection and at other times to distorted peak profiles.

Similarly the test which was devised to check reproducibility of the sampling system seems unduly complex. However, it was found early in the research that a set of conditions which apparently gave reproducible samples behaved anonymously under high speed conditions, i.e., when the sampling interval was decreased below some minimum. Synthesizing the expected output under correlation conditions using the experimentally obtained single pulse chromatograms was found to be quickest way of identifying instrumental contributions to unsatisfactory correlograms.

Finally, the results obtained with this system which are summarized in Figure 6 demonstrate the effectiveness of the correlation procedure for recovering signals which are buried in the noise of the detection system. Certainly 50-ppm concentrations of hydrocarbons do not normally constitute a detection problem but under the conditions of this experiment conducted in a laboratory where the progress of

many other experiments contributed to a particularly dirty electrical environment, the improvement exhibited by the correlation mode of operation is rather remarkable.

ACKNOWLEDGMENT

We are deeply indebted to Guy Preau for his technical advice and assistance.

LITERATURE CITED

(1) Raymond Annino, "Signal and Resolution Enhancement Techniques in Chromatography" in "Advances in Chromatography", Vol. 15, Marcel Dekker, New York, 1977, pp 33-63.
(2) J. B. Phillips and M. F. Burke, *J. Chromatogr. Sci.*, **14**, 495 (1976).
(3) Raymond Annino and Eli Grushka, *J. Chromatogr. Sci.*, **14**, 265 (1976).
(4) Raymond Annino and L. E. Bullock, *Anal. Chem.*, **45**, 1221 (1973).
(5) Gyula Gaspar, Patrick Arpino, and Georges Guiochon, *J. Chromatogr. Sci.*, **15**, 256 (1977).
(6) Gyula Gaspar, Raymond Annino, Claire Vidal-Madjar, and Georges Guiochon, *Anal. Chem.*, **50**, 1512 (1978)
(7) Gyula Gaspar, Jean-Pierre Olivo, and Georges Guiochon, *Chromatographia*, in press.
(8) Robert L. Wade and Stuart P. Cram, *Anal. Chem.*, **44**, 131 (1972).
(9) Stuart P. Cram and Stephen N. Chesler, *J. Chromatogr.*, **99**, 267 (1974).
(10) Raymond Annino, Joseph Franko, and Harry Keller, *Anal. Chem.*, **43**, 107 (1971).

RECEIVED for review October 25, 1978. Accepted December 1, 1978.

Combination of Size Exclusion and Normal-Phase Partition Modes in High Performance Liquid Chromatography

Sadao Mori* and Akira Yamakawa

Department of Industrial Chemistry, Faculty of Engineering, Mie University, Tsu, Mie 514, Japan

Size exclusion chromatography (SEC) and normal-phase partition chromatography (NPPC) were performed on the same column packed with polystyrene gels used for SEC of small molecules. Chloroform was used as the mobile phase in SEC in order to measure the approximate numbers of components. Then, chloroform–*n*-hexane mixture was used for the complete separation. The potential utility of the SEC-NPPC technique was illustrated by application of phthalate esters, alkylbenzenes, and ketones. The combined use of SEC and NPPC on the same column may extend their advantages and compensate their disadvantages.

Recent improvements in high performance size exclusion chromatography (SEC) (conventional GPC) have advanced the separation of low molecular weight materials (*1*). Polystyrene gels with small pore and particle sizes permitted the complete separation of *n*-alkanes (*1*), phthalate esters (*2*), alkylbenzenes (*3*), oligostyrenes (*4*), and various other materials. In the separation of these materials by "true" SEC with polystyrene gels as packing materials, it is essentially necessary to use solvents as the mobile phase which minimize the interactions between the gels and solute molecules, i.e., good solvents for uncross-linked polystyrenes (*5*).

When solvents having solubility parameters much different from that of the polystyrene gel are used as the mobile phase, the separation mode may be regarded as liquid–solid, i.e., adsorption chromatography (*5*). *n*-Hexane has a solubility parameter less than that for the polystyrene gel and the separation mode is normal-phase adsorption chromatography (henceforth referred to as NPAC) where the elution order of the homologous series is in the order of decreasing molecular weight. Chloroform and tetrahydrofuran are eluents often used for SEC with the polystyrene gel. The separation mode of the mixtures of chloroform and *n*-hexane is regarded as normal-phase partition chromatography (henceforth referred to as NPPC), the elution order being the same as SEC and NPAC.

Among advantages and disadvantages in SEC, NPAC, and NPPC, those for low molecular weight materials are itemized as follows from a comparison standpoint. Advantages in SEC are the following four factors: (a) As a molecule of the largest size elutes first from the SEC column in principle, the information on the size or molecular weight of the separated molecules can be obtained without difficulty. (b) As no solute elutes after the total permeation limit, it is suitable for the preliminary analysis of unknown samples. (c) Columns of 8-mm i.d. are normally used, which enables a large sample load and application of a refractive index detector. (d) Compared to the other separation modes, the separation time is short. The need for greatly increased column length in the case of insufficient separation and the high cost of columns are disadvantages in SEC. Advantages in NPAC and NPPC are (a) the capability of the increased resolution of two adjacent bands by selecting the mobile phase or the constituents and (b) less costly columns with small volume of packing materials. A lower sample load than SEC and the difficult prediction of the existence of retarded solutes in the case of unknown samples are the disadvantages in NPAC and NPPC.

High performance liquid chromatography utilizes one of the four basic separation modes (adsorption, partition, ion exchange, and size exclusion) without combination of the other three modes. In SEC, for example, the information from the chromatogram is analyzed under the condition that adsorption or partition modes are not incorporated. On the other hand, the combined use of two separation modes will make it possible to extend their advantages and to compensate their disadvantages if the combination is adequate for the samples. Recently, coupled column chromatography using SEC and reversed-phase chromatography has been reported (*6*). In the method, SEC was used as the preliminary separation technique and some fractions which need more separation were transferred to other secondary columns(s) for further separation.

In our study, SEC and NPPC are performed on the same column packed with polystyrene gels used for SEC of low molecular weight materials. Chloroform was used in the first elution as SEC and then, the mobile phase was changed to the chloroform–*n*-hexane mixture as NPPC in order to obtain better separation. NPPC was performed on the SEC column (henceforth referred to as SEC-NPPC). The potential utility of the SEC-NPPC technique was illustrated by applications of three different homologous series.

0003-2700/79/0351-0382$01.00/0 © 1979 American Chemical Society

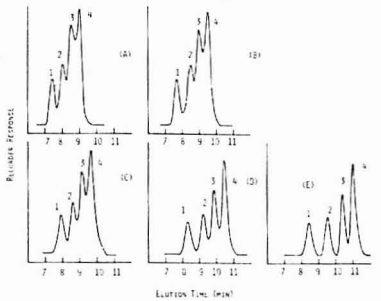


Figure 1. Size exclusion and normal-phase partition chromatograms of phthalates on the 4.5-mm i.d. column packed with Shodex A801 polystyrene gel. Flow rate: 0.48 mL/min. Attenuation: 0.64 AUFS. Sample volume: 10 μL. Mobile phase: (A) chloroform (pump pressure, 18 atm), (B) chloroform–*n*-hexane (9:1 v/v), (C) (8:2), (D) (7:3), (E) (5:5) (pump pressure, 10 atm). Solutes: (1) DNP, (2) DBP, (3) DEP, (4) DMP

EXPERIMENTAL

Apparatus. A Jasco (Japan Spectroscopic Co. Ltd., Hachioji, Tokyo, Japan) TRIROTAR high performance liquid chromatograph was used with a Jasco Model UVIDEC-100 variable-wavelength UV detector. The detector was operated at 254 nm. Mixed solvents were prepared using a solvent programmer Model GP-A30. Sample solutions were injected using a variable loop injector Model VL-611.

Columns. Three stainless steel columns of 50-cm length and different inside diameter were used. In a 2.3-mm i.d. column, Shodex HP-255 porous polystyrene gel of 25 ± 3 μm was packed by the slurry packing procedure using methanol–water (1:1) mixed solvent under a flow rate of 0.5 mL/min first and finally 1.0 mL/min. This packing material is used for adsorption or partition chromatography. A 4.5-mm i.d. column was packed with Shodex A801 polystyrene gel of 15–20 μm. This packing material is used for SEC of small molecules. Both packing materials are composed of the same matrix, but have different physical properties (5). The gel was suspended in a toluene–chloroform mixed solvent and packed into the column by the slurry packing procedure using the same solvent under a flow rate of 0.5 mL/min, followed by changing the solvent into chloroform and finally into chloroform–*n*-hexane (1:1) mixture. The final flow rate was 1.0 mL/min. A 8-mm i.d. column was a Shodex A 801 GPC column with A801 gel of about 10 μm packed by the manufacturer (Showa Denko Co. Ltd., Minato-ku, Tokyo, Japan). These packing materials and the column were provided by courtesy of Hikari Kogyo Co. Ltd., Chuo-ku, Tokyo, Japan.

Samples and Procedure. All compounds used as solutes (samples) were guaranteed reagents purchased from several chemical supply houses and used as received. They were phthalate esters, alkylbenzenes, and ketones as follows: dimethyl- (DMP), diethyl- (DEP), dibutyl- (DBP), and di-*n*-nonyl- (DNP) phthalates, benzene, toluene, ethyl- and *n*-octyl benzenes, acetone, methyl ethyl- (MEK), methyl isobutyl- (MIBK), and diisobutyl- (DIBK) ketones. A sample concentration was selected between 0.1 and 0.5% (w/v) to obtain suitable responses. Sample injection volumes, flow rates, and pump pressure are indicated in the figure captions. The mobile phase was chloroform, *n*-hexane, and mixtures of the two. All measurements were performed at room temperature.

RESULTS AND DISCUSSION

Figure 1 shows the chromatograms of phthalates achieved on SEC and SEC-NPPC using the 4.5-mm i.d. column. Figure 1A is the example of SEC and the phthalates were sufficiently resolved to make a tentative identification based on molecular size. However, more complete separation was accomplished by adding *n*-hexane to the mobile phase. Figures 1B–1E are the examples of SEC-NPPC and the increasing *n*-hexane content in the mobile phase resulted in increasing the resolution of the adjacent peaks. With the mixture of chloroform–*n*-hexane of the same volume content, all the phthalates were separated almost completely (Figure 1E).

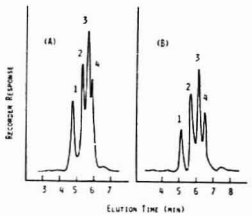


Figure 2. Chromatograms of alkylbenzenes on the same column as in Figure 1. Flow rate: 0.48 mL/min. Attenuation: 0.64 AUFS. Sample volume: 2 μL. Mobile phase: (A) chloroform, (B) chloroform–*n*-hexane (6:4 v/v). Solutes: (1) *n*-octylbenzene, (2) ethylbenzene, (3) toluene, (4) benzene

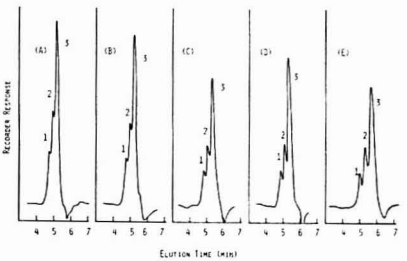


Figure 3. Chromatograms of ketones on the same column as in Figure 1. Flow rate: 1.0 mL/min. Attenuation: 0.08 AUFS. Sample volume: 10 μL. Mobile phase: (A) chloroform, (B) chloroform–*n*-hexane (9:1 v/v), (C) (8:2), (D) (7:3), (E) (6:4). Solutes: (1) DIBK, (2) MIBK, (3) MEK + acetone

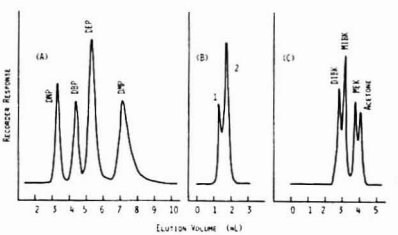


Figure 4. Normal-phase adsorption chromatograms on the 2.3-mm i.d. column packed with Shodex HP-255. Flow rate: 0.48 mL/min. Attenuation: 0.16 AUFS. Sample volume: 5 μL. Mobile phase: *n*-hexane (pump pressure 18 atm). Solutes: (A) phthalate esters, (B) alkylbenzenes (1. *n*-octylbenzene, 2. benzene, toluene, and ethylbenzene), (C) ketones

Figures 2 and 3 are the chromatograms of alkylbenzenes and ketones on the 4.5-mm i.d. column, respectively. Figures 2A and 3A are the examples of SEC and Figures 2B and 3B to 3E are those of SEC-NPPC. The increased resolution of alkylbenzenes by SEC-NPPC is predominant. The insufficient resolution of ketones by SEC (Figure 3A) was somewhat improved by adding *n*-hexane to the mobile phase, though peaks of acetone and MEK were still unresolved.

Phthalate esters were completely separated on the NPAC system employing the 2.3-mm i.d. column using *n*-hexane as an eluent. The result is shown in Figure 4 together with those of alkylbenzenes and ketones. Similar separation on SEC as in Figure 4 could be done using two Shodex A801 SEC col-

Table I. Peak Half-Width and the Resolution of Adjacent Peaks of Phthalate Esters on the SEC-NPPC System

mobile phase		DNP	DBP	DEP	DMP
chloroform	half-width, mL	0.18	0.17	0.18	0.17
	resolution[a]	1.04	0.61	0.64	
chloroform-*n*-hexane 9:1	half-width, mL	0.18	0.18	0.18	0.17
	resolution	1.18	0.59	0.94	
chloroform-*n*-hexane 8:2	half-width, mL	0.19	0.19	0.19	0.20
	resolution	1.24	0.77	0.94	
chloroform-*n*-hexane 7:3	half-width, mL	0.21	0.20	0.21	0.21
	resolution	1.26	0.90	0.90	
chloroform-*n*-hexane 5:5	half-width, mL	0.24	0.23	0.21	0.23
	resolution	1.33	1.12	0.93	

[a] Resolution = $1.177\ (V_2 - V_1)/(W_{(0.5)_1} + W_{(0.5)_2})$. V = elution volume (mL); $W_{(0.5)}$ = peak half-width.

umns of 8 mm i.d. × 50 cm length (2). However, total separation time by SEC was about 26 min under a flow rate of 1 mL/min. The cost of the SEC columns is about ten times that of the other two columns. Sample load on a 4.5-mm i.d. column increases 3.8 times that on a 2.3-mm i.d. column, but an eluent consumed by adsorption chromatography employing a 4.5-mm i.d. column would be about 5 times that by SEC-NPPC with the same column dimensions. This value was calculated by considering column size and the retardation of sample elution due to adsorption (compare the elution time of DMP in Figure 1E and Figure 4A). Hence, combination of SEC and NPPC would have proved advantageous over a single usage of SEC, NPAC, or NPPC.

Benzene, toluene, and ethylbenzene were not separated on the NPAC system employing a 2.3-mm i.d. column (Figure 4B). However, their elution volumes determined individually were not identical (5) and they could be separated by SEC-NPPC. A longer column is required for further separation. The case of acetone and MEK was the opposite. Though acetone and MEK could be separated on the NPAC system (Figure 4C), they were hardly separated on the SEC system (Figure 3A) and SEC-NPPC system (Figure 3B–3E).

Partial separation of adjacent peaks on SEC and NPAC systems are required for the success of the SEC-NPPC technique. Separation on the SEC system is the first requisite. Table I gives peak half-width and the resolution of adjacent peaks for phthalate esters on the SEC-NPPC system. The resolution increases with increasing *n*-hexane content, followed by the increase of peak half-width. The space between adjacent peaks must increase enough to compensate for the decrease of the resolution accompanied by the increase of peak width.

Figure 5 illustrates the results of SEC and NPPC of phthalate esters on the Shodex A801 GPC column of 8-mm i.d. Separation of the esters by SEC on one column was insufficient, but separation by SEC-NPPC was complete. However, the number of theoretical plates of the column decreased rapidly after this experiment, because the column was packed under the swollen state and the addition of nonsolvents such as *n*-hexane resulted in shrinkage of the gel in the column. In the SEC-NPPC step, the gel must be packed into the column with the solvent including *n*-hexane. In our experiment, the gel was packed with a mixture of chloroform and *n*-hexane (5:5). Table II indicates the reproducibility of the SEC-NPPC technique by successive change of the mobile phase in the order of chloroform, chloroform–*n*-hexane (5:5), chloroform, and finally chloroform–*n*-hexane (5:5). Consistent

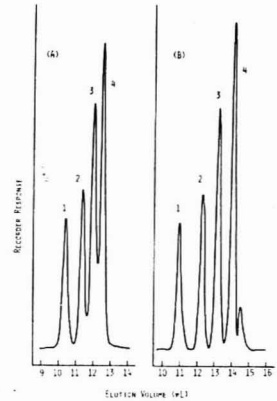


Figure 5. Size exclusion and normal-phase partition chromatograms of phthalate esters on the Shodex A801 GPC column of 8-mm i.d. Flow rate: 1.0 mL/min. Attenuation: 0.16 AUFS. Sample volume: 100 μL. Mobile phase: (A) chloroform (pump pressure 30 atm), (B) chloroform–*n*-hexane (7:3 v/v) (pump pressure 21 atm). Solutes: (1) DNP, (2) DBP, (3) DEP, (4) DMP

Table II. Reproducibility in SEC-NPPC Technique

run no.	mobile phase	elution volume,[a] mL DNP	DBP	DEP	DMP	N^b
1	chloroform	3.57	3.88	4.06	4.25	7700
2	chloroform–*n*-hexane (5:5)	4.05	4.58	5.00	5.34	6300
3	chloroform	3.56	3.89	4.11	4.27	7600
4	chloroform–*n*-hexane (5:5)	4.02	4.52	4.97	5.29	6700

[a] Average in triplicate measurements. Relative average deviation is within 0.8%. [b] Number of theoretical plate measured by benzene.

elution volumes and numbers of theoretical plates prove that this technique is the reproducible and powerful method in high performance liquid chromatography.

The technique of SEC-NPPC will be proved to be effective when unknown samples are separated. The SEC technique provides information about the number of components in the unknown sample. As the elution order of solutes in SEC and NPPC will not reverse each other, the number of components in the unknown sample can be estimated precisely by SEC-NPPC and the solute eluted behind will not be overlooked. The preparation of more rigid polystyrene gels for small molecules will increase the effectiveness of the SEC-NPPC technique, because the *n*-hexane content can be increased more than 50%. The SEC-NPPC technique will be applied to the separation of mixtures of several compound types besides homologues.

LITERATURE CITED

(1) A. Krishen and R. G. Tucker, *Anal. Chem.*, **49**, 898 (1977).
(2) S. Mori, *J. Chromatogr.*, **129**, 53 (1976).
(3) M. Popl, J. Coupek, and S. Pokorny, *J. Chromatogr.*, **104**, 135 (1975).
(4) Y. Kato, S. Kido, H. Watanabe, M. Yamamoto, and T. Hashimoto, *J. Appl. Polym. Sci.*, **19**, 629 (1975).
(5) S. Mori, *Anal. Chem.*, **50**, 745 (1978).
(6) E. L. Johnson, R. Gloor, and R. E. Majors, *J. Chromatogr.*, **149**, 571 (1978).

RECEIVED for review September 11, 1978. Accepted November 14, 1978.

Salting-Out Chromatography Applied to Separation and Analysis of Mixtures of Thioureas and Thioacetamide by High Performance Liquid Chromatography

Akio Hashimoto

Water Quality Research Section, Kitakyushu Municipal Institute of Environmental Health Science, 1-2-1 Shin-ike, Tobataku, Kitakyushu City, 804, Japan

Salting-out chromatography was applied to the separation of thiourea, ethylenethiourea, 1,3-dimethyl-2-thiourea, 1-allyl-2-thiourea, 1,3-diethyl-2-thiourea, and thioacetamide by high performance liquid chromatography. The best results were obtained when the flow rate is 18 mL/h, and the column temperature 60 °C, using 1.0–1.1 M of ammonium sulfate aqueous solution as a mobile phase. This method was applied to the analysis of field soil samples spiked with thiourea. A recovery of 99.3 ± 2.66% (n = 5) was obtained at the level of 160 ng/mL. The limits of detection were estimated to be 2.7 ng.

Thiourea (TU), one of the most widely used nitrification inhibitors in a compound fertilizer, has been reported to be a potential carcinogen in rats (*1–4*). In 1976 in Japan, 2714 tons of fertilizer containing TU was produced (*5*). Because of the widespread usage of the fertilizer, data were needed to see whether the compound would be a residue problem in the environment. To obtain such data, a new method of analysis had to be developed.

Several methods for the determination of TU such as colorimetric procedures (*6–9*), and chromatographic procedures, i.e., paper chromatography (*10*), thin-layer chromatography on silica gel (*11, 12*), on alumina (*13*), and column chromatography on ion-exchange resins (*14–16*), etc. have been reported. However, these methods have not succeeded in complete separation of thioureas and thioacetamide, and also are insufficient for monitoring trace amounts of TU in the environment.

In this paper, application of salting-out chromatography to the separation of a mixture of thioureas [thiourea (TU), ethylene-thiourea (ETU), 1,3-dimethyl-2-thiourea (DMTU), 1-allyl-2-thiourea (ATU), and 1,3-diethyl-2-thiourea (DETU)], and thioacetamide (TAA) in water by HPLC, and application of this procedure to the determination of TU spiked to field soil samples are described. The method is simple, rapid, and sensitive.

EXPERIMENTAL

Apparatus. Chromatographic separations were carried out with a chromatographic system consisting of a Hitachi model 635 pumping system (Hitachi, Ltd., Tokyo, Japan), a Hitachi sampling injection valve (catalogue no. 645-0435) and a Hitachi Wavelength Tunable Effluent Monitor (catalogue no. 634-0514). Temperature of the column was controlled with a Hitachi Circulating Water Bath Temperature Controller (catalogue no. 635-0203). Retention time and peak area were measured by a Hitachi Model J211A Digital Integrator. The columns were 2.6 mm i.d. × 500 mm length stainless steel with a water jacket. Ultraviolet spectra were measured with a Shimadzu Multi-purpose Recording spectrophotometer Model MPS 5000 (Shimadzu, Ltd., Kyoto, Japan).

Reagents and Materials. All reagents used were of analytical grade. Ethylene thiourea (2-imidazolidine thione), 1,3-dimethyl-2-thiourea, 1,3-diethyl-2-thiourea, and thioacetamide were supplied by Tokyokasei, Ltd., Tokyo, Japan. Thiourea was supplied by Kishida Chemical Ltd., Osaka, Japan. 1-Allyl-2-thiourea was supplied by Kanto Chemical Co., Tokyo, Japan. A Hitachi custom cation-exchange resin with most probable pore size 17.5 μm (catalogue no. 2610) was supplied by Hitachi Ltd., Tokyo, Japan.

Preparation of Mobile Phase. The ammonium sulfate aqueous solution used as the mobile phase was filtered with a Toyo No. 5C filter paper and the filtrate was degassed ultrasonically for 2 h.

Packing of Cation-Exchange Resin. The cation-exchange resin was packed with the conventional method, wet packing at a pressure of 100 kg/cm^2, suspending in 1.0 M ammonium sulfate solution and equilibrating for 30 min.

Preparation of Standard Solution. Thioureas except for ETU and TAA were weighed accurately to 100.0 mg and were dissolved in water purified by ion-exchange and distillation. ETU was weighed and dissolved in 20 mL of methanol, subsequently in water purified by ion exchange and distillation. Each solution was made up to 50 mL with water in a calibrated flask, and then these mother solutions were diluted to appropriate concentrations.

Procedure. A 5-μL aliquot of an aqueous solution containing the mixture of thioureas and thioacetamide (40 μg/mL each) was injected by syringe with sampling injection valve in the separation experiments, and also in the sensitivity and precision section; 100 μL was injected with a loop type sampling system. In the separation section, three factors were varied: (1) the column temperature from 23 to 60 °C; (2) the flow rate of mobile phase from 18 to 42 mL/h; and (3) the concentration of ammonium sulfate from 0.05 to 1.5 M. The eluate was monitored at 240 nm.

Extraction Procedure for Field Soil Sample. To 5 g of field soil sample spiked with 4.0 μg of TU was added 20 mL of pure water and stirred well with a magnetic mixer, then filtered with a dried 5C Toyo filter paper. Twenty μg of 1,3-dimethylthiourea as an internal standard was added to the filtrate and the total volume was made up to 25 mL in a calibrated flask. A 100-μL aliquot of the sample was injected into HPLC.

RESULTS AND DISCUSSION

The ultraviolet absorption curve for each compound in aqueous solution is shown in Figure 1. Absorption maximum and the molar absorptivity are 237 nm (1.02×10^4), 234 nm (1.05×10^4), 236 nm (1.06×10^4), 234 nm (1.37×10^4), 239 nm (1.05×10^4), and 264 nm (1.11×10^4) for TU, DMTU, DETU, ETU, ATU, and TAA, respectively. To detect all the compounds tested, the absorption at 240 nm was selected for monitoring the eluate throughout the experiments.

To evaluate some characteristics of salting-out chromatography using HPLC, the usual formulas for capacity factor k', the height equivalent to a theoretical plate HETP, enthalpy ΔH, and salting-out constant K_s (*17*), were used. The limits of detection were estimated as twice the signal-to-noise ratio.

Effect of Concentration of Ammonium Sulfate. The logarithms of k' are plotted against the concentration of ammonium sulfate in Figure 2. These plots follow fairly closely Equation 1.

$$\log k' = \log k'_0 + K_s M \quad (1)$$

where k'_0 is the capacity factor with water as mobile phase, k' is the capacity factor with the aqueous salt solution of

0003-2700/79/0351-0385$01.00/0 © 1979 American Chemical Society

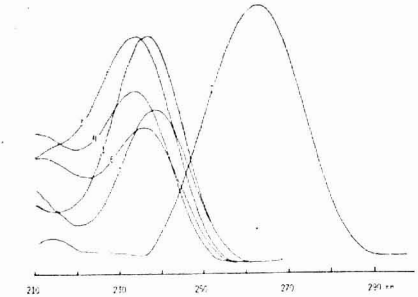


Figure 1. Ultraviolet absorption curve for each compound in water. 1, TU; 2, TAA; 3, ETU; 4, DMTU; 5, ATU; and 6, DETU. Concentration is 8 μg/mL each

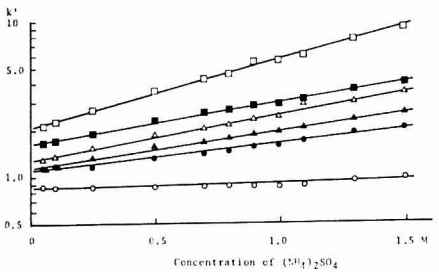


Figure 2. log k' vs. concentration of ammonium sulfate. -□—□- DMTU, -■—■- ATU, -△—△- DMTU, -▲—▲- ETU, -●—●- TAA, -○—○- TU. Conditions: column, 500 mm × 2.6 mm, Hitachi cation-exchange resin #2610; flow rate, 18 mL/h (570 psi); column temperature, 60 °C; concentration, 200 ng for each compound with 5-μL injection; sensitivity, 0.16 AUFS

Table I. Salting-Out Constants[a] and ΔH

compound	log k''_0	K_s	ΔH kcal/mol
TU	−0.071	0.038	1.88
TAA	0.037	0.18	2.33
ETU	0.049	0.24	2.82
DMTU	0.097	0.29	2.65
ATU	0.20	0.27	2.87
DETU	0.32	0.45	3.22

[a] The constants listed were calculated from the mean value of at least two measurements.

molarity M, and K_s is the salting-out constant. These constants are listed in Table I. Increasing the concentration of ammonium sulfate from 0.05 to 1.5 M, the k' value for each compound, except for TU, increased, i.e., the higher the concentration of ammonium sulfate, the stronger are the compounds, except for TU, absorbed on the column. The salting-out constant K_s, calculated from the slopes of Figure 2, shows the relative magnitude of the salting-out effect of ammonium sulfate on each compound. The K_s is largest for DETU, DMTU, ATU, ETU, TAA, and smallest for TU, which is little affected by the concentration of ammonium sulfate as is the K_s value shown.

In order to obtain some insight into the nature of an interaction in this system, enthalpies of transfer from the stationary phase to the mobile phase were determined, ΔH was obtained by plotting the logarithm k' against $1/T$, and the values are given in Table I. The ΔH is largest for DETU,

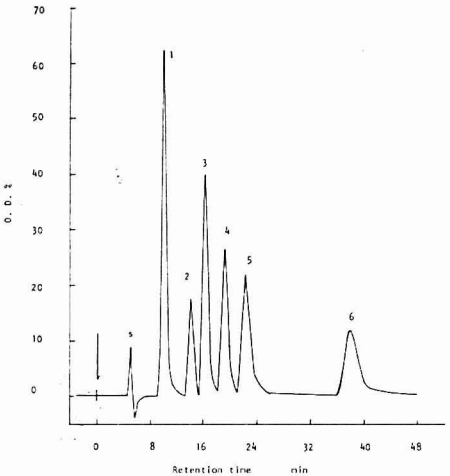


Figure 3. Typical chromatogram of compounds. Numbering of compounds as in Figure 1. S = solvent. Conditions as in Figure 2. Mobile phase is 1.1 M ammonium sulfate

ATU, DMTU, ETU, TAA, and is smallest for TU. The magnitude of the ΔH of this system is similar to that of usual absorption chromatography (*18*). The magnitude of K_s of each compound is proportional to that of the steric effect of N-substituted functional group of thioureas, i.e., 1,3-diethyl of DETU is bulkiest among the compounds tested and 1,3-dimethyl of DMTU, 1-allyl of ATU, ethyl of ETU, and hydrogen of TU is smallest. These facts give a good explanation for the elution sequence of the compounds studied, i.e., the elution sequence is determined by k'_0 and K_s in the salting-out chromatography.

Effect of Flow Rate on Column Efficiency. The logarithm of HETP, calculated from the data of DETU on the last peak of the chromatogram, was plotted against the logarithm of flow rate. The relationship between HETP and v follows closely the equation, $H = Av^n$ (*19*). The calculated n value is 0.935, and this value is higher than that of the other chromatographic systems reported (*18, 20*). The result means that the resin used is not suitable for higher speed operation than that described in this paper in the column system of salting-out chromatography, because the high flow rate of the mobile phase causes the decrease of column efficiency. As was the result shown, the HETP of the column is improved about twofold from 0.671 at 42 mL/h to 0.313 at 18 mL/h.

Effect of Column Temperature on Column Efficiency. The HETP, calculated from the data of DETU, was improved about fourfold from 1.28 at 23 °C to 0.29 at 60 °C.

In conclusion, when the concentration of ammonium sulfate, the flow rate, and the column temperature were 1.0–1.1 M, 18 mL/h, and 60 °C, respectively, the complete separation of five thioureas and TAA was obtained as shown in Figure 3.

With the chromatographic conditions described, the relationship between peak height and concentration of each compound is linear within the range of 0 to 300 ng with 5-μL injections. The relative standard deviation calculated from a series of 10 replicate determinations at the level of 200 ng of each compound, in the form of standard solution, was 2.6%, 2.4%, 3.4%, 2.4%, 2.6%, and 2.2% for TU, TAA, ETU, DMTU, ATU, and DETU, with 5-μL injections, respectively.

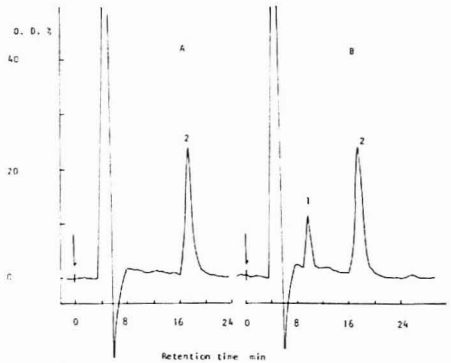


Figure 4. HPLC of (A) blank of field soil and (B) field soil spiked TU at the level of 160 ng/mL. (1) TU, (2) DMTU as internal standard. Conditions as in Figure 3. Sample volume injected: 100 μL, UV monitored: 237 nm, AUFS: 0.08

The limits of detection were estimated to be 1.5 ng, 8.8 ng, 2.3 ng, 3.7 ng, 3.7 ng, and 9.1 ng for TU, TAA, ETU, DMTU, ATU, and DETU, for a standard solution, with 100-μL injections, respectively.

Analysis of TU Spiked to Field Soil Sample. Typical chromatograms of field soil samples are shown in Figure 4A and 4B. Control field soil samples showed no interfering peaks (Figure 4A). A recovery of 99.3 ± 2.66% (mean ± rel. stand. dev., $n = 5$) was obtained when TU was spiked to field soil samples at the level of 160 ng/mL. The limits of detection were estimated to be 2.7 ng in this case. The method was also applied to industrial waste, river water, seawater, and secondary treated sewage effluent, and none of the samples showed interfering peaks; TU was not detected.

ACKNOWLEDGMENT

The author thanks T. Akiyama, Research Director of the Kitakyushu Municipal Institute of Environmental Health Sciences, for his valuable advice and encouragement. He also thanks the authority of the institute, for permission to publish this paper.

LITERATURE CITED

(1) H. J. Morris, *J. Natl. Cancer Inst.*, **7**, 159 (1946).
(2) H. D. Purves and F. W. Grissbach, *Br. J. Exp. Pathol.*, **27**, 24 (1946).
(3) H. D. Purves, *Br. J. Exp. Pathol.*, **27**, 294 (1946).
(4) A. Rosin and M. Bachmilewitz, *Cancer Res.*, **14**, 494 (1954).
(5) M. Watanabe, *Hiryo Nenkan (in Japanese)*, 1978, p 337.
(6) R. C. Hoseney and K. F. Finny, *Anal. Chem.*, **36**, 2145 (1964).
(7) Association of Official Analytical Chemists, "Official Methods of Analysis", 11th ed., Washington D.C., 1970, p 350, 29.099.
(8) E. T. Raktzes, *Anal. Chim. Acta*, **78**, 495 (1975).
(9) S. Goto, O. Ogawa, I. Asakawa, and C. Oshima, *Nippon Kogyo Kaishi*, **88**, 1067 (1972).
(10) W. P. Mckinley and R. Yasin, *J. Assoc. Off. Anal. Chem.*, **43**, 829 (1960).
(11) J. H. Onley and G. Yip, *J. Assoc. Off. Anal. Chem.*, **54**, 165 (1971).
(12) M. B. Devani, C. J. Shishoo, and B. K. Dadia, *J. Chromatogr.*, **105**, 186 (1975).
(13) I. M. Kovina and N. K. Rozhkova, *Dokl. Akad. Nauk. Uzb. SSR*, **25**, 25 (1968).
(14) K. Seiffarth and W. Aldelt, *Plaste Kautsch.*, **15**, 818 (1968).
(15) E. N. Boitsov, Yu. I. Mushkin, and V. M. Kavlik, *Zavod. Lab.*, **35**, 790 (1969).
(16) N. Nomura, D. Shiho, K. Osuga, and M. Yamato, *J. Chromatogr.*, **42**, 226 (1969).
(17) R. N. Sargent and W. Rieman III, *J. Phys. Chem.*, **61**, 354 (1957).
(18) K. Fujita, Y. Arikawa, and S. Ganno, *Nippon Kagaku Kaishi*, **3**, 463 (1975).
(19) J. L. Waters, J. N. Little, and D. F. Horgan, *J. Chromatogr. Sci.*, **7**, 293 (1969).
(20) L. R. Snyder, *J. Chromatogr. Sci.*, **7**, 352 (1969).

RECEIVED for review March 25, 1977. Resubmitted September 7, 1978. Accepted November 8, 1978. This work was financially supported by the Environment Agency of Japan.

High Gas Temperature Furnace for Species Determination of Organometallic Compounds with a High Pressure Liquid Chromatograph and a Zeeman Atomic Absorption Spectrometer

Hideaki Koizumi,*[1] Ralph D. McLaughlin, and Tetsuo Hadeishi

Lawrence Berkeley Laboratory, University of California, Berkeley, California 94720

A new furnace has been constructed that allows atomic absorption detection of volatile organometallic compounds. The operation of this furnace is demonstrated by analyzing the eluent of a high pressure liquid chromatograph utilizing Zeeman atomic absorption spectrometry. The content of tetraethyllead in National Bureau of Standards gasoline standards was determined. Data are presented on the ability of this furnace to suppress interference with cadmium and lead determinations by $MgCl_2$, $CuCl_2$, and $CaCl_2$. It was found that two orders of magnitude more interferent can be tolerated. The determination of lead in automotive exhaust is also described.

Species determination of organometallic compounds is nowadays one of the most important subjects in analytical chemistry. This is because the toxicity of metals depends upon the binding conditions in the compound (*1*). Speciation of organometallic compounds is also important in physiology and biology. Up to now, more than 1000 enzymes and coenzymes have been found and about one third of them are "metalloenzymes" or "metal-substrate complexes" (*2*).

It is a well known fact that commercial gasoline contains alkyllead compounds. In the United States, leaded gasoline contains around 0.1% of alkyllead, and commercial unleaded gasoline is defined as gasoline having not more than 0.05 g Pb/gal (13.16 μg/mL) (*3*). This paper describes the use of a special furnace Zeeman atomic absorption (ZAA) combination as a detector for a high pressure liquid chromatograph (HPLC) for the determination of organometallic lead com-

[1] Permanent address, Naka Works, Hitachi Ltd., Katsuta, Ibaraki 312, Japan.

0003-2700/79/0351-0387$01.00/0 © 1979 American Chemical Society

pounds in gasoline.

Various types of organic solvents are used as eluents for HPLC columns: aromatic compounds such as benzene and toluene, alcohols, ketones, and nitro compounds. Therefore, we are obliged to determine trace amounts of metals in a variety of organic solvents. With conventional techniques of trace element detection, including atomic emission and absorption spectroscopy and mass spectroscopy, it is very difficult to avoid interferences caused by large amounts of organic solvent. In many cases, the organic solvent cannot be eliminated by vaporization before the measurement because many organometallic compounds have boiling points below 200 °C and a considerable part of the organometallic compound escapes with vaporization of the solvent. For example, the mercury signal from methylmercuric chloride in benzene solution cannot be obtained by mass spectrometry, because this compound evaporates at around 100 °C (*4*).

Several researchers have used atomic absorption methods as detectors for HPLC (*5–7*). These methods generally have many advantages over other techniques. However, interference caused by the eluent was still a problem, because ashing temperatures had to be kept as low as possible to avoid evaporation of organometallic compounds. Strictly speaking, furnace ashing should not be used for organometallic compounds because of their volatile nature.

The Zeeman atomic absorption (ZAA) technique has features that make it attractive for determinations of this kind (*8*). ZAA can measure accurate values of atomic absorption signals with 500–1000 times larger background absorption (*9–11*). The stability of the base line is also a desirable feature for long time measurement with HPLC (*12*). However, at times, there is a problem in the determination of organometallic compounds, even though the ZAA technique provides excellent background correction. For example, the absorption signal of Pb in alkyllead compounds cannot be observed with the conventional graphite furnace because highly volatile alkyllead escapes from the cuvette before atomization.

There are also problems that arise when the flame is used for atomization of alkyllead in gasoline which require special treatment of the sample to obtain accurate results. These problems arise because tetramethyllead (TML) produces a different absorbance value than does the same amount of tetraethyllead (TEL) (*13*). It is much more difficult to get the same absorbance response from the various species in conventional furnace AA than in flame AA. Therefore, a different furnace is necessary to atomize the metal in organometallic compounds and for speciation studies in conjunction with HPLC.

One way to minimize the different response of different species is to dissociate the organometallic compound as completely as possible into individual atoms by heating to high temperatures. Conventional furnaces are not very effective because the gas temperature of the furnace is much lower than the wall temperature and the sample vapor easily diffuses out of the hot part of the cuvette before reaching a high temperature (*14*, *15*).

Figure 1 shows various possible furnace designs to achieve high gas temperatures. Figure 1a shows the type of furnace used in this work. Figure 1b shows a double chamber furnace (*10*) cuvette which can be used in commercially available Massmann type furnaces. The same high temperature can be obtained with this arrangement as with the conventional graphite tube cuvettes because the surface area of the cuvette is kept small to minimize radiation loss. The recovery of the element in a sample with a complex matrix is highly improved compared with conventional cuvettes. However, this cuvette cannot achieve 100% recovery for highly volatile organometallic compounds such as TML and TEL. Figure 1c shows

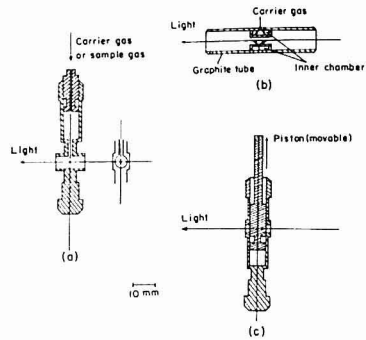


Figure 1. Various types of high gas temperature (HGT) furnaces

Table I. Instrumentation for HPLC-ZAA System

HPLC	
	high performance liquid chromatograph, Hitachi M633, 0-350 kg/cm², 0.36 ~ 3.6 mL/min
	column, Hitachi, 2.5 × 500 mm
	resin, Hitachi Gel No. 3010
Furnace	
	graphite, Ultra Carbon 0.5-in. diameter
	porous graphite, RVC 100 PPI porosity grade
	furnace power supply, reactor controlled, 20 V, 700 A
ZAA spectrophotometer	
	light source, magnetically confined lamp (dc + rf (50 MHz))
	magnet, permanent, 12 kg
	variable retardation plate, 0 ~ λ/2, 30 Hz
	polarizer, Rochon prism (quartz, optical contact)
	monochromator, Hitachi M100 spectrophotometer
	photomultiplier, Hamamatsu T.V., YA 7122
	chopper, Bulova L2C, 1.0 KHz
electronics	
	lock-in amplifier (including log convertor, AGC)
	recorder, Honeywell Electronik 17

a closed system furnace. A sample is atomized in a closed space and kept there for a while to achieve complete dissociation. The piston is moved with the thermal expansion of the sample vapor, and just after the piston passes by the windows, an absorption measurement is made. The properties of this cuvette are now being investigated. The circular cavity furnace (*16*), which was recently developed by L'vov, is also a kind of high gas temperature furnace.

If a furnace could be constructed to raise the gas temperature high enough, the dissociation of all organometallic compounds would occur and the signal would be independent of species. In this paper, we will report the species determination of organometallic lead compounds by utilizing a HPLC-ZAA system with a new furnace that can efficiently atomize these highly volatile compounds.

EXPERIMENTAL

Table I lists the experimental apparatus and parameters. The same ZAA spectrophotometer as reported before was used through this experiment (*11*).

Figure 2 shows the cross section of the present furnace, which is called the high gas temperature (HGT) furnace. This furnace consists of several separate parts; the sample cup, the thermal converter and reactor of porous graphite, a narrow hole (which at high temperatures also acts as a thermal converter), and the absorption cell. The sample vapor flows through the thermal converter and its temperature is raised sufficiently to decompose the compound and to atomize the metal. After that, the sample vapor is carried to the absorption cell for ZAA measurement.

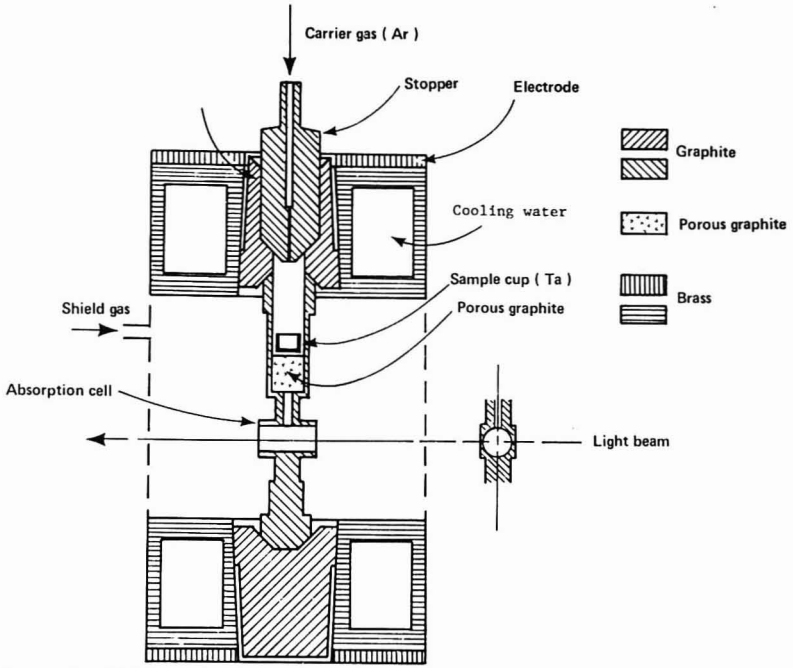


Figure 2. Cross section of HGT furnace

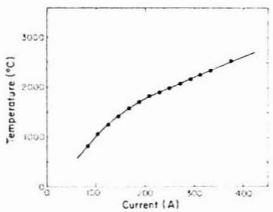


Figure 3. Relationship between current and temperature of hottest region of HGT furnace

In the case of the present furnace, the center portion of the cuvette is heated to a high temperature first because of the small heat capacity and the large electrical resistance. Conductive heating causes the porous graphite to be heated next and, finally, the tantalum cup is heated. A few seconds after the current is turned on, the temperature difference between the three sections begins to decrease. Vaporized sample in the cup follows the flowing argon gas through the porous graphite where its temperature is raised by coming into intimate contact. It then passes through a small hole, the walls of which have the highest temperature. Because of intimate contact with these surfaces, the gas temperature becomes equal to the wall temperature before passing into the absorption cell.

Figure 3 shows the relationship between the temperature of the regions just above the absorption cell and the current supplied to the cuvette. The surface area and the heat capacity of this cuvette are as small as the Massmann furnace (*17*). It is easy to raise the temperature of the cuvette to 2800 °C by supplying about 5 kW of electric power. This high temperature makes it possible to atomize various types of elements that are not possible with the Woodriff type furnace (*18*, *19*). This furnace is small enough to fit between the poles of a permanent magnet if the polarized Zeeman AA technique is utilized (*12*).

Table II. Properties of Selected Pb Compounds (*20*)

compound	formula	critical temperatures, °C melting	boiling	dissociation
lead nitrate	$Pb(NO_3)_2$			470
lead chloride	$PbCl_2$	501	950	
lead monoxide	PbO	888	1740	
lead chloride	$PbCl_2$	501	950	
tetramethyllead	$Pb(CH_3)_4$	−27.5	110	
tetraethyllead	$Pb(C_2H_5)_4$	−136.8	200[a]	200
tetraphenyllead	$Pb(C_6H_5)_4$	227.7		270

[a] Decomposition temperature

The system used to separate alkyllead compounds is described in Table I. Methyl alcohol was used as the eluent. The pressure was about 30 kg/cm², and the flow rate was 0.67 mL/min. A sample of 10 μL was injected into the HPLC while the flow was stopped. A 10-μL aliquot from each 250-μL portion of column effluent was intermittently introduced into the HGT furnace.

RESULTS AND DISCUSSION

Table II shows the properties of lead and some lead compounds (*20*). Usually, $Pb(NO_3)_2$ is used for the lead standard in atomic absorption spectrometry. $Pb(NO_3)_2$ decomposes into PbO around 470 °C, and atomic Pb is produced from the dissociation of PbO. In the graphite furnace, the following reduction process also proceeds on the surface of graphite.

$$C + PbO = Pb + CO$$

Atomic lead appears at around 770 °C, and the change of free energy, ΔG, for this reaction is −22 kcal/mol at this tem-

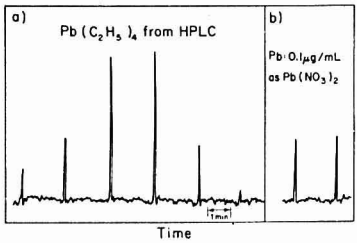


Figure 4. (a) ZAA signals of tetraethyllead peak from HPLC column showing distribution in 1.5 mL of eluent, (b) signal from standard lead solution (0.5 N HNO_3)

Table III. Results of Direct Determination[c] of Pb in NBS Gasoline Standard by ZAA with High Gas Temperature Furnace

standard used	solvent	Pb in NBS SRM 1636, μg/mL[a] result[b]	certified value
$Pb(NO_3)_2$	HNO_3 [0.5 N]	19.1 ± 0.5	19.15
$Pb(C_6H_5)_4$	C_6H_6	19.3 ± 0.5	

[a] At 20 °C. [b] Solvent: MIBK. [c] Number of determinations, 6.

perature. Usually, the ashing temperature for Pb is chosen to be below 600 °C, and the atomizing temperature is around 1500 °C (*21*).

TML and TEL are liquid at room temperature. TML boils at 110 °C and TEL decomposes at 200 °C. They are easily vaporized, even at the drying temperature. With the conventional furnace, if we try to atomize these organometallic compounds without drying, they vaporize before the gas temperature becomes high enough to produce lead atoms.

The organometallic lead compounds listed in Table II were introduced into the present furnace and the signals were compared with those from an inorganic lead standard: $Pb(NO_3)_2$ 0.1 μg/mL in HNO_3 (0.5 N). The alkyllead compounds were dissolved in benzene, such that the final concentration was 0.1 μg/mL; 10-μL aliquots were directly atomized without drying and ashing. The strong background absorption interference was corrected by using ZAA technique. The same peak height of lead atomic absorption was observed for each sample. Examples of the signal shape for organic and inorganic lead compounds are presented in Figure 4. The similarity in peak shape supports the idea that the metal organic compound is totally atomized in the furnace.

The concentration of Pb was determined in the NBS standard fuel SRM-1636 which contains the lead in the TML and TEL forms in 91 octane number reference fuel (a mixture of about 91% 2,2,4-trimethylpentane and 9% *n*-heptane). This NBS standard was diluted by a factor of 1/200 with methyl isobutyl ketone, and 10 μL of the sample was directly atomized using the HGT furnace. Both inorganic and organic lead solutions were employed as standards: $Pb(NO_3)_2$ in HNO_3 (0.5 N), and tetraphenyllead (TPL) in benzene. The reason TPL was used as the organic lead standard is that TPL is crystalline at room temperature and is comparatively stable. This aids in the preparation of an accurate standard solution. Table III shows the results of the analysis. Good agreement was obtained with the certified NBS value, both when the inorganic and organic lead standard solutions were used. From these results, we can safely conclude that both the same accuracy and the same sensitivity is obtained for the inorganic lead and organic lead compounds in spite of a big difference

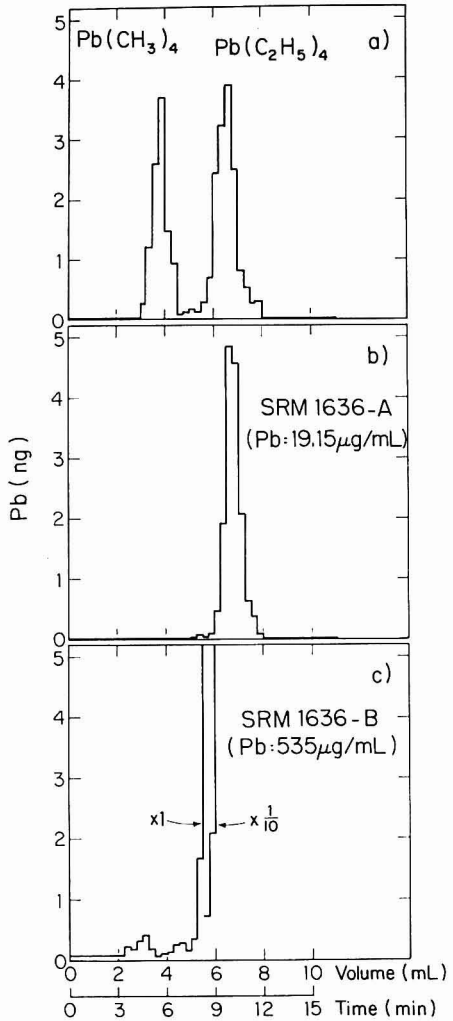


Figure 5. Elution chromatograms for alkyllead compounds: (a) 80 μg/mL tetramethyllead and 20 μg/mL tetraethyllead, (b) and (c) NBS standard lead in gasoline samples

in vaporization temperatures. Now, the determination of the concentration of various organometallic species is possible with the HGT furnace because the sensitivity is independent of species.

Figure 5a shows the histogram of lead concentration in various portions of the eluent. The peaks of TML and TEL appear at retention times of 5.5 and 10 min, respectively. The histogram in Figure 5a shows that TML and TEL can be separated without overlap. The recovery (the ratio of the amount of injected lead to the total amount of the observed lead in the elutent from the column) was 97% for TEL, and 25% for TML; 75% of TML might be dissociated and trapped in the resin. In the GC-Flame AA system, several TML peaks

Table IV. Comparison of Chemical Interferent Levels between High Gas Temperature Furnace and Conventional Furnaces

element	interferent	concentration of interferent, μg/mL	recovery, % conventional furnace	ref.[b]	high gas temperature furnace
Pb	$MgCl_2$	100	63 (95)[a]	*25, 26*	
		1 000	6 (29)[a]	*25*	
		5 000	18	*27*	93
		10 000			68
	$CaCl_2$	100	74 (98)[a]	*25*	
		1 000	0 (45)[a]	*25*	
		5 000	48	*23*	
		10 000			100
	$CuCl_2$	100	0	*24*	
		10 000			82
Cd	$CaCl_2$	10 000	0	*23*	97

[a] CTA. [b] Ref. 23: HGA70, HGA2000. Ref. 24: CRA63. Ref. 25: CRA63 (a.CTA). Ref. 26: HGA.70. Ref 27: HGA2200.

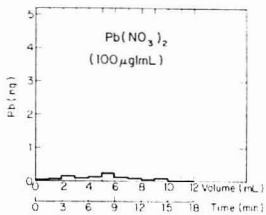


Figure 6. Chromatogram showing spreading of $Pb(NO_3)_2$ by the Hitachi Gel No. 3010 column

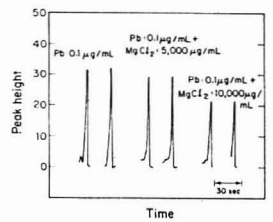


Figure 7. Lessening of suppressions of Pb signal by $MgCl_2$ through the use of the HGT furnace

were observed (22). This shows that TML is very unstable. When the inorganic lead solution $Pb(NO_3)_2$ was introduced into the HPLC containing Hitachi No. 3010 resin, almost no lead was recovered (Figure 6). In order to separate organic lead from inorganic lead, the Hitachi ion-exchange column No. 2611 should be used. We have already reported on the use of this column to separate Co bound to vitamin B_{12} from inorganic Co (8).

Next, the determination of TML and TEL in the NBS standard was performed using the HPLC-ZAA system. Ten μL of NBS 1636-A (10.15 μg Pb/mL) was introduced into the system. A clear peak (Figure 5b) was obtained at the retention time at 10 min. The concentration of lead in the elutent is also shown in this figure. The content of lead integrated over this peak is 187 ng, which is 97.6% of the lead in the injected NBS standard (191.5 ng). No peak could be observed at the retention time corresponding to TML at 5.5 min. A higher concentration standard (NBS 1636-B, 535 μg Pb/mL) was introduced into the system to check the existence of TML. However, a peak for TML could not be observed as shown in Figure 5c. We also confirmed that inorganic lead and TPL do not cause a peak near the TEL position (Figure 6). Therefore, we can conclude that the NBS standards which were used in this experiment contain more than 95% of one lead species (TEL). (These NBS standard Pb in gasoline samples were purchased in 1975 and the unopened ampules were stored in a dark box until used.)

Decrease of Chemical Interferences Caused by Large Quantities of Salts. Chemical interference by metal halides causes serious problems in conventional furnace AA (*23–30*). The use of the high gas temperature (HGT) furnace greatly reduces this type of interference. A typical case of this kind of interference occurs when $MgCl_2$ is present during the determination of Pb. Sometimes only 50 μg/mL of $MgCl_2$ causes a 30% depression of the Pb signal. Molecular absorption and scattering by $MgCl_2$ is not large at 283.3 nm (the wavelength of the Pb resonance line). Therefore, this phenomenon is totally due to chemical interference. Figure 7 shows the effect of $MgCl_2$ upon the Pb signal using the HGT furnace. Table IV lists the magnitude of signal suppression for several salts. It can be seen that $MgCl_2$ is the strongest suppressing agent.

This ability of the HGT furnace to prevent signal suppression cannot be explained by the high temperature of the sample vapor. The change of free energy, ΔG, for the dissociation of PbCl is still large at a temperature of 2500 °C. Hence, thermal dissociation would not be expected to occur. A possible explanation would be that a reduction process is accelerated because of the large surface area of the porous graphite.

Other Applications of the High Gas Temperature Furnace. The lead concentration in exhaust gases can be measured by using the HGT furnace. Automobile exhaust gas was collected in a polyethylene bag and was forced to flow through the HGT furnace carrier gas inlet port at a flow rate of 90 cm^3/min. The lead concentration in the exhaust gas was determined from the area under the absorption signal to be 0.3 ng/cm^3. Hence, this furnace is capable of on-line monitoring of trace elements in gas or ambient air.

Another important area of application is to the direct analysis of solid samples. Because this furnace tends to prevent molecular formation, solids can be volatized and the elements in that sample can be atomized, and the sensitivity will be largely independent of organometallic species. This will be true, even for highly volatile compounds. Preliminary work on metal organic lead compounds in oil have indicated complete recovery when the oil is injected directly into the furnace.

In this paper, the problems that cause difficulties in species determination of organometallic compounds have been discussed. HPLC is a very powerful technique for the nondestructive separation of organometallic compounds. However,

if this technique is used, the problems of interference caused by the organic eluent and losses of highly volatile organometallic compounds still remain. It is very difficult to separate the eluent from volatile organometallic compounds. Our approach is to vaporize the sample in a quasi-closed space and to raise the temperature of the sample vapor as high as possible to highly dissociate the molecules. The interference caused by background absorption is avoided by utilizing the Zeeman AA technique. When more complete dissociation of molecules is necessary, a dc or rf discharge in the furnace might be effective.

ACKNOWLEDGMENT

We thank S. Hanamura of the National Bureau of Standards for helpful discussions and suggestions.

LITERATURE CITED

(1) "A Review of the Physiological Impact of Mercurials", EPA-660/3-73-022 (1974).
(2) A. Nakahara, *Chem. Ind., (Japan)*, **30**, 153 (1977).
(3) *Fed. Regist.*, **38** (6), 1254 (Jan. 10, 1973).
(4) S. Hanamura, Private communications (1978).
(5) J. C. Van Loon, B. Radziuk, N. Kahn, J. Lichwa, F. J. Fernandez, and J. D. Kerber, *At. Absorp. Newsl.*, **16**, 79 (1977).
(6) D. R. Jones and S. E. Manaham, *Anal. Chem.*, **48**, 502 (1976).
(7) F. E. Brinckman, W. R. Blair, K. L. Jewett, and W. P. Iverson, *J. Chromatogr. Sci.*, **15**, 493 (1977).
(8) H. Koizumi, T. Hadeishi, and R. D. McLaughlin, *Anal. Chem.*, **50**, 1700 (1978).
(9) T. Hadeishi, *Appl. Phys. Lett.*, **21**, 438 (1972).
(10) T. Hadeishi and R. D. McLaughlin, *Anal. Chem.*, **48**, 1009 (1976).
(11) H. Koizumi and K. Yasuda, *Spectrochim. Acta, Part B*, **31**, 237 (1976).
(12) H. Koizumi, K. Yasuda, and M. Katayama, *Anal. Chem.*, **49**, 1106 (1977).
(13) J. W. Robinson, *Anal. Chim. Acta*, **24**, 451 (1961).
(14) R. E. Sturgeon and C. L. Chakrabarti, *Spectrochim. Acta, Part B*, **32**, 231 (1977).
(15) R. E. Sturgeon and C. L. Chakrabarti, *Anal. Chem.*, **49**, 1100 (1977).
(16) B. V. L'vov, *Talanta*, **23**, 109 (1976).
(17) H. Massmann, *Spectrochim. Acta, Part B*, **23**, 215 (1968).
(18) R. Woodriff and G. Ramelow, *Spectrochim. Acta, Part B*, **23**, 665 (1968).
(19) R. Woodriff and R. Stone, *Appl. Opt.*, **7**, 337 (1968).
(20) "Handbook of Chemistry and Physics", 53rd ed., R. C. Weast, Ed., The Chemical Rubber Co., Cleveland, Ohio, 1973.
(21) R. E. Sturgeon, C. L. Chakrabarti, and C. H. Langford, *Anal. Chem.*, **48**, 1792 (1976).
(22) D. T. Coker, *Anal. Chem.*, **47**, 386 (1975).
(23) R. B. Cruz and J. C. Van Loon, *Anal. Chim. Acta*, **72**, 231 (1974).
(24) E. J. Czobik and J. P. Matousek, *Anal. Chem.*, **50**, 2 (1978).
(25) M. D. Amos, P. A. Bennett, K. G. Brodie, P. W. Y. Lung, and J. P. Matousek, *Anal. Chem.*, **43**, 211 (1971).
(26) C. W. Fuller, *At. Absorp. Newsl.*, **16**, 106 (1977).
(27) D. C. Manning and W. Slavin, *At. Absorp. Newsl.*, **17**, 43 (1978).
(28) F. J. Fernandez and D. C. Manning, *At. Absorp. Newsl.*, **10**, 65 (1971).
(29) J. S. Verbeke, Y. Michotte, P. V. Winkel, and D. L. Massart, *Anal. Chem.*, **48**, 125 (1976).
(30) J. Aggett and A. J. Sprott, *Anal. Chim. Acta*, **72**, 49 (1974).

RECEIVED for review July 21, 1978. Accepted October 10, 1978.

Gas–Liquid Chromatographic Study of the Thermodynamics of Solution in Dipropionitriles

R. K. Kuchhal and K. L. Mallik*[1]

Indian Institute of Petroleum, Dehradun-248005, India

Gas–liquid chromatography has been employed to study the thermodynamic solution properties of a number of hydrocarbons and oxygenated compounds in β,β′-oxydipropionitrile, β,β′-thiodipropionitrile, and β,β′-iminodipropionitrile. Comparative data on these three solvents are reported for three temperatures 40, 50, and 60 °C. The data in TDPN for some solutes are compared with previously published data. The activity coefficient data are presented after correction for surface effects (solute adsorption at the gas–liquid interface). The $\gamma_{2,1}^{\infty}$ data are correlated with a linear relation between the partial molar excess free energy and the hydrocarbon chain length of the solute for a homologous series in a given solvent. The results are also discussed in terms of statistical approaches (thermal and athermal contribution) and partial excess molar thermodynamic quantities.

The high selectivity for aromatic hydrocarbons over paraffins exhibited by propionitriles like β,β′-oxydipropionitrile (ODPN), β,β′-iminodipropionitrile (IDPN), and β,β′-thiodipropionitrile (TDPN) was first indicated by Saunders (*1*) and subsequently further explored by Medcalf et al. (*2*) in their studies on ODPN as a selective solvent for aromatic recovery by solvent refining. Soon after the introduction of the gas chromatographic technique in the mid-fifties, these nitriles, especially ODPN, had gained wide popularity and have been in use as stationary phase in gas–liquid chromatography (GC) as evidenced in the subsequent numerous publications (*3–13*). In the intervening years, with gradual perfections in the technique (*14*), GC has provided the chemist with a rapid and convenient means to obtain a large volume of data on solute–solvent interactions, which was useful for studying the thermodynamics of solutions. The activity coefficient data determined by the GC technique have been found to be thermodynamically reliable and the data compare quite favorably with those extrapolated from static measurements under well-defined equilibrium conditions.

The objective of the present work is to provide carefully determined GC equilibrium data on the three nitrile stationary phases over a limited temperature range for diverse types of solutes. Although, as stated earlier, some workers have used these solvents in GC for several purposes, systematic studies on the thermodynamics of solution on these nitriles have not been carried out. Utilizing the solute–solvent interaction information available through the GC technique, it was felt interesting to study the changes in thermodynamic parameters, if there are any, with the systematic change in the structure of the solvents with introduction of different groupings such as O<, S<, or HN< in the propionitrile molecules. This information is perhaps also necessary to complement the observation of Saunders (*1*) that the key for high selectivity of these nitriles is supposed to be associated with $CNCH_2CH_2S$–, $CNCH_2CH_2NH$–, or $CNCH_2CH_2O$– structures.

The widely used expression (*15–17*) which relates $\gamma_{2,p}^{\infty}$, the activity coefficient of a solute at infinite dilution in a stationary

[1] Present address: Research & Development Centre, Indian Oil Corporation Limited, Sector-13, Faridabad-121002, Haryana, India.

0003-2700/79/0351-0392$01.00/0 © 1979 American Chemical Society

phase, to the GC measured specific retention volume $V_g°$ is given by the equation

$$\gamma_{2,p}^{\infty} = \frac{RT}{V_g° p_2 M} = \frac{1.704 \times 10^7}{V_g° p_2 M} \quad (1)$$

where M and p_2 stand for the molecular weight of the solvent and the saturated vapor pressure of pure solute, respectively, and T is the column temperature.

It was observed by Martin (6) that the adsorption of solutes at the gas–liquid interface affected markedly the elution orders and retention volumes because of the existence of a mixed retention mechanism in the system. Subsequently several workers (7, 8, 18–29) confirmed the contribution of adsorption at the gas–liquid interface and support surface to the retention volume. Conder, Locke, and Purnell (23) and later Liao and Martire (27) had shown that the corrected net retention volume per gram of packing material V_N is given by

$$V_N = K_L V_L + K_A A_L + K_S A_S \quad (2)$$

where K_L, K_A, and K_S are gas–liquid bulk partition coefficient, adsorption coefficient at gas–liquid interface and solid support interface, respectively. In the case of polar solvents, the term $K_S A_S$ is almost negligible, hence Equation 2 can be written in the form

$$\frac{V_N}{A_L} = K_L \frac{V_L}{A_L} + K_A \quad (3)$$

The terms, K_L and K_A can be determined from a series of experiments measuring V_N for a particular binary system on a number of columns having varying amounts of solvent. The value of K_A and K_L can be obtained from the intercept and slope of the straight line from V_L/A_L vs. V_N/A_L curve. Thus obtained K_L values were used in the computing of activity coefficients at infinite dilution employing the following relation

$$\gamma_{2,p}^{\infty} = \frac{RT\rho}{K_L M p_2} \quad (4)$$

where ρ denotes the density of the solvent and other terms have the usual significance. Activity coefficient corrected for vapor phase nonideality (γ_{2f}^{∞}) is given (30–32) by

$$\ln \gamma_{2,f}^{\infty} = \ln \gamma_{2,p}^{\infty} + \frac{(V_2 - \beta_{22})(p_2 - p_1)}{RT} + \frac{\beta_{22}^2 (p_2^2 - p_1^2)}{(RT)^2} \quad (5)$$

where V_2 is the molar volume of solute in mL, β_{22} is the second virial coefficient for pure solute at temperature T in $cm^3\ mol^{-1}$, p_2 and p_1 are vapor pressures of pure solute and solvent, respectively, in Torr. The last term of Equation 5 can be ignored as β_{22}^2 makes an insignificant contribution. The solvent's saturation vapor pressure term p_1 is also negligible in gas chromatographic conditions, and thus the reduced form of the equation may be indicated as

$$\ln \gamma_{2,f}^{\infty} = \ln \gamma_{2,p}^{\infty} + \frac{(V_2 - \beta_{22}) p_2}{RT} \quad (6)$$

Excess thermodynamic functions, $\Delta\bar{g}_{2,e}^{\infty}$ and $\Delta\bar{h}_{2,e}^{\infty}$ were determined from the standard relationships.

EXPERIMENTAL

The gas chromatograph used in this investigation was a modified Chrome Alyser-100 equipped with a thermal conductivity detector. All columns employed were of 2-m length having 3-mm i.d. copper tubings. The column packings were prepared in conventional manner using known amounts of support material (–60 + 80 mesh) and stationary solvents. The stationary phases, β,β′-oxydipropionitrile and β,β′-thiodipropionitrile were obtained from Applied Science Labs, State College, Pa., and β,β′-iminodipropionitrile from Analabs, North Haven, Conn., and were used without further treatment. The solvent loadings were 5, 10, 15, 21, and 30% for each solvent. Studies were made at three different temperatures 40, 50, and 60 °C. A thermostatic water bath was used for precise thermal control of the column to ±0.1 °C. The solutes used were of AR grade chemicals.

In order to minimize the depletion of the solvent, use of a presaturator before the analytical column has often been recommended (33). We have also observed (34, 35) that, irrespective of the nature of volatility of the stationary phase, the use of a presaturator had helped us to obtain consistent GC data. In our present studies, the carrier gas hydrogen (99.9% purity) was saturated with solvent by putting a precolumn before the point of injection. The precolumns used were of 30 cm in length (3-mm i.d.) packed with 35% solvent-coated solid support. The carrier gas was throttled down to 2–5 psig using a pressure regulator. To have a fine regulation of flow rate, a fine needle control valve was also used in the series. The pressure difference across the column was measured with a mercury manometer and the gas flow was monitored by a calibrated soap film (flow rate) meter at the outlet. The outlet pressure was always atmospheric.

The densities of all three dipropionitriles were measured using a calibrated pycnometer in a constant temperature bath controlled to ±0.05 °C, at various different temperatures. The densities at required temperatures were determined by interpolation.

The retention volumes were determined by taking an average of at least three runs for each solute. The procedure for the determination of corrected net retention volume (V_N) per gram of packing was followed as per Martire's computation method (8). The surface area of the packing (exposed liquid surface area, A_L) were taken from Pecsok et al.'s data (7).

RESULTS AND DISCUSSION

$V_g°$ data were determined at three temperatures, 40, 50, and 60 °C for 16 solutes at five different concentrations of the three stationary phases ODPN, IDPN, and TDPN. Each solute was injected three times, and the mean $V_g°$ values were used for the calculation. The repeatability of $V_g°$ data was always within 1%. The effect of solute sample size and carrier gas flow rate on $V_g°$ were found to be almost negligible. Figure 1 demonstrates the variation in $V_g°$ with the liquid phase concentration at 40 °C for some selected solutes. For the sake of brevity $V_g°$ data at three temperatures for these three solvents are not reported here. It is evident from the figure that for the *n*-paraffin solutes (and to some extent naphthenes), $V_g°$ decreased with the increase in the percentage coating of liquids for all the solvents studied. For polar solutes, the retention volume was fairly independent of the liquid loading. It is also interesting to note that the elution pattern of the few solutes even changed with the increase or decrease in column temperature; this property has often been utilized by various authors for the analysis of aromatics in the presence of saturates (12). As mentioned earlier, Martin (6a, 6c) had first reported this kind of variation in the retention volume of nonpolar solutes in highly polar solvent, and polar solutes in nonpolar solvents where the contribution of gas–liquid interface absorption is quite significant.

Tables I–III show the relative contributions of bulk solution and adsorption to the retention volumes for six solutes, representing different types like *n*-hexane, cyclohexane, cyclohexene, benzene, methanol, and 2,2,4-trimethyl pentane in ODPN, IDPN, and TDPN, respectively, at 40 °C. It is evident that the adsorption contribution at the gas–liquid interface is largest for a branched chain paraffin, followed by *n*-paraffin, cycloparaffin, cycloolefin, and aromatic compound. This observation is in agreement with that of Karger et al. (36). As the polarizability of the solute increased, the adsorption coefficient K_A decreased. For oxygenated compounds, K_A values were found to be quite low which is again in agreement with Martire's observation (8).

From an analytical point of view, the knowledge of the mixed mechanism leads to an attractive method for finding the separation abilities of a stationary phase. For example, Figure 1 depicts how 3-methyl hexane and *n*-heptane can be

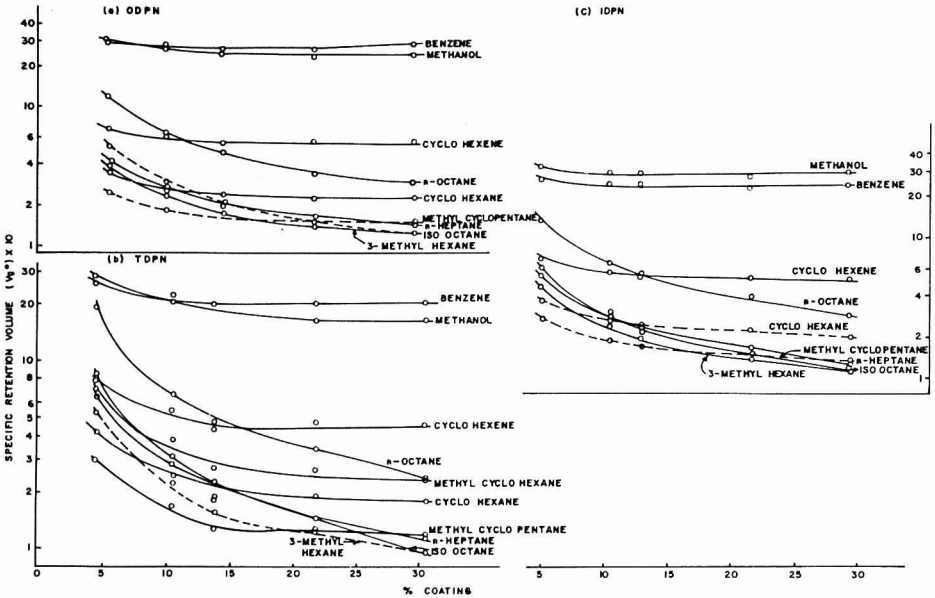


Figure 1. Variation of specific retention volume with stationary liquid loading at 40 °C

Table I. Contributions of Solution and Adsorption to the Retention Volumes for Selected Solutes on β,β'-Oxydipropionitrile at 40 °C

solute	liquid phase on Chromosorb P, %	extent of retention: solution $K_L V_L$	extent of retention: adsorption $K_A A_L$	total V_N	adsorption, %
n-hexane	5.65	3.35	0.72	4.07	17.7
	10.05	6.66	0.60	7.26	8.3
	14.57	10.71	0.49	11.20	4.4
	21.77	19.22	0.33	19.55	1.7
	29.76	25.55	0.17	25.72	0.7
cyclohexane	5.65	10.97	0.64	11.61	5.5
	10.05	22.34	0.54	22.88	2.4
	14.57	33.00	0.44	33.44	1.3
	21.77	63.02	0.30	63.32	0.5
	29.76	83.77	0.15	83.92	0.2
cyclohexene	5.65	28.47	0.55	29.02	1.9
	10.05	57.97	0.46	58.43	0.8
	14.57	85.64	0.37	86.01	0.4
	21.77	163.5	0.25	163.75	0.2
	29.76	217.4	0.13	217.53	0.1
benzene	5.65	140.7	−0.69	140.0	−0.5
	10.05	286.7	−0.58	286.1	−0.2
	14.57	423.3	−0.47	422.8	−0.1
	21.77	808.5	−0.32	808.2	0.0
	29.76	1074.5	−0.17	1074.3	0.0
methanol	5.65	121.1	3.36	124.5	−2.7
	10.05	246.6	2.81	249.4	−1.2
	14.59	364.3	2.30	366.6	−0.6
	21.77	695.6	1.56	697.2	−0.2
	29.76	924.7	0.81	925.5	0.0
isooctane	5.65	5.20	2.64	7.84	33.8
	10.05	10.58	2.21	12.79	17.3
	14.57	15.63	1.80	17.43	10.4
	29.76	39.68	0.63	40.31	1.6

Table II. Contribution of Solution and Adsorption to the Retention Volumes for Selected Solutes on β,β'-Iminodipropionitrile at 40 °C

solutes	liquid phase on Chromosorb P, %	extent of retention: solution $K_L V_L$	extent of retention: adsorption $K_A A_L$	total V_N	adsorption, %
n-hexane	4.94	3.59	1.02	4.61	22.2
	10.50	7.57	0.82	8.39	9.7
	13.03	9.69	0.73	10.42	7.0
	21.72	14.21	0.47	14.68	3.2
	29.51	27.30	0.24	27.54	0.9
cyclohexane	4.94	12.83	1.22	14.05	8.7
	10.50	27.06	0.97	28.03	3.5
	13.03	34.60	0.87	35.47	2.5
	21.72	50.80	0.55	51.35	1.1
	29.51	97.60	0.29	97.90	0.3
cyclohexene	4.94	33.37	1.59	34.96	4.6
	10.50	70.40	1.27	71.67	1.8
	13.03	90.13	1.14	91.27	1.2
	21.72	132.2	0.73	132.9	0.6
	29.51	253.9	0.38	254.3	0.2
benzene	4.94	171.4	−10.3	161.1	−6.4
	10.50	361.6	−8.2	353.4	−2.3
	13.03	462.9	−7.4	455.5	−1.6
	21.72	678.7	−4.7	674.0	−0.7
	29.51	1304.1	−2.5	1301.6	−0.2
methanol	4.94	195.5	−0.23	195.3	−0.1
	10.50	412.6	−0.19	412.4	0
	13.03	528.2	−0.17	528.0	0
	21.72	774.5	−0.11	774.4	0
	29.51	1488.0	−0.06	1488.0	0
isooctane	4.94	6.43	4.09	10.52	38.86
	10.50	13.57	3.25	16.82	19.30
	13.03	17.37	2.91	20.28	14.30
	29.51	48.93	0.98	49.9	1.96

Table III. Contribution of Solution and Adsorption to the Retention Volumes for Selected Solutes on β,β'-Thiodipropionitrile at 40 °C

solute	liquid phase on Chromosorb P, %	extent of retention: solution $K_L V_L$	extent of retention: adsorption $K_A A_L$	total V_N	adsorption, %
n-hexane	4.61	2.27	1.03	3.30	31.2
	10.58	5.30	0.80	6.10	13.2
	13.74	6.80	0.70	7.50	9.3
	21.83	13.35	0.46	13.81	3.3
	30.46	18.96	0.22	19.18	1.1
cyclohexane	4.61	8.28	0.89	9.17	9.8
	10.58	19.35	0.69	10.04	3.5
	13.74	24.84	0.60	25.44	2.4
	21.83	48.72	0.40	49.12	0.8
	30.46	69.18	0.19	69.37	0.3
cyclohexene	4.61	21.86	0.96	22.82	4.2
	10.58	51.08	0.74	51.82	1.4
	13.74	65.58	0.65	66.23	1.0
	21.83	128.60	0.42	129.02	0.2
	30.46	229.90	0.20	230.1	0.1
benzene	4.61	98.13	1.81	99.94	1.8
	10.58	229.3	1.41	230.7	0.6
	13.74	294.3	1.22	295.5	0.4
	21.83	577.3	0.80	578.1	0.1
	30.46	819.8	0.38	820.2	0.0
methanol	4.61	78.54	5.05	83.6	6.0
	10.58	183.3	3.93	187.3	2.1
	13.74	235.6	3.41	239.0	1.4
	21.83	462.1	2.23	464.3	0.5
	30.46	657.5	1.06	658.6	0.2
isooctane	4.61	3.50	3.79	7.29	52.0
	10.58	8.17	2.95	11.12	26.5
	13.74	10.49	2.56	13.05	19.6
	30.46	29.22	0.79	30.01	2.6

Table IV. Contribution of Solution and Adsorption to the Retention Volumes for Various Solutes on β,β'-Thiodipropionitriles at Different Temperatures

	40 °C			50 °C			60 °C		
solute	K_LV_L	K_AA_L	adsorption, %	K_LV_L	K_AA_L	adsorption, %	K_LV_L	K_AA_L	adsorption, %
n-hexane	2.27	1.03	31.2	1.84	0.43	18.9	1.76	0.63	26.3
isooctane	3.50	3.79	52.0	2.92	2.85	49.4	2.53	1.93	43.3
cyclohexene	21.86	0.96	4.2	17.90	0.76	4.00	14.87	0.85	5.4
benzene	98.13	1.81	1.8	72.68	1.78	2.4	59.28	1.18	1.95
methanol	78.54	5.05	6.0	57.46	4.91	7.8	48.09	2.11	4.20

Table V. Comparison of Bulk Partition Coefficient K_L Data with Reported Values at 50 °C, in β,β'-TDPN

			our data	
solutes	Martin's data (Ref. 6a) 49 °C	Pecsok's data (Ref. 7) 50 °C	uncorrected for adsorption (50 °C) at 21% loading	corrected for adsorption (50 °C)
n-pentane	2.2	3.2	3.2	2.35
n-hexane	4.7	4.8	6.9	4.75
n-heptane	8.5	9.1	14.3	9.4
methylcyclopentane	11.0	10.8	13.5	11.3
methylcyclohexane	20.9	-	26.5	23.0
cyclohexane	17.0	16.3	19.7	17.2
cyclohexene	43.4	40.4	47.4	46.2
benzene	186.0	170.5	190.0	187.7
2,2,4-trimethylpentane	6.6	7.3	-	7.5

resolved successfully from isooctane at different liquid loadings. The behavior, namely the change of the elution order, may be of great interest in trace analysis, e.g., in the elution of a minor component before the major one (*37*) (quantitative estimation of *n*-heptane in isooctane or vice versa is of industrial application).

The effect of temperature on the mixed mechanism can be considered interesting from the analytical point of view. Table IV, for example, shows that the increase in temperature has comparatively less effect on K_A values for benzene as compared to paraffins. It is interesting here to note that at a higher column temperature, some higher boiling paraffins could be eluted earlier with respect to benzene.

All calculations for K_L and K_A were carried out using a computer-aided least-square refinement. For the sake of brevity, K_A and K_L values are not reported here. To check the reliability and accuracy of our data, a comparison of bulk partition coefficient at infinite dilution (K_L) in β,β'-thiodipropionitrile was made with those of Martin (*6a*) and Pecsok et al. (*7*). Table V shows that our values are in fair agreement with these authors' data. Table V also includes the K_L values at 21% loading in which the gas–liquid interface adsorption correction factor was not taken into account. It is clear that these values are higher as compared to the true bulk partition coefficient. The data suggest that even 21% solvent loading is insufficient to provide the true bulk partition coefficient data in these types of polar stationary solvents.

Table VI shows the infinite dilution activity coefficients for 16 solutes in these solvents at three temperatures, 40, 50, and 60 °C. The data represent at least three runs on each binary system. The $\gamma_{2,p}^{\infty}$ and $\gamma_{2,f}^{\infty}$ values were computed employing Equation 4 and subsequently Equation 6. The second virial coefficient data (β_{22}) at different temperatures were estimated by a modified corresponding state of the equation (*38*, *39*), for hydrocarbon solutes.

$$\frac{\beta_{22}}{V_c} = 0.430 - 0.886\left(\frac{T_c}{T}\right) - 0.694\left(\frac{T_c}{T}\right)^2 - 0.0375\,(n-1)\left(\frac{T_c}{T}\right)^{4.5} \quad (7)$$

where V_c and T_c are the critical volume and critical temperatures of solutes, respectively. For the cycloheptane system no experimental T_c and V_c values were available, and so the data were computed using van der Waal's constant (*40*). For oxygenated compounds, like acetone, diethyl ether, and methanol, β_{22} data were obtained from interpolation of literature (*41*, *42*) data (reported at different temperatures).

The validity of any data under the equilibrium conditions can be substantiated by comparison with well established literature results. No direct data are available in the literature for checking the accuracy of our data except for few solutes in β,β'-thiodipropionitrile. The $\gamma_{2,p}^{\infty}$ data for solutes such as methyl cyclohexane, cyclohexene, diethyl ether, acetone, isooctane, and benzene in TDPN were reported in the literature, though at different temperatures for the sake of comparison; these $\gamma_{2,p}^{\infty}$ were extrapolated to the same temperature at which we used our columns. Our $\gamma_{2,p}^{\infty}$ data were found to be in fair agreement with those reported by Martin (*6a*) (reproduced by Martire (*8*)) and Pecsok et al. (*7*). The $\gamma_{2,f}^{\infty}$ values reported by Bonastre et al. (*9*) for a few solutes at 80 and 100 °C were fairly high compared to ours. It is interesting to note that the $\gamma_{2,f}^{\infty}$ values for cyclohexane and benzene at 30 °C determined by the static method (*18*) are in excellent agreement with our data. Sheehan and Langer (*43*) reported $\gamma_{2,p}^{\infty}$ for *n*-heptane, *n*-octane, benzene, and toluene in an ODPN system at 80 °C. For the *n*-paraffin data, the values were in good agreement, though those for aromatics were found to be slightly higher (Figure 2). Interestingly again, Korol's (*44*) data for benzene in ODPN determined by static as well as GLC methods are in good agreement with ours. Meen et al. (*13*) have reported $\gamma_{2,f}^{\infty}$ values for benzene and toluene in ODPN, TDPN, and IDPN at 60 °C; in the cases of benzene and toluene in IDPN, the data are in good agreement (within 4%) but in other cases the deviation was as high as 19%. Deal and Derr (*45*) had studied different solvents for aromatic recovery and determined the limited activity coefficient data from empirical theoretical relations. Their $\gamma_{2,p}^{\infty}$ data in IDPN at 60 °C for *n*-hexane and benzene were 54 and 2.7 as compared to our 62.5 and 2.87, respectively, but the values in ODPN were found to disagree with ours, 90 and 4.95 as compared to 57.3 and 2.61, respectively.

Table VI. Activity Coefficients at Infinite Dilution for Hydrocarbons at 40, 50, and 60 °C

solute	β,β′-oxydipropionitrile						β,β′-thiodipropionitrile						β,β′-iminodipropionitrile					
	40 °C		50 °C		60 °C		40 °C		50 °C		60 °C		40 °C		50 °C		60 °C	
	$\gamma_{2,p}^{\infty}$	$\gamma_{2,f}^{\infty}$	$\gamma_{2,p}^{\infty}$	$\gamma_{2,f}^{\infty}$	$\gamma_{2,p}^{\infty}$	$\gamma_{2,f}^{\infty}$	$\gamma_{2,p}^{\infty}$	$\gamma_{2,f}^{\infty}$	$\gamma_{2,p}^{\infty}$	$\gamma_{2,f}^{\infty}$	$\gamma_{2,p}^{\infty}$	$\gamma_{2,f}^{\infty}$	$\gamma_{2,p}^{\infty}$	$\gamma_{2,f}^{\infty}$	$\gamma_{2,p}^{\infty}$	$\gamma_{2,f}^{\infty}$	$\gamma_{2,p}^{\infty}$	$\gamma_{2,f}^{\infty}$
n-pentane	48.7	51.3	42.7	46.1	37.4	40.5	59.5	62.7	57.5	61.3	43.6	47.1	61.3	64.6	46.7	49.8	42.9	46.4
n-hexane	77.4	79.4	68.0	70.3	57.3	59.8	93.1	95.5	74.8	77.3	66.6	69.5	93.5	95.9	69.2	71.5	62.6	65.3
n-heptane	122.0	123.5	101.3	103.0	85.1	87.0	137.5	139.0	121.0	123.0	99.8	102.1	139.5	141.3	102.1	103.9	92.0	94.1
n-octane	187.0	188.1	166.1	167.5	126.1	127.6	212.0	213.2	158.8	160.2	136.2	137.8	195.9	197.0	147.9	149.1	130.3	131.8
methylcyclopentane	38.8	39.7	34.0	35.0	29.3	30.4	42.8	43.0	38.5	39.5	31.9	33.1	44.1	45.1	35.4	36.5	32.0	33.2
cyclohexane	35.8	46.5	31.0	31.7	26.9	27.7	38.6	39.3	34.5	35.3	29.1	30.0	39.6	40.3	31.8	32.6	29.0	29.9
cyclohexene	14.6	14.8	12.7	13.0	11.4	11.7	15.6	15.8	13.0	13.3	11.5	11.8	16.2	16.5	13.3	13.6	12.4	12.8
methylcyclohexane	57.9	58.6	48.3	49.1	41.6	42.5	62.4	63.1	49.5	50.3	42.7	43.6	63.3	64.0	48.5	49.3	43.8	44.7
cycloheptane	52.3	52.6	43.4	43.7	34.8	35.2	53.7	54.0	42.1	42.4	34.1	34.5	54.8	55.1	43.4	43.7	36.4	36.8
3-methylhexane	106.1	107.7	90.0	91.9	78.6	80.8	124.6	126.6	97.3	99.3	85.5	87.9	120.4	122.3	91.0	92.9	80.6	82.9
2,2,4-trimethylpentane	142.0	144.3	110.4	112.8	100.4	103.2	156.4	159.0	119.7	122.3	114.0	117.2	146.5	148.9	111.2	113.6	104.7	107.6
benzene	2.81	2.85	2.72	2.78	2.61	2.68	3.29	3.34	3.09	3.15	2.89	2.97	2.99	3.04	2.95	3.01	2.88	2.96
toluene	4.70	4.74	4.44	4.49	3.72	3.77	5.05	5.09	4.42	4.47	4.13	4.19	5.17	5.21	5.03	5.09	4.79	4.86
acetone	1.13	1.17	1.16	1.21	1.13	1.19	1.47	1.52	1.42	1.49	1.34	1.42	1.38	1.43	1.35	1.41	1.34	1.42
diethyl ether	6.60	6.93	6.09	6.48	5.72	6.19	8.42	8.84	7.74	8.23	6.67	7.21	7.64	8.02	7.24	7.70	6.81	7.36
methanol	2.39	2.44	2.12	2.17	2.06	2.12	3.01	3.07	2.65	2.72	2.35	2.42	1.92	1.96	1.72	1.76	1.73	1.78

Figure 2. Log of activity coefficients at infinite dilution vs. reciprocal of temperature on β,β′-ODPN system

The data in Table VI indicate that all the solutes exhibit a positive deviation from Raoult's law. There is a marked decrease in $\gamma_{2,f}^{\infty}$ values for paraffins, cycloparaffins, and cyclolefins with the increase in column temperature in all three solvents. In the case of aromatic and oxygenated solutes, however, the rate of decrease is considerably smaller. In a system where a compound containing active donor or acceptor atoms and having high cohesive energy density is mixed with a compound containing no active sites, it would generally lead to the limited solubility of the latter in the former, thus giving rise to positive deviations from ideality as indicated by the $\gamma_{2,f}^{\infty}$ values for paraffins and naphthenes.

Aromatics have been observed to show high affinity toward these propionitriles (*1*, *2*). The $\gamma_{2,f}^{\infty}$ data for naphthenes were found to be in between paraffins and aromatics. This behavior is consistent with the mechanism of intermolecular interactions reported by Anderson and Prausnitz (*46*). The relatively lower $\gamma_{2,f}^{\infty}$ values of aromatics in dipropionitriles may be attributed to the presence of π electrons which exhibit a tendency to form π-complexes of varying degree of stability. In these complex systems however, a single interaction parameter cannot explain the mechanism. The hetero atoms of the solvents –Ö–, –N̈(H)–, –S̈– also act as donors (n → π interactions). There is also the possibility of interaction of the nitrile group (electrophillic in character) with π electrons of the benzene ring. The deviation from Raoult's law can be expressed as the combination of two completely independent factors (*47*),

$$\ln \gamma_{2,f}^{\infty} = \ln \gamma_{2,f}^{\infty\ \text{combin.}} + \ln \gamma_{2,f}^{\infty\ \text{interaction}}$$

where $\ln \gamma_{2,f}^{\infty\ \text{combin.}}$ accounts for the effects due to difference in size of solvent and solute molecules (also known as athermal or configurational contribution), and the $\ln \gamma_{2,f}^{\infty\ \text{interaction}}$ factor (interaction parameter χ) indicates the interaction energies between the molecules in mixture (thermal contribution). There are several treatments (*48*) for the evaluation of $\ln \gamma_{2,f}^{\infty\ \text{combin.}}$. Employing the Flory–Huggins equation (which corresponds formally to the Miller–Guggenheim treatment with $z \to \infty$) the combinatory (athermal) part and the interaction parameter (χ) were calculated. The χ and combining contribution data are not included in this paper for the sake of

Table VII. Excess Enthalpy of Mixing in Kilocalories at 50 °C

solute	β,β′-oxydipropionitrile	β,β′-thiodipropionitrile	β,β′-iminodipropionitrile
n-pentane	2.42	3.04	3.35
n-hexane	2.86	3.65	3.89
n-heptane	3.53	3.23	4.22
n-octane	3.81	3.85	4.23
methylcyclopentane	2.69	3.12	3.95
cyclohexane	2.69	2.82	3.27
cyclohexene	2.46	3.10	2.57
methylcyclohexane	3.27	4.13	4.12
cycloheptane	4.16	4.75	4.36
3-methylhexane	2.91	4.08	4.09
2,2,4-trimethylpentane	3.88	3.73	4.36
benzene	0.69	1.05	0.23
toluene	2.18	1.88	0.71
acetone	−0.38	0.73	0.00
methanol	1.43	2.43	1.11
diethyl ether	1.14	1.93	1.16

Table VIII. Selectivity Factors ($S_{A,B}^{\infty}$) at Three Temperatures (°C)

	$\gamma_{CH}^{\infty}/\gamma_{BZ}^{\infty}$			$\gamma_{nC_7}^{\infty}/\gamma_{MCH}^{\infty}$			$\gamma_{nC_7}^{\infty}/\gamma_{Tol.}^{\infty}$		
solvents	40 °C	50 °C	60 °C	40 °C	50 °C	60 °C	40 °C	50 °C	60 °C
ODPN	12.8	11.4	10.3	2.11	2.10	2.05	26.0	22.9	23.1
TDPN	11.8	11.2	10.1	2.20	2.45	2.34	27.3	27.5	24.4
IDPN	13.3	10.8	10.1	2.21	2.21	2.10	27.1	20.4	19.4

brevity. The athermal part, as expected, indicated negative contribution to solution nonideality. The interaction parameter (χ) data are positive and greater than unity for all the studied systems, except for acetone, indicating that overall interchange free energies are positive. In the case of acetone, the χ values were around 0.2 to 0.5 which indicate that the contact energy dissimilarity is small. It is interesting to note that χ increases uniformly for *n*-paraffins in a particular solvent, which means that as the number of contact sites or segments increase in a system, the interaction parameter also increases. With increase of temperature, the χ data decrease for a particular solute–solvent pair.

Evaluation of excess thermodynamic properties: partial molar excess free energy ($\Delta\bar{g}_{2,e}^{\infty} = RT \ln \gamma_{2,f}^{\infty}$) and enthalpy of mixing

$$(\Delta\bar{h}_{2,e}^{\infty} = R\mathrm{d} \ln \gamma_{2,f}^{\infty}|\mathrm{d}t) \qquad (8)$$

were computed. Figure 3 shows a linear relationship between excess partial molar free energy at infinite dilution and molecular structure, for all the three solvents studied. When a methyl group is added in the *n*-paraffin series, there is a change in $\Delta\bar{g}_{2,f}^{\infty}$ by about 0.28 ± 0.04 kcal/mol per methyl group in the solvents studied; in the case of naphthenes and aromatics also, the change is almost the same order. However, as Langer and Purnell (*49*) had mentioned, this is a greatly simplified view since $\Delta\bar{h}_{2,e}^{\infty}$ and $\Delta\bar{s}_{2,e}^{\infty}$ are not additive in this fashion but are intererelated in a linear fashion and compensating which gives a resultant additivity to $\Delta\bar{g}_{2,e}^{\infty}$ for the series. The thermal dependance of $\gamma_{2,f}^{\infty}$ as presented in Table VII indicates positive values for all the systems studied which might be attributed to loss in cohesive energies of solvent molecules. The general trend in the increase of $\Delta\bar{h}_{2,e}^{\infty}$ values with increase in carbon number is in agreement with the observations of earlier workers (*45*, *50*). The excess partial molar free energy, $\Delta\bar{g}_{2,e}^{\infty}$ was found to be almost the same for a particular solute in these three solvents but the $\Delta\bar{h}_{2,e}^{\infty}$ values were in general found to be lower in ODPN. The Table further indicates the lower values of $\Delta\bar{h}_{2,e}^{\infty}$ for aromatics. The reduced endothermicity of mixing indicates the presence of enhanced specific interaction between propionitriles and aromatics. Acetone data also indicate enhanced solute–solvent

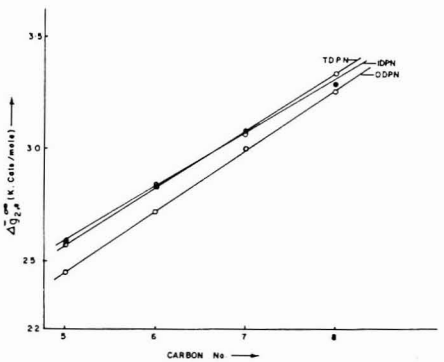


Figure 3. Incremental relation between excess free energy and molecular structure for *n*-paraffins in propionitriles, at 40 °C

interactions with these propionitriles.

The GC technique has also provided a rapid and convenient means of examining the efficacy of potential solvents for extractive distillation. It is well known that good performance, with respect to efficiency and economy of operation in the extraction processes, can only be achieved with solvents having high selectivity for the desired components. It was considered worthwhile to compare the selectivity of these three well-known solvent for the aromatics. The infinite dilution relative volatility ($\alpha_{A,B}^{\infty}$) is related with activity coefficients as follows:

$$\alpha_{A,B}^{\infty} = \frac{\gamma_A^{\infty}}{\gamma_B^{\infty}} \cdot \frac{p_A}{p_B} \qquad (9)$$

In the case of separation of close boiling compounds ($p_A \approx p_B$), which are often encountered in petroleum fractions, the selectivity of the solvent can be represented as

$$S_{A,B}^{\infty} = \frac{\gamma_A^{\infty}}{\gamma_B^{\infty}} \qquad (10)$$

Table VIII provides the selectivity data at three temperatures on these three solvents for typical pairs like cyclohexane–benzene, methyl cyclohexane–*n*-heptane, and *n*-heptane–toluene systems as these are of industrial importance. Deal and Derr (*45*) reported the selectivity for the *n*-hexane–benzene system in ODPN and IDPN solvents; their values, 18 and 20, are in fair agreement with our data, 21.9 and 21.7, respectively, at 60 °C, although Kononov et al. (*51*) reported the value of 34.0 for the same pair of solutes at the same temperature in IDPN. It is evident from Table VIII that all three solvents show the same trend and selectivity for the binary mixtures studied, which is in conformity with the observations of Kononov et al. (*51*) and Tenney (*3*).

It would be interesting to correlate the selectivity factor $S_{A,B}^{\infty}$ with the structural parameter of these solvents. Three more solvents were chosen which have the same basic structure but differ by a functional group or alkyl chain length. The binary pair cyclohexane and benzene were chosen and our $S_{A,B}^{\infty}$ data from ODPN, IDPN, and TDPN were compared with those of β-hydroxypropionitrile (HPN) and β-methoxypropionitrile (MOPN), and adipic dinitrile (ADPN) obtained from Kononov et al. (*51*). The selectivity for the benzene–cyclohexane pair on these solvents, ODPN, TDPN, IDPN, HPN, MOPN, ADPN was 12.9, 11.6, 12.1, 12.5, 8.0, and 5.7, respectively, at 30 °C. All the data reported here are taken from reference 35 except that of ADPN which is taken from reference 51. The reported values do not include any corrections for gas–liquid interface adsorption. However, the higher liquid loadings were chosen in order to minimize the surface area/volume of the stationary liquid ratio. The data suggest that ODPN, TDPN, IDPN and hydroxypropionitrile (HPN) are almost identical in selectivity for benzene with respect to cyclohexane; however the selectivity of TDPN is lowest among the four. Methoxypropionitrile (MOPN) and adipic dipropionitrile (ADPN) both seem to be less efficient than the rest of the solvents. It is interesting to point out here that the substitution of a $-CH_2CH_2CN$ group in the ODPN by a $-CH_3$ group (as in the case of MOPN) lowers the selectivity for benzene, wherein the replacement by –H (as in the case of HPN) causes an increase in the selectivity. In the case of ADPN, where the O, S, and NH groups are absent, the selectivity again drops down. As discussed earlier, the enhanced selectivity for aromatics in all the three dipropionitriles (having hetero atoms) may arise due to ($n \rightarrow \pi$) interactions. In the case of ADPN, the nitrile linkage alone can act as donor and so it is not very effective for the extraction of aromatics from the petroleum fraction in spite of the fact that it has high dipole moment. Rowlinson (*52*) had also pointed out that nitriles are not good proton acceptors; our data also show that in conjunction with hetero atoms such as O, S, or groups like NH, the nitrile linkage develops good affinity for aromatic hydrocarbons.

LITERATURE CITED

(1) K. W. Saunders, *Ind. Eng. Chem.*, **43**, 121 (1951).
(2) E. C. Medcalf, A. G. Hill, and G. N. Vriens, *Pet. Refiner*, **30** (7), 97 (1951).
(3) H. M. Tenney, *Anal. Chem.*, **30**, 2 (1958).
(4) H. S. Knight, *Anal. Chem.*, **30**, 9 (1958).
(5) L. Rohrschneider, *Fresenius Z. Anal. Chem.*, **170**, 256–263 (1959).
(6) R. L. Martin, *Anal. Chem.*, (a) **33**, 347 (1961); (b) **34**, 896 (1962), (c) **35**, 116 (1963).
(7) R. L. Pecsok, A. Yllana, and A. Abdul-Karim, *Anal. Chem.*, **36**, 452 (1964).
(8) D. E. Martire, *Anal. Chem.*, **38**, 244 (1966).
(9) J. Bonastre, P. Greneier, and P. Gazenave, *Bull. Soc. Chim. Fr.*, **3885** (1968).
(10) A. Grobler, T. Kada, and I. Czalik, *J. Chromatogr.*, **27**, 239 (1967); **27**, 63 (1967).
(11) K. L. Mallik and R. K. Kuchhal, *Chem. Ind. (London)*, 260 (1973).
(12) R. K. Kuchhal and K. L. Mallik, *Chromatographia*, **5**, 278 (1972); **6**, 202 (1973); *Ind. J. Chem.*, **12**, 1322 (1974).
(13) D. L. Meen, F. Morris, J. H. Purnell, and O. P. Srivastava, *Trans. Faraday, Soc. 1*, **69**, 2080 (1973).
(14) K. L. Mallik, "An Introduction to Nonanalytical Applications of Gas Chromatography", Peacock Press, New Delhi, India, 1976.
(15) A. B. Littlewood, C. S. G. Phillips, and D. T. Price, *J. Chem. Soc.*, 1480 (1955).
(16) D. Ambrose, A. I. M. Keulemans, and J. H. Purnell, *Anal. Chem.*, **30**, 1582 (1958).
(17) M. R. Hoare and J. H. Purnell, *Trans. Faraday Soc.*, **52**, 222 (1956).
(18) D. E. Martire, R. L. Pecsok, and J. H. Purnell, *Nature (London)*, **203**, 1279 (1964).
(19) D. L. Camin, R. W. Wing, and S. D. Showhan, *Anal. Chem.*, **36**, 1174 (1964).
(20) M. Rogozinski and I. Kautman, *J. Gas Chromatogr.*, **4**, 413 (1966).
(21) R. L. Pecsok and B. H. Gump, *J. Phys. Chem.*, **70**, 2202 (1967).
(22) J. R. Conder, *J. Chromatogr.*, **39**, 273 (1969).
(23) J. R. Conder, D. C. Locke, and J. H. Purnell, *J. Phys. Chem.*, **73**, 700 (1969).
(24) D. F. Cadogan, J. R. Conder, D. C. Locke, and J. H. Purnell, *J. Phys. Chem.*, **73**, 708, 3849 (1969).
(25) L. J. Lorenj and L. B. Rogers, *Anal. Chem.*, **43**, 1593 (1971).
(26) J. W. King, A. Chatterjee, and B. L. Karger, *J. Phys. Chem.*, **76**, 2769 (1972).
(27) H. Liao and D. E. Martire, *Anal. Chem.*, **44**, 498 (1972).
(28) J. F. Parcher and C. L. Hussey, *Anal. Chem.*, **45**, 188 (1973).
(29) R. C. Castells, *J. Chromatogr.*, **111**, 1 (1975).
(30) A. J. B. Cruickshank, M. L. Windsor, and C. L. Young, *Proc. R. Soc. London, Ser. A*, **295**, 271 (1966).
(31) B. W. Gainey and C. L. Young, *Trans. Faraday Soc.*, **64**, 349 (1968).
(32) A. J. Ashworth, *J. Chem. Soc., Faraday Trans. 1*, **69**, 459 (1973).
(33) R. E. Pecsar and J. J. Martin, *Anal. Chem.*, **38**, 1661 (1966).
(34) R. K. Kuchhal and K. L. Mallik, *J. Appl. Chem. Biotechnol.*, **26**, 67 (1976); *J. Chem. Eng. Data*, **17**, 49 (1972).
(35) R. K. Kuchhal, Ph.D. thesis, University of Meerut, 1973.
(36) B. L. Karger, R. C. Castells, P. A. Sewell, and A. Hartkopf., *J. Phys. Chem.*, **75**, 3870 (1971).
(37) H. Hachenburg, "Industrial Gas Chromatographic Trace Analysis", Heyden and Sons, Ltd., London, 1973.
(38) M. L. McGlashan and D. J. B. Potter, *Proc. R. Soc. London, Ser. A*, **267**, 478 (1962).
(39) M. L. McGlashan and C. J. Wormald, *Trans. Faraday Soc.*, **60**, 646 (1964).
(40) G. Thodos, *AIChE J.*, **2**, 508 (1956).
(41) C. N. Kretschnur and R. Wiebe, *J. Am. Chem. Soc.*, **76**, 2582 (1954).
(42) R. E. Pennington and K. A. Kobe, *J. Am. Chem. Soc.*, **79**, 300 (1957).
(43) R. J. Sheehan and S. H. Langer, *Ind. Eng. Chem., Proc. Des. Dev.*, **10**, 44 (1971).
(44) G. V. Filonenko and A. N. Korol, *J. Chromatogr.*, **119**, 159 (1976).
(45) C. H. Deal and E. L. Derr, *Ind. Eng. Chem., Proc. Des. Dev.*, **3**, 394 (1964).
(46) R. Anderson and J. M. Prausnitz, *Ind. Chem., Eng.*, 67, (1962).
(47) D. H. Everett and M. F. Penney, *Proc. R. Soc. London, Ser. A*, **212**, 164 (1952).
(48) E. A. Guggenheim, "Mixtures", Oxford University Press, 1952, Chap. X and XI.
(49) S. H. Langer and J. H. Purnell, *J. Phys. Chem.*, **67**, 263 (1963); **70**, 904 (1966).
(50) D. H. Desty and W. T. Swanton, *J. Phys. Chem.*, **68**, 766 (1961).
(51) N. F. Kononov, Ya. I. Maharovskii, M. I. Rosengart, and V. G. Kogan, *J. Appl. Chem. USSR*, **38**, 2464 (1965).
(52) J. S. Rowlinsons, "Liquids and Liquid Mixtures", Butterworths, London, 1959, p 160.

RECEIVED for review September 2, 1977. Resubmitted September 25, 1978. Accepted November 3, 1978.

Graphitized Carbon in Gas–Liquid–Solid Chromatography and Gas Chromatography/Mass Spectrometric Analysis of High Boiling Hydrocarbon Mixtures

Paolo Ciccioli[1] and John M. Hayes

Departments of Chemistry and Geology, Indian University, Bloomington, Indiana

Gianfranco Rinaldi[2] and Kenneth B. Denson

Department of Geology, Indiana University, Bloomington, Indiana

Warren G. Meinschein*

Department of Geology and School of Public and Environmental Affairs, Indiana University, Bloomington, Indiana

Gas–liquid–solid chromatography (GLSC) employing a poly(phenyl ether) (PPE 20) liquid phase on graphitized carbon black (GCB) is applicable to the analyses of crude oils and distillates of sedimentary rocks. The elution of C_4 to C_{40} hydrocarbons which consist of *n*-alkanes, isoprenoid-type alkanes, steranes, olefins, and aromatic hydrocarbons can be handled in a single GC run. A GLSC column in tandem with a mass spectrometer provides an excellent means for the identification of geochemically significant organic compounds in complex natural mixtures.

The surface properties generally and the gas chromatographic behavior specifically of graphitized carbon black (GCB) have been studied (*1–4*). These studies have recently been extended to investigations of changes in the adsorption characteristics of GCB caused by various amounts of different liquid coatings (*5–7*). Such investigations have indicated that the resolution of a GCB column can be tailored for a specific separation by coating GCB with an appropriate quantity of liquid phase which has the proper polarity and thermal properties.

Because the liquid phase influences the separations occurring on the GCB surface, the process of resolving mixtures of volatile compounds on columns packed with liquid coated GCB is called gas–liquid–solid chromatography (GLSC). Many applications of GLSC are cited (*8–11*). GLSC analyses of particular interest include separations of complex mixtures of organic compounds of different isomeric structures and isotopic compositions (*8*), and of trace pollutants in air (*9*). Most applications of GLSC have been restricted to low-boiling compounds, but a few GLSC analyses have been performed on high-boiling compounds (*10–12*). Some of the reasons that have limited the use of GLSC for separations of high-boiling compounds may be summarized as follows: (1) The elution temperatures of high boiling compounds frequently exceed the maximum temperatures to which most widely used liquid phases may be heated; (2) The knowledge of the gas chromatographic properties of GCB is limited to coating of only a few molecular layers in thickness; and (3) Data are lacking about the maximum operating temperatures of most liquid phases on GCB.

This paper presents evidence that GLSC using GCB and certain liquid coatings can provide a selective and versatile method of analyzing organic mixtures containing compounds which boil over a wide range of temperatures. For example, data are reported on the GLSC separations of alkanes isolated from the New Albany Shale by: (1) solvent extraction and (2) pyrolysis at 500 °C. Although GLSC analyses are presented which show that alkanes ranging in size from C_4 to C_{40} can be readily handled in a single temperature-programmed run, major emphasis in this paper will be paid the GLSC and tandem gas chromatographic–mass spectrometric (GC-MS) analyses of the C_{15} and larger alkanes which include isoprenoid alkanes and steranes that structurally resemble constituents of biological lipids (*13*). Special attention will be given the steranes in the carbon tetrachloride (CCl_4) extract of the shale. Some of these steranes have different gas chromatographic retention times and mass spectrometric fragmentation patterns than do either 5α- or 5β-steranes. Alternative structures to those recently proposed for apparently equivalent steranes in geological samples (*14*) are suggested.

EXPERIMENTAL

Column Materials and Preparation. Packed columns were constructed from 3.2 mm o.d. × 2 mm i.d. stainless steel tubing. Stainless steel micropacked columns were constructed from 1.6 mm o.d. × 1.0 mm i.d. tubing, while glass micropacked columns used 6 mm o.d. × 1 mm i.d. Pyrex tubing. All columns were 2 m in length, and each column was cleaned with 3:1 benzene/methanol and dried over-night at 110 °C prior to being packed.

Carbopack A with a surface area of 15 m^2/g and Carbopack C with a surface area of 12 m^2/g were purchased from Supelco (Bellefonte, Pa). These graphitized carbon blacks (GCB) were used as GC supports. The packed columns were filled with 80/100 mesh supports, and 100/120 mesh supports were used for the micropacked columns.

Coating of the solid support was carried out by dissolving the liquid phase in a suitable solvent, such as chloroform, and adding it to the support in a Teflon container. After gentle mixing, the solvent was allowed to evaporate at room temperature under a stream of nitrogen, and the dried and coated GCB was sieved prior to use.

Apparatus. Varian 1400 Series Gas Chromatographs equipped with linear temperature programmer and injectors modified to reduce dead volume and to decrease septum temperature were used for all gas chromatographic analyses. The two chromatographs used for GC analyses were each equipped with a flame ionization detector (FID). FID and an electron capture detector (ECD) could be interchanged on the chromatograph used in tandem with the mass spectrometer. When the ECD was used, the air flame gas inlet was capped off, and a supplementary flow of about 100 mL/min of 95% argon–5% methane (Matheson, East Rutherford, N.J.) was added to the detector via the inlet used for hydrogen when the FID was operative. Helium was used as the carrier gas.

[1]Present address: Laboratorio Sull'Inguinamento, Atmosferico del C.N.R., Via Montorio Romano 36, Roma, Italy
[2]EXXON Research Center, Houston, Texas

0003-2700/79/0351-0400$01.00/0 © 1979 American Chemical Society

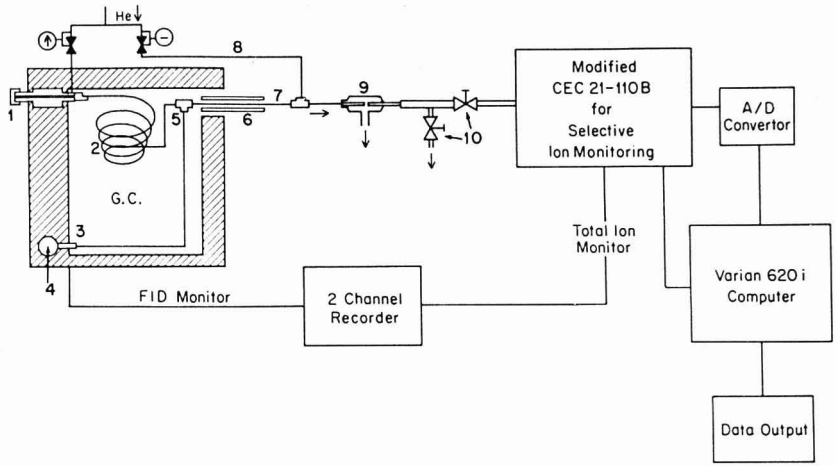


Figure 1. Schematic of tandem GC-MS system. (1) Injector, (2) micropacked column, (3) connection tube, (4) GC detector, (5) splitter, (6) heater, (7) capillary, (8) make-up gas line, (9) jet separator, (10) valves

Table I. Temperature Limits and McReynold's Indices of the Liquid Phases Commonly Used in the Analyses of High Boiling Compounds

name	chemical composition	°C min/max	X'	Y'	Z'	U'	S'
Dexsil 400	poly(carborane siloxane)	50/500	072	108	118	166	123
PPE 20	poly(phenyl ether)	125/375	257	355	348	433	---
OV 17	50% phenyl-50% methyl silicone	0/375	119	158	162	243	202

A modified Consolidated Electrodynamics 21-110B mass spectrometer was coupled with the GC for GC-MS analyses. The ion source housing was modified to accommodate an Edwards EO-4 600 L/s oil diffusion pump, VT-4 cold trap, and QV-4 butterfly valve (Edwards High Vacuum, Inc., Grand Island, N.Y).

A diagram of the GC-MS coupling is shown in Figure 1. The line running from the splitter to the GC detector is a 30 cm in length × 0.25 mm i.d. stainless steel tube (see 3 in Figure 1), while the 60-cm coiled length of the same tubing (see 7 in Figure 1) serves as a flow restrictor. The make-up gas is added in order to maintain a positive pressure at the splitter. The separator is a glass single-stage jet (Vacumetrics, Inc., Ventura, Calif.) which is attached using Vespel ferrules (Supeltex M-2, Supelco). The valves are Nupro SS-6BW-TWS metal bellows valves (Nupro Co., Cleveland, Ohio).

For GC-MS analysis, the carrier gas flow through the micropacked column and make-up gas line were each maintained at approximately 6 mL/min. The make-up gas flow rate was set so that approximately 10% of the column effluent flowed to the FID detector. The lines between the GC and the mass spectrometer were maintained at 250 °C. Solvent peaks were vented by closing the metal bellows valve to the MS and opening the metal bellows valve to a diffusion pump (see 10 in Figure 1). The mass spectrometer operating conditions were as follows: ion source temperature, 200 °C; electron energy, 70 eV; and emission current, 300 μA.

The mass spectrometer was interfaced to a Varian MAT Spectro-system 100 for the acquisition and recording of low resolution mass spectra. This data system consists of a Varian 620/i minicomputer with 8K of core memory, dual 9-track tape drives, a Tektronix 4010-1 graphic display terminal with 4610 hard copy unit, and a Varian MAT N101 interface unit. The N101 contains a 50-kHz 14-bit analog-to-digital converter, a Hall-effect probe, and associated electronics. Spectra were acquired using Varian MAT's KOS II software, supplemented with a program written in our lab for plotting spectra on the Tektronix 4010. The mass spectrometer accelerating voltage was set at 8 kV and the magnet was scanned from m/e 450 to m/e 25 at 0.074 decade/s, resulting in a 17-s scan time, with another 13 s required for magnet recovery before another scan could be made.

For selected ion monitoring, ion beam switching was accomplished electrically. As reported previously (*15*), the ion accelerator and electric sector power supplies on our instrument can be replaced with computer-controllable power supplies constructed in our laboratory. In this way the 620/i computer can control the focusing of ion beams onto the detector. The signal from the electron multiplier is sent to a current-to-frequency converter and then to an ion counting interface in the computer, as described elsewhere (*16*). For the work reported here, single ion monitoring traces at masses 372, 386, and 400 were obtained in three separate GC runs, although software for multiple ion monitoring is currently being written.

Sample Preparation. Extractions were carried out in a Soxhlet extractor using 3/2 v/v of benzene–methanol on 100-g samples of the New Albany Shale that were ground to pass a 200-mesh sieve. After removal of the extraction solvent in a stream of nitrogen at 40 °C, the shale extracts were chromatographed on silica gel columns and/or thin-layer plates (*17*). The alkane fractions studied in this investigation correspond to either the carbon tetrachloride (CCl_4) eluates from column chromatograph or the TLC fractions with the largest R_f values.

RESULTS AND DISCUSSION

Gas Chromatographic Column. The liquid phases considered for this investigation of GLSC using GCB are listed with their McReynold's constants (*18*) in Table I. These phases were selected on the basis of their stabilities at temperatures up to 350 °C or higher. Preliminary thermal stability tests were carried out by coating 1.5% of the liquid phases in Table I on Carbopack A, a well studied modification of GCB having a surface area of 15 m^2/g. The results indicate that both Dexsil 400 and PPE 20 are almost completely retained on the surface of GCB up to 380 °C, while OV 17 is

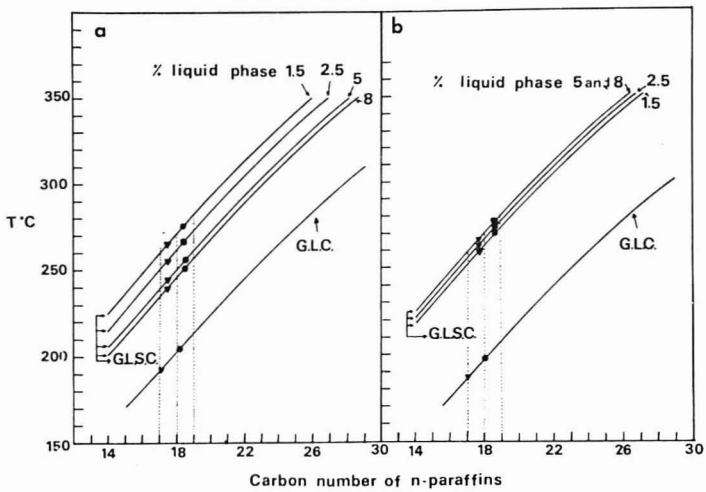


Figure 2. Effect of various degrees of liquid coatings on the GLSC elution temperatures of *n*-alkanes from Carbopack A coated with (a) PPE 20 and (b) Dexsil 400 and a GLC column packed with Chromosorb WAW coated with 3% w/w of (a) PPE 20 and (b) Dexsil 400. Elution temperatures of pristane and phytane are denoted by ▼ and ●, respectively

rapidly desorbed above 300 °C. The effect of the degree of coating on elution temperature of *n*-alkanes was measured for both Dexsil 400 and PPE 20. Amounts of Dexsil 400 and PPE 20 corresponding to 1.5, 2.5, 5, and 8% w/w on GCB were employed in GLSC analyses to determine the effect of the degree of coating on the elution temperatures of *n*-alkanes. The smallest of these amounts (1.5%) corresponds to two complete monolayers; whereas the largest amount (8%) corresponds to approximately 13 monolayers (*19*). Since GCB is a nonporous adsorbent exhibiting a geometrically homogeneous surface, the 8% coating closely approaches the amount of liquid phase usually used in GLC. For comparison purposes, GLC columns were constructed using Chromosorb WAW as solid support and this support was separately coated with 3% w/w each of Dexsil 400 and PPE 20. All columns were 2 m long.

Figures 2a and 2b are plots of the elution temperatures for alkanes on PPE 20 and Dexsil 400 coated Carbopack A (GLSC) and Chromosorb WAW (GLC). The positions of the reference pristane and phytane peaks relative to the positions of the C_{17}, C_{18}, and C_{19} *n*-alkanes are indicated in these plots because it is difficult to separate these isoprenoid alkanes from C_{17} to C_{19} *n*-alkanes on most packed columns. The following information may be deduced from Figures 2a and 2b: (1) GLC columns employing either Dexsil 400 or PPE 20 do not adequately separate pristane and phytane from *n*-C_{17} and *n*-C_{18} alkanes; (2) The resolutions determined for the GLC columns indicate that a capillary column approximately 30 m in length would be required to completely isolate pristane and phytane from *n*-alkanes with comparable boiling points; (3) Pristane and phytane can be completely separated on a 2-m packed column by GLSC using Carbopack A coated with either Dexsil 400 or PPE 20; and (4) The GLSC elution temperatures decrease as the amount of the polar coating (PPE 20) is increased, but this trend is reversed when a nonpolar liquid phase (Dexsil 400) is employed.

Similar observations on the separations obtained using polar and nonpolar coatings on GCB (*9, 12*) and on Chromosorb W (*20*) have been reported. These studies have shown that the separations obtained between nonpolar compounds on GCB coated with a nonpolar liquid are slightly reduced by increasing the amount of coating; however, an increase in the amount of polar coating on GCB sharply decreases the retention volumes for nonpolar compounds without a reduction in the separation factor (α).

Table II. Reference Hydrocarbons Coinjected with the Mixture of Utah *n*-Alkanes

Branched Chained and Cyclic Alkanes	
a. cyclohexane	m. anteiso-C_{24}
b. adamantane	n. squalene
c. farnesane	o. squalane
d. octylcyclohexane	p. coprostane
e. C_{18} isoprenoid	q. α-cholestane
f. pristane	r. 17α-trisnorhopane
g. phytane	s. 17α-trisnormohopane
h. C_{21} isoprenoid	t. lupene
i. androstane	u. fernene
j. iso-C_{21}	v. moretane
k. anteiso-C_{22}	w. 17α-homohopane
l. heptadecylcyclohexane	y. 17β-homohopane

n-Alkanes

C_4-C_{12}, C_{32}, C_{34}, C_{36}, C_{38} and C_{40}

Figure 3 shows a GLSC analysis of *n*-alkanes isolated by use of 5-Å molecular sieves from a Utah (Uinta) crude oil to which were added the reference compounds listed in Table II. As the chromatogram presented in Figure 3 clearly demonstrates, PPE coated Carbopack A provides a versatile and selective packing for the analysis of alkanes. This packing permits the relatively rapid chromatographic analyses of alkanes with a wide range of carbon numbers and the separation of isoprenoid-type hydrocarbons, steranes, and *n*-alkanes at a preparative scale. The column bleeding of either PPE 20 or Dexsil 400 coated GCB is remarkably low at high operating temperatures.

Carbopack C was used in place of Carbopack A after our supply of Carbopack A was exhausted. As previously reported (*19*), the chromatographic properties of liquid coated Car-

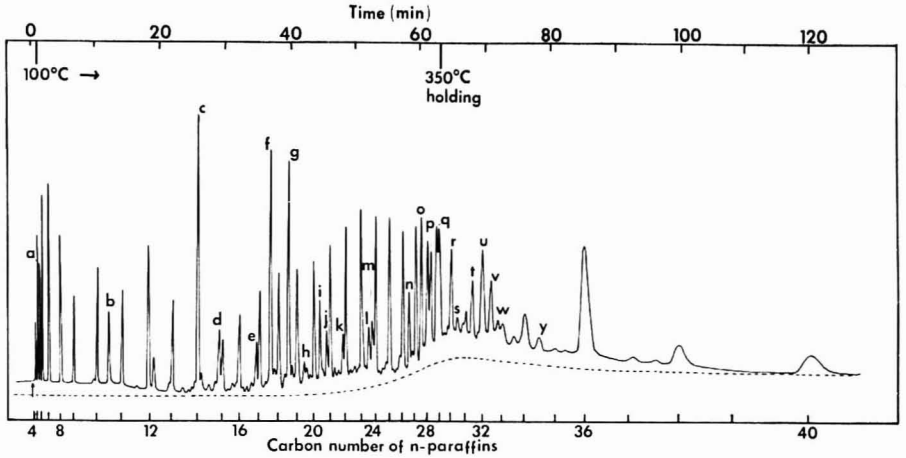


Figure 3. Chromatogram of a hydrocarbon mixture obtained by adding the reference compounds listed in Table II to C_{13} to C_{35} *n*-alkanes from a Utah (Uinta Basin) crude oil. Column: 2 m × 2 mm. Packing: 100–120 mesh Carbopack A + 8% w/w PPE 20. ϕ = 25 mL/min. Temperature programmed at 4 °C/min.

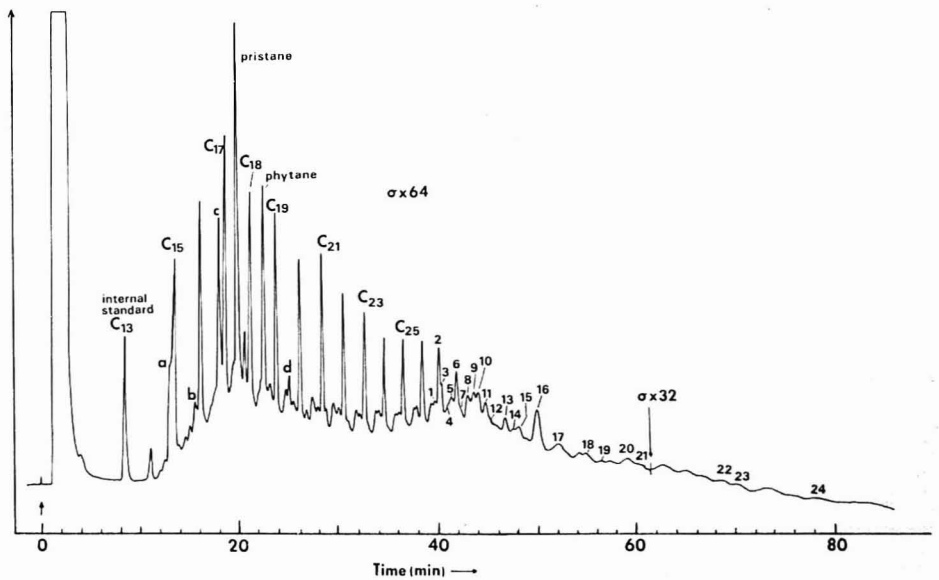


Figure 4. FID trace from GC-MS analysis of alkane fraction of the New Albany Shale extract. (a) C_{16} isoprenoid, (b) C_{17} isoprenoid, (c) C_{18} isoprenoid, (d) C_{21} isoprenoid. Column: 2 m × 1 mm. Packing: 100–120 mesh Carbopack A + 8% PPE 20. ϕ = 6 mL/min. Temperature programmed at 4 °C/min from 170 to 350 °C

bopack C and Carbopack A are similar, but these GCB's require different amounts of a liquid phase. Carbopack C coated with 4% w/w of PPE 20 is chromatographically equivalent to Carbopack A coated with 8% w/w of PPE 20 for alkane analysis, but Carbopack C columns operate at lower temperatures than do Carbopack A columns. Specifically, the *n*-C_{40} alkane elutes at 340 °C and 350 °C, respectively, from chromatographically equivalent PPE 20 coated Carbopack C and Carbopack A columns. In subsequent discussions, no distinction will be made between applications of Carbopack C and Carbopack A columns.

GC-MS Coupling. Micropacked columns can be operated at high linear gas velocities ($\bar{u}$) while maintaining low flow rates (*21*, *22*). This capability enhances the potential of micropacked columns for use in conjunction with mass spectrometry and the low bleed rate and high efficiency of PPE 20 coated

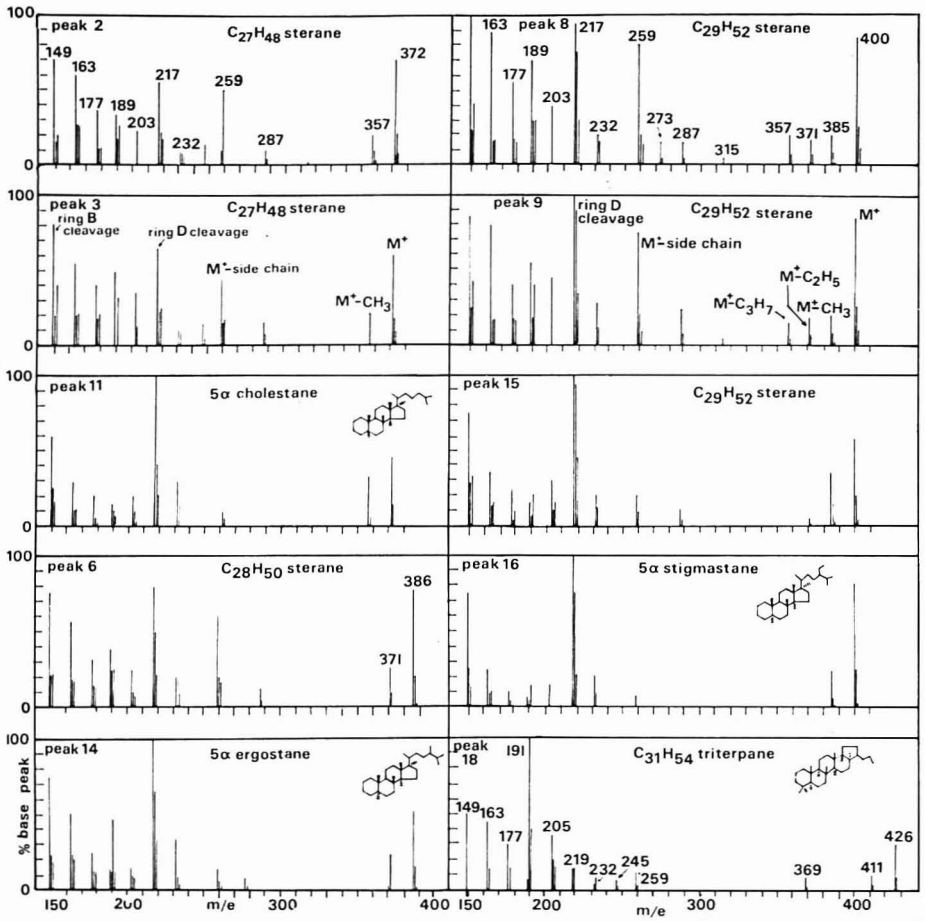


Figure 5. Mass spectra of steranes and triterpanes collected during the GC-MS analysis of the New Albany Shale. Peak numbers correspond to those in the chromatogram in Figure 4

GCB recommend its use in micropacked columns. An original GC-MS coupling shown in Figure 1 joins a micropacked column to a CEC21-110 B mass spectrometer. This novel coupling permits simultaneous recording of a gas chromatogram using any type of gas chromatographic detector and the beam monitor of the mass spectrometer. The splitter makes it possible to operate the column exit at atmospheric pressure, as in standard GLSC, rather than at a vacuum as is the case for most GC-MS couplings (*23*). The addition of make-up gas may be varied to adjust the split ratio between the GC and MS detectors without changing the linear gas velocity ($\bar{u}$) of the column. When the flow of the make-up gas is properly set, signals from the two detectors are coincident and the recorded peak widths are equal. The two metal valves, labeled as 10 in Figure 1, permit the isolation of the ion source during the venting of the GC solvent peak. Efficient removal of the carrier gas (He) is achieved by the separator. The ion source is maintained at approximately 9×10^{-7} Torr (uncorrected) and the beam monitor gives a stable base-line signal during operation of the coupled system at 70-eV ionization potential.

ANALYTICAL APPLICATIONS

GC-MS Analyses of Branched Chain and Cyclic Alkanes from the New Albany Shale. The FID trace, obtained during the GC-MS analysis of the total alkane fraction of the benzene–methanol extract of a New Albany Shale sample is shown in Figure 4. The high abundances of the C_{15}, C_{17}, and C_{19} *n*-alkanes and of pristane indicate that the remains of marine organisms are major constituents of the organic materials in this shale (*24*). As suggested above, the analysis of the steranes and triterpanes present in this shale are of special interest because these compounds have been used in investigations of the migration and maturation of petroleum (*25, 26*). The empirical formulas of the compounds for which the peaks are numbered in Figure 4 are listed by these numbers in Table III. Mass spectra are recorded in Figure 5 for some of the steranes and a triterpane in these

Table III. Steranes and Triterpanes Identified in the Alkane Fraction of the New Albany Shale Extract

peak number (Figure 4)	formula	hydrocarbon type
1.	$C_{27}H_{48}$	steranes
2.	$C_{27}H_{48}$	steranes
3.	$C_{27}H_{48}$	steranes
4.	$C_{27}H_{48}$	steranes
5.	$C_{28}H_{50}$ + $C_{27}H_{48}$	steranes
6.	$C_{28}H_{50}$	steranes
7.	$C_{29}H_{52}$	steranes
8.	$C_{29}H_{52}$	steranes
9.	$C_{29}H_{52}$	steranes
10.	$C_{29}H_{52}$ + $C_{27}H_{48}$	steranes
11.	5α-cholestane	
12.	$C_{28}H_{50}$ + $C_{29}H_{52}$ + $C_{30}H_{54}$	steranes
13.	$C_{29}H_{52}$ + $C_{30}H_{54}$	steranes
14.	5α-ergostane	
15.	$C_{29}H_{52}$	steranes
16.	5α-stigmastane	
17.	$C_{29}H_{50}$	pentacyclic triterpanes
18.	$C_{30}H_{52}$	pentacyclic triterpanes
19.	$C_{31}H_{54}$	pentacyclic triterpanes
20.	$C_{31}H_{54}$	pentacyclic triterpanes
21.	$C_{31}H_{54}$	pentacyclic triterpanes
22.	$C_{33}H_{58}$	pentacyclic triterpanes
23.	$C_{33}H_{58}$	pentacyclic triterpanes
24.	$C_{34}H_{60}$	pentacyclic triterpanes

alkanes. The peak numbers listed in Figure 5 correspond with those in Figure 4 and Table III.

Marked differences may be observed between the mass spectra of 5α-cholestane, 5α-ergostane and 5α-stigmastane and the mass spectra of other types of steranes in Figure 5. One noteworthy difference is the presence of an intense peak at m/e 259 coupled with a decreased intensity of the peaks at m/e 217 and 218. The m/e 259 peak is formed as a consequence of the cleavage of the large alkyl side chain at the 17 position, and the m/e 217 and 218 ions are formed by the cleavage that removes ring D. The loss of the side chain fragments is particularly evident in the mass spectra of the steranes in GC peaks 8 and 9 of Figure 5, where large peaks may be observed at m/e 371, 357, 315, 287, and 273. The appearance of the peak at m/e 259 is associated with a general increase in the sizes of the peaks at m/e 177, 163 and m/e 149 which result from cleavages in ring B. None of the steranes have a base peak at m/e 231 that is characteristic of the 4-methyl substituted steranes. The distributions of some of the C_{27}, C_{28}, and C_{29} steranes may be clearly observed in the single ion monitor traces recorded at m/e 372, 386, and 400 in Figure 6. The shaded area indicates the presence of a compound that has a m/e 259 peak which is >50% as large as the base peak (m/e 217). The symbols α and β denote 5α and 5β isomers of cholestane, ergostane, and stigmastane that were present in these eluates. The identifications of these steranes were confirmed by coinjecting standard compounds.

The single ion monitor traces in Figure 6 indicate similar distributions for the C_{27}, C_{28}, and C_{29} steranes. Furthermore, the relative concentrations of steranes that have and do not have intense m/e 259 peaks in their spectra are approximately constant. Steranes with large m/e 259 peaks comprise between 35 and 45% of the total C_{27}, C_{28}, and C_{29} steranes in the New Albany Shale extract. As shown by the positions of the shaded areas in the Figure 6 traces, the steranes with large m/e 259 peaks have shorter GC retention times than do the other steranes.

Seifert et al. (*14*) have observed distributions and fragmentation patterns for steranes from California crude oils

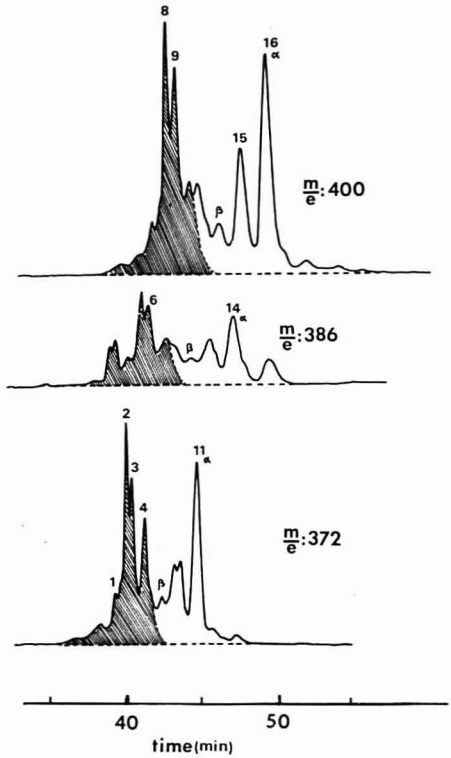


Figure 6. Single ion monitor traces for C_{27}, C_{28}, and C_{29} steranes collected during the GC-MS analysis of the New Albany Shale extract. The shaded areas indicate the presence of m/e 259 peaks that are larger than 50% base peak. Peak numbers correspond to those in the chromatogram in Figure 4

which resemble those reported above for the steranes from the New Albany Shale. They propose that the crude oil steranes with intense m/e 259 peaks are rearrangement products of sterols in which the bridge methyl groups are attached to carbon atoms 5 and 14 rather than at the 10 and 13 positions. Laboratory experiments have established that cholestanol undergoes a "backbone rearrangement" (*27*) under strongly acidic conditions at 145 °C to yield a 5,14-dimethyl substituted sterol ring system. Seifert et al. (*14*) cite these experiments and the fact that the mass spectrum of the sterene product has a strong m/e 257 peak as evidence for the presence of the 5,14-dimethyl sterane in the crude oil. This interpretation presumes that hydrogenation of the steranes with a large m/e 257 peak would produce a sterane with an intense m/e 259 peak, and their interpretation is indirectly supported by the similarity in the mass spectra of the stereoisomers of cholestane reported by Mulheirn and Ryback (*28*).

Recently, Ensminger et al. (*29*) have found backbone rearranged steranes, which they refer to as diasteranes, in the Dontrien Shale. Their identifications of βα- and αβ-diasteranes were accomplished by comparisons of the retention times and the mass spectra of the natural products isolated from shales and crude oils with those of diasteranes prepared

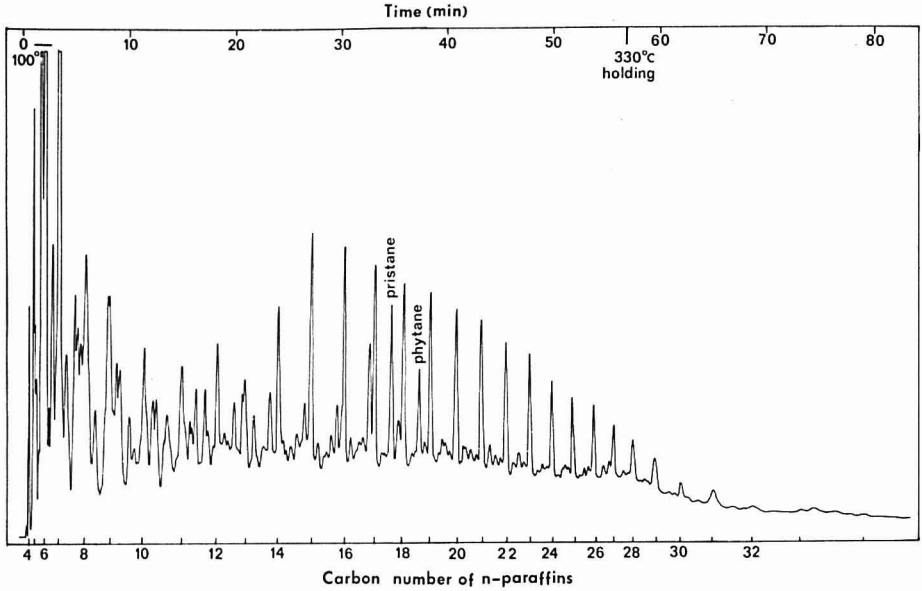


Figure 7. Chromatogram of a total Devonian crude oil from Lowry Indiana. Column: 2 m × 1 mm. Packing: Carobpack C + 4% PPE 20. ϕ = 10 mL/min. Temperature programmed at 4 °C/min

by synthesis. An intense m/e 259 peak was observed in the mass spectra of $\beta\alpha$-diacholestanes as reported by these authors. Moreover, the fragmentation patterns of peaks 2 and 3 of Figure 5 closely resemble the data presented for $\beta\alpha$-diacholestanes (*29*), and in this respect, some of our mass spectral analyses support the presence of backbone rearranged products in the sterane fractions from the New Albany Shale. However, it is conceivable that rearrangements requiring less severe conditions than methyl group migrations (*13*) may have been favored relative to the backbone rearrangement in the New Albany Shale which has a mild thermal history. For instance, Petrov (*30*) has noted that the cis CD ring fusion in the steroid ring system is the thermodynamically preferred configuration. At equilibrium, up to 90% of cholestanes may be converted to cholestanes with cis CD ring junctures, and similar conversions are observed in the hopanes (*31*). The mechanism for the formation of the m/e 217 peak in the mass spectra of 5 steranes involves a hydrogen rearrangement from position 14 to 17 and from positions 12, 8, and 13 to position 14 (*32*). Seemingly, isomerizations at ring and side chain junctures may reasonably be expected to diminish cleavages in the D ring of steranes. In this regard, it is interesting to note that m/e 218 is the base peak of 5α,14β-cholestane (*28*). Moreover, a small but detectable increase in m/e peaks 259, 149, 163, and 173 in the mass spectrum of 5α,14β-cholestane can be observed relative to these peaks in the mass spectrum of 5α,14α-cholestane.

Although we suggest that structural rearrangements other than those involving methyl group migrations may provide an explanation of the gas chromatographic–mass spectrometric analyses of unidentified compounds in the sterane fractions of the New Albany Shale and similar geological samples, we recognize that our suggestion cannot be evaluated until suitable reference compounds are available.

Table IV. Compounds Identified in the New Albany Shale Distillate

FID Trace

1 C_7 olefin + C_7 n alkane + benzene
2 C_8 olefin + C_8 n-alkane + toluene
3 C_9 olefin + m-xylene
4 C_9 olefin + o- and p-xylene
5,6 C_{10} olefin
7 methylethylbenzene
8
9
10
11 C_{11} olefin
12,13
14
15
16
17 C_1
18
19 C_2
20,21 C_3
22
23 C_3
24 C_4
25 C_2
26 C_5
27 C_3
28 C_3
29,30 C_4
31 C_5

ECD Trace

a thiophene
b C_2 + C_3 benzothiophenenes
c benzodithiophenes

Fingerprint Analysis of the Total Organic Fractions of Geological and Industrial-type Samples. Crude oils and organic extracts and distillates of sedimentary rocks are generally complex mixtures. Definitive analyses of these carbonaceous substances are commonly preceded by sequential

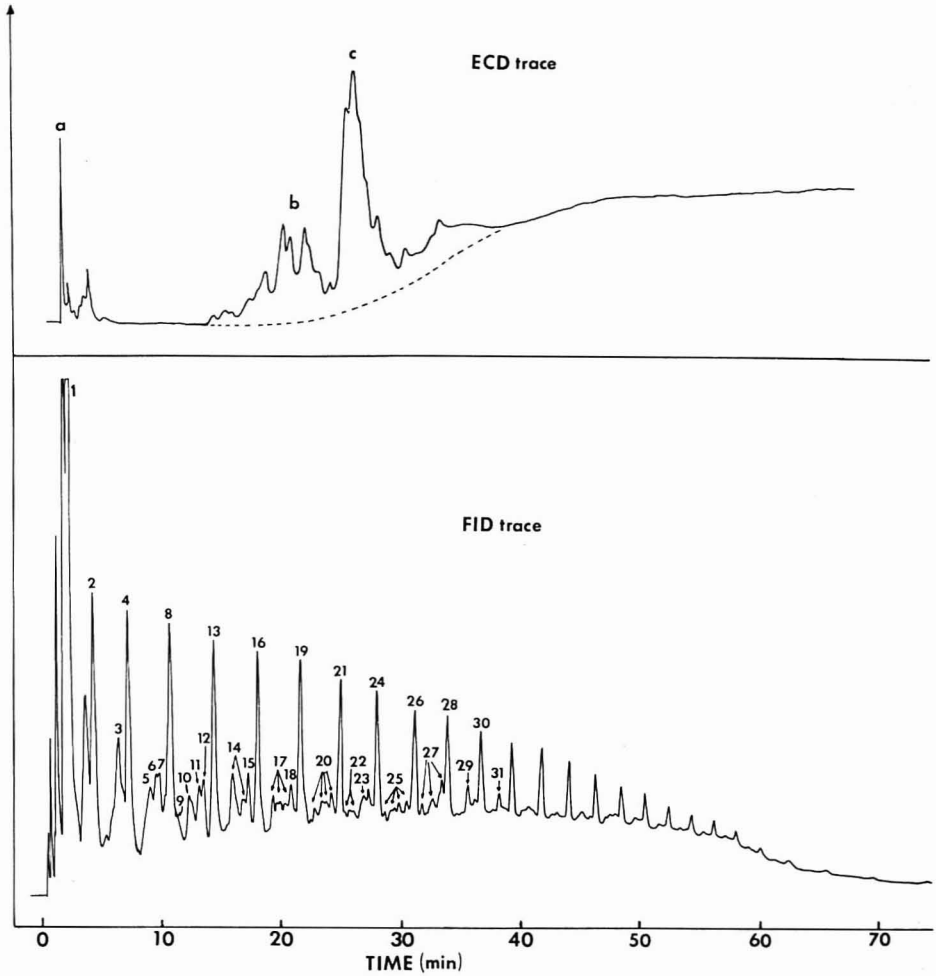


Figure 8. Chromatograms of two equivalent samples of a distillate obtained from the New Albany Shale in a Fischer Retort operated at 500 °C. Column: 2 m × 1 mm. Packing: Carbopack C + 4% PPE 20. ϕ = 6 mL/min. Temperature programmed at 4 °C/min from 100 to 340 °C

separations which divide these complex mixtures into relatively simple fractions that are amenable to analyses. Unless elaborate precautions are taken, substantial portions of such organic samples are lost during the exchanges of solvent involved in the extractions, chromatographic fractionations, and recoveries of these samples. For instance, the gasoline and kerosene portions of crude oils are lost when crude oil is separated by LSC or TLC.

GLSC employing GCB affords a means of resolving complex mixtures composed of organic compounds with widely different molecular weights and functional groups or polarities. For example, the GC analyses of samples of a Devonian crude oil from Indiana and a 500 °C Fischer Retort distillate of the New Albany Shale are presented in Figures 7 and 8. As the GC analyses of a total crude oil in Figure 7 shows, the pristane/phytane, n-C_{17}/pristane, and n-C_{18}/phytane ratios as well as the carbon preference indices, which are extensively used in organic geochemical investigations (*33*), can be measured. GC data acquired with GLSC columns packed with GCB exhibit a large capacity in addition to high resolution. For this reason, these columns may employ multidetection systems (*34*) thus making it possible to obtain GC "fingerprints" and mass spectral analyses in a single run.

Figure 8 shows the FID and ECD traces recorded during two separate GC-MS analyses of the New Albany Shale distillate. Table IV lists the compounds tentatively identified by the GC-MS analysis of this distillate which is predominantly composed of aromatic hydrocarbons (*17*). Both the intensity of the ECD signal and the distributions of ^{32}S and ^{34}S containing ions in the mass spectra provide evidence relating to the number of sulfur atoms in the thiophenes listed in Table IV.

ACKNOWLEDGMENT

The authors thank G. Eglinton of the University of Bristol (England) for providing some of the reference compounds, W. B. Wimberg for technical assistance, and G. E. Von Unruh and E. Brancaleoni for helpful discussions. We also thank P. J. Arpino of the Ecole Polytechnique (France) for calling to our attention the recent work by Ensminger et al. (29).

LITERATURE CITED

(1) D. M. Young and A. D. Crowell, "Physical Adsorption of Gases", Butterworths, London, 1962, and references therein.
(2) S. Ross and J. P. Olivier, "On Physical Adsorption", Interscience, New York, 1969, and references therein.
(3) A. V. Kiselev and Y. I. Yashin, "Gas Adsorption Chromatography", Plenum Press, New York, 1969, p 128.
(4) G. M. Petov and K. D. Sherbakova, in "Gas Chromatography 1966", A. B. Littlewood, Ed. Institute of Petroleum, London, 1967, p 50.
(5) A. V. Kiselev, N. V. Kovaleva, and Y. S. Nikitin, *J. Chromatogr.*, **58**, 19 (1971).
(6) F. Bruner, P. Ciccioli, G. Crescentini, and M. T. Pistolesi, *Anal. Chem.*, **45**, 1851 (1973).
(7) A. DiCorcia and A. Liberti, *Adv. Chromatogr.*, **14**, 305-363 (1974).
(8) F. Bruner, P. Ciccioli, and A. DiCorcia, *Anal. Chem.*, **44**, 894 (1972).
(9) F. Bruner, P. Ciccioli, and F. DiNardo, *Anal. Chem.*, **47**, 141 (1975).
(10) C. Vidal-Madjar and G. Guiochon, *Nature (London)*, **215**, 1372 (1967).
(11) F. Bruner, P. Ciccioli, and F. DiNardo, *J. Chromatogr.*, **99**, 661 (1974).
(12) C. Vidal-Madjar, S. Bekassy, M. F. Gonnord, P. J. Arpino, and G. Guiochon, *Anal. Chem.*, **49**, 768 (1977).
(13) W. G. Meinschein, *Bull. Am. Assoc. Petrol. Geologists*, **43**, 925 (1959).
(14) W. K. Seifert and J. M. Moldowan, *Geochim. Cosmochim. Acta*, **42**, 77 (1978).
(15) K. B. Denson, S. P. Taylor, and J. M. Hayes, *Proc. 24th Annu. Conf. Mass Spectrom. Allied Topics, San Diego Calif.*, 548 (1976).
(16) D. E. Matthews, K. B. Denson, and J. M. Hayes, *Anal. Chem.*, **53**, 681 (1978).
(17) G. Rinaldi, P. Ciccioli, W. B. Wimberg, and W. G. Meinschein, Paper presented at the "First Eastern Gas Shales Symposium", Morgantown, W.Va., 1977, pp 734-747, in press.
(18) W. O. McReynold, *J. Chromatogr. Sci.*, **8**, 685 (1970).
(19) F. Bruner, G. Bertoni, and P. Ciccioli, *J. Chromatogr.*, **120**, 307 (1976).
(20) P. Urone, Y. Takahashi, and G. H. Kennedy, *J. Phys. Chem.*, **74**, 2326 (1970).
(21) F. Bruner, P. Ciccioli, G. Bertoni, and A. Liberti, *J. Chromatogr. Sci.*, **12**, 758 (1974).
(22) M. Novotny, J. M. Hayes, F. Bruner, and P. G. Simmonds, *Science*, **189**, 215 (1975).
(23) F. Bruner, P. Ciccioli, and S. Zelli, *Anal. Chem.*, **45**, 1002 (1973).
(24) P. Albrecht and G. Ourisson, *Angew. Chem., Int. Ed. Engl.*, **10**, 209, (1971).
(25) R. C. Clark, Jr., and M. Blumer, *Limnol Oceanogr.*, **12**, 70 (1967).
(26) W. K. Seifert, *Geochim. Cosmochim. Acta*, **42**, 473 (1978).
(27) I. Rubinstein, O. Sieskind, and P. Albrecht, *J. Chem. Soc., Perkin Trans. 1*, 1833 (1975).
(28) L. J. Mulheim and G. Ryback, "Advances in Organic Geochemistry", (Madrid, 1975), R. Campos and J. Soni, Ed., 1977, p 211.
(29) A. Ensminger, G. Joly, and P. Albrecht, *Tetrahedron Lett.*, **18**, 1575 (1978).
(30) A. A. Petrov, D. S. Pustilnikova, and N. N. Abriutina, "8th International Congress on Organic Geochemistry" held in Moscow 10-13 May, 1977; Volume 1, Abstracts of Reports, p 162.
(31) A. Ensminger, P. Albrecht, G. Ourisson, and B. Tissot, "Advances in Organic Geochemistry" (Madrid, 1975), R. Campos and J. Soni, Ed., 1977, p 45.
(32) L. Tokes, G. Jones, and C. Djerassi, *J. Am. Chem. Soc.*, **90**, 5465, (1968).
(33) R. E. Kreider, 1971 Joint Conference on Prevention and Control of Oil Pollution, p 119.
(34) P. Ciccioli, G. Bertoni, E. Brancaleoni, R. Fratarcangeli, and F. Bruner, *J. Chromatogr.*, **126**, 757, (1976).

RECEIVED July 17, 1978. Accepted December 8, 1978. This work was partially supported by DOE Grant EY-76-C-05-5204 and funding from NSF Grant EAR 76-13463, NASA Grant NGR 15-003-118, and OWRT Grant 14-31-0001-5143 contributed to the maintenance of the laboratory facilities used in this study.

Development and Characterization of a Miniature Inductively Coupled Plasma Source for Atomic Emission Spectrometry

R. N. Savage and G. M. Hieftje*

Department of Chemistry, Indiana University, Bloomington, Indiana 47401

A miniature inductively coupled plasma source for atomic emission spectrometry is described and a preliminary evaluation of its analytical capabilities is presented. The mini-ICP is very economical to sustain and works well with less than 1 kW of rf power and 8 L min^{-1} of argon coolant gas. In addition, the new source possesses some unique operating characteristics which simplify sample introduction. In this paper, detection limits, multielement capabilities, and other analytical features of the mini-ICP are compared with those demonstrated by a conventional ICP source and shown to be comparable. In addition, the two plasmas are shown to exhibit similar excitation temperatures in their respective analyte observation regions (i.e., plasma tail flames). These results suggest that the mini-ICP possesses the same desirable atomization and excitation characteristics as conventional ICP sources.

During the past decade, the radio-frequency inductively coupled plasma (ICP) has emerged as a very promising excitation source for atomic emission spectrometry (AES) and many investigators have examined both the physical nature (*1-4*) and analytical capabilities (*5-7*) of ICP sources for simultaneous multielement optical emission analysis. However, one of the main impediments to the acceptance of these ICP-AES systems has been the high operational cost and complexity associated with the ICP source itself. In addition, the high-power rf equipment required by conventional ICP sources increases their initial cost, requires a lot of laboratory space, and can produce strong radio-frequency interference (RFI), unless proper shielding techniques are employed.

Many of these limitations should be overcome merely by shrinking the physical dimensions of the ICP. Such a mini-ICP, if operated at similar power densities to its larger counterpart, should exhibit the same high sensitivity, working curve linearity, and freedom from interferences; these desirable features are largely a result of high plasma temperature, which is itself a function of power density (*8*). In turn, the smaller ICP would require a lower input power to maintain equivalent power density and would consume less coolant gas (argon) during operation. Attendant savings in the cost of the rf power supply, impedance matching device, and transmission lines would be expected. In addition, lower power requirements would reduce necessary laboratory space and expected interference from radiated rf energy.

In the present study, such a mini-ICP was developed and its operational characteristics and analytical capabilities were evaluated and compared to a conventional ICP source. The conventional source is a commercially available system containing a 20-mm o.d. torch. This kind of system is found

0003-2700/79/0351-0408$01.00/0 © 1979 American Chemical Society

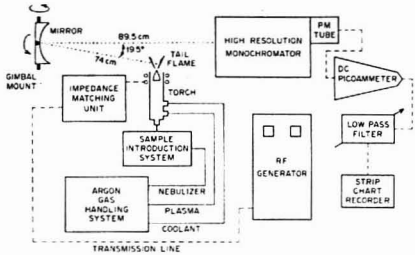


Figure 1. Schematic diagram of ICP-AES experimental system. (....) optical path; (---) electrical path; (—) gas flow

in many laboratories today (*2*, *4*, *7*).

Torch design was found to play a critical role in the process of stabilizing the smaller plasma, and hydrodynamic techniques were devised (*9*) to aid in torch development. The plasma supported by the new mini-torch demonstrated excellent stability and was easier to ignite than its larger brother (the commercial plasma source). In addition, the mini-plasma was operated at 33% lower rf power levels and consumed 50% less high-purity argon than the conventional ICP system employed for comparison. Significantly, while operating under these conditions the mini-ICP demonstrated that it possessed the same highly acclaimed analytical capabilities (i.e., low detection limits, high excitation temperatures, simultaneous multielement capabilities, and linear analytical calibration curves covering 4–5 orders of magnitude) as the conventional ICP.

EXPERIMENTAL

Instrumentation. A schematic diagram of the apparatus used in this study is shown in Figure 1. Details concerning the individual components are summarized below.

Radio-frequency Power System. Radio-frequency power is developed by a crystal-controlled air-cooled power amplifier (Model HFP-2500 D with Model APCS-1 power control, Plasma-Therm Inc., Kresson, N.J.) operating at 27.12 MHz. The rf power is continuously variable up to a maximum of 2.5 kW and is transmitted via a coaxial cable (RG 8/U) to the load coil of an automatic impedance matching unit (Model AMN-2500E, Plasma-Therm Inc., Kresson, N.J.). The water-cooled load coils are fabricated of $^1/_8$-in. (3.175-mm) o.d. copper tubing. For mini-ICP operation, a 2-turn load coil with a diameter of ~2 cm is used; when operating the conventional ICP, a 3-turn coil is employed with a diameter of ~3 cm. Primary ignition of the plasma is accomplished by applying to the torch a spark from a Tesla coil.

Torch, Nebulizer, and Housing. In general, the mini-ICP torch has the same features and operates on the same basic principles as conventional ICP torches (*10–15*). However, the mini-torch is 33% smaller than conventional torches (*16*, *17*) and possesses some unique features, as revealed in the diagram of Figure 2. In this diagram, dimensions of the torch are given and its orientation with respect to the load coil is shown. A quartz bonnet, positioned around the end of the torch, aids in electrically screening the conductive plasma gases from the load coil.

As in conventional torches, both the plasma and coolant gases (high-purity argon) are introduced tangentially (*10*) into the torch. Therefore, the central axes of the gas inlet tubes must lie on tangent lines to the coolant tube. For the mini-torch, this orientation was established empirically using hydrodynamic techniques (*9*). In addition, the gas inlet tubes were constricted to increase the swirl velocity of the gases as they spiral up the torch. With this technique, a stable vortex is formed at low gas flows; a similar effect has been examined in some detail by Barnes (*18*). A mini-torch employing this design can stably support a plasma using less than 8 L min^{-1} of argon coolant gas.

The shape and position of the central injection tube plays a critical role in assuring that the sample is directed into the hottest

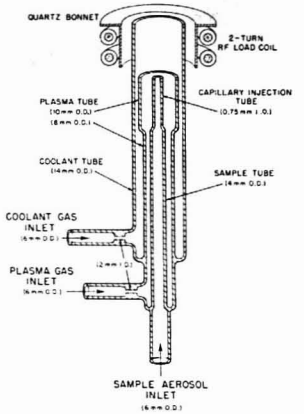


Figure 2. Mini-ICP torch construction. Quartz wall thickness = 1 mm. All features are drawn to scale

part of the plasma. In our torch, the injection tube is tipped with a length of capillary tubing adequate to create a laminar flow (*19*) of exiting sample aerosol. This laminar flow readily penetrates the plasma and reduces the chances of sample being swept around the plasma periphery. A laminar flow design of this nature also enables the injection tube to be positioned as far as 2 mm below the end of the plasma tube, where the chances of its overheating and melting are reduced.

The internal diameter of the injection tube is also important because it determines the size of the hole that is punched through the plasma. This hole should be kept small to ensure that the sample channel is electrically screened from the energy addition region (defined as the skin depth) of the plasma (*12*), and that the sample flow cools the plasma as little as possible. Under these conditions, the addition of sample to the plasma will cause only minimal variations in the plasma's impedence and not affect materially the plasma's stability. This consideration is particularly important in the mini-ICP since the energy addition region occupies a large portion of the plasma. In this study, excellent plasma stability was obtained using a 0.75-mm i.d. capillary injection tube.

The sample introduction system consists of a simple concentric pneumatic nebulizer attached to a dual-tube spray chamber, similar to the one described by Fassel (*16*). Ordinarily, the nebulizer is operated at an argon flow rate of 1 L min^{-1} and sample solution is delivered to the nebulizer by a peristaltic pump at a rate of 0.36 mL min^{-1}. The resulting spray is fed directly into the torch (i.e., no desolvation apparatus is employed).

To shield other instrumentation from RFI, a custom-designed copper housing enclosed the load coil, torch, nebulizer, and spray chamber. Access ports for the necessary support facilities (i.e., argon gas, cooling water, drain, etc.) are provided and windows are cut into the housing for optical access. A piece of welding glass ($A \approx 4$) has been inserted into one window to enable the operator to monitor plasma operation.

Support Gas Handling. Delivery of the large quantities of prepurified argon gas (99.998%) needed to sustain the plasma requires a special gas handling system. To reduce the frequency with which gas supplies required changing, three argon tanks are interconnected by a manifold equipped with station and check valves (Matheson Gas Products, Joliet, Ill.). A single stage pressure regulator (Air Products, Allentown, Pa.) and a sensitive line regulator (Model 40H, Matheson Gas Products, Joliet, Ill.) combined in series, serve to reduce the tank pressure and maintain a constant upstream pressure of 30 psig. The argon gas is then delivered through toggle valves (Nupro Co., Cleveland, Ohio) to three rotameters (Series 7600, Matheson Gas Products, Joliet, Ill.). Each rotameter is equipped with a high accuracy needle valve (Series 4170, Matheson Gas Products, Joliet, Ill.) for controlling

Table I. General Operating Conditions for ICP-AES System

	conventional ICP	mini-ICP
rf power[a]	1.5 kW	1.0 kW
gas flows, L min^{-1}		
coolant (starting)	18.4	9.8
coolant (operating)	14.7	7.9
plasma (starting)	1.1	0.3
plasma (operating)	1.1	0
monochromator	entrance slits = exit slits	
	width = 50 μm	width = 50 μm
	height = 5 mm	height = 5 mm
time constant	1 s	1 s

[a] Forward power output from the rf generator.

the rates at which argon is delivered to the nebulizer and torch. Each rotameter tube was calibrated using a wet-test meter (Precision Scientific Co., Chicago, Ill.).

Optical Design. The entire optical system, the impedance matcher and plasma housing, and the monochromator are kinematically mounted onto an eight-foot lathe bed which serves as an optical support and alignment platform. As shown in Figure 1, optical radiation emitted in the tail flame of the plasma is collected by a 6-inch (15.2-cm) spherically concave first-surface mirror (f.l. = 40.5 cm, Al-MgF_2/2000 coating, Oriel-Corp., Stamford, Conn.) which is held by a gimbal mount (Model 760, Newport Research Corp., Fountain Valley, Calif.). The light is imaged onto the entrance slit of a high resolution monochromator (magnification = 1.25) so the entire acceptance angle of the monochromator is filled. By rotating the mirror on its axes, the image of the plasma can be translated horizontally and vertically across the entrance slit to spatially select the region in the plasma being observed. The size of the observation region is thus determined by the width and height of the entrance slit. In preliminary tests and in routine use, this optical system was found to provide good spatial resolution and was simple to align and operate. In addition, the use of only one reflective surface to transfer the optical radiation from the plasma to the monochromator minimizes light losses and chromatic aberration. However, monochromatic aberrations (e.g., coma and astigmatism) can be a problem in such an off-axis system and careful attention must be paid to its design if high-fidelity imaging is desired (*20, 21*). To reduce these aberrations, all off-axis angles should be minimized; in our system, the off-axis angles employed limited spatial resolution to approximately 5 mm in the plasma.

Detection System. Radiation transferred by the optical system is dispersed by a high resolution monochromator (Model HR1000, I.S.A. Inc., Metuchen, N.J.) employing a 120 × 140 mm holographic grating with a groove density of 2400 g mm^{-1} and a reciprocal linear dispersion of 3.9 Å mm^{-1}. The dispersed radiation is detected by a photomultiplier tube (Model R636, Hamamatsu Corp., Middlesex, N.J.) operating at −1000 V dc (Model 245 High Voltage Power Supply, Keithley Instruments Inc., Cleveland, Ohio) and mounted in a RFI-shielded housing (Model PR 1405, Products for Research Inc., Danvers, Mass.). The resulting photocurrent is monitored by a picoammeter (Model 414S, Keithley Instruments Inc., Cleveland, Ohio) which converts it into a proportional voltage. This voltage signal is passed through a variable time constant low-pass filter and displayed on a strip-chart recorder (Model SR204, Heath Company, Benton Harbor, Mich.).

Operating Procedure for Detection Limit Determinations. Detection limits were determined for a number of elements using the experimental system just described and also with a conventional ICP torch (Model T-1, Plasma-Therm Inc., Kresson, N.J.). Typical operating conditions for both the mini and the conventional ICP systems are outlined in Table I. Under these conditions, detection limits were determined using the following general operating procedure.

First, all electronic equipment including the rf generator was warmed up for at least one-half hour. The torch and nebulizer were then flushed with argon, and the coolant and plasma gas flows cited on Table I were established. These gas flows were found to provide the best conditions for stable plasma formation and operation. The slightly greater gas flows used in starting a plasma minimized the chances of torch devitrification during the ignition process. In the case of the mini-ICP, the nebulizer gas flow could be set at approximately 1 L min^{-1} before plasma initiation, while for the conventional ICP the nebulizer gas must be initially shut off or the plasma could not be ignited. Next, the forward rf power level was set and the plasma ignited. After the plasma was formed, sample was introduced and the monochromator was scanned onto the peak of the analyte emission line of interest. Both observation height (defined as the vertical distance from the center of the observation zone to the top of the load coil) and sample introduction rate (i.e., nebulizer flow rate) were optimized for maximum signal-to-noise ratio for each element. At this point 1 μg mL^{-1} sample solutions and blank solutions (i.e., distilled-deionized H_2O) were alternately introduced; each signal was recorded 5 times for at least ten time constants each run. Signal-to-noise ratios were calculated from these measurements and detection limits were determined using the procedure described by Winefordner (*22*).

Table II. Fe Emission Line Data

wavelength of transition, nm	wavenumber of emitting level, cm^{-1}	statistical weight of upper level	A_λ[a]
382.043	33096	9	3.91
382.444	26140	7	0.174
382.588	33507	7	3.48

[a] Relative transition probability normalized to the Fe 371.994 nm line by $A_{371.994} = 0.163$; taken from ref. 32.

Plasma Excitation Temperature Measurements. Excitation temperatures experienced by analyte species in both the mini and conventional ICP sources were determined using essentially the same experimental system and operating conditions as outlined above and in Table I. However, nebulizer gas flow rates were set at 1.18 L min^{-1} for the conventional ICP and 0.97 L min^{-1} for the mini. In both cases the thermometric species (Fe) was nebulized into the plasma as a 1000 μg mL^{-1} solution. The relative intensities of the three Fe emission lines (cf. Table II) of interest were measured in the tail flames of both the conventional and mini plasmas at observational heights of 29.9 and 20.1 mm, respectively. The entrance slit width of the monochromator was decreased to 40 μm for these measurements to ensure that the three Fe spectral lines were properly resolved. Spectral backgrounds at each emission line were measured while distilled-deionized water was aspirated into each plasma. The net emission line intensities of the Fe lines were determined by averaging three background-corrected values for each line.

Operating Conditions for Dynamic Range Experiments. Analytical calibration curves were determined for several analyte species in the mini-ICP, employing the same experimental system outlined in the previous sections and operating conditions given in Table I. The solution delivery rate was changed to 0.49 mL min^{-1} for these measurements and the nebulizer gas flow was set at 0.86 L min^{-1}. Emission signals were measured at an observation height of 20 mm. Spectral background measurements were made at each emission line while distilled-deionized water was aspirated, and the net emission intensity for each solution was determined by averaging four background-corrected values.

Reagents. Stock solutions were prepared as suggested by Dean and Rains (*23*), using reagent grade salts and acids as required. Analytical standards were prepared by suitable dilution of these stock solutions with freshly distilled-deionized water.

RESULTS AND DISCUSSION

Operating Characteristics of Mini-ICP. Radio-frequency Power. One of the anticipated advantages of the mini-ICP was its ability to perform usefully at reduced rf power levels. In our studies, the mini-ICP could easily be

sustained with as little as 300 W of forward rf power when no sample was introduced (Ar gas flows: coolant, 7.9 L min^{-1}; plasma, 0.3 L min^{-1}); moreover, while aqueous samples were being introduced, the mini-ICP remained stable with as little as 500 W of rf power (Ar gas flows: coolant, 9.8 L min^{-1}; plasma, 0 L min^{-1}; nebulizer, 0.68 L min^{-1}). Significantly, these power levels do not represent the lowest possible but are only those at which the present mini-ICP system can easily operate; with improved torch and load coil configurations, still lower operating levels should be obtainable.

In the present study, the mini-ICP was ordinarily operated at 1 kW (33% less rf power than the conventional plasma); this value was selected on the basis of ease and stability of operation and on an approximate power density calculation. To perform this calculation, the plasmas were modeled geometrically as toroids and a constant coupling efficiency was assumed (coupling efficiency is defined as the percentage of the rf power which is transferred from the load coil to the plasma). The skin depth was determined (*16*) to be approximately 2 mm and taken to be the same for each plasma. Assuming that all of the rf power is coupled into the skin depth region, the conventional ICP (15-mm diameter) can be modeled as a toroid with an inner radius of 5.5 mm and an outer radius of 7.5 mm. Correspondingly, the mini-ICP (10-mm diameter) can be modeled as a toroid with an inner radius of 3 mm and an outer radius of 5 mm. The resulting volume of the conventional-sized toroid is 128 mm^3; the mini-toroid has a volume of 79 mm^3. If 1.5 kW of the rf power is transferred to the conventional plasma (i.e., 100% coupling efficiency), a power density of 11.7 W mm^{-3} will be established. To obtain the same power density within the mini-plasma, 926 W of rf power must be delivered from the generator (also assuming 100% coupling efficiency). Of course, this calculation is only approximate but indicates that a 1-kW mini-ICP could have the same characteristics as the conventional ICP operated at 1.5 kW.

Plasma Initiation and Sample Introduction. The ignition and stabilization of a mini-plasma was found to be extremely simple using the operating procedure outlined earlier and under the conditions shown in Table I. Significantly, the mini-plasma could be ignited under either the "operating" or "starting" gas flows listed in Table I. Of course, ignition under the "operating" conditions would be preferable, because no flow adjustments would then be necessary between initiation and operation. However, occasionally (approximately one out of ten ignitions) plasma instability and torch damage occurred when "operating" (cf. Table I) gas flows were used during torch firing; to prolong the lifetime of the mini-torch, we ignite the plasma at the slightly higher (starting) gas flows. By comparison, plasma instability and damage to the conventional torch occurred much more frequently (approximately one out of three times) when the plasma was initiated using the lower (operating) gas flows. Consequently, the conventional plasma should *only* be ignited at the higher (starting) gas flows. In our experience, the lifetime of a mini-torch was much longer than a conventional one, primarily because of the better stability of the mini-ICP during ignition. For example, during all our analytical investigations, the same mini-torch was used while two conventional-sized torches suffered extensive damage.

The mini-plasma could also be struck while the nebulizer gas was flowing and distilled water was being aspirated, with an annular-shaped plasma being formed immediately. The entire plasma ignition and sample introduction process is thus very straightforward and could easily be automated. Importantly, only deionized-distilled water can be aspirated during plasma initiation, and instabilities result if a sample solution is aspirated at that time. In contrast, the conventional ICP could not be initiated at all when the nebulizer gas was flowing. In fact, introducing sample into the conventional plasma was not easily accomplished; it often caused plasma extinction and required an operator with considerable experience.

Plasma Stability. After the mini-plasma is struck, it can be sustained easily for long periods of time, demonstrates excellent stability, and accepts samples readily. Significantly, 50% less high-purity argon is consumed during this operation than with the conventional ICP (cf. Table I). The quantitative stability of the entire mini-plasma system is revealed by the reproducibility of the signal from a 1 ppm Fe solution, monitored at 3719.9 Å. The signal was measured from a series of 5 sample and 5 blank solutions run over a 20-min period, with a measurement time constant of 1 s. A relative standard deviation of 0.8% was calculated.

Sample Residence Time in Plasma. The velocity of sample injection into an ICP is significant, because it determines the time during which the analyte species can interact with the plasma. In turn, this interaction time should influence both the degree of matrix interferences and signal strength. Approximate injection velocities were calculated (*16*) from injection tip orifice sizes and average flow rates for the mini-ICP (orifice size = 0.75-mm i.d.; flow rate = 0.92 L min^{-1}) and the conventional ICP (orifice size = 1.0-mm i.d.; flow rate = 1.32 L min^{-1}) and were determined to be 3453 cm s^{-1} and 2806 cm s^{-1}, respectively. Although these velocities are not the lowest usable with each plasma, it is not surprising that the injection velocity for the mini-plasma appears higher. Higher injection velocities would be required to overcome the greater magnetohydrodynamic (MHD) thrust velocity expected in the mini-plasma (*8, 24*). Higher injection velocities for smaller diameter torches were also predicted by Barnes (*15*); however, the observed magnitude appears to be much smaller than those predicted by Barnes' computer model.

Neglecting MHD effects and assuming that the velocities of the particles remain constant and equal to the injection velocities, particle residue times will be approximately 1.5 ms for the conventional ICP and 0.8 ms for the mini for observation heights of 30 and 20 mm, respectively. Even though the residence times appear to be shorter in the mini-ICP, the results presented in the following sections indicate that the analyte residence times are adequate for the analyte species to be efficiently desolvated, vaporized, atomized, and excited.

Background Spectra. High-resolution recordings of the background radiation emitted by both the mini and the conventional ICP sources revealed highly structured spectra, containing many prominent features of both line and broad band character. The structure and intensities of the background spectra of the two sources were identical; however, their complex nature suggests that spectral interferences might be a problem for both sources. Studies directed at examining the mini-plasma's background in detail are currently underway in our laboratories.

Detection Limits. A useful indication of the analytical utility of the mini-ICP can be obtained by comparing its limits of detection with those of a conventional ICP source. However, because detection limits are affected by *every* component in an AES system, comparisons between different systems are somewhat ambiguous. Consequently, detection limits were determined in this study for both a mini and a conventional ICP source on the *same* AES spectrometer (described in the Experimental section), and under essentially the same operating conditions (cf. Table I).

Detection limits for ten elements are listed in Table III. Because an uncertainty factor of 2 or 3 is inherent in detection limit determinations, the data in Table III indicate that the sensitivity available with a mini-ICP is comparable to that

Table III. Comparison of Detection Limits,[a] ng mL^{-1}

element	spectral line[b]	conventional ICP	mini-ICP	literature
Al	3961.5	5	3	2 (*5*)
Ca(II)	3933.7	0.04	0.07	0.07 (*31*)
Cd	2288.0	13	42	30 (*5*)
Cu	3247.5	2	8	1 (*31*)
Fe	3719.9	12	10	5 (*5*)
Mg	2852.1	2	6	0.7 (*31*)
Na	5889.9	0.2	0.7	0.2 (*31*)
Ni	3524.5	15	4	6 (*5*)
Pb	4057.8	40	33	8 (*5*)
Zn	2138.6	23	71	10 (*16*)

[a] Detection limits were defined as that concentration of analyte which produced a signal equal to 2.122 times the standard deviation of the blank signal. This factor was derived on the basis of five sample–background pair measurements and 99% confidence limits (*22*). See Table II for operating conditions. [b] Used in present study.

of a conventional ICP. Significantly, the same detection limits were obtained for both torches over a 4-month period, during which reproducibility checks were performed. Literature values are also listed in Table III and are comparable in most cases to those from the ICP–AES system described in this report.

Conditions for Simultaneous Multielement Analysis. An important feature of ICP sources is their applicability to simultaneous multielement analysis, a capability which is rendered more significant by the fact that a single set of operating conditions can be employed for a large number of elements (*25*). The results shown in Table III indicate that both the mini and conventional ICP sources can be used to determine a variety of elements with low limits of detection. However, these detection limits were not obtained under identical operating conditions; the observation height and nebulizer gas flows were optimized for each element.

The range of optimal conditions for different elements in ICP sources can be conveniently portrayed using diagrams like those of Boumans (*25*). Figures 3A and 3B are diagrams of this nature which illustrate the range of optimal conditions found for both the conventional and the mini-ICP sources, respectively. These figures show that the choice of compromise conditions for the mini-ICP would be no more difficult than for the conventional ICP.

In fact, compromise conditions may be easier to establish using the mini-ICP source. Figures 3A and 3B demonstrate that the range of optimal observation heights and nebulizer gas flows for different elements is smaller for the mini-ICP. As a result, compromise conditions can be selected which are closer to optimal for a larger number of elements in the mini-ICP than in the conventional ICP.

Excitation Temperatures. Excitation temperatures of both mini and conventional ICP sources were determined using the Atomic Boltzmann Plot method (*26*, *27*), with neutral iron being used as the thermometric species (*2*). The wavelengths, excitation energies, statistical weights of the upper levels, and relative transition probabilities of the appropriate lines are summarized in Table II.

From these measurements, an excitation temperature of 5100 K is assigned to the conventional ICP at an observation height of 30 mm and a 4300 K temperature to the mini-ICP at an observation height of 20 mm. These observation regions are located in the cooler tail flames of the plasmas and represent the excitation temperatures experienced by analyte species during their observation. Although these observation heights differ by a factor of 1/3, so do the sizes of the two plasmas. Therefore, these temperatures should characterize the same relative regions in each source.

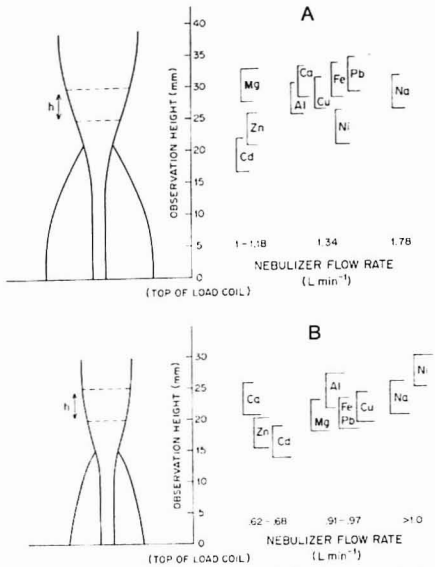


Figure 3. Operating conditions for greatest signal-to-noise ratio for several elements (After Boumans and DeBoer (*25*)). (A) Conventional ICP. (B) Mini-ICP. h = Height of observation zone (5 mm). Over the entire range of conditions, measured detection limits for most elements changed by no more than a factor of 5, an amount considered insignificant in a practical analysis

Because an uncertainty of ±10% or more can be assigned to each plasma temperature measurement (*2*), the two plasmas cannot be assumed to possess dissimilar excitation temperatures. The temperatures determined in this study agree with values determined by other workers (*1*, *2*). However, it would not be surprising for the mini-ICP to be slightly cooler than the conventional ICP, in view of the different aerosol injection velocities of the two sources. This temperature similarity coupled with the similarity of the optimal observation regions for the mini and conventional plasmas (cf. Figures 3A and 3B) argues that the atomization and excitation behavior of the plasmas should not differ significantly.

Analytical Calibration Curves. Another important characteristic of conventional ICP sources is their ability to produce analytical calibration curves covering 4 to 5 orders of magnitude (*12*). Figure 4 shows analytical calibration curves for CuI (3247 Å), FeI (3719 Å), NaI (5889 Å), BaI (5536 Å), and BaII (4554 Å) which demonstrate the wide linear dynamic range available with the mini-ICP source. The plots are linear over concentration ranges covering 4 to 5 orders of magnitude and have slopes of approximately unity. In Figure 4, curves are drawn between concentrations approximately one order of magnitude above the detection limit to concentrations of 10000 μg/mL (1% wt) and above in some cases, demonstrating that the mini-ICP can accept high salt content solutions for analysis.

CONCLUSIONS

Through proper torch design and operation, a stable miniature inductively coupled plasma can be formed which readily accepts sample and exhibits many of the same analytical characteristics associated with conventional ICP sources. At present, it appears that the mini-ICP will be just as powerful a source for atomic emission spectrometry as

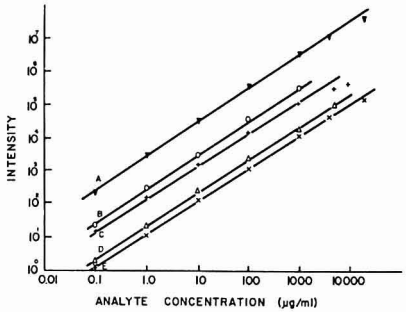


Figure 4. Analytical calibration curves obtained with the mini-ICP. (A) Ba(II) (4554 Å), (B) Cu(I) (3247 Å), (C) Na(I) (5889 Å), (D) Fe(I) (3719 Å), (E) Ba(I) (5536 Å)

conventional ICP sources while offering improved operating characteristics and reduced cost. Clearly, additional investigations into the analytical utility of this new source are warranted.

Experiments to examine the complete thermal nature of the mini-ICP are presently underway in our laboratories. The results of these investigations will provide insight into the physical nature of the source and the mechanisms controlling analyte atomization and excitation. Interference effects in conventional ICP sources have been shown to be minimal but when present they are complex and are directly related to the conditions under which they are generated (*28–30*). Future work will include a careful examination of the spectral, vaporization, and ionization interferences associated with the mini-ICP source. This area is particularly interesting because of the reduced residence times of the analyte species expected in the mini-ICP. In addition, progress is currently being made toward developing an improved miniature ICP source which will operate at even lower rf powers and reduced argon support gas flows.

ACKNOWLEDGMENT

The authors are indebted to R. L. Cochran and J. M. Ramsey for their suggestions and constructive criticism in the course of this project. We also acknowledge with pleasure the assistance of E. Sexton in the design and construction of the miniature torch.

LITERATURE CITED

(1) D. J. Kalnicky, V. A. Fassel, and R. N. Kniseley, *Appl. Spectrosc.*, **31**, 137 (1977).
(2) D. J. Kalnicky, R. N. Kniseley, and V. A. Fassel, *Spectrochim. Acta, Part B*, **30**, 511 (1975).
(3) K. Visser, F. M. Hamm, and P. B. Zeeman, *Appl. Spectrosc.*, **30**, 34 (1976).
(4) G. R. Kornblum and L. de Galan, *Spectrochim. Acta, Part B*, **32**, 71 (1977).
(5) G. W. Dickinson and V. A. Fassel, *Anal. Chem.*, **41**, 1021 (1969).
(6) S. Greenfield, I. L. Jones, H. McD. McGeachin, and P. B. Smith, *Anal. Chim. Acta*, **74**, 225 (1975).
(7) P. W. J. M. Boumans and F. J. de Boer, *Spectrochim. Acta, Part B*, **30**, 309 (1975).
(8) R. C. Miller and R. J. Ayen, *J. Appl. Phys.*, **40**, 5260 (1969).
(9) R. N. Savage and G. M. Hieftje, to be submitted for publication, *Appl. Spectrosc.*
(10) T. B. Reed, *J. Appl. Phys.*, **32**, 2534 (1961).
(11) S. Greenfield, I. L. Jones, and C. T. Berry, *Analyst (London)*, **89**, 713 (1964).
(12) S. Greenfield, H. McD. McGeachin, and P. B. Smith, *Talanta*, **23**, 1 (1976).
(13) V. A. Fassel and R. N. Kniseley, *Anal. Chem.*, **46**, 1155A (1974).
(14) P. W. J. M. Boumans, F. J. de Boer, and J. W. de Ruiter, *Philips Tech. Rev.*, **33**, 50 (1973).
(15) C. D. Allemand and R. M. Barnes, *Appl. Spectrosc.*, **31**, 434 (1977).
(16) R. H. Scott, V. A. Fassel, R. N. Kniseley, and D. E. Nixon, *Anal. Chem.*, **46**, 75 (1974).
(17) R. H. Scott and M. L. Kokot, *Anal. Chim. Acta*, **75**, 257 (1975).
(18) J. L. Genna and R. M. Barnes, *Anal. Chem.*, **49**, 1450 (1977).
(19) A. G. Gaydon and H. G. Wolfhard, "Flames", Chapman and Hall, Ltd., London, 1970.
(20) S. A. Goldstein and J. P. Walters, *Spectrochim. Acta, Part B*, **31**, 201 (1976).
(21) S. A. Goldstein and J. P. Walters, *Spectrochim. Acta, Part B*, **31**, 295 (1976).
(22) J. D. Winefordner, P. A. St. John, and W. J. McCarthy, *Anal. Chem.*, **39**, 1495 (1967).
(23) J. A. Dean and T. C. Rains, "Standard Solutions for Flame Spectrometry", Chap. 13 in "Flame Emission and Atomic Absorption Spectrometry", Vol. 2, J. A. Dean and T. C. Rains, Ed., Marcel Dekker, New York, 1971, p 332.
(24) J. D. Chase, *J. Appl. Phys.*, **42**, 4870 (1971).
(25) P. W. J. M. Boumans and F. J. de Boer, *Spectrochim. Acta, Part B*, **27**, 391 (1972).
(26) R. H. Tourin, "Spectroscopic Gas Temperature Measurements", Elsevier, New York, 1962, pp 47–48.
(27) P. E. Walters, T. L. Chester, and J. D. Winefordner, *Appl. Spectrosc.*, **31**, 1 (1977).
(28) T. E. Edmonds and G. Horlick, *Appl. Spectrosc.*, **31**, 536 (1977).
(29) G. R. Kornblum and L. de Galan, *Spectrochim. Acta, Part B*, **32**, 455 (1977).
(30) G. F. Larson, V. A. Fassel, R. H. Scott, and R. N. Kniseley, *Anal. Chem.*, **47**, 238 (1975).
(31) V. A. Fassel and R. N. Kniseley, *Anal. Chem.*, **46**, 1110A (1974).
(32) I. Reif, "Spectroscopic Temperature Measurements of Flames and Their Physical Significance", Ph.D. Thesis, Iowa State University, Ames, Iowa, 1971.

RECEIVED for review June 14, 1978. Accepted December 6, 1978. Supported in part by the National Science Foundation through grant CHE 76-10896 and by the Office of Naval Research.

Determination of Organic (Methyl) Mercury in Fish by Graphite Furnace Atomic Absorption Spectrophotometry

Gerald T. C. Shum,* Harry C. Freeman, and John F. Uthe

Department of Fisheries & the Environment, Fisheries and Marine Service, Technology Branch, 1707 Lower Water Street, P.O. Box 550, Halifax, Nova Scotia B3J 2S7

A method to determine organic (methyl) mercury in fish using graphite furnace atomic absorption spectrophotometry is described. Following initial acetone extraction, methylmercury is released from samples by acid cupric bromide, and extracted into toluene. Addition of dithizone to the extract allows the determination of mercury in the furnace. The average recovery of added methylmercuric chloride at 2.00- and 4.00-μg levels is 97.7 ± 5.5%. Detection limit is 0.08 μg Hg/g sample. Determination of methylmercury in aqueous sodium thiosulfate after partitioning from toluene, permits an autosampler to be used. Results of the analyses of several fish samples by this technique are compared to those of gas–liquid chromatography and Magos' selective atomic absorption method.

The determination of low concentrations of total mercury in biological and environmental samples has become routine with the development of the cold vapor atomic absorption spectrophotometric method (*1*). However, it has been shown that the major form of mercury accumulated in most fish and shellfish edible tissue is methylmercury (*2*) and not the less toxic inorganic form (*3*). Therefore the need to distinguish the chemical form of mercury in samples is obvious.

Several gas–liquid chromatography based methods for the determination of methylmercury in fish have been published (*4–7*), but these are tedious and still subject to review (*8*). A selective atomic absorption method to determine inorganic and methylmercury in biological materials was described by Magos (*9*), and was modified by Kacprzak and Chvojka (*10*). Matsunaga and Takashashi determined organic mercury by the cold vapor method using solvent extraction and back extraction into a reagent suitable for reduction (*11*).

The rapid development of heated furnace atomization for atomic absorption offered new opportunities in trace metal analysis. Inorganic mercury was first determined by this technique by Ediger (*12*), who used ammonium sulfide as a stabilizing agent. Alder and Hickman (*13*) demonstrated the stabilizing effect of hydrochloric acid and hydrogen peroxide on mercury determination in the graphite furnace. The work of these earlier researchers on standard solutions demonstrated the potential of the graphite furnace for use in developing a method for determining trace quantities of mercury in fish. The graphite furnace, unlike the cold vapor technique which could be applied to mercury only, could be used to determine other trace elements.

The purpose of this study was to develop a simple and reliable method that can be used to determine methylmercury in fish tissue by laboratories with atomic absorption capability. In this method, a modified toluene extraction adapted from the method of Uthe et al. (*5*) was used, and the methylmercury content in the toluene was directly determined in the graphite furnace, using dithizone as a stabilizing agent. An aqueous system was adapted by extracting the methylmercury from the toluene with sodium thiosulfate and determining its concentration in the graphite furnace.

EXPERIMENTAL

Apparatus. A Perkin-Elmer Model 403 atomic absorption spectrophotometer equipped with background corrector and a Perkin-Elmer Model HGA 2100 heated graphite furnace were used for all methylmercury determinations. The furnace control settings were: drying at 100 °C for 40 s, charring at 180 °C for 40 s, and atomizing at 950 °C for 30 s with the purging argon gas interrupted. Total mercury was determined by the semiautomated method of Armstrong and Uthe (*14*), using a Perkin-Elmer Model 306 atomic absorption spectrophotometer, Technicon autosampler, and proportioning pump.

Reagents. All chemicals used were ACS reagent grade and solvents were "distilled-in-glass" grade.

Methylmercuric chloride (95+%) from Ventron Alpha Products was used to prepare 100 μg/mL (as Hg) stock solution in toluene. A second stock of 10.0 μg/mL was prepared weekly by dilution. Both solutions were stored in a refrigerator. Working standard solutions (0.05 to 0.80 μg/mL) were prepared for each run by diluting with freshly prepared 0.10% dithizone in toluene.

Extraction solutions were: 0.10 M $CuSO_4 \cdot 5H_2O$ (aqueous and in 4 N H_2SO_4) and 3.0 M KBr (in 4 N H_2SO_4).

Procedure. The fish samples were homogenized by a Waring blender or a Brinkmann Polytron unit. Two grams (wet weight) of samples were weighed into 40-mL pyrex conical centrifuge tubes fitted with Poly-Seal screw caps (A. H. Thomas). The homogenized sample was shaken vigorously by hand with two 25-mL aliquots of acetone. Each time the mixture was centrifuged for 5 min at 1500 rpm, and the acetone was removed by aspiration. Tilting the tube during the second aspiration facilitated the removal of the acetone. Five mL of acid bromide and 10 mL of $CuSO_4$ (4 N H_2SO_4) solution were added to the residue and the mixture was shaken gently by hand. Ten mL of toluene was added next, the tube was shaken vigorously by hand for 1 min, and then centrifuged for 10 min at 1500 rpm. The solution was prepared for analysis in the furnace by pipetting 0.5 mL of the toluene extract and 0.5 mL of 0.10% dithizone into a glass stoppered tube and mixing on a Vortex mixer. Standards were prepared in the same manner, using 0.05–0.40 ppm methylmercury in the dithizone–toluene solution. Twenty to forty μL of the solution was injected into the furnace for each determination. The peak heights were measured and were used to calculate the mercury concentration by the method of standard addition.

When freeze-dried and powdered fish samples were analyzed, an aqueous rather than acidic $CuSO_4$ solution was used.

RESULTS AND DISCUSSION

Stabilization of Methylmercury in the Furnace. Methylmercury was stabilized in the furnace by the addition of dithizone in toluene added to an equal volume of sample extract. It was noted that the atomic absorption of methylmercury in a swordfish extract reaches a maximum and plateau at 0.08% dithizone added (Figure 1). The optimum charring temperature to give the maximum absorption at atomization was fairly narrow and ranged from 175–200 °C (Figure 2), but the signals were reproducible. This low charring temperature caused some buildup of residue in the graphite tube, but this was reduced by prewashing the fatty samples with acetone and by atomizing the samples for 30 s. The graphite tube was given a high temperature burn two or three times a day to ensure no significant residue buildup, and it could be used for 400–500 injections. The standard curve

0003-2700/79/0351-0414$01.00/0 © 1979 American Chemical Society

Table I. Determination of Methylmercury (MeHg) in Fish and Shellfish (in μg Hg/g) by the Heated Graphite Furnace (Authors' Lab), with Comparative Analyses Data

	authors' lab			external lab 1		external lab 2	
sample	MeHg in toluene ext.	MeHg in $Na_2S_2O_3$ ext.	total Hg	MeHg by GLC	total Hg	inorganic Hg by Magos'	total Hg
freeze-dried							
oyster	N.D.[a]	0.06, 0.06	0.18 ± 0.02[b]	0.02	0.25	-	-
halibut	5.37, 5.68	5.49, 5.55	5.79 ± 0.07	4.55	4.77	0.200	5.85
canned tuna	0.76 ± 0.05 (6)	0.78, 0.74	0.92 ± 0.03	0.60	0.80	0.034	0.95
scallop muscle	N.D.	0.06, 0.06	0.06 ± 0.02	0.05	0.11	-	-
lobster tomalley	N.D.	0.05, 0.06	0.74 ± 0.02	0.09	0.64	-	-
swordfish muscle 1	0.43 ± 0.06	0.40, 0.42	0.41 ± 0.02	-	-	0.022	0.42
swordfish muscle 2	2.37 ± 0.06	2.52, 2.48	2.54 ± 0.07	-	-	0.109	2.45
swordfish muscle 3	3.00 ± 0.10	-	3.34 ± 0.06	2.75	3.03	0.143	3.31
canned tuna 1	0.40, 0.40	0.41, 0.42	0.50 ± 0.01				
canned tuna 2	1.90, 1.95	-	2.23 ± 0.19				
frozen							
swordfish liver 1	0.41, 0.42		1.05, 1.00				
swordfish liver 2	8.67, 8.25	9.14, 8.39	19.1 ± 0.72				
swordfish liver 3	1.50, 1.62	1.38, 1.81	2.27 ± 0.12				
swordfish muscle 1	1.96 ± 0.15 (4)	-	2.02, 1.99				
swordfish muscle 2	3.98, 4.22	-	4.40, 4.41				
swordfish muscle 3	1.60, 1.50	-	1.71, 1.70				
swordfish muscle 4	0.87, 0.87	-	0.92 ± 0.12				

[a] Not detectable. [b] Figures are the mean and standard deviation of triplicate analyses except otherwise indicated.

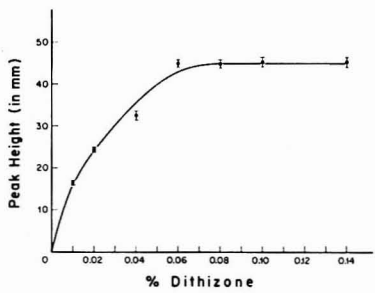


Figure 1. Atomic absorption of swordfish muscle toluene extract with the addition of dithizone. Equal volume of extract and dithizone in the indicated concentration were mixed and 20 μL of solution was used for determination in the heated graphite furnace. Each point is presented as the mean and standard deviation of 3 to 5 injections (100 mm is equivalent to 0.2 absorbance unit)

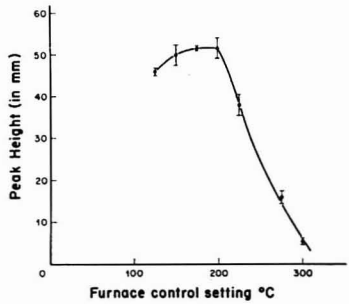


Figure 2. Optimization of charring temperature for swordfish muscle toluene extract. 0.10% dithizone solution was added to an equal volume of extract. Two to three injections of 20 μL solution. Furnace controls were: drying at 100 °C for 40 s, and atomizing at 950 °C for 30 s

was linear from 1 to 6 ng of mercury, but the samples showed a slight suppression of absorption signal (Figure 3). Much lower sensitivity was obtained with pyrolytically coated graphite tubes (Perkin-Elmer), in contrast to the enhancement effect found for the difficult-to-volatilize elements (*15*).

Extraction of Methylmercury. The extraction procedure is an adaptation of the method of Uthe et al. (*5*), combined with an acetone prewashing technique of Watts et al. (*7*). Prewashing with acetone was necessary with oyster and fatty samples such as liver tissue and tuna canned in oil. Nonfatty muscle tissue did not require this pretreatment but, to be consistent and to standardize the method, the prewashing was carried out on all samples. When the extraction was carried out in a glass centrifuge tube under the present conditions, the acid concentration of the aqueous mixture had to be increased to 4.0 N for a more complete extraction, except in the case of freeze-dried and powdered samples, where the original 1.3 N was used to avoid formation of a gel at the interface.

Analysis of Fish Samples. A number of fish samples were analyzed for methylmercury using this procedure. Total mercury content of these samples were also determined for

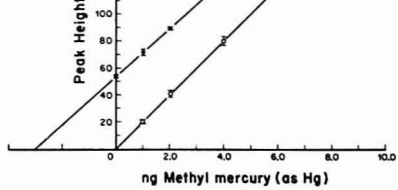


Figure 3. Standard (–O–) and sample (–●–) calibration curves of toluene extract stabilized with dithizone. The sample was tuna canned in oil. 10 μL of standards and 20 μL of spiked samples were used

comparison (Table I, Authors' Lab.). Recovery was determined by adding 2.00–4.00 μg methylmercury to samples after prewashing with acetone, and comparing results with unspiked samples. The average recovery for nine different samples in

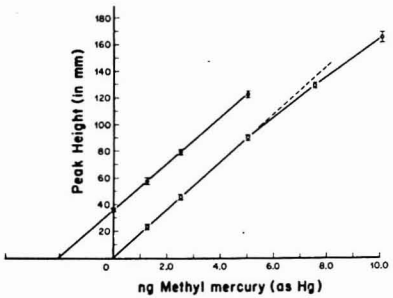


Figure 4. Standard (-O-) and sample (-●-) calibration curves of 0.005 M $Na_2S_2O_3$ extract. The sample was tuna canned in oil. 10 μL of standards was determined, while the sample was determined by overlaying 10 μL of standard solution onto 10 μL of sample in the furnace. Furnace controls were: drying at 100 °C for 40 s, charring at 150 °C for 30 s, and atomizing at 1200 °C for 30 s with purge gas interrupted

duplicate was 97.7 ± 5.5%. The detection limit was 0.08 μg/g sample, using 20 μL of sample plus 20 μL spiking standard. The calculation was based on an absorbance signal of 3-mm peak height and an average slope of several sample calibration curves. An average of 92.2% of the mercury in muscle samples was methylmercury. This showed that prewashing the samples with acetone did not remove appreciable amounts of tightly bound organic mercury, confirming the results of Watts and co-workers (*7*). The swordfish liver samples, however, contained a much lower percentage of methylmercury than muscle. This was not surprising because the liver had been suggested as one of the sites for demethylation of methylmercury (*16*, *17*).

Adaptation to Aqueous System. In order to allow laboratories to utilize autosamplers (e.g., Perkin-Elmer AS-1) which cannot handle organic solvents, the methylmercury in the toluene extract was partitioned into aqueous sodium thiosulfate, and then determined by the graphite furnace. It was found that a simple one-step partitioning gave excellent recovery. Two to six mL of the toluene extract was pipetted into a 15-mL glass stoppered conical centrifuge tube, and then 2.0 mL of 0.005 M aqueous $Na_2S_2O_3$ (freshly diluted from 0.05 M stock) was added. The mixture was shaken 40 times by hand, and centrifuged to separate the layers. The toluene layer on top was aspirated off and the mercury concentration in the aqueous solution was determined by the method of standard additions (Figure 4). The standards for spiking were prepared in toluene and extracted with the thiosulfate solution.

The standards were linear to about 5.5 ng at the optimal sample atomization temperature (Figure 4). However, the sample calibration curves were linear to a wider range, for example, canned tuna as shown in the same figure. The extraction of methylmercury from toluene into thiosulfate was complete in most cases (Table I). The average recovery of 14 extractions of 5 different types of samples was 102 ± 5.1%. Sample extracts that were low in methylmercury, for example, oyster and lobster tomalley (Table I) were concentrated two to three times by the partitioning, thus increasing the sensitivity of the method.

Check Sample Study. Six of the freeze-dried samples were sent to an external laboratory for methylmercury determination by the gas–liquid chromatographic method of Uthe et al. (*5*), and also for total mercury determination. Except for the halibut sample, the results (Table I, External Lab 1) were in good agreement. The low percentage of methylmercury in oyster and lobster tomalley found by us was verified. The halibut results indicated a difference in the quantitation of mercury but confirmed that most of the mercury in this fish was methylmercury.

The same halibut, tuna, and three freeze-dried swordfish samples were analyzed in a third laboratory using a modified Magos' (*9*) selective reduction atomic absorption method. Total and inorganic mercury in the fish were determined and organic mercury was calculated by difference (Table I, External Lab 2). The mercury results obtained by this laboratory were almost identical to ours, and thus substantiated our finding, that these samples had very little inorganic mercury.

CONCLUSIONS

The furnace atomic absorption method for the analysis of methylmercury in fish presented here, does not distinguish the different forms of organic mercury, but is based on the findings that with rare exception (*18*), the organic form of mercury found in fish has been methylmercury (*2*). When in doubt, the species of organic mercury can be identified by a thin-layer chromatographic technique similar to the one described by Westöö (*4*) or Tatton and Wagstaff (*19*). The present method enables laboratories engaged in trace metal analyses to carry out methylmercury determinations in fish without having to install separate gas–liquid chromatographic equipment which is costly to operate and maintain (*20*). In addition, use of an autosampler allows methylmercury determination at a much faster rate than gas–liquid chromatographic methodology.

ACKNOWLEDGMENT

The authors express their gratitude to A. Lutz of the Freshwater Institute, Fisheries and Oceans Canada, and A. S. Hall of the National Marine Fisheries, U.S. Department of Commerce for their cooperation in the comparative studies.

LITERATURE CITED

(1) W. R. Hatch and W. L. Ott, *Anal. Chem.*, **40**, 2085 (1968).
(2) G. Westöö, "Chemical Fallout", M. W. Miller and G. G. Berg, Eds., Charles C Thomas, Springfield, Ill., 1969, p 75.
(3) P. L. Bidstrup, "Toxicity of Mercury and Its Compounds", Elsevier, New York, 1964.
(4) G. Westöö, *Acta Chem. Scand.*, **20**, 2131 (1966).
(5) J. F. Uthe, J. Solomon, and B. Grift, *J. Assoc. Offic. Anal. Chem.*, **55**, 583 (1972).
(6) M. L. Schafer, U. Rhea, J. T. Peeler, C. H. Hamilton, and J. E. Campbell, *J. Agric. Food Chem.*, **23**, 1079 (1975).
(7) J. O. Watts, K. W. Boyer, A. Cortez, and E. R. Elkins, Jr., *J. Assoc. Offic. Anal. Chem.*, **59**, 1226 (1976).
(8) A. J. Malanoski, K. Helrich, S. Williams, B. J. Prima, and S. W. Butler, *J. Assoc. Offic. Anal. Chem.*, **61**, 397 (1978).
(9) L. Magos, *Analyst (London)*, **96**, 847 (1971).
(10) J. L. Kacprzak and R. Chvojka, *J. Assoc. Offic. Anal. Chem.*, **59**, 153 (1976).
(11) K. Matsunaga and S. Takahaski, *Anal. Chim. Acta*, **87**, 487 (1976).
(12) R. D. Ediger, *At. Absorpt. Newsl.*, **14**, 127 (1975).
(13) J. F. Alder and D. A. Hickman, *Anal. Chem.*, **49**, 336 (1977).
(14) F. A. J. Armstrong and J. F. Uthe, *At. Absorpt. Newsl.*, **10**, 101 (1971).
(15) R. E. Sturgeon and C. L. Chakrabarti, *Anal. Chem.*, **49**, 90 (1977).
(16) W. D. Burrows and P. A. Krenkel, *Environ. Sci. Technol.*, **7**, 1127 (1973).
(17) K. R. Olson, K. S. Squibb, and R. J. Consins, *J. Fish. Res. Board Can.*, **35**, 381 (1978).
(18) S. Yamanaka and K. Ueda, *Bull. Environ. Contam. Toxicol.*, **14**, 409 (1975).
(19) J. O'G. Tatton and P. J. Wagstaffe, *J. Chromatogr.*, **44**, 284 (1969).
(20) J. F. Uthe and F. A. J. Armstrong, *Toxicol. Environ. Chem. Rev.*, **2**, 45 (1974).

RECEIVED for review September 5, 1978. Accepted November 29, 1978.

Fiber Optic Waveguides for Time-of-Flight Optical Spectrometry

W. B. Whitten* and H. H. Ross

Analytical Chemistry Division, Oak Ridge National Laboratory, Oak Ridge, Tennessee 37830

Transit time and pulse broadening within an 1100-m optical fiber have been studied with single photon time-correlation techniques at a number of wavelengths. The results confirm that a fiber optic waveguide can be used as the dispersing element in a time-of-flight optical spectrometer.

In conventional optical spectrometry, information about the intensity of polychromatic light as a function of wavelength is obtained parametrically via a spatial coordinate. This coordinate might be the distance light is deflected by a prism or grating, or the displacement of an interferometer reflector, for example. A spectrum covering a range of wavelengths is measured by translating the light beam or detector, or with a position-sensitive detector such as a photographic plate, sensor array, etc. Recently, Orofino and Unterleitner (*1*) proposed that the variation of photon velocity with wavelength in a fiber optic waveguide could be used to provide spectroscopic dispersion in the time domain. With time instead of distance as the spectral parameter, spectra could be measured with a single detector in a rigid system. Experiments by Franks et al. (*2, 3*) on the time-dispersion of Cerenkov light pulses in optical fibers showed that useful spectral resolution could be obtained with commercially available fibers. The purpose of this paper is to show how single photon time-correlation techniques can be used in conjunction with a fiber optic waveguide for optical time-of-flight spectrometry.

For a well designed multimode graded index optical fiber (*4*), the transit time, τ, of a pulse of monochromatic light is chiefly determined by the photon group velocity, v_g, of the central core material

$$\tau = L/v_g \tag{1}$$

$$v_g = \frac{c}{n}\left(1 + \frac{\lambda}{n}\frac{dn}{d\lambda}\right) \tag{2}$$

where L is the length of the fiber, c and λ are the speed and wavelength of light in vacuum, and n is the wavelength-dependent index of refraction. The spectral dispersion of the fiber, commonly called material dispersion in contrast to modal dispersion, is determined by the variation of τ with wavelength

$$\frac{d\tau}{d\lambda} = -\frac{\lambda L}{c}\frac{d^2n}{d\lambda^2} \tag{3}$$

The data of Malitson (*5*) for the index of refraction of fused silica can be used to estimate the spectral resolution that can be obtained for a fiber of given length. From Malitsons's equation for n vs. λ, the group dispersion from Equation 3 was found to range from 6.6×10^{-11} s nm^{-1} km^{-1} at 900 nm to 1.1×10^{-9} s nm^{-1} km^{-1} at 400 nm. The transit time for 400-nm photons in 1 km of fused silica was calculated to be 163 ns longer than that of 900-nm photons.

Practical limits on the length of a fiber for spectrometric measurements are set by the attenuation. While fiber attenuation is continually being reduced by improvements in purity and fabrication techniques, high values of attenuation in the blue region of the spectrum make fibers of much over 1 km in length impractical for spectral measurements in this wavelength region. Consequently, time resolution of better than 1 ns is required for adequate (~1 nm) wavelength separation over most of the visible spectral region.

Single photon time-correlation techniques provide a convenient way to achieve the desired time resolution as long as the samples to be studied are stable under multiple flashes of weak light. The exciting light is attenuated so that, after traversing the fiber, sample, etc., at most a single photon is detected per flash. The time delay between the flash and the detection of the photon is measured and stored digitally. The transmission spectrum in the time domain is then merely the histogram of photons counted vs. their transit time. Some advantages of the method are that the exciting flash can be of low intensity and the timing signals are converted as early as possible into digital logic levels for high timing precision. The principal disadvantage is that a large number of flashes is required to accurately define a complete spectrum, since the standard deviation of a given channel count will be equal to the square root of the number of counts in the channel.

EXPERIMENTAL

The optical fiber studied in the present investigation was a Corning Glass Works Model 5050 fiber with a nominal attenuation at 820 nm of 5 dB km^{-1} and a bandwidth of 500 mHz at 900 nm. The 1119-m fiber was wound from the shipping spool in a single layer on a Lucite drum 30 cm in diameter. The drum had a movable plate in the circumference so that the winding tension could be relieved. For mechanical protection, the drum and fiber were placed inside an aluminum box with the fiber ends brought out through opaque Teflon sleeving. The fiber ends and sleeving were secured to 0.3-cm diameter phenolic rods with heat-shrinkable plastic tubing for convenience of manipulation.

The instrumentation was assembled from commercially available components. Light pulses from an Ortec Model 9352 nanosecond light pulser were, after suitable filtering, focused by a 20X microscope objective onto one end of the fiber. A timing signal from the pulser was delayed for 5.4 μs by a digital delay generator and applied to the start input of a time to pulse height converter. Photons emerging from the fiber were detected by an RCA C31034 photomultiplier in a cooled housing (-30 °C). The photomultiplier output was converted to a timing signal by a fast discriminator and applied to the stop input of the time to pulse height converter, whose output was stored in a pulse height analyzer. In this way, the time difference between the delayed trigger and detected photon is converted into a proportional voltage and these voltage pulses are sorted into a histogram of the number of photons vs. time.

It is essential that at most a single photon is detected per flash with the present experimental setup because the first photon detected after the flash stops the time to pulse height converter. If more than one photon per flash were detected, the resulting spectrum would be biased in favor of shorter time delays. This problem can be avoided by attenuating the light with neutral density filters until the average number of photons counted during a scan of the time to pulse height converter is 0.05. At this rate, the probability of two photons arriving within the same scan is about 0.001 (2% error).

The time calibration of the time to pulse height converter–pulse height analyzer combination was performed with the crystal-controlled digital time delay generator and checked by inserting an additional cable of known length between the discriminator and the stop input of the time to pulse height converter. Interference filter bandwidths were determined on a Cary 14

0003-2700/79/0351-0417$01.00/0 © 1979 American Chemical Society

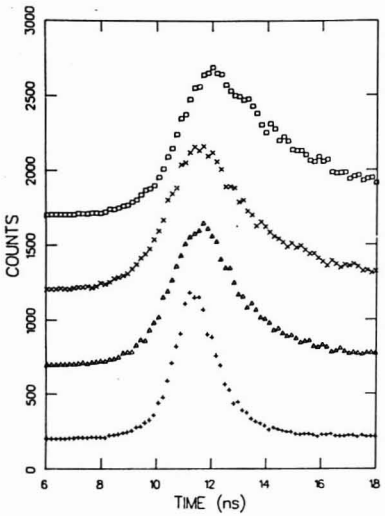


Figure 1. Time response of 1-m fiber at a number of wavelengths: 436 nm (+) 590 nm (△), 800 nm (×), 900 nm (□)

Spectrophotometer. To ensure that the photomultiplier was counting single photon events, the linearity of counting rate with light intensity was checked with neutral density filters.

A series of ten interference filters with nominal bandwidths at 50% transmission from 5 to 10 nm and with central wavelengths ranging from 900 to 436 nm were placed between the source and microscope objective lens to determine the transit time and pulse broadening of the fiber as a function of wavelength. Measurements of photon counts vs. delay time were made for both the 1119-m fiber and for a 1-m fiber so that the time response of the measuring system could be separated from the combined system/fiber response.

The absorption spectrum of a solution of $KMnO_4$ in 1 N H_2SO_4 (0.2 g L^{-1}) was measured from 450 to 700 nm. The sample was placed in a quartz cuvette with 0.5-cm path length and run alternately with a 1 N H_2SO_4 blank. A Corning CS 4-70 and two CS 1-75 filters were placed behind the sample to remove the red and near infrared light. If this weakly absorbed light were allowed to pass through to the detector, the flash intensity, and hence the counting rate, for visible region photons would have to be much lower to avoid pulse pileup. For these measurements, the flashlamp was run with O_2 instead of air to obtain somewhat higher time resolution at longer wavelengths. The absorbance was calculated as the logarithm of the ratio of blank counts to sample counts, the correction for dark counts being negligible. The wavelengths were obtained by linear interpolation between the ten transit times obtained with the interference filters. For comparison, the absorption spectrum of the same sample was measured with the Cary 14 spectrophotometer.

RESULTS AND DISCUSSION

The response of the measuring system with the 1-m fiber at various wavelengths is shown in Figure 1. There is a marked increase in the width at half maximum of the response on going to the longer wavelengths, from 1.8 ns at 436 nm to 3.7 ns at 900 nm. These results represent the combined time resolution of the flash, photomultiplier, and electronics without the long fiber optic waveguide. The contribution to the timing error of the electronics alone can be determined by measuring the response at high light intensity. Under these conditions, the stop pulse will be due to a large number of photons arriving nearly simultaneously at the photomultiplier and all coming

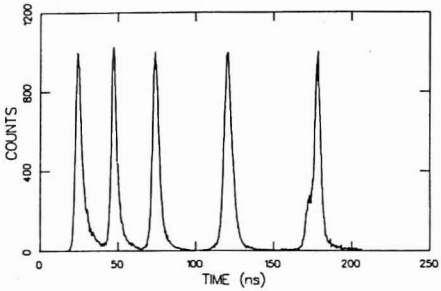


Figure 2. Combined transmission spectrum of five interference filters with central wavelengths from left to right of 900, 700, 600, 500, and 436 nm

from the initial portion of the flash. The time spread found in this way was less than 0.3 ns. The timing error of the RCA C31034 photomultiplier has been studied by Reisse et al. (6). They obtained a timing resolution of 0.6 ns with 660-nm light. The timing error of the photomultiplier would be expected to decrease with increasing wavelength because the electrons from the photocathode would have less spread in kinetic energy (7, 8). Since the various independent contributions to the timing error should add quadratically, by far the largest contribution to the width of the time response must come from the spark source.

When the 1-m fiber is replaced by the 1119-m fiber, the counting peaks for the various interference filters are displaced in time because of the dispersion of the fiber. The combined time domain spectra of five interference filters are shown in Figure 2. It can be seen that the spectral dispersion is much more pronounced in the short wavelength region. The transit times for the different wavelengths are within a few percent of those calculated for fused silica.

The transmission spectra in the time domain of the ten interference filters studied are shown in more detail in Figures 3a and 3b. The time scales are all measured relative to the transit time of peak intensity. There is a considerable variation in widths and shape among the various peaks with prominent shoulders in some cases. As discussed below, the shapes of the output peaks may not be entirely due to the fiber.

It should be possible to deconvolute the output peaks to remove the broadening due to the flash duration, photomultiplier response, and electronics (determined with the 1-m fiber), and due to the material dispersion of the fiber. Unfortunately, the spectrum of the spark source is not perfectly flat with wavelength but shows some sharp lines. If such a line has a wavelength within or near the interference filter passband, this spectral peak passing through the interference filter may be wider or narrower than the transmission spectrum of the filter itself. The shoulders on the 800-nm peak, for example, do not appear when oxygen is used instead of air in the spark source. The 436-nm peak is distorted by a spectral line close to the filter transmission maximum. This distortion does not appear at all wavelengths, however. At 700 nm, the istrumental broadening and material dispersion can be subtracted off quadratically, giving a value for modal dispersion of 1.4 ns. This value is not far from what would be expected based on the manufacturer's specification of 500 MHz km^{-1} for the bandwidth at 900 nm.

The absorption spectrum of the $KMnO_4$ sample is shown in Figure 4. It can be seen that the principal features of the spectrum are reproduced very well by the time-of-flight method, although the resolution is not as high as that for the

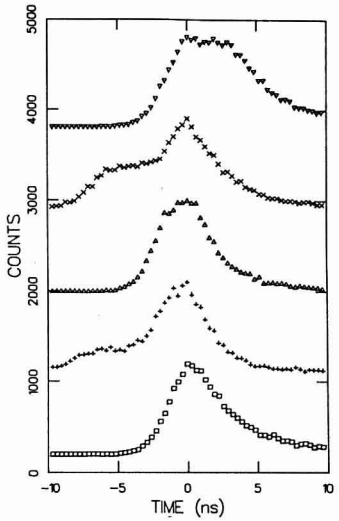


Figure 3a. Transmission spectra in time domain of interference filters: 436 nm (+), 590 nm (△), 800 nm (×), 850 nm (▽), 900 nm (□)

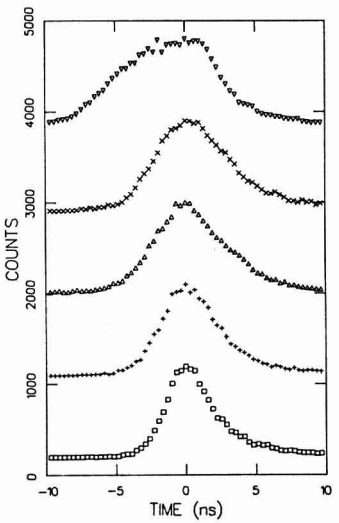


Figure 3b. Transmission spectra in time domain of interference filters: 460 nm (▽), 500 nm (△), 540 nm (×), 600 nm (+), 700 nm (□)

Cary 14. The random noise in the spectral data is much more pronounced in the blue region where the total number of counts is low. Because of the increased attenuation of the fiber in this region, the counting rate was 100 times less than at 600 nm. Thus, for Poisson counting statistics, the relative fluctuations should be 10 times larger at the shorter wavelengths. Such a variation is qualitatively borne out in Figure 4.

We have shown that in addition to providing a convenient way to study light pulse propagation in fiber waveguides, single

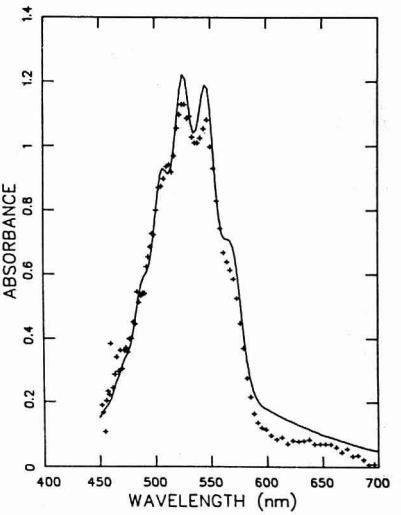


Figure 4. Absorption spectrum of $KMnO_4$ in 1 N H_2SO_4. The crosses represent time-of-flight data while the solid curve is the spectrum measured with the conventional spectrophotometer

photon time correlation techniques in conjunction with an optical fiber can be used for absorption spectrometry. The method could be used to study transient phenomena on a nanosecond time scale. For example, if the source were synchronized to an external stimulus (an actinic laser flash or orienting electric field pulse, for example), it would be possible to obtain transmission spectra as a function of time by varying the delay of the flash with respect to the stimulus. There are analytical applications as well, particularly where time resolution is important, such as monitoring flow spectra, and in situations where a rugged system with no moving parts is desired. The method seems particularly suitable for studying the spectra of fast discharges.

One obstacle which must be overcome is the high attenuation of the commercially available fibers at the shorter wavelengths. The problem may be alleviated by improving the overall time resolution of the system and reducing the fiber length. Because the attenuation of the fiber increases exponentially with length while spectral resolution is linear, the useful wavelength region could then be extended toward the near ultraviolet.

LITERATURE CITED

(1) T. A. Orofino and F. C. Unterleitner, *Appl. Opt.*, **15**, 1907 (1976).
(2) L. A. Franks, M. A. Nelson, and T. J. Davies, *Appl. Phys. Lett.*, **27**, 205 (1975).
(3) L. A. Franks, M. A. Nelson, T. J. Davies, P. Lyons, and J. Golob, *J. Appl. Phys.*, **48**, 3639 (1977).
(4) R. Olshansky and D. B. Keck, *Appl. Opt.*, **15**, 483 (1976).
(5) I. H. Malitson, *J. Opt. Soc. Am.*, **55**, 1205 (1965).
(6) R. Reisse, R. Creecy, and S. K. Poultney, *Rev. Sci. Instrum.*, **44**, 1666 (1973).
(7) R. Nathan and C. H. B. Mee, *Phys. Status Solidi A*, **2**, 67 (1970).
(8) B. Sipp, J. A. Miehe, and R. Lopez-Delgado, *Opt. Commun.*, **16**, 202 (1976).

RECEIVED for review October 11, 1978. Accepted November 30, 1978. Oak Ridge National Laboratory is operated for the U.S. Department of Energy by Union Carbide Corp. under Contract W-7405-eng-26. This article was supported by the Basic Energy Sciences.

Influence of Errors and Matching Criteria upon the Retrieval of Binary Coded Low Resolution Mass Spectra

Geert van Marlen

Department of Analytical Chemistry, Delft University of Technology, Jaffalaan 9, Delft, The Netherlands

Auke Dijkstra* and Henk A. van't Klooster

Department of Analytical Chemistry, State University of Utrecht, Croesestraat 77A, Utrecht, The Netherlands

The influence of coding errors and the matching criterion being used upon the performance of a retrieval system for binary coded spectra has been investigated. A file of 9628 mass spectra, including 773 doublets, originating from an MSDC collection, was used. The spectra were reduced to 120 binary coded m/e values, selected by using the information content as a criterion. It is concluded that the performance of the retrieval primarily depends on the extent of errors occurring in the coded spectra and is hardly affected by the matching criterion being used.

Since the introduction of computers in analytical chemistry, automated methods for data processing and retrieval have become common tools in the analytical laboratory (*1*). As many search systems have been proposed, including commercially available data bases and systems, such as MSSS (*2*) and STIRS (*3*), it has become desirable to evaluate the possibilities and limitations of such systems (*4*). For this evaluation, both empirical and statistical approaches have been published (*5–13*).

The performance of a retrieval procedure is determined by several factors of which the number of features used for the retrieval, the errors in the selected features, and the matching criterion are expected to be of major importance. In a previous paper, a feature selection procedure has been described based upon information theoretical concepts (*14*), which has resulted in a compressed binary code to be used for retrieval purposes. In this paper the influence of errors occurring in binary coded spectra and of the matching criterion on the performance of a retrieval system are reported.

MATCHING CRITERIA AND ERRORS

In formulating matching criteria, usually intensity errors resulting from the measurement, the recording, and the coding of the spectra are not incorporated. Including these errors in the matching criterion is expected to lead to an improvement of the retrieval procedure (*3*). It is, however, virtually impossible to take the correlations between the errors for the different m/e values into account. Therefore, as far as the errors are concerned, channel independency has been assumed in this study.

Binary coding of spectra implies a reduction of the spectrum to a "bitstring" of "1"s and "0"s, where a "1" denotes "peak present" and "0" "no peak present". The degree of (dis)similarity or (mis)match between unknown spectrum U and reference spectrum R can easily be obtained by using a simple Boolean truth table $\alpha(u,r)$, with u and r as binary values for one channel (peak position) in U and R, respectively. The operator between u and r usually is a logical AND [$\alpha(1,1) = 1$, $\alpha(0,0) = \alpha(0,1) = \alpha(1,0) = 0$] an EXCLUSIVE OR (XOR), [$\alpha(0,1) = \alpha(1,0) = 1$, $\alpha(1,1) = \alpha(0,0) = 0$], or a linear combination of both (*10*). Addition of the value of $\alpha(u,r)$ for every channel and introduction of a scaling generate a wide range of (dis)similarity criteria (*15*). In this study the following criteria are used.

XOR. This similarity criterion is equal to the distance or the number of "bitmismatches".

COSINE.

$$\mathrm{COS} = \frac{\mathrm{U\ AND\ R}}{\sqrt{|\mathrm{U}|\cdot|\mathrm{R}|}} \tag{1}$$

The values |U| and |R| denote the total number of peaks coded with a "1" in the spectra U, respectively R. The use of this criterion has been suggested by Gray (*15*) because of a possible improvement of the retrieval procedure.

Truth Probability. Probabilities of occurring errors have been taken into account by replacing the Boolean values with the "probabilities of truth" in the truth table α. The overall probability for an unknown spectrum matching a reference spectrum becomes:

$$P(\mathrm{U,R}) = \prod_n \alpha(u,r) \tag{2}$$

where n is the number of channels. However, it is easier to calculate

$$\log P = \sum_n \log \alpha(u,r) \tag{3}$$

with

$$\alpha(0,0) = 1 - p_{1/0}$$

$$\alpha(1,0) = p_{1/0}$$

$$\alpha(0,1) = p_{0/1}$$

$$\alpha(1,1) = 1 - p_{0/1}$$

and $p_{1/0}$ and $p_{0/1}$ being the error probabilities of finding a "0" or a "1" when the reference channel of the same compound contains a "1" or a "0" respectively. Defining p as the probability of finding a "1" in the reference file and p_d as the probability of a mismatch for one channel between two spectra of the same compound, the following equations can be derived:

$$p_d = p\cdot p_{1/0} + (1 - p)\cdot p_{0/1} \tag{4}$$

Since two spectra of the same compound are mutually interchangeable the following relationship exists:

$$p\cdot p_{1/0} = (1 - p)\cdot p_{0/1} \tag{5}$$

The combination of Equations 4 and 5 leads to:

$$p_{1/0} = p_d/2\cdot p \tag{6}$$

$$p_{0/1} = p_d/2\cdot(1 - p) \tag{7}$$

The parameters p and p_d may be estimated from a large set of doublets. When the measurement, the recording, and the coding of the spectra is highly reproducible ($p_d = 0$), the

0003-2700/79/0351-0420$01.00/0 © 1979 American Chemical Society

Table I. Mismatch Probabilities for 120 Selected *m/e* Values

m/e	prob.	*m/e*	prob.	*m/e*	prob.	*m/e*	prob.	*m/e*	prob.	*m/e*	prob.
14	0.18	42	0.10	63	0.10	83	0.06	104	0.04	131	0.04
15	0.25	43	0.12	64	0.08	84	0.06	105	0.06	133	0.03
16	0.06	44	0.14	65	0.10	85	0.08	106	0.04	135	0.04
18	0.18	45	0.09	66	0.09	86	0.07	107	0.05	138	0.03
19	0.05	46	0.03	67	0.08	87	0.07	109	0.06	139	0.03
25	0.07	47	0.03	68	0.06	88	0.05	111	0.05	141	0.03
26	0.24	49	0.08	69	0.06	89	0.06	112	0.04	143	0.02
27	0.20	50	0.14	70	0.05	90	0.05	113	0.05	145	0.02
28	0.25	51	0.15	71	0.07	91	0.08	114	0.03	149	0.04
29	0.17	52	0.13	72	0.04	92	0.05	115	0.06	152	0.03
30	0.13	53	0.13	73	0.07	93	0.07	117	0.05	155	0.02
31	0.09	54	0.09	74	0.08	94	0.06	118	0.04	163	0.03
32	0.14	55	0.09	75	0.08	95	0.06	119	0.06	165	0.03
33	0.03	56	0.09	76	0.07	97	0.05	120	0.05	167	0.02
36	0.08	57	0.10	77	0.08	98	0.06	121	0.05	169	0.02
37	0.15	58	0.10	78	0.10	99	0.05	123	0.04	178	0.01
38	0.20	59	0.08	79	0.09	100	0.04	125	0.05	189	0.02
39	0.11	60	0.08	80	0.07	101	0.06	126	0.04	212	0.01
40	0.17	61	0.08	81	0.06	102	0.05	127	0.03	222	0.01
41	0.09	62	0.08	82	0.06	103	0.04	128	0.04	262	0.00

probabilities $p_{1/0}$ and $p_{0/1}$ become 0 and the truth table becomes an inverted XOR truth table. Although a similar approach has been reported by Grotch (*13*), a comparison of the results is hardly possible because of the completely different method of binary coding.

EXPERIMENTAL

Data Base. The data base used contains 9628 low resolution mass spectra from the Mass Spectral Data Centre in Aldermaston. These spectra were binary coded using an intensity threshold of 1% of the base peak. Data reduction was further obtained by selecting 120 peak positions in the *m/e* range 1–300. This selection was based upon the information contents of the peak positions, taking correlations into account (*14*). The same binary coded file was converted into another by removing all 14 masses below *m/e* value 34, as these are often omitted in recording the spectra. A slightly different file was obtained by deleting those *m/e* values for which a high mismatch probability was found.

The organization of the data base enabled an easy extraction of double or multiple spectra of the same compound (spectra doublets or multiplets). A set of 773 spectra doublets was extracted from the file, from which a testset of 773 "unknown" spectra was composed by taking one spectrum from each doublet, leaving the "alternative" spectrum in the reference file.

Search System. In this study, a disk resident system running on a PDP 11/45 mini-computer has been used. Programs were written in PDP 11 FORTRAN IV PLUS, with additional assembler coded matching routines. A comparison of two spectra requires about 2 ms. The search time is linearly dependent on the number of reference spectra needed to be searched, which in turn is related to the quality of the unknown spectrum, and on the number of best matches to be produced. The search for a perfect or near perfect match is performed in less than 2 s. By allowing a higher error rate and/or a longer list of possible solutions to be generated, the search time increases to 4–10 s. In order to decrease the number of reference spectra to be compared, the system utilizes an optimized search strategy. This strategy implies that a comparison of an excessive number of spectra is avoided by setting limits to the allowed absolute and relative distances, and to the number of best matches (nearest neighbors) to be generated (*16*). (The *absolute distance* (*W*), hereafter in short called "*distance*", is defined as the number of bitmismatches between unknown and reference spectrum; the *relative distance* (*E*) is equal to *W* divided by the number of peaks ("1"s) in the unknown spectrum).

RESULTS

The average probability p_d of a mismatch for one channel has been estimated for every selected mass from the set of 773 doublets. These errors are compiled in Table I. From this table it appears that errors occur to a large extent (up to 25%) in the low mass range. This is probably due to the fact that from many reference spectra, low mass peaks are

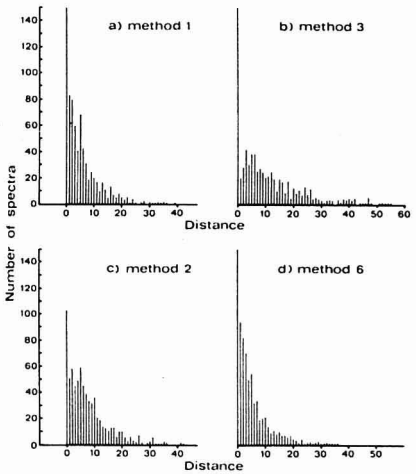


Figure 1. Distribution of distances between spectra of the same compound (773 spectra doublets)

omitted. The effects of the errors upon the degree of (dis)similarity between spectra of the same compound can be derived from the same set of doublets. The distribution of (scaled) distances has been plotted in Figure 1 for some methods, i.e., some combinations of masses and matching criteria. The characteristics of these methods are given in Table II.

The average number of bitmismatches per spectrum for 120 preselected masses is 8.9 (Figure 1c). The removal of masses with a high error probability yields an improvement; the average number of bitmismatches decreases to 6.5 for 107 selected masses (Figure 1d).

In order to evaluate the *performance* of the retrieval procedures with the binary codes and matching methods as compiled in Table II, the *percentage of the unknown spectra recovered* as a function of the *confusion* has been taken as a criterion. (In conformity with Grotch (*10*), "confusion" is defined as the number of reference spectra/compounds with a degree of similarity as good as or better than the correct answer.) The degree of similarity depends only upon the number of errors, whereas the performance of the retrieval

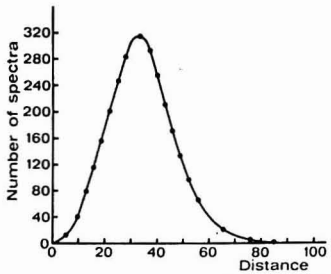


Figure 2. Distribution of distances between "unknown" and reference spectra (method 1)

Table II. Number of Masses and Matching Criteria Used

method	number of masses	matching criterion
1	106, Table I, $m/e \geq 34$	exclusive or
2	120, Table I	exclusive or
3	106, Table I, $m/e \geq 34$	cosine
4	120, Table I	cosine
5	120, Table I	truth probabilities
6	107, Table I, minus m/e 14, 15, 18, 26, 27, 28, 29, 30, 32, 37, 38, 40, 51	exclusive or

system is also affected by the distances between the unknown spectrum and all the reference spectra. The distribution of these distances, averaged for all 773 "unknown" spectra, is given in Figure 2.

An ideal performance requires the distance between the unknown and the correct reference spectrum to be smaller than the distance of the unknown to all other reference spectra. This ideal situation, however, cannot be obtained for the file under consideration as is clearly shown by comparing Figures 1 and 2. Apparently, the actual performance of the retrieval system, when applying the six methods given in Table II for some values of the confusion is far from ideal, as shown in Table III. For some spectra the effect of a large number of errors upon the confusion is given in Table IV. An extreme example is formed by 3-butylcholestane with a disagreement of 99 peaks, in which case it is not surprising to find a complete mismatch.

The number of spectra to be searched can be decreased appreciably without significant loss of performance by setting a limit to the distance (Figure 3). With the use of such a presearch parameter, the number of spectra to be searched, and consequently the search time, may decrease to about 40%. The influence of errors upon the performance can be studied by using subsets of spectra with different numbers of coding errors (average distances). The results are plotted in Figure 4 for several values of the average distance and the confusion.

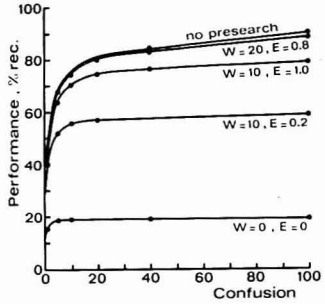


Figure 3. Percentage of "unknowns" recovered (with method 1) as a function of the confusion for some distance limits. (W = maximum absolute distance = maximum number of bitmismatches between unknown and reference spectrum; E = maximum relative distance = W divided by the number of peaks ("1"s) in the unknown spectrum)

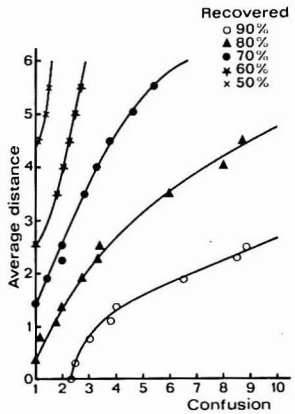


Figure 4. Percentage recovered as a function of the average distance (derived from Figure 1a) and the confusion

From this figure it appears that, for example, with an average distance of 2, 80 to 90% of the correct answers will be among the five best matches, whereas for an average distance of 6, the percentage recovered is about 65.

Figure 5 shows the performance at four values of the confusion if the distance is limited to a certain value.

DISCUSSION

Typically, a retrieval with the file of 9628 binary coded mass spectra with an average number of 6.9 bitmismatches for 106 preselected masses is expected to yield the correct identity to be among the three best matches with a probability of about 60%. This result applies to any file with these characteristics, whereby it should be observed that for larger files, the

Table III. Percentage Recovered as a Function of the Confusion

confusion	method 1	method 2	method 3	method 4	method 5	method 6
1	45	41	46	42	48	48
3	61	59	61	59	64	63
5	67	65	68	66	71	69
10	75	71	75	73	78	76
20	80	79	80	78	83	83
40	85	84	84	84	87	87
100	89	88	88	89	91	90

Table IV. Distance and Confusion for Doublet Spectra of Some Reference Compounds (Method 1)

distance	confusion	formula	name
34	1168	C10.H14.0	thymol
36	2546	C16.H32.02	palmatic acid
53	9029	Ci5.H16.04	allopeucenin
62	9326	C15.H16.04	isopeucenin
69	9450	C21.H32.02	5-β-pregnan-3,20-dione
73	4983	C29.H50.0	β-sitosterol
80	9604	C19.H36.02	methyloleate
99	9626	C31.H56	3-butylcholestane

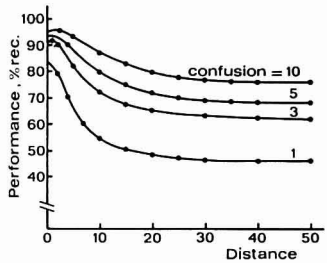


Figure 5. Percentage recovered as a function of the cumulative distance distribution (derived from Figure 1a)

performance will be worse. At first sight this unsatisfactory performance is surprising because the information content of the retrieval procedure, without taking into account the errors, was found to be about 40 bit (*14*), allowing $2^{40} \sim 10^{12}$ compounds to be distinguished by their coded spectra. However, it can be calculated (*17*) that, because of the high error probability as estimated in this study, the information content decreases to as little as 11 or 12 bit which enables a distinction of not more than 1000 or 2000 compounds. Similar results were found for the retrieval with binary coded infrared spectra (*17*).

To improve the performance of the retrieval procedure, the information content has to be raised. In principle this can be achieved by (1) applying more than two intensity levels, (2) including a more or less independent presearch criterion in the retrieval procedure, (3) using more than 106 m/e values and/or (4) reducing the error probabilities and consequently the mismatch probabilities.

The use of more intensity levels will lead to a higher information content and the influence of errors upon the information content and consequently upon the performance of the retrieval procedure is expected to be (relatively much) smaller. However, binary coded spectra are attractive because of the compactness of the code and the fast searching algorithms for such codes (*16*). Similarly, the application of an independent presearch criterion such as the m/e value of the base peak (*11*) will increase the information content and improve the performance of the retrieval at the cost of the compactness of the code.

Using more than 106 m/e values does not increase the information content, mainly because of the correlations between the features (*14*). Even in the absence of such correlations the additional features would merely add noise. A reduction of the errors has a pronounced influence upon the performance of the retrieval procedure. As shown by Figure 4, a decrease of the average error probability to a level corresponding with 1 mismatch for the 106 selected peaks will cause an increase of the probability of finding the correct answer among the three best matches from about 60% to 90%. Obviously, in order to achieve such, or a better performance, a rigorous standardization of measuring, recording, and coding the spectra is required. The performance of a retrieval system employing binary coded spectra is hardly influenced by the choice of the matching criterion. Preference should be given to the criterion that enables the fastest comparison of spectra.

ACKNOWLEDGMENT

The authors are indebted to P. Cleij and J. H. van den Hende for valuable discussions.

LITERATURE CITED

(1) R. G. Ridley, "Biochemical Applications of Mass Spectrometry", G. R. Waller, Ed., Wiley, New York, 1972, Chap. 6.
(2) R. S. Heller, G. W. A. Milne, R. J. Feldman, and S. R. Heller, *J. Chem. Inform. Comput. Sci.*, **16**, 176 (1976).
(3) K. S. Kwok, R. Venkataraghavan, and F. W. McLafferty, *J. Am. Chem. Soc.*, **95**, 4185 (1973).
(4) F. W. McLafferty, *Anal. Chem.*, **49**, 1441 (1977).
(5) R. J. Mathews and J. D. Morrison, *Aust. J. Chem.*, **27**, 2167 (1974).
(6) R. J. Mathews, *Int. J. Mass Spectrom. Ion Phys.*, **17**, 217 (1975).
(7) K. Varmuza, *Fresenius' Z. Anal. Chem.*, **282**, 129 (1976).
(8) R. J. Mathews and J. D. Morrison, *Aust. J. Chem.*, **29**, 689 (1976).
(9) G. M. Pesyna, R. Venkataraghavan, H. E. Dayringer, and F. W. McLafferty, *Anal. Chem.*, **48**, 1362 (1976).
(10) S. L. Grotch, *Anal. Chem.*, **43**, 1362 (1971).
(11) S. L. Grotch, *Anal. Chem.*, **45**, 2 (1973).
(12) S. L. Grotch, *Anal. Chem.*, **46**, 526 (1974).
(13) S. L. Grotch, *Anal. Chem.*, **47**, 1285 (1975).
(14) G. van Marlen and A. Dijkstra, *Anal. Chem.*, **48**, 595 (1976).
(15) N. A. B. Gray, *Anal. Chem.*, **48**, 1420 (1976).
(16) G. van Marlen and J. H. van den Hende, to be published.
(17) P. F. Dupuis and A. Dijkstra, *Fresenius' Z. Anal. Chem.*, **290**, 357 (1978).

RECEIVED for review July 17, 1978. Accepted November 27, 1978.

Application of Microporous Membranes to Chemiluminescence Analysis

Vance Nau and Timothy A. Nieman*

School of Chemical Sciences, University of Illinois, Urbana, Illinois 61801

A novel approach to reagent introduction into flowing streams is accomplished by using a microporous membrane to separate a reagent reservoir from an analyte stream. Reagent addition rates as low as a few μL/min are possible and can be controlled by the membrane porosity, membrane surface area, concentration of reagents in the reagent reservoir, and applied pressure gradient. The reaction zone is probably near, but not confined to the membrane surface; reagent concentrations in the reaction zone appear to be one tenth of that in the reagent reservoir. With Co(II) as the analyte, efficient rinsing of the cell is limited by adsorption at the membrane surface, but can be improved if EDTA is present in the rinse solution. Sensitivity is maximized for analyte solutions of pH 7–9. Determinations of Co(II) using luminol have a detection limit of about 10^{-10} M (10 part per trillion); typical precision is ±3%.

Solution chemiluminescence (CL) has received increased interest as a method for determination of certain species (notably, metal ions, hydrogen peroxide, and certain other inorganics and organics) at trace concentration levels. However, routine use of CL in analysis is rare, due in part to a lack of straightforward methodology and suitable instrumentation. Recent applications of CL have in large part been directed to measurements in flowing streams (*1*), either in continuous flow systems (*2–6*) or in liquid chromatography detectors (*7–10*). Such flow systems, while generally popular, require elaborate or expensive instrumentation to deliver the analyte and reagent streams, and, in general, are not very conservative of reagents.

We have investigated the application of recently available microporous plastic membranes to CL analysis. In this approach, the membrane separates a reservoir of CL reagent from an analyte flow stream. The CL reagent is delivered through the membrane at a very low flow rate (about 1–10 μL per minute). The initial attraction to use of such membranes in CL instrumentation was to evaluate several anticipated advantages: (1) small reagent volumes, (2) simplification of reagent delivery system, (3) negligible contamination of the analyte stream with the CL reagent, (4) minimization of interference from self-absorbance due to a very low concentration of CL reagent in the bulk of the analyte solution, and (5) physical localization of the emission near the surface of the membrane.

A continuous flow system using a microporous membrane was developed and characterized using the well known luminol–H_2O_2–Co(II) reaction. This initial report on microporous membranes in CL instrumentation discusses that system and the investigation and optimization of the composition of the reagent and the analyte streams (concentrations, auxiliary complexing agents, pH), the absolute and relative flow rates of reagent and analyte, and the cell geometry. Future papers will be concerned with both specific applications and fundamental investigation of the emission properties of the membrane system.

EXPERIMENTAL

Reagents and Solutions. Luminol (Pfaltz and Bauer) and all other reagents (Mallinckrodt, Analytical Reagent) were used without further purification.

Stock solutions of luminol (10^{-4}–10^{-3} M) were prepared in 4 × 10^{-3} M KOH, then adjusted to pH 9.5 and stored under refrigeration. No deterioration was noted over the lifetime of the stock solution (about one month). Excluding the final working curve and the luminol concentration study, a small amount of EDTA (10^{-6} M) was added to the luminol stock solution to reduce the background emission level.

Working solutions of Co(II) were prepared by serial dilution from a 10^{-3} M stock solution of $Co(NO_3)_2{\cdot}6H_2O$ that contained 1% nitric acid. Concentrations below 10^{-8} M were achieved by diluting known aliquots of the 10^{-8} M solution and using the resulting solution within 30 min after preparation. In general, the procedure outlined by Subramanian et al. (*11*) was used to construct the working curve. Each Co(II) solution was adjusted to near neutral pH immediately before use (reason discussed in Results and Discussion section).

Glass distilled deionized water (DDW) was used to prepare all solutions.

Flow Cell. Figure 1 gives a schematic representation of the operational aspects of the flow cell. The reagent reservoir holds an essentially stagnant solution containing luminol, H_2O_2, and KOH at their selected concentrations. Because this reservoir is pressurized, a one-way flow of reagent is established, through the membrane, into the analyte flow chamber. Reaction occurs where the reagent and analyte mix and yields emission at an intensity which is characteristic of the level of analyte present.

The actual flow cell is shown in Figure 2. This design minimizes the surface area that requires sealing, permits the large surface area to volume ratio desired in CL flow cells, and allows easy and reproducible assembly. Nylon was used for the construction because it is relatively inert, structurally rigid, and easy to machine. Because of the pressure required for proper sealing, the front window was Plexiglas, instead of glass. The cell holder was very similar to one previously described (*1*). All solution ports have $^1/_4$ - 28 threads for compatibility with commercially available tube fittings.

Delivery System. The analyte stream delivery system used in these studies is shown in Figure 3. Separate vessels for the analyte and the rinse (or background) solutions are connected through a three-way Teflon solenoid valve, V1, (Angar Model 250) to the analyte flow chamber. Valve V1 automatically switches between the two solutions according to the preset pulse width (analyte volume) and duty cycle (ratio of analyte volume to total analyte plus rinse volumes). The vessels are pressurized with nitrogen to about 3 psi (20 kPa) to provide smooth, stable, and continuous flow, subject to only minor long-term drift of either rinse or analyte solutions. When the analyte solution is changed, valve V2 is activated to release the pressure from the analyte vessel without any perturbation to the rinse line. Release of V2 and activation of V3 permits bleeding of any air that may have become lodged within the associated tubing. If air becomes trapped within the analyte flow chamber, the flow characteristics are substantially altered and the precision is degraded.

This analyte delivery system is quite useful for characterization studies because it allows automatic control of the number of repetitions of a given sample, the rate of repetition, the duty cycle, and the sample volume per injection. For routine work or with small volumes of sample, the system could easily be simplified

0003-2700/79/0351-0424$01.00/0 © 1979 American Chemical Society

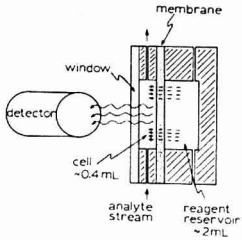


Figure 1. Schematic diagram of membrane flow cell. Dashed arrows indicate direction of reagent flow through membrane

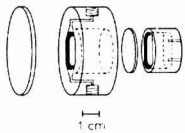


Figure 2. Construction of membrane flow cell

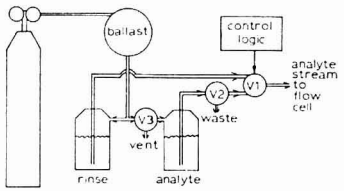


Figure 3. Analyte flow system

to syringe injection of sample into the flowing rinse stream.

The reagent reservoir is filled by delivering and mixing equal volumes of stock solutions of luminol, H_2O_2, KOH, and DDW using a four-syringe stopped-flow solution delivery system as previously described (*12*). The reservoir is then pressurized to the desired level (about 10 psi or 70 kPa) and maintained at that pressure using a regulated tank of nitrogen. The total amount of reagent consumed can be accurately measured with a modified graduated pipet positioned between the gas regulator and the reagent reservoir. Since the pipet is within the pressurized reagent system, it therefore increases the effective volume of the reagent reservoir.

Membrane. The microporous membranes used in this study were manufactured by Moleculon Research Corporation (Cambridge, Mass.) and sold under the trade name of Poroplastic.

Detection. The light emission was observed directly by a 1P28 PMT, without wavelength discrimination.

MEMBRANE CHARACTERISTICS

Poroplastic membranes are an ultramicroporous network of cellulose triacetate with molecular size pores. Initially, the pores contain water, but a wide variety of solvents, both polar and nonpolar, can be substituted. The transparent membrane sheets are strong, flexible, non-ionic, and stable over a wide pH range. The membrane is available in a variety of thicknesses (50–500 μm) pore sizes (14–200 Å). Pore size and structural strength are inversely related and are both dependent upon the water content (70–97%) included in the original manufacture of the membrane (*13*).

Diffusion through the membrane depends mainly upon its pore diameter and thickness. A controlled net flow, however, can be easily enforced by adjusting an applied pressure gradient, the upper limit of which is set by the structural rigidity of the membrane. Using a Tyvek (spunbound polyethylene fibers) reinforced membrane, pressure differentials of up to 20 psi (140 kPa) can be applied across the membrane without significant deformation. Reverse diffusion against the net flow is negligible at pressure gradients greater than 4 psi (28 kPa). In general, mid-range pressures (9–10 psi) were used.

Characterization studies revealed that the flow rates of both the solvent and the solute are equivalent, with no observed discrimination against any reagent used, irrespective of concentration, and that all flow rates are proportional to the applied pressure gradient. At 6 psi (42 kPa), the flow rate is 2.2 μL/min/cm^2; at 14 psi (98 kPa), the flow rate is 5.0 μL/min/cm^2. (The membrane surface area in our cell is 1 cm^2.) Substitution of membranes available with other porosities and thicknesses allows the flow-rate range to be shifted higher or lower by 1–2 orders of magnitude.

There are, then, four methods to control the reagent flow rate (in moles per unit time) through the membrane: the porosity of the membrane (limited by structural rigidity), the total membrane surface area (limited by detector geometry and the rinsing efficiency of the cell), the concentration of the reagent solution (limited by reagent solubility and membrane integrity), and the applied pressure (limited by membrane rigidity).

RESULTS AND DISCUSSION

Explanation of the optimization of variables for this system can be readily divided into two separate although not entirely independent parts: (1) the reagent flow system, including the relative concentrations of luminol, H_2O_2, and OH^-, as well as the flow rate through the membrane, and (2) the analyte flow system, including the necessity for a complexing agent in the rinse solution, the sample volume, the duty cycle, the sample pH, and the sample flow rate. Optimization was complicated by trade-offs between the signal intensity and either the background emission level or precision. All experiments used the luminol–H_2O_2–OH^-–Co(II) system. The order of the following discussion does not reflect the order in which the variables were investigated.

Reagent Flow System. Exact knowledge of reagent concentrations is limited to those concentrations in the reagent reservoir. On the other side of the membrane, in the analyte flow chamber at the position where reaction occurs, knowledge of reagent concentrations is less certain. If reaction is confined to a narrow region near the surface of the membrane, the reagent concentration at that position will be the same as in the reagent reservoir. However, if reaction occurs in the bulk of the solution in the analyte chamber, the reagent concentration will be 3 to 4 orders of magnitude lower due to dilution. (The reagent flow rate is only a few μL per minute while the analyte/rinse flow rate is about 10 mL per minute.) It is most likely that the reaction will occur in a continuum of conditions between these two extremes. To demonstrate that the effective reagent concentrations in the reaction zone more closely approximate those at the membrane surface than in the bulk, the emission intensity from this reaction was measured using conventional stopped flow reagent delivery and compared to the intensity observed with the membrane. When the stopped flow delivered reagents (H_2O_2, OH^-, and luminol) that were at the same concentration as in the membrane reservoir (see below), the observed intensity was 8 times larger than that observed with the membrane. When the stopped flow delivered reagents diluted by 1000 (to reproduce the bulk solution conditions with the membrane), the observed intensity was less than 0.1% of that observed with the membrane. (The above measurements all used 10^{-6} M Co(II).) Experiments are planned to directly measure the emission intensity profile as a function of the distance from the membrane surface.

Comparison of observed emission intensity as a function of reagent concentrations for the membrane flow system with

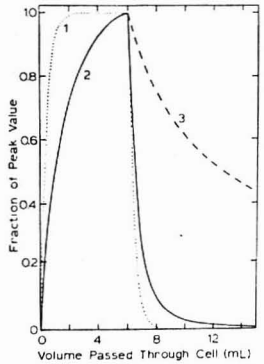


Figure 4. Ideal and observed rinsing efficiences of the analyte flow chamber. Flow chamber volume = 0.4 mL; analyte volume = 6 mL; volume ratio = 15. (1) Computer simulation of ideal peak shape; (2) observed peak with EDTA in the rinse solution; (3) observed peak without EDTA in the rinse solution; curves 2 and 3 are identical from 0–6 mL. For curve 1, the ordinate is in units of concentration of Co(II). For curves 2 and 3, the ordinate is in units of observed photocurrent

published reports on this same chemical system using a conventional flow stream can offer probable upper limits on the effective reagent concentration in the reaction zone. It has been reported for the Co(II)–luminol system that plots of CL emission intensity vs. reagent concentration pass through a maximum at about 10^{-4} M for luminol and 10^{-3} M for both OH^- and H_2O_2 (*15*). Because such plots for the membrane system show CL intensity still increasing at concentrations nominally ten times higher, it is probable that the effective reagent concentration in the reaction zone is no greater than one tenth of the concentration in the reagent reservoir.

Incomplete dissolution of luminol or precipitation, once the solution had been adjusted to a relatively neutral pH, became a problem at concentrations greater than 10^{-3} M. Any trials using OH^- at or below 10^{-4} M or using both OH^- and H_2O_2 simultaneously at or below 10^{-3} M yielded either comparatively no response or substantially reduced response. To ensure the integrity of the membrane, concentrations of OH^- and H_2O_2 were limited to 10^{-2} M or lower, although no specific tests have been conducted to determine the necessity of this limitation. Thus, the reagent concentrations chosen for the remainder of this study were 10^{-2} M OH^-, 10^{-2} M H_2O_2, and 2×10^{-4} M luminol. Unless stated otherwise, all reagent concentrations are those within the reagent reservoir.

Addition of a small amount of EDTA, at concentrations approximately two orders of magnitude less than that of luminol, to the reagent solution was found to reduce the background emission level by a factor of 50, without significantly degrading the response to the higher concentrations of cobalt. The loss of linearity at the lower Co(II) concentrations, due to a finite amount of EDTA emerging from the membrane on the analyte side and tying up a significant portion of the total analyte present, precluded use of EDTA in the reagent solution during construction of a working curve.

Analyte Flow System. Experimental verification of the rinsing efficiency of the analyte chamber was accomplished by comparing the observed response to a 6-mL "slug" of 10^{-6} M Co(II) analyte rinsed through the chamber (curve 3 in Figure 4) with that theoretically derived by computer simulation (curve 1 in Figure 4). The simulation assumed that the only variable involved in the signal intensity was the instantaneous Co(II) concentration in the chamber and that

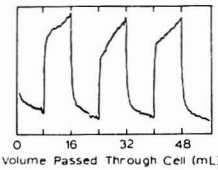


Figure 5. Observed peak shape for large analyte volumes. Flow chamber volume = 0.1 mL; analyte volume = 8 mL; volume ratio = 80

the Co(II) concentration was homogeneous through the analyte chamber. The mathematical model used was that described by Seitz (*14*) for a CL reaction in a continuously stirred tank, but excluded depletion of Co(II) due to reaction. This model differs slightly from our experimental situation but is quite useful because it provides a "best case" upper limit for comparisons. The observed (curve 3) and predicted (curve 1) peak shapes show much better agreement as the analyte enters the chamber than as it leaves the chamber. (Since the predicted curve has not been corrected for nonlinearity in the Co(II) working curve, nor for Co(II) depletion due to reaction, the actual agreement is somewhat better than is apparent.) It was speculated that adsorption of the Co(II) analyte on the interior surfaces of the cell, most probably at the relatively polar membrane surface, caused the Co(II) to be rinsed from the cell more slowly than predicted and produced the highly unsymmetrical, tailing peaks. EDTA (about 10^{-5} M) was added to the rinse solution to remove adsorbed Co(II) from the cell walls by complexation. The resulting peak (curve 2 in Figure 4) followed the predicted exponential decay very closely. This method of establishing the rinsing efficiency of a continuous flow cell (by comparison to ideal peak shapes) could serve as a means to directly compare the rinsing efficiencies of many flow cells appearing throughout the literature.

Figure 5 shows the peak shape obtained with an analyte volume to flow chamber volume ratio more than five times larger than that used in Figure 4. The peaks begin with the expected exponential approach to a maximum value, then abruptly change to a slower, linear increase that continues beyond the anticipated maximum. This behavior has been attributed to slow diffusion of the Co(II) analyte into the pores of the membrane (against the reagent flow). The EDTA rinse is not able to remove the Co(II) from the cell until the Co(II) has diffused out of the membrane pores into the flow chamber. The mirror-image behavior during the rinse cycle demonstrates the diffusion of Co(II) out of the membrane. This effect can be minimized by use of smaller analyte volumes and of rinse volumes two to five times larger than the analyte volume. If neither restriction is desirable, addition of a small amount of EDTA to the reagents (as discussed earlier) will help keep the Co(II) analyte from accumulating within the membrane pores.

It is obvious that the analyte pulse width (analyte volume) affects not only the peak heights, but also the rinsing efficiency and therefore the total rinse volume required to adequately flush out the analyte chamber. Figure 6 verifies that a 1:3 duty cycle with a 10^{-5} M EDTA rinse solution was sufficient to completely flush out all traces of analyte from a 6-mL pulse. Each series of peaks was produced by an initial Co(II) analyte pulse, at the indicated concentration, followed by the EDTA rinse solution and then a DDW pulse. If any Co(II) remained in the analyte chamber after one complete cycle, either because of poor rinsing or desorption from the cell surfaces, the substitution of DDW for the next sample pulse would have shown some response (as in the first two traces in Figure 6); the cycle would repeat itself until eventually DDW gave no

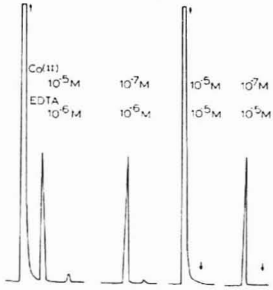


Figure 6. Effects of EDTA, in the rinse solution, on the rinse efficiency. Analyte volume = 6 mL (30-s pulse at a flow rate of 12 mL/min), flow chamber volume to analyte volume ratio = 15, duty cycle = 1:3. The upward arrows on the first and third traces indicate that the peak is considerably off scale; the two peaks are of equal height. The downward arrows in the third and fourth traces indicate the point at which a DDW pulse was injected

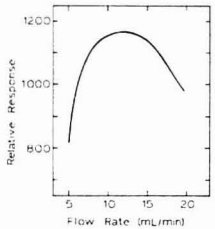


Figure 7. Effect of analyte stream flow rate on peak intensity. Analyte Co(II) pulse width = 30 s

response. The fact that increasing the rinse EDTA concentration from 10^{-6} to 10^{-5} M had no effect on the response to 10^{-7} M Co(II) (second and fourth traces) provided further evidence that complete rinsing of the flow chamber occurred within the 6-mL analyte volume and that the additional time required for rinsing was likely due to analyte adsorption/desorption.

The volume of analyte solution introduced per pulse was governed by the time that V1 remained activated and by the analyte flow rate. It was expected that response would increase with flow rate until a sufficient volume of analyte had been delivered to the cell to quantitatively displace the EDTA rinse solution. Figure 7 shows that the response does increase over the region of 4–10 mL/min. The reduction in signal intensity at flow rates greater than 12 mL/min is due to the reduced residence time, relative to the rate of reaction, within the flow chamber reaction zone.

The effect of the analyte solution's pH on the signal intensity is seen in Figure 8. In general, a plateau or maximum is observed at values just basic of neutral (pH 7–9). Accordingly, in the construction of the working curve, all analyte solutions were adjusted to between pH 7 and 8 for maximum sensitivity. The pH yielding maximum response provides additional data concerning the location of the reaction zone within the analyte chamber and the effective reagent concentrations within that zone. The pH at the membrane surface will be governed by the OH^- concentration in the reagent solution (pH 12). The pH in the bulk of the solution will be determined by the analyte solution (about pH 8 at the maximum sensitivity), the reagent solution (pH 12), and their relative flow rates. The flow rates in Figure 8 differ by $3^1/_2$ orders of magnitude, yielding a bulk solution pH of 8.6. It

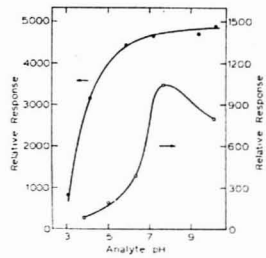


Figure 8. Effect of analyte pH on peak intensity. Analyte flow rate at 12 mL/min; 30-s analyte pulse width, reagent flow rate at 3.6 μL/min. (●-●-●) 10^{-6} M Co(II); (O-O-O) 10^{-8} M Co(II)

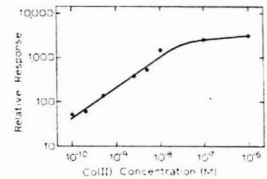


Figure 9. Co(II) working curve for the membrane CL system. All conditions given as in Figure 8

has been reported for the Co(II)–luminol system that the CL intensity decreases at pH values lower than pH 11 (*15*). This fact supports the earlier observation that the reaction zone is near to, but not confined to, the membrane surface, and that the effective reagent concentrations in the reaction zone are about one tenth of the concentrations in the reagent reservoir.

Analytical Results. The optimum operating conditions, as indicated by Figures 4 and 7, consisted of a 6-mL analyte pulse driven at a flow rate of 12 mL/min. (The sample volume requirements can be lowered by designing a smaller volume cell.) Accordingly, to establish the stability of the reagents within the reagent reservoir, as well as the precision of the technique, 6-mL pulses of a 10^{-8} M solution of Co(II) were repeatedly introduced into the flow stream for $2^1/_2$ hours. The overall precision was 4.1% RSD, with the worst case for any 30-min period being 3% RSD.

Operation at a 1:3 duty cycle and an analyte stream flow rate of 12 mL/min yields an analytical throughput of 40 samples (6 mL each) per hour. In one hour, 500 mL of rinse solution would be consumed, but, at a typical reagent reservoir pressure of 10 psi (70 kPa), only 0.25 mL of reagent solution would be consumed. Reduction of analysis time could be made by improving the rinsing efficiency of the cell and/or by reducing the volume of the analyte sample.

A working curve for Co(II) determinations is given in Figure 9. The change in slope at about 2×10^{-8} M is of interest, and is perhaps related to the question of the reagent concentration in the reaction zone. The slope of a plot of CL intensity vs. Co(II) concentration has been reported to change dramatically at a luminol-to-metal ratio of about 1:1, presumably because of complex formation (*16*). However, in the present study, the luminol concentration (in the reaction zone) was between 2×10^{-3} M (at the surface) and 6×10^{-7} M (in bulk solution) and the luminol-to-metal ratio (at the bend in the working curve) is at least 30:1 and possibly as high as 10^5:1.

At present, the practical limit of detection for Co(II) is slightly less than 10^{-10} M (10 parts per trillion) using the membrane flow cell. It should be noted that this is the lowest measured detection limit for Co(II) with luminol reported to

date; a previously reported value of 10^{-11} M was obtained by extrapolation from higher concentrations (2).

The linear range (on a log–log plot) extends from 2×10^{-10} M to 2×10^{-8} M. The onset of leveling off can be seen below 2×10^{-10} M; however, significant slope still remains to push the detection limit below 10^{-10} M (17). The authors believe that the linear range can be extended to include a wider concentration range through knowledge of, and control of, reagent and analyte concentrations and residence times in the reaction zone.

CONCLUSIONS

The reported method of reagent addition has been shown to provide the anticipated advantages, with reagent economy and good precision important in general, and localization of emission and high sensitivity of particular utility in CL analysis.

The membrane system offers certain present advantages and possibilities for future applications that are not readily feasible with conventional use of a peristaltic pump for reagent delivery (although a peristaltic pump certainly has the advantages of wider availability, applicability, and general acceptance). Flow rates through the membrane are below the normal flow rates available with peristaltic pumps. Also, the membrane system is able to allow a reaction to take place under conditions where the "effective" reagent concentration is orders of magnitude higher than in the bulk.

Future studies will examine storage and/or immobilization of reagents within the membrane pores. In addition, because of the localization of emission, it should be possible to have a sample stream containing several analytes flow along a row of membrane strips, where each membrane contains different reagents, which respond to different analytes (or categories of analytes). Such an approach would extend CL to simultaneous multicomponent analysis. Finally, pressurizing a microporous membrane system using the energy stored in an inflatable elastomeric reservoir (18) could provide a portable reagent delivery system.

LITERATURE CITED

(1) S. Stieg and T. A. Nieman, *Anal. Chem.*, **50**, 401 (1978).
(2) W. R. Seitz and D. M. Hercules in "Chemiluminescence and Bioluminescence", M. J. Cormier, D. M. Hercules, and J. Lee, Ed., Plenum Press, New York, 1973, pp 427–49.
(3) D. Slawinska and J. Slawinski, *Anal. Chem.*, **47**, 2101 (1975).
(4) U. Isacsson and G. Wettermark, *Anal. Chim. Acta*, **83**, 227 (1976).
(5) T. L. Sheehan and D. M. Hercules, *Anal. Chem.*, **49**, 446 (1977).
(6) S. N. Lowery, P. W. Carr, and W. R. Seitz, *Anal. Lett.*, **10**, 931 (1977).
(7) B. M. Strom, M.S. Thesis, Iowa State University, Ames, Iowa, 1974.
(8) M. P. Neary, R. Seitz, and D. M. Hercules, *Anal. Lett.*, **7**, 583 (1974).
(9) R. Delumyea and A. V. Hartkopf, *Anal. Chem.*, **48**, 1402 (1976).
(10) R. L. Veazey and T. A. Nieman, 29th Pittsburgh Conference on Analytical Chemistry and Applied Spectroscopy, Cleveland, Ohio, 1978, paper 99.
(11) K. S. Subramanian, C. L. Chakrabarti, J. E. Sueiras, and I. S. Maines, *Anal. Chem.*, **50**, 444 (1978).
(12) S. Stieg and T. A. Nieman, *Anal. Chem.*, **49**, 1322 (1977).
(13) Poroplastic Data Sheets, Moleculon Research Corp., Cambridge, Mass.
(14) W. R. Seitz, *Proc. Conf. Anal. Appl. Biolum. Chemilum.*, Brussels, 1978, to be published.
(15) T. G. Burdo and W. R. Seitz, *Anal. Chem.*, **47**, 1639 (1975).
(16) R. G. Delumyea, Ph.D. Thesis, Wayne State University, Detroit, Mich., 1974.
(17) J. D. Ingle, Jr., and R. L. Wilson, *Anal. Chem.*, **48**, 1641 (1976).
(18) *Chem. Eng. News*, **55**, 30 (July 11, 1977).

RECEIVED for review July 28, 1978. Accepted December 8, 1978. Acknowledgment is made to the donors of the Petroleum Research Fund, administered by the American Chemical Society, and to Research Corporation for support of this research.

Trace Element Laser Microanalyzer with Freedom from Chemical Matrix Effect

H. S. Kwong and R. M. Measures*

Institute for Aerospace Studies, University of Toronto, 4925 Dufferin Street, Downsview, Ontario M3H 5T6, Canada

A study on the susceptibility of TABLASER—Trace (element) Analyzer Based on Laser Ablation and Selectivity Excited Radiation to various chemical interference effects has been carried out. Tests were made on a diverse range of chromium doped samples to study source interference; anion–anion interference; cation–anion interference, and ionization interference. The observed laser induced fluorescence signal was found to be relatively independent of the source materials used, even under conditions of doping with high concentrations of compounds such as copper sulfate and potassium sulfate. The calibration curves for chromium in three different matrix materials are linear with a 45° slope. These observations provide evidence that our TABLASER is relatively free from chemical interference effects. The absence of these undesirable effects is attributed to (a) the extremely high temperature of the laser generated plasma (enabling complete dissociation of the compounds) and (b) the subsequent rapid expansion of the laser ablated plasma into the low vacuum region (which minimizes molecular association through interspecies collisions). This new technique has the potential for development into a new form of laser trace element microanalyzer that could be used for in situ high sensitivity measurements.

Evaluation of trace concentrations of heavy metals in biological, medical, industrial and environmental materials has become a major analytical task (1). The impact of heavy metal contamination on the biosphere is slowly being recognized as a potential health hazard of growing proportions (2). Consequently, there is an increasing demand for a trace element microprobe that can be used to rapidly monitor the concentration of a select group of elements in a wide variety of material samples. The ideal characteristics of such a trace element microprobe are:

(1) Selective microsampling capability.
(2) No sample preparation—in situ measurement.
(3) Real time analysis.
(4) High relative and absolute concentration sensitivity.
(5) Freedom from matrix effects (chemical or physical) so that calibration is independent of substrate containing element.
(6) Highly selective for element of interest.
(7) Linearity of response over wide dynamic range of concentrations.
(8) Minimum variation in sensitivity between elements.
(9) Depth profiling capability.
(10) Simultaneous multielement measurement possible.
(11) Capable of distinguishing between isotopes.
(12) Insensitive to the nature of substrate material.

0003-2700/79/0351-0428$01.00/0 © 1979 American Chemical Society

Table I. Principal Microtrace Element Analysis Techniques

technique	principle	potential and limitation	sensitivity limit
Ion Microprobe Mass Analyzer (IMMA)[3]	high energy ion sputtering of secondary ions for analysis in mass spectrometer	surface, in situ element analysis; sample preparation required; contamination is possible through preparation; experiences severe matrix effects; isotope measurement feasible; operates at high vacuum (10^{-6} Torr); all elements are detectable; simultaneous multielement analysis is, in principle, possible.	sensitivity varies over several orders of magnitude for wide range of elements; background interference limits sensitivity; ppm for most elements.
Emission Laser Microprobe (ELM)[4, 5]	laser ablation combined with spark excitation, subsequent line emission of specific element monitored	surface, in situ element analysis; sample preparation not required; contamination is introduced through cross-excitation electrodes; experiences severe matrix effects; isotope measurement not possible; operates in atmospheric condition; all elements are, in principle, detectable; simultaneous multielement analysis is feasible.	sensitivity varies slightly for all elements; background plasma emission limits sensitivity; from 10 to 100 ppm.
Laser Microprobe Mass Analyzer (LAMMA)[6]	laser ablation generating ions for analysis in time of flight mass spectrometer	thin film element analysis; sample preparation required; contamination is introduced via sample preparation; experiences moderate matrix effects; isotope measurement feasible; operates at high vacuum (10^{-6} Torr); all elements are, in principle, detectable; simultaneous multielement analysis is feasible.	sensitivity varies over two orders of magnitude for most elements; background interference limits sensitivity and accuracy; ppm range for most elements.

Although there are several sensitive trace element microprobes currently available for quantitative element analysis, each has its drawbacks and limitations, see Table I. We intend to present evidence that the combination of laser ablation and laser selective excitation spectroscopy represents a new form of laser ultra-trace element microprobe that possesses the potential to closely approach the ideal analytical tool outlined above. We have named our technique TABLASER—an acronym for "trace (element) analyzer based (on) laser ablation (and) selectively excited radiation".

Laser ablation has long been used as a method for microsampling materials (*4*) and is the preferred approach used in many microprobe systems in use today (*5*). On the other hand laser selective excitation spectroscopy (*7*) (or laser induced resonance fluorescence) can achieve extremely high sensitivity (*8*). In essence, a fan of vaporized target material is created by laser ablation within a vacuum chamber. The rapidly expanding vapor cloud is then probed by a pulse of dye laser radiation that is tuned to selectively saturate one of the resonance transitions within the element of interest. The subsequent enhanced spontaneous emission is monitored and found to be proportional to the original concentration of the element within the target material. We have previously demonstrated that this approach can be used to accurately and conveniently measure the radiative lifetime of atomic transitions (*9*).

In the course of developing this new approach we have discovered that operation with a low background pressure (10^{-3} to 10^{-4} Torr) results in an additional attractive feature; a freedom from chemical matrix effects. In the preliminary work reported herein, our TABLASER was used to detect trace concentrations of chromium in several diverse materials ranging from metal alloys to organic substances. Chromium was chosen in this initial investigation for two reasons: its resonance transitions are directly accessible by the nitrogen pumped dye laser available in our laboratory and chromium is one of the elements that has recently been recognized to be of importance (*10*).

EXPERIMENTAL

Material and Sample Preparation. Stock solution I ($K_2Cr_2O_7$) and stock solution II ($Cr(NO_3)_3$) were both prepared from reagent grade salts using 10 mg of chromium in 1 mL of solution. Dilutions of 10, 100, 1000 were made from each stock solution. Twenty milliliters of each diluted solution was mixed with 20 g (dry weight) of Carnation skim milk powder to generate samples; S10, S100, S1000 containing $K_2Cr_2O_7$ and SC10, SC100, and SC1000 containing $Cr(NO_3)_3$. Their concentrations are outlined in Table II. Diluted stock solution I, 20 mL, was also mixed with 20 g (dry weight) of flour powder to generate F10, F100, and F1000. In addition to the above samples, 2 samples of the 20-mL, 100 times diluted stock solution I and II were separately mixed with 20 g (dry weight) of Carnation skim milk powder; 200 mg of anhydrous reagent grade copper sulfate ($CuSO_4$) was added to one and 200 mg of potassium sulfate (K_2SO_4) was added to the other generating two additional samples: S100-$CuSO_4$ (containing 100 times more by weight of $CuSO_4$ than its chromium content) and SC100-K_2SO_4 (containing 100 times more by weight of K_2SO_4 than its chromium content). In all cases, the mixtures were thoroughly blended into paste form. The samples were frozen before undergoing the freeze-drying process to avoid foaming. After the drying process, which took about 48 h, the solid samples were broken down and ground into a fine powder in an alumina mortar to ensure homogeneous mixing. Sample powder was then pelleted into small tablets and mounted onto the sample holder and kept dry for later use. In order to

Table II. Doped Chromium Content in Skim Milk Powder and Flour Samples

sample no.	substrate	chromium source	calculated relative concentration, ppm
S10	skim milk powder	potassium dichromate, $K_2Cr_2O_7$	10
S100			100
S1000			1000
SC10[a]	skim milk powder	chromic nitrate, $Cr(NO_3)_3$	10
SC100			100
SC1000[a]			1000
S100-$CuSO_4$[b]	skim milk powder	$K_2Cr_2O_7$, $Cr(NO_3)_3$	99
SC100-K_2SO_4[c]			99
F10	flour	potassium dichromate, $K_2Cr_2O_7$	10
F100			100
F1000			1000

[a] Not used in this measurement. [b] Addition of 1% by weight of copper sulfate ($CuSO_4$). [c] Addition of 1% by weight of potassium sulfate (K_2SO_4).

Table III. Comparison between Values of Chromium Concentrations in Skim Milk Powder Obtained by Calculation and Neutron Activation Analysis

sample no.	calculated relative concentration, ppm[a]	neutron activation analysis relative concentration, ppm
S10	10	9.6 ± 0.4[b]
S100	100	103. ± 2[b]
S1000	1000	1000. ± 20[b]

[a] Uncertainty is expected to be less than 1%. [b] Standard deviation.

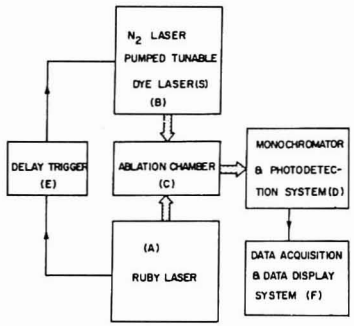


Figure 1. TABLASER block diagram

ensure the accuracy of this sample preparation, samples S10, S100, and S1000 containing 10, 100, and 1000 ppm of chromium were checked by the neutron activation technique. The result confirmed the calculated value as presented in Table III. This test, however, did nothing to evaluate the homogeneity of the sample.

Steel samples obtained from NBS were also used to test our new technique. These were designated: SRM 665, SRM 664, SRM 663, SRM 662, and SRM 661 and contained 0.007%, 0.06%, 1.31%, 0.3%, and 0.69% of chromium by weight, respectively. Since these standards are designed for microanalysis such as electron and laser probe analysis, we assumed that the homogeneity of these standard samples was sufficient for our measurements (*11*).

Apparatus. A block diagram of our TABLASER system is presented as Figure 1. A detailed description of this facility is published elsewhere (*12*). Basically the TABLASER comprises six major components: A Q-switched ruby laser (A) served for ablation and delivered an energy pulse of 10 to 20 mJ at 694.3 nm with a duration of about 30 ns. A nitrogen laser pumped dye laser (B) was employed for the selective excitation of the ablated vapor cloud. The wavelength of the dye laser was tuned to the 428.9 nm ($^7P_2°$–$^7S_3$) resonance line of chromium (Figure 2). Its peak power was about 1 kW its duration was close to 6 ns, and its spectral line width was better than 0.01 nm. An ablation chamber (C) was used in which the chromium doped samples were mounted onto a sample holder. The pressure within the chamber was kept between 10^{-4} and 10^{-3} Torr by a diffusion and rotary pump combination.

The dye laser axis, the ruby laser axis, and the axis of the receiver optics were mutually orthogonal and intersected 5.5 mm in front of the target surface, Figure 3. A fraction of the laser induced resonance fluorescence emanating from the ablated vapor cloud was captured by a lens and focused onto the entrance slit of a Czerny-Turner Monochromator (SPEX ±1700 II). The resulting spectrally filtered radiation (2-nm linewidth) was focused onto the photocathode of a RCA-C31034 photomultiplier tube (D). The output of the PMT was subsequently displayed on a Tektronix 7704 oscilloscope (E) where it was photographed. A Tektronix 556 oscilloscope (F) was used for delaying the dye laser pulse to optimize the signal observed.

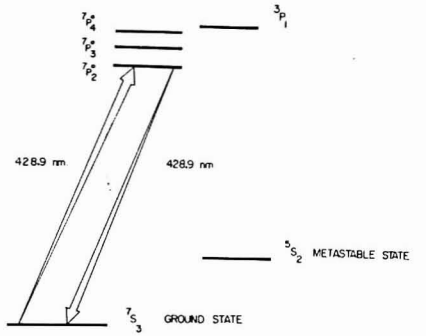


Figure 2. Partial energy diagram for chromium(I)

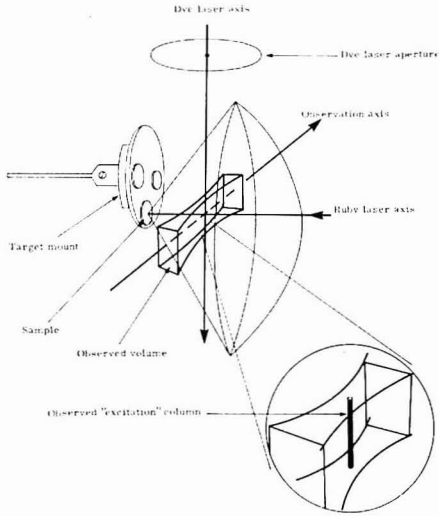


Figure 3. Relative positions of the observed volume, excitation column, and target sample

RESULTS AND DISCUSSION

Ablation of the sample target generates a plume of dense, high temperature plasma that is contaminated with particulate debris. The ions within this plasma rapidly recombine as the plume expands and cools. The atomic species formed by plasma recombination and the remaining ionic species expand into the low pressure background region faster than the heavier particulates. This separation of the ablated cloud creates a particulate free zone of atomized material suitable for dye laser probing. The Tektronix 556 oscilloscope provided the delay trigger necessary to synchronize the arrival of the dye laser pulse with that of this particulate-free window at the region of observation. Mie scattering was in this way essentially eliminated. A more detailed discussion of this problem is provided elsewhere (*12*).

It should be noted that the very short duration of the dye laser pulse, relative to the radiative lifetime of the laser pumped transition, made it possible to rely upon temporal discrimination to distinguish between laser scattered signals

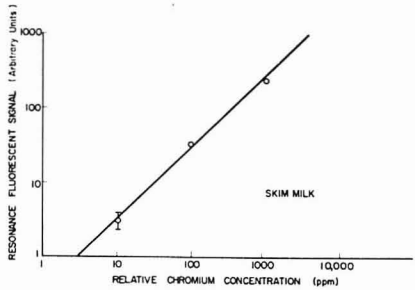


Figure 4. Resonance fluorescent signal vs. relative chromium concentration (ppm) for skim milk powder. Error bar indicates standard deviation, typical uncertainty is ≃ 20%

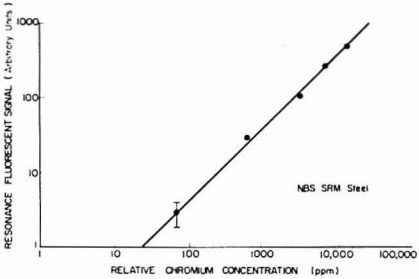


Figure 5. Resonance fluorescent signal vs. relative chromium concentration (ppm) for NBS-SRM steel standards. Error bar indicates standard deviation, uncertainty ranges between 15% and 30%

and those arising as a result of laser enhanced emission (resonance fluorescence) (*12*). Laser saturation of the resonance transition was employed (i), to maximize the enhanced emission signal and (ii) to reduce its dependence upon intensity fluctuation of the dye laser pulse (*13*).

A linear relation has been established between the laser induced resonance fluorescent signal and the relative concentration of chromium over several orders of magnitude Figure 4, 5, and 6. The slope of the log–log plot is 45° for each of the three types of sample material studied, i.e., flour, skim milk powder, and NBS SRM steel. The typical uncertainty of the signal intensity is around 20% to 30%. For extremely powdery materials such as flour, it tends to be somewhat higher.

There are several factors that influence the signal intensity on a shot to shot basis. (i) Piepmeier et al. (*14*) reported that the amount of material sampled is a function of ruby laser energy. The ruby laser output of our system was, unfortunately, somewhat irreproducible. The variation in its energy could be as high as ±30% over a given experimental run. (ii) There was also a jitter of ±20 ns in the delay of firing of the thyratron of the N_2 laser. This led to a spread in the time of probing the vapor at a given location, which in turn created a spread in the amplitude of resonance fluorescence since the density in the vapor cloud is a function of time because of its rapid expansion. (iii) There may also have been some degree of inhomogeneity in the distribution of the doped element. This would also contribute to variations in the observed signal. Inhomogeneity of NBS steel samples has been discussed at length by Yakowitz et al. (*11*). (iv) Variation of power density or the dye laser may have also contributed to the spread in the observed signal amplitude. However, this should have only

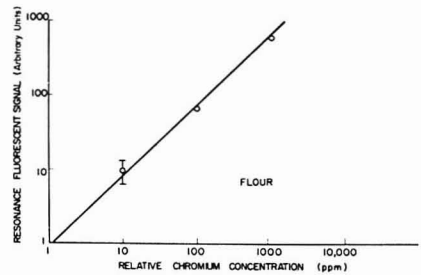


Figure 6. Resonance fluorescent signal vs. relative chromium concentration (ppm) for flour. Error bar indicates standard deviation, typical uncertainty is ≃ 30%

Table IV. Effect on Signal Intensity by Changing the Chemical State of Chromium and Adding Additional Chemical Compounds

	SC100	SC100·K_2SO_4	S100	S100·$CuSO_4$
signal intensity, V	0.86 ± 0.24	0.88 ± 0.18	0.88 ± 0.14	0.81 ± 0.24
ruby laser energy, mJ	18 ± 3.6	17 ± 2.6	18.3 ± 4.2	16 ± 2.4

given rise to a second-order effect since the power density of the dye laser was high enough to approach saturation of the atomic transition (*15*).

Chemical matrix effects (*16*) represent one of the major complicating factors that plague the trace element atomic fluorescent technique. To evaluate the susceptibility of our TABLASER to this type of matrix effects, several tests were undertaken. These included a comparison of the signal response from several samples with the same concentration of chromium, albeit that the chromium was in two different chemical states i.e., Cr^{3+} and $Cr_2O_7^{2-}$. Furthermore, two of the samples were prepared with excess (100:1) amounts of copper sulfate or potassium sulfate to produce the four different skim milk powder samples indicated in Table II.

The use of two different chromium salts allows the source interference effect to be evaluated. Potassium and copper were chosen as added cation contaminants to study the vulnerability of this technique to cation–cation interference. Furthermore, the use of potassium with its lower ionization potential (K, 4.34 eV; Cr, 6.76 eV) should reveal the severity, if any, of the change in the sampling efficiency of the refractory metals due to the change in the plasma temperature as suggested by Ahrens et al. (*17*). Sulfate and nitrate were chosen as the concomitant anion because of their severe cation–anion interference, reported widely in other trace element techniques (*16*, *18*). In this way, we hoped to determine if the TABLASER was prone to major variations in the chemical composition of the target material.

Table IV clearly indicates that there is no significant variation of the induced fluorescent signal, (a) when different chromium compounds were used, (b) when different chemical states of chromium were used, and (c) when 1% by weight of an additional compound, such as copper sulfate or potassium sulfate was added to the sample. The slightly lower signal intensity for S100·$CuSO_4$ was mainly due to lower ruby laser energy used in that series of measurements.

These results suggest the following three major observations: (1) Complete atomization of the ablated material occurs. Consequently, the laser induced fluorescent signal is independent of the chemical state or the form of the chromium while within the target.

(2) The degree of breakup of the chromium compound and the sampling efficiency of the ablation laser appears to be insensitivity to the presence of other elements having significantly different ionization potentials (concomitant concentrations higher than 1% by weight were not used because this might alter the physical properties of the substrate).

(3) The added cation and anion did not induce chemical removal of the atomic chromium or introduce spectral interference to the induced fluorescent signal. Furthermore, the immunity of this technique from cation–cation interference effect is reinforced by the linearity of the log–log plot for the NBS-SRM steel standards where the chemical composition varied over two orders of magnitude for individual impurity elements such as carbon, manganese, silicon, and molybdenum.

Since the key to eliminate chemical matrix effects is high temperature (Kirkbright, 1974) (*19*), it is worth estimating the approximate temperature of the laser generated plasma. To achieve this, the mean speed of the neutral chromium atoms was monitored and was estimated to be around 5×10^5 cm s^{-1} which corresponded to 6.5 eV. In fact, since a substantial amount of energy of the plasma was lost in the early phase of expansion through plasma emission, it is reasonable to assume that the initial plasma temperature for the heavy species (such as atoms and ions) was estimated to be in excess of 10^5 K. At such high temperatures, molecular association is highly unlikely. Furthermore, the streaming motion of the neutrals and ions (*20*) drastically reduces interaction between them as they expand and cool thus minimizing molecular association between the neutral chromium and concomitant atoms, that constitute the major ingredients of the matrix materials used in the analysis.

The sensitivity of our current facility, albeit rather crude, is in the case of flour around 1 ppm which corresponds to an absolute detection limit of 10^{-13} g. The present sensitivity is limited by signal shot noise and stray dye laser light from the reaction chamber. The ultimate sensitivity limit of this technique, however, can be improved by several orders of magnitude if the system is carefully optimized. A detailed discussion of the expected limits of sensitivity to be achieved in practice is provided elsewhere (*12*). It is worthy pointing out, however, that a relative sensitivity of close to 1 ppb should easily be attained for most elements.

At present the spatial resolution is less than 100 μm. This, however, does not reflect the resolution capability of this technique. Spatial resolution down to 1 μm has been achieved by LAMMA (*6*) using essentially the same sampling mechanism.

Monitoring of specific trace elements in water samples is also possible with our TABLASER approach. Sample treatment, in this instance, will be necessary. The sample preparation procedure would be similar to that adopted for the skim milk and flour reference pellets. The carrier substrate should be chosen so as to minimize the interference with regard to the elements of interest. Powdery material (such as flour) should, however, be avoided since we suspect that with such targets the ratio of particulate to atomized vapor produced varies on a shot to shot basis.

The sensitivity for water analysis would be considerably greater than that for a solid sample because of the preconcentration that takes place during sample preparation. In view of the relative freedom of various interference effects associated with our TABLASER, the adoption of a common substrate might enable a single calibration curve to be used for most elements under investigation. This would make monitoring of trace elements in water samples extremely simple.

Extension of our TABLASER to multielement analysis could be achieved in one of two ways. Either one dye laser could be tuned to one resonance line of each element successively or several suitably tuned dye lasers (pumped by a common nitrogen laser) would be used simultaneously. The photodetection system would be correspondingly different in the two cases. The range of elements accessible by the TABLASER approach is limited by the availability of suitable laser radiation. In essence, almost all elements, that are likely to be of interest as a trace constituent, can be included if nonlinear optics, such as second harmonic generation, is employed.

LITERATURE CITED

(1) *Chem. Eng. News*, **49**, 29 (July 1971).
(2) W. R. Wolf, *Anal. Chem.*, **50**, 190A (1978).
(3) K. F. J. Heinrich and D. E. Newbury, Ed., "Secondary Ion Mass Spectrometry", *Natl. Bur. Stand. (U.S.), Spec. Publ.*, **427**, 191 (1975); T. Hall et al., Eds., "Microprobe Analysis as Applied to Cells and Tissues", Academic Press, London, New York, 1974, p 23.
(4) F. Brech and L. Cross, *Appl. Spectrosc.*, **16**, 59 (1962); E. F. Runge et al., *Spectrochim. Acta*, **20**, 733 (1964).
(5) K. W. Marich et al., *J. Phys. E*, **7**, 830 (1974).
(6) F. Hillenkamp et al., *Appl. Phys.*, **8**, 341 (1975).
(7) S. J. Weeks, H. Haraguchi, and J. D. Winefordner, *Anal. Chem.*, **50**, 360 (1978).
(8) W. F. Fairbank, Jr., et al., *J. Opt. Soc. Am.*, **65**, 199 (1975).
(9) R. M. Measures, N. Drewell, and H. S. Kwong, *Phys. Rev. A*, **16**, 1093 (1977).
(10) M. S. Black and R. E. Sievers, *Anal. Chem.*, **48**, 1872 (1976). H. A. Laitinen, *Anal. Chem.*, **43**, 809 (1971).
(11) H. Yakowitz et al., "Standard Reference Materials: Homogeneity Characterization of NBS Spectrometric Standards II: Cartridge Brass and Low-Alloy Steel", *Natl. Bur. Stand. (U.S.), Misc. Publ.* **260-10**, (1965); R. F. Michaelis et al. "Standard Reference Materials: Metallographic Characterization of an NBS Spectrometric Low-Alloy Steel Standard", *Natl. Bur. Stand. (U.S.), Misc. Publ.*, **260-3**, (1964).
(12) R. M. Measures and H. S. Kwong, "TABLASER—Trace (element) Analyser Based on Laser Ablation and Selectively Excited Radiation", *Appl. Opt.*, in press.
(13) R. M. Measures, *J. Appl. Phys.*, **39**, 5232 (1968); J. W. Daily, *Appl. Opt.*, **17**, 225 (1978).
(14) E. H. Piepmeier and D. E. Osten, *Appl. Spectrosc.*, **25**, 642 (1971).
(15) J. W. Daily, *Appl. Opt.*, **16**, 568 (1977).
(16) W. G. Schrenk, "Analytical Atomic Spectroscopy", Plenum Press, New York and London, 1975.
(17) L. A. Ahrens and S. R. Taylor, "Spectrochemical Analysis", 2nd ed., Addison-Wesley Publishing Co., Reading, Mass., 1961, p 119.
(18) J. Smeyers-Verbeke, Y. Michotte, and D. L. Massart, *Anal. Chem.*, **50**, 10 (1978); E. J. Czobik and J. P. Matousek, *Anal. Chem.*, **50**, 2 (1978).
(19) G. F. Kirkbright et al., "Atomic Absorption and Fluorescence Spectroscopy", Academic Press, London, New York, 1974, p 507.
(20) H. S. Kwong, "Free expansion of atomic species in vacuum after laser ablation", in preparation.

RECEIVED for review August 11, 1978. Accepted November 6, 1978. The support of the National Research Council of Canada and Environment Canada (the Atmospheric Environment Services Branch) is greatly appreciated.

Resolution of the Optical Isomers of Dansyl Amino Acids by Reversed Phase Liquid Chromatography with Optically Active Metal Chelate Additives

James N. LePage, Wolfgang Lindner, Geoffrey Davies, David E. Seitz, and Barry L. Karger*

Institute of Chemical Analysis and Department of Chemistry, Northeastern University, Boston, Massachusetts 02115

The technique of ligand exchange chromatography through addition of lipophilic metal chelates to the mobile phase of a reversed phase column has been extended to the separation of the optical isomers of dansyl amino acids using an optically active metal chelate. Remarkably high α values approaching 2.0 are achieved while maintaining high performance conditions. It is hypothesized that the metal center, in addition to imposing a rigid environment at the exchange site, also induces proton loss from the sulfonamide group of the dansyl derivatives, since retention and selectivity are strongly dependent upon pH and the metal ion selected. Stereoisomeric selectivity is shown to be dependent upon the particular dansyl amino acid and the optically active metal chelate employed.

Recent studies in our laboratory have shown that addition of the metal chelate C_{12}-dien-M(II) (C_{12}-dien = 4-dodecyldiethylenetriamine; M = Zn or Cd) to the mobile phase can dramatically influence selectivity in reversed phase liquid chromatography, while at the same time not significantly degrading the high performance obtainable using chemically bonded phases on small diameter particle supports (*1*, *2*). The metal imposes a conformational rigidity on the atoms of the chelating agent (dien), and this structuring undoubtedly plays a significant role in the selectivity observed.

Of particular interest has been the steric and geometric selectivity found with this metal chelate additive. For example, the relative retention of maleic vs. fumaric acid was 2.5 with C_{12}-dien-Zn(II), whereas a value of only 0.90 was observed with the simple ion-pairing reagent, *n*-dodecyltrimethylammonium (*3*). Moreover, the dansyl derivative of glycine was retained roughly twice as long as that of alanine (*2*), an indication of a substantial steric effect on selectivity.

From the excellent selectivities found, it was logical to extend this work toward the separation of enantiomeric solutes. In this paper we report the successful resolution of a number of D,L-dansyl amino acids using optically active metal chelates.

Stereoisomeric selectivity generated by metal chelate complexation has been previously achieved. Recent examples of this approach have been from the work of Davankov and Zoltarev (*4*) and of Lefebvre et al. (*5*). Moreover, inert optically active metal chelates such as $Co(en)_3^{3+}$ have been separated and in addition utilized for separating optically active anions (*6–8*). The technique of ligand exchange chromatography has also been recently reviewed (*9*). To our knowledge, the present paper reports for the first time the use of optically active counterions for the successful high performance reversed phase separation of optical isomers.

EXPERIMENTAL

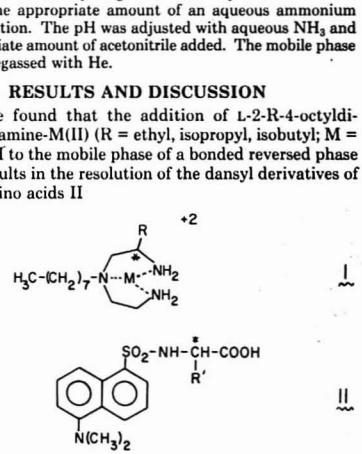
Apparatus. The modular liquid chromatographic system used consisted of a Waters M 6000-A pump and Model U6K injector and a Laboratory Data Control Model 1206 V (254 nm) ultraviolet absorbance detector. The columns were thermostated at 30 ± 0.1 °C using a Haake type NBE circulator.

Chemicals and Packing. The optically active chelating agents were synthesized in four steps. The optically active amino alcohols, L-2-amino-1-butanol, L-2-aminovalinol, and L-2-aminoleucinol (Sigma reagent grade), were converted to their corresponding aziridines according to (*10*). The aziridines were then reacted with ethylenediamine to form the L-2-alkyldiethylenetriamine (*11*). This material was reacted with benzaldehyde to form the corresponding Schiff base at the primary amine sites and then with *n*-octyl bromide which added the *n*-octyl group at the four position. The Schiff base was finally reconverted to the primary amino group (*12*). Further details of the synthesis will be described elsewhere. The DNP and dansyl amino acids were Sigma reagent grade or were synthesized according to Bayer et al. (*13*). Approximately 1 μg of each standard substance was injected onto the LC column. Hypersil 5 μm silica was obtained from Shandon Southern Products Limited. Reagent grade *n*-octyldimethylchlorosilane and hexamethyldisilazane were obtained from Silar Labs. The silica was bonded, exhaustively silanized, and packed into 15 cm × 4.6 mm i.d. columns (Analabs), as described in (*2*). The UV grade acetonitrile was obtained from Burdick and Jackson.

Preparation of Mobile Phases. The synthesized dien and metal salt were carefully weighed on an analytical balance and added to the appropriate amount of an aqueous ammonium acetate solution. The pH was adjusted with aqueous NH_3 and the appropriate amount of acetonitrile added. The mobile phase was then degassed with He.

RESULTS AND DISCUSSION

We have found that the addition of L-2-R-4-octyldiethylenetriamine-M(II) (R = ethyl, isopropyl, isobutyl; M = Zn or Cd), I to the mobile phase of a bonded reversed phase column results in the resolution of the dansyl derivatives of the D,L-amino acids II



where R′ denotes the particular amino acid and * indicates the asymmetric centers of I and II. Typical separations of racemic mixtures of II for a number of amino acids are shown in Figures 1 and 2 using the isopropyl derivative of I at pH 9.0. As can be seen, excellent resolutions have been achieved for various D,L pairs with relative retention values approaching 2.0 in certain cases (e.g., dansyl cysteic acid in Figure 1). Peak identification was made by separately injecting the dansyl derivatives of the optically pure D and L amino acids.

0003-2700/79/0351-0433$01.00/0 © 1979 American Chemical Society

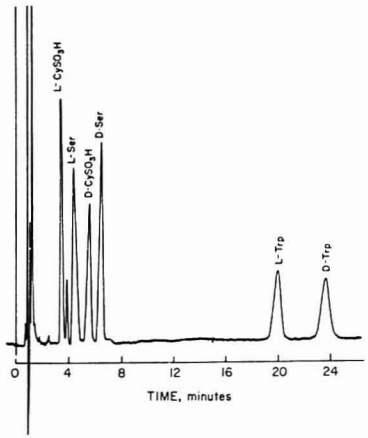


Figure 1. Separation of D,L-dansyl amino acids. Conditions: 0.65 mM L-2-isopropyl-dien-Zn(II); 0.17 M NH_4Ac to pH 9.0 with aqueous NH_3; 35/65 AN/H_2O; T = 30 °C; flow-rate 2mL/min; column: 15 cm by 4.6 mm i.d. Hypersil 5 μm C_8; solutes: $CySO_3H$ = cysteic acid; Ser = serine; Trp = tryptophan

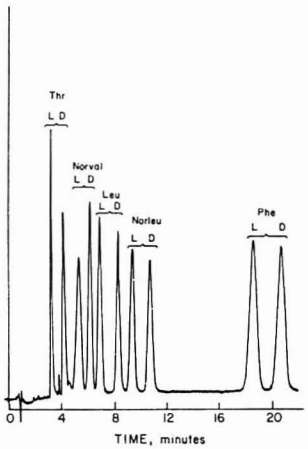


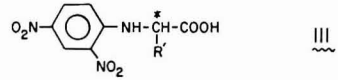
Figure 2. Separation of D,L-dansyl amino acids. Conditions as in Figure 1. Solutes: Thr = threonine; Norval = norvaline; Leu = leucine; Norleu = norleucine; Phe = phenylalanine

The requirements for resolution of racemic mixtures of II were established by comparing the retention and selectivity in reversed phase (R.P.) and ion-pair (I.P.) (C_{12}-$N(CH_3)_3^+$ counterion) chromatography with those observed in the presence of I under otherwise identical chromatographic conditions. Increasing pH in the range ca. 7–9 had little effect on the retention of anionic solutes (including II) in the R.P. or I.P. modes. Ligand I with no added metal ion behaved quite similarly to the I.P. mode at pH 9, and no resolution of racemic II was observed. However, increasing pH in this range greatly increased the retention and steric selectivity in the presence of I with added metal, the effect being much more marked for Zn than for Cd. This effect of mobile phase pH was, however, not observed for dansyl amino acids which did not contain an ionizable proton on the sulfonamide group (e.g., Pro whose k' ranged between 1.4 and 2.4 for conditions in Table I) or for 2,4-DNP amino acid derivatives III.

Table I. Retention and Selectivity Parameters for Dansyl Amino Acid Derivatives[a]

	R[d] = ethyl		R = isopropyl		R = isobutyl	
solute[b]	k'	α[c]	k'	α[c]	k'	α[c]
α-Ala	3.4	1.00	3.65	0.79	6.5	0.86
	3.4		4.6		7.6	
α-NH_2 butyric	2.5	1.00	2.85	0.88	4.8	0.89
	2.5		3.25		5.4	
Norleu	8.25	0.96	10.0	0.86	18.0	0.92
	8.60		11.6		19.5	
Leu	6.15	0.94	7.3	0.84	14.2	1.08
	6.50		8.7		13.1	
Thr	2.55	1.19	2.7	0.71	5.1	0.82
	2.15		3.8		6.2	
Ser	4.0	1.25	4.1	0.67	7.8	0.74
	3.2		6.1		10.5	
Asp	1.9	1.00	2.9	1.16	5.4	1.00
	1.9		2.5		5.4	

[a] Common conditions: 0.65 mM L-2-R-dien-Zn, other conditions as in Figure 1. [b] Solutes are dansyl amino acids: α-Ala = α-alanine; α-NH_2 butyric = α-NH_2 butyric acid; Asp = aspartic acid. Other amino acid abbreviations may be found in Figures 1 and 2. [c] $\alpha = k_L'/k_D'$. [d] R = alkyl substituent on metal chelate in I.



III

We suggest that in addition to imposing a rigid conformation at the exchange site, the metal center effectively competes with the proton on the sulfonamide group for negative charge. The driving force for this association would then involve the formation of a multidentate ligand capable of "chelation" through the carboxylate and sulfonamide groups. As expected, the effect of pH was more pronounced for Zn than Cd because of greater polarization of the solute N–H group by the smaller metal center (2).

Chromatographic data for enantiomeric dansyl amino acids are shown in Table I for different R in the Zn(II) chelate system (I). Under identical mobile phase conditions relative retention, α, clearly depends on R. It appears that the greatest selectivity is found with R = isopropyl, and moreover, its use is crucial for the resolution of D,L-aspartic acid in the mobile phase under the conditions employed. Table I further demonstrates that changes in R can influence the D,L elution order for a particular amino acid. For example, D-Ser elutes before L-Ser using R = ethyl, and the opposite order is observed for R = isopropyl or isobutyl. It is unclear why the elution order for the D,L pairs is dependent upon the particular amino acid for a given metal chelate (I); however, additional binding between the solute and metal chelate (e.g., through hydrogen bonding) may take place.

As previously found (*1, 2*) the efficiency obtained with these metal chelate additives is quite good. We have also found, in agreement with Wehrli et al. (*14*), that column stability at high pH can be extended with NH_3/NH_4^+ buffers using high coverage bonded phases. Moreover, the use of a precolumn before the injector may also prolong column lifetime. Column lifetimes appear to be in excess of three months with continual use.

We have also found the above metal chelate system to be effective in the D,L separation of certain drugs of pharmaceutical interest (e.g., substituted hydantoins). Preliminary work indicates that the use of ternary phase systems (e.g.,

AN/EtOH/H_2O) offers large (but still unpredictable) changes in D,L selectivity. These results will be reported at a later date.

LITERATURE CITED

(1) N. H. C. Cooke, R. L. Viavattene, W. S. Wong, G. Davies, and B. L. Karger, *J. Chromatogr.*, **149**, 391 (1978).
(2) B. L. Karger, W. S. Wong, R. L. Viavattene, J. N. LePage, and G. Davies, *J. Chromatogr.*, to be published in the Proceedings of the 12th International Symposium on Chromatography, Baden-Baden, September, 1978.
(3) J. N. LePage and B. L. Karger, unpublished results.
(4) V. A. Davankov and Yu. A. Zolotarev, *J. Chromatogr.*, **155**, 285, 295, 303 (1978).
(5) B. Lefebvre, R. Audebert, and C. Quivorom, *Isr. J. Chem.*, **15**, 69c (1977).
(6) J. Gaál and J. Inczédy, *Talanta*, **23**, 78 (1976).
(7) G. H. Searle, *Aust. J. Chem.*, **30**, 2625 (1977).
(8) H. Nakazawa and H. Yoneda, *J. Chromatogr.*, **160**, 89 (1978).
(9) V. A. Davankov and A. V. Semechkin, *J. Chromatogr.*, **141**, 313–353 (1977).
(10) H. Wenker, *J. Am. Chem. Soc.*, **57**, 2328 (1935).
(11) L. B. Clapp, *J. Am. Chem. Soc.*, **70**, 184 (1948).
(12) F. Vasileva, O. Y. Laurova, N. M. Dyatlova, and V. G. Yashunskii, *Zh. Obsheh. Khim.*, **36**, 724 (1966)
(13) E. Bayer, E. Grom, B. Kaltenegger, and H. Uhmann, *Anal. Chem.*, **48**, 1106 (1976).
(14) A. Wehrli, J. C. Hildenbrand, H. P. Keller, R. Stampfli, and R. W. Frei, *J. Chromatogr.*, **149**, 199, (1978).

RECEIVED for review November 6, 1978. Accepted December 18, 1978. The authors gratefully acknowledge the National Science Foundation for support of this work. Contribution #55 from the Institute of Chemical Analysis.

Effect of Oxygen on Composition of Light Hydrocarbons Evolved in Oil Shale Pyrolysis

Mark V. Robillard, Sidney Siggia, and Peter C. Uden*

Department of Chemistry, GRC Tower I, University of Massachusetts, Amherst, Massachusetts 01003

The changes in the absolute and relative levels of light alkane and alkene hydrocarbons evolved during the thermal degradation of oil shale have been studied with respect to pyrolysis atmosphere for milligram samples. Programmed temperature gas–solid chromatography on Spherocarb carbon molecular sieve gives effective resolution of alkane–alkene pairs up to the C_5 compounds. *n*-Alkane formation is favored over that of 1-alkenes under inert pyrolysis, but the alkane/alkene ratios decrease as the atmospheric oxygen content is raised to the 10% level. Thereafter they change relatively little up to 20% oxygen atmosphere. Absolute amounts of alkanes evolved increase up to a 5% oxygen level as do those of alkenes, which however exhibit the effect to a considerably greater degree. Absolute amounts of all the light hydrocarbon gases evolved decrease markedly above the 5% oxygen level.

The continually increasing efforts to discover and develop alternative energy sources have led to a renewed interest in the world's oil shale deposits as potential alternatives to crude oil resources. In the United States, the Green River oil shale deposits have been estimated to contain the equivalent of 600 billion barrels of obtainable oil in high grade deposits (*1*), this being the equal of all presently known United States crude oil reserves.

The major organic component of oil shale is known as kerogen and comprises up to 15/20% by weight of the shale. It is a macromolecular organic material bound to the inorganic shale matrix and is not extractable by organic solvents. When oil shale is heated to 500–550 °C, degradation of the kerogen occurs, releasing smaller organic molecules. These organic vapors are collected and condensed as shale oil, this being the basis for the process known as "retorting".

The possibilities for using shale oil as a fuel material are real; however, its potential as a petrochemical feedstock is equally important. Shale oil has a large hetero-atom content as well as high olefinic and aromatic character; this greater variety of organic constituents of differing functionality may be a positive feature with regard to feedstock possibilities. If oil shale is to be used thus, the question arises whether the retorting process is a viable means to produce commercially useful petrochemicals. It has now been reported that oil shale that is retorted by the entrained-solids method permits control of the composition as well as of the quantity of volatile products (*2*). It has also been found that the rate at which oil shale is heated affects the nature of the oil produced (*3*); the slower the heating rate, the higher the paraffin and the lower in olefin content the shale oil becomes. Slower heating also results in increased naphtha and light distillates. Variations in retorting temperature result in changes in the amount of oil produced, the boiling range of the oil, and its chemical character (*4*).

The major retorting parameters that can affect the composition of shale oil are: shale particle size, retorting temperature and heating rate, the velocity of the flue gases, and the retorting atmosphere (*3*), but the effect of the latter has been the subject of little investigation. From the petrochemical point of view, the ability to control the character of the oil during the retorting process by means of temperature and atmosphere is an important concept; by allowing a controlled stream of air to enter the retort system, it may prove possible to effect changes in the quantity and character of the resulting shale oil.

Interest has arisen recently in the determination of alkane/alkene ratios of hydrocarbons present in shale oil. The ratio of 1-alkene to the *n*-alkane at the same carbon number has been correlated linearly with the percent oil yield of the oil shale (*5*). Also the ratios of acetylene and methane to ethylene generated have been employed in the characterization of oil shale (*6*). Through observation of changes in alkane/alkene ratios, it may be possible to determine the effect of variations in the amount of oxygen in the shale pyrolysis atmosphere on the overall character of the resulting oil. The effect on the light hydrocarbon gases (C_1–C_5) released on pyrolysis of oil shale is discussed in this paper.

The gas chromatographic analysis of such gases has been a challenging problem. Many liquid stationary phases and adsorbing media have been tried without total success. The use of complex substrate mixtures and extensive treatment

0003-2700/79/0351-0435$01.00/0 © 1979 American Chemical Society

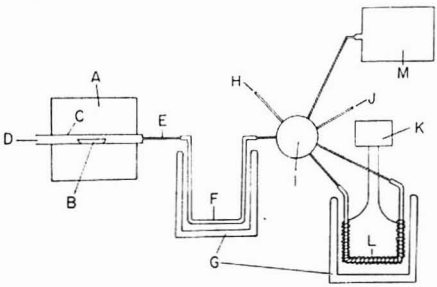


Figure 1. System used for the pyrolysis of oil shale and the analysis of the evolved hydrocarbons: (A) MP-3 pyrolysis furnace, (B) sample in quartz boat, (C) $^1/_4$-inch quartz pyrolysis tube, (D) pyrolysis atmosphere, (E) $^1/_{16}$-inch stainless steel transfer line, (F) $^1/_8$-inch stainless steel trap at 0 °C, (G) Dewars, (H) vent, (I) Valco switching valve, (J) helium backflush, (K) trap heater, (L) $^1/_8$-inch stainless steel Porapak Q trap at −196 °C, (M) Varian 2760 gas chromatograph with 4 ft × $^1/_8$ inch Spherocarb column

of solid supports, as well as application of multiple columns, has often proved laborious and difficult. Gas–liquid chromatography is generally unsatisfactory due to the wide range of component boiling points encountered and the subambient temperatures needed to gain adequate separations. Both pure and modified alumina and silica substrates have been tried, but their main problem is their affinity for water, which ultimately results in changing retention times for hydrocarbons. *n*-Octane bonded Poracil C has been employed but it suffers from similar drawbacks. Porous polymer substrates have shown reasonable success, in that separations can be accomplished above 50 °C, but complete resolution of the alkane and alkene is not always obtained. Guiochon (*7*) and DiCorcia (*8*) have employed graphitized carbon black supports, modified with various liquid phases with good success.

In the study now described, short columns of unmodified Spherocarb, (Analabs Inc., North Haven, Conn.) a carbon molecular sieve, have been used for the separation and resolution of light alkane and alkene hydrocarbon gases utilizing temperature programming to 400 °C. The ease and reproducibility of column packing with this material has made this analysis simple and efficient.

EXPERIMENTAL

Oil Shale. Green River oil shale (SGR-1 grade) obtained from the Oil Shale Corporation (TOSCO) was used throughout the analysis. The partial elemental composition of the shale used was approximately: carbon (total) 28%, hydrogen 3.3%, nitrogen 0.9%, and sulfur 1.0%. Samples were prepared by crushing and sieving several gram-size pieces, collecting only the 20/40 mesh material; this was then further crushed and sieved to a final mesh size of 80/100. Milligram range samples were weighed by microbalance into small quartz boats for pyrolysis.

Pyrolysis. An MP-3 Thermal Chromatograph (Spex Industries, Inc., Metuchen, N.J.) (*9*) was used for oil shale pyrolysis. Small quartz boats containing the shale were placed in the quartz tube furnace, purged for 5 min under the test atmosphere and then heated from ambient to 600 °C at 40 °C per minute. The gas stream atmosphere flowing over the sample was varied from sample to sample from pure helium to air (ca. 20% oxygen) by means of a constant flow gas metering system. Various flows of air and helium were combined to give the desired level of oxygen and an overall final flow rate of 30 mL/min.

The products from pyrolysis were swept to a trapping system through a $^1/_{16}$-inch stainless steel transfer line maintained at 300 °C. The trapping system consisted of a 12 inch × $^1/_8$ inch empty stainless steel tube held at 0 °C whose purpose was to trap all of the higher boiling components and allow only lower boiling gases to continue to a second trap; this consisted of a similar tube packed

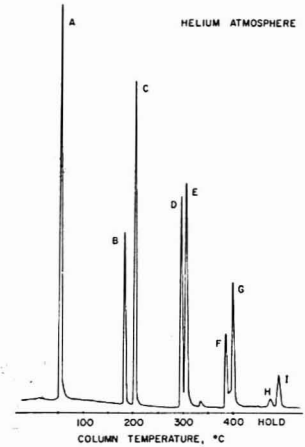


Figure 2. Chromatogram of the light hydrocarbon gases pyrolytically released from oil shale under an inert helium atmosphere: (A) methane, (B) ethene, (C) ethane, (D) propene, (E) propane (F) 1-butene (G) *n*-butane, (H) 1-pentene, (I) *n*-pentane. Conditions: 4 ft × $^1/_8$ inch stainless steel Spherocarb column. Flow; 55 mL/min helium. Temperature program; 50–400 °C @ 20 °C/min

with 80/100 mesh Porapak Q (Waters Associates) held at liquid nitrogen temperature. The latter trap has been found to retain methane for more than 30 min under the noted conditions. A block diagram of the system is depicted in Figure 1.

Gas Chromatography. After pyrolysis was completed, the Porapak Q trap was heated to 150 °C and the light gases backflushed to a Varian 2760 gas chromatograph equipped with flame ionization detection. Helium was used as backflush and carrier gas at a flow rate of 55 mL/min. The gas chromatographic column consisted of 4 ft × $^1/_8$ inch stainless steel packed with 80/100 mesh Spherocarb and was maintained at 50 °C until the methane eluted. The oven was then programmed to 400 °C at 20 °C/min and held until pentane eluted.

Another quartz tube pyrolysis unit was constructed in similar fashion to the MP-3 unit, utilizing Valco high temperature valves and a pyrolysis furnace temperature programmer (PC 6011, Valley Forge Instrument Co., Inc., Phoenixville, Pa.). This unit could be interfaced to a GC-Vapor Phase Infrared (GC-VIPR) system consisting of a Varian 2760 gas chromatograph and a Norcon 201 vapor phase infrared spectrophotometer (Norcon Instrument Co., South Norwalk, Conn.) (*9*).

The total amount of hydrocarbons released per gram of oil shale was determined by injecting and trapping known volumes of standardized hydrocarbon mixtures (Supelco, Inc.) utilizing a gas tight microsyringe. Narrow symmetrical peaks enabled peak height to be used as a basis for quantitation.

RESULTS AND DISCUSSION

Chromatograms of the light hydrocarbon gases released pyrolytically from oil shale under atmospheres containing pure helium and 10% oxygen in helium are shown in Figures 2 and 3, respectively. At each carbon number from 2 to 5, the peak attributable to the 1-alkene is fully or almost completely resolved from the *n*-alkane eluting before it. Under the conditions of inert pyrolysis, the *n*-alkane is seen to be the predominant species at each carbon number. However, as the oxygen content of the pyrolysis atmosphere is increased, the alkene to alkane ratio increases, most notably for the ethene–ethane and propene–propane pairs. In addition, as oxygen content increases, other small component peaks become evident indicating a greater degree of fragmentation to be occurring under oxidative conditions. This tendency is also

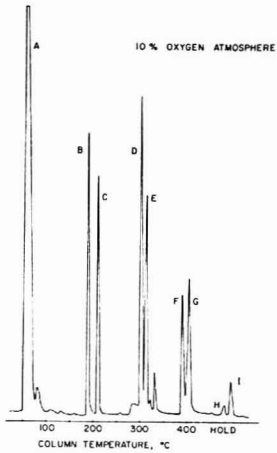


Figure 3. Chromatogram of the light hydrocarbon gases pyrolytically released from oil shale under a 10% oxygen atmosphere. Peaks and conditions as in Figure 2

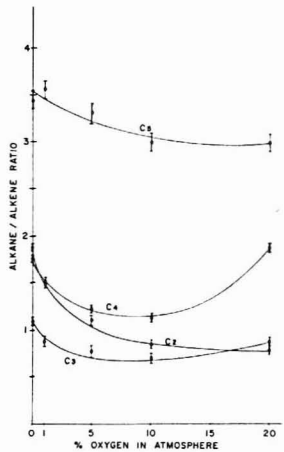


Figure 4. Plot of alkane/alkene ratios for carbon numbers C_2 through C_5 released from oil shale under increasingly oxidizing pyrolysis conditions

substantiated by a corresponding relative increase in methane production as is seen in Figure 3. Figure 4 shows alkane/alkene ratios for carbon numbers 2 through 5 as a function of the percent oxygen in the pyrolysis atmosphere; data were obtained from peak height measurements and showed a relative standard deviation of approximately 3%. Each ratio favors the alkane under inert pyrolysis conditions. The effect of small proportions of oxygen is to cause an immediate decrease in the alkane/alkene ratios. These ratios continue to decrease as the level of oxygen in the pyrolysis atmosphere increases, to about the 10% level. Atmospheres containing oxygen levels above 10% have little further effect on the alkane/alkene ratios for some pairs or appear to cause slight reversals of the alkane/alkene ratio trend for other pairs.

A quantitative study of absolute amounts of alkane and alkene produced was then undertaken to determine what

Table I. Total Micrograms of (a) Alkane and (b) Alkene Produced per Gram of Oil Shale under Increasingly Oxidizing Pyrolysis Conditions

(a) Micrograms of Alkane Produced per Gram of Oil Shale

carbon #	He	1% O_2	5% O_2	10% O_2	20% O_2
C_1	1030	1500	1220	2420	3150
C_2	815	858	780	510	383
C_3	568	681	702	508	453
C_4	368	440	460	338	224
C_5	26	31	36	25	26

(b) Micrograms of Alkene Produced per Gram of Oil Shale

C_2	423	513	620	531	439
C_3	522	719	828	672	475
C_4	215	309	381	310	130
C_5	53	91	106	85	5

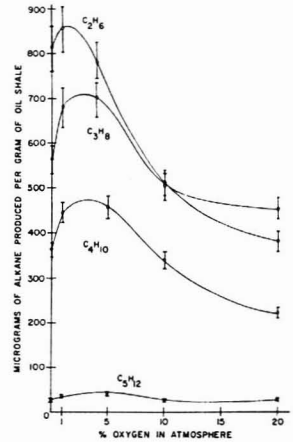


Figure 5. Plot of total micrograms of alkane produced per gram of oil shale under increasingly oxidizing conditions

changes were responsible for the variation in alkane/alkene ratios. Known volumes of a standard hydrocarbon gas mixture with components at the 100-ppm level were thus injected into the pyrolysis system without heating, trapped, and chromatographed under the same conditions as for the shale pyrolysis. The total quantities of hydrocarbons produced under the various atmospheres were then determined from the standard curves, the results being given in Table I. The quantity of alkane from ethane to pentane increased on the average 20–30% as the pyrolysis oxygen content was raised to 1 to 5%. Above 5% oxygen, the absolute quantities of alkane produced decreased significantly and at 20% oxygen levels, less alkane was invariably produced than under the inert conditions. A similar trend is observed for the alkenes, except that the relative increase in amounts of alkene produced are much greater than seen for the alkanes. This factor accounts for the initial trend in the alkane/alkene ratios. Again, above 5% oxygen atmosphere levels, the amounts of alkene produced begin to decrease until at the 20% oxygen level, less alkenes are generally produced than under the inert conditions. The trends in total quantities of C_2–C_5 hydrocarbons produced are indicated in Figure 5 for the alkanes and in Figure 6 for the alkenes with appropriate precision ranges being indicated.

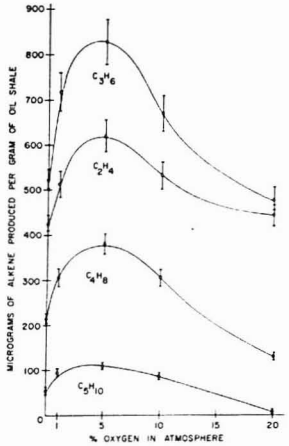


Figure 6. Plot of total micrograms of alkene produced per gram of oil shale under increasingly oxidizing conditions

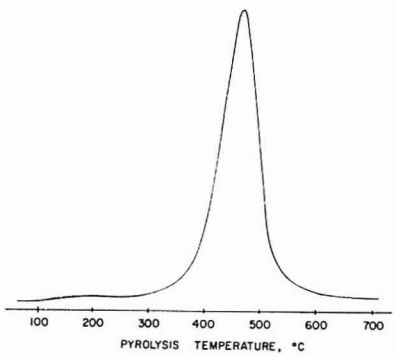


Figure 7. Flame ionization detection thermogram of the organics pyrolytically released from oil shale under an inert helium atmosphere

The temperature range over which evolution of organics took place under different atmospheres was then investigated. In this study, all of the evolved pyrolysis products were passed into a flame ionization detector without prior separation as they were continually released from the oil shale. A typical resulting evolution thermogram is shown in Figure 7 for pyrolysis in the absence of oxygen. The integrated flame response which indicates the amount of organic material being produced under the helium atmosphere shows maximum release rate at around 465 °C. As the level of oxygen in the pyrolysis atmosphere was increased, the temperature at which maximum organic evolution took place decreased to around 330 °C for pyrolysis in air (20%, oxygen). The total integrated area under the evolution thermogram also decreased continually with increased oxygen level showing again that diminishing amounts of organics were being produced.

It should be noted that with regard to the temperatures quoted, the actual surface temperature at which reaction occurs may differ considerably because of surface reaction and could be markedly higher than those noted.

Further evidence of the change in pyrolysis products with atmosphere, both quantitatively and qualitatively, was obtained by vapor phase infrared spectral monitoring of the evolution thermogram. Clear evidence was found for the presence of carbon dioxide and water for pyrolysis in the presence of higher proportions of oxygen, throughout the evolution profile. These were not observed below 500 °C under inert gas pyrolysis conditions. This indicates that partial combustion of organics is occurring during pyrolysis explaining the decrease in both alkanes and alkenes found at higher oxygen levels.

It might be expected that for gas phase oxidations, the alkenes would have reacted at faster rates than the alkanes; as this was not seen experimentally, it is likely that the oxidation reactions occur as surface–gas phase processes coupled into the kerogen degradation processes.

CONCLUSIONS

The light hydrocarbon gases evolved upon oil shale pyrolysis may be readily resolved with respect to alkane and alkene content by gas–solid chromatography on packed Spherocarb carbon molecular sieve columns. Hydrocarbons as high as five and six carbon species may be quantitatively separated in this mode with good precision, and both changes in ratios and absolute amounts evolved measured with changes in the oxygen content of the pyrolysis atmosphere. The effect of oxygen is manifested in three different ways with regard to the nature of the pyrolytic release of light gases. The relative proportion of alkene to alkane for a given number increases with atmospheric oxygen content to around the 10% O_2 level but thereafter remains fairly constant or may decrease in some cases. The total quantity of light hydrocarbons released increases significantly under slightly oxidizing conditions but decreases above the 10% level as combustion becomes significant. Parallel evidence exists for the increased fragmentation of kerogen in the presence of oxygen, to give more methane and possibly other small nonhydrocarbon molecules. Thirdly, an effect of oxygen is to lower the temperature at which the maximum level of organic gas evolution occurs.

This observation may represent another thermal effect, namely that gas yields are strongly dependent upon heating rate. The higher oxygen levels will result in higher surface temperatures due to oxidative kinetics. Separate analysis for carbon monoxide and carbon dioxide levels would aid in elucidating these effects further.

While it must be noted that the pyrolysis system used in this study may not replicate conditions present in a large scale retorting process, particularly as regards particle size and atmospheric gas velocities, it has been shown (*10*) that, in general, gas chromatographic profiles of shale oil produced in this pyrolysis system are closely similar to those for commercial samples. The reproducibility gained in this study and the general effects noted do serve to indicate trends in the content of shale light gases as pyrolysis atmospheres are varied. Further details of these changes are under present investigation, notably with regard to changes in the composition of liquid oil fractions.

LITERATURE CITED

(1) S. Siggia and P. C. Uden, Ed., "Analytical Chemistry Pertaining to Oil Shale and Shale Oil", Report of a Conference Workshop of the National Science Foundation, Washington, D.C., June 24–25, 1974.
(2) H. W. Sohns, E. E. Jokkola, R. J. Fox, F. E. Brantley, W. G. Collins, and W. I. R. Murphy, *Ind. Eng. Chem.*, **47**, 461 (1955).
(3) H. B. Jensen, R. E. Poulson, and G. L. Cook, *Prepr. Div. Fuel Chem., Am. Chem. Soc.*, **15**(1), (1971)
(4) S. S. Thien, J. F. Brown, H. B. Jensen, P. R. Tisot, N. M. Melton, and W. I. R. Murphy, *Ind. Eng. Chem.*, **47**, 464 (1955).
(5) T. T. Cobern, R. E. Bozak, J. E. Clarkson, and J. H. Campbell, *Anal. Chem.*, **50**, 958 (1978).
(6) R. L. Hanson, D. Brookins, and N. E. Vanderborgh, *Anal. Chem.*, **48**, 2210 (1976).
(7) C. Vidal-Madjar, S. Bekassy, M. F. Gonnord, P. Arpino, and G. Guiochon, *Anal. Chem.*, **49**, 768 (1977).
(8) A. DiCorcia and R. Samperi, *J. Chromatogr.*, **107**, 99 (1975).
(9) P. C. Uden, D. E. Henderson, and R. J. Lloyd, *J. Chromatogr.*, **126**, 225 (1976).

(10) F. P. DiSanzo, M. V. Robillard, S. Siggia, and P. C. Uden, unpublished observations.

RECEIVED for review October 25, 1978. Accepted January 2, 1979. This work was supported by the National Science Foundation through grant CHE74-15244, and through Research Instrument grant GP 42542 to the University of Massachusetts.

Membrane-Covered, Rotated Disc Electrode

David A. Gough* and John K. Leypoldt

Department of Applied Mechanics and Engineering Sciences, Bioengineering Group, University of California at San Diego, La Jolla, California 92093

A rotated disc electrode that can be used to evaluate mass transport in membranes is described. In this design, both a disc electrode and reference electrode are mounted in a rotating shaft over which the membrane is placed. A transport model is given for solutes that diffuse through the membrane and undergo simple reaction at the electrode surface. With membrane in place, the diffusion current at low rotation rates approaches the theoretical (Levich) current that would be seen without membrane. At high rotation rates, however, the current is dependent on membrane permeability.

In recent years, there has been a growing interest in the development of chemical-specific electrodes for monitoring chemical concentrations (*1-4*). Sensors for a variety of chemicals have been reported, and some have reached a relatively practical state of development for certain monitoring applications (e.g., *3*, *4*). One type of electrochemical sensor that has received some attention is the amperometric electrode, in which current is produced when electrochemically active species react at the electrode surface. In this type of sensor, selectivity for the chemical of interest is promoted by operating at a particular electrode potential (*5*) and by placing a semipermeable membrane between the electrode surface and the sample. In addition, immobilized catalysts can be incorporated in the membrane to extend the range of chemicals that can be monitored. In this way, certain chemicals for which selectivity is not readily obtainable on the basis of transport or electrode potential alone can be converted to other measurable species (*6*). A variety of potentially useful sensors based on these electrode designs is conceivable.

However, the amperometric-type sensor has had relatively limited application in biochemical monitoring situations because of an inadequate understanding of the complex physicochemical phenomena involved in its operation. An example is the lack of information about the electrochemical reaction. The mechanisms of reaction of most organics at solid electrodes have not been thoroughly studied. These processes at the electrode surface may include: formation of multiple intermediates, adsorption and electrode poisoning, electrochemical reactions in which the number of electrons exchanged is variable, or competitive reactions of other biochemicals that are not completely excluded by the membrane (*5*). Mass transfer is another example. Chemical transport in the external medium to the membrane surface must be quantitatively defined. The membrane must be designed to provide selectivity for the biochemical of interest and an acceptable response time. For diffusants that saturate the electrode surface, membrane permeability must necessarily be limited in order to promote linearity of the current with concentration. Additionally, for sensors with catalytically active membranes, account must be taken of such properties as kinetics, catalyst loading, and catalyst inactivation.

A rotated disc electrode on which a membrane could be mounted would offer some unique advantages for sensor development. With such an electrode, a well-defined transport regime could be established that would be analogous to that of the classical rotated disc electrode first described by Levich (*7*), in which the disc surface is uniformly accessible to reactant and the diffusion boundary layer thickness precisely determined. At low rotation rates, the diffusion boundary layer would be relatively large, so that transport through solution would be a major contribution to total diffusional resistance. Under such conditions, the current would be proportional to the square root of rotation rate. At high rotation rates, however, where the diffusion boundary layer would be small, the resistance of the solution would be negligible making the diffusion current independent of rotation rate and determined by the properties of the membrane. Thus, transport in the membrane could be evaluated quantitatively without complications of external mass transfer. This feature would be particularly useful where the membrane is permeable enough to the solute that transport in membrane is comparable to transport in solution, or where carefully defined conditions are essential for distinguishing the effects of diffusion from chemical reaction in catalyst-containing membranes. This electrode could therefore be used for characterization of membranes that are to be used in nonrotating sensors or, as appropriate, employed directly as a sensor in the rotated configuration.

Two previous investigations with a membrane-covered, rotated disc electrode have been reported. Chien, Olson, and Sokoloski (*8*) employed fixed potential voltammetry and a carbon rotated disc electrode with a Millipore VC membrane to qualitatively study transport of *p*-nitrophenol. The other electrode was a stationary combination reference/counter electrode. These investigators found that, at steady state, the limiting current was approximately linear with the square root of rotation rate at low rotation rates (although unexplainedly lower than the Levich current), and independent of rotation rate at high rotation rates. No theoretical treatment was proposed to describe the effect of rotation rate on current. Determinations of membrane permeability were made at high rotation rate by injecting a known amount of the reactant and measuring the time to establish a new steady state. In a subsequent publication by the same authors (*9*), this system was used to determine the relative concentrations of bound

0003-2700/79/0351-0439$01.00/0 © 1979 American Chemical Society

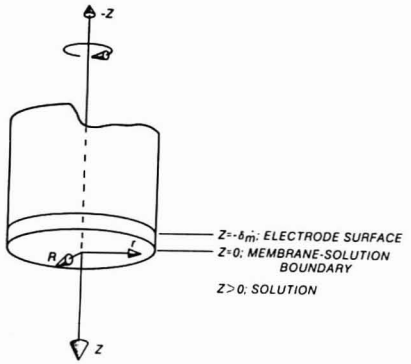


Figure 1. Coordinate system for mass transfer to a rotated, membrane-covered disc

and unbound drug in studies on drug interaction with macromolecules.

We are employing a similar type of rotated disc electrode to characterize transport in new membranes that may eventually be used in biochemical-specific sensors. In this communication, we discuss the construction of this novel electrode system and demonstrate its application to evaluate permeability of certain commercial hydrophilic membranes using solutes that undergo an uncomplicated reaction at the electrode surface. We develop an analytical model for this system and compare its predictions with experimental results. This limited study provides a basis for future work employing solutes of physiological significance and new membranes.

THEORETICAL

We consider steady-state mass transfer of a solute that is consumed quantitatively at the surface of the disc electrode. As shown in Figure 1, the disc is covered by a homogeneous gel membrane of thickness δ_m and rotated at a steady angular frequency ω. The radius R of the disc is large compared to the diffusion boundary layer so that edge effects can be neglected and only variations of chemical concentration in the Z-direction need be considered. The liquid-filled space between the membrane and the electrode surface is assumed negligible. Employing a coordinate system similar to that of Levich (7), we let $Z = 0$ at the membrane-solution boundary with Z positive in the downward direction. Assuming no convective flow within the membrane, the diffusion equation is

$$\frac{d^2C_m}{dZ^2} = 0 \qquad -\delta_m \le Z \le 0 \tag{1}$$

where C_m is the solute concentration in the membrane. In the solution, the convective diffusion equation is

$$v_z(Z)\frac{dC}{dZ} = D\frac{d^2C}{dZ^2} \qquad 0 \le Z < \infty \tag{2}$$

where C is the solute concentration, D is the diffusion coefficient in solution, and $v_z(Z)$ is the fluid velocity in the Z-direction. Far from the disc, the concentration of the reacting solute equals the bulk solute concentration C_B

$$C = C_B \qquad \text{as } Z \to \infty \tag{3}$$

and in the limit of complete diffusion control, the concentration at the electrode surface is zero

$$C = 0 \qquad \text{at } Z = -\delta_m \tag{4}$$

Conservation of mass at the membrane–solution interface requires

$$D_m\left(\frac{dC_m}{dZ}\right) = D\left(\frac{dC}{dZ}\right) \qquad \text{at } Z = 0 \tag{5}$$

where D_m is the molecular diffusion coefficient within the membrane. A partition coefficient α is defined as the equilibrium ratio at the membrane–solution interface of solute concentration in the membrane divided by concentration in solution. Thus,

$$\frac{C_m}{C} = \alpha \qquad \text{at } Z = 0 \tag{6}$$

We assume both D_m and α to be constants. Integration of Equations 1 and 2 in their respective domains analogously to the method of Levich (7), and evaluation of the integration constants by the boundary conditions given in Equations 3 through 6 yield the following concentration profiles

$$C_m(Z) = \frac{DC_B}{D_m\delta_d}\left[\frac{Z + \delta_m}{1 + \dfrac{D\delta_m}{\alpha D_m\delta_d}}\right] \tag{7}$$

and

$$C(Z) = C_B\left\{\frac{1}{\delta_d}\left[\frac{1}{1 + \dfrac{D\delta_m}{\alpha D_m\delta_d}}\right]\int_0^Z \exp\left[\frac{1}{D}\int_0^\xi v_z(u)du\right]d\xi + \frac{1}{1 + \dfrac{\alpha D_m\delta_d}{\delta_m D}}\right\} \tag{8}$$

where δ_d is the thickness of the diffusion boundary layer

$$\delta_d = 1.6\, D^{1/3}\nu^{1/6}\omega^{-1/2} \tag{9}$$

with kinematic viscosity ν, and $v_z(Z)$ is obtained from the solution of the hydrodynamic problem (7). A first approximation of $v_z(Z)$ used in the evaluation of the constants from the boundary conditions is

$$v_z(Z) \simeq -0.51\,\omega^{3/2}\nu^{-1/6}Z^2 \tag{10}$$

The resulting diffusion current i_d can then be obtained

$$i_d = n\mathcal{F}\pi R^2 D_m\left(\frac{\partial C}{\partial Z}\right)_{Z=-\delta_m} = i_L\left[\frac{1}{1 + \dfrac{P_s}{P_m}}\right] \tag{11}$$

where n is the number of electrons transferred, $\mathcal{F}$ is the Faraday constant, i_L the current in the absence of a membrane as described by Levich (7)

$$i_L = 0.62n\mathcal{F}\pi R^2 D^{2/3}\nu^{-1/6}\omega^{1/2}C_B \tag{12}$$

and P_m and P_s are, respectively, the permeability of the membrane and solution,

$$P_m = \frac{\alpha D_m}{\delta_m} \tag{13}$$

$$P_s = \frac{D}{\delta_d} \tag{14}$$

The solution permeability is here well defined and is directly amenable to experimental manipulation by varying the rotation rate.

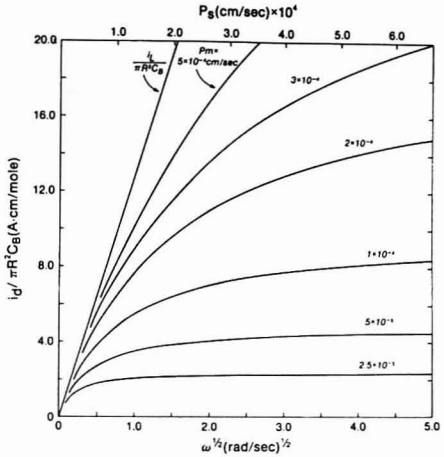


Figure 2. Predicted effects of mixed membrane and solution transport control with representative values for P_s and P_m. Current density normalized by concentration is plotted as a function of rotation rate. The values used in this figure are: $D = 1 \times 10^{-6}$cm^2/s, $\nu = 1 \times 10^{-2}$cm^2/s, $n = 1$, and P_m as shown. $i_L/\pi R^2 C_B$ is the normalized current density without membrane

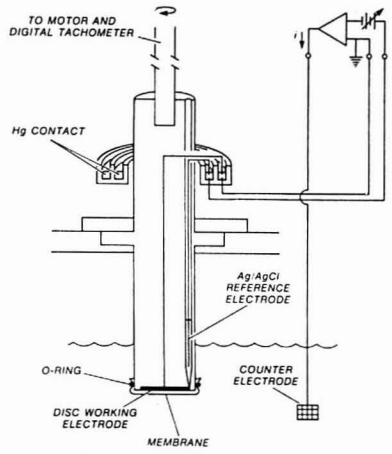


Figure 3. Design schematic of a membrane-covered, rotated disc electrode

The anticipated effects of mixed membrane and solution transport control are shown in Figure 2. Here, the diffusion current density normalized by bulk concentration is given as a function of representative values for membrane permeability, solution permeability, and rotation rate. The normalized Levich current is linear with rotation rate and solution permeability. Membranes with different representative permeabilities are expected to demonstrate characteristic effects. At sufficiently low rotation rates such that $P_s/P_m \ll 1$, the diffusion current approaches the Levich current and in the limit the system is in solution transport control

$$\lim_{\omega^{1/2}\to 0} i_d = i_L \tag{15}$$

However, at high rotation rates where $P_s/P_m >> 1$, the current becomes limited by membrane permeability and

$$\lim_{\omega^{1/2}\to \infty} i_d = n\mathcal{F}\pi R^2 P_m C_B \tag{16}$$

This effect becomes more apparent with decreasing membrane permeability as shown in Figure 2. Thus, a possible explanation might be afforded for the observation previously reported in the literature (*8*) of the effect of rotation rate on current density: slight inaccuracy in the measurement of diffusion current might lead to the incorrect conclusion that the current density is linear with rotation rate at low rotation rates but proportionally lower than the Levich current.

It should be emphasized that, in this derivation, membrane permeability appears only as a function of the product of the partition coefficient and the diffusion coefficient in the membrane, and that these two latter properties represent different mechanisms of transport control by the membrane. Nevertheless, if the partition coefficient can be determined by an independent measurement, the diffusion coefficient in the membrane can be found.

ELECTRODE DESIGN

It may be difficult in practice to demonstrate these theoretical predictions because of certain technical considerations. For example: when employing conventional electrochemical instrumentation with the standard three-electrode configuration, the potential of the disc working electrode is usually determined by a Luggin capillary, located very close to the electrode surface to minimize iR drop in solution (*10*). With a hydrophilic membrane placed over the disc electrode, potential determinations would be of questionable accuracy because of possible iR drop in the membrane and accurate conpensation would be difficult. For membranes of substantial electrical resistivity, reliable measurement by such an arrangement would be impossible.

This objection could be resolved by mounting both the disc and reference electrodes behind the membrane on the rotating shaft. This configuration would eliminate iR drop through the membrane, and any remaining iR drop in the thin layer of solution between the membrane and the electrode surface could be reduced by using high conductivity electrolyte or could be compensated by conventional methods. The compliance voltage of the counter electrode would be sufficient to pass current through membranes of low and moderate electrical resistivity. Distribution of the current between the disc working electrode and the external counter electrode could be made symmetrical by using high conductivity background electrolyte and properly positioning the counter electrode far enough away from the membrane. Thus, the membrane-covered disc electrode would be uniformly accessible to both reactant and background electrolyte, thereby ensuring a uniform potential distribution across the disc. This arrangement requires an independent measurement of membrane conductivity and the assurance that membrane resistance is always lower to electrolyte flux than to reactant transport.

We have constructed a new electrode system incorporating these features. As shown schematically in Figure 3, the working disc electrode and an internal silver–silver chloride reference electrode (ISSCE) are mounted in the rotated shaft over which the membrane is placed. The liquid junction of the reference electrode is a small opening in the inactive region of the disc near the edge of the working electrode. A background electrolyte of sufficiently high conductivity is used and the counter electrode can be positioned as appropriate for symmetrical current distribution. In this configuration, noise-free electrical contact established through mercury pools

is essential for maintenance of a stable reference electrode.

EXPERIMENTAL

Electrode Construction. The electrode body was precision machined from a 1.9-cm diameter Lucite rod. A disc electrode of 0.80-cm diameter was machined from 0.5-mm thick platinum plate (Engelhard Industries, Los Angeles, Calif.). A length of platinum wire was spot welded to the center of the disc, passed through the central cavity of the electrode body, and attached to the ring fixture described below for electrical contact. The disc and wire were cemented into the electrode body, and the disc surface was polished to a mirror finish. The reference electrode was a chlorided silver wire with saturated KCl as the internal electrolyte. A linen fiber was inserted at the liquid junction of the reference electrode to minimize the rate of convective outflow of electrolyte.

A two-piece fixture was designed for the electrical contact. The lower, immobile piece contained two concentric channels with a precision-fitted stainless steel ring cemented into the bottom of each channel, and a wire from the back of the rings for connection to the potentiostat. A small volume of mercury was placed in each channel. The upper piece, which was fastened to the rotated shaft, contained two protruding stainless steel rings, each connected from above to the respective electrode and mated into the channels below. The shaft was fitted with Teflon bearings and mounted, together with the electrical contact fixture, onto the vessel lid. The electrode could be rotated freely while maintaining uninterrupted electrical contact.

Apparatus. The shaft was coupled directly to a model M-062 stepper motor (Minarik Corp., Los Angeles, Calif.), and rotation rate was controlled by a corresponding model TBM regulator of the same manufacturer that had been modified to allow continuously variable rotation rate from 0 to 3000 rev/min as dictated by a voltage input. Rotation rate was monitored by a digital tachometer of our own construction employing a photo transistor sensor, and was found to be precisely maintainable over the entire range.

Voltammetric measurements were made with a model 173/178 potentiostat (Princeton Applied Research Corp., Princeton, N.J.). Other equipment included a model 176 programmer (Princeton Applied Research), a model ABA-26 slow sweep generator (Elsinct Ltd., Haifa, Israel) for producing linear voltage sweep, and an X-Y recorder (Hewlett-Packard, Palo Alto, Calif.). The sealed vessel was thermostated to 30 ± 0.5 °C and equilibrated with prepurified nitrogen gas. The two different background electrolyte solutions used in this study were 1 N KCl in 10^{-2} M sodium phosphate buffer, pH 7.3, and 1 N NaOH. Solutions were prepared fresh daily from analyzed reagent grade chemicals and double distilled water.

A special conductivity cell was constructed for estimation of ionic resistance in the membrane. Two rectangular platinum plate electrodes, each of 0.5 cm^2 geometric area were spot welded to respective platinum leads, and each lead was sealed into the end of a 1-cm diameter glass tube. Two pieces of such tubing were joined through a ball and socket, ground glass joint in which the membrane could be clamped. The electrodes were platinized and provision made for filling the cell.

Membrane. Bemberg Cuprophane PT-150 was used in this study. This is a regenerated cellulosic membrane that contains about 65 vol % water at equilibrium. Other properties have been reported elsewhere (*14*). Membranes were discarded after 1-h use to minimize any effects of possible membrane degradation in the alkaline electrolyte.

Procedure. The electrode surface was prepared prior to each day's experiment by 10 to 20 repeated cyclic polarizations in 1 N H_2SO_4 until a reproducible scan was obtained. The membrane was equilibrated in the background electrolyte and held in place taut across the disc surface with an O-ring. The limiting current was recorded at individual rotation rates, allowing adequate time after adjusting the rotation rate to attain steady state. The partition coefficient for $Fe(CN)_6^{3-}/Fe(CN)_6^{4-}$ in Cuprophane was estimated by equilibrating a 30-inch square piece of membrane in background electrolyte solutions that contained 10^{-2} M of each salt, then superficially drying to remove excess solution from the surface, and transferring into exactly 50 mL of the solute-free electrolyte solution. After reequilibration the concentration was determined from the limiting current. Thickness of the wet membrane was determined to within ±0.0005 cm with a precision micrometer. Conductivity measurements of the background electrolyte were made by the conventional method (*11*) with and without the membrane in place.

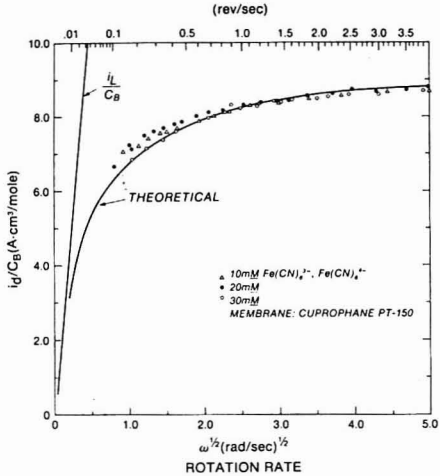


Figure 4. Normalized limiting current at a membrane-covered, rotated disc electrode. i_L/C_B is the normalized Levich current in the absence of membrane. The theoretical curve was calculated from Equation 11 using permeability data obtained in this study

RESULTS AND DISCUSSION

The $Fe(CN)_6^{3-}/Fe(CN)_6^{4-}$ couple was chosen for this study because it reacts in a simple, reversible electrochemical process and the diffusion properties in solution have been well documented (*12*, *13*). Cuprophane was used because its permeability to a variety of solutes representing a spectrum of molecular weight is known (*14*). Although the transport of $Fe(CN)_6^{3-}/Fe(CN)_6^{4-}$ in Cuprophane has not been studied, a correlation has been reported between molecular dimensions and membrane permeability that may be applicable to these solutes (*14*).

The properties of the electrode with no membrane were first studied using a Luggin capillary for the reference electrode. It was observed that at rotation rates greater than 2 rev/s the theoretical Levich current could be obtained to within 1% accuracy, with deviations becoming increasingly larger at lower rotation rates because of natural convection. The current was also recorded at much higher rotation rates and concentrations in order to reveal any possible kinetic limitation. The Levich current was obtained at all rotation rates and concentrations, confirming that the process was under complete diffusion control in the conditions of our experiment. The anticipated difference in magnitude of anodic and cathodic limiting currents due to the difference in diffusivities of ferro- and ferricyanide was also observed.

Results shown in Figure 4 were obtained with the membrane over the electrode. The data points represent the steady-state diffusion current i_d normalized by concentration for individual values of rotation rate. As predicted, the diffusion current approaches the theoretical normalized Levich current i_L/C_B at low rotation rates, and is limited by membrane at high rotation rates. It is difficult to demonstrate more definitive correlation with this membrane at low rotation rates because of natural convection. Although certain other

Table I. Mass Transfer Properties of Ferricyanide in Cuprophane ($\delta_m = 25 \times 10^{-4}$ cm, $T = 30$ °C)

electrolyte	R_m min/cm	P_m, cm/s × 10^4	α, cm³/cm³	D, cm²/s × 10^7	D_{eff}, cm²/s × 10^7	D_m, cm²/s × 10^7	D_{eff}/D
1 N NaOH	86.6	1.92	0.82	65.2 (*12*)	4.80	5.85	0.07
1 N KCl in 0.01 M sodium phosphate buffer, pH 7.3	99.7	1.67	0.74	63.2 (*13*)	4.18	5.65	0.07

commercial membranes are expected to be somewhat more permeable than Cuprophane (*14*), predictions based on Figure 2 suggest that these relatively small differences would still not permit a significant improvement in correlation at low rotation rates. The effect had a linear concentration dependence over the concentration range studied. The theoretical curve was calculated using Equation 11, with membrane permeability obtained as follows. The membrane molecular resistance R_m was taken from plots of C_B/i_L vs. $1/\omega^{1/2}$ as the intercept at $1/\omega^{1/2} = 0$. The membrane permeability and D_{eff}, the effective diffusion coefficient within the membrane, were calculated from the formula

$$1/R_m = P_m = D_{eff}/\delta_m \quad (17)$$

With a value for the partition coefficient obtained from an independent measurement, the true diffusion coefficient within the membrane was estimated from the relation

$$D_{eff} = \alpha D_m \quad (18)$$

Experimentally obtained values for these parameters are summarized in Table I. The method used here for determination of α may, in principle, be subject to relatively large experimental error. Thus, the values reported for α and D_m, while reasonable, must be considered as only approximate. Previous studies (*14*) based on solutes of comparable molecular dimensions suggest an anticipated value of 0.07 to 0.09 for the ratio D_{eff}/D. The agreement of our data suggests that no significant artifacts were introduced by either the membrane mounting procedure or possible membrane degradation in the alkaline solution.

Although we have studied a number of commercial hydrophilic membranes by this technique, the permeability of most has not been adequately characterized by conventional methods to allow confident comparison of results. Nevertheless, in every case, the limiting current showed the characteristic response with rotation rate, and membrane permeability for these solutes was readily obtainable. It should be noted that relative membrane permeability as judged by one solute may not reflect permeability properties in general. The latter should be estimated by employing a variety of solutes representing a range of molecular sizes.

Some important technical points must be remembered when working with the membrane–electrode system. First, there may be a lag time due to diffusion in the membrane. Time must be allowed for the current to reach steady state after a change in rotation rate, concentration, or electrode potential. As an illustration, Figure 5 shows the effect of electrode scan rate on current density in the presence of membrane. In this experiment rotation rate was held constant at 3 rads/s and the electrode potential scanned linearly in one direction at successive scan rates. At the lowest scan rate, current density procedes monotonically from the anodic ferrocyanide oxidation current to the cathodic ferricyanide reduction current. This curve closely approximates the steady-state current density that would be obtained upon application of fixed, discrete electrode potentials in this potential range. With increasing scan rates, however, the current density passes through a

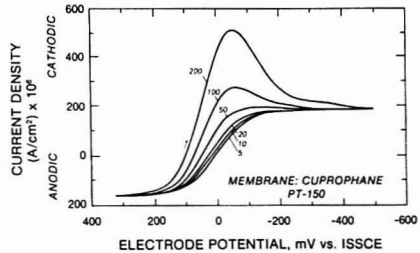


Figure 5. Effect of electrode potential scan rate on the reduction of ferricyanide at the membrane-covered, rotated disc electrode. Curves are shown for a rotation rate of 3 rads/s and scan rates of 5, 10, 20, 50, 100, and 200 mV/min. The arrow indicates the direction of scan. The solution was 10 mM $Fe(CN)_6^{3-}/Fe(CN)_6^{4-}$ in 1 N NaOH

prominent maximum before returning to the cathodic plateau. Equivalent anodic peaks can be demonstrated with linear potential scans in the opposite direction. This transient phenomenon is analogous to the familiar peaks formed with linear scan voltammetry using conventional, nonrotated electrodes. Here, the solute immediately adjacent to the electrode is vigorously consumed when the electrode potential becomes sufficiently cathodic, thus momentarily producing a high current density. As the solute in this region is depleted, the diffusion distance for subsequent reactant becomes larger and the current density falls off to the cathodic plateau value. This process occurs more rapidly with increasing scan rates resulting in greater peak current densities and, for a given scan rate, peak formation is promoted by greater diffusional resistance such as that provided by the membrane. Thus, studies done under the same conditions as in Figure 5, but without membrane, demonstrated no peaks or effect of scan rate, even at the highest scan rates. Thus, the membrane can cause dramatic time-dependent effects.

A second practical consideration that can cause considerable frustration of the investigator if ignored, is the likelihood of forming bubbles under the membrane by gas evolution. While this problem can be ameliorated by operating only at intermediate potentials, it is nevertheless significant because it may limit the use of certain electrochemical pulsing pretreatments for activation of the electrode surface (*5*).

The nature of the electrochemical reaction must also be considered. In this basic model, we have limited our treatment to simple, diffusion-limited processes, involving no intermediates or side reactions. Few solutes of analytical interest are expected to be similarly uncomplicated. For most gases and low molecular weight organics, the electrochemical processes have not yet been well defined or, where information is available, the reactions are often complex. The membrane may alter these processes in many ways, in addition to the effect on solute transport. For example, the rate of transport of intermediates or products from the electrode may be reduced. This could result in a variable number of electrons exchanged, enhanced side reactions, or electrode poisoning.

Thus, the effect of membrane on the electrochemical process must be carefully evaluated for each solute.

This study prepares the way for characterization of transport of physiologic solutes in membranes and for evaluation of the potential usefulness of new membranes for chemical-specific sensors.

ACKNOWLEDGMENT

We thank Mark Davis for technical assistance.

LITERATURE CITED

(1) R. P. Buck, *Anal. Chem.*, **48**, 23R (1976).
(2) P. J. Elving, *Bioelectrochem. Bioeng.*, **2**, 251 (1975).
(3) G. A. Rechnitz, *Science*, **190**, 234 (1975).
(4) I. Fatt, "Polarographic Oxygen Sensors", CRC Press, Cleveland, Ohio, 1976.
(5) D. A. Gough, F. L. Anderson, J. Giner, C. K. Colton, and J. S. Soeldner, *Anal. Chem.*, **50**, 941 (1978).
(6) D. A. Gough and J. D. Andrade, *Science*, **180**, 380 (1973).
(7) V. G. Levich, "Physicochemical Hydrodynamics", Prentice-Hall, Englewood Cliffs, N.J., 1962.
(8) Y. W. Chien, C. L. Olson, and T. D. Sokoloski, *J. Pharm. Sci.*, **62**, 435 (1973).
(9) Y. W. Chien, T. D. Sokoloski, C. L. Olson, D. T. Witiak, and R. Nazareth, *J. Pharm. Sci.*, **62**, 440 (1973).
(10) A. P. Delahay, "New Instrumental Methods in Electrochemistry", Interscience Publishers, New York, 1954.
(11) D. P. Shoemaker and C. W. Garland, "Experiments in Physical Chemistry", McGraw-Hill, New York, 1962.
(12) J. C. Bazan and A. J. Arvia, *Electrochim. Acta*, **10**, 1025 (1965).
(13) M. von Stackelberg, M. Pilgram, and V. Toome, *Z. Electrochem.*, **57**, 342 (1953).
(14) C. K. Colton, K. A. Smith, E. W. Merrill, and P. C. Farrell, *J. Biomed. Mater. Res.*, **5**, 459 (1971).

RECEIVED for review April 11, 1978. Resubmitted August 8, 1978. Accepted December 18, 1978. We gratefully acknowledge support from NIH grants HL-10881 and HL-22118 to B. W. Zweifach, and from the U.C.S.D. Biomedical Research Support Fund and the Academic Senate Research Fund.

Amperometric Enzymatic Determination of Total Cholesterol in Human Serum with Tubular Carbon Electrodes

Younghee Hahn[1] and Carter L. Olson*

College of Pharmacy, 500 West 12th Avenue, The Ohio State University, Columbus, Ohio 43210

An amperometric enzymatic assay for total cholesterol in human serum has been developed. The assay utilizes cholesterol esterase, cholesterol oxidase, and peroxidase. H_2O_2 produced by the oxidase is coupled via peroxidase to produce $K_3Fe(CN)_6$ which is measured at a tubular carbon electrode. The reactions go all the way to completion and the $K_3Fe(CN)_6$ formed can be stoichiometrically related to total cholesterol concentration. Therefore, the assay can be calibrated with standard $K_3Fe(CN)_6$. (The reaction time is minimized by running the esterase reaction at 60 °C.) The method shows very good reproducibility, accuracy, and sensitivity. Bilirubin and hemoglobin show no interference and ascorbic acid up to 4 mg/dL did not interfere with the assay. Results obtained by the amperometric method show excellent agreement (correlation coefficient = 0.995) with those obtained by the Leffler method.

The analysis of total cholesterol (free cholesterol plus cholesterol esters) in human serum is a routine clinical diagnostic test that has been somewhat of a problem for clinical chemists (*1*, *2*). In traditional methods, cholesterol is treated to produce colored reaction products which are measured spectrophotometrically. The most common reactions are the Liebermann–Burchard reaction, the iron salt–sulfuric acid reaction (Kiliani or Zak), and the *p*-toluene sulfonic acid reactions. Color development is usually preceded by extraction and saponification steps. These methods have the disadvantages that the color reactions are very dependent on experimental conditions, other substances interfere with cholesterol, and a fairly large sample volume is required (*1*).

[1]Present address: Department of Pathology, University of Wisconsin, Madison, Wisconsin 53706.

More recently, Flegg (*3*) and Richmond (*4*) developed enzymatic methods for analyzing cholesterol utilizing cholesterol oxidase isolated from soil bacteria. Since that time, many enzymatic methods have appeared in the literature (*5–17*). All these enzymatic cholesterol assays were claimed to be more specific, sensitive, precise, and simple than the direct chemical ones.

A variety of analytical detection methods have been used for the enzymatic methods. These include spectrophotometry (*5–12*), fluorometry (*13*), potentiometry (*17*), and amperometry (*14–16*). The enzymatic spectrophotometric methods seemed to have some problems with bilirubin and ascorbic acid interferences, and most of the enzymatic procedures required calibration with cholesterol standards which sometimes have questionable reliability.

This paper describes a new amperometric enzymatic method for the analysis of total serum cholesterol that is highly sensitive, relatively free from interferences, and which does not require a cholesterol standard for calibration purposes.

THEORY

The assay for total cholesterol utilizes the following reaction scheme. When total serum cholesterol is measured, the cholesterol present in the form of esters must be hydrolyzed since cholesterol esters are not suitable substrates for the enzyme cholesterol oxidase. The two initial reactions are written as follows:

$$\text{cholesterol esters} + H_2O \xrightarrow{[CEH]} \text{cholesterol} + \text{fatty acids} \quad (1)$$

$$\text{cholesterol} + O_2 \xrightarrow{[CO]} \text{cholest-4en-3-one} + H_2O_2 \quad (2)$$

where CEH is the enzyme cholesterol ester hydrolase (CEH: EC 3.1.1.13) and CO is the enzyme cholesterol oxidase (CO:

0003-2700/79/0351-0444$01.00/0 © 1979 American Chemical Society

EC 1.1.3.6). The hydrogen peroxide produced by Equation 2 is measured using the following reaction:

$$H_2O_2 + 2K_4Fe(CN)_6 + 2H^+ \xrightarrow{PO} 2H_2O + 2K_3Fe(CN)_6 + 2K^+ \quad (3)$$

where PO is the enzyme peroxidase (PO: EC 1.11.1.7). The concentration of $K_3Fe(CN)_6$ produced is directly proportional to the concentration of total cholesterol present in the sample. The $K_3Fe(CN)_6$ is measured amperometrically by reduction at a tubular carbon electrode according to the following equation:

$$K_3Fe(CN)_6 + e^- \xrightarrow[\text{vs. SCE}]{E \text{ app} = -75 \text{ mV}} K_4Fe(CN)_6 \quad (4)$$

When the voltage applied to the electrode is in the vicinity of −75 mV vs. a saturated calomel electrode (SCE), the current is in the diffusion limited current region for the reduction of $K_2Fe(CN)_6$ and there is little interference from other constituents normally present in human serum.

All the enzymatic reactions are permitted to come to equilibrium. The assay is an equilibrium, not a kinetic assay.

The coupled enzymatic reactions can be carried out under a variety of conditions, among which are the following: (a) The three enzyme reactions may be carried out as a single operation at some specified temperature. (b) The cholesterol ester hydrolase reaction may be carried out at an elevated temperature, followed by the cholesterol oxidase and peroxidase reactions which are performed together at a lower temperature. (c) The cholesterol ester hydrolase and cholesterol oxidase reactions may be run at an elevated temperature followed by the peroxidase reaction which is run at a lower temperature. (d) The three enzyme reactions may be run separately and at different temperatures.

The peroxidase reaction is carried out in the presence of $K_4Fe(CN)_6$ and O_2. In order to prevent a high blank due to the oxidation of $K_4Fe(CN)_6$, the reaction temperature should be low and the time during which $K_4Fe(CN)_6$ oxidation could occur should be held as short as possible. The cholesterol ester hydrolase reaction is the slow step which can be speeded by either using more enzyme or elevating the temperature. Since the enzyme is somewhat expensive, a higher temperature is favored. Procedure (b) is favored over procedure (c) because, if it is desired, the measurement of free cholesterol can be obtained by simply omitting the initial elevated temperature cholesterol ester hydrolase reaction. Procedure (d) is overly complex and susceptible to error.

EXPERIMENTAL

Apparatus. *Electrodes and Cell.* A three-electrode cell with a tubular carbon working electrode (TCE) is described in Figure 1. The electrode design is similar to that used in previous work (*18–20*). A brass screw is used to make electrical contact to the TCE. Both the platinum counter electrode and calomel reference electrode are located downstream from the TCE. The plastic cell bodies can be made from Kel-F, Teflon, or Lucite. Kel-F is the material of choice when both machinability and inertness are considered. The salt bridge is closed by a dialysis membrane. The TCE is prepared by machining a graphite rod into an electrode of the following dimensions (length = 0.5 cm, outside diameter = 0.48 cm, and inside diameter = 0.16 cm). The dimensions are not critical and shorter electrodes should yield an improved signal-to-noise ratio. The graphite tube was washed with hexane and dried. It was then placed in Nujol for 5 h under a vacuum. After removal, the excess Nujol sticking to the electrode was absorbed on tissues.

Flow System. A pull system was used with a single peristaltic pump (Scientific Industries Model 403) placed downstream from the electrode cell. A short piece of Teflon tubing about 2 inches long served as a low holdup volume inlet line from the sample solution. A three-way stopcock was placed immediately downstream from the electrode cell. This permits sample solutions to be changed without pulling air bubbles through the cell or turning off the pump. A length of large Tygon tubing (15 cm long, 1.1-cm o.d., 0.95 cm i.d.) was placed between the stopcock and the pump to act as a pulse damper which smooths out the solution flow rate through the electrode. The volume flow rate of the solution was normally adjusted to about 0.5 mL/min.

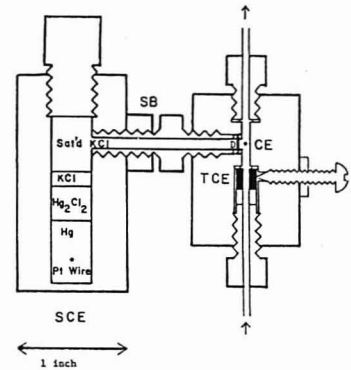


Figure 1. Electrode assembly. TCE: tubular carbon working electrode, SCE: saturated calomel reference electrode, CE: platinum wire counter electrode, SB: salt bridge, D: dialysis membrane

Measurement System. All electrochemical measurements were made using a Princeton Applied Research, Model 174A Polarograph. Currents were recorded on a Houston Instrument, Omniscribe stripchart recorder.

Reagents. All chemicals were reagent grade unless otherwise specified. A stock buffer solution, pH 7.0, was prepared by dissolving 19.94 g of Na_2HPO_4 (J. T. Baker, 99.3%), 9.39 g of $NaH_2PO_4 \cdot H_2O$ (J. T. Baker, 99.3%), and 14.98 g of KCl (Mallinckrodt, 99.5%) in double-distilled water to make 2 L of solution. All aqueous solutions were made with this buffer solution.

A solution of $K_4Fe(CN)_6$ was prepared by dissolving $K_4Fe(CN)_6$ crystals (J. T. Baker) in deaerated buffer. This solution was stored under purified N_2 as prepared by passing prepurified grade nitrogen through two glass scrubbing towers containing acidified vanadous sulfate solution (*21*) to remove oxygen traces followed by a third scrubbing tower containing buffer to remove acid.

Cholesterol ester hydrolase (0.28 unit/mg) and cholesterol oxidase (30 units/mL) were obtained from Miles Laboratories, Elkhart, Ind. Horseradish peroxidase (156 units/mg) was obtained from Worthington Biochemical Corporation, Freehold, N.J. The unit activity definitions for the enzymes used are as follows: One unit of cholesterol esterase (3.1.1.13) is that amount of enzyme catalyzing the decomposition of 1 μmol of cholesterol ester per minute at 37 °C and pH 6.7. One unit of cholesterol oxidase (1.1.3.6) is that amount of enzyme liberating 1 μmol of H_2O_2 per minute at 37 °C, pH 7.0, using a cholesterol substrate. One unit of peroxidase (1.11.1.7) decomposes 1 μmol of peroxidase per minute at 25 °C and pH 6.0.

RESULTS AND DISCUSSION

In addition to the enzymes required for the coupled reactions, the reagent solutions contain additional reagents. Triton X-100 was shown to help solubilize cholesterol (*14*), and sodium cholate was added because it was shown to facilitate the esterase reaction (*5*). Sodium azide was added because serum samples often contain some catalase which will destroy peroxide. Sodium azide has been shown to inhibit catalase (*17*). If the azide concentration is low enough, it will not seriously inhibit peroxidase during the normal reaction times (*22*).

There are several factors that influence the final choice of experimental conditions. In the enzymatic assay of cholesterol and its esters, the required enzymes are somewhat expensive.

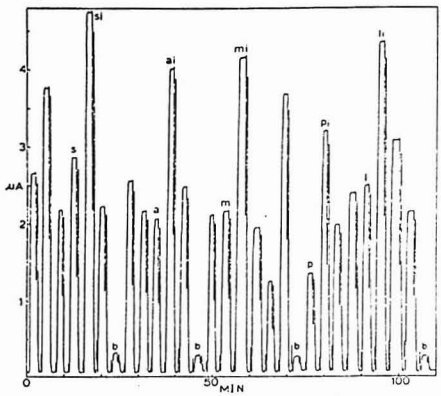


Figure 2. Electrode response for serum cholesterol assays

It would be desirable, therefore, to use as small an amount of enzymes as possible per assay. However, as the amount of enzyme is decreased, the reaction time becomes longer. It is often possible to substantially increase the reaction rate without enzyme deactivation by increasing the temperature. The same factors that facilitate the enzyme reaction may unfortunately increase the effect of interference. An example in the cholesterol assay described here is the air oxidation of ferrocyanide which increases rapidly with temperature.

The following results and discussions describe different conditions for the assay of cholesterol, some of the problems observed for the assay, and how these problems can be minimized.

The most simple procedure is to incubate all the enzymes and reagents simultaneously. When the reaction is complete, the ferricyanide produced is measured and the total cholesterol concentration is calculated. After studying the kinetics and successfully analyzing standards, the following correlation study was conducted using analyzed patient samples furnished by the clinical chemistry laboratory of the Ohio State University Hospital. The exact procedure is the following.

The reaction mixture is prepared as follows. One milliliter of a reagent containing 15 mM sodium cholate, 0.75% (v/v) Triton X-100, 3 mM sodium azide, 300 units/mL horseradish peroxidase, 0.1 unit/mL cholesterol ester hydrolase, and 0.15 unit/mL cholesterol oxidase is mixed with 20 μL of buffer followed by 1 mL of deaerated 20 mM $K_4Fe(CN)_6$. Twenty μL of sample is then added to the reaction mixture. If a blank is to be run, the sample is replaced by 20 μL of buffer. If a $K_3Fe(CN)_6$ standard addition experiment is run, the 20 μL of buffer in the reagent is replaced by 20 μL of 10 mM $K_3Fe(CN)_6$. The reaction mixture was incubated for 18 min at 36.5 °C. The incubated reaction mixture was pumped through the electrode cell and the $K_3Fe(CN)_6$ was measured amperometrically at −75 mV vs. a SCE using a Nujol-impregnated tubular carbon electrode. Experimental recordings are shown in Figure 2. Currents for the serum samples are indicated by letters "s, a, m, p, and l", and currents for samples containing a standard addition of $K_3Fe(CN)_6$ are indicated by "si, ai, mi, pi, and li". Blank currents are indicated by "b".

Analytical results obtained using the amperometric method were compared with results obtained by the Ohio State University Hospital using the Leffler method (*23*). The 130 patient samples tested covered a wide range of total cholesterol concentrations. The correlation between the two methods was fairly good. The linear equation was found to be: amperometric method (mg/dL) = (1.036 ± 0.026) × (Leffler value − (13.8 ± 5.9) The correlation coefficient was 0.962.

Table I. i_{dc} as a Function of Total Cholesterol Concentrations

total cholesterol, mg/dL	i_{dc}, μA	i_{dc}/total cholesterol, μA/(mg/dL)
1.15	0.79	0.687
1.15	0.78	0.678
2.29	1.60	0.699
3.43	2.39	0.697
2.29	1.60	0.697
3.43	2.35	0.685
4.56	3.11	0.682
5.69	3.85	0.677

These results are encouraging but it was felt that they were not satisfactory. There may be several reasons for a less than satisfactory correlation between the methods. For example, during the course of the reaction, air oxidation of $K_4Fe(CN)_6$ takes place as a competitive reaction for forming $K_3Fe(CN)_6$. On the other hand, oxidizable species in the serum may reduce some of the $K_3Fe(CN)_6$ that is produced by enzymatic reactions. The extent of these competitive reactions is both time and temperature dependent and is maximized by introducing the peroxidase–ferrocyanide system at the start of the overall reaction sequence.

A second approach, which should minimize the problem of the competitive redox reactions, is to separate the peroxidase–ferrocyanide reaction from the esterase–oxidase reactions. Since the peroxidase reaction is relatively fast, it can be run at a lower temperature than the esterase–oxidase reactions. The following study describes the results that can be obtained using this type of procedure. A cholesterol concentration study was conducted by adding 5 to 25 μL of Serachol (general diagnostic), a total cholesterol standard, to 1 mL of a reagent mixture and incubating for at least 10 min at 37 °C. The reagent consists of 25 mM sodium cholate, 1.25% (v/v) Triton X-100, 0.75 mM sodium azide, 0.2 unit/mL cholesterol ester hydrolase and 0.3 unit/mL cholesterol oxidase. After incubation, 0.5 mL of deaerated 5 mM $K_4Fe(CN)_6$ and 0.5 mL of 1000 units/mL peroxidase were added to the mixture. The final solution was immediately pumped through the cell and the $K_3Fe(CN)_6$ determined amperometrically. The results are shown in Table I. These results are very good; however, two additional improvements were desired: first to lower the amount of cholesterol esterase required per assay and, second, to shorten the time for cholesterol ester hydrolysis.

Since experiments showed that the esterase reaction was much slower than the oxidase reaction, it was decided that the optimum procedure would be to conduct the esterase reaction separately at an elevated temperature. After completion, the reaction mixture would be cooled and the oxidase and peroxidase reactions run concurrently at the lower temperature. This should minimize interfering reactions with both the H_2O_2 produced by the oxidase and the ferro-ferricyanide coupled to the peroxidase.

An initial study was conducted to determine the feasibility of running the esterase reaction at elevated temperatures. One hundred and sixty μL pooled patient serum was added to 16 mL of a reagent solution containing 7.5 mM sodium cholate, 0.38% (v/v) Triton X-100, 1.5 mM sodium azide, 150 units/mL peroxidase and 10 mM $K_4Fe(CN)_6$. The reaction mixture was slowly pumped through the tubular electrode to follow the reaction progress. The times required for the reaction to go to completion at temperatures from 38 to 60 °C are shown in Table II. It was decided that 60 °C should be used for the cholesterol esters hydrolysis in all further studies.

Table II. Time Required as a Function of Temperature to Reach Equilibrium for the Cholesterol Ester Hydrolase Reaction

temperature, °C	time, min
38	12
43	10
50	8
60	3

Table III. i_{dc} as a Function of Enzymatic Hydrolysis Time

time, min	i_{dc}, μA	normalized, $i_{dc}/3.80$ μA
1.2	2.69	0.708
2.0	3.09	0.813
3.0	3.28	0.863
4.0	3.65	0.961
5.0	3.78	0.995
6.0	3.80	1.000
7.0	3.79	0.997

Table IV. i_{dc} as a Function of Enzymatic Oxidation and Coupling Reaction Time

time, min	i_{dc}, μA	normalized, $i_{dc}/3.90$ μA
1.0	3.52	0.903
2.0	3.72	0.954
3.0	3.80	0.974
4.0	3.87	0.992
5.0	3.90	1.000
6.0	3.85	0.987

The following set of reagent solutions were used for all subsequent studies. The pH 7.0 buffer solution was prepared to contain 0.5% (v/v) Triton X-100. The hydrolysis reagent contained 0.05 unit/mL cholesterol ester hydrolase (Miles Laboratories, 0.28 unit/mg), 10 mM sodium cholate (Sigma Chemical Co.), and 3 mM sodium azide (Sigma Chemical Co.) in pH 7.0 buffer. The reagent for enzymatic oxidation and coupling contained 0.2 unit/mL cholesterol oxidase (Miles Laboratories, 30 units/mL) and 156 units/mL peroxidase (Worthington Biochemicals, 156 units/mg) in pH 7.0 buffer. The enzyme reagents remained stable for at least 40 days when stored at 4 °C. A 20 mM $K_4Fe(CN)_6$ (J. T. Baker Chemical Co.) solution was made in deoxygenated pH 7.0 buffer and stored under nitrogen. The ferrocyanide solution did not contain Triton X-100 to prevent foaming during deaeration. For calibration purposes, a 10 mM $K_3Fe(CN)_6$ (J. T. Baker Chemical Co.) solution was prepared in pH 7.0 buffer.

The enzyme incubation times were studied for this final set of reagents. To establish the necessary enzymatic hydrolysis time, 20 μL of human serum containing 300 mg/dL cholesterol was mixed with 0.18 mL buffer and 0.8 mL of esterase reagent. The mixture was incubated at 60 °C for time periods ranging from 1.2 to 7 min. The hydrolyzed mixture was cooled to room temperature (23 °C) after which 0.5 mL of the oxidation and coupling reagent and 0.5 mL of $K_4Fe(CN)_6$ reagent were added. The final solution was incubated for about 3 min and then pumped through the electrode. The results are shown in Table III. A similar study was conducted to determine how much time was required for the oxidase-coupling reaction. The same solutions were used as in the hydrolysis study. The esterase reaction was incubated for 7 min at 60 °C to assure completion. The solution was cooled to room temperature and the oxidase reaction was allowed to incubate for 1 to 6 min before pumping through the flow cell. The results are shown in Table IV. In order to be sure that any total cholesterol concentration likely to be encountered in human serum samples would react to completion with some safety margin, all subsequent assays were run using 7 min at 60 °C for the esterase reaction and 5 min at 25 °C for the oxidase–peroxidase reactions.

One of the major concerns with the analysis of cholesterol is to obtain accurately known calibration standards. It was felt that it would be much simpler if a standard ferricyanide solution could be used to replace the cholesterol standard. In order to prove this possibility, a study was conducted to determine the stoichiometry of the reaction sequence. The electrode response is easily calibrated with standard ferricyanide solution. Assuming 2 mol of ferricyanide are produced for each mole of cholesterol present, the current can be used to calculate the cholesterol concentration. A cholesterol diluant was prepared as follows: Ten mL of isopropyl alcohol (Isopropanol, anhydrous, Chemical Samples Co.) was mixed with 5 mL of Triton X-100 and then diluted to 100 mL with double-distilled water. A stock cholesterol solution was prepared by transferring 26.42 mg cholesterol (99% Sigma Chemical Co.) to a 25-mL volumetric flask. The cholesterol was dissolved in 1 mL of isopropanol and then diluted to 25 mL with the cholesterol diluant. This stock solution was used to make the standard cholesterol solutions.

The assays were conducted as follows. One hundred μL of cholesterol standard was mixed with 0.9 mL of 0.5% Triton X-100 buffer solution containing 10 mM sodium cholate and 3 mM sodium azide. To this mixture, 0.5 mL of ferrocyanide reagent and 0.5 mL of oxidase–peroxidase reagent, were added. The resulting mixture was incubated for 5 min at 25 °C. During incubation either 20 μL of buffer, as a sample volume correction, or 20 μL of $K_3Fe(CN)_6$ was added as a standard addition. To obtain a blank correction, 100 μL of diluant was substituted for the cholesterol sample. The results for the conversion studies shown in Table V indicate that standard $K_3Fe(CN)_6$ can be used to calibrate the assay.

The procedure for the final studies was standardized as follows. A 20-μL aliquot of serum was added to a small glass vial. One mL of esterase reagent was then added after which the vial was stoppered and incubated in a water bath set at 60 °C for 7 min. The vial was then placed in a water jacketed cooler for 2 min. After cooling, 0.5 mL of $K_4Fe(CN)_6$ reagent

Table V. Percentage of Cholesterol Conversion

prepared [cholesterol] in final soln mg/dL	i_{dc}, av ± S.D. (n),[a] μA	measured [cholesterol] in final soln mg/dL	stoichiometric conversion, %
1.04	0.94 ± 0.05 (8)	1.06	101.9
2.07	1.84 ± 0.04 (7)	2.07	100.0
3.11	2.77 ± 0.02 (7)	3.11	100.0
4.14	3.65 ± 0.04 (7)	4.10	99.0
5.18	4.59 ± 0.05 (8)	5.16	99.6

[a] n = the number of experiments averaged for each sample, i_{dc} for the 9.12 μM $K_3Fe(CN)_6$ standard addition trial was 1.57 μA ± 0.02 (*18*) (20 μL of 9.21 mM $K_3Fe(CN)_6$ solution was added to 2.0 mL of enzyme catalyzed reaction mixture resulting in a $K_3Fe(CN)_6$ final solution concentration of 9.12 μM).

Table VI. Within-Day Precision of the Amperometric Enzymatic Method for Total Cholesterol

av value, mg/dL	std. dev., mg/dL	% rel std dev	no. of assays
127.3	3.17	2.49	22
210.3	4.68	2.23	23
381.3	6.90	1.81	22

Table VII. Effect of Some Potentially Interfering Compounds on the Amperometric Enzymatic Method for Total Cholesterol

compound	concn, mg/dL	total cholesterol in serum, mg/dL: with compound	total cholesterol in serum, mg/dL: without compound
ascorbic acid	4	192	190
hemoglobin	200	199	200
bilirubin	500	188	189

and 0.5 mL of oxidase–peroxidase were added. Twenty μL of buffer was added for volume correction. The sample was incubated at 25 °C for 5 min and then pumped through the electrode. For calibration purposes, the 20 μL of standard $K_3Fe(CN)_6$ was substituted for the 20 μL of buffer. For blank determination, 20 μL of buffer was substituted for the serum sample.

In order to verify that total serum cholesterol is being measured, a recovery study was made. One hundred μL of standard cholesterol solution containing 31.39, 62.78, and 94.18 mg/dL, respectively, were added to 20-μL samples of pooled patient serum. The samples were assayed in triplicate using the described procedure. The percent recovery for the added cholesterol concentration in the final solutions were 101.4% for 1.47 mg/dL, 102.4% for 2.93 mg/dL, and 98.2% for 4.40 mg/dL.

Within-day precision was studied for three concentrations of pooled patient sera. The results shown in Table VI indicate very acceptable precision, especially considering the small sample volume utilized.

Since bilirubin and hemoglobin interfere with conventional colorimetric methods, and ascorbic acid interferes with the enzymatic spectrophotometric method (*11*), these substances were studied for interferences with the amperometric enzymatic assay for total cholesterol. Reported normal values for ascorbic acid, bilirubin, and hemoglobin in human serum are, respectively, 0.2–2.0 mg/dL, 0–1.5 mg/dL, and 0.03–0.89 mg/dL (2). For the interference tests, ascorbic acid (Merck) and hemoglobin (Sigma Chemical Co., Human Type IV) were dissolved in buffer pH 7.0, and bilirubin (Sigma Chemical Co.) was dissolved in 0.1 N NaOH. Twenty μL of a serum cholesterol sample is mixed with 20 μL of a solution containing the interference and assayed for total cholesterol. The results are shown in Table VII. It can be seen that there is no interference from bilirubin or hemoglobin. Normal ascorbic acid concentrations also do not interfere. However, very high concentrations much higher than normal, of ascorbic acid do interfere, presumably by reducing the ferricyanide that is measured electrochemically.

Since sterols other than cholesterol may be present in human serum, a brief selectivity study was conducted. It was reported that dihydrocholesterol, lathosterol, and 7-dehydrocholesterol are found in human serum at concentrations ranging from about 1–3%, 0.4–1.4%, and 2.5–20%, respectively, of the total cholesterol present (2). Dihydrocholesterol and 7-dehydrocholesterol were purchased from the Sigma Chemical Co. However, a source for lathosterol was not found. Approximately 2 mM solutions were prepared for dihydrocholesterol, 7-dehydrocholesterol, and cholesterol by dissolving an appropriate amount of sterol in 5 mL of isopronol and adding diluant to 50 mL. Twenty μL of sterol was assayed using the standard procedure. Rates for the oxidation of cholesterol, dihydrocholesterol, and 7-dehydrocholesterol were approximately in the ratio 1:0.97:0.65. These other sterols will be measured as cholesterol by the enzymatic assay. This is in reasonably good agreement with previous work (*5*).

Table VIII. Comparison of the Amperometric Enzymatic Analysis of Patient Serum with the Leffler Method Analysis

patient no.	total cholesterol, mg/dL: Leffler method	total cholesterol, mg/dL: amperometric enzymatic method	
4239	80	76	76
4117	350 (310)[a]	333	330
3939	225 (224)[a]	203	206
4255	124	128	131
4201	190	189	187
4279	170	179	180
4686	146	155	161
4719	186	189	193
4807	240	245	244
4825	260	260	256
4905	255 (244)[a]	262	263
1645	440 (410)[a]	454	454
1895	125	123	124
2350	305	309	309
2361	364 (340)[a]	384	385
1631	130	134	132
2444	145	137	136
2605	125	123	126
2556	180	177	176

[a] Values originally furnished by the clinical laboratory of The Ohio State University Hospital before reanalysis.

A correlation study was made between human serum samples assayed by the final enzymatic amperometric method and the Leffler method used by the Ohio State University Hospital. The results are shown in Table VIII. Duplicate results reported for the electrochemical method illustrate the excellent reproducibility of this method. Five of the samples seemed to show too much discrepancy and were returned to the Hospital Laboratory for reanalysis. The initial values are shown in parentheses and the second assay is listed in the column under the Leffler method. The correlation between the two methods is excellent. The linear equation was found to be: amperometric enzymatic method (mg/dL) = (1.021 ± 0.016) × (Leffler method) − (3.24 ± 3.55) with a correlation coefficient of 0.995.

In conclusion, the advantages of the amperometric enzymatic assay for total serum cholesterol can be summarized as follows. The method is highly sensitive and requires only a small sample per assay. It is also quite selective and relatively free from normal interferences. The instrumentation required is very simple and low cost. It is also very reliable. For example, the Nujol impregnated graphite rod electrode was used for over a period of ten months without replacement. The ability to calibrate the assay with standard $K_3Fe(CN)_6$ seems very attractive since it is low cost, easily soluble, and available in high purity. It was fortunate that the esterase reaction could be run at 60 °C because this permits the hydrolysis step to be carried out rapidly with a minimum amount of enzyme. And finally, the assay proved to be precise, accurate, and was found to give excellent correlation with results obtained by the standard Leffler method.

ACKNOWLEDGMENT

We are particularly grateful to the Clinical Chemistry Laboratory of the Ohio State University Hospital for providing

us with analyzed patient serum samples and their results.

LITERATURE CITED

(1) D. B. Tonks, *Clin. Biochem.*, **1**, 12 (1967).
(2) R. J. Henry, D. C. Cannon, and J. W. Winkelman, Ed., "Clinical Chemistry Principles and Technics", Bio-Science Laboratories, 2nd ed., Harper & Row, New York, 1974.
(3) H. M. Flegg, *Ann. Clin. Biochem.*, **10**, 79 (1973).
(4) W. Richmond, *Clin. Chem. (Winston Salem, N.C.)*, **19**, 1350 (1973).
(5) C. C. Allain, L. S. Poon, C. S. G. Chan, W. Richmond, and P. C. Fu, *Clin. Chem. (Winston-Salem, N.C.)*, **20**, 470 (1974).
(6) P. N. Tarbutton and C. R. Gunter, *Clin. Chem. (Winston-Salem, N.C.)*, **20**, 724 (1974).
(7) D. L. Witte, D. A. Barrett II, and D. A. Wycoff, *Clin. Chem. (Winston-Salem, N.C.)*, **20**, 1282 (1974).
(8) P. W. Wentz, R. E. Cross, and J. Savory, *Clin. Chem. (Winston-Salem, N.C.)*, **22**, 188 (1976).
(9) R. J. Morin, *Clin. Chim. Acta*, **71**, 75 (1976).
(10) F. Zoppi and D. Fenili, *Clin. Chem. (Winston-Salem, N.C.)*, **22**, 690 (1976).
(11) C. A. Robinson, Jr., L. M. Hall, and J. Vasiliades, *Clin. Chem. (Winston-Salem, N.C.)*, **22**, 1542 (1976).
(12) R. Haeckel and M. Perlick, *J. Clin. Chem. Clin. Biochem.*, **14**, 411 (1976).
(13) H. Huang, J. W. Kuan, and G. G. Guilbault, *Clin. Chem. (Winston-Salem, N.C.)*, **21**, 1605 (1975).
(14) A. Noma and K. Nakayama, *Clin. Chem. (Winston-Salem, N.C.)*, **22**, 336 (1976).
(15) F. Williams, A. Brunsman, J. Huntington, J. Johnson, and D. Newman, "Amperometric-Oxidase Enzyme Probes for Biochemical Analysis", Yellow Springs Instrument Company., Inc., Technical paper, Yellow Springs, Ohio, March 1976, p 12.
(16) *Chem. Eng. News*, January 5, 1976, p 19.
(17) D. S. Papastathopoulos and G. A. Rechnitz, *Anal. Chem.*, **47**, 1972 (1975).
(18) W. D. Mason and C. L. Olson, *Anal. Chem.*, **42**, 488 (1970).
(19) M. D. Smith and C. L. Olson, *Anal. Chem.*, **46**, 1544 (1974).
(20) M. D. Smith and C. L. Olson, *Anal. Chem.*, **47**, 1074 (1975).
(21) L. Meites and T. Meites, *Anal. Chem.*, **20**, 984 (1948).
(22) M. Dixon and E. C. Webb, "Enzymes", 2nd ed., Academic Press, New York, 1964, p 338.
(23) H. H. Leffler, *Am. J. Clin. Pathol.*, **31**, 310 (1959).

RECEIVED for review April 12, 1978. Accepted December 18, 1978. This work was partially supported by the National Institue of General Medical Sciences Grant GM 15821.

Determination of Quinidine and Dihydroquinidine in Plasma by High Performance Liquid Chromatography

Berry J. Kline,* Vilma A. Turner, and William H. Barr

Department of Pharmacy and Pharmaceutics, Medical College of Virginia, Virginia Commonwealth University, Richmond, Virginia 23298

A rapid, specific and sensitive high performance liquid chromatographic method has been developed for the determination of quinidine (Q) and dihydroquinidine (DHQ) in human plasma. Plasma samples are extracted with a benzene–isoamyl alcohol mixture (1:1) followed by separation on a microparticulate reverse-phase column. Quinidine, dihydroquinidine, and their metabolites are detected by fluorescence in acid medium using post-column addition of sulfuric acid. Plasma concentrations as low as 0.05 μg/mL can be measured with a relative standard deviation less than 10%. The complete assay procedure takes about 30 min. Recovery from plasma is at least 95%. A linear response is obtained in the concentration range of 0.05 to 10 μg/mL of quinidine in plasma. The minimum detectable quantity is 1 ng on column.

To study quinidine pharmacokinetics in human subjects, a specific method for the separation and determination of quinidine, dihydroquinidine, and their metabolites is needed. Quinidine may contain up to 20% of a natural contaminant, dihydroquinidine, depending on the source (*1*). Dihydroquinidine is an analogue of quinidine with similar if not greater antiarrhythmic effect (*2, 3*). Drayer et al. have reported that three metabolites of quinidine found in man are pharmacologically active in mice and rabbits (*4*). Until this activity, or lack thereof, is verified in humans, plasma level determinations of quinidine for the purpose of therapeutic dosage adjustment should be specific with minimal contribution from dihydroquinidine or metabolites. The analytical method commonly used to determine quinidine in plasma is that of Cramer and Isaksson (*5*). This method is based on extraction of alkalinized plasma samples with benzene, which excludes the more polar metabolites, and then back extraction into H_2SO_4 for fluorimetric quantitation of the quinidine. However, Huynh-Ngoc and Sirios (*6*) have found that some metabolites are being measured along with the quinidine in this method. They recommend washing the benzene layer with NaOH to eliminate interferences from less polar metabolites.

Numerous chromatographic procedures have been developed for the determination of quinidine (*7–19*). Several of them (*7–10*) are specific but time-consuming TLC procedures which we did not consider suitable for routine clinical monitoring. Some of them (*11, 12*) have been applied only to pharmaceutical preparations. Several others (*13–15*) did not separate quinidine from dihydroquinidine. The method presented here provides good separation of quinidine, dihydroquinidine, and their metabolites, is sensitive enough to determine low concentrations of quinidine and dihydroquinidine, and is rapid enough for routine clinical monitoring of plasma levels.

EXPERIMENTAL

Apparatus. A Waters Model ALC202 liquid chromatograph fitted with a Model 6000 constant flow pump, a 30 cm × 3.9 mm i.d. μBondapak C_{18} column (Waters Associates, Milford, Mass.) and a Rheodyne Model 7120 syringe loading sample injector with a 175-μL sample loop was used. A 5 cm × 2 mm i.d. guard column packed with C_{18} Corasil (37–50 μm particle size) was added to the system to prevent clogging of the main column. A T-union (Altex, #200-22) was used to combine the column eluate with 2 N sulfuric acid supplied by a peristaltic pump (Manostat Cassette pump) through Teflon tubing (0.8-mm i.d.). The sulfuric acid and the column eluate were introduced into the T-union at a 180° angle so that the opposing flows created turbulence, thus eliminating the need for a long mixing coil. A second Teflon tube (75 cm × 0.8 mm i.d.) connected the T-union to the detector flow cell. Acid-resistant flexible tubing (0.056-inch i.d.) was used to pump the sulfuric acid to the Teflon tubing. The detector was a filter fluorimeter (Aminco Fluoro-Monitor) equipped with a 70-μL flow cell, 350-nm excitation, and 450-nm emission filters (Turner, #7-60 and 2A). The areas under the chromatographic peaks were measured with a Spectra Physics Autolab Minigrator.

Reagents. Water was single-distilled, and acetonitrile was 99 mol % pure (Fisher Scientific Co.). All other chemicals and

0003-2700/79/0351-0449$01.00/0 © 1979 American Chemical Society

organic solvents were reagent grade and were used as received. Quinidine sulfate dihydrate and dihydroquinidine were obtained as gifts from A. H. Robins Co. Although the batch of quinidine sulfate used contained approximately 5% dihydroquinidine and, likewise, the dihydroquinidine was contaminated with about 1.4% of quinidine, analytical results were not corrected for these because the same batches of each were used in all experiments. Correction of the actual amounts weighed and measured for these contaminants made no difference in recovery or precision data because of internal consistency. When patient samples are analyzed using standards with significant levels of contamination, this correction should be applied. Since quinidine and dihydroquinidine give equivalent responses in the chromatographic system (as will be discussed later), estimates of the contamination levels of these two compounds in each other may be obtained by chromatographic peak area normalization.

A stock solution containing 2 mg/mL of quinidine was prepared by dissolving and diluting 24.2 mg of quinidine sulfate dihydrate to 10 mL with distilled water. A similar solution of dihydroquinidine, 1 mg/mL was prepared in methanol. A quinidine plasma stock solution (10 μg/mL) was prepared by the addition of 50 μL of quinidine stock solution (2 mg/mL) to 10 mL of drug-free plasma. Quinidine standard solutions in the 5 to 0.05 μg/mL range were prepared by serial dilution of the 10 μg/mL quinidine stock solution with drug-free plasma.

Procedure. Pipet 0.5 mL of plasma into a 5-mL stoppered test tube, alkalinize with 0.5 mL of 5N NaOH, add 2 mL of benzene–isoamyl alcohol (1:1 mixture), mix gently by rocking for approximately 10 min on a mechanical mixer, and centrifuge at 2000 rpm for 10 min. Inject 175 μL of the organic layer into the HPLC column (full-loop injection). The concentration of quinidine in the plasma sample is determined from a calibration curve of quinidine peak area vs. quinidine concentration.

Chromatographic Conditions. The mobile phase was prepared to contain 4% (v/v) of a 1% (w/v) aqueous $(NH_4)_2CO_3$ solution, 31% (v/v) of methanol, and 65% (v/v) of acetonitrile. It was degassed and filtered through a 0.45-μm membrane filter before use. The flow rate of the mobile phase was 3.5 mL/min (1000 psi). The sulfuric acid flow rate was approximately 0.45 mL/min.

RESULTS AND DISCUSSION

Fluorescent Detection. After development of the HPLC column–solvent system which separates quinidine from dihydroquinidine and their metabolites, it was obvious that ultraviolet photometric detection was not sensitive enough for quantitation of the low plasma levels of dihydroquinidine and its metabolites. Since Cramer and Isaksson (5) utilized the fluorescence of quinidine in its determination, it was anticipated that fluorescence detection might improve sensitivity. Although quinidine did not fluoresce in the HPLC mobile phase, addition of aqueous sulfuric acid restored the fluorescence characteristics of the quinidine. Therefore, post-column addition of aqueous sulfuric acid to the column eluate was introduced by use of a peristaltic pump and a simple T-joint. Since the quality of the HPLC separation is determined by the flow rate of the mobile phase, the only other variables which could be manipulated to improve detectability were the concentration and the post-column addition rate of sulfuric acid. Fluorescence was optimized at a sulfuric acid concentration of 2 N and a flow rate of approximately 0.45 mL/min. Since the mobile phase contains ammonium carbonate, the possibility of CO_2 bubble formation during the addition of the aqueous acid was a concern because the bubbles could cause detector noise. However, this anticipated problem never appeared.

Extraction. During the initial investigation, direct injection of plasma into the HPLC column was attempted (*14*), but precipitated plasma proteins tended to clog the column. Several protein precipitation methods were then investigated. Precipitation of plasma proteins with trichloroacetic acid (TCA) yielded low recovery of quinidine. Other protein precipitants such as methanol and tungstic acid were tested, also with unsatisfactory results. Since direct injection after protein precipitation did not appear promising, several solvent extraction methods were then investigated. However the main disadvantage with them was a lengthy solvent evaporation step, and/or adsorption of quinidine by the glassware. The latter could be reduced by adding a small amount of isoamyl alcohol, but that increased the evaporation time. The highly fluorescent characteristics of quinidine and its affinity for the benzene–isoamyl alcohol solvent system made it possible to avoid the evaporation step by direct injection of the extract onto the column. The analysis can then be performed in 30 min. The advantage of this solvent system over others investigated is that it extracts quinidine, dihydroquinidine, and their metabolites (*8*) since it was desired to determine all of these in this laboratory. Identification and quantitation of the metabolites by this method are currently under investigation.

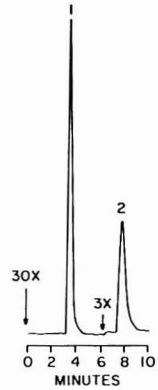


Figure 1. Chromatogram of human plasma spiked with quinidine (1), 10 μg/mL containing dihydroquinidine (2) at the natural contaminant level (~0.5 μg/mL). The arrows indicate the relative sensitivity of the fluorimetric detector at those points

Quantitation. Because the internal standard method is preferred in quantitative chromatography, initial investigations were directed at finding a compound which would serve as an internal standard in this procedure. However, the severe constraints placed upon an internal standard by the analytical system drastically restricted the choice of compounds. For example, the internal standard must (1) be extracted efficiently from plasma under the same conditions as quinidine in this procedure; (2) elute from the HPLC column with a retention time different from that of quinidine, dihydroquinidine, and their metabolites; and (3) have the same fluorescence characteristics as quinidine in the column eluate–sulfuric acid mixture. Dibucaine met conditions 1 and 3, but interfered with one of the metabolites. Thiopropazate met conditions 2 and 3, but was poorly extracted from plasma in this procedure. Numerous other compounds were investigated, but none of them conformed to the constraints of the analytical system. Therefore, external standardization was adopted after it was proved that acceptable precision was obtainable with that technique in this procedure.

Figure 1 is a chromatogram of a 10 μg/mL standard plasma solution of quinidine with dihydroquinidine at the natural contaminant level (~5% in this batch). Although it is not necessary to increase detector sensitivity when determining dihydroquinidine by electronic integration, it was increased for purposes of clarity in this figure. Figure 2 shows a chromatogram for the plasma from a patient who was dosed

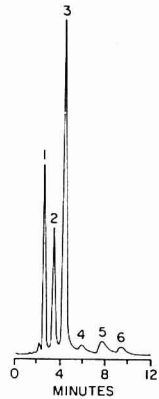


Figure 2. Chromatogram of plasma from a patient dosed with quinidine sulfate. Peaks represent 3-hydroxyquinidine (a quinidine metabolite) (1), as yet unidentified metabolites of quinidine or dihydroquinidine (2, 4, and 5), quinidine, 3.8 μg/mL (3), and dihydroquinidine (6)

Table I. Relative Recovery of Dihydroquinidine from Plasma Using Quinidine Standards

concn added, μg/mL	0.246	0.493	0.983	4.93
concn found, μg/mL	0.233	0.496	0.973	5.23
mean recovery, %	94.7	100	98.7	106

Table II. Absolute Recovery of Quinidine and Dihydroquinidine from Plasma

drug	Q[a]	Q	DHQ	DHQ
concn added, μg/mL	0.1	10.0	0.1	1.0
concn found, μg/mL	0.095	9.73	0.107	1.04
% recovered	95.0	97.0	107	104

[a] Q: Quinidine. DHQ: Dihydroquinidine.

with quinidine sulfate. This figure illustrates the separation of metabolites and the parent compounds.

Calibration Curve. A calibration curve was constructed with quinidine concentrations of 10, 5, 2, 0.1, and 0.05 μg/mL in drug-free plasma. A linear curve of peak area vs. quinidine concentration was obtained with a correlation coefficient of 0.999. The same curve can be used to measure the concentration of dihydroquinidine in plasma since it was found that the peak areas for equal concentrations of quinidine and dihydroquinidine are the same. This was determined by measuring the relative recovery of dihydroquinidine from plasma spiked at 0.25 to 5 μg/mL, using quinidine as the standard. As can be seen in Table I, the recovery is within experimental error of 100% at all levels.

Recovery. The absolute recoveries of quinidine and dihydroquinidine were determined by comparing chromatographic peak areas from extracted plasma solutions with areas generated by direct injection of aqueous or methanolic solutions of the two drugs. As shown in Table II, absolute recoveries are within experimental error of 100%. Recoveries were significantly lower when 0.05 mL of 5 N NaOH was used for alkalinization. Further experiments indicated that the recovery was improved when plasma samples were diluted with an equal volume of water. Therefore, 0.5 mL of 0.5 N NaOH was used to alkalinize and dilute plasma samples.

Since the absolute recoveries approximate 100%, it should be possible to substitute water for drug-free plasma in the preparation of standard solutions, although this has not been tested experimentally.

Table III. Reproducibility for the Determination of Quinidine and Dihydroquinidine in Plasma

drug	Q[a]	Q	Q	DHQ	DHQ
mean concn, μg/mL	1.82	0.10	0.051	0.91	4.96
no. of determinations	20	10	15	6	6
std. dev.	0.067	0.007	0.0032	0.045	0.185
rel. std. dev., %	3.7	7.3	6.3	4.9	3.7

[a] Q: Quinidine. DHQ: Dihydroquinidine.

Reproducibility. Drug-free plasma spiked with quinidine and dihydroquinidine at three different concentrations was analyzed over a period of several days. As shown in Table III, the relative standard deviation is less than 10% at all levels.

Sensitivity. Quinidine and dihydroquinidine concentrations of 0.05 μg/mL are easily measurable by this method. It is possible to increase the detector sensitivity or the sample volume so that as little as 1 ng of quinidine or dihydroquinidine on column can be detected.

Interferences. No attempt was made to screen a large number of drug compounds which might be coadministered with quinidine and interfere with this determination. It became obvious during the search for an internal standard that the constraints placed upon other drugs (and their metabolites) by this analytical system would limit the number of compounds which could interfere. Because of these constraints, the method is considered to be quite specific. However, the potential for interference by other compounds should be recognized.

To investigate the possibility that metabolites were eluting with the quinidine or dihydroquinidine, a sample of urine from a patient dosed with quinidine sulfate was analyzed by this procedure, and the eluate fractions containing the quinidine and dihydroquinidine were collected. The solvent was evaporated, and the residues were analyzed by mass spectrometry. The spectra obtained were identical to those of pure quinidine and dihydroquinidine.

LITERATURE CITED

(1) "The United States Pharmacopeia", XIX rev., Mack Publishing Co., Easton, Pa., 1975 p 435.
(2) T. Lewis, *Am. J. Med. Sci.*, **163**, 781 (1922).
(3) F. Alexander, H. Gold, L. N. Katz, R. L. Levy, R. Scott, and P. D. White, *J. Pharmacol. Exp. Ther.*, **90**, 191 (1947).
(4) D. E. Drayer, C. E. Cook, and M. M. Reidenberg, *Clin. Res.*, **24**, 623-A (1976).
(5) G. Cramer and B. Isaksson, *Scand. J. Clin. Lab. Invest.*, **15**, 553 (1963).
(6) T. Huynh-Ngoc and G. Sirois, *J. Pharm. Sci.*, **66**, 591 (1977).
(7) C. T. Ueda, D. S. Hirschfeld, M. M. Scheinman, M. Rowland, B. J. Williamson, and B. S. Dzindzio, *Clin. Pharmacol. Ther.*, **19**, 30 (1976).
(8) G. Härtel and A. Korhonen, *J. Chromatogr.*, **37**, 70 (1968).
(9) B. Wesley-Hadzija and A. M. Mattocks, *J. Chromatogr.*, **144**, 223 (1967).
(10) J. M. Steyn and H. K. L. Hundt, *J. Chromatogr.*, **111**, 463 (1975).
(11) E. Smith, S. Barkan, B. Ross, M. Malenthal, and J. Levine, *J. Pharm. Sci.*, **62**, 1151 (1973).
(12) N. J. Pound and R. W. Sears, *Can. J. Pharm. Sci.*, **10**, 122 (1975).
(13) J. L. Valentine, P. Driscoll, E. L. Hamburg, and E. D. Thompson, *J. Pharm. Sci.*, **65**, 96 (1976).
(14) K. A. Conrad, B. L. Molk, and C. A. Chidsey, *Circulation*, **55**, 1 (1977).
(15) J. L. Powers and W. Sadee, *Clin. Chem. (Winston-Salen, N.C.)*, **24**, 299 (1978).
(16) B. A. Persson, and P. O. Lagerström, *J. Chromatogr.*, **122**, 305 (1976).
(17) M. A. Moulin and H. Kinsun, *Lin. Chim. Acta*, **75**, 491 (1977).
(18) K. K. Midha and C. Charette, *J. Pharm. Sci.*, **63**, 1244 (1974).
(19) R. G. Achari, J. L. Baldridge, T. R. Koziol, and L. Yu, *J. Chromatogr. Sci.*, **16**, 271 (1978).

RECEIVED for review June 26, 1978. Accepted December 8, 1978.

Determination of Trace Silica in Industrial Process Waters by Flameless Atomic Absorption Spectrometry

Judith A. Rawa* and Earl L. Henn

Calgon Corporation, P.O. Box 1346, Pittsburgh, Pennsylvania 15230

A method for determining trace concentrations of silica in industrial process waters by flameless atomic absorption spectrometry (FAAS) is described. The method incorporates the addition of calcium to samples and standards to minimize the formation of silicon carbide, thereby enhancing sensitivity. Lanthanum is also added to minimize the negative interference caused by orthophosphate. Good correlation between the FAAS method and the heteropoly blue colorimetric test has been demonstrated. Average recovery of silica added to various industrial waters was 102%. The relative standard deviation of the test at the 25 μg/L SiO_2 level is 6.1%. The detection limit is 2.5 μg/L SiO_2.

Control of silica in boiler feedwater and boiler water is essential in minimizing the formation of scale-forming silicates, which reduce heat transfer in the boiler. Also, volatilization and carryover of silica with the steam may cause hard, glassy siliceous deposits to form on turbine blades, thereby drastically reducing turbine efficiency. Treatment of high pressure boiler systems (>1500 psi) often requires the control of silica in the boiler feedwater at the 10–20 μg/L SiO_2 level. Boiler feedwater is often purified through a demineralization process involving anion and mixed bed exchangers. The silica content of the demineralizer effluents requires monitoring to determine regeneration needs. Control limits for silica in the boiler feedwater are determined by the boiler operating pressure, pH of the boiler water, and cycles of concentration. Generally, silica concentrations in excess of 50 μg/L SiO_2 in the boiler feedwater would not be acceptable in a high pressure boiler system.

The classical approach to trace silica (<250 μg/L SiO_2) testing in the water treatment industry has been utilization of the colorimetric heteropoly blue method (*1, 2*). This method was used successfully in our laboratory for a number of years. Recently, we have found that an unknown substance in current supplies of ammonium molybdate used in preparing an essential reagent for the colorimetric test causes a positive interference in this test. Apparently, the recent change in the quality of the ammonium molybdate is due to a change in the process used in manufacturing molybdenum oxide. The change in processsing was due to OSHA requirements. We have been unable to locate a supply of ammonium molybdate which does not contain the interfering substance. The nature of this interference is such that it cannot be compensated for by the usual blank determination, thereby necessitating establishment of a correction factor for each batch of ammonium molybdate reagent prepared. Because of the reduced confidence in the accuracy of the colorimetric method, our laboratory sought an alternate method for trace silica analysis.

Flameless atomic absorption spectrophotometry (FAAS) is commonly used for the determination of trace metals in water (*3, 4*). However, there are few references in the literature describing the application of FAAS to silicon analysis. Silicon is a relatively refractory element which tends to form a carbide in the graphite tube during FAAS analysis, resulting in relatively poor sensitivity and reproducibility.

In 1975, Thompson et al. (*5*) found that addition of 1000 mg/L Ca (as the nitrate) enhanced the silicon signal. The enhancement was thought to be due to preferential formation of a calcium carbide. Comparable signal enhancement was noted when an uncoated and pyrolytically coated tube were used. Lo and Christian (*6*) later evaluated possible mechanisms for the formation of the silicon atom population in the graphite atomizer. Because of formation of silicon carbide with an uncoated graphite tube, sensitivity and memory effects were found to be dependent on the age of the graphite tube. Pretreatment of the graphite tube with La, Zr, and Mo to form their respective carbides resulted in sensitivity improvements in the silica test.

Ortner and Kantuscher (*7*) reported that silicon carbide formation was minimized by the use of graphite tubes impregnated with solutions of Ta, Ti, Hf, or Na_2WO_4. Recently Lagas (*8*) noted sensitivity improvements and a reduction in memory effects for some refractory materials by conditioning a pyrolytically coated graphite tube with lanthanum prior to injection of samples or standard solutions.

Despite the apparent difficulties associated with FAAS analysis of silicon, this technique appeared to offer a number of attractive advantages. FAAS analysis is amenable to automation with direct readout in concentration. In addition, FAAS provides a simple and direct method of determining silica in the deionized water used for the preparation of calibration standards. Consequently, our laboratory decided to pursue the possibility of developing a method for determining trace concentrations of silica by FAAS.

Our initial investigation into the use of FAAS for trace silica analysis was discouraging because of poor sensitivity and poor reproducibility, as well as memory effects. Acquisition of a new graphite atomizer with temperature controlled maximum power heating appeared to provide an improvement in sensitivity and a reduction in memory effects, thereby prompting further development of this method.

The method described herein permits analysis of silica in the concentration range of 5-250 μg/L SiO_2. The method utilizes flameless atomic absorption and is applicable to high purity waters, such as high pressure boiler waters and boiler feedwaters, and condensates. Calcium and lanthanum are added to samples and standards at a concentration of 1.0 mg/L CaO and 25 mg/L La to enhance the sensitivity of the test and to minimize interference from orthophosphate.

EXPERIMENTAL

Apparatus. A Perkin-Elmer Model 603 Atomic Absorption Spectrophotometer equipped with an HGA-2200 Heated Graphite Atomizer, a maximum power accessory which provides temperature controlled maximum power heating, and pyrolytically coated graphite tubes was used for all measurements. Readout was displayed simultaneously on a strip chart recorder and a PRS-10 Printer Sequencer. Both automatic sampling with an AS-1 Automatic Sampling Device and manual sampling with Eppendorf microliter pipets were used.

Instrument Settings. The 251.6-nm resonance line with a spectral band pass of 0.2 nm was used for all measurements. The line source was a silicon hollow cathode lamp operated at a current setting of 40 mA.

0003-2700/79/0351-0452$01.00/0 © 1979 American Chemical Society

Controls on the HGA-2200 were experimentally optimized to provide the following drying, charring, and atomizing times and temperatures: dry, 100 °C for 80 s; char, 1400 °C for 30 s; atomize, 2800 °C for 7 s. Argon was used as a purge gas. The purge gas flow was interrupted for 3 s from the beginning of the atomization stage to increase the residence time for silica atoms in the graphite tube, thus providing improved sensitivity. A 4-s integration time was used to measure silicon absorbance in the peak height mode. A 100-μL sample size was used throughout. The absorbance was expanded about 2.5 times and results were recorded directly in terms of concentration as μg/L SiO_2.

Reagents. Low-silica water was prepared by passing tap water through large beds of strongly acidic cation-exchange resin (Amberlite IR-120) and strongly basic anion-exchange resin (Amberlite IRA-402) followed by an identical cation/anion train for polishing. Low-silica water was stored in a preconditioned high density polyethylene container.

A stock 50 mg/L (as SiO_2) silica solution was prepared from sodium silicate pentahydrate obtained from Calgon Corporation, Pittsburgh, Pa. Standard silica solutions for instrument calibration were prepared by dilution of the stock solution with low-silica water. Standard solutions were stored in pre-rinsed polystyrene containers to avoid silica contamination.

The calcium–lanthanum reagent was prepared by adding 5.5 mL concentrated nitric acid to 2.90 g of 99.99% pure lanthanum oxide (obtained from Ventron-Alfa Products, Danvers, Mass.) wetted with about 50 mL of low silica water followed by dissolution of 0.100 g of calcium oxide (obtained from Fisher Scientific, Pittsburgh, Pa.). The solution was diluted to 1 L in a polypropylene volumetric flask with low-silica water.

Procedure. The pyrolytically coated graphite tube was conditioned before use by initiating the preset drying, charring, and atomizing cycle several times without sample injection until a low, reproducible absorbance value was obtained. The spectrophotometer was zeroed on this furnace blank.

The silica content of the low-silica water was determined by the method of standard additions. One hundred milliliters of low-silica water was transferred to a prerinsed polystyrene container and analyzed by FAAS. Appropriate aliquots of the 50 mg/L SiO_2 stock solution were added to the 100 mL of low-silica water to provide an equivalent of 25 and 50 μg/L SiO_2 and subsequently analyzed. The contribution of silica to the standards and samples by the calcium–lanthanum reagent was also determined by the method of standard additions. An equivalent of 1.0 mg/L CaO and 25 mg/L La was added to a 100-mL aliquot of deionized water and analyzed as above.

The standards used for instrument calibration, as well as samples, were pretreated by adding 100 μL of the calcium–lanthanum reagent to 10 mL of sample or standard in a pre-rinsed polystyrene container. This was equivalent to adding 1.0 mg/L CaO and 25 mg/L La. Pretreated standards and samples were transferred to pre-rinsed 2.0-mL polystyrene sampling cups for automatic sample injection. The instrument was calibrated with standard solutions containing a nominal concentration of 100 and 250 μg/L SiO_2. The actual concentration of silica in the standards was determined by adding the amount contributed by the water and reagents to the nominal concentration. The response was linearized by use of microprocessor-controlled automatic curvature correction to 250 μg/L SiO_2. Sample readings were corrected for the silica concentration contributed by the calcium–lanthanum reagent.

RESULTS AND DISCUSSION

Preliminary Investigation. Poor reproducibility and sensitivity, as well as memory effects, were noted when trace silica analysis was attempted with heated graphite atomizers not equipped with a maximum power accessory. Markedly improved sensitivity and reproducibility were obtained when a maximum power accessory equipped with an optical temperature sensor was used, although some memory effects were still present. The estimated detection limit of the test without matrix modification was about 5 μg/L SiO_2.

A number of chemicals were investigated as potential matrix modifiers in an attempt at improving sensitivity and reproducibility as well as achieving a detection limit <5 μg/L SiO_2. Addition of fluoride, iron, magnesium, manganese, and ammonium molybdate were tested as possible matrix modifiers to determine whether they would preferentially react with silica, thereby inhibiting carbide formation. In most cases, additions of these compounds resulted in a negligible increase in sensitivity. In addition, silica contamination in these reagents prevented their effective use as matrix modifiers.

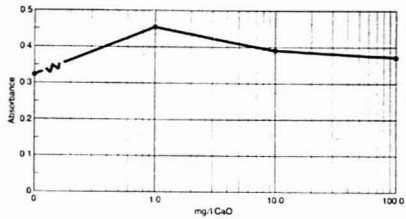


Figure 1. Effect of calcium oxide concentration on the silica signal by flameless atomic absorption. Silica concentration, 100 μg/L SiO_2

Evaluation of Calcium Addition. Thompson et al. (5) reported that addition of 1000 mg/L Ca as calcium nitrate enhanced the sensitivity of the silica test by FAAS. We found that addition of 1000 mg/L Ca as calcium nitrate resulted in some improvement in sensitivity. However, a high test blank was noted and background correction was required to compensate for the background absorption caused by the high concentration of calcium nitrate.

It was determined that the addition of calcium as calcium oxide did enhance the silica signal 40–50% at CaO concentrations as low as 1.0 mg/L when an optimum charring temperature of 1400 °C was used. The optimum addition of CaO was determined experimentally as indicated in Figure 1 by adding the equivalent of 0, 1.0, 10, and 100 mg/L CaO to separate 100 μg/L SiO_2 solutions. The enhancement effect (47%) noted when an equivalent of 1.0 mg/L CaO was added, was nearly twice the enhancement effect noted when an equivalent of 10 or 100 mg/L CaO was added. The enhancement effect of calcium is attributed to the formation of a calcium silicide, thus minimizing the formation of silicon carbide. The reaction of calcium with silicon to form a calcium silicide is known to occur above 1000 °C (9). The formation of calcium silicide is evidenced by the increase in silica response as the char temperature is increased from 1000 to 1500 °C. A plot of silica absorbance with increased char temperatures is indicated in Figure 2.

Phosphate Interference. Since some high pressure boiler systems or medium pressure boiler systems with low silica content are phosphate treated, the effect of orthophosphate on the silica signal was evaluated. To test the possible interference of phosphate in these waters, standards were prepared by adding an equivalent of 0.1 to 50 mg/L PO_4 (added as NaH_2PO_4) to separate solutions of 100 μg/L SiO_2 containing an equivalent of 1.0 mg/L CaO and analyzed by the flameless atomic absorption method. The presence of as little as 1.0 mg/L PO_4 was found to suppress the silica signal by 22%.

It is possible that this interference effect is due to the reaction of phosphate with added calcium to form a calcium phosphate, thereby inhibiting the formation of the calcium silicide. In the flame atomic absorption analysis of calcium, lanthanum is used as a releasing agent to suppress formation of calcium phosphate (*10*, *11*). The use of lanthanum to minimize phosphate interference in the flameless atomic absorption test for silica was investigated on the basis of its

Table I. Comparison of Silica Results Obtained by Flameless Atomic Absorption and the Heteropoly Blue Colorimetric Method

		SiO_2, μg/L					
			flameless atomic absorption				
test no.	sample type	colorimetric	found	amount added	found after addition	recovered	recovery, %
1	superheater outlet	40	42	50	92	50	100
2	superheater outlet	38	36	50	78	42	84
3	boiler feedwater	10, 11	3	25	28	25	100
4	anion effluent	20, 19	19	50	75	56	112
5	deionized water	19, 22	36	50	89	53	106
6	polisher effluent	<5	<5	50	46	46	92
7	demineralized water	12	11	25	38	27	108
8	steam before superheater	25	15	50	65	50	100
9	condensate	50, 50	45	50	95	50	100
10	boiler feed water	21	24	25	48	24	96
11	anion outlet	22	28	50	74	46	92
12	condensate	45	46	50	97	51	102
13[a]	condensate	46, 56	68	50	117	49	98
14	anion effluent	13. 10	9	25	41	32	128
15	boiler water	42, 40[c]	37	50	82	45	90
16	deionized water	78	85	50	130	45	90
17	condensate	200, 200	112	50	172	60	120
18	condensate	37	37	50	96	59	118
19[b]	condensate	400, 300	130	50	178	48	96
20	anion outlet	<5	<3	-	-	-	-
21	saturated steam	10	3	-	-	-	-
22	mixed bed outlet	5	4	-	-	-	-
23	condensate pump discharge	<5	<3	-	-	-	-

[a] Suspended solids present. [b] Colloidal material present. [c] Double reagents added for PO_4 interference.

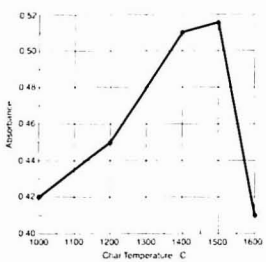


Figure 2. Effect of varying char temperature on silica sensitivity with 1.0 mg/L CaO added (100 μg/L SiO_2)

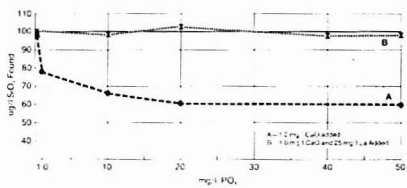


Figure 3. Effect of orthophosphate on silica analysis by flameless atomic absorption with and without lanthanum addition. (100 μg/L SiO_2)

tendency to preferentially react with phosphate, thereby freeing calcium to form the desired calcium silicide. Addition of an equivalent of 25 mg/L lanthanum was found to essentially eliminate the phosphate interference. Figure 3 indicates the effectiveness of lanthanum addition in eliminating phosphate interference. The enhancement effect of the calcium addition was not significantly altered by the addition of lanthanum. The optimum char temperature with the 25 mg/L La addition was 1400 °C.

Evaluation of the Method. The silica reponse with addition of 1.0 mg/L CaO and 25 mg/L La was linear to about 100 μg/L SiO_2.

The single-operator precision of the method was determined by performing at least nine replicate analyses of standard silica solutions prepared with low-silica water of known silica content. Automatic sample injection was used. The relative standard deviation as percent was 15.4, 6.1, 7.7, and 3.3 for 10, 25, 50, and 150 μg/L SiO_2, respectively.

The detection limit of the silica test was determined by 10 sequential analyses of a blank solution (low-silica water), 10 μg/L SiO_2 standard, and a 25 μg/L SiO_2 standard solution. The calculated detection limit was 2.5 μg/L SiO_2.

Industrial water samples which had been previously analyzed by the heteropoly blue colorimetric method were also analyzed by flameless atomic absorption and the results compared. The comparative data for the colorimetric and FAAS methods are listed in Table I. Comparison was good considering that silica results obtained by either method may vary as much as ±5 μg/L SiO_2.

The recovery of added silica from the previously analyzed water samples was determined by fortification with known amounts of silica and analysis by FAAS. The recovery data are also listed in Table I. The recovery ranged from 84–128%. Most of the recovery data were within 100% ± 10.

Precautions Concerning the Method. Precise and accurate results using the FAAS method for trace silica analysis are dependent upon careful technique and awareness of potential problems unique to this test.

When autosampling is used, misalignment of the pipet tip on the AS-1 Auto Sampler may adversely affect the precision of the method if the distance of the pipet tip from the bottom of the furnace during sample injection is not correctly adjusted to 2–3 mm. If the tip repeatedly strikes the bottom of the

graphite tube, the pyrolytic coating is eroded and some reduction in sensitivity results.

The sensitivity of the silica test varies somewhat from day to day due to variation in the quality of the pyrolytic coating on the graphite tube. The properties of the pyrolytically coated tube are more important for the silica test, in which charring and atomizing temperatures are somewhat higher than for many other FAAS tests.

Because a 100-μL sample is required for the trace silica test, it is important to carefully control the drying time and temperature to avoid loss of sample by boiling during the drying stage. A drying time of 80 s was chosen to ensure proper drying of the sample even if the drying temperature needs to be set slightly less than 100 °C. A lower drying temperature may be required when the autosampling device is used for an extended period of time for sample injection, since the graphite atomizer is not cooled as efficiently after numerous sample analyses as in the initial sample injections. The analyst must monitor the drying stage after about 10 sample analyses to make certain the sample is slowly evaporating, not boiling during the drying stage.

Sometimes a spurious peak is observed immediately following the silica atomization peak. Since the highest atomization peak within the preset integration time (usually 4 s) is recorded by the spectrophotometer, the integration time may need to be set between 3 and 4 s to assure that only the silica atomization signal is measured.

The wavelength must be carefully adjusted on the spectrophotometer to properly set the wavelength at 251.6 nm. There are several other sensitive wavelengths in the same region — 250.7, 252.4, and 252.8 nm. Improper wavelength adjustment will result in loss of sensitivity.

Care must be exercised to avoid silica contamination. No glassware should be used in the preparation of silica standard solutions or samples. All receptacles, e.g., such as polyethylene pipet tips, polystyrene beakers, and 2.0-mL cups for the automatic sampling device, must be pre-rinsed with either low-silica water and/or the solution the receptacle is to contain. The flush water used for the AS-1 autosampler must be low-silica water. Samples requiring trace silica analysis should be collected in high density polyethylene bottles.

LITERATURE CITED

(1) J. T. Woods and M. G. Mellon, *Ind. Eng. Chem., Anal. Ed.* **13**, 760 (1941).
(2) American Public Health Association "Standard Methods for the Examination of Water and Wastewater", 14th ed., 1975, p 490.
(3) J. C. Guillaumin, *At. Absorpt. Newsl.*, **13**, 135 (1974).
(4) H. L. Kahn, M. Bancroft, and R. H. Emmel, *Res./Dev.*, **23** (7), 30 (1976).
(5) K. C. Thompson, R. G. Godden, and D. R. Thomerson, *Anal. Chim. Acta*, **74**, 289 (1975).
(6) David B. Lo and Gary D. Christian, *Can. J. Spectrosc.*, **22**, 45 (1977).
(7) H. M. Ortner and E. Kantuscher, *Talanta*, **22**, 581 (1975).
(8) P. Lagas, *Anal. Chim. Acta*, **98**, 261 (1978).
(9) "Encyclopedia of Industrial Chemical Analysis", Snell and Ettre, Ed., Interscience Publishers, New York 1973, pp 18, 39.
(10) Joseph L. Dinnin, *Anal. Chem.*, **32**, 1475 (1960).
(11) J. B. Willis, *Spectrochim. Acta*, **16**, 259 (1960).

RECEIVED for review November 9, 1978. Accepted December 21, 1978.

Fluorescence Photometric Determination of Disopyramide and Mono-*N*-dealkylated Disopyramide in Plasma after Separation by Thin-Layer Chromatography

Ram N. Gupta,* Francis Eng, and Diane Lewis

Department of Laboratory Medicine, St. Joseph's Hospital, Hamilton, Ontario, Canada

Cyrus Kumana

Department of Medicine, McMaster University, Hamilton, Ontario, Canada

A thin-layer chromatographic method for the estimation of disopyramide and its metabolite, mono-*N*-dealkylated disopyramide is described. The method involves a simple extraction of 200 μL of plasma at alkaline pH with benzene. An aliquot of the extract is quantitatively spotted on a TLC plate. The plate is developed in the solvent (ethyl acetate:methanol:ammonia, 40:30:0.5) which allows good separation of the two compounds from one another, from plasma constituents, and from other drugs which are prescribed along with disopyramide. The plate is dipped in 20% sulfuric acid in methanol to make these compounds fluorescent. Densitometric scanning of the separated compounds provides a precise quantitative estimation. The procedure is linear up to 10 mg/L and the calibration curve passes through the origin.

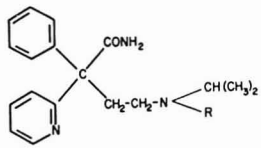
Disopyramide (DIS) is an anti-arrhythmic drug effective in the treatment of a broad spectrum of atrio-ventricular arrhythmias (*1*), and has recently been introduced in North America. It is metabolized primarily to mono-*N*-dealkylated disopyramide (MND) (*2*), which probably has less therapeutic activity than DIS. In most instances, it has been the practice to correlate clinical effect solely with plasma concentrations of the parent drug, but for several reasons knowledge of plasma MND concentrations may also be useful. If treatment failure is associated with low DIS levels, high plasma MND levels would favor rapid metabolism as the cause rather than noncompliance.

Data on the plasma concentration effect of the MND metabolite is still relatively meagre in the clinical setting and the MND metabolite, although less active than DIS, could be important in patients having a high proportion of metabolite; particularly if the dosage of DIS administered is being titrated to yield a given plasma concentration. Individual differences in sensitivity may exist between patients both for plasma concentration of DIS and/or MND. In long-term therapy, the metabolizer status of the patient could prove helpful where side effects emerge.

Initially, DIS was evaluated by a spectrofluorometric procedure (*3*). This procedure measures both the parent drug and its metabolite as both of them are nearly equally fluorescent in the presence of strong acid (λ_{ex} = 275 nm; λ_{fl} = 410 nm). For clinical use, this procedure lacks specificity

0003-2700/79/0351-0455$01.00/0 © 1979 American Chemical Society

as other compounds present may produce fluorescence under the experimental conditions.



R = $-CH(CH_3)_2$ = DISOPYRAMIDE
R = H = MONO-N-DEALKYLATED DISOPYRAMIDE

In the past few years, gas chromatographic procedures have been described using either a flame ionization detector (*4–7*) or a nitrogen-selective detector (*8*). However, only one of these procedures (*4*) describes the simultaneous estimation of the parent drug and its metabolite. The sample preparation of this procedure is complex, tedious, and not suitable for a routine laboratory.

To overcome the problems of analysis of these compounds by gas chromatography, high performance liquid chromatographic procedures using paired-ion techniques for the simultaneous estimation of DIS and MND have been described (*9*). After separation, these compounds are estimated by their UV absorption at 254–258 nm. We describe a procedure in which DIS and MND are separated by TLC and then estimated by fluorometric densitometry.

EXPERIMENTAL

Instrumentation. A TLC scanning spectrophotometer, model KM3 (Carl Zeiss, Canada Ltd., Don Mills, Ontario) was used in the fluorescent (M-Pr) mode with a mercury vapor lamp as the light source for excitation. A Turner filter, No. 110-812, narrow pass, 405 nm (Fisher Scientific Co., Toronto) with a holder improvised to fit the Zeiss scanner was used for isolation of the emitted light. It was inconvenient to use Zeiss M-405 filter in M-Pr mode. Both a strip-chart recorder, model 355 (Linear Instrument Corp., Irvine, Calif.) and an Autolab System IV computing integrator (Spectra Physics, Santa Clara, Calif.) were used for calculation.

Silica gel 60 glass plates, 20 × 20 cm, without fluorescent indicator (E. Merck, No. 5763) were developed in TLC tanks with twin chambers (Terochem Laboratories, Edmonton, Alberta). The extracts were applied to the TLC plates using a TLC multispotter equipped with 250-μL syringes and a nitrogen flow system (Analytical Instrument Specialties, Libertyville, Ill.). A dipping tank (Whatman Inc., Clifton, N.J.) was used to acidify the plate. All volume measurements were made with SMI micro-pettors (Scientific Manufacturing Industries, Emeryville, Calif.).

Reagents. All reagents were of analytical grade and were used without further purification. Disopyramide, chlordisopyramide and mono-*N*-dealkylated disopyramide were obtained as gifts from Searle Canada Ltd., Oakville, Ontario.

Stock standards (1 mg/mL) of each of these compounds were prepared by dissolving appropriate amounts of the hydrochloride salts in 0.1 N HCl.

Plasma Standards. Combined plasma standards containing 2.5, 5, 7.5, and 10 mg/L of both DIS and MND were prepared by adding appropriate volumes of the stock standards of DIS and MND to drug-free pooled plasma. The plasma standards were divided into 2-mL aliquots and frozen until assay.

Patients' Samples. One hour after the last dose, venous blood from patients receiving regular disopyramide therapy was drawn into evacuated, sterile, heparinized, blood collection tubes. Plasma was separated within 2 h of collection and stored at 4 °C until analyzed. The samples were frozen when they were to be stored for more than 48 h.

Procedure. To 0.2 mL of spiked plasma standards or patient plasma in 13 × 100 mm glass culture tubes, with Teflon-lined screw caps, 50 μL of 6 N NH_4OH and 1 mL of benzene were added. The tubes were shaken on a mechanical shaker at low speed for 5 min and were then centrifuged. Before loading the 250-μL syringes onto the TLC multispotter, each syringe was rinsed with a benzene extract and then filled accurately to the 100-μL mark with the same extract. The spotter heater was maintained at 50–60 °C in a gentle atmosphere of nitrogen. The plunger drive was driven at medium speed to complete the spotting in about 5 min. The extracts of all standards were spotted on each plate if more than one plate was used.

The plate was developed in solvent, ethyl acetate/methanol/ammonia (40:30:0.5), to a height of about 12 cm and air-dried for 10 min. The plate was then dipped in 20% sulfuric acid in methanol. The back of the plate was wiped dry with tissue paper and allowed to stand in air in subdued light for 45 min. The plate was then scanned in the fluorescence mode (λ_{ex} = 266 nm, λ_{em} ≃ 405 nm; slit length = 10 mm, and slit width = 2 mm).

The emission peaks were recorded on the strip chart recorder and simultaneously integrated by the electronic integrator. Under these conditions, peaks only due to DIS, MND, and the solvent front were observed.

The plasma DIS and MND levels were determined from standard curves established by plotting peak areas of the standards against the DIS and MND concentrations of the standards.

RESULTS AND DISCUSSION

It is common practice to use internal standards for the assay of drugs in body fluids by chromatographic procedures to obviate the need of accurate measurements at various steps. *p*-Chlorodisopyramide (Cl-DIS) has been used as internal standard in GC (*4*) and HPLC procedures (*9*). In our initial experiments, we also used this compound as an internal standard, which was added to plasma prior to extraction. It was found that the intensity of fluorescence of Cl-DIS was about 5 times that of DIS. Further, it proved difficult to select a suitable solvent for ideal separation of the three compounds from each other and from other fluorescent anti-arrhythmic drugs, particularly quinidine. The procedure described in this report is simple and does not involve many volume measurements and evaporation of extracts. When the assay of DIS and MND without the addition of an internal standard was attempted, better precision overall was achieved than that found with the initial procedure including the internal standard.

It was decided to use a solvent which would provide the upper layer to facilitate the collection of extracts. A number of solvents less dense than water were tested for extraction efficiency and for ease of spotting and benzene was found to be the most suitable solvent. Recovery from plasma spiked with DIS and MND was found to be about 90%. This was determined by comparing the peak areas of DIS and MND in extracted plasma standards to the peak areas of unextracted methanolic standards of the same concentration. The extraction efficiency is unaffected by change in pH between the range of 9–13. To minimize exposure to benzene vapor, spotting is carried out in the fume hood.

In the present procedure, an auto-spotter is used for convenience and speed. However, it is not essential to do so. Plasma (0.2 mL) can be extracted with less volume (0.2 mL) of benzene and 20 μL can be spotted manually in a current of nitrogen without loss of precision. However, it is tedious to do so when a large number of samples are to be spotted.

Disopyramide has been estimated fluorometrically in the presence of strong acid with the excitation at 275 nm (*3*). In the present procedure, high fluorescence was observed when λ_{ex} = 266 nm was used. However, the mercury line at 266 nm is weak and requires a wide slit width (1.5–2 mm). The base line is still quite stable under these conditions (Figure 1).

Different concentrations of aqueous and alcoholic solutions of sulfuric acid, perchloric acid, and phosphoric acid were compared for the development of optimum fluorescence of disopyramide and its metabolite. The reagent used in the present procedure, 20% methanolic sulfuric acid, gave the best

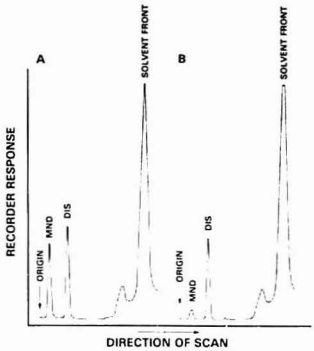


Figure 1. Chromatogram of extracts: (A) of plasma spiked with 4 mg/L each of DIS and MND; (B) of plasma from a patient receiving 4 × 200 mg/day of DIS. Fluorescence mode: λ_{ex} = 266 nm, λ_{em} = 405 nm, slit width = 2 mm

Table I. Estimation of Precision

	DIS			MND		
A. Within-batch variation						
mean, mg/L	2.11	4.09	5.94	2.02	4.01	6.02
1 S.D., mg/L	0.11	0.13	0.13	0.12	0.07	0.12
N	10	10	10	10	10	10
C.V., %	5.3	3.1	2.2	5.8	2.0	2.0
B. Between-batch variation						
mean, mg/L	2.02	4.01	5.90	2.04	4.01	6.01
1 S.D., mg/L	0.04	0.10	0.18	0.08	0.17	0.11
N	10	10	10	10	10	10
C.V., %	2.4	2.6	3.1	4.0	4.4	1.9

results. Initially, the fluorescence continues to increase while the plate is drying and then after 3 h there is a gradual decrease in fluorescence. The fluorescence of MND is about 80% that of DIS.

The procedure is linear to 10 mg/L for both DIS and MND and the standard curve passes through the origin. When a test sample shows a level greater than 10 mg/L, TLC quantitation is repeated using 50 μL of the extract.

The precision of this procedure for both DIS and MND is satisfactory when compared to current methodology (*5*, *9*). Within-batch and between-batch precision was tested with plasma samples spiked with different concentrations of these compounds within the therapeutic range (2, 4, and 6 mg/L) and the results are summarized in Table I.

Twenty-five blind serum samples, spiked with DIS by G. D. Searle and Company, Oakville, Ontario, were submitted for analysis by the TLC procedure. The data are presented in Table II. After evaluation, the TLC method was considered to be acceptable for the analysis of DIS in plasma.

A number of plasma constituents and other drugs, if present, could also be extracted due to the simple benzene extraction employed. Therefore, plasma spiked with a number of drugs which may be administered with disopyramide was carried through the procedure. As shown in Table III, these drugs do not interfere with the assay of disopyramide or its metabolite. Fluorescence adds to the specificity of the thin-layer chromatographic procedure. Chromatographic procedures are not absolutely specific and it is not possible within the scope of this study to exclude all potential interferences. In the last six months, we have analyzed more than 50 samples from patients receiving disopyramide and we have not observed any interference (distorted peaks or

Table II. Blind Sample Study

concn of spiked samples, μg/mL	no. of samples	observed values
0.5	2	0.45, 0.45
1.0	2	0.76, 0.84
1.8	2	1.92, 2.08
2.0	2	2.12, 2.17
2.5	4	2.52, 2.73
		2.42, 2.62
2.75	6	2.88, 2.86
		2.81, 2.64
		2.91, 2.92
3.0	2	3.50, 3.34
3.5	2	3.47, 3.50
8.0	3	7.01, 7.18
		7.10

Table III. Interference Studies

compound	concn mg/L of plasma	R_f[a] solvent 1	R_f[a] solvent 2
DIS		0.40	0.51
MND		0.20	0.39
Cl-DIS		0.48	0.58
caffeine	20	- -	- -
codeine	5	- -	- -
chlordiazepoxide	10	- -	- -
diazepam	5	- -	- -
diphenylhydantoin	40	- -	- -
flurazepam	5	- -	- -
lidocaine	10	- -	- -
procainamide	10	- -	- -
propranalol	5	- -	- -
quinidine	10	0.57	0.67

[a] Solvent 1 = ethyl acetate/methanol/ammonia (40:30:0.5). Solvent 2 = methanol/ammonia (100:1.5). (- -) = Not detected; stays at origin or migrates with solvent front.

Table IV. Steady-State Plasma Concentrations (Pre-dose level, i.e., 6 hours post-dose)

patient	6 hourly dose, mg	DIS, mg/L	MND, mg/L	DIS/MND
1	200	1.8	1.8	1.0
2	200	4.9	0.3	16.3
3	200	3.0	1.2	2.5
4	150	0.6	2.3	0.7
5	150	2.9	0.4	7.3
6	100	1.7	0.1	17.0

unusually high values for DIS or MND). If an interference is suspected, TLC would be repeated using an alternate solvent #2: methanol/ammonia (100:1.5). When more than one chromatographic system is employed, the combined discriminating power increases (*10*). As shown in Table IV, there is a wide variation in the plasma levels of DIS and MND in patients receiving similar doses of disopyramide and in the ratio of MND/DIS.

The procedure is sensitive. DIS or MND can be quantitated at a concentration of 0.5 mg/L of plasma. The quantitative TLC procedure described here for the estimation of DIS and MND is an acceptable, efficient method for incorporation into a routine laboratory.

ACKNOWLEDGMENT

We are indebted to F. Louman, G. D. Searle & Co., for providing pure compounds and spiked samples.

LITERATURE CITED

(1) L. A. Vismara, D. T. Mason, and E. A. Amsterdam, *Clin. Pharmacol. Ther.*, **16**, 330 (1974).
(2) A. Karim, R. E. Ranney, and S. Kraychy, *J. Pharm. Sci.*, **61**, 888 (1972).
(3) R. E. Ranney, R. R. Dean, A. Karim, and F. M. Radzialowski, *Arch. Int. Pharmacodyn.*, **191**, 162 (1971).
(4) T. C. Hutsell and S. J. Stachelski, *J. Chromatogr.*, **106**, 151 (1975).
(5) J. W. Daniel and S. Subramanian, *J. Int. Med. Res. Suppl. 1*, **4**, 2 (1976).
(6) A. Johnston and D. McHaffie, *J. Chromatogr.*, **152**, 501 (1978).
(7) A. M. Hayler and R. J. Flanagan, *J. Chromatogr.*, **153**, 461 (1978).
(8) A. M. J. A. Duchateau, F. W. H. M. Merkus, and E. Schobben, *J. Chromatogr.*, **109**, 432 (1975).
(9) P. J. Meffin, S. R. Harapat, and D. C. Harrison, *J. Chromatogr.*, **132**, 503 (1977).
(10) A. C. Moffat and K. W. Smalldon, *J. Chromatogr.*, **90**, 9 (1974).

RECEIVED for review September 15, 1978. Accepted December 9, 1978.

CORRESPONDENCE

Improved Timing Resolution in Time-Correlated Photon Counting Spectrometry with a Static Crossed-Field Photomultiplier

Sir: Time-correlated photon counting is a power analytical technique for studying a variety of properties of chemical systems. Recently, reported experimental measurements using gated detection techniques have an overall timing uncertainty (light source plus detection system) of 1 ns or less, limited principally by the transit time dispersion in conventional photomultiplier tubes (*1–4*). Because many physiochemical processes of interest display a temporal behavior requiring time-correlated measurements for analysis and/or to improve signal-to-noise ratio, even small reductions in timing uncertainty on the subnanosecond time scale can extend significantly the applicability of this analytical method to, inter alia (1) the study of fluorescent molecules with very short lifetimes, (2) the elimination of Raman background-scattering from fluorescence emission spectra, (3) time-resolved emission spectra of transient species, and (4) the enhancement of Raman spectra by rejection of fluorescence background emission.

Previously, we reported the use of a synchronously pumped tunable dye laser producing very short light pulses (<35 ps fwhm), coupled with a modified Ortec 9200 photon counting system (*1, 2*). In this communication, we report a detection system with improved timing performance using a Varian VPM-154 static crossed-field photomultiplier (SCFP). The important advantages of the SCFP are: the transit time dispersion is <30 ps, the anode pulse risetime and FWHM are 120 ps and 160 ps, respectively, with very little pulse-to-pulse shape variation, and there is very good pulse height resolution within a relatively narrow dynamic range (*5–7*). These characteristics indicate that the SCFP can be used to substantially decrease timing uncertainty, such that the limiting factor will be the bandwidth of the remaining electronic devices in the detection circuit.

EXPERIMENTAL

A synchronously-pumped cavity-dumped Rhodamine 6G dye laser was used as the light source. The manner in which the laser is interfaced with the photon counting system has been described previously (*1*). Replacing the Ortec 473A in the stop channel with an Ortec (leading edge) 924 Quad Discriminator, the timing resolution of the photon counting electronics (without photomultiplier and amplifier) was determined to be <15 ps.

Pulse profile measurements were made using a VPM-154A.6D SCFP, with an InGaAsP photocathode, in the detection channel. Mounted in a Products for Research TE-165RF housing and cooled to −78 °C, the SCFP had a gain of 1×10^5 when operated at cathode and rail potentials of −3300 VDC and +320 VDC, respectively. The anode signal was terminated in a 50-Ω load at the input to a HP 35005A amplifier with 0.1- to 2.0-GHz bandwidth and 40-dB gain. The amplifier output was connected directly to the Ortec 924 Quad Discriminator. By using a Tektronix CT-3 Signal Pickoff to obtain a CRT display of the amplified anode signal input to the discriminator, the threshold trigger point could be observed by comparing the internally triggered display with the trace externally triggered by the negative logic output from the discriminator.

The pulse profile presented in Figure 1 was recorded by scattering the 580-nm laser output from a Ludox solution. Experimental repetition and data acquisition rates were ca. 60 and 3 kHz, respectively. The data collection rate was 5% of the experimental repetition rate in order to achieve good single photon counting statistics. With 40 000 counts in the peak channel, the spectrum was obtained in ~3 min. The small cavity-dumped trailing pulse, separated from the main peak by the mode-locker drive period of 13.020 ns, was used for time scale calibration. The minimum pulse width recorded with this system was 228 ps fwhm.

As a test of this experimental procedure, we determined the fluorescence lifetime of 10^{-6} M Rhoadmine B in water. The result of 1.52 ns was within experimental error compared to the previous value of 1.48 ns, obtained with our conventional photomultiplier detection system (*1*).

DISCUSSION

We have achieved significant reduction in the timing uncertainty for the photon counting detection system. When compared with previous subnanosecond measurements (with a picosecond laser) using an RCA 31034 photomultiplier (*3*), which has a spectral response similar to the SCFP, the improvement is 72%. Relative to the measurements of Raman enhancement factors using an Amperex PM2106 photomultiplier (*4*), the improvement is 77%. Lastly, in relation to our previous studies using an RCA 8850 photomultiplier (*1*), the improvement is 35%.

With regard to analytical applications, such reductions in timing uncertainty can significantly extend measurement capabilities of gated detection systems. The analysis of subnanosecond fluorescence lifetime parameters and the enhancement of fluorescence emission spectra by eliminating Raman (and diffuse) background-scattering are greatly improved when the excitation profile approximates a "delta function" impulse in relation to the relaxation time. In addition, time-resolved emission spectra of transient species may be obtained within subnanosecond time intervals subsequent to the light pulse. Relevant to these points is the fact that the full-width-tenth-maximum occurs ~380 ps from the excitation peak (Figure 1a).

Furthermore, significant enhancements of Raman spectra by the rejection of fluorescence background emission may be obtained. Using a 1.0 ns fwhm excitation pulse, Raman

0003-2700/79/0351-0458$01.00/0 © 1979 American Chemical Society

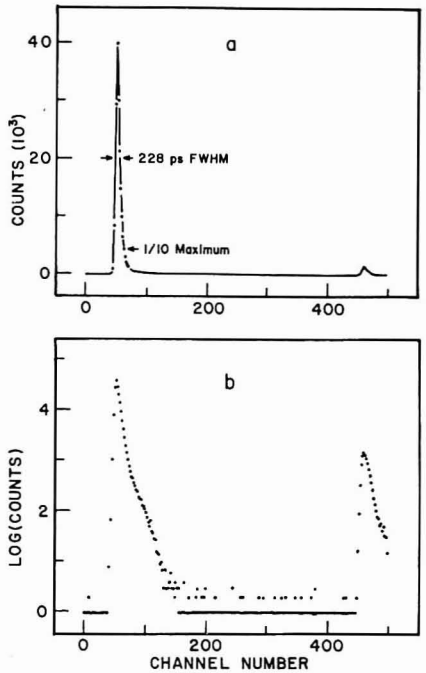


Figure 1. Static crossed-field photomultiplier measurement of excitation pulse profile: (a) linear, (b) semi-log. Time scale calibration is 31.7 ps/channel

enhancement factors of 34 and 115 were reported for benzene in the presence of fluorophores with lifetimes of 4.5 ns (acridine orange) and 15.6 ns (rubrene), respectively (*4*). For the excitation pulse width of 228 ps, we calculated (theoretical) enhancement factors of 118 and 392, corresponding to the fast and slow emitters, respectively.

The principal reason for the displayed pulse width being greater than the actual laser light pulse is the timing walk introduced into the detection channel by the leading edge discriminator. This situation is to be contrasted with recent publications where the photomultiplier transit time dispersion was the limiting factor in determining the timing uncertainty (*1–3*).

The system could potentially be further improved using constant fraction timing. However, present bandwidth limitations in our constant fraction discriminator (Ortec 473A) prevented its use. Likewise, it may be possible by using a higher gain amplifier–SCFP combination, in which case the discriminator can be adjusted to trigger at a point much closer to the leading edge fast risetime portion of the anode signal, to decrease timing walk and further optimize timing performance. Such improvements, in order to ultimately reach the timing resolution limit imposed principally by the transit time dispersion in the SCFP, will in our view justify the ~$15 000 cost of the SCFP.

ACKNOWLEDGMENT

The author gratefully appreciates technical assistance from T. J. Paules and J. Mougianis, E. G. & G. Ortec, Inc.; M. R. Cole, Products for Research; S. J. Green, McDonnell Douglas Astronautics Company—East; J. B. Abshire, NASA Goddard Space Flight Center; and R. Enck and J. R. Klein, Varian LSE Division.

LITERATURE CITED

(1) V. J. Koester and R. M. Dowben, *Rev. Sci. Instrum.*, **49**, 1186 (1978).
(2) V. J. Koester and R. M. Dowben, *Biophys. J.* **24**, 245 (1978).
(3) K. G. Spears, L. E. Cramer, and L. D. Hoffland, *Rev. Sci. Instrum.*, **49**, 255 (1978).
(4) J. M. Harris, R. W. Chrisman, F. E. Lytle, and R. S. Tobias, *Anal. Chem.*, **48**, 1937 (1976).
(5) J. B. Abshire, *NASA Tech. Memo.*, **78027** (1977).
(6) J. B. Abshire and H. E. Rowe, *NASA Tech. Memo.*, **78028** (1977).
(7) J. B. Abshire and H. E. Rowe, *NASA Tech. Memo.*, **78029** (1977).

Vaughn J. Koester
Department of Physiology and Graduate Program in Physiology and Biophysics
University of Texas Health Center at Dallas
5323 Harry Hines Boulevard
Dallas, Texas 75235

RECEIVED for review October 5, 1978. Accepted December 18, 1978. This work was supported by grants from the Robert A. Welch Foundation, the National Heart, Lung, and Blood Institute (HL-16678), and the Sid W. Richardson Foundation.

Ligand Exchange Chromatography of Amino Acids on Copper(II) Modified Silica Gel with Ultraviolet Spectrophotometric Detection at 210 Nanometers

Sir: Ligand exchange chromatography evolved in 1961 (*1*) from the fundamental work of Walton and Stokes, "Metal Amine Complexes in Ion Exchange" (*2*) published in 1954. Although it seemed to be a powerful tool, ligand exchange chromatography (*3*) has remained marginal because of two major drawbacks. First, the slow kinetics of mass transfer during the exchange of ligands in the sorbed metal coordination sphere, in addition to the slow diffusion of mobile ligands in the resin particles of the stationary phase lead to poor efficiency for the columns and subsequently broad peaks.

Second, exchangers of the polystyrene divinylbenzene type have poor mechanical properties. High pressures cannot be used; otherwise, the resins deform or collapse and column permeability decreases.

Good results have been recently obtained as well by deposited metal on or incorporated metal into pure silica gel (*4, 5*), ligands chemically bonded to silica and then copper(II) loaded (*6, 7*), and by metal ions coordinated to an hydrophobic

0003-2700/79/0351-0459$01.00/0 © 1979 American Chemical Society

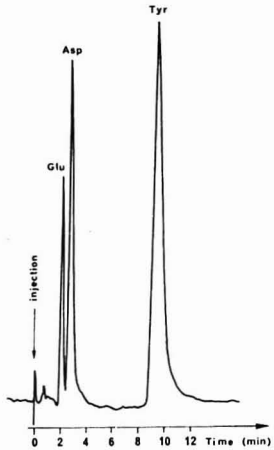


Figure 1. Separation of Glu, Asp, and Tyr by ligand exchange chromatography on Cu(II) modified silica gel. Column: L = 15 cm, i.d. = 0.48 cm. Packing: Cu(II) modified silica gel (Partisil, dp = 7 μm). Mobile phase: water–acetonitrile (70:30 v/v), with $(NH_3) = 10^{-1}$ M. Flow rate = 1.7 mL min^{-1}. Inlet pressure = 100 atm. Temperature: ambient

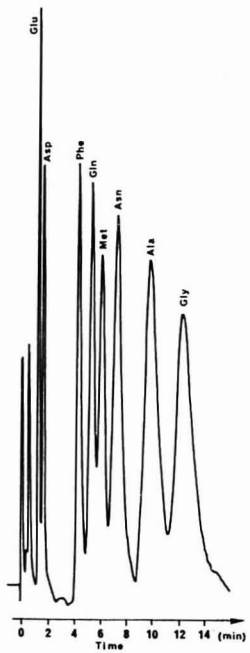


Figure 2. Separation of eight amino acids by ligand exchange chromatography on Cu(II) modified silica gel. Conditions as in Figure 1, except $(NH_3) = 1.4\ 10^{-1}$ M

chelating agent in the mobile phase in conjunction with a reversed phase packing (*8*, *9*). An application of ligand exchange chromatography is the resolution of optical isomers on chiral bonded phases loaded with a transition metal (*10–12*).

The following results in high performance liquid chromatography of amino acids have been obtained in our laboratory by using a Cu(II) modified silica gel as stationary phase.

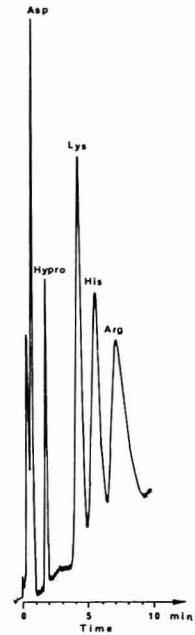


Figure 3. Separation of Asp, Hypro, and basic amino acids by ligand exchange chromatography on Cu(II) modified silica gel. Conditions as in Figure 1, except L = 5 cm, and (NH_3) = 1 M. Remarks: NH_3 slowly attacks the silica gel matrix, and we observe a decreae in efficiency with time. The drift base line is then caused by slow apparition of Cu(II) ions in the eluate

EXPERIMENTAL

Columns. Stainless steel columns of variable length and 4.8-mm i.d. were packed by the slurry technique with silica gel Partisil 5 (mean particle size, 7 μm) (Whatman).

A $CuSO_4$ 10^{-2} M, NH_3 1 M aqueous solution was then allowed to percolate slowly through the columns. Equilibrium was reached when 0.75 mmol of Cu(II) per gram of silica gel was fixed. After washing, the analysis of the modified silica gel revealed a total lack of sulfate ions, which meant that formation of cupric silicates did occur. Cu(II) ions were strongly fixed since further elution with an ammonia–water–acetonitrile mixture ((NH_3) up to 1 M) did not reveal Cu(II) ions in the eluate (as we checked with an atomic absorption instrument (Varian AA6)).

Columns were then ready for ligand exchange chromatography and fitted on the liquid chromatograph.

Chromatographic Runs. Liquid chromatography was performed using a Varian Model 8510. Typical sample size of 2 μL were introduced with a 5-μL Hamilton syringe via a stop-flow injector. The spectrophotometric detector was a Varichrom (Varian) with a flow cell of 8 μL. The wavelength was 210 nm. The eluant was a mixture of water (bidistilled)–acetonitrile (spectrograde) (70:30 v/v), with ammonia as the competing ligand. Chemicals were from Merck (Darmstadt, West Germany) and Prolabo (Paris, France).

RESULTS

Typical chromatograms are shown in Figures 1 to 3. (In these figures, the following abbreviations are used: Asp, aspartic acid; Glu, glutamic acid; Tyr, tyrosine; Phe, phenylalanine; Gln, glutamine; Met, methionine; Asn, asparagine; Ala, alanine; Gly, glycine; Hypro, hydroxyproline; Lys, lysine; His, histidine; Arg, arginine.) The acidic amino acids are eluted first, followed by the neutral ones. The concentration of ammonia must be adjusted carefully because of its strong influence. As a rule, a higher concentration of ammonia reduces the capacity factors and improves the column efficiency, i.e., affects both thermodynamic and kinetic phenomena. Basic amino acids are strongly fixed and need very short columns (5 cm long) and concentrated solutions of ammonia (1 M), so that the lifetime of the columns is shortened. These preliminary results already proved comparable with those obtained by ion-exchange chromatography (*13*) or by reversed phase chromatography (*14*), thus giving the way to very promising developments.

Let us note the following advantages of the method: (1) The pure silica gel is cheap and exhibits high mechanical properties. (2) The procedure for Cu(II) modification is very simple. (3) The detection of amino acids without derivatization is easy. (4) The columns are highly efficient, as a result of the small particle size (7 μm). (For example, the plate height evaluated on the lysine peak is about 0.07 mm). (5) The time for an analysis is short.

A disadvantage is the very slow attack of the silica gel matrix by ammonia. The use of other competing ligands, like aliphatic amines, alcohol amines, and polyamines could probably delay the loss in efficiency (*15*). Further investigation is in progress on the influence of other parameters: temperature, nature and proportion of organic solvents, nature of the metal ion, and modification of the stationary phase by added chemically bonded materials.

LITERATURE CITED

(1) F. Helfferich, *Nature (London)*, **189**, 1001–1002 (1961).
(2) H. F. Walton and R. H. Stokes, *J. Am. Chem. Soc.*, **76**, 3327–3331 (1954).
(3) For reviews on Ligand Exchange Chromatography, see: H. F. Walton, *Sep. Purif. Methods*, **4**, 189–214 (1975); V. A. Davankov and A. V. Semechkin, *J. Chromatogr.*, **141**, 313–353 (1977).
(4) R. Aigner, H. Spitzy, and R. W. Frei, *Anal. Chem.*, **48**, 2–7 (1976).
(5) D. Kunzru and R. W. Frei, *J. Chromatogr. Sci.*, **14**, 381–385 (1974).
(6) F. K. Chow and E. Grushka, *Anal. Chem.*, **49**, 1756–1761 (1977).
(7) F. K. Chow and E. Grushka, *Anal. Chem.*, **50**, 1346–1353 (1978).
(8) N. H. C. Cooke, R. L. Viavattene, R. Eksteen, W. S. Wong, G. Davies, and B. L. Karger, *J. Chromatogr.*, **149**, 391–415 (1978).
(9) B. L. Karger, W. S. Wong, R. L. Viavattene, J. N. Le Page, and G. Davies, "12th International Symposium, Baden-Baden", *J. Chromatogr.*, 73–92 (1978).
(10) V. A. Davankov, S. V. Rogozhin, and A. V. Semechkin, *J. Chromatogr.*, **93**, 363–367 (1974).
(11) B. Lefebvre, Thesis, University of Pierre and Marie Curie, Paris, 1977. B. Lefebvre, R. Audebert, and C. Quivoron, *Isr. J. Chem.*, **15**, 69–73 (1976/77).
(12) I. S. Krull, *Adv. Chromatogr.*, **16**, 175–210 (1978).
(13) C. Murren, A. Stelling, and G. Felstead, *J. Chromatogr.*, **115**, 236–239 (1975).
(14) I. Molnar and C. Horvath, *J. Chromatogr.*, **142**, 623–640 (1977).
(15) A. Wehrli, J. C. Hildenbrand, H. P. Keller, R. Stampfli, and R. W. Frei, *J. Chromatogr.*, **149**, 199–210 (1978).

M. Caude
A. Foucault*
Laboratoire de Chimie Analytique de l'Ecole Superieure de Physique et de Chimie Industrielles de la ville de Paris
10 rue Vauquelin
75231 Paris, Cedex 05, France

RECEIVED for review September 11, 1978. Accepted November 27, 1978.

Comments on Determination of Acetate in Biological Material by Vacuum Microdistillation and Gas Chromatography

Sir: Vreman et al. in their article "Determination of Acetate in Biological Material by Vacuum Distillation and Gas Chromatography" (*1*) have emphasized the important advantages of vacuum distillation for the isolation of acetic acid prior to gas chromatography on Carbopack B coated with Carbowax 20M and H_3PO_4. They employed propionic acid as an internal standard, stating that propionic acid is found only in the blood plasma of patients with propionic acidemia.

I would like to point out that we have also found vacuum distillation after acidification of plasma, cerebrospinal fluid, or urine with sulfosalicyclic acid to be the ideal isolation procedure for volatile short chain acids of chain lengths from acetic to valeric and have published our method in detail (*2, 3*). We formerly employed Porapak PS for gas chromatography but we now use the Carbopack, Carbowax, H_3PO_4 phase because of minimal ghosting and the excellent separation of 2-methylbutryic and isovaleric acids. Although propionic, isobutyric, butyric, and isovaleric acid are one-twentieth or less the concentrations of acetic acid, they are normal constituents of plasma and other physiological fluids (*4*). Furthermore, propionic acid is elevated in the plasma of patients with Reye's syndrome (*5*). We have found the level of propionic acid and other volatile acids in peritoneal-dialysis fluid to be about one-third the plasma levels.

The method of Vreman et al. is an excellent one for acetic acid, but propionic acid should not be used as an internal standard without ensuring that its concentration is negligible in the samples being analyzed. One step in their procedure can be simplified. The sulfosalicylic acid can be added directly without separating the protein. By increasing the sample volume to 500–1000 μL and concentrating the distillate, as the sodium salts, then re-acidifying, the procedure of Vreman et al. could readily be extended to analysis of propionic, isobutyric, butyric, and 2-methylbutyric, isovaleric, and valeric acids as well as acetic acid.

LITERATURE CITED

(1) H. J. Vreman, J. A. Dowling, R. A. Raubach, and M. W. Weiner, *Anal. Chem.*, **50**, 1138–1141 (1978).
(2) T. Ando, K. Rasmussen, W. L. Nyhan, G. N. Donnell, and N. D. Barnes, *J. Pediatr.*, **78**, 827–832 (1971).
(3) L. Sweetman, "Heritable Disorders of Amino Acid Metabolism", W. L. Nyhan, Ed., Wiley, New York, 1974, pp 730–751.
(4) T. L. Perry, S. Hansen, S. Diamond, B. Bullis, C. Mok, and S. G. Malancon, *Clin. Chim. Acta*, **29**, 369–374 (1970).
(5) D. Trauner, L. Sweetman, J. Holm, S. Kulovich, and W. L. Nyhan, *Ann. Neurol.*, **2**, 238–241 (1977).

Lawrence Sweetman
Department of Pediatrics M-009
University of California–San Diego
La Jolla, California 92093

RECEIVED for review September 29, 1978. Accepted November 20, 1978.

0003-2700/79/0351-0461$01.00/0 © 1979 American Chemical Society

AIDS FOR ANALYTICAL CHEMISTS

Simultaneous Determination of Trace Amounts of Hydrogen, Oxygen, Nitrogen, Carbon Monoxide, Carbon Dioxide, Methane, Ethane, Ethylene, and Acetylene by Two Gas Chromatographic Columns in Parallel and One Detector

Fikry F. Andrawes*

Lockheed Electronics Co., Inc., 1830 Nasa Road 1, Houston, Texas 77058

Everett K. Gibson, Jr.

SN7, Geochemistry Branch, NASA Johnson Space Center, Houston, Texas 77058

The determination of trace amounts of H_2, O_2, N_2, CO, CO_2, CH_4, and C_2 hydrocarbons has wide application and is of interest to many analysts. Unfortunately, this suite of gases cannot be separated isothermally using a single chromatographic column. Analysis and separation of this group of gases can be carried out using temperature programming with carbon molecular sieve (*1*) or various Porapak columns (*2*). However, temperature programming suffers from some limitations and is not suitable for all applications. Isothermal methods of analysis using a combination of multiple columns with one or more detectors have been previously described (*3, 4*). For example, two columns with two detectors connected in parallel (commonly called a dual system) are frequently used to separate the gases mentioned above. A molecular sieve column is used to separate H_2, O_2, N_2, CH_4, and CO while a Porapak or carbon molecular sieve column is used to separate CO_2 and the C_2 hydrocarbons. The use of a dual system requires the use of a dual channel recorder and two integrators if quantitative analysis is required. The use of two columns connected in series with two nondestructive detectors has been reported (*3*), but this arrangement is not always suitable for trace analysis and it also requires two detectors. The use of more than one chromatographic column with one detector has previously been reported (*4*). In this arrangement a switching, valving system is used to allow insertion of independent columns in the carrier gas circuit. A distinct disadvantage of this system is the complicated switching required to carry out an analysis. This method of analysis cannot be used with the highly sensitive helium ionization detector because of different gas compositions at the outlet of different chromatographic columns. This difference changes the background current in the detector and prevents proper operation.

Our laboratory has been carrying out trace gas analysis in terrestrial and extraterrestrial materials (e.g., volcanic rocks, meteorites, and lunar samples). We have recently developed a gas chromatographic analysis system in which the trapped gases are released upon crushing of the sample and analyzed using a dual column–dual helium ionization detector system (*5*). With the present analytical system, it is difficult to perform simultaneous analysis of any sulfur gases that may be released from the samples. Because of this difficulty, we have attempted the separation of H_2, O_2, N_2, CO, CO_2, CH_4, and C_2 hydrocarbons using separate molecular sieve and Porapak columns operating in parallel with a single detector; the second detector is then available for the analysis of the sulfur gases on a separate column. The molecular sieve and Porapak columns have been tailor-made so that the gases eluted from the two columns would not overlap in the detector.

EXPERIMENTAL

A Varian 1700 gas chromatograph equipped with helium ionization detector was used in this study. The detector was operated at an applied potential of 480 V. A Valco 8-port sample injection valve was adapted to the gas chromatograph with a 100-μL sample loop. In order to obtain positive responses for all of the gases of interest, 1 5 ppm hydrogen was added to the purified helium carrier gas using the permeation tube technique described previously (*6*).

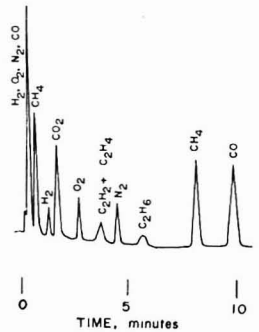


Figure 1. Analysis using 3 m Porapak Q with flow of 40 mL/min, and 6 m molecular sieve with flow of 55 mL/min

Chromatographic columns were made of stainless steel and of the following specifications: two columns of 6 m and 4.5 m long of 2.1-mm i.d. by 3.2-mm o.d. packed with molecular sieve 13X 60/80 mesh; one column of 3 m of 1.8-mm i.d. and 3.2-mm o.d. packed with Porapak Q 80/100 mesh; and one 1.5-m column of 2.1-mm i.d. and 3.2-mm o.d. packed with Porapak N 80/100 mesh. The columns were conditioned at 200 °C with helium flowing at 40 mL/min. The columns were operated at room temperature during this study.

The helium carrier gas line from the gas sampling valve was split into two fractions, (1) the Porapak column and (2) the molecular sieve column, via a two-way sample splitter. Between the sample splitter and chromatographic columns, a fine metering valve was placed in the line. The Swagelok connections at the outlets of the two chromatographic columns were connected using a Swagelok union modified by drilling into the center of the union (normal to the gas flow) and silver soldering a 1-cm stainless steel tubing of 3.2-mm o.d. to the union. The modified union was attached to the helium ionization detector using a Swagelok connection.

The standard reference gas contained the following concentrations of gases: 11 ppm H_2, 20 ppm O_2, 29 ppm N_2, 23 ppm CO, 5 ppm CO_2, 14 ppm CH_4, 5 ppm C_2H_2, 4 ppm C_2H_4, and 5 ppm C_2H_6.

RESULTS AND DISCUSSIONS

Typical analyses of H_2, O_2, N_2, CH_4, and CO using a molecular sieve column are achieved with columns of 1- to 2.5-m

0003-2700/79/0351-0462$01.00/0 © 1979 American Chemical Society

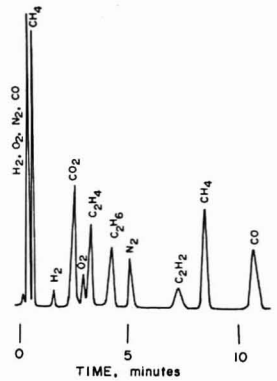


Figure 2. Analysis using 1.5 m Porapak N with flow of 43 mL/min, and 4.5 m molecular sieve with flow of 46 mL/min

length. However, in our work, we used molecular sieve columns of 4.5- to 6-m length in order to obtain a wide separation of the elution peaks to permit the gases eluted from the Porapak column to "fit" between the gases eluted from the molecular sieve column. In order to determine the operating parameters required for the operation of the dual columns–single detector system, both columns (molecular sieve and Porapak) were connected to the helium ionization detector. The needle valve on one of the columns is closed. The sample is analyzed on the open column. Chromatograms for the analysis are obtained using gas flow rates of 30 to 60 cm^3/min. After the analysis is completed on the first column, the needle valve on the first column is closed. The needle valve of the second column is opened and the analysis is carried out on the second column at different flow rates, and a second set of chromatograms is obtained. With the proper matching between the two sets of chromatograms, the appropriate flow rates can be determined. When the two columns are operated together (at the experimentally determined flow rates), small adjustments in the flow rate of either column may be required to enhance separation. The analysis of a mixture of gases is shown in Figure 1 with the flow through the 3-m Porapak Q column at 40 cm^3/min and the 6-m molecular sieve 13X column at 55 cm^3/min. The flow rate measured at the detector was 95 cm^3/min. The Porapak Q does not separate C_2H_2 from C_2H_4. If this separation is required, a Porapak N column can be used as shown in Figure 2. The flow rate through the 1.5-m Porapak N column was 43 cm^3/min and 46 cm^3/min through the 4.5-m molecular sieve 13X column. The flow rate measured at the detector was 89 cm^3/minute.

The use of two parallel columns with one detector has been previously described by Lysyj and Newton (7) for the separation of oxygen, nitrogen, and carbon dioxide. Brenner and Cieplinski (8) also describe the use of two parallel columns to separate oxygen, nitrogen, methane, propane, *n*-butane, and isobutane. The system we describe here utilizes molecular sieve and Porapak columns to analyze nine gases in about 10 min. The system is simple and can be used with either the sensitive helium ionization detector or the thermal conductivity detector. The use of two columns in parallel connected to one detector could be employed whenever two columns are needed for the analysis.

LITERATURE CITED

(1) A. Zlatkis, H. R. Kaufman, and D. E. Durbin, *J. Chromatogr. Sci.*, **8**, 416 (1970).
(2) O. L. Hollis, *Anal. Chem.*, **38**, 309 (1966).
(3) E. W. Cieplinski, W. Averill, and L. S. Ettre, *J. Chromatogr.*, **8**, SSO (1962).
(4) A. Di Lorenzo, *J. Chromatogr. Sci.*, **8**, 224, (1970).
(5) F. F. Andrawes and E. K. Gibson, *Am. Mineral.*, in press.
(6) F. F. Andrawes and E. K. Gibson, *Anal. Chem.*, **50**, 1146 (1978).
(7) I. Lysyj and P. R. Newton, *J. Chromatogr.*, **11**, 173 (1963).
(8) N. Brenner and E. Cieplinski, *Ann. N.Y. Acad. Sci.*, **72**, 705 (1959).

RECEIVED for review October 2, 1978. Accepted November 10, 1978. This work was performed in part under the auspices of the National Aeronautics and Space Administration, Contract NAS 9-15200 to Lockheed Electronics Co., Inc.

Preparing Nitrogen Gas for Nitrogen-15 Analysis

Richard J. Volk* and William A. Jackson

Department of Soil Science, North Carolina State University, Raleigh, North Carolina 27607

Ammonium nitrogen can be converted to N_2 for mass spectrometric ^{15}N analysis by oxidation with NaOBr (*1*) or LiOBr (*2*). Both reagents contain dissolved N_2 which must be removed just prior to use. This is commonly achieved by evacuating the hypobromite reagent either in a Rittenberg Y tube (*1*) or in a glass dispensing apparatus (*2, 3*). We have recently developed a freeze-layering procedure which eliminates the need for specialized glass apparatus. It consists of separating a dry NH_4Cl sample from N_2-free NaOBr by a layer of N_2-free ice. Nitrogen is subsequently generated from the sample by evacuating the container (a disposable test tube) and thawing its contents.

EXPERIMENTAL

Two reagents are required: ammonia-free redistilled water and NaOBr solution (*1*). The latter contains KI to minimize O_2 liberation (*4, 5*) and is diluted with 1.5 volumes of water to hasten subsequent freezing. Dissolved gases are displaced from both reagents by bubbling with argon for 10 min prior to and during sample preparation. The samples, consisting of 0.2 to 1.0 mg N as NH_4Cl, are evaporated to dryness at 95 °C in disposable, 12 mm o.d. × 75 mm borosilicate glass test tubes. During freeze-layering, the sample tubes are cooled in ethanol–dry ice slush, and are continuously flushed with argon (Figure 1). Each NH_4Cl sample is covered with 0.3 mL of N_2-free water, which freezes rapidly, followed by 0.5 mL of N_2-free NaOBr solution. Two 6-mm

Table I. Atom % ^{15}N Analysis of N_2 Samples Prepared by the Rittenberg Procedure (*1*) and by the Proposed Freeze-Layering Method

			atom % ^{15}N	
sample	tissue	N/sample, mg	Ritten-berg	freeze-layer
A	shoot	1.10	0.639	0.641
B	shoot	1.05	0.681	0.678
C	shoot	0.80	0.512	0.514
D	root	0.55	1.898	1.891
E	root	0.50	2.990	2.992
F	root	0.45	1.878	1.881

0003-2700/79/0351-0463$01.00/0 © 1979 American Chemical Society

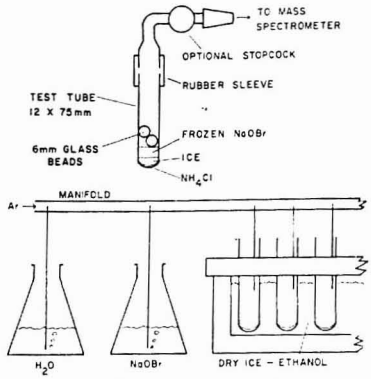


Figure 1. Preparation of freeze-layered samples using an argon manifold to minimize contamination with atmospheric nitrogen

diameter borosilicate glass beads are then placed on the frozen NaOBr to prevent its upward movement during subsequent N_2 generation. When sufficient samples have been prepared, they are stoppered and stored on dry ice until analyzed.

Just prior to analysis, a sample tube is attached to the mass spectrometer inlet system with a short length of 3-mm wall rubber tubing and an appropriate standard taper joint, which may include a stopcock for convenience (Figure 1). Applying a light coat of high vacuum grease improves the seal between the rubber and glass parts and minimizes leakage of air into the sample tube. The tube is evacuated, either with the mass spectrometer pump or with an auxiliary pumping system, thawed to permit NaOBr oxidation of the NH_4Cl, and refrozen prior to admitting N_2 into the instrument.

To test the procedure, six corn tissue samples, known to be enriched in ^{15}N, were digested using a semi-micro Kjeldahl procedure (6). The ammonia was recovered by distillation into 0.1 N HCl, using a silver condenser to avoid ^{15}N cross contamination between samples (7). Half of the distillate was analyzed by a Rittenberg procedure (1) and half by the proposed freeze-layering procedure, using an electron ionization mass spectrometer. When the oxygen peak in any sample exceeded the residual level, it was assumed that the sample contained air, and the nitrogen peaks were corrected accordingly. Correction factors were obtained from the mass spectrum of ambient air (5, 8). These corrections, although commonly used, are only approximate because the N_2/O_2 ratio in ambient air may differ from that in the contaminant air, especially if part of the latter came from the solutions.

RESULTS AND DISCUSSION

Comparable atom % ^{15}N values were obtained on samples run by the Rittenberg (1) and freeze-layering procedure (Table I). In no case was the Δ atom % ^{15}N greater than 0.007, nor was there a tendency for one method to exhibit higher values than the other.

The freeze-layering procedure as described here has proven to be both rapid and precise during six months of routine use. In addition, the oxygen values obtained with the proposed method are usually so low (e.g. m/e 32 < 0.1% of the m/e 28) that correction of the m/e 28 peak for air leakage is unnecessary. This is not the case with the Rittenberg tube procedure, where the oxygen values are considerably higher (e.g., m/e 32 > 0.3% of m/e 28). When using the latter procedure, we routinely correct for air leakage, based on the m/e 32 value obtained.

ACKNOWLEDGMENT

The authors gratefully acknowledge the technical assistance of Penelope V. Windsor.

LITERATURE CITED

(1) D. B. Sprinson and D. Rittenberg, *J. Biol. Chem.*, **180**, 707 (1949).
(2) P. J. Ross and A. E. Martin, *Analyst, (London)*, **95**, 817 (1970).
(3) L. K. Porter and W. A. O'Deen, *Anal. Chem.*, **49**, 514 (1977).
(4) M. P. Fleury, *Compt. Rend.*, **171**, 957 (1920).
(5) A. P. Sims and E. C. Cocking, *Nature (London)*, **181**, 474 (1958).
(6) H. A. McKenzie and S. Wallace, *Aust. J. Chem.*, **7**, 55 (1954).
(7) A. C. D. Newman, *Chem. Ind. (London)*, 115 (1966).
(8) D. Rittenberg in "Preparation and Measurement of Isotopic Tracers", D. W. Wilson, A. O. C. Nier, and S. P. Reimann, Ed., J. W. Edwards, Ann Arbor, Mich., 1948, pp 31–42.

RECEIVED for review October 31, 1978. Accepted December 8, 1978. Paper number 5806 of the Journal Series of the North Carolina Agricultural Experiment Station, Raleigh, N.C. This research was supported in part by National Science Foundation grant PCM 77-03152.

Author Index

Ammann, D. 351
Andrawes, F. F. 462
Annino, R. 379

Bajo, S. 376
Barr, W. H. 449
Blount, H. N. 327
Bond, A. M. 337

Caude, M. 459
Chow, L. H. 322
Ciccioli, P. 400
Curran, D. J. 353

Davies, G. 433
Denson, K. B. 400
Dijkstra, A. 420

Elving, P. J. 346
Eng, F. 455
Evans, J. F. 358
Ewing, G. W. 322

Foucault, A. 459
Freeman, H. C. 414
Freiser, H. 366, 373

Gibson, E. K., Jr. 462
Gonnord, M-F. 379
Gough, D. A. 439
Grabaric, B. S. 337
Guiochon, G. 379
Gupta, R. N. 455

Hadeishi, T. 387
Hahn, Y. 444
Hashimoto, A. 385
Hayes, J. M. 400
Henn, E. L. 452
Hieftje, G. M. 408

Jackson, W. A 463
Jagner, D. 342
Jezorek, J. R. 366, 373

Karger, B. L. 433
Kline, B. J. 449
Koester, V. J. 458
Koizumi, H. 387
Kuchhal, R. K. 392
Kumana, C. 455
Kuwana, T. 358
Kwong, H. S. 428

LePage, J. N. 433
Lewis, D. 455
Leypoldt, J. K. 439
Lindner, W. 433

McLaughlin, R. D. 387
Mallik, K. L. 392
Measures, R. M. 428
Meinschein, W. G. 400
Moiroux, J. 346
Mori, S. 382

Nau, V. 424
Nieman, T. A. 424

Oehme, M. 351
Olson, C. L. 444

Rawa, J. A. 452
Rinaldi, G. 400
Robillard, M. V. 435
Ross, H. H. 417

Savage, R. N. 408
Seelig, P. F. 327
Seitz, D. E. 433
Shum, G. T. C. 414
Siggia, S. 435
Simon, W. 351
Steiner, R. A. 351
Strohl, A. N. 353
Sweetman, L. 461

Turner, V. A. 449

Uden, P. C. 435
Uthe, J. F. 414

van Marlen, G. 420
van't Klooster, H. A. 420
Volk, R. J. 463

Whitten, W. B. 417
Wyttenbach, A. 376

Yamakawa, A. 382

Future Articles

Nanosecond Time-Resolved Spectrometry with a Tunable Dye Laser and a Simple Pulse-Gated Photon Counter

T. Imasaka, T. Ogawa, and N. Ishibashi

Determination of Individual Ubiquinone Homologues by Mass Spectrometry and High Performance Liquid Chromatography

S. Imabayashi, T. Nakamura, Y. Sawa, J. Hasegawa, K. Sakaguchi, T. Fujita, and K. Kawabe

Determination of Sulfur-Containing Gases by a Deactivated Cryogenic Enrichment and Capillary Gas Chromatographic System

S. O. Farwell, S. Gluck, W. L. Bamesberger, T. M. Schutte, and D. F. Adams

X-ray Fluorescence Determination of Uranium as the Barium Diuranate Precipitate

B. B. Jablonski and D. E. Leyden

Voltammetric Ion-Selective Electrode for the Determination of Nitrate

J. A. Cox and G. R. Litwinski

Surface Analyses by a Triboelectric Charging Technique

H. W. Gibson, J. M. Pochan, and F. C. Bailey

Metallized-Plastic Optically Transparent Electrodes

R. Cieslinski and N. R. Armstrong

Thin-Layer Spectroelectrochemistry for Monitoring Kinetics of Electrogenerated Species

E. A. Blubaugh, A. M. Yacynych, and W. R. Heineman

Determination of Nitrogen in Atmospheric Aerosols by Proton Activation Analysis

M. Clemenson, R. Novakov, and S. S. Markowitz

Laser-Induced Thermal Lens Effect for Calorimetric Trace Analysis

N. J. Dovichi and N. M. Harris

Spectroscopic and Chemical Characterization of Superoxide

S. Kim, R. Di Cosimo, and J. San Filippo, Jr.

Determination of Carbon in Steel by Secondary Negative Ion Mass Spectrometry

N. Yamaguchi, K.-i. Suzuki, K. Sato, and H. Tamura

Determination of Lead in Seawater by Furnace Atomic Absorption Spectrometry after Concentration with Yield Tracer

Y. Hirao, K. Fukumoto, H. Sugisaki, and K. Kimura

Two-Dimensional Chemical State Plots: A Standardized Data Set for Use in Identifying Chemical States by X-ray Photoelectron Spectroscopy

C. D. Wagner, L. H. Gale, R. H. Raymond

Determination of Proton Types in Solid Pitch by Wide Line Nuclear Magnetic Resonance Spectrometry

R. M. Pearson

Simultaneous Determination of Mixtures in Liquid by Laser-Induced Photoacoustic Spectrometry

S. Oda, T. Sawada, H. Kamada, and M. Nomura

Effect of Sample Thickness of the Magnitude of Optoacoustic Signals

M. J. Adams, G. F. Kirkbright, and D. R. Menon



Want the only dispenser with a Teflon®-coated plunger?

Ask for the 'Teflon Dispenser.'

Why does a Brinkmann Dispensette seem to work more smoothly than other bottle-top dispensers?

The secret is its Teflon-coated plunger.

Dispensers with glass or polypropylene plastic plungers often 'freeze' or 'stick' when used with alkaline reagents. On a Dispensette, the Teflon coating on the plunger insures smooth operation with most reactive chemicals (except HF), even with many concentrated acids and bases.

Of course, it takes more than a smoothly-working plunger to make a dependable dispenser. Instead of external glass tubing that could break or chip, Dispensettes are equipped with flexible Teflon filling and discharge tubes that can easily be cut to any desired length. Simply pull them off and a Dispensette is ready for autoclaving at 120°C without further disassembly.

Dispensette offers a wide selection of models for fast, accurate dispensing of volumes from 0.1 to 50ml, with better than ±1.0% accuracy and ±0.1% reproducibility. There is hardly a standard size screw-neck reagent bottle, can or container (even STJ 24/40 and 29/42 glassware) which a Dispensette will not fit, either directly or with optional screw-in adapters.

Some Dispensette design features have been copied by other dispensers, but none has its smooth, foolproof operation. That's because only Dispensette has a Teflon-coated plunger. Write for literature: Brinkmann Instruments, Inc., Cantiague Rd., Westbury, N.Y. 11590. In Canada: Brinkmann Instruments (Canada), Ltd.

Brinkmann Dispensette®

Available from: Ace Scientific
Beckman Instruments, Science Essentials Operations
Bio-Rad Laboratories/Cole-Parmer Instrument Co.
Curtin Matheson Scientific/Fisher Scientific
General Scientific/Markson Scientific/Preiser Scientific
Sargent Welch/Scientific Products/SGA Scientific
Arthur H. Thomas/VWR Scientific/Wilkens-Anderson Co.

Dispensette® is a registered trademark of R. Brand Co.
Teflon® is a Du Pont trademark.

CIRCLE 20 ON READER SERVICE CARD